DEPARTMENT OF THE INTERIOR
U.S. GEOLOGICAL SURVEY

Geological, Geochemical, Geophysical, and Oceanographic Data and Interpretations of Seamounts and Co-rich Ferromanganese Crusts from the Marshall Islands, KORDI-USGS R.V. *Farnella* Cruise F10-89-CP

by

James R. Hein[1], Jung-Keuk Kang[2], Marjorie S. Schulz[1], Byong-Kwon Park[2], Herbert Kirschenbaum[3], Suk-Hoon Yoon[2], Renee L. Olson[1], Virginia K. Smith[1], Dong-Won Park[2], George O. Riddle[4], Paula J. Quinterno[1], Yoon-Oh Lee[5], Alicé S. Davis[1], Seong Ryul Kim[2], Malcolm S. Pringle[1], Dong-Lim Choi[2], LedaBeth Pickthorn[1], Seymour O. Schlanger[6], Frederick K. Duennebier[7], Douglas D. Bergersen[7], and Jonathan M. Lincoln[6]

Open File Report 90-407

[1]U.S. Geological Survey, Menlo Park, CA
[2]Korea Ocean Research and Development Institute, Seoul
[3]U.S. Geological Survey, Reston, VA
[4]U.S. Geological Survey, Denver, CO
[5]Korea Research Institute of Energy and Resources, Seoul
[6]Northwestern University, Evanston, IL
[7]University of Hawaii, Honolulu, HI

INTRODUCTION

From 6 September to 3 October 1989, the Korea Ocean Research and Development Institute (KORDI) and the U.S. Geological Survey (USGS) participated in a cooperative cruise (F10-89-CP) to the Marshall Islands (Figs. 1, 2). Eight scientists from Korea, twelve from the United States, and one observer from the Republic of the Marshall Islands comprised the scientific staff (Table 1). The two main purposes of this cruise were: 1. To determine the geological, oceanographic, and geochemical controls on the origin and evolution of Co-rich Fe-Mn crusts that occur on seamounts in the Marshall Islands Exclusive Economic Zone (EEZ), and 2. To determine the origin and evolution of the seamounts and atolls in the Marshall Islands region.

Shipboard operations comprised 46 stations which included 28 dredges, 18 temperature-oxygen profiles in the water column, and 2 bottom camera-video surveys (Table 2). In addition, 2107 km of 3.5 and 10 kHz bathymetry, single-channel airgun, gravity, and magnetic surveys were completed (Table 3). In addition to the work in the Marshall Islands, one dredge was taken on Karin Seamount in the Johnston Island EEZ during the transit from Hawaii to the Marshall Islands. This report also includes chemical data for ferromanganese crusts and petrographic and age data on substrate rocks from dredges collected during University of Hawaii-Northwestern University cruise MW-88-05. MW-88-05 was a surveying and sampling cruise in the Marshall Islands that originated and ended in Guam between 24 April and 30 May, 1988.

A total of 20 seamounts in the Marshall Islands EEZ were sampled for Fe-Mn crusts and 22 seamounts and one atoll for basalts; outside the EEZ, 1 seamount was sampled for Fe-Mn crusts and 2 for basalts. On cruise F10-89-CP, 12 seamounts and 1 atoll were studied in the Marshall Islands EEZ and 1 seamount in the Johnston Island EEZ. The most extensive surveys were completed on Ujlañ volcanic complex, which comprises five volcanic peaks: Ujlañ, Ļalibjet, Ļōtab, Likelep, and Ļajutōkwa (Fig. 1; Tables 2, 3). In addition, 6 temperature-oxygen profiles were taken in the open-ocean between seamounts. An additional 8 seamounts from the Marshall Islands EEZ were sampled for Fe-Mn crusts from cruise MW-88-05, and those same 8 plus 2 others for basalts . We subsampled a dredge for basalts from an eleventh MW-88-05 seamount located in international waters about 550 km west of the Marshall Islands EEZ boundary.

With the data presented here, the Marshall Islands becomes the most extensively studied of the Pacific nations EEZs for Co-rich Fe-Mn crusts. Besides the seamounts listed in the previous paragraph, the flanks of 4 seamounts, 2 atolls, and an island were sampled in the eastern Ratak chain of the Marshall Islands in 1984 during USGS cruise L9-84-CP (Schwab et al., 1986; Hein et al., 1988). Five of these volcanic edifices yielded Fe-Mn

crusts for study. Hein et al. (1988) also reported chemical analyses completed by the USGS on crusts collected from 2 additional seamounts by the University of Hawaii. These same two seamounts were sampled by the F.R. Germany R.V. Sonne cruise SO 46/1 in 1986, but no results have been published on the collected samples. Thus, chemical analyses and other information are available for crusts from 25 seamounts within the Marshall Islands EEZ. This compares with the approximately 90 seamounts and 30 atolls located within the Marshall Islands EEZ. In terms of resource exploration, this is a remarkably thorough reconnaissance sampling of the Marshall Islands EEZ, especially when considering that the flanks of atolls do not have thick or widespread Fe-Mn crusts, because the crusts are destroyed by gravity movement of reef debris down the atoll flanks. This destructive process operates to water depths as great as 3000 m (Hein et al., 1987). So, excluding atolls, 25% of the seamounts in the EEZ have been surveyed; this percentage is closer to 75 if small seamounts and seamounts close to major atolls are eliminated, as these edifices would also have little potential for thick or extensive crusts.

This report presents all shipboard data and land-based laboratory data: 1. Track line, seismic-gravity-magnetic line, station, and bathymetric maps; 2. Location map with geographic names; 3. Seismic, gravity, magnetic, and bathymetric lines; 4. Temperature and oxygen profiles of the water column; 5. Paleontological age dating of sediments and sedimentary rocks; 6. Ferromanganese crust and substrate descriptions; 7. Mineralogy and major, minor, Pt-group, and rare earth element chemistry of Fe-Mn crusts; 8. Statistical analyses of crust chemistry; 9. Major element chemistry of substrate rocks; 10. Radiometric age dates of several basalts from MW-88-05; 11. Seafloor photographs; 12. Discussions and comparisons with other data.

Seamount is used as a general term in this report. Some of the seamounts (for example Look and Ruwitūñtūñ) have flat or nearly flat summits and could be designated as guyots.

Most of the seamounts and submarine volcanic complexes within the Marshall Islands EEZ have been given traditional Marshallese names, that were compiled by Alfred Capelle and Kanki Amlej, Alele Museum, Mājro. These seamount names have historical significance within certain defined corridors originating from nearby atolls (Appendix). The officially sanctioned seamount names are used in this report (Fig. 1). The Republic of the Marshall Islands has also adopted the traditional spelling of the atoll names, and we also use those officially sanctioned names here (Fig. 1; Appendix).

METHODS

The two main types of shipboard navigation used were GPS (the U.S. Navy's Global Positioning System) and Rhorho, which is the name of a

software program developed at the U.S. Geological Survey to do direct ranging on Loran C stations (Gann, 1988). The Japanese Loran chain was used while in the Marshall Islands area. Seismic surveys included 3.5 and 10 kHz bathymetry, and analog single-channel seismics collected with 40 in^3 and 160 in^3 airguns (Table 3). The velocity of sound used to calculate sediment thicknesses was 1600 m/s. CTD-oxygen profiles and water samples were taken with a Neil Brown rosette. Two or three water samples were taken per CTD cast and analyzed for oxygen content to calibrate the oxygen profiles. Standard Winkler titrations were done to determine oxygen contents.

X-ray diffraction analyses were completed on a Phillips diffractometer, with Ni-filtered, Cu kα radiation and a curved-crystal carbon monochrometer. Abundances of major oxides of substrate rocks were determined by X-ray fluorescence and FeO, H_2O, and CO_2 by wet chemical techniques (see Taggart et al., 1987 for details). For ferromanganese oxyhydroxides, most major and minor elements were determined by inductively coupled plasma-atomic emission spectrometry. K, Zn, and Pb were determined by flame atomic-absorption spectroscopy, and As, Cr, and Cd by graphite-furnace atomic absorption spectroscopy on air dried samples (Aruscavage et al., 1989). Pt-group elements and rare earth elements were determined by inductively coupled plasma-atomic emission spectrometry-mass spectrometry (Lichte et al., 1987).

For Q-mode factor analysis, each variable percentage was scaled to the percent of the maximum value before the values were row normalized and the cosine theta coefficients calculated. The factors were derived from orthogonal rotations of the principal component eigenvectors using the Varimax method (Klovan and Imbrie, 1971). All communalites are ≥0.94.

BATHYMETRY AND GEOPHYSICS

Generally, two seismic lines were run at nearly right angles across each seamount studied in order to choose dredge sites. However, two lines are not enough to produce bathymetric maps. A more detailed seismic and sampling survey over the Ujlañ volcanic complex allowed us to construct a bathymetic map of that area (Figs. 3-5). Ujlañ volcanic complex consists of 5 large volcanic edifices (6 counting Ujlañ Atoll) and several minor volcanic cones. Ujlañ Seamount is a composite edifice with three peaks, whereas, the other seamounts in the Ujlañ volcanic complex have only one peak each. The bathymetry suggests that northwest-southeast and northeast-southwest trending rift zones cut the Ujlañ volcanic complex. The bathymetry for Look Seamount was collected during cruise MW-88-05 with swath bathymetry and side-scan sonar using the SeaMARC II system (Fig. 6; Duennebier and Schlanger, 1988). Small volcanic cones rest on the flanks of the main volcanic edifice. The extensively rilled slopes are

characteristic of mid-plate Cretaceous seamounts. The channels act as conduits for sediment and talus debris. The bathymetry shown for the other seamounts (Figs. 7-12) is modified from Chase and Menard (1973) by changing the water depths from fathoms to meters (Chase, Seekins, and Young, U.S. Geological Survey, unpublished data, 1988).

Airgun and 3.5 kHz Lines

This section provides a brief description of each of the 37 seismic lines collected on F10-89-CP (Table 3; Figs. 13-79). The 156 km long **Line 1** crosses Ruwitūñtūñ and Look Seamounts from the southeast to the northwest (Figs. 13-17). The shallowest water depth over the summit of Ruwitūñtūñ Seamount is 1215 m. The rugged summit platform of Ruwitūñtūñ Seamount consists of a series to basement knolls and basins filled or partly filled with sediment. Craters can be distinguished on the volcanic pinnacles to the southeast. Sediment thickness varies from 104 m in the summit-edge basins to 32 m for interior basins. The sediment drape is thicker on the southeast sides of volcanic pinnacles. The summit platform may tilt slightly to the southeast. The upper to lower flank slope angles increase from 11° to 28° for the southeast flank and from 13° to 17° for the northwest flank.

The pass between the two seamounts is rugged, showing volcanic pinnacles, sediment fill, slump deposits, and talus. The summit of Look Seamount shallows to 1000 m water depth and consists of mostly small volcanic pinnacles draped by a thin layer of sediment. Sediment thickness varies from 0 m to 40 m on the summit and slumps and talus occur on the lower slopes. Slope angles range between 11 and 14°, although the lower northwest slope is 33°.

The 33 km long **Line 2** crosses the lower north-northwest flank of Look Seamount (Figs. 18, 19). The line shows mostly talus debris and slump structures, with abyssal sediment covering the lowermost slope at the northeast end of the line.

The 46 km long **Line 3** crosses Look Seamount from north to south (Figs. 20, 21). The summit shallows to 999 m water depth, consistent with the line 1 crossing. The summit topography is irregular with small sediment-filled basins. Maximum sediment thickness is 32 m. The sedimentary section is nearly transparent with few internal reflectors. Pelagic sediment at least several hundred meters thick laps up on the lower south flank. The water depth to abyssal sediment is about 400 m deeper on the north flank than on the south flank.

Lines 4 through 9 total 241 km and cross North and South Ļāānmōjānjān Seamounts (Figs. 22-32), which are elongated in a north-south direction. The summit of South Ļāānmōjānjān is about 7 km west-northwest of its position on the Chase and Menard (1973) base map. Little or no sediment occurs on the summit or upper flanks of these generally very

rugged seamounts (see Line 6; Figs. 26, 27). The shallowest water depth, 1090 m, was recorded at the end of line 9 (Figs. 31, 32), which ended at the summit of North Ļāānṃōjānjān. Upper and lower slope angles vary from 9 to 17° and from 9 to 25°, respectively.

The west flank of North Ļāānṃōjānjān shows a series of well-defined terraces, whereas the east flank shows two large slumps, the lowermost of which covers abyssal deposits at about 5400 m water depth (Line 4, Figs. 22, 23). Talus occurs at the base of at least two of the terraces on the west flank and on all the lower seamount flanks crossed by lines. The north and south flanks of North Ļāānṃōjānjān also show several terraces (Line 6, Figs. 26, 27).

Lines 10 through half of 12 cross Ļami Seamount, which is elongate in a northwest-southeast direction (Figs. 33-37). The shallowest water depth is 1295 m. The flat summit supports small basement knolls and sediment-filled basins (Figs. 36, 37). Maximum sediment thickness is 64 m. Upper and lower flank slope angles vary from 13 to 19° and from 11 to 21°, respectively. A broad terrace characterizes the southeast flank while a narrower, shallower-water terrace is located on the northwest flank; this configuration of terraces is a mirror image of the terraces on the adjoining Lọmilik Seamount (Fig. 37). In other words, the broad terraces occur on the adjoining (facing) flanks and the narrow terraces on the outer flanks (Line 12, Figs. 36, 37). The summit of Ļami is slightly shallower than the summit of Lọmilik. Slumps are prevalent along the east and west flanks and the saddle between the two seamounts.

Half of Line 12 through 14 cross Lọmilik Seamount, which is joined to Ļami Seamount by a shallow-water pass (Figs. 36-41). The flat summit consists of volcanic knobs with sediment to 72-m thick infilling basins between knobs. Two of the knobs project above the sediment (Figs. 40, 41). The broad terrace on the north flank extends around the east side of the seamount, in contrast to the steep west flank which lacks a terrace. Volcanic knobs, sediment, slumps, and talus occur on the broad terrace in several places. Slumps and talus characterize the lower flanks. Upper and lower flank slope angles vary between 9 and 19° and between 9 and 27°, respectively.

Line 15 crosses Ļōjemeja Seamount, whose summit shallows to a depth of 1750 m (Fig. 42). A large volcanic pinnacle separates the sediment cap from a sediment-covered terrace to the southwest. Maximum sediment thicknesses on the cap and terrace are 139 m and 48 m, respectively. The upper flanks are very steep, with slope angles from 40 to 58°.

Line 16 traverses the Ujlañ volcanic complex from north to south, crossing three seamounts (Ļajutōkwa, Ļotab, and Ujlañ Seamounts) and the western flank of Ujlañ Atoll (Figs. 43-46). The water depth to the summit of Ļajutōkwa, Ļotab, and Ujlañ Seamounts is 1585 m, 1560 m, and 1670 m, respectively; the maximum thickness of the sediment cap for each

seamount is 320 m, 160 m, and 0 m, respectively. Ujlañ has a sediment cap farther to the west (see lines 17 and 22; Figs. 47, 48, 57, 58). Most of the passes between seamounts appear to contain little pelagic sediment, but substantial talus and slump deposits. Abyssal sediments occur in the pass at the northern end of the line and are at least several hundred meters thick. The northeast flank of Ļōtab Seamount shows a number of large structural failures (Figs. 44, 45). Ujlañ Seamount has a terrace on the southwest side. The southern seamounts are more rugged, with less pelagic sediment than the northern seamounts. Flank slope angles of Ļajutōkwa vary from 9 to 15° and those of Ļōtab and Ujlañ, from 9 to 20°.

Line 17 crosses two of the three peaks of Ujlañ Seamount (see line 22 for the other) and Ļalibjet Seamount of the Ujlañ seamount complex (Figs. 47, 48). The water depth to the summits of south Ujlañ peak, north Ujlañ peak, and Ļalibjet Seamounts is 1250 m, 1590 m, and 1453 m, respectively; the maximum thickness of the sediment cap for each seamount is 208 m, 0 m, and 190 m, respectively. The southern half of the Ļalibjet sediment cap has either been eroded, or, more likely, has slumped into the depression between the two seamounts, making the pass between Ļalibjet and north Ujlañ peak shallower than the one between north and south Ujlañ peaks. Camera run 1 overlaps with the area of dredges 14 and 15 (Figs. 47 and 48) and extends just beyond the edge of the sediment cap. Little limestone was recovered by the 5 dredges taken along this line and we expect that reefs are either small or do not cap these volcanic structures. The flanks and passes of these seamounts are characterized by slump deposits and the north flank of the southern Ujlañ peak has a small terrace. The acoustic basement beneath the sediment cap of Ujlañ and Ļalibjet Seamounts is flat. The flanks of Ujlañ and Ļalibjet Seamounts have slope angles of 6 to 21° and 9 to 17°, respectively.

Lines 18 and 19 cross Likelep Seamount, the northernmost seamount in the Ujlañ complex (Figs. 49-52). The shallowest water depth over the summit is 1545 m (line 19). The summit is characterized by volcanic knolls, a perched sediment cap, and possibly outward dipping beds on the northeast side (Figs. 51, 52). Maximum sediment thickness on line 18 is 176 m and on line 19, 336 m. Line 18 shows a volcanic cone outcropping from the pelagic cap. Southwest of the cone, the sediment appears to be scoured and eroded. The beds are turned down immediately adjacent to the cone. Line 18 also shows a prominent terrace on the northeast flank. To the northeast of Likelep on line 19 is a small adjoining seamount (Figs. 51, 52). Slumps are common on the flanks of Likelep Seamount. Flank slope angles vary between 10 and 27°.

Line 20 crosses Likelep and Ļajutōkwa Seamounts (Figs. 53, 54). Cross sections of the two peaks are nearly mirror images. The shallowest water depth over the summits of Likelep and Ļajutōkwa is 1570 m (compared to 1545 m on line 19) and 1585 m (identical to line 16), respectively; the maximum thickness of the sediment caps is 288 m (compared to 336 m on line 19) and 208 (compared to 320 on line 16),

respectively. Both peaks have volcanic knolls beneath the sediment caps. The sediment cap on Ļajutōkwa thins from east to west. Abyssal sediments occur to the east of Ļajutōkwa Seamount. Flank slope angles vary between 7 and 15° for Likelep and between 9 and 19° for Ļajutōkwa.

Line 21 crosses Ļōtab and Ļalibjet Seamounts (Figs. 55, 56). The shallowest water depth over the summits of Ļōtab and Ļalibjet is 1557 m (nearly the same as 1560 m on line 16) and 1439 m (close to the 1453 m on line 17), respectively; the maximum thickness of the sediment caps is 152 m (nearly the same as 160 m on line 16) and 184 m (nearly the same as 190 m on line 17), respectively. The acoustic basement across both summits is nearly flat, although it dips slightly to the northeast on Ļalibjet. A small seamount adjoins the lower northeast flank of Ļōtab. Flank slope angles vary between 6 and 20° for Ļōtab and Ļalibjet.

Line 22 crosses two of the three peaks (northwest and south peaks; the north peak is seen on line 17) composing Ujlañ Seamount (Figs. 57, 58). The shallowest water depth over the summits of the northwest and south peaks is 1295 m and 1254 m, respectively; for comparison, water depths of summits on lines 16 and 17 are 1250 m (south peak) and 1590 m (north peak). The maximum sediment thickness on the northwest peak is 184 m (line 22) and on the south peak is 208 m (line 17; 200 m on line 22). The pelagic cap thins symmetrically across the acoustic basement of the northwest peak. The northwest flank shows numerous slumps. The pelagic cap on the south peak is asymmetrical, thickening to the southeast; the acoustic basement dips slightly to the northwest. A small slump scar or terrace marks the upper southeast flank. Flank slope angles vary between 7 and 15°.

Line 23 crosses the lower south flank of Ujlañ Seamount (Fig. 59). The topography is rough and probably consists of talus, slumps, and debris flows.

Lines 24, 25, and 26 cross Mij-Lep Seamount, which shallows to 1105 m (Figs. 60-62). The sediment cap has a maximum thickness of 184 m (Fig. 62) and thins toward the margins. A flat-topped volcanic pinnacle outcrops from the pelagic cap (Fig. 60). The western flank of the seamount is steeper than the eastern flank and shows many hyperbolic reflections that we interpret to be either slumps or basement outcrops. Other volcanic pinnacles occur, such as on the northwest flank (line 25) and the lowermost south flank. Flank slope angles vary between 9 and 23°.

Line 27A extends from Jālwōj Atoll to Jebro Seamount, but only the part that crosses Ṃaanjidep Seamount is discussed (Fig. 63). The apparent summit of this seamount rises to within 2215 m of the sea surface. The peak morphology and the absence of sediment suggest that the track line crosses one of the upper flanks of the seamount rather than the summit. Volcanic knobs characterize the middle and lower flanks. The abyssal sedimentary section on the north side is disrupted at the contact with the seamount, where an erosional(?) moat is seen.

Lines 27 through 32 cross Jebro Seamount, which has two peaks, one to the southwest and the other to the northeast (Figs. 64-69). The shallowest water depth over the summit of the southwestern and northeastern peaks is 1530 m (line 31) and 1253 m (Line 27), respectively; the maximum thickness of the sediment cap is 256 m (line 30; 240 m on lines 27 and 31) and 224 m (line 27), respectively. The pelagic cap on the southwest summit thickens toward the east. The upper part of the sedimentary section is apparently bedded, whereas the lower part is transparent. The pass between the southwest and northeast peaks contains pelagic sediment as well as slump deposits. A basement outcrop marks the north edge of the summit of the southwest peak. Talus and slumps characterize the flanks. Flank slope angles vary between 7 and 24°.

Lines 33 through 37 were taken on the central part of the archipelagic apron between Jebro Seamount and Majro Atoll (Figs. 70-79). Line 33 (Figs. 70 and 71) begins at the summit of Jebro Seamount and shows about 200 m of apron sediments that thin against the east flank of the seamount. The sediment section also thins over basement highs. Several erosional channels are present on the seafloor, one of which has levees and occurs above the north flank of a basement high (line 35, Figs. 74, 75). Another channel shows an asymmetric cross section and occurs over the south flank of a basement high; this channel is bounded to the east by sediment and to the west by basement (north end of line 36, Figs. 76, 77). Several small basement highs protrude through the sediment (lines 35 and 36, Figs. 74-77). The maximum sediment thickness for the 6 lines is 240 m (line 34, Figs. 72, 73), averaging about 210 m. The average water depth is about 4100 m.

Many of the characteristics of seamount morphology and structure described here have also been noted by Duennebier et al. (1988a) for other seamounts in the Marshall Islands region. Their conclusions are based on both seismic records and SeaMARC II side-scan sonar records.

Gravity and Magnetic Profiles

Gravity was logged continuously during the cruise, but magnetics were recorded only during geophysical lines 1 through 37. The magnetic and gravity profiles are organized according to each seamount surveyed (Figs. 80-89). The eotvos corrections used to process the gravity have been run through a standard low-pass filter. The magnetics were not run through a filter. The navigation used to calculate the eotvos corrections was sampled from the approved navigation file at 20 second intervals. The gravity land ties used to calculate the free air corrections were: 968747.1 mGal on 001/0101 for meter S-53 (assumed, no first tie made) and 968747.1 mGal on 275/2220 for meter S-53 at New Pier, Majro. The gravity constant used for converting from digital meter units to mGals for meter S-53 is 0.9972.

The gravity and magnetics are currently being processed and modeled; the interpretations will be presented elsewhere. Mean magnetizations of the seamounts and paleomagnetic polarities and poles will be determined using both least-squares and semi-norm inversion modeling techniques. Comparison of the paleomagnetic poles determined from these inversions with the apparent polar wander path (APWP) for the Pacific plate will enable us to: 1. constrain the age of the volcanism that formed the seamounts, especially those seamounts for which radiometric ages are not available; 2. constrain the possible tectonic histories of the Pacific plate, and 3. determine the Pacific APWP with greater reliability, using those seamounts with radiometric ages.

The magnetics and gravity versus time are presented here (Figs. 80-89). All of the seamounts have a negative magnetic anomaly over their summits, although in detail the anomaly patterns are more complex. The negative anomaly is not necessarily centered over the summit, or it may be a small negative anomaly superimposed on an overall positive anomaly, such as on parts of the Ujlañ volcanic complex (Figs. 85, 86). The magnetic profiles and preliminary modeling indicate that the seamounts surveyed are probably all normally magnetized, and that the resultant paleomagnetic poles lie along the Late Cretaceous part of the Pacific APWP. The magnetic data are consistent with the hypothesis that all of the seamounts studied formed during normal polarity periods in the Late Cretaceous, and that there has been little if any volcanism since that time.

The positive gravity anomalies over the summits of the seamounts are also quite variable, but average about 200 mGals and range up to about 350 mGals. Such gravity anomalies are usually indicative of relatively uncompensated volcanoes that formed in a mid-plate environment significantly removed from a mid-ocean ridge. Further gravimetric modeling will quantify the degree of compensation, determine the effective elastic thickness of the lithosphere at the time of volcanic loading, and enable us to compare the Marshall Islands volcanoes to other seamounts throughout the ocean basins.

WATER COLUMN STUDIES

Thirteen CTD-oxygen profiles were taken over the summit and/or flanks of each seamount studied as well as 5 profiles in deep water between seamounts (Figs. 90-107). The conductance module failed on the CTD, so salinity data are not available and we report only oxygen content and temperature versus water depth (Figs. 90-107). The water depth to the top of the oxygen-minimum zone varies throughout the area and ranges from 205 m for southernmost station CTD 17 (open ocean; Fig. 106), to 420 m for CTD 5 (Fig. 94) located on the western edge of the summit of North Ḷāānṃōjānjān Seamount, the northernmost seamount with CTD data (Table 4). In fact, the water depth to the top of the oxygen-minimum zone has a

strong positive correlation (correlation coefficient = 0.823) with latitude of the 18 stations, but does not correlate with longitude or water depth of the stations. This change with latitude is especially clear in the eight stations along a north-south traverse over Ujlañ seamount complex (from south to north, stations 9, 10, 11, 12, 13, 14, 8). The change with latitude is due to the equatorial zone of high biological productivity. The greater quantities of organic matter produced to the south are oxidized in the water column and, combined with zooplankton respiration, deplete the seawater in oxygen, thereby raising the top boundary of the oxygen-minimum zone. From our 18 stations, the regional mean water depth of the top of oxygen-minimum zone is 305 m.

In addition to the water depth to the top of the oxygen-minimum zone increasing to the north, the maximum amount of depletion of oxygen in the seawater decreases to the north and west (lower oxygen contents to the south and east), and the water depth of the greatest oxygen depletion increases to the west.

In order to compare temperature profiles from the 18 stations, we looked at the water depth at each station corresponding to 10°C; the 10°C isotherm corresponds roughly to the boundary between the seasonal and permanent thermocline in the region and occurs at water depths near the top of the oxygen-minimum zone (Table 4). This isothermal boundary has the same pattern of distribution as the layer marking the top of the oxygen-minimum zone. The water depth of the temperature boundary has a positive correlation with latitude with a correlation coefficient of 0.809. The water depth of the 10°C isotherm varies from 200 m for open ocean CTD 16 (Fig. 105), to 310 m for CTD 5 (Fig. 94) taken over North Ḷāānṃōjānjān Seamount in the northernmost part of the area. The average regional water depth of the 10°C isotherm is 247 m. The water depth of the isothermal boundary deepens somewhat over the summits (CTD 10, 11, 12; Figs. 99-101) and flanks (CTD 13, 14; Figs. 102, 103) of the Ujlañ volcanic complex relative to the off structure profiles to the north (CTD 8; Fig. 97) and south (CTD 9; Fig. 98).

SEAMOUNT GEOLOGY, PETROLOGY, AND GEOCHEMISTRY

As noted in the previous section, most of the seamounts are capped by various amounts of sediment, predominantly foraminiferal sand and ooze (Fig. 108). Based on nannofossils and Foraminifera, sand recovered in dredges D10, 18, 22, 24, and 25 is Pleistocene or Holocene in age, which is probably characteristic of most of the foraminiferal sand and ooze that caps the seamounts and covers the upper slopes in the Marshall Islands area (Table 5). One sand sample from interior vugs in a substrate rock (D22-1-1) contains microfossils that indicate a Pliocene or Quaternary age. A few questionably identified specimens of *Globoquadrina venezuelana* (middle

Eocene through early Pliocene) are present. Talus debris with a thin coating of Fe-Mn oxyhydroxides and Fe-Mn nodules rests on the sediment in places. The two bottom-photographic surveys on Ujlañ volcanic complex show that outcrops on the upper flanks of the seamounts may be dusted with sediment or covered with a thin layer of sediment. Exposed outcrops alternate with sections of sediment-covered outcrops. The exposed outcrops commonly include one or more nearly vertical cliffs several meters to tens of meters high. Outcrops commonly contain sediment ponds that fill lows and sediment-filled troughs oriented both parallel to and perpendicular to the slope.

The first bottom camera-video survey was on Ļalibjet peak in the Ujlañ seamount complex, where the 6 hr survey traversed 6.6 km at 0.5 knots (Figs. 109-111). The survey began at 1725 m water depth. From **1725 m to 1650 m** (0.99 km), rock outcrops occur that are covered with apparently thick botryoidal Fe-Mn crusts and that contain sediment ponds (Fig. 109). These outcrops alternate with sediment troughs that have talus debris resting on the surface adjacent to the margins of the outcrops. The sediment is prominently rippled (Fig. 110). In places the outcrops are dusted with sediment (Fig. 110B). At about 1650 m, the nearly flat summit platform begins. From **1650 m to 1630 m** (2.33 km), sediment-covered outcrops occur alternating with sediment troughs up to 60 m wide (Fig. 111). Little or no talus debris occurs on or adjacent to outcrops. From **1630 m to 1600 m** (2.82 km), large sediment covered outcrops occur alternating with sediment troughs as before, however, sections to tens of meters wide contain sparse to moderate amounts of talus debris. The talus debris includes pebble- to cobble-sized Fe-Mn crust-coated rock fragments and spherical Fe-Mn nodules (Fig. 111). These large Fe-Mn nodules were collected in dredge D16. The margin of the sediment cap on the seamount was crossed at a water depth of about 1600 m. From **1600 m to 1597 m** (0.25 km, end of survey), rippled sediment occurs (Fig. 111). The ripples are elongate, straight crested to sinuous, and asymmetric. The ripples are more symmetric where the crests are sinuous. Tracks and trails modify the ripples to various degrees.

The second bottom camera-video survey was on Ļajutōkwa Seamount in the Ujlañ volcanic complex, where the 5 hr survey traversed 5.6 km at about 0.6 knots (Figs. 112-114). The survey began at about 3225 m water depth. From **3225 m to 2345 m** (2.59 km), linear outcrops striking parallel to the slope occur that are rarely sediment free (Fig. 112). Talus-free outcrops alternate with outcrops containing talus debris; sediment troughs; and sediment troughs with talus resting on the sediment surface. The linear outcrops generally are flanked on both the downslope and upslope margins by cobble- and pebble-sized talus debris that decreases in amount and size away from outcrops. The Fe-Mn crusts coating the rocks are not botryoidal and are probably thin; the outcrops are apparently being buried by pelagic sediment (Figs. 112, 113A). The sediment is not rippled and apparently is not actively being transported by bottom currents. The

steep upper seamount flank from **2345 m to 2014 m** (0.63 km) shows linear outcrops with distinctly botryoidal Fe-Mn crusts on the rock surfaces (Figs. 113B,C). The outcrops alternate with sediment ponds and troughs (Fig. 113C). Rare outcrops are fractured and fragmented, but fragments have not been transported. From **2014 m to 1870 m** (1.00 km), a major hard-rock outcrop occurs with small sediment ponds on the down-slope margin, but very little talus or sediment is noted (Fig. 114A). This section includes at least two and perhaps three vertical 10-m-high cliffs. This outcrop ends near the edge of the summit platform. From **1870 m to 1845 m** (0.15 km), predominantly talus debris resting on sediment occurs with small outcrops at the upslope margin (Fig. 114). Talus ranges from boulders to pebbles and includes many siliceous sponge fragments. This section marks the transition from outcrops to the sediment cap. From **1845 m to 1820 m** (1.20 km, end of the survey), the camera sled crossed the edge of the sediment cap. The sediment is rippled, but the ripples become more degraded upslope (Fig. 114D).

Rock Types and Ages

Rock types in decreasing order of abundance are breccia, basalt, hyaloclastite (and volcanic ash), limestone (much of it partly phosphatized), volcaniclastic sandstone-siltstone-mudstone, phosphorite, and ironstone (Tables 6, 7, 8). Breccia is overwhelmingly the predominant rock type and comes in many varieties (Table 7). Most commonly breccia consists of a variety of basalt clasts in various kinds of cement, or with a matrix composed of altered fine-grained volcanic debris or carbonate sediment. Cements in decreasing order of abundance are phosphorite, phillipsite, calcite, Fe-Mn oxyhydroxide, and Fe hydroxide. Smectite forms a rim cement on some clasts. Invariably, the phosphorite cement is replaced foraminiferal limestone, with the foraminifers also replaced, but ranging from well preserved to ghosts. A few samples were recrystallized before being replaced (D21-6, 7, and 8). The age of the breccia from Likelep Seamount (D19-16) is probably Campanian, as determined from the Foraminifera in the matrix (Table 5). The calcite cements are void-filling cement and are not obviously related to a foraminiferal sediment precursor. Phillipsite most commonly forms a rim cement, but may extend out to completely fill void space. The crystals are most commonly tabular and radiate from clast boundaries. In one sample (RD63-D), large single phillipsite crystals fill each void space, and in another (D20-1), it forms a radial-fibrous rim cement. Phosphorite and phillipsite (consisting of cross twins) may be finely mixed, with the phillipsite replacing the phosphorite (D21-7). Goethite cement is probably hydrothermal and forms wavy laminations and a swirled texture; it can be thoroughly mixed with phosphorite cement, although cross-cutting veins contain only phosphorite, indicating two generations of phosphorite (D21-9). The order of formation

of cements varies in different samples: D20-1, smectite-calcite-phillipsite, in places phillipsite replaced calcite; D21-6, phillipsite-phosphorite; D21-19-1, phillipsite-phosphorite-Fe-Mn oxyhydroxide; D26-9A, phillipsite-calcite-phosphorite(?), in places calcite replaced phillipsite, forming pseudomorphs. Clast types in decreasing order of abundance are basalt, hyaloclastite, phosphorite, sandstone, limestone, Fe-Mn crust fragments, rarely abundant ironstone fragments (D21-2, D21-8), mollusk fragments (D10-17A), and fish debris (D1-1). Basalt clasts are commonly partly replaced by smectite and goethite.

Hyaloclastites are almost completely replaced by smectite and goethite and rarely by celadonite. Grains were predominantly highly vesicular glass shards. Phillipsite and phosphorite are common cements, with phillipsite forming first when they occur together. Laminated and bedded deposits of hyaloclastite, volcanic ash, and volcaniclastic sandstone, siltstone, and mudstone are common. All gradations exist among hyaloclastite, volcaniclastic sandstone, and breccia. Most sandstones consist of grains of volcanic rock fragments, however, mollusk fragments (D18-20-1), plagioclase, pyroxene, and amphibole crystals also occur. Some clastic beds display cross bedding and parallel laminations. The nannofossil age of a laminated hyaloclastite-sandstone sequence (D11-3G) from Ḷami Seamount is Eocene or Oligocene (Table 5). A pocket of foraminiferal ooze (D11-3F) exposed by cutting through the center of the laminated rock is Pliocene in age. Two calcareous mudstones from Jālwōj Atoll (D24, D25) give a nannofossil age of late Campanian or Maastrichtian, between 66 and 80 m.y. old (Table 5).

Foraminiferal limestone is the dominant type of limestone, and rarely occurs without some replacement by phosphorite; some samples are completely replaced by phosphorite (Tables 7, 8). Planktonic and benthic Foraminifera and rudist ages of limestones from six seamounts sampled on cruise MW-88-05 yield Cretaceous ages (Lincoln, 1990): Ḷọ-Eṇ Seamount (RD33), latest Albian or early Cenomanian; Ruwitūñtūñ Seamount (RD40), Albian rudists redeposited in Campanian limestone; Wōdejebato Seamount (RD50), Albian rudists redeposited in Campanian limestone; Ḷōbbadede Seamount (RD56), Cenomanian; Ḷewa Seamount (RD58), latest Albian or earliest Cenomanian; Ḷōmtal Seamount (RD59), Santonian; Unnamed (RD67), early Cenomanian or older (see also Lincoln et al., 1989). Rarely, radiolarians, echinoids, and other fossils occur with the foraminifers in the limestones. Various amounts of volcanogenic grains may contaminate the limestones and limestone may be interbedded with volcaniclastic beds. Limestone beds rarely show recrystallization and neomorphism. Little compaction took place before cementation of the foraminiferal sands.

Volcanic rocks are predominantly alkalic basalt. Some samples are strongly alkalic (basanite and/or nephelinite) and some are extensively differentiated (hawaiite and/or mugearite). No chemical analyses are available at this time and rock names are based on the kind and abundance

of minerals present. The alkalic basalts have abundant olivine in the groundmass and typically contain pinkish-brown clinopyroxene, which are presumed to be Ti-rich. Many different rock types were commonly recovered within a single dredge. Lithologies range from aphyric to highly porphyritic. Phenocrysts when present are predominantly plagioclase with variable amounts of clinopyroxene and olivine pseudomorphs, but in some samples, large (centimeter-size), resorbed clinopyroxene are more abundant than plagioclase and olivine. The plagioclase and clinopyroxene occur most frequently as glomerocrysts and are typically unaltered. The olivine pseudomorphs are commonly single, euhedral crystals that were completely replaced by iddingsite, clay minerals, or more rarely by calcite. The groundmass of the basalts is also highly variable. In some samples, the groundmass is holocrystalline, consisting of plagioclase microlites, accompanied by variable amounts of small iddingsite crystals (replaced olivine) and fresh granules of clinopyroxene and opaque minerals. In other samples, significant amounts of intersertal glass is present that is typically altered to palagonite and/or clay minerals and iron hydroxides. Some samples from a guyot west of the Marshall Islands (RD67) contain fresh sideromelane and only partly altered olivine. Textures range from intersertal or intergranular to hyalopilitic.

The more differentiated samples (e.g. hawaiite or mugearite) include two petrographic groups. One group consists of sparsely plagioclase phyric rocks with large (centimeter-size) phenocrysts in a matrix of trachytic plagioclase microlites and abundant opaque minerals, accompanied by only traces of granular clinopyroxene. The other group is amphibole-phyric with rounded amphibole phenocrysts, plus rare clinopyroxene and/or plagioclase phenocrysts, in a groundmass of sub-trachytic plagioclase and opaque minerals in devitrified glass. Apatite commonly occurs in trace amounts.

The strongly alkalic compositions are highly vesicular ankaramites with an abundance of clinopyroxene phenocrysts plus olivine pseudomorphs, in a groundmass of granular clinopyroxene accompanied by minor feldspathoids or traces of plagioclase and variable amounts of altered glass. The feldspathoids are typically replaced by analcime.

All samples are altered. The samples containing unaltered glass (RD67) and the holocrystalline hawaiite and mugearite samples are the least altered. Highly vesicular ankaramites, with amygdules of zeolites, clay minerals, and calcite, and samples containing a large proportion of devitrified glass are the most altered.

Except for the ankaramites that appear strongly alkalic in composition, the samples are typically non-vesicular or only sparsely vesicular (< 5%). The absence of vesicles can indicate either eruption in deep water with hydrostatic pressure great enough to prevent degassing or it may indicate subaerial eruption of degassed lavas. The ubiquitous oxidation of opaque minerals, and the high abundance of reddish brown iron oxides in veinlets and disseminated throughout the groundmass of some samples, suggest that some of these samples may have been exposed to subaerial weathering. The

presence of abundant palagonite in other samples suggest rapid quenching in water and may indicate submarine eruption, or the flow may have erupted subaerially and then flowed into the ocean. The presence of abundant vesicles in strongly alkalic rocks does not necessarily indicate eruption in shallow water. Studies of some submarine lavas (Moore et al., 1982; Gill et al., 1989) showed that volatile-rich lavas may be highly vesicular despite eruption under great hydrostatic pressure. The composition of the rocks must be taken into account when attempting to relate vesicle abundance to eruption depths. The presence of multiple lithologies in a single dredge suggests compositionally diverse flows of limited areal extent. The petrologic diversity is similar to that observed for edifices in the Ratak chain of the Marshall Islands (Davis et al., 1989) and for edifices in the Line Island chain (e.g. Natland, 1976).

Radiometric ages for 19 volcanic complexes are presently being determined (Table 9). Four preliminary radiometric ages for three edifices range between 75 and 85 Ma: RD56, Ļōbbadede Seamount; drill core from Ānewetak Atoll (E-1-4-3b, E-1-5-6a); and D67 from the unnamed seamount west of the Marshall Islands (Table 9). The age of Ļōkkwōrkwōr and Wōden-Kōpakut Seamounts in the eastern Marshall Islands are 87.3 ± 0.6 Ma and 82.2 ± 1.6 Ma, respectively (Davis et al., 1989). Thus, four seamounts and two atolls in the Marshall Islands area give Late Cretaceous ages (Santonian, Campanian, and Maastrichtian), including the Cretaceous mudstones from Jālwōj Atoll, which must be close in age to the basalts from which they were derived; and the ages of limestones from six seamounts, probably close to the age of the seamounts on which they occur, are Late Cretaceous (perhaps as old as Albian) (Lincoln et al., 1989; Lincoln, 1990). No volcanic edifices in this area have been dated as younger than Cretaceous, consistent with the paleomagnetic data.

Mineralogy and Chemistry

Primary volcanogenic or sedimentary minerals include plagioclase, pyroxene, amphibole, and calcite, and secondary minerals include carbonate fluorapatite, smectite, calcite, phillipsite, celadonite, goethite, and K-feldspar (Table 10). Secondary carbonate fluorapatite is the most abundant mineral and occurs in major to moderate amounts in 70% of the rocks, regardless of rock type (Table 10). It occurs as replacement cement, vein and vesicle infillings, and replacement of primary grains. The most P_2O_5 rich sedimentary rocks have CaO/P_2O_5 ratios that range from 1.6 to 1.9 (Table 11), whereas the theoretical chemical compositions for carbonate fluorapatites range from 1.5 to 1.6 (Manheim and Gulbrandsen, 1979). The excess Ca over P in some of our samples is due to Ca associated with plagioclase in the basalt clasts and phillipsite cement in the breccias and to relict calcite in the phosphatized limestone. Some of the phosphorites are

very pure, consisting of over 80% carbonate fluorapatite (e.g. D9-9A, D19-3, RD43-1E, RD44-1B; Tables 10, 11).

Phillipsite is also a common mineral, occurring in major to moderate amounts in 30% of the rocks, primarily in volcaniclastic breccia, sandstone, and hyaloclastite. Three (D14-3B, D24-1-4, RD63D) of the six samples with abundant phillipsite for which chemistry is available have Si/Al ratios that vary from 2.3 to 2.9; these ratios are mostly within the range of other marine phillipsites (2.3-2.8) and greater than the ratio for phillipsite in mafic igneous rocks (1.3-2.4) (Kastner, 1979). The other three have Si/Al ratios of 3.3 to 4.7, reflecting contamination by other Si and Al bearing minerals.

Smectite occurs in major to moderate amounts in 27% of the rocks. It commonly occurs with primary volcanogenic minerals as well as secondary phillipsite and goethite. Smectite is the sole mineral in D9-16, an altered hyaloclastite and ash, and is probably an Fe-rich montmorillonite with some intermixed illite layers.

We use the term ironstone for dense compact rocks containing over 15% Fe (21% Fe_2O_3). All the ironstones are from D21, although rocks from D10, D24, D25, and RD47 contain high concentrations of Fe.

Ironstones contain up to 50% hydrous iron oxide, $Fe_2O_3 \cdot nH_2O$ (D21-2; Table 11), in contrast to those from the Johnston Island EEZ, which consist of more than 90% hydrous iron oxide (Hein et al., 1990a). All crystalline iron oxide is goethite, which occurs as a replacement of volcanogenic minerals and rocks and as a cement. Eleven percent of the rocks contain moderate to major amounts of goethite (Table 10). Ironstones are Fe-hydroxide replaced and cemented volcanic breccia and Fe-hydroxide replaced basalt. Ironstones probably formed during the late history of seamount growth when volcanism and hydrothermal processes were active. Gradations exist among breccia, ironstone, and phosphorite. The phosphorite that occurs with goethite as a cement may also be hydrothermal and is texturally different than phosphorite found in the other seamount rocks.

Most of the basalt and basalt clasts in breccia are altered to smectite and goethite and rarely are replaced by phosphorite and phillipsite. Alteration is best characterized by increases in ferric Fe and water and decreases in ferrous Fe and K_2O contents (Table 11). The volcaniclastic mudstones, siltstones, and hyaloclastites have compositions comparable to those of the highly altered basalts.

FERROMANGANESE CRUSTS

Crusts vary in thickness from a patina to 180 mm. Dredge haul D11 has the thickest Co-rich crust known (180 mm) and the thickest crust average (110 mm) for an entire dredge haul known to the authors (Tables 6,

7, 8). The previous record thickness is from the Johnston Island EEZ where the thickest crust is 160 mm and the dredge average is 75 mm (Hein et al., 1990a). Thicker crusts are composed of two or more layers, 7 being the maximum, and three the most common number. Layers may be laminated, massive and dense, porous and Fe stained, porous with vugs infilled with phosphorite, or composed of crystallites oriented perpendicular to crust-growth layers; they may contain columnar structures, inclusions of substrate grains, large fractures, abundant phosphorite veins, or may be minutely fractured (Tables 7, 8). Phosphorite laminae occur in some crusts and separate the crust from the substrate in other samples.

The surface texture of crusts is predominantly botryoidal. Many botryoidal surfaces have been smoothed, polished, or fluted by bottom current activity. In addition, botryoids may have been modified by erosion or dissolution at their bases, forming mushroom-like forms; botryoids may merge to form a rippled surface; and a complete gradation exists from unmodified botryoidal surfaces to smooth surfaces. Other surface textures include granular, which is the predominant type on the sides and underside of substrate rocks; lizard skin, which consists of very fine-scale botryoids; irregular; and smooth.

Growth Rates and Ages

Based on the Co, Mn, and P contents and the equations of Puteanus and Halbach (1988), the growth rates of bulk crusts varied from 1.5 to 16.0 mm/m.y. The average growth rate was 4.7 mm/m.y., whereas the average growth rate for the ≤0.5 mm surface layer was 1.7 mm/m.y. Growth rates of about 1 to 10 mm/m.y. are common for hydrogenetic crusts (Hein et al., 1987, 1990b) and this study suggests that the range of common growth rates should be extended to about 15 mm/m.y.; faster growth rates may indicate a hydrothermal or detrital input (Hein et al., 1990b). The five thickest crusts analyzed, D11-15 (140 mm), D12-1 (120 mm), D14-1 (120 mm), D16-2 (105 mm), and RD60 (105 mm) began growing about 23, 18, 31, 20, and 16 m.y. ago, respectively, based on the growth rates of individual layers and the thickness of each layer. These ages of initiation of crust growth are minimum ages because the technique does not take into account dissolution and erosional unconformities, which can add another several million years to the age of the crusts (Futa et al., 1988; Ingram et al., 1990). The oldest crust (31 m.y.) is early Oligocene, and with the time represented by unconformities included, this crust may be as old as late Eocene. It is clear that even though we analyzed a set of remarkably thick crusts, the oldest among them is still 35 to 65 m.y. younger than the age of seamounts in the Marshall Islands (75-105 Ma) upon which they grew. More accurate crust ages will be determined using Sr isotope analyses (Futa et al., 1988; Ingram et al., 1990).

X-ray Diffraction Mineralogy

Great care was taken in sampling crusts for chemical and mineralogical analyses. All contamination from recent sediments was removed, which was especially critical in the porous crust layers. Also, special attention was paid to obtaining a clean separation of the lower crust layers from the substrate. Any minerals or elements determined to exist in the various crust layers were incorporated into those layers during deposition or diagenesis and are not due to sampling procedures or postdepositional infiltration of sediment. Finally, all encrusting organisms and other debris were cleaned from the crust surfaces before sampling. Bulk always refers to the entire crust thickness, whether composed of layers or not.

All but four of 65 bulk crusts analyzed are composed of over 90% δ-MnO_2 (vernadite), which has only two X-ray reflections at about 2.42Å and 1.41Å (Table 12). X-ray amorphous Fe oxyhydroxide epitaxially intergrown with δ-MnO_2 is also a dominant phase. This Fe phase crystallized to goethite in 8% of the bulk crusts and 15% of the individual layers analyzed (Table 12). It is not clear why goethite occurs predominantly in the second layer out from the substrate, rather than in the innermost layer; however, goethite is relatively common in the innermost layer, which would be expected to show the most advanced stages of diagenesis. Most crust and nodule layers are also predominantly δ-MnO_2, but some contain up to 27% carbonate fluorapatite. Carbonate fluorapatite occurs in 65% of the bulk crusts and 44% of the layers. Invariable carbonate fluorapatite occurs in the innermost 1-3 layers depending on the thickness of the crust. If carbonate fluorapatite occurs in more than just the innermost layer, then it always increases in abundance towards the base of the crust (e.g. D11-13D,E,F; Table 12). This continuous increase in the lower layers toward the substrate differs from crusts in the Johnston Island area, where layers not immediately adjacent to the substrate may contain more carbonate fluorapatite than deeper (older) layers (Hein et al., 1990a).

Quartz is ≤1% in all but one sample (2%), and plagioclase is ≤1% in all but three samples (2%,3%,3%, Table 12). The quartz is most abundant in the surface layers and plagioclase in the inner layers. Quartz occurs in 50-60% of the bulk crusts, bulk nodules, and the uppermost surface layer of crusts, whereas plagioclase occurs in only 15% of the bulk crusts and uppermost surface layers. The quartz and some of the plagioclase are of eolian origin, carried by the westerlies from Asia. There is no local or regional source for quartz in the west-central Pacific. The Marshall Islands are south of the main westerlie wind belt which is reflected in lower quartz contents compared to crusts from higher latitudes (Hein et al., 1985a,b, 1987, 1990a). The remainder of the plagioclase, as well as the phillipsite,

pyroxene, and calcite are reworked from local outcrops and incorporated into the crusts during precipitation of the Fe-Mn oxyhydroxides.

Calcite occurs predominantly at the crust surface (≤0.5 mm surface scrapes) and disappears after one or two millimeters of burial by accretion of Fe-Mn oxides. The calcite is probably derived from pieces of encrusting Foraminifera tubes included in the surface layer.

Todorokite is rare in seamount crusts (Hein et al., 1987) and occurs in only 3% of the 162 crust samples analyzed here, but occurs in 56% of the 9 nodule samples. Todorokite also occurs in the hydrothermal stratabound layer (D21-3B), the fossil crust clast from a breccia (D9-1F), and 43% of the 7 underside crust samples analyzed. Todorokite in the crusts may have formed under different redox conditions than the more oxidized δ-MnO_2 phase, either during initial precipitation or during diagenesis. The todorokite in the nodules may reflect a diagenetic origin as it does in abyssal nodules; however, such an origin is rare for seamount nodules, which have compositions similar to the adjacent hydrogenetic crusts. The stratabound hydrothermal layer contains goethite, phosphorite, todorokite, and δ-MnO_2. These hydrothermal deposits are relatively rare on seamounts and, in addition to the Mn oxides, the goethite and phosphorite may have a hydrothermal origin, unlike their diagenetic origin in crusts. Crusts formed much later in the history of the seamounts than did the hydrothermal deposits, commonly 35-65 m.y. after cessation of volcanism and hydrothermal activity.

Chemistry

Bulk Crusts

Chemical analyses for 164 samples and subsamples of crusts and nodules from the Marshall Islands and 8 analyses for deposits from Karin Seamount are presented in Table 13. The mean Fe and Mn contents of 61 bulk crusts from the Marshall Islands are 12.2% and 18.8%, respectively, yielding a Mn/Fe ratio of 1.54 (Tables 13-15). Crusts RD40-1 and RD59-3 were not included in the bulk crust average because one is missing the outer layers and the other accreted onto an older crust fragment (Table 13); therefore, they do not clearly represent bulk crusts. The Mn/Fe ratio is higher than the average ratio for the entire central Pacific region (1.46), and both Fe and Mn are lower than their regional averages of 15.7 and 23.0%, respectively (Hein et al., 1987, 1990c). Most of the other metals are also below the central Pacific regional average (Table 14 and 15), except for Pt, which is significantly enriched over the regional average. The mean contents of the potential economically important metals Co (0.51%), Ni (0.42%), and Pt (0.49 ppm), are significantly below (0.79%), about the

same (0.47%), and, as mentioned, significantly above (0.24 ppm) their regional averages, respectively (Table 15). Phosphorous, a potential byproduct of mining has a high mean value of 1.51% compared to 0.91% for the regional average, which is consistent with the large amounts and ubiquitous carbonate fluorapatite found in substrate rocks.

Analysis of a large number of thick crusts lowers the mean content of many of the metals, especially Co (Table 15), and that is why this study and that of Hein et al. (1990a) show mean concentrations below the regional average. Studies that include analyses of only thin crusts yield mean concentration higher than the regional average (for example, Pichocki and Hoffert, 1987; see Hein et al., 1990c for a discussion). Bulk crusts with high Co contents yield Mn and Ni values very close to the regional mean, but Fe is still below the mean (Table 15). Mean Al contents, indicative of clastic input, decrease with crust thickness (Table 15), except for the surface of the crusts, which has very low Al contents. Mean P contents increase markedly with crust thickness because P is concentrated in the older crust layers. Mean Cu contents do not vary with crust thickness (Table 15).

Adsorbed water (H_2O^-) measured in the crusts varies with the humidity in the laboratory where the samples were analyzed. Unless all of the samples are analyzed in the same laboratory at the same time, H_2O^-, and consequently the abundances of the other elements, will vary accordingly. Therefore, compositions normalized to 0% H_2O^- can be more readily compared and may indicate the composition of ore, if the crusts are eventually mined and can be easily separated from their substrates, because the water can be easily removed. The mean compositions of Fe, Mn, P, Co, Cu, Ni, and Pt for bulk crusts normalized for adsorbed water are 16.6%, 25.6%, 2.06%, 0.70%, 0.11%, 0.57%, and 0.67 ppm, respectively. With this normalization for adsorbed water, the concentrations of all the metals are near or greater than the regional mean (including adsorbed water), except Co, which is lower (Table 15). the Pt content is very high compared with other areas of the Pacific (Hein et al., 1990c).

A marked difference between the Marshall Islands and Karin Seamount crusts is consistently higher Ce, Pb, and Pd contents in Karin Seamount crusts (Table 13).

Layers

It has been well established that Co content in general decreases from outer crust layers to inner crust layers (Halbach et al., 1982; Hein et al., 1985b). This relation can also be demonstrated here (Table 15) where Co increases with decreasing crust thickness and Co is greater in outer layers relative to inner layers of the crusts (Table 13). Other metals also vary with depth in the crusts. Ni, Pb, and Mn commonly decrease and Fe and Pt increase toward the substrate. The variation in Co content with depth in the

crusts is especially evident for the surface of the crusts (≤0.5 mm) where the mean Co content is 0.99% (Tables 15 and 16). Two (D21-11; D25-3A) of the 19 surface scrapes listed in Table 13 were left out of the calculations, because shipboard observations indicated that the outer surfaces were not recent growth surfaces; there has been some period of nondeposition or dissolution, and the chemical compositions support that conclusion. The other surface scrapes fall into two groups based on Co contents, 1.10% to 1.60% and 0.70% to 0.86% with one intermediate value of 0.94%. We suggest that the first group is representative of very slow contemporary precipitation at relatively shallow water depths in the more eastern parts of the Marshall Islands, whereas the second group is representative of precipitation at deeper water depths in the western Marshall Islands. The correlation coefficients support these conclusions (see below).

In detail, the metal concentrations vary widely among the layers of individual crusts and among different crusts (note the variations in the layers listed in Table 13). For example, the 3 layers of D1-1 (Table 13) show decreases toward the substrate in Mn, Na, Mg, K, Al, Co, Mo, As, and Pb, increases in Ca, P, Ni, and Zn, and an increase from both margins toward the center in Fe, Si, Ti, V, and Ce. As another example, the 5 layers of D9-7 (Table 13) show decreases toward the substrate in Fe and As, an increase in Cd, and an increase from both margins toward the center in Mn, Na, Ba, Co, Mo, Ni, V, Ce, Cr, and Zn; other elements fluctuate in other patterns through the crust.

Thinner crusts are chemically equivalent to the outer parts of thicker crusts (Tables 13 and 15). It is the inner, older parts of thick crusts that are missing in thinner crusts because they were eroded prior to deposition of the younger crust layers. It is rare to find crusts consisting solely of the older growth layers without the more Co-rich younger layers. However, many of the crusts collected on Karin Seamount in the Johnston Island area, KSD-1, recovered such crusts (Table 7); the younger crust layers were removed by a turbidity current flow. More typically, thinner crusts exist because the earlier-formed crusts were destroyed by gravity flows and accretion had to begin again (Hein et al., 1985a, 1988).

Samples With Atypical Compositions

Some crust layers show atypical Mn/Fe ratios and corresponding compositions. For example, D10-1-1C (Table 13) has the lowest Mn/Fe ratio; very low Mn, H_2O^-, Co, Mo, Sr, V, Ce, As, Cd, and Pb, most of which are associated with the Mn phase; and high Si, P, Ca, CO_2, Cu, and Y, which are associated with the detrital and carbonate fluorapatite phases. D19-1C has a similar composition and low Mn/Fe ratio. A crust with a high Mn/Fe ratio defined by low Mn and very low Fe concentrations yield similar enrichments and depletions as a crust with a low Mn/Fe ratio, because few elements are associated with the Fe phase. The sample with the

highest Mn/Fe ratio (2.87; RD59-2H) has an average Mn content and low Fe content; the elements other than Fe are typical of the crust average from the Marshall Islands. Compositional banding in crusts is common and probably reflects the Mn/Fe ratio of the Fe and Mn oxyhydroxide flocs in seawater at the time of accretion (Aplin and Cronan, 1985). Some metals may be concentrated by diagenesis or by input of clastic debris. For example, sample RD33-1A is enriched in Ni (0.84%), Zn (0.11%), and Cr (95 ppm), which reflect diagenetic concentration for Ni and Zn and input of Cr-rich detritus. High Cu (0.23%) in RD47-A may reflect input and subsequent diagenesis of large amounts of biogenic debris.

Hydrothermal ferromanganese deposits have been rarely recovered from Cretaceous mid-plate seamounts (Hein et al., 1990a,c; De Carlo et al., 1987). Sample D21-6 (Table 13) is an example of a hydrothermal stratabound layer that occurs below a hydrogenetic crust and within the substrate rock. This stratabound layer has a very high carbonate fluorapatite content (Ca, P, CO_2) and Si, Al, and especially Cr (210 ppm) that are either detrital or were leached from the substrate rocks by hydrothermal fluids. Ba (1.79%), Cu (0.15%), and Sr (0.195) are strongly enriched. In contrast, H_2O^-, Co (0.09%), Mo (47 ppm), Ce (65 ppm), As (18 ppm), and Pb (160 ppm) are strongly depleted. It is not clear whether the apatite is also hydrothermal or whether the hydrothermal deposit was phosphatized later, at the same time as the older part of the overlying hydrogenetic crust. A possible hydrothermal Fe, Mn, and P association has been noted previously for seamount deposits from the Pacific (Hein et al., 1990a) and the Atlantic (Varentsov et al., 1990).

Platinum Group Elements (PGEs) and Gold

We report the concentrations of Pt, Pd, Rh, Ru, Ir and Au for 34 crust samples, including 21 bulk samples and 13 layers (Table 13). This is the first published report of Ru and Ir in Fe-Mn crusts, although Ir concentrations in Fe-Mn nodules have been published (Hodge et al., 1986). PGEs in bulk crusts from the Marshall Islands show significant enrichments over lithospheric and seawater abundances, but not over solar system abundances (mean composition of C1 chondrites). Relative to the lithosphere, the mean composition of bulk crusts is enriched in Ru, Rh, Ir, and Pt, by 14, 23, 6, and 98 times, respectively, whereas Pd and Au concentrations are slightly depleted and slightly enriched, respectively. Ru, Pd, Ir, Pt, and Au are enriched over surface seawater (Hodge et al., 1986; Goldberg, 1987) by $7x10^6$, $1x10^5$, $4x10^6$, $5x10^6$, and about $3x10^4$ times, respectively (Fig. 115). Most of these metals increase in seawater with increasing water depth, so at about 1500 to 2000 m water depth, where many of these crusts formed, the enrichment factors may be less by as much as one-half (Hodge et al., 1986; Goldberg, 1987). We are not aware of any reports of the concentration of Rh in seawater and the value used in Figure

115 is arbitrarily set at 50 pg/l, half the concentration of Pt. However, based on the ratios of Rh and Pt to Ir in the crusts and Pt and Ir in seawater, the seawater value of Rh may by as low as 6 pg/l. Pd and Au show negative anomalies on an otherwise relatively flat seawater normalized plot (Fig. 115). Rh would also show a significant negative anomaly if its seawater concentration is around 6 pg/l. Mean concentrations of Ru, Rh, Pd, Ir, Pt, and Au in crusts are depleted relative to their solar system abundances (Anders and Ebihara, 1982) by 51, 6, 217, 80, 2, and 14 times, respectively (Fig. 115). Rh and Pt show positive anomalies on an overall trend of heavy metal enrichment, increasing depletion with decreasing atomic number (Fig. 115). The mean Au content in the crusts in all of these comparisons is set at 1.0 ppb. Twenty of the 34 Au analyses are less than the limit of detection of 20 ppb and the other 14 values are less than the limit of detection of 10 ppb. However, the mean concentration of 1.0 ppb of Au we use is probably close to the actual mean. The only other reported Au values for crusts that we are aware of are much higher than 1.0 ppb, averaging 82 ppb for 7 analyses of crusts from French Polynesia (Le Suave et al., 1989), however, these high values are suspect.

The highest Pt, Rh, Ru, and Ir concentrations occur in bulk crust D8-1-1A, which in all its other elemental concentrations is unremarkable. Bulk crust D10-1-1A contains high concentrations of Pd and Ru and elements indicative of clastic input, whereas crust layer D11-15E contains low concentrations of Pd and Ru and elements indicative of clastic input. Karin Seamount crusts are depleted in Pt, Rh, Ir, and Ru and enriched in Pd relative to Marshall Islands crusts.

Crust RD59-2D shows increasing Pt, Rh, and Ir contents and decreasing Ru contents through four layers, toward the substrate (Table 13); Pd is below the detection limit in all four layers. The underside crust on the same rock also has four layers, but Pt, Rh, and Ir are high in the first and third layers and low in the second and forth layers (Table 13); Ru decreases through the outer three layers and then increases in the layer next to the substrate. Pd is again below the detection limit in all four layers.

Comparisons of the ratios of each of the PGEs to Ir and Pt for crusts, seawater, the lithosphere, and the solar system indicate that Pt, Ir, and probably Rh in the crusts are derived predominantly from seawater, and that Pd and Ru are derived from both seawater and clastic debris. The extraterrestrial component (meteorite debris) in the bulk crusts must be very small, certainly no more than 20% of the PGEs could have been derived from an extraterrestrial source; however, meteorite debris may be concentrated locally in various horizons or layers in the crusts by formation of dissolution unconformities or by proximity of the crust to meteorite fallout during formation of the layer. These localized extraterrestrial debris-rich horizons, however, do not significantly alter the overall hydrogenetic signature of the crusts.

Rare Earth Elements (REEs)

Eighty-six samples, 21 bulk crusts and 65 layers, were analyzed for REEs (Table 17). For bulk crusts, ΣREEs ranges from 0.09% to 0.28%, with a mean of 0.16%. ΣREEs for individual layers ranges from 0.09% to 0.37%. The highest ΣREEs is for the innermost layer (53-63 mm) in crust RD59-2L, which is an underside crust with high Mn/Fe ratio, low clastic component, and is carbonate fluorapatite rich. The lowest ΣREEs is for the innermost layer (95-105 mm) in crust D16-2F, which has a high clastic component, no carbonate fluorapatite, and high Ni, Zn, Mn, and Cd.

Chondrite-normalized REE patterns (Haskin et al., 1968) are shown in Figures 116-137. Different REEs are enriched from about 60 to 3000 times over chondrites (Fig. 116). Most of the chondrite-normalized patterns are typical of Fe-Mn oxyhydroxide crusts and nodules (Piper, 1974; Elderfield et al., 1981; Aplin, 1984; Hein et al., 1988, 1990a), with heavy REE (HREE) depletion, nearly flat HREE pattern, positive Ce anomaly, and small positive Gd anomaly (the occurrence of the Gd anomaly has been reported only for crusts; Hein et al., 1988). However, 21% of the samples are not characteristic: 9 of the 86 analyses show essentially no Ce anomaly; 4 samples show strong negative Ce anomalies (Table 17; Figs. 117, 120-122, 124-127, 131); and 5 samples show very small positive anomalies. As will be shown in the next section, these Ce anomaly variations are related to geographic position (and associated oxidation potential) and to the amount of authigenic phases present that have negative Ce anomalies (carbonate fluorapatite, zeolites, etc.). The characteristic chondrite-normalized patterns have some aspects in common with seawater (Gd anomaly; also in some samples a small negative Tb anomaly, Hein et al., 1988) and others opposite to those of seawater (HREE depletion, positive Ce anomaly). This variation in characteristics relative to seawater indicates that the REEs were scavenged by several different phases within the crusts, predominantly phosphorite, Fe and Mn oxyhydroxides, barite, zeolites, and others.

Unlike the other REEs, soluble Ce^{+3} is oxidized to insoluble Ce^{+4} at the Fe-Mn surface and fixed in Fe, Mn, and other phases, thus creating a large positive Ce anomaly on both shale- and chondrite-normalized plots (Goldberg et al., 1963; Piper, 1974). The Ce anomaly, Ce* (normalized Ce/La+Pr), ranges from 0.11 to 2.51 for all samples analyzed and averages 0.97 for the bulk crusts.

Nearly all the crusts have a small positive Gd anomaly and a few samples have a very small negative Tb anomaly. These results are similar to those obtained by Hein et al. (1988) for crusts from the eastern chain of the Marshall Islands, but contrasts with the results for crusts from the Johnston Island EEZ, where the Gd anomaly is rarely present (Hein et al., 1990a). DeBaar et al. (1985) attributed the Gd/Tb fractionation in seawater to anomalous properties associated with the shift from an exactly half-filled 4f electron shell.

The HREE depletion results from the formation of more stable complexes by the HREEs in seawater than by the light REEs (LREEs), and consequently, the HREEs are more difficult to fix in the crusts than the LREEs (Cantrell and Byrne, 1987).

The REE compositions and chondrite-normalized patterns change with depth in the crusts, but the changes are not consistent from one crust to another. Three of the four crusts consisting of only two layers has the highest ΣREEs in the inner layer and the largest Ce* in the outer layer. Beyond those relationships there is no consistency to the REE distributions; ΣREES and Ce* can be high or low in any of the crust layers, although there is some preference for greater ΣREEs in the inner layers. Several crusts show internally consistent REE trends: RD59-2E-H, increasing ΣREEs with increasing depth toward the substrate; D8-1B-D, RD36-1C-E, and RD59-2I-L, decreasing Ce* with increasing depth; D14-1B-E and RD60B-E, increasing Ce* with increasing depth. The absence of a consistent trend in the distribution or the REEs contrasts with other areas, where the highest ΣREEs occurs at the base of the crusts (Hein et al., 1990a). There is no consistent relationship between the REEs and the various crusts phases, again indicating that the REEs are associated with several phases. However, within individual crusts, REEs may covary with phosphorite or Mn/Fe.

ΣLREEs shows the same pattern of distribution among layers within individual crusts as the ΣREEs, because both are dominated by the high Ce contents. However, ΣHREEs may show trends that are the same as those of the ΣLREEs (D9-7, D12-1, D14-1); the opposite to those of the ΣLREEs (D1-1, D16-5, D27-2, RD43-1, RD50; or some other variation (Table 17). These relationships contrast with those in crusts from the Johnston Island EEZ to the east, where the ΣHREEs always shows an opposite trend to that of the ΣLREEs, and invariably has its highest concentration in the outermost crust layer (Hein et al., 1990a).

Interelement Relationships: Correlation Coefficient Matrix

Eighteen correlation coefficient matrices were calculated, one on the total Marshall Islands data set and 17 on various subsets of the Marshall Islands data. Ten of these 18 matrices are presented here: All bulk crusts, Table 18; crust surfaces (≤0.5 mm), Table 19; all bulk crusts ≤20 mm, Table 20; all bulk crusts ≥20 mm, Table 21; all bulk crusts ≥100 mm, Table 22; all bulk crusts with REE analyses, including selected major elements, Table 23; layers from sample D9-7 including REEs, Table 24; layers from sample D11-15 including REEs, Table 25; layers from sample D12-1 including REEs, Table 26; and layers from sample RD59-2 top crust including REEs, Table 27.

Bulk Crusts

For the 61 bulk crusts, statistically significant strong to moderate positive correlations are found among the following selected elements (table 18): **Fe**: Ti, Si, As, Ru; **Mn**: Co, Cd, Na, Pb, Mo, As; **Si**: Al, Fe, K, Ti, Ru, Pd; **Ca**: P, CO_2, Y; **Al**: Si, K, Pd, Cu, Ru; **P**: Ca, CO_2, Y; **Co**: Mn, Na, As, Cd; **Cu**: Pd, Al; **Ni**: Mg, Cd, Zn; **Sr**: V; **As**: Na, Mn, Co, Ti, Fe, V; **Pt**: Rh, Ir, Pd; **Pd**: Cu, Al, Si Ru; **Rh**: Ir, Pt; **Ru**: Ti, K, Si, Pd, Cr, Fe, Al; **Ir**: Rh, Pt; **latitude**: Pt, Rh, Ir. **Water depth** shows weak positive correlations with Si, Cu, Al and weak negative correlations with Cd, Ni, Rh, Ir, Mo. **Crust thickness** shows weak negative correlations with Na, Co, Mg, Ru. Many statistically significant weak correlations also exist among the various elements. All of the elements are associated with one or more mineral phases within the crusts. We interpret the correlations in Table 18 to indicate the following phases and their associated elements: **δ-MnO_2**: Mn, Co, Cd, Na, Pb, Mo, As, Mg, V, Ni, Ti(?); **Fe-oxyhydroxide** phase: Fe, As, Na(?), V(?); **aluminosilicate** component: Al, Si, Fe, Ti, K, Pd, Ru, Cu, Na, Cr(?), Zn(?); **carbonate fluorapatite** component: Ca, P, CO_2, Y, Cr(?); **residual biogenic** component: Ba, Ce, Sr, V, Ru, Pd, Pb(?), Mo(?). Elements of the aluminosilicate, Fe-oxyhydroxide, and δ-MnO_2 phases vary inversely with the carbonate fluorapatite phase. These interelement associations are similar to those determined for crusts from other areas of the central Pacific, although regional differences do occur (Hein et al., 1990a,c).

Other than Ce, the **REEs** are not correlated with any of the other elements, indicating that the REEs in bulk crusts must be distributed among most of the constituent phases. The individual REEs and ∑REEs show positive correlations among themselves, except for Ce, which is not correlated with Eu, Ho, Er, or Yb (Table 23). The significance of the correlations among the REEs is generally high for correlations with La, low for correlations with Ce, and then the significance increases toward higher atomic numbers for each element; the strongest correlations are with the REE with the atomic number just above and just below its own; then the significance decreases slightly and levels out through the remaining REEs of higher atomic number. ∑REES, Ce*, and many of the individual REEs have weak positive correlations with latitude and strong to weak positive correlations with H_2O^-. Ce and Ce* also have weak positive correlations with longitude. Thus, the height of the positive Ce anomaly increases with increasing latitude and longitude (to the east). All samples with negative Ce* occur in the southeast part of the area, around the Ujlañ complex. The abundance of the REEs increases with increasing latitude. These geographic distributions probably reflect the regional oxidation potential. As mentioned above, the water depth to the top of the oxygen-minimum zone increases to the north; the maximum amount of depletion of oxygen in

the seawater decreases to the north and west (lower oxygen contents to the south and east), and the water depth of the greatest oxygen depletion increases to the west (Tables 4 and 21).

The **PGEs** form two groups, Pt, Rh, Ir and Ru, Pd. The first group is apparently distributed in many of the crust phases, with perhaps some minor preference for the carbonate fluorapatite and residual biogenic phases. This group also increases in abundance with increasing latitude. The second group, Ru and Pd are distributed mainly in the aluminosilicate phase and secondarily in the residual biogenic phase, with minor amounts occurring in the other phases. Rh and Ir contents in crusts increase with decreasing water depth. Ru contents increase with decreasing crust thickness.

The correlations change somewhat when only thin (≤20 mm) bulk crusts are considered (Table 20). The thin crusts have fewer and weaker interelement correlations. The most interesting difference is that the elements representative of the carbonate fluorapatite and residual biogenic phases are combined (all of them correlate for the thin crust subset). This indicates that for crusts that were not phosphatized (typical of young, thin crusts) the elements associated with the apatite compose part of an undifferentiated biogenic phase. Another interesting and related difference is that Ba, Cu, Ca, and P all increase with increasing crust thickness within the 0-20 mm thick crusts. Again, this indicates either differentiation of the apatite and residual biogenic phases with increasing crust growth and/or the addition of carbonate fluorapatite with longer periods of growth. Co still decreases with increasing crust thickness as with the all bulk crust data set.

The element correlations for the subset of crusts ≥20 mm are very similar to the those for all bulk crusts (Table 21). Co shows the greatest difference with positive correlations with Ni, LOI, Rh, and Mo as well as with Mn, Na, Mg, As, Cd, and Ti as in the all bulk crust data set. Another difference is that no correlation exists between Co and crust thickness, but the abundances of K, Mg, Ru, and Pd, elements characteristic of the aluminosilicate fraction, all decrease with increasing crust thickness.

Most of the element correlations for the subset of crusts ≥100 mm are different from any of the other subsets of data (Table 22). Most of the correlations show mixing of the elements characteristic of the different phases, strong evidence for diagenetic modification of these thick crusts. The carbonate fluorapatite phase with correlations among Ca, P, CO_2, and Y and the aluminosilicate phase remain mostly unchanged. No correlations exist with water depth. Fe decreases with increasing latitude and longitude, which controls the increase in the Mn/Fe ratio with increasing latitude and longitude. During the 20 to 40 m.y. history of growth of the thick crusts, their geographic position has changed because of plate motions, and their water depth has changed because of subsidence due to cooling of the oceanic crust and changes in sealevel. Changes in all of these oceanographic and geological conditions over long periods of time would produce crusts with many chemical signatures representative of many

different environments. Analysis of thick bulk crusts averages all these individual characteristic signatures.

These elemental correlations and variations with different groups of bulk crusts indicate that: 1. Diagenesis may significantly affect thick crusts. 2. Growth rates affect element associations. 3. P is associated with apatite only in thick crusts, suggesting at least two mechanisms of incorporation of P into crusts. The significance of the P, Ca, and CO_2 correlations increases with increasing crust thickness. 4. The REEs and PGEs vary significantly with latitude and longitude. 5. The aluminosilicate fraction varies directly and the Mn phase inversely with water depth. 6. Co varies inversely with crust thickness.

Layers

Nine correlation coefficient matrices were constructed to determine interelement associations among layers within individual crusts. Four of those matrices are presented here (Tables 24-27). Each crust shows minor to major differences in the element correlations as compared with the other crusts. In general, the number of correlations decreases for some elements and increases for others compared to bulk crusts; but in most crusts, the number of correlations decreases for all of the elements. The paucity of correlations of elements among crust layers is partly due to the high zero correlation for 4 or 5 points, and partly due to the smaller compositional variability among the layers compared to all the bulk crusts considered together. However, many of the strong and moderate interelement correlations in the complete data set for bulk crusts occur for the elements in the layers of crust D9-7 (75 mm thick; Table 24). A major difference is that the Fe and Mn phases are not clearly separated for D9-7. Also, Na, Mg, Ba, As, and Zn, commonly associated with the residual biogenic and Mn phases, show many more correlations than they do for all bulk crusts. For example, Zn is positively correlated with Mo, V, Na, Mg, H2O+, Mn, As, Co, Ba, Cd, Ti, Pb, Fe, Ni, and K, indicating association with the Mn, Fe, and residual biogenic phases. Also, for D9-7, Cu is associated with the residual biogenic phase rather than the aluminosilicate phase as with the all bulk crust data set, and Cr is with the aluminosilicate phase rather than the carbonate fluorapatite phase. Three REE groups are associated with different crust phases. Ce, Gd, Dy, ΣREEs are associated with several crust phases; La, Ho, Er, Tm, Yb are predominantly with the apatite phase; and Pr, Nd, Sm, Eu, Tb are predominantly with the Fe-Mn phase.

In contrast, D11-15, the thickest crust (138 mm) analyzed, shows very few correlations for elements among the layers (Table 25). However, the correlations that do occur are the same as those for all bulk crusts, with the exception of Ba, which has positive correlations with Cu and Zn. The REEs have very few correlations with other elements including other REEs.

Correlations are few for elements in the 4 layers of crust D12-1 (120 mm thick; Table 26). However, the correlations that do occur are the same as those for all bulk crusts, with the exception of Ba, which is similar to crust D11-15. Positive correlations exist among Ba, Cu, Sr, and Zn. However, unlike D11-15, individual REEs are correlated with the other REEs and, except Ce, are associated with the Fe-oxyhydroxide phase (Fe, Cu). Ce is associated with several phases and Yb may be associated with the Mn phase.

Correlations are also few for elements in the 4 layers of crust RD59-2 (top crust, 65 mm thick; Table 27). A number of distinctions exist compared to the all bulk crust data set. As, Cr, and Na are associated with the aluminosilicate phase. Sr and Ce are included in the carbonate fluorapatite phase. Again, Ba is correlated with Zn and Cu. Pt is correlated with Ce. All of the REEs show a consistent coherent pattern of strong correlations with other REEs. Also, all the REEs have positive correlations with elements characteristic of the carbonate fluorapatite phase, not the Fe-oxyhydroxide phase as in D12-1; in fact, four of the nine matrices of elements in crust layers show associations of the REEs with apatite; three show associations with several crust phases; and one shows an association with Fe-oxyhydroxide. Crusts that show REE correlations with elements associated with the carbonate fluorapatite phase are not necessarily enriched in P.

Crusts Surfaces and Seawater Oxygen

It has been assumed by most researchers studying ferromanganese crusts that the strong enrichment of Co, and perhaps other metals, in crusts is related to the oxygen-minimum zone, because Fe and Mn are more soluble in low oxygen seawater. However, this assumption has not been tested. In order to test it, we scraped the surface ($\leq$0.5 mm) of a crust from each dredge haul immediately after collection in order to obtain a sample representative of the most recently precipitated oxides. We also measured the temperature and oxygen content of the water column in several places over the seamounts in order to correlate the oxygen content of the seawater with the Co content of the crust surface. This is not an ideal test, because the observed oxygen profile may exist for only a short time, whereas the outer 0.5 mm of the crust may integrate as many as 0.3 m.y. of precipitation from seawater. However, correlations exist between the crust surface chemistry and water depth to the top of the oxygen-minimum zone (A), the lowest oxygen content in each profile (B), and the water depth of the lowest oxygen content in each profile (C) (Table 19). (A) shows a positive correlation with (B), latitude (of the CTD stations), Si, Fe, Cu, Al and a negative correlation with Co, Mn/Fe, Mn, Cd, Na, Mg, and Zn. (B) shows a positive correlation with latitude (of the CTD stations), Cu, Y, As, and Fe, and a negative correlation with Co, Cd, longitude (of the CTD

stations), Mn, Mn/Fe, K, and Ti. (C) shows a positive correlation with Si and Al. The strongest correlation is between Co and (B) (correlation coefficient = 0.711). These correlations indicate that there is a direct correspondence between low oxygen in the water and high Co, Cd, Mn, K, and Ti (δ-MnO_2 phase) in the crusts; and between low oxygen in the water and low Cu, Y, As, and Fe (Fe-oxyhydroxide phase) in the crusts. However, these correlations may be fortuitous, as (B) and both groups of elements are correlated with longitude. Two relationships, however, suggest that they are not fortuitous. First, (B) is also correlated with latitude, whereas Cd is the only element within the two groups that correlates with latitude. Second, many other elements (Si, Mg, Mo, Ni, Al, and CO_2) correlate with longitude, but not with oxygen content of the water column. Consequently, we suggest that these data support a direct relationship between oxygen content of seawater and metal content of crusts.

Fe compounds are less soluble than Mn compounds and the ferrous ion more easily oxidized than the manganous ion under most naturally occurring pH-Eh conditions (Krauskopt, 1957). Our results indicate that partial Fe-Mn fractionation must occur within the oxygen-minimum zone where Fe is preferentially concentrated in crusts forming in areas of higher oxidation potential and Mn in the areas where seawater has the lowest oxygen contents. However, the fractionation is never complete, but is extensive enough so that the crust compositions reflect the enrichment or depletion of the minor metals associated with the Fe and Mn phases.

Substrate-Crust Element Correlations

Hein et al. (1990a) tested the assumption that substrate rocks do not have an influence on crust chemistry by analyzing the innermost 5 mm of crusts and the adjacent substrate rocks and then subjecting those analyses to statistical studies. Here we calculated a correlation coefficient matrix for 17 bulk crusts and associated substrate chemistry. The only correlations between crust chemistry and substrate chemistry are: weak positive, Mn* (* denotes substrate element) with Cu and water depth; very weak positive, K* with Ru; weak negative, Mn* with Sr; very weak negative Mn/Fe* with Rh. These correlations are fewer than those determined by Hein et al. (1990a) for the Johnston Island crust study, because bulk crusts were used here rather than the crust layer adjacent to the substrate. However, these few correlations support their conclusions that, overall, the substrate rocks do not contribute greatly to crust chemistry, but may have partly exchanged some of the most mobile elements with the crusts; exchange probably occurs in both directions as both crusts and most substrates are very porous and water saturated. Substrate rocks have been the major contributor of the minor detrital phases (except quartz) to the crusts.

Grouping of Elements: Q-Mode Factor Analysis

Q-mode factor analysis was completed for the 61 bulk crusts and for 13 subsets of data. Five of the factor score sets are presented here (Figs. 138-142): All bulk crusts (Fig. 138); crust surface chemistry (Fig. 139); all bulk crusts ≥100 mm (Fig. 140); layers for crust D11-15 (Fig. 141); and layers for crust RD59-2 (Fig. 142). The elements determined by Q-mode can be assigned to essentially the same crust phases as determined from analysis of the correlation coefficient matrices. Some differences do occur. For example, the Fe phase is not distinguished for some data subsets or may be included as part of the δ-MnO_2 factor in others. More specific differences regarding the placement of individual elements in different phases are also noted.

The 5 factors determined for the 61 bulk crusts are interpreted to be δ-MnO_2 (including some Fe), carbonate fluorapatite, aluminosilicate, Fe-oxyhydroxide, and residual biogenic (Fig. 138). The elements associated with each of these phases are predominantly the same as those interpreted from the correlation coefficients. However, the differences include for the Q-mode: δ-MnO_2, add Fe, exclude Ni; carbonate apatite, add Mo, Sr, and Ce; aluminosilicate, exclude Na, Cr, and Zn; Fe-oxyhydroxide, add Sr and Ce; residual biogenic, add Cu and exclude Sr and Pb. The main difference is the redistribution of some of the biogenic elements into the carbonate fluorapatite, Fe-oxyhydroxide, and residual biogenic phases.

In contrast, Q-mode factor analysis of the crust surface chemistry produces only two factors, which we interpret as δ-MnO_2 and a combination of aluminosilicate and biogenic (Fig. 139). The δ-MnO_2 phase includes: Co, Cd, Mo, Ni, Mn, Na, Pb, Mg, K, and Ti. The aluminosilicate plus biogenic phase includes: Si, Al, Cr, Cu, CO_2, Fe, Y, Ba, Ca, P, Sr, and As. Mineralogically, this second phase includes aluminosilicate minerals, quartz, calcite, and X-ray amorphous residual biogenic debris.

Three factors were determined for bulk crusts ≥100 mm (Fig. 140). But, as with the element correlations, the phases determined by Q-mode show a mixing of elements characteristic of one phase among other phases, again attesting to the occurrence of diagenesis in thick crusts. For example, the carbonate fluorapatite phase includes not only P, Ca, CO2, and Y, but also, Sr, Ba, Cu, Mo, Ni, Ce, and Zn. The δ-MnO_2 phase does not include the characteristic elements Co, Ni, and Cd, but rather Mn, Mo, V, As, Sr, and Na, which, except for Sr, are also common in this phase.

Three factors were determined for the grouping of elements among layers of crust D11-15 (138 mm thick; Fig. 141). However, a large amount of mixing exists of elements characteristic of one phase among the other phases. For example, one factor includes: As, Si, Fe, Ti, Al, Co, Cr, Mn, Na, Mg, K, Ba, Mo, Ni, V, Cd, and Pb. This factor includes elements

characteristic of the δ-MnO_2, Fe-oxyhydroxide, aluminosilicate, and residual biogenic phases, again attesting to the occurrence of diagenesis in this very thick crust. Similarly, the second factor, carbonate fluorapatite includes not only P, Ca, CO_2, and Y, but also Ni, Sr, and Ce. In contrast, the third factor, aluminosilicate, includes only Si, Al, and Cr.

Three factors were determined for the grouping of elements among layers of crust RD59-2 (65 mm thick; Fig. 142). The aluminosilicate factor includes: Si, Al, Cr, Fe, As, K, Na, Ti, Mg, V, Pb, Ru, and, anomalously, Co; the carbonate fluorapatite phase includes: P, Ca, CO_2, Y, Ce, Sr, Pt, Rh, and Ir; the δ-MnO_2 phase includes, Mn, Ni, Co, Cu, Mo, Cd, Ba, and Zn, all characteristic of this phase except Ba and Cu. The PGEs are divided between the aluminosilicate phase (Ru and probably Pd, not included in this analysis) and carbonate fluorapatite (Pt, Rh, Ir).

RESOURCE CONSIDERATIONS

Based on limited information, we considered the Marshall Islands EEZ as having a high potential for Co-rich Fe-Mn crusts (Hein et al., 1987, 1988, 1990c). The Marshall Islands EEZ and the Johnston Island EEZ have been the most extensively surveyed areas for potential crust resources. Based on the interrelationships of Mn, Fe, Co, Ni, and Cu, the Marshall Islands crusts fall within the range of central Pacific hydrogenetic crusts, as shown on the Bonatti diagram (Fig. 143; Bonatti, et al., 1972).

The commonly cited cut off grade for potential economic development is 0.8% Co. On a water-free basis, crusts in the Marshall Islands are very high in platinum (0.67 ppm); high in manganese (26%), phosphorous (2.1%), and nickel (0.57%); and moderate in the most economically important element, cobalt (0.70%), as well as copper (0.11%). Cobalt content in crusts in the Marshall Islands EEZ increases to the east (also relatively high in a few places in the central Marshall Islands; Fig. 144), along with the oxygen content of the water column. The correlation of Co in the outer crust layer with oxygen content of the seawater offers an important exploration tool for Co-rich crusts.

Several areas in the Marshall Islands EEZ have remarkably thick crusts (large tonnage), including Lọmilik, Ļōjemeja, Ujlañ, and Ļalibjet, Seamounts, which all have crusts over 100 mm thick and average thickness from individual dredges of over 50 mm. The commonly cited cut off thickness for potential economic development is 40 mm. Seamounts with average crust thicknesses for individual dredges of more than 40 mm include Lọmilik, Ļōjemeja, Ujlañ, Ļalibjet, Mij-Lep, and Jebrọ. The two dredges from Mij-Lep have especially impressive average thicknesses of 60 and 70 mm and the one dredge from Lọmilik Seamount with a 110 mm average thickness. However, surveys within the Marshall Islands have not been extensive enough to delineate the extent of these areas of thick crusts.

Because the mining of crusts from the rugged flanks and summit of seamounts and ridges will be a difficult endeavor, crust thickness (tonnage) may turn out to be a more important factor in economic and site selection considerations than grade. The weak negative correlation that exists between crust thickness and Co content means that tonnage has an inverse relationship with Co content and choice of potential mine sites will have to balance these two critical factors. Crust thickness does not correlate with either Ni or Pt.

The areas that warrant further work include the Ujlañ volcanic complex, especially Ujlañ and Ļalibjet Seamounts, Lǫmilik, Mij-Lep, and Jebrǫ Seamounts. The sediment-free, flat, southern summit area of Ļalibjet Seamount warrants attention because of the relatively subdued topography. Without detailed, site specific surveys, it is difficult to assess the long term economic potential of the Marshall Islands, or any other Pacific EEZ. However, results from the three reconnaissance cruises to the Marshall Islands suggest that the area probably holds the highest potential for Co-rich crust resources in the central Pacific, especially if Pt can be recovered as a byproduct (Table 28). Identification of areas with favorable grade, tonnage, and seafloor characteristics will also have to correspond with the appropriate world markets and metals prices before mining can be accomplished. The technological problems of mining can be solved if the other factors are favorable.

CONCLUSIONS

1. The Marshall Islands is the most extensively studied area for Co-rich Fe-Mn crusts and for the structure and morphology of seamounts.
2. The Marshall Islands, Johnston Island, and French Polynesia EEZs have the highest long-term resource potential for Co-rich ferromanganese crusts.
3. Crusts from the Marshall Islands have the highest mean Pt value of all central Pacific areas. Co content (grade) varies inversely with crust thickness (tonnage).
4. Seamounts do not show simple or uniform morphologies and structures, but rather vary significantly, even between adjacent seamounts. The summit platforms are complex, commonly rugged, and may be tilted. Summits may or may not have a sediment cap, but when present, the sediment shows evidence of erosion and slumping. Seamounts may have multiple terraces that vary in water depth and width from place to place on the flanks; other seamounts may not have terraces. Seamount flanks are sites of extensive slumping and mass failures.
5. All dated seamounts are of Cretaceous age, predominantly Late Cretaceous. The abundance of rock types, in decreasing order, are breccia, basalt, hyaloclastite, limestone (much of it partly phosphatized), volcaniclastic sandstone-siltstone-mudstone, phosphorite, and ironstone.

Volcanic rocks are predominantly alkalic basalt; some are strongly alkalic and others are extensively differentiated.

6. Oxygen and temperature profiles in the water column vary with latitude and longitude, showing greater depletion in oxygen to the east and to the south.

7. Secondary carbonate fluorapatite is the most abundant mineral in substrate rocks, occurring in major to moderate amounts in 70% of the rocks.

8. Hydrothermal ironstones contain up to 50% hydrous iron oxide.

9. The thickest Co-rich crusts known, up to 180 mm, were collected in the Marshall Islands. Growth rates vary from 1.5 to 16 mm/m.y. and average 4.7 mm/m.y. The age of initiation of growth of the thickest crusts began between about 16 and 31 Ma; the ages of these remarkably thick crusts are 35 to 65 m.y. younger than the ages of the seamounts upon which they grew.

10. Fe-Mn crusts are composed predominantly of δ-MnO_2, but the inner layers of crusts can contain up to 27% carbonate fluorapatite.

11. On a adsorbed water-free basis, bulk crusts average 16.6% Fe, 25.6% Mn, 2.06% P, 0.70% Co, 0.11% Cu, 0.57% Ni, and 0.67 ppm Pt. Analysis of a large number of thick crusts lowers the regional mean content of many of the metals, especially Co.

12. Oxygen content of seawater influences the metal contents of the crusts. There is a direct correspondence between low oxygen in the water and high Co, Cd, Mn, K, and Ti in the crusts and between low oxygen in the water and low Y, Cu, As, and Fe in the crusts.

13. Q-mode factor analysis and correlation coefficients indicate that bulk crusts are composed of 5 phases with characteristic associated elements: δ-MnO_2--Mn, Co, Cd, Na, Pb, Mo, As, Mg, V, Ni, Ti(?); Fe-oxyhydroxide--Fe, As; aluminosilicate--Al, Si, Fe, Ti, K, Pd, Ru, Cu, Na; carbonate fluorapatite--Ca, P, CO_2, Y; residual biogenic--Ba, Ce, Sr, V, Ru, Pd. Thick crusts show strong evidence that diagenesis has changed the interelement associations.

14. The PGEs (Pt, Rh, Pd, Ru, and Ir) in bulk crusts show significant enrichments over their lithospheric averages and over seawater abundances. PGE ratios indicate that Pt, Ir, and probably Rh are primarily derived from seawater and that Pd and Ru are derived from seawater and clastic debris. The extraterrestrial component (meteorite debris) in the bulk crusts must be very small, certainly no more that 20% of the PGEs could have been derived from that source.

15. ΣRREs ranges from 0.09% to 0.28% for bulk crusts and up to 0.37% for individual crust layers. Many chondrite-normalized REE patterns show either a small positive anomaly, or no Ce anomaly (several have a negative Ce anomaly), in contrast to other central Pacific crusts. The REE compositions and chondrite-normalized patterns change with depth in the crusts, but the changes are not consistent from one crust to

another nor are the REEs consistently associated with the same crust phases. The geographic distribution of the REEs reflects the regional oxidation potential.

ACKNOWLEDGMENTS

We thank Jack Halkena, Ministry of Foreign Affairs, who was very helpful in providing coordination with the Republic of the Marshall Islands and Alfred Capelle, Alele Museum and National Archives, who was essential in providing the seamount names and post-cruise coordination of activities. We thank the Government and people of the Republic of the Marshall Islands for their kindness, help, and encouragement of our work. We thank Captain John Cannan and the crew of the R. V. *Farnella* for excellent support. We thank Marlene A. Noble, Shawn V. Dadisman, Heidi L. Dieffenbach, William S. Weber, Joanne C. Thede, George B. Tate, Carolyn H. Degnan, Edward J. Maple, Michael E. Boyle, J. Kevin O'Toole, and Ward R. Ozanne of the U.S. Geological Survey and Yong Joo and Sang-Dai Seo of the Korea Ocean Research and Development Institute for technical help on various aspects of this project. Randolph Koski, U.S. Geological Survey, kindly and bravely reviewed this report. The following U.S. Geological Survey analysts provided chemical data: Ardith J. Bartel, Robert R. Carlson, H. Neil Elsheimer, Laureano F. Espos, Herbert Kirschenbaum, John W. Marinenko, Clara S.E. Papp, Cynthia L. Prosser, Norma Rait, George O. Riddle, David F. Siems, Hezekiah Smith, Joseph E. Taggart.

REFERENCES

Anders, E. and Ebihara, M., 1982, Solar-system abundances of the elements: Geochimica et Cosmochimica Acta, v. 46, p. 2363-2380.

Aplin, A.C., 1984, Rare earth element geochemistry of central Pacific ferromanganese encrustations: Earth and Planetary Science Letters, v. 71, p. 13-22.

Aplin, A.C. and Cronan, D.S., 1985, Ferromanganese oxide deposits from the central Pacific, I. Encrustations from the Line Islands Archipelago: Geochimica et Cosmochimica Acta, v. 49, p. 427-436.

Aruscavage, P.J., Kirschenbaum, H., and Brown, F., 1989, Analytical methods: The determination of 27 elements in ferromanganese materials: in Manheim, F.T. and Lane-Bostwick, C.M. (eds.), Chemical Composition of Ferromanganese Crusts in the World Ocean: A Review and Comprehensive Database. U.S. Geological Survey Open File Report 89-020, 200 p. plus 3 appendices.

Bonatti, E., Kraemer, T., and Rydell, H., 1972, Classification and genesis of submarine iron-manganese deposits: in Horn, D.R. (ed.), Ferromanganese

Deposits On the Ocean Floor. Washington, D.C., National Science Foundation, p. 149-166.
Cantrell, K.J. and Byrne, R.H., 1987, Rare earth element complexation by carbonate and oxalate ions: Geochimica et Cosmochimica Acta, v. 51, p. 597-605.
Chase, T.E. and Menard, H.W. (compilers), 1973, Bathymetric atlas of the North Pacific Ocean: U.S. Naval Oceanographic Office, Washington, D.C., Publication 1301-2-3.
Cook, H.E., Johnson, P.D., Matti, J.C., and Zemmels, I., 1975, Methods of sample preparation and X-ray diffraction data analysis (X-ray mineralogy laboratory, Deep Sea Drilling Project, University of California Riverside): in Hays, D.E., Frakes. L.A., et al., Initial Reports of the Deep Sea Drilling Project, U.S. Government Printing Office, Washington, D.C., v. 28, p. 999-1007.
Davis, A.S., Pringle, M.S., Pickthorn, L.B., and Clague, D.A., 1989, Petrology and age of alkalic lava from the Ratak chain of the Marshall Islands: Journal Geophysical Research, v. 94, p. 5757-5774.
DeBaar, H.J.W., Brewer, P.G., and Bacon, M.P., 1985, Anomalies in rare earth distributions in seawater: Gd and Tb: Geochimica et Cosmochimica Acta, v. 49, p. 1961-1969.
De Carlo, E.H., McMurtry, G.M., and Kim, K.H., 1987, Geochemistry of ferromanganese crusts from the Hawaiian Archipelago--I. Northern survey areas: Deep Sea Research, v. 34, p. 441-467.
Duennebier, F. K. and Schlanger, S.O., 1988, MW88-05 Marshall Islands guyots cruise report, April 24-May 30, 1988, Guam to Guam, 80 p. (unpublished report).
Duennebier, F.K., Bergersen, D.D., and Icay, W., 1988a, Structure and evolution of guyots in the Marshall Islands guyot province: EOS, Transactions of the American Geophysical Union, v. 69, no. 44. p. 1441.
Elderfield, H., Hawkesworth, C.J., Greaves, M.J., and Calvert, S.E., 1981, Rare earth element geochemistry of oceanic ferromanganese nodules and associated sediments: Geochimica et Cosmochimica Acta, v. 45, p. 513-528.
Futa, K., Peterman, Z. E., and Hein, J.R., 1988, Sr and Nd isotopic variations in ferromanganese crusts from the central Pacific: Implications for age and source provenance: Geochimica et Cosmochimica Acta, v. 52, p. 2229-2233.
Gann, J.T., 1988, Integrated GPS, range-range and hyperbolic Loran C marine navigation system for use on IBM AT or compatible microcomputer: U.S. Geological Survey Open File Report 88-562.
Gill, J., Torssander, P., and Koyama, M., 1989, Deep water fire fountaining in a backarc rift: EOS,Transactions of the American Geophysical Union, v. 70, p. 1408.
Goldberg, E.D., Koide, M., Schmitt, R.A., and Smith R.H., 1963, Rare earth distribution in the marine environment: Journal of Geophysical Research, v. 68, p. 4209-4217.

Goldberg, E.D., 1987, Heavy metal analyses in the marine environment--approaches to quality control: Marine Chemistry, v. 22, p. 117-124.
Halbach, P., Manheim, F.T., and Otten, P., 1982, Co-rich ferromanganese deposits in the marginal seamount regions of the central Pacific basin--results of the Midpac '81: Erzmetall, v. 35, p. 447-453.
Haskin, L.A., Haskin, M.A., Frey, F.A., and Wildeman, T.R., 1968, Relative and absolute terrestrial abundances of the rare earths: in Ahrens, L.H. (ed.), Origin and Distribution of the Elements, 1, Pergamon, Oxford, p. 889-911.
Hein, J.R., Manheim, F.T., Schwab, W.C., and Davis, A.S., 1985a, Ferromanganese crusts from Necker Ridge, Horizon Guyot, and S.P. Lee Guyot: Geological considerations: Marine Geology, v. 69, p. 25-54.
Hein, J.R., Manheim, F.T., Schwab, W.C., Davis, A.S., Daniel, C.L., Bouse, R.M., Morgenson, L.A., Sliney, R.E., Clague, D.A., Tate, G.B., and Cacchione, D.A., 1985b, Geological and geochemical data for seamounts and associated ferromanganese crusts in and near the Hawaiian, Johnston Island, and Palmyra Island Exclusive Economic Zones: U.S. Geological Survey Open-File Report 85-292, 129 p.
Hein, J.R., Morgenson, L.A., Clague, D.A., and Koski, R.A., 1987, Cobalt-rich ferromanganese crusts from the Exclusive Economic Zone of the United States and nodules from the oceanic Pacific: in Scholl, D.W., Grantz, A. and Vedder, J.G. (eds.), Geology and Resource Potential of the Continental Margin of Western North America and Adjacent Ocean Basins-Beaufort Sea to Baja California. Circum-Pacific Council for Energy and Mineral Resources, Earth Science Series, Houston, Texas, v. 6, p. 753-771.
Hein, J.R., Schwab, W.C. and Davis, A.S., 1988, Cobalt and platinum-rich ferromanganese crusts and associated substrate rocks from the Marshall Islands: Marine Geology, v. 78, p. 255-283.
Hein, J.R., Kirschenbaum, H., Schwab, W.C., Usui, A., Taggart, J.E., Stewart, K.C., Davis, A.S., Terashima, S., Quinterno, P.J., Olson, R.L., Pickthorn, L.G., Schulz, M.S., Morgan, C.L., 1990a, Mineralogy and geochemistry of Co-rich ferromanganese crusts and substrate rocks from Karin Ridge and Johnston Island, *Farnella* Cruise F7-86-HW, 80 p.
Hein, J.R., Schulz, M.S. and Kang, J.K., 1990b, Insular and submarine ferromanganese mineralization of the Tonga-Lau Region: Marine Mining (in press, v. 9, no. 3).
Hein, J.R., Schulz, M.S., and Gein, L.M., 1990c, Central Pacific cobalt-rich ferromanganese crusts: Historical perspective and regional variability: in Keating, B. and Bolton, B. (eds.), Geology and Offshore Mineral Resources of the Central Pacific Region, Circum-Pacific Council for Energy and Mineral Resources, Earth Science Series, Houston, Texas, in press.

Hodge, V., Stallar, M., Koide, M., and Goldberg, E.D., 1986, Determination of platinum and iridium in marine waters, sediments, and organisms: Analytical Chemistry, v. 58, p. 616-620.

Ingram, B.L., Hein, J.R., and Farmer, G.L., 1990, Age determinations and growth rates of Pacific ferromanganese deposits using strontium isotopes: Geochimica et Cosmochimica Acta, v. 54, no. 6, in press.

Kastner, M., 1979, Zeolites: in Burns, R.G. (ed.), Marine Minerals, Mineralogical Society of America Short Course Notes, v. 6, p. 111-122.

Klovan, J.E. and Imbrie, J., 1971, An algorithm and FORTRAN-IV program for large-scale Q-mode factor analysis and calculation of factor scores: Mathematical Geology, v. 3, p. 61-77.

Krauskopf, K.B., 1957, Separation of manganese from iron in sedimentary processes: Geochimica et Cosmochimica Acta, v. 12, p. 61-84.

Le Suave, R., Pichocki, C., Pautot, G., Hoffert, M. Morel, Y., Voisset, M., Monti, S., Amosse, J., and Kosakevitch, A., 1989, Geological and mineralogical study of Co-rich ferromanganese crusts from a submerged atoll in the Tuamotu Archipelago (French Polynesia): Marine Geology, v. 87, p. 227-247.

Lichte, F.E., Golightly, D.W., and Lamothe, P.J., 1987, Inductively coupled plasma-atomic emission spectrometry: in Baedecker, P.A. (ed.), Methods for Geochemical Analysis. U.S. Geological Survey Bulletin 1770, p. B1-B10.

Lincoln, J.M., Schlanger, S.O., Bergersen, D., Coogan, A.H., and Premoli Silva, I., 1989, Cretaceous foundations and multiple periods of uplift in the northern Marshall Islands, west central Pacific. Geological Society of America Annual Meeting, St. Louis, Missouri, Abstracts with Program, v. 21, no. 6, p. A195.

Lincoln, J.M., 1990, Regional tectonic history and Cenozoic sea levels deduced from drowned carbonate banks and atoll stratigraphy in the Marshall Islands, west central Pacific Ocean: Ph.D. dissertation, Northwestern University, Evanston, Illinois, 245 p.

Manheim, F.T. and Gulbrandsen, R.A., 1979, Marine Phosphorites: in Burns, R.G. (ed.), Marine Minerals, Mineralogical Society of America Short Course Notes, v. 6, p. 151-173.

Moore, J.G., Clague, D.A., and Normark, W.R., 1982, Diverse basalt types from Loihi seamount, Hawaii: Geology, v. 10, p. 88-92.

Natland, J.H., 1976, Petrology of volcanic rocks dredged from seamounts in the Line Islands: in Schlanger, S.O., Jackson, E.D., et al., Initial Reports of the Deep Sea Drilling Project, U.S. Government Printing Office, v. 33, p.749-777.

Pichocki, C. and Hoffert, M., 1987, Characteristics of Co-rich ferromanganese nodules and crusts sampled in French Polynesia: Marine Geology, v. 77, p. 109-119.

Piper, D.Z., 1974, Rare earth elements in ferromanganese nodules and other marine phases: Geochimica et Cosmochimica Acta, v. 38, p. 1007-1022.

Puteanus, D., and Halbach, P., 1988, Correlation of Co concentration and growth rate: a method for age determination of ferromanganese crusts: Chemical Geology, v. 69, p. 73-85.

Schwab, W.C., Hein, J.R., Davis, A.S., Morgenson, L.A., Daniel, C.L., and Haggerty, J.A., 1986, Geological and geochemical data for seamounts and associated ferromanganese crusts in the Ratak chain, Marshall Islands: U.S. Geological Survey Open File Report 86-338, 36 p.

Taggart, J.E., Lindsay, J.R., Scott, B.A., Vivit, D.V., Bartel, A.J., and Stewart, K.C., 1987, Analysis of geologic materials by wavelength-dispersive X-ray fluorescence spectrometry: in Baedecker, P.A. (ed.), Methods for Geochemical Analysis. U.S. Geological Survey Bulletin 1770, p. E1-E19.

Varentsov, I., Drits, V.A., Gorshkov, A.I., Sivtsov, A.V., and Sakharov, B.A., 1990, Mn-Fe oxyhydroxide crusts from Krylov Seamount (Atlantic Ocean): Mineralogy, Geochemistry, and Genesis: Marine Geology, in press.

Table 1. Scientific personnel on R.V. *Farnella* cruise F10-89-CP.

James R. Hein	Co-chief scientist	USGS[1]
Jung-Keuk Kang	Co-chief scientist	KORDI[2]
Michael E. Boyle	Electronics technician	USGS
Dong-Lim Choi	Watch stander	KORDI
Shawn V. Dadisman	Watch chief	USGS
Heidi L. Dieffenbach	Watch stander	USGS
Jack Halkena	Observer	Marshall Islands
Yong Joo	Marine technician	KORDI
Seong Ryul Kim	Watch stander	KORDI
Yoon-Oh Lee	Watch stander	KIER[3]
Renee L. Olson	Watch stander	USGS
J. Kevin O'Toole	Marine technician	USGS
Ward R. Ozanne	Marine technician	USGS
Dong-Won Park	Watch stander	KORDI
LedaBeth Pickthorn	Watch chief	USGS
Malcolm S. Pringle	Watch chief	USGS
Marjorie S. Schulz	Watch stander	USGS
Sang-Dai Seo	Photographer	KORDI
Joanne C. Thede	Watch stander	USGS
William S. Weber	Watch stander	USGS
Suk-Hoon Yoon	Watch stander	KORDI

[1]United States Geological Survey
[2]Korea Ocean Research and Development Institute
[3]Korea Research Institute of Energy and Resources

Table 2. Station locations and operations for cruise F10-89-CP.

Station	Operation	Seamount	Station	Operation	Seamount
KS	D 1	Karin			
1	D 1	Look	23	D 15	Ļalibjet
2	*CTD* 1	Look	24	*CTD* 11	Ļalibjet
3	D 2	Look	25	CAM 1	Ļalibjet
3	D 3	Look	26	D 16	Ļalibjet
4	D 4	Look	27	D 17	Ļalibjet
5	*CTD* 2	Look	28	*CTD* 12	Ļōtab
6	*CTD* 3	Open ocean	29	D 18	Ļōtab
7	*CTD* 4	Open ocean	30	*CTD* 13	Likelep
8	*CTD* 5	N. Ļāānṃōjānjān	31	D 19	Likelep
9	D 5	N. Ļāānṃōjānjān	32	*CTD* 14	Likelep
10	D 6	N. Ļāānṃōjānjān	33	D 20	Likelep
10	D 7	N. Ļāānṃōjānjān	34	CAM 2	Ļajutōkwa
11	D 8	N. Ļāānṃōjānjān	35	D 21	Ļajutōkwa
12	D 9	Ļami-Lọmilik	36	D 22	Mij-Lep
13	D 10	Ļami	37	D 23	Mij-Lep
14	*CTD* 6	Lọmilik	38	*CTD* 15	Mij-Lep
15	D 11	Lọmilik	38	*CTD* 16	Open Ocean
16	*CTD* 7	Lọmilik	39	*CTD* 17	Open Ocean
17	D 12	Ļōjemeja	40	----	----
18	*CTD* 8	Open ocean	41	D 24	Jālwōj Atoll
19	*CTD* 9	Open ocean	42	D 25	Jālwōj Atoll
20	D 13	Ujlañ	43	*CTD* 18	Jebrọ
21	*CTD* 10	Ujlañ	44	D 26	Jebrọ
22	D 14	Ujlañ	45	D 27	Jebrọ

D = dredge; *CTD* = temperature and oxygen profiles;
CAM = camera survey.

Table 3. Single-channel airgun and 3.5 kHz bathymetry lines.

Seamount Name	Line Number	Airgun Volume	Nautical Miles	Kilo-meters
Karin	KS-1	3.5 only	27.0	50.0
Subtotal	----	----	**27.0**	**50.0**
Ruwitūñtūñ & Look	1	40 in^3	84.0	155.6
Look	2	40 in^3	17.6	32.6
Look	3	40 in^3	24.6	45.6
Ḷāānṃōjānjān	4	160 in^3	24.6	45.6
Ḷāānṃōjānjān	5	160 in^3	20.5	38.0
Ḷāānṃōjānjān	6	160 in^3	46.8	86.7
Ḷāānṃōjānjān	7	160 in^3	4.0	7.4
Ḷāānṃōjānjān	8	160 in^3	12.4	23.0
Ḷāānṃōjānjān	9	160 in^3	22.0	40.7
Ḷami	10	160 in^3	20.0	37.0
Ḷami	11	160 in^3	12.0	22.2
Ḷami&Ḷomilik	12	160 in^3	43.0	79.6
Ḷomilik	13	160 in^3	14.0	25.9
Ḷomilik	14	160 in^3	24.5	45.4
Ḷōjemeja	15	3.5 only	23.0	42.6
Ujlañ Group	16	160 in^3	85.3	158.0
Ujlañ Group	17	160 in^3	51.0	94.5
Ujlañ Group	18	160 in^3	42.3	78.3
Ujlañ Group	19	160 in^3	43.0	79.6
Ujlañ Group	20	160 in^3	55.2	102.2
Ujlañ Group	21	160 in^3	63.0	116.7
Ujlañ Group	22	160 in^3	37.0	68.5
Ujlañ Group	23	160 in^3	10.5	19.5
Mij-Lep	24	3.5 only	28.0	51.9
Mij-Lep	25	3.5 only	22.0	40.7
Mij-Lep	26	3.5 only	29.5	54.6
Maanjidep	27A	3.5 only	19.2	35.6
Jebro	27	3.5 only	30.0	55.6
Jebro	28	3.5 only	16.0	29.6
Jebro	29	3.5 only	19.0	35.2
Jebro	30	3.5 only	25.0	46.3
Jebro	31	3.5 only	18.0	33.3
Jebro	32	3.5 only	11.0	20.4
Subtotal	----	----	**998.0**	**1848.4**
Archipelagic Apron	33	160 in^3	31.0	57.4
Archipelagic Apron	34	160 in^3	17.0	31.5
Archipelagic Apron	35	160 in^3	25.0	46.3
Archipelagic Apron	36	160 in^3	13.5	25.0
Archipelagic Apron	37	160 in^3	26.0	48.1
Subtotal	----	----	**112.5**	**208.3**
Total	----	----	**1137.5**	**2106.7**

Table 4. Oxygen and temperature data from CTD casts, see Figs. 90-107.

	Location	Top of O_2 Min. Zone (m)	Lowest O_2 Contents (ml/l)	Water Depth of lowest O_2 (m)	Water Depth of 10°C Isotherm (m)
CTD 1	Look, central summit	315	0.510	356	250
CTD 2	Look, mid-east flank	300	0.562	358	249
CTD 3	Open ocean	350	0.687	420	290
CTD 4	Open ocean	400	0.603	473	270
CTD 5	N.Ļāānṃōjānjān summit	420?	0.686	515	310
CTD 6	Lọmilik, summit	320	0.861?	347?	260
CTD 7	Lọmilik, summit	320	0.558?	315?	270
CTD 8	Open ocean	350	0.696	748	235
CTD 9	Open ocean	300	0.454	703	225
CTD 10	Ujlañ, NW upper flank	290	0.449	705	240
CTD 11	Ļalibjet, summit	275	0.730 0.748	386 885	230
CTD 12	Ļōtab	305	0.716 0.733	362 866	240
CTD 13	Likelep, NW lower flank	350	0.726 0.792	904 421	250
CTD 14	Likelep, N lower flank	375	0.765	895	251
CTD 15	Mij-Lep, N upper flank	275	0.400 0.419	519 746	220
CTD 16	Open ocean	230	0.258	246	200
CTD 17	Open ocean	205	0.264	624	215
CTD 18	Jebrọ, summit of south peak	230	0.123 0.157	509 600	240

Table 5. Foraminifer and calcareous nannofossil ages of sediments and sedimentary rocks.

Dredge/ Sample	Rock/Sediment	Nannofossils	Foraminifers	Age	Comments
D10-6	Foraminiferal ooze	*Ceratolithus telesmus* *Discolithina sp.* *Emiliania huxleyi* *Gephyrocapsa spp.* *Helicosphaera sp.* *Rhabdosphaera claviger* *Sphenolithus? sp.*	*Bolliella adamsi* *Globigerinoides extremus* *Globorotalia truncatulinoides* *Orbulina universa*	late Pleistocene or Holocene	Minor Pliocene reworking
D11-3F	Foraminiferal ooze filling internal vug in laminated rock	*Discoaster asymmetricus* *D. berggreni?* *D. brouweri* *D. challengeri?* *D. pentaradiatus* *D. surculus* *D. tamalis* *D. triradiatus* *Calcidiscus macintyrei* *Ceratolithus cristatus* *Emiliania annula* *Gephyrocapsa spp.*	*Globigerina nepenthes?* *Globigerinoides conglobatus* *G. quadrilobatus immaturus* *G. triloba* *G. ruber* *G. sacculifer* *Globorotalia tosaensis?* *G. tumida* *Neogloboquadrina dutertrei* *Pulleniatina praecursor?* *Sphaeroidinella dehiscens* *Sphaeroidinellopsis spp.*	late Pliocene	Some contamination by Pleistocene fossils
D11-3G	Mudstone lamina	--	--	Indeterminate	Few phosphatized nannofossils
D11-3G	Phosphatized foraminiferal limestone lamina	*Coccolithus eopelagicus?* *Chiasmolithus sp.?* *Cyclicargolithus floridanus?* *Discoaster sp.* *Dictyococcites bisectus* *Fasciculithus? sp.* *Sphenolithus sp.* *Zygrhablithus sp.*	Not analyzed	Eocene or Oligocene	--
D18-1-1	Foraminiferal ooze from fracture in limestone	*Calcidiscus leptoporus* *C. macintyrei* *Ceratolithus cristatus* *C. telesmus* *Discoaster brouweri (fragment)* *Emiliania huxleyi* *Gephyrocapsa spp.* *Helicosphaera sp.* *Rhabdosphaera claviger*	*Candiena nitida* *Globigerinella calida* *Globigerinoides conglobatus* *G. immaturus* *G. mitra?* *G. ruber* *G. sacculifer* *Globigerinita glutinata* *Globorotalia truncatulinoides* *G. tumida tumida* *G. tumida flexuosa?* *Hastigerina aequilateralis* *Neogloboquadrina dutertrei* *Pulleniatina obliquiloculata* *Sphaeroidinella dehiscens*	late Pleistocene or Holocene	fossils abundant and well preserved
D19-16	Matrix of breccia	Not analyzed	*Globotruncana bulloides* *G. elevata* *G. stuartiformis* *G. arca* *Heterohelix globulosa*	Campanian	basalt, echinoid, bryozoan, algal, & *Inoceramus* clasts in foram. matrix
D22-1-1	Foraminiferal sand from vugs in breccia	--	*Globigerinoides conglobatus* *G. ruber* *G. sacculifer* *Globoquadrina venezuelana?* *Globorotalia tumida* *G. menardii* *Hastigerina aequilateralis* *Orbulina universa* *Orbulina sp.* *Pulleniatina obliquiloculata* *P. sp.* *Sphaeroidinella dehiscens*	Pliocene or Quaternary	Nannofossils rare and unidentifiable; sand was winnowed during sampling or on the seafloor

Table 5 continued

D24-1-1,2	Foraminiferal ooze infilling borings in mudstone	*Calcidiscus leptoporus* *C. macintyrei* *Ceratolithus cristatus* *C. telesmus* *C. sp.* *Emiliania huxleyi* *Gephyrocapsa spp.* *Helicosphaera sp.*	*Globigerinita glutinata* *Globigerinoides conglobatus* *G. immaturus* *G. ruber* *G. sacculifer* *Globorotalia menardii* *G. tumida* *Pulleniatina obliquiloculata*	late Pleistocene or Holocene	Foraminifers & nannofossils are abundant
D24-1-3	Pale brown calcareous mudstone	*Eiffellithus turriseiffelii* *Lithraphidites carniolensis* *Microrhabdulus belgicus* *M. decoratus* *M. elongatus?* *Micula? sp.* *Quadrum trifidum* *Tetrapodorhabdus decorus?* *Watznaueria barnesae*	*Globigerinelloides ferreolensis?* *Globotruncana ventricosa?* *Hedbergella simplex?* *Heterohelix globulosa* *Pseudoguembelina costulata*	Late Cretaceous: late Campanian or Maastrichtian	Some Early Cretaceous reworking
D25-5	Yellow-brown calcareous mudstone	*Ahmuellerella sp.* *Ceratolithoides sp.* *Cribrosphaerella ? sp.* *Lithraphidites carniolensis* *Microrhabdulus decoratus* *M. belgicus* *Micula sp.* *Nannoconus multicadus* *Quadrum trifidum* *Tetralithus nitidus* *Tetrapodorhabdus decorus* *Watznaueria barnesae* *W. biporta?*	*Globotruncana bulloides* *Globotruncanita stuartiformis* *Heterohelix globulosa* *H. moremani* *Pseudoguembelina costulata* *Rugotruncana subcircumnodifer* *R. subpennyi?*	Late Cretaceous: late Campanian or Maastrichtian	Some early Cretaceous reworking
D25-8	Foraminiferal ooze	*Calcidiscus leptoporus* *C. macintyrei* *Ceratolithus cristatus* *C. telesmus* *C. sp.* *Discolithina sp.* *Emiliania huxleyi?* *Gephyrocapsa spp.* *Helicosphaera sp.* *Sphenolithus tribulosus?*	*Globigerina conglobata?* *Globigerinita glutinata* *Globigerinoides conglobatus* *G. immaturus* *G. ruber* *G. sacculifer* *Globorotalia menardii* *G. tumida* *Hastigerina aequilateralis* *Neogloboquadrina dutertrei* *Pulleniatina obliquiloculata* *Sphaeroidinella dehiscens*	late? Pleistocene or Holocene	Reworked Early Tertiary sphenolith
RD50-E	Phosphatized foraminiferal limestone	*Fasciculithus sp.* *Chiasmolithus sp. aff. C. grandis* *Cyclicargolithus sp. aff. C. Abisectus?* *Helicosphaera sp.*	Not analyzed	Paleogene (E. Tertiary)	Nannofossils are few & are phosphatized, & identifications questionable, but all are Early Tertiary

Table 6. Dredge summary for cruise F10-89-CP.

Dredge Number	Seamount Name	Water Depth On-Off Bottom (m)	Water Depth Corrected (m)[1]	Recovery (kg)	Crust Thickness (Max., mm)	Crust Thickness (Av., mm)	Dominant Substrate	Comments
D 1	Look	1565-1190	1540-1250	25	70	40	Breccia	Phosphorite; calcite veins
D 2	Look	-----	-----	-----	-----	-----	-----	No recovery
D 3	Look	1450-1300	1450-1400	4	57	25	Breccia	Calcite cement
D 4	Look	2060-1190	2025-2000	70	45	5	Basalt	Calcite; phosphorite; limestone in basalt
D 5	North Ļaānmōjānjān	1900-1870	2000-1900	1.5	25	10	Breccia	-----
D 6	North Ļaānmōjānjān	-----	-----	-----	-----	-----	-----	No recovery
D 7	North Ļaānmōjānjān	-----	-----	-----	-----	-----	-----	No recovery
D 8	North Ļaānmōjānjān	1550-1180	1550-1180	2.5	40	30	Tr. Breccia?	-----
D 9	Ļami	2530-2495	2530-2525	250	80	10	Limestone	Phosphorite; polished crusts; sandst., mudst.
D 10	Ļami	1945-1575	2000-1800	80	35	10	Limestone	Foraminiferal ooze
D 11	Ļomilik	1870-1465	1870-1690	450	180	110	Breccia	Mega crusts
D 12	Ļōjemeja	1910-1780	1910-1800	15	125	60	None	Nodules
D 13	Ujlan	2130-2280	2130-2050	55	95	30	Breccia	Polished & fluted crusts; phosphorite
D 14	Ujlan	2000-1825	2000-1825	35	130	60	Breccia	Phosphorite
D 15	Ļalibjet	2075-2040	2075-2040	6	35	15	Breccia	Phosphorite
D 16	Ļalibjet	1610-1605	1610-1600	50	105	50	Basalt	Mega nodules
D 17	Ļalibjet	2025-1850	2000-1850	4	55	35	None	-----
D 18	Ļōtab	1975-1940	1925-1800	125	150	20	Limestone	Phosphorite
D 19	Likelep	2160-2030	2160-1900	80	32	5	Breccia	Phosphorite
D 20	Likelep	2140-1920	2140-1920	40	75	30	Breccia	Phosphorite
D 21	Ļajutōkwa	2300-1850	2100-1850	275	65	15	Breccia	Phosphorite; hydrothermal Fe & Mn
D 22	Mij-Lep	1270-1245	1270-1245	46	80	60	Breccia	Phosphorite
D 23	Mij-Lep	1405-1305	1390-1300	70	92	70	Breccia	-----
D 24	Jālwōj Atoll	3030-2730	3030-2730	200	2	1	Mudstone	1 kg of crust
D 25	Jālwōj Atoll	3550-3380	3600-3380	200	3	2	Sandstone	Hornblende crystals
D 26	Jebrọ	1740-1700	1740-1700	100	64	35	Breccia	Smoothed crusts
D 27	Jebrọ	1670-1570	1670-1570	15	70	50	Breccia	Crust fragments
KS D1	Karin	1815-1705	1800-1705	125	50	3	Basalt	Missing outer layers

[1]Depth interval samples were probably recovered from, based on 12 kHz bathymetry at the times of high tension on the wire

Table 7. Location and description of dredge hauls, cruise F10-89-CP.

Dredge No.	Latitude (°N)	Longitude (°E)	Total Recovery (Kg)	% Broken From Outcrop	% Talus	% of Rocks in Dredge Encrusted	Description of Ferromanganese Oxides	Substrate Description
D 1	12°07.0' 12°07.3'	166°13.9' 166°13.4'	25	100	0	100	fine-scale botryoidal surfaces; 3 layers: 1, outer, botryoidal; 2, porous, Fe oxides line vugs; 3, inner, massive, blebs & veins of phosphorite; some eroded crusts; porous granular crusts on sides; thickness: max.=70mm, av.=40mm	90% breccia: angular to subrounded, moderate to poorly sorted, altered basalt clasts in phosphorite cement, with lesser altered hyaloclastite matrix, & minor calcite cement; phosphorite veins; 10% altered basalt
D 2	---	---	0	---	---	---	No recovery	---
D 3	12°11.5' 12°11.7'	166°17.2' 166°17.6'	4	100	0	99	medium-sized botryoids on surfaces; layers as in D1; rock fragment inclusions in layer 3; mostly crust fragments without substrate; thickness: max.=57mm, av.=25mm	75% altered porphyretic and vesicular basalt; calcite & rare phosphorite amygdules; 20% breccia with granule- to pebble-sized highly altered basalt clasts in calcite cement; 5% basalt(?) completely altered to clay minerals, Fe oxides, zeolites
D 4	12°10.8' 12°11.2'	166°18.6' 166°18.4'	70	100	0	95	botryoidal, granular, irregular, & smooth surface textures; mostly thin, dense, black crusts with 1 layer; thicker crusts have 3 layers as in D1, although layer 2 is thicker & distinctly columnar in D4; thickness: max.=45mm, av.=5mm; thicker on breccia, thinner on basalt & limestone	80% amygdaloidal to vesicular, gray-green, hornblende phyric basalt, with calcite amygdules; associated with limestone; 5% very altered basalt with phosphorite; 10% breccia with clasts of altered & fresh basalt, limestone, phosphorite, & crust fragments in carbonate matrix & phosphorite cement; 5% silty micritic limestone; phosphorite layer between crust & substrate of many samples
D 5	13°00.2' 13°00.2'	62°44.0' 162°43.9'	1.5	100	0	100	complete crusts absent; fragmented during dredging; granular, porous, & subdued botryoidal surfaces; thickness: max.=25mm, av.=10mm	small fragments of breccia composed of altered basalt clasts in phosphorite cement
D 6	---	---	0	---	---	---	Lost bag	---
D 7	---	---	0	---	---	---	Lost bag	---
D 8	13°03.9' 13°04.6'	162°46.0' 162°45.6'	2.5	100	0	100	medium botryoids on surface; same 3 layers as in D1; thickness: max.=40mm, av.=30mm	only traces of yellow-brown breccia or hyaloclastite attached to base of crusts
D 9	1°45.1' 11°45.4'	161°33.6' 161°33.6'	250	90	10	50	granular, rarely botryoidal & smooth, surface textures; some surfaces current polished & fluted; patina on limestone, thicker on sandstone, thickest on breccia; 4 layers: 1, outer, thin, dense; 2, porous, radial columnar; 3, dense, vertical cracks; 4, dense, fine dendritic Fe oxide veinlets; but number of layers varies from 1 to 6; much reworking of crusts by breccia formation forming crust clasts in breccia; 2 nodules; thickness: max.=80mm, av.=10mm	45% partly phosphatized limestone with animal borings on top surface & fractures lined with Mn oxides; 45% yellow-green hyaloclastite & volcaniclastic sandstone-siltstone-mudstone composed of completely altered glassy volcanic grains; commonly pebbly; normal size-graded beds; contains Mn chips and Mn diffusion gradient at top surface; 10% breccia composed of crust fragments, sandstone, & phosphorite, with carbonate matrix and phosphorite cement; pale brown dense phosphorite

Table 7 continued

D 10	11°50.0' 11°51.3'	161°28.7' 161°28.3'	80	100	0	80	medium sized, high relief botryoids on surfaces, some granular, some current polished; patina on limestone, thin granular on basalt, thickest on breccia; many crusts without substrates; 1 to 3 layers: 1, outer, black, porous, with pores between coalesced botryoids; 2, black, laminated with porous areas between laminae; 3, black, porous with botryoids composed of columns, Fe enriched between the botryoids; thickness: max.=35mm, av.=10mm	65% limestone, predominantly foraminiferal, partly to completely replaced by phosphorite, in places with basalt sand & pebble clasts; fractures and animal borings lined with Mn oxide; 25% massive olivine (some also plagioclase and pyroxene) phyric basalt; olivine altered to orange iddingsite, rest of rock fresh; <10% crusts without substrate; <2% breccia composed of basalt clasts in carbonate matrix; several Kg of foraminiferal sand also recovered
D 11	11°37.0' 11°39.0'	161°41.1' 161°39.8'	450	100	0	100	medium size botryoids on surface; some smoothed & polished by currents; granular on sides; 3 to 7 layers: 1, outer, massive, botryoidal; 2, vuggy, Fe oxide stained; 3, massive, black; 4, vugs infilled with phosphorite & carbonate; 5, massive, black; 6, porous, Fe stained; 7, massive, black, laced with phosphorite veins; thickness: max.=180mm, av.=110mm	60% breccia composed of altered brown & yellow-green, granule- to pebble-sized basalt clasts with phosphorite & Mn oxide cements; phosphorite & carbonate lenses & veins; 40% volcaniclastic sandstone & hyaloclastite with graded and laminated beds; completely altered yellow-green glassy volcanic grains; carbonate & phosphorite lenses
D 12	11°28.1' 11°27.8'	161°10.4' 161°09.1'	15	95	1	99	medium botryoids on surfaces; 17 crust fragments without substrates & 15 nodules; 4 layers: 1, outer, black, dense, vitreous; 2, porous, vugs filled with sediment & Fe stained; 3, porous, columnar-radiating, Fe stained; 4, dense, fractured with phosphorite blebs; thickness: max.=125mm, av.=60mm	none; nodule nuclei composed of Fe-Mn oxide fragments; <1kg pumice, probably not of local origin; <1 kg siliceous sponge fragments
D 13	09°37.2' 09°37.3'	160°32.6' 160°33.0'	55	98	2	95	irregular, current polished & fluted, botryoidal, and granular surfaces; 1 to 4 layers: 1, outer, porous, Fe stained; 2, massive, dense, black; 3, porous, micro-fractured, Fe stained, small basalt & phosphorite grains; 4, massive, dense, black, phosphorite veins; Mn oxide diffusion fronts along fractures in limestone; thickness: max.=95mm, av.=30mm	60% breccia: 1, with olivine & pyroxene phyric basalt clasts in phosphorite & Mn oxide cements; 2, highly altered red-brown, sand- & pebble-sized basalt clasts in phosphorite cement; 3, yellow-brown with gray patches, olivine & pyroxene phyric basalt clasts in calcite cement; 30% limestone: 1, micrite with animal borings, peppered with Mn oxide grains & dendrites; 2. bioclastic, reefal debris; 10% crust fragments without substrates
D 14	09°46.1' 09°45.3'	160°31.2' 160°31.8'	35	100	0	100	botryoidal-granular & subdued botryoidal surfaces; 1 to 4 layers: 1, outermost, dense, massive, laminated; 2, porous, columnar, vugs filled with sediment; 3, moderately porous; 4, innermost, dense, massive, botryoidal surface in sharp contact with layer 3; thickness: max.=130mm, av.=60mm	80% breccia: 1, yellow-green & brown completely altered basalt clasts in altered hyaloclastite matrix & minor phosphorite cement; 2, gray-brown basalt & pinkish micrite clasts in white & cream micrite matrix; 3, Mn nodules in phosphorite cement; 5% brown, vesicular, olivine & plagioclase phyric basalt; 5% phosphorite with Mn dendrites; 10% crust fragments

Table 7 continued

D 15	09°56.9'	160°30.2'	6	100	0	100	mostly crust fragments with botryoidal, lizard skin (microbotryoidal), and granular surfaces; 1 or 2 layers: 1, porous, massive; 2, very porous, massive; thickness: max.=35mm, av.=15mm	1 substrate rock: brown, altered, olivine, pyroxene, & plagioclase phyric basalt; basalt pebbles in phosphorite attached to one edge; also recovered 1 pebble of pumice & 1 of volcaniclastic sandstone
	09°56.7'	160°30.0'						
D 16	09°58.2'	160°29.2'	50	60	25	100	botryoidal & smooth surfaces; crusts 1 to 4 layers: 1, outermost, massive, dense; 2, porous, Fe stained; 3, crudely laminated; 4, massive, black, dense; many fragments without substrates; 3 cobble-sized (to 170mm diameter) nodules make up 15% of dredge; 2 with 5 layers & 1 with 6: 1, outermost, porous, botryoidal; 2, dense, massive; 3, porous, vugs infilled with sediment; 4, wavy laminated with phosphorite laminae; 5, porous, laminated; 6, dense, massive; thickness: max.=105mm, av.=50mm	100% gray olivine phyric basalt; olivine altered to orange iddingsite; same basalt type is the nuclei of nodules; phosphorite, Mn & Fe oxides, and calcite infill fractures; also recovered a few pebbles of pumice, siliceous sponge fragments, & one whale ear bone
	09°58.3'	160°29.0'						
D 17	10°07.6'	160°27.5'	4	100	0	100	crust fragments without substrates; botryoidal & granular surfaces; incomplete crusts, 1 to 3 layers: 1, black, massive; 2, porous, vugs with sediment; 3, porous massive; the commonly present innermost dense layer is missing, suggesting the dredge parted the crusts at mid-thickness; thickness: max.=55mm, av.=35mm	none; recovered 3 pumice pebbles, siliceous sponge fragments, and one basalt pebble
	10°07.2'	160°27.2'						
D 18	10°15.5'	160°40.4'	125	98	2	95	botryoidal, current polished & fluted, rarely smooth, granular on sides; thin crusts with 1 massive, dense, submetallic layer; thicker crusts with 2 or 3 layers: 1, outer, dense, massive; 2, porous, Fe stained, columnar; 3, radial crystallites in columnar botryoids; more substrate grains & thick pervasively porous crusts than in other dredges; many crust fragments without substrates; thickness: max.=150mm, av.=20mm	80% foraminiferal limestone, burrowed and bored, with Mn & Fe stained areas & dendrites; burrow-fill replaced by phosphorite; some contacts with crusts are gradational with Mn diffusion fronts; 20% miscellaneous: 1, breccia with clasts of gray, brown, yellow-green basalt, hornblende crystals in altered hyaloclastite matrix & Mn oxide cement; 2, pebbly sandstone with basalt, shell, hornblende grains in calcite cement; 3, gradations of 1 & 2; 4, aphyric to olivine, hornblende, plagioclase phyric altered basalt; also pumice pebbles & siliceous sponge fragments
	10°15.5'	160°40.7'						

Table 7 continued

D 19	10°36.0' 10°35.9'	160°22.1' 160°22.5'	80	100	0	100	smooth, botryoidal (small to large), lizard skin, & granular surfaces; 1 porous layer, rarely 2 layers: 1, massive, porous, Fe stained; 2, very porous, Fe stained, inclusions of small rock fragments; Mn oxide lines animal borings and forms dendrites in limestone; thickness: max.=32mm, av.=5mm	80% breccia, matrix or cement supported, sand to pebble size, angular to subrounded basalt clasts: 1, yellow-brown basalt in yellow-green altered hyaloclastite matrix with veins of phosphorite; 2, gray-brown basalt in brown altered hyaloclastite matrix with calcite veins; 3, altered to fresh basalt in phosphorite cement; 4, rust-red basalt in altered hyaloclastite matrix & phosphorite cement; 5, gray & brown basalt in carbonate matrix; 20% basalt (probably clasts from breccia); aphyric to olivine, pyroxene, hornblende, plagioclase phyric, moderately altered, massive
D 20	10°48.0' 10°48.3'	160°29.6' 160°29.7'	40	100	0	100	botryoidal to granular surfaces; thin crusts highly porous, Fe stained, with 1 layer; thicker crusts have 2 to 7 layers: 1, outer, crudely laminated, Fe oxides partly fill surface lows; 2, porous, massive, Fe stained; 3, porous, laminated, Fe stained; 4, very highly porous, pores infilled with phosphorite; 5, massive, dense; 6, highly porous, pores infilled with Fe oxide & minor phosphorite; 7, massive, dense; many crust fragments without substrates; thickness: max.=75mm, av.=30mm	95% breccia, clast supported, pale brown, dark brown, & gray altered basalt pebbles with: 1, calcite & zeolite cement, partly phosphatized; 2, calcite rim cement on clasts with carbonate matrix or phosphorite cement; 3, phosphorite cement; 4% basalt: 1, brown-gray to rust, aphanitic; 2, massive, olivine & plagioclase phyric; 1% micritic limestone; also recovered siliceous sponge and gorgonian coral fragments
D 21	10°30.2' 10°30.1'	160°51.1' 160°51.5'	225	70-100	0-30	70, much as patina	many of the crusts were completely removed by dredging or only the inner parts of the crusts remained on the substrates of others; many of those recovered are fossil crusts, having been buried by a pebbly limestone debris flow; many rocks only with patina; porous, granular, & botryoidal surfaces; many phosphorite laminae; included rock fragments; 1 or 2 layers: outer porous, inner massive; Mn diffusion front extending into limestone; thickness: max.=65mm, av.=15mm	most of the basalt cobbles were probably disaggregated from breccia during dredging & thus represent outcrop rather than talus; 20%, pebbly limestone is attached to many rocks & overlies some crusts & grades from sparse basalt clasts to clast-supported breccia; 75% breccia, (including disaggregated basalt clasts); brown-altered to gray-fresh basalt clasts, rare phosphorite & Mn oxide clasts, grain supported, sand- to pebble-size, angular to subrounded in phosphorite cement ± calcite cement ± zeolite cement ± altered hyaloclastite matrix ± Mn oxide cement, rarely with hydrothermal Fe oxide & Mn oxide cement; 5% miscellaneous: 1, ironstone, hydrothermally replaced basalt & breccia; 2, exhalite, hydrothermal Fe-Mn rock; 3, phosphorite

Table 7 continued

D 22	08°43.7' 08°43.6'	163°11.4' 163°12.9'	46	100	0	100	1 large slab & many fragments, probably broken from the slab; botryoidal surface, smooth on one edge; 3 layers: 1, porous, vugs with Fe stains; 2, massive, black, small vugs either empty or infilled with geopedal phosphorite; 3, massive, black, laced with microfractures stained by Fe; thickness: max.=80mm, av.=60mm	100% breccia to granulestone; yellow-green, granule- to small-pebble-sized clasts of completely altered glassy volcanic grains, phosphorite, & limestone in altered hyaloclastite matrix & phosphorite, zeolite, & Mn oxide cements; large vugs infilled with geopedal phosphorite or foraminiferal sand; also recovered large siliceous sponge, stock and spicules; 40 cm long reddish flexible whip-like organism; 60 pumice pebbles
23	08°52.0' 08°51.7'	163°10.3' 163°10.6'	70	100	0	100	many crusts without substrates; botryoidal & smooth surfaces; 1 to 4 layers: 1, outer, massive, porous in places; 2, highly porous, Fe stained; 3, massive, microfractured; 4, massive, black, dense, in places with included rock fragments; rare type with 3 layers: 1, outer, dense, laminated; 2, wavy laminations, microfractured; 3, dense, massive, phosphorite partings in lower part and botryoids in upper part; thickness: max.=92mm, av.=70mm	85% breccia composed of brown basalt clasts, granule to cobble size, with phosphorite & zeolite cements & phosphorite veins; 15% altered basalt, fractures filled with phosphorite; plagioclase, olivine, & pyroxene phyric; olivine altered to iddingsite; also recovered siliceous sponge fragments
D 24	06°17.2' 06°17.5'	1 69°18.5' 169°18.5'	200	100	0	100	granular patina on surface & lining animal borings; thickness: max.=2mm, av.=1mm	100% bedded calcareous mudstone; bioturbated with large & small borings; dark & pale brown beds; foraminiferal sand fills large borings
D 25	06°18.2' 06°18.0'	169°16.1' 169°16.4'	200	80	20	25	lizard skin, cauliflower botryoids, granular, & smooth surfaces; 1 black massive layer; thickness: max.=3mm, av.=2mm	40% yellow-green to red-brown volcaniclastic sandstone to pebbly sandstone; completely altered brown basalt grains & hornblende crystals (to 15mm long) in altered hyaloclastite matrix & minor calcite cement; 20% gray sandstone to pebbly sandstone; poorly sorted, angular to subrounded basalt grains & hornblende crystals in calcite cement & gray mud matrix; to 10mm, clasts of yellow-green waxy mud; 40% basalt, vesicular, hornblende & olivine phyric; <1%: mudstone as in D24; 2 pumice pebbles; a limestone pebble; foraminiferal sand
D 26	07°25.7' 07°25.5'	169°45.0' 169°44.8'	100	100	0	100	current smoothed & polished, botryoidal, & granular surfaces; upper mm's missing due to current abrasion; inclusions of rock fragments; highly fractured; phosphorite veins; many crust fragments without substrates; 1 or 2 layers: 1, massive, slightly to moderately porous; 2, massive, dense, gray; thickness: max.=64mm, av.=35mm	80% breccia, grain supported, poorly sorted, angular to subrounded, sand- to cobble-size, brown or gray altered basalt clasts in calcite, zeolite, and phosphorite cements; phosphorite veins; some have altered hyaloclastite matrix; 20% basalt, fresh to altered, brown-gray to rust-red, aphanitic, aphyric, massive to sparsely vesicular; also recovered 32 pumice pebbles;

Table 7 continued

D 27	07°31.4' 07°31.4'	169°39.9' 169°40.7'	15	100	0	100	botryoidal, irregular, & granular surfaces; many crust fragments without substrates; 2 layers: 1, outer, massive, finely porous; 2, black, massive, dense; thickness: max.=70mm, av.=50mm	100% breccia, altered brown, sand- to pebble-size, vesicular basalt pebbles in yellow-brown altered hyaloclastite matrix with phosphorite cement & veins; vugs infilled with phosphorite; some without matrix, only phosphorite cement; also recovered brittle stars & branching coral
KS D1	18°02.0' 18°01.5'	168°55.5' W 168°57.1' W	125	30	70	99	upper crust layers stripped by seafloor gravity flow processes; smooth, subdued botryoidal, & granular surfaces; phosphorite veins near base of crusts; 1 to 3 layers: 1, outer, laminated, 2, massive, dense; or 1, outer, black, vitreous, fractured; 2, dense, massive, black, parallel fractures, 3, dense massive, black, vitreous; also crust clasts floating in phosphorite=crust breccia; thickness: max.=50mm, av.=3mm, although originally probably averaged 30-40mm	98% basalt, aphanitic, moderately altered, massive; glassy rinds; plagioclase & rarely pyroxene phyric; phosphorite veins; 2% breccia, altered basalt & phosphorite clasts in altered hyaloclastite matrix & phosphorite cement, rarely with Mn oxide cement; breccia composed of crust fragments in phosphorite cement; also, one cobble-sized fragment of dark brown to gray phosphorite with Mn dendrites

Table 8. Location and description of dredge hauls, cruise MW-8805.

Dredge Number	Seamount Name	Latitude (°N)	Longitude (°E)	Water Depth On-Off Bottom (m)	General Description[1]	Subsample Descriptions
RD33	Lo-En	10°00.1' 10°01.8'	162°43.0' 162°42.1'	2440-1547	Much Fe-Mn oxides, basalt, & dense limestone; breccia with hyaloclastite & crust fragment clasts in phosphorite & Fe-Mn oxide cement; volcaniclastic sandstone; phosphorite veins & amygdules	1, cobble with max. 95mm, av. 65mm crust with smoothed botryoidal surface; 3 layers; 2, nodule, smooth surface, 48-67mm thick crust on moderate-sized nucleus; 2 layers; 3, crust on basalt cobble, max. 34mm, av. 26mm thick, smooth surface; 3 layers; phosphorite veins and vug infillings in all 3 crusts
RD34	Lo-En	10°02.6' 10°03.2'	162°42.1' 162°41.1'	1390-1292	Vesicular basalt, limestone, crust fragments, breccia	Max. 6mm, av. 4.5 mm crust with botryoidal surface on breccia with altered basalt clasts in carbonate replaced phosphorite cement
RD35	Lo-En	09°56.4' 09°59.5	162°52.4' 162°51.8'	1789-1243	Fe-Mn crusts & breccia with basalt & crust clasts in foraminiferal matrix; gray pumice	Fragment of large crust; smooth surface that was once botryoidal; max. 95mm, av. 80mm; 2 layers: 1, 30mm, outer, porous; 2, 65mm dense, black, massive; lamina with phosphorite vug infillings separates the two layers;
RD36	Lo-En	10°03.1' 10°02.5'	162°49.8' 162°51.3'	1124-1104	Basalt with calcite veins; Fe-Mn crusts; some limestone	1: max. 35mm, av. 28mm thick crust with botryoidal surface; 3 layers: 1, porous, large vugs; 2, dense, massive; 3, porous, phosphorite infilled vugs, included fragments to 10mm of substrate; basalt-clast breccia with phosphorite cement; 2: crust fragment with missing layers, no substrate; 3: basalt cobble surrounded by crust that is missing outer layers
RD38	Lo-En	10°19.3' 10°20.1'	162°46.8' 162°46.9'	1462-1452	Fe-Mn crusts & nodules with basalt nuclei	Nodule with 45-55mm thick crust with smoothed botryoidal surface; nucleus is 60mm diameter, vesicular, altered basalt cobble; some phosphorite amygdules

Table 8 continued

RD40	Ruwitūñtūñ	11°46.2' 11°47.0'	167°02.2' 167°01.9'	1385-1331	About 90 kg (2 large blocks) of altered foraminiferal, molluscan, algal limestone with 100mm Fe-Mn crusts	Max. 69mm, av. 48mm crust with botryoidal surface & 3 layers: 1, porous, Fe stained; 2, dense, massive, accretion parallel fractures; 3, wavy to botyroidal laminations; phosphorite infilled vugs span the contact of layers 1 & 2; phosphatized bioclastic limestone substrate, moldic porosity
RD41	Ruwitūñtūñ	11°42.7' 11°44.1'	167°01.0' 167°01.4'	1962-1583	About 35 kg altered vesicular basalt with Fe-Mn crusts; one breccia cobble with altered basalt clasts & carbonate matrix; 1 small cobble of pumice	Max. 27mm, av. 15mm thick crust with botryoidal surface & 3 layers: 1, dense, massive; 2, porous, Fe stained; 3, dense, massive, phosphorite veins; highly altered, vesicular, basalt substrate, with vesicles infilled with phosphorite
RD43	Ruwitūñtūñ	11°51.2' 11°51.4'	166°46.9' 166°47.1'	2248-2177	Fe-Mn encrusted, altered, vesicular basalt; tabular fragments of hyaloclastite with 2-3mm crust & carbonate ooze infilled borings; 1 cobble of basalt-limestone clast breccia	All 3 crusts with smoothed botryoidal surface; 1: 50mm thick crust with 4 layers: 1, dense, black; 2, porous, large vugs; 3, dense, black; 4, porous, Fe stained, included substrate clasts; phosphorite breccia, replaced foraminiferal sand; 2: 30mm crust, dense, black; cross-bedded sandstone with phosphorite lens between crust & sandstone; 3: 22mm crust with 2 layers: 1, black, dense; 2, porous Fe-stained; highly vesicular basalt substrate
RD44	Look	12°07.7' 12°07.8'	166°08.7' 166°08.9'	2376-2040	Fe-Mn crusts on: gray vesicular basalt; yellow green hyaloclastite; breccia with basalt clasts; foraminiferal limestone & pale-brown soft nannofossil chalk	Max. 40mm, av. 30mm crust with granular sides & botryoidal top & 2 layers: 1, porous, Fe stained; 2, denser, but still porous, black; both layers with vertical-oriented Mn-oxide crystallites; phosphorite breccia substrate
RD45	Look	12°08.2' 12°08.9'	166°09.4' 166°09.7'	1771-1532	2-3mm crusts on: highly altered vesicular basalt; 2 breccia boulders with vesicular basalt clasts & hyaloclastite matrix cut by calcite veins	Sampled only for basalt age dating & petrology

Table 8 continued

RD46	Look	12°07.9' 12°07.4'	166°10.6' 166°09.8'	1609-1087	1 small cobble of altered basalt with Fe-Mn crust	Sampled only for basalt age dating & petrology
RD47	Wōdejebato	11°43.3' 11°44.0'	164°45.5' 164°45.7'	2691-2414	Fe-Mn crusts on: basalt; brown-gray chalk; salmon-colored, hard limestone; nodules with nuclei of pelagic sediment; hyaloclastite	Smoothed botryoidal surface on porous, Fe-stained crust with included sand-sized substrate grains; max. 17mm, av. 12mm; surrounds a hyaloclastite talus cobble
RD48	Wōdejebato	11°54.4' 11°54.6'	164°42.8' 164°42.4'	1639-1592	Boulder-sized breccia block and many smaller pieces, with basalt clasts in a foraminiferal limestone matrix	1: smoothed botryoidal crust; max. 62mm, av. 50mm thick; 2 layers: 1, porous, Fe stained; 2, black, dense, conchoidal fracture; altered basalt substrate; 2: botryoidal, black, massive crust; max. 12mm, av. 7mm thick; phosphorite-cement-supported, basalt-clast breccia; replaced foraminiferal ooze
RD49	Wōdejebato	11°50.4' 11°50.7'	164°53.7' 164°53.6'	1568-1556	Up to 50mm thick Fe-Mn crusts on: basalt; breccia with basalt clasts, carbonate matrix	Sampled only for basalt age dating & petrology
RD50	Wōdejebato	11°51.0' 11°51.3'	164°53.5' 164°53.5'	1428-1401	Up to 150mm thick Fe-Mn crusts on rudist reef limestone with mulluscs, foraminifers, & algae	Botryoidal surface, max. 65mm, av. 40mm thick crust with 3 layers: 1, dense, black; 2, porous, large vugs, Fe stained; 3, dense, black, microfractured; partly phosphatized foraminiferal limestone substrate
RD53	Bwewa-Kaṇ	13°29.7' 13°29.8'	164°23.3' 164°22.7'	1600-1575	Fe-Mn crusts on: basalt; breccia boulder with basalt clasts in hyaloclastite matrix; breccia, phosphorite & salmon-colored limestone clasts in carbonate matrix	Smoothed & polished botryoidal surface, 32mm-thick crust with 5 layers: 1, fractured, dense, black; 2, porous, Fe stained; 3, dense, black; 4, dense, black, small vugs, botryoidal lower surface; 5, dense, black; breccia with altered basalt clasts, poorly sorted, angular, in calcite, phosphorite, & phillipsite cement

Table 8 continued

RD56	Ļōbbadede	13°52.6' 13°51.4'	163°36.5' 163°36.6'	2475-2375	Crust fragments; Fe-Mn crusts on: basalt, some with fresh olivine; dense foraminiferal limestone with basalt fragments; 3 small pieces of breccia with vesicular basalt clasts	Smoothed botryoidal surface, max. 53 mm, av. 40mm thick crust, Fe stained, phosphorite in small vugs, porous with 2 large vugs infilled with carbonate ooze; no substrate
RD59	Ļōmtal	14°42.2' 14°42.7'	163°27.1' 163°27.0'	1930-1475	Fe-Mn nodules up to 250mm diameter with basalt nuclei; Fe-Mn crusts on: vesicular basalt; breccia with basalt & breccia clasts in carbonate matrix	1: altered vesicular basalt talus cobble asymmetrically surrounded by 20-55mm of Fe-Mn crust with 5 layers: 1, dense, black, Fe stained; 2, porous, Fe-stained, large vugs; 3, dense, black, micro-fracturing with phosphorite; 5, dense, black; 2: phosphorite cement-supported, altered basalt-clast breccia surrounded on 3 sides by crust, av. 38mm, max. 65mm thick with 5 layers as in #1; 3: cement supported, phosphorite- & Mn oxide-cemented, altered basalt- & phosphorite-clast breccia with 42mm thick crust that is missing its outer layers
RD60	South Wōd-Ẹn	15°17.3' 15°17.3'	162°56.3' 162°56.7'	1575-1475	Up to 100mm Fe-Mn crusts on: basalt with foraminiferal limestone filling fractures; fractured olive green volcaniclastic sandstone with phosphorite veins	Vesicular altered basalt with Fe oxides infilling vesicles & phosphorite veins; smoothed botryoidal surface, max. 108mm, av. 90mm crust with 5 layers: 1, dense, black; 2, very porous, vugs with phosphorite; 3, dense, black, few phosphorite-infilled vugs; 4, porous, small vugs infilled with phosphorite grading into 5, dense, black, laminated
RD61	South Wōd-Ẹn	15°07.5' 15°07.7'	162°58.9' 162°58.8'	1649-1450	Thin Fe-Mn crusts on: basalt boulders with fractures infilled with foraminiferal ooze; breccia with basalt clasts & little matrix	Sampled only for basalt age dating & petrology

Table 8 continued

RD62	North Wōd-Eṇ	15°57.9' 15°58.6'	162°56.0' 162°55.8'	1700-1490	Thin Fe-Mn crusts on: breccia with ironstone & basalt clasts in Fe oxide cement; calcite-phosphorite veins	Sampled only for basalt age dating & petrology
RD63	Neen-Koiaak	14°18.8' 14°19.3'	160°59.1' 160°59.9'	1490-1363	Up to 70mm Fe-Mn crusts on: hyaloclastite; boulders of altered basalt; foraminiferal-molluscan limestone is matrix for hyaloclastite-clast breccia	Altered basalt clasts in hyaloclastite matrix with phosphorite veins; smoothed botryoidal surface on max. 82mm, av. 57mm thick crust with 2 layers: 1, porous, Fe stained; 2, dense, black, phosphorite veins at the base
RD65	Aeañ-Kaṇ	14°43.7' 14°43.8'	160°26.1' 160°26.2'	1303-1259	Gray basalt; breccia with basalt clasts & foraminiferal carbonate matrix with some shell fragments	Sampled only for basalt age dating & petrology
RD67[2]	Unnamed	15°29.3' 15°30.3'	155°01.4' 155°01.4'	1643-1548	Gray basalt with pinkish carbonate ooze in fractures; many types of breccia including limestone clasts in foraminiferal carbonate matrix; basalt clasts	Sampled only for basalt age dating & petrology

[1]Mostly from cruise report, Dunnebier and Schlanger (1988)
[2]Located to the west of the region shown in Figure 1

Table 9. Fresh basalt samples being processed for radiometric age dating, stable isotopes, and chemistry.

Seamount/ Atoll	Dredge/ Sample	$^{40}Ar/^{39}Ar$ Dating[1]	Sr, Nd, Pb isotopes	Whole Rock Chemistry
Look	D1-3	Hbl, Plag?	Hbl?, Plag?	X
	D4-2	Hbl, Plag?	Hbl, Plag?	X
	D4-17	Plag?	Pyx	X
	RD44-1	Hbl	Hbl	X
	RD45-1	--	Pyx	X
	RD46-1	--	Pyx	X
Lọmilik	D10-7	Plag?	Plag?	X
	D10-9	Plag?	Pyx, Plag?	X
	D10-10	Plag	Plag	X
	D10-11-2	--	--	X
	D10-12	Plag?	Pyx, Plag?	X
Ujlañ	D13-2	Plag?	pyx	X
	D14-1	Plag	Plag	--
Ḷalibjet	D15-1	--	Pyx	X
	D16-1	--	Pyx	X
	D16-6	WR, Plag?	WR, Plag?	X
Ḷōtab	D18-14-1	--	Pyx	X
	D18-22-1	Plag?	Pyx	X
Likelep	D19-18	WR, Plag, Hbl	Plag, Hbl	X
	D19-19	WR, Plag, Hbl	Plag, Hbl	X
	D19-20	WR, Plag, Hbl	Plag, Hbl	X
	D20-14-1	Plag?	Plag?	X
	D20-14-2	Plag?	Plag?	X
Ḷajutōkwa	D21-11	WR, Plag	Pyx, Plag	X
	D21-25-3	Plag?	Pyx	X
	D21-26-1	Plag?	Plag?	X
	D21-27-1	Plag?	Plag, Pyx?	X
	D21-27-2	Plag?	Plag, Pyx?	X
	D21-27-3	Plag?	Plag, Pyx?	X
	D21-28-1	Plag?	Pyx	X
	D21-30-1	--	--	X
	D21-30-2	--	--	X
	D21-30-3	--	--	X
Mij-Lep	D23-3	Plag	Plag	X

Table 9 continued

Jālwōj	D25-1	--	Pyx	--
	D25-4-2	--	Pyx	--
	D25-9-1	WR	Pyx	X
Jebrọ	D26-3	--	--	X
	D26-4	--	--	X
	D26-8	--	--	X
Ḷọ-Eṇ	RD35-2	--	--	X
	RD35-3	--	--	X
Ruwitūñtūñ	RD41-2	--	--	X
Wōdejebato	RD48-1	--	--	X
	RD48-2	--	--	X
	RD49-1	--	--	X
Bwewa-Kaṇ	RD53-1	Plag?	Pyx	X
Ḷōbbadede	RD56-1	WR, Plag?	Pyx, Plag?	X[2]
South Wōd-Eṇ	RD60-1	Plag?	Pyx, Plag?	X
	RD61-1	Plag	Pyx, Plag	X
North Wōd-Eṇ	RD62-1	Plag	Plag, Pyx?	X
	RD62-4	WR, Plag?	WR, Plag?	X
Aeañ-Kaṇ	RD65-1	WR?, Plag?	WR?, Plag?	X
Unnamed	RD66-1	Plag	Pyx, Plag	X
	RD67-2	WR	WR	X[2]
	RD67-4	WR?	WR?	X
Anewetak Drill Core	E-1-4-3b	WR	WR	X[2]
	E-1-5-6a	WR	WR	X[2]

[1]WR, whole rock; Plag, plagioclase; Pyx, pyroxene; Hbl, hornblende; ?, denotes analysis possible if enough sample can be separated.
[2]Preliminary dates range between 75 and 85 Ma.

Table 10. X-ray diffraction mineralogy of substrate rocks from cruises F10-89-CP and MW-88-05.

Sample	Major[1]	Moderate	Minor/Trace	Rock/Sediment
		F10-89-CP		
D1-1F	Apatite	K-feldspar, Calcite	-	Phosphorite and calcite cemented sandstone
D1-20	Plagioclase, Apatite	Smectite	-	Altered basalt with phosphorite veinlets
D3-8	Calcite	Smectite	-	Altered breccia with calcite and phosphorite cement
D4-2B	Plagioclase, Pyroxene, Calcite	Smectite	Apatite	Altered amygduloidal basalt with calcite amygdules
D4-3E	Calcite	Apatite	-	Calcite and phosphorite cement of breccia
D4-20	Calcite	Apatite	-	Partly phosphatized foraminiferal limestone
D9-1G	Apatite	Smectite	-	Phosphorite cemented breccia
D9-9A	Apatite	-	-	Phosphorite (replaced foraminiferal sand)
D9-9B	Apatite	Smectite	-	Phosphorite cemented and replaced hyaloclastite
D9-11	Calcite, Apatite	-	-	Partly phosphatized limestone
D9-15	Apatite	-	-	Phosphorite (replaced foraminiferal sand)
D9-16	Smectite	-	-	Interbedded altered hyaloclastite and reworked ash
D9-25-1	Calcite	Smectite	-	Calcite cemented sandstone with calcite veins
D9-26-1	Phillipsite, Smectite	-	-	Zeolite cemented altered hyaloclastite
D9-29-1	Calcite	Apatite	-	Slightly phosphatized limestone
D10-17A	Apatite	Calcite	Phillipsite	Phosphorite cemented breccia
D10-17B	Apatite	-	-	Phosphorite (replaced foraminiferal sand)
D11-3E	Apatite	Plagioclase, Calcite	-	Phosphorite and calcite cemented laminated hyaloclastite-ash-sandstone
D11-3F	Calcite	-	-	Foraminiferal sand filling central vug in laminated rock
D11-3G	Apatite	Plagioclase	Smectite	Phosphatized ash lamina
D11-3H	Apatite	Plagioclase, Calcite, Smectite, Celadonite	-	Phosphorite and calcite cemented sandstone lamina
D11-3I	Apatite	Plagioclase	Smectite	Phosphorite cemented altered hyaloclastite lamina,
D11-13G	Apatite	Smectite	Plagioclase	Phosphorite cemented breccia
D14-3B	Phillipsite	Apatite, Calcite	Smectite	Zeolite, phosphorite, and calcite cemented breccia
D16-6A	Plagioclase	Smectite	-*	Basalt
D18-1B	Apatite, Calcite	Phillipsite	-	Partly phosphatized foraminiferal limestone
D18-20-1	Calcite, Plagioclase	Apatite, Phillipsite	Smectite	Calcite, phosphorite, and zeolite cemented pebbly sandstone
D19-1D	Plagioclase, Apatite	-	Smectite	Phosphorite cemented breccia
D19-3	Apatite	-	K-feldspar	Phosphorite cemented breccia
D20-1	Plagioclase, Calcite	Phillipsite	Smectite	Calcite and zeolite cemented breccia
D21-2	Goethite	Plagioclase	Apatite	Goethite and apatite cemented, goethite replaced breccia--ironstone
D21-3C	Goethite, Apatite, Plagioclase	-	-	Goethite and apatite replaced basalt--ironstone
D21-5	δ-MnO_2	Apatite, Plagioclase	-	δ-MnO_2 and phosphorite cemented breccia
D21-6	Apatite	Plagioclase, Phillipsite	-	Phosphorite and zeolite cemented breccia
D21-7	Apatite	Plagioclase, Phillipsite	-	Phosphorite and zeolite cemented breccia

Table 10 continued

D21-8	Goethite, Plagioclase, Apatite	Phillipsite	-	Phosphorite, goethite, and zeolite cemented, goethite replaced breccia--ironstone
D21-9A	Apatite	Goethite, Plagioclase	Phillipsite	Phosphorite and goethite cemented breccia
D21-9B	Goethite	Plagioclase, Apatite	Trace Phillipsite	Phosphorite and goethite cemented, goethite replaced breccia--ironstone
D21-9C	Apatite	Plagioclase	Goethite, Trace Phillipsite	Phosphorite cemented breccia
D21-12	Plagioclase	Apatite, Goethite	Phillipsite	Phosphorite cemented, goethite replaced breccia
D21-19-1	Plagioclase, Apatite	Phillipsite	-	Phosphorite and zeolite cemented breccia
D21-24-1	Plagioclase	Apatite	Smectite	Altered basalt with phosphorite veins
D21-24-2	Plagioclase	Smectite	-	Altered basalt
D21-24-3	Plagioclase	Phillipsite	Apatite, Smectite	Altered basalt
D22-1E	Apatite	-	Smectite, Phillipsite	Phosphatized hyaloclastite
D23-6F	Plagioclase	Phillipsite, Apatite	Smectite	Zeolite cemented breccia with phosphorite veins
D24-1-1,2	Calcite	-	-	Foraminiferal sand in borings in mudstone
D24-1-3	Calcite	Phillipsite, Plagioclase	-	Pale brown calcareous mudstone bed
D24-1-4	Plagioclase, Phillipsite	Smectite, Pyroxene		Dark brown mudstone bed
D25-1A	Phillipsite	-	Smectite	Cement / Fracture fill
D25-1B	Phillipsite	-	Smectite	Hyaloclastite
D25-3B	Plagioclase, Pyroxene	Goethite	-	Altered vesicular basalt
D25-4A	Plagioclase, Pyroxene	Phillipsite	Smectite, Goethite	Zeolite cemented volcaniclastic sandstone
D25-4B	Celadonite	-	-	Clay clasts in sandstone
D25-5	Calcite	Phillipsite	Smectite, Plagioclase	Calcareous mudstone
D26-9A	Calcite, Plagioclase	Apatite	Smectite, Phillipsite	Calcite and phosphorite cemented breccia
D27-5-1	Apatite, Plagioclase	Goethite, Phillipsite	Smectite	Phosphorite and zeolite cemented, altered breccia
KSD1-19B	Apatite	Smectite	Plagioclase	Phosphorite cemented breccia
		MW8805		
RD33-2B	Apatite	Plagioclase	Smectite	Phosphorite cemented sandstone
RD36-1B	Plagioclase	Smectite, Apatite	Phillipsite	Altered basalt clast from breccia
RD43-1E	Apatite	-	-	Phosphorite
RD43-2B	Apatite	-	-	4mm phosphorite layer
RD43-2C	Phillipsite	Apatite, Smectite	-	Phosphorite and zeolite cemented sandstone
RD44-1B	Apatite	-	Smectite	Phosphorite cemented breccia
RD47B	Phillipsite, Smectite	-	-	Altered hyaloclastite
RD48-2B	Apatite	-	Plagioclase	Phosphorite cement of breccia
RD50E	Apatite, Calcite	-	-	Phosphorite cemented and partly replaced foraminiferal sand
RD59-2C	Apatite	-	Smectite, Plagioclase	Phosphorite (replaced breccia)
RD60-F	Plagioclase	Apatite	Smectite	Altered porous basalt with phosphorite veins
RD63-D	Apatite, Phillipsite	Smectite	-	Zeolite cemented altered breccia, with phosphorite veins.

1. Major: >25%, Moderate: >5% to <25% , Minor: <5%.
2. All apatite is Carbonate Fluorapatite.
3. All breccias are sedimentary, and most are volcaniclastic.

Table 11. Chemical composition in weight percent of substrate rocks from cruises F10-89-CP and MW-88-05.

	D1-1F[3]	D1-20	D3-8	D4-2B	D4-3E	D4-20	D9-1G	D9-9A[3]	D9-9B	D9-16	D9-25-1	D9-26-1	D9-29-1	D10-10
SiO_2	9.57	35.60	22.00	29.10	10.40	5.60	17.70	1.84	19.60	45.20	20.70	51.30	1.55	38.30
Al_2O_3	3.35	16.10	7.44	11.90	3.44	1.58	5.47	0.53	5.49	12.20	6.35	13.90	0.35	13.50
FeO	nd	nd	nd	nd	nd	nd	nd	nd	nd	nd	nd	nd	nd	nd
Fe_2O_3	3.74	11.80	7.42	7.10	3.79	1.42	6.85	0.54	6.14	10.30	6.42	12.40	0.28	16.70
MgO	1.36	1.27	2.01	1.64	0.90	0.93	1.49	0.47	1.56	4.45	1.92	4.78	0.54	5.82
CaO	42.10	14.30	27.90	24.30	41.20	50.30	30.60	51.90	29.00	0.61	29.00	0.47	54.70	11.10
Na_2O	1.26	1.81	1.14	2.04	1.19	0.46	1.41	1.03	1.54	1.92	0.97	2.66	0.25	1.67
K_2O	0.91	2.63	1.05	0.99	0.85	0.34	1.07	0.07	1.02	2.28	1.12	2.63	0.03	0.76
TiO_2	0.73	1.42	1.89	2.64	0.77	0.35	0.87	0.07	0.90	1.85	0.99	2.20	< 0.02	3.89
P_2O_5	21.10	7.84	6.01	1.43	16.10	7.45	18.80	30.00	18.20	0.29	0.67	0.08	4.34	1.15
MnO	0.06	< 0.02	0.42	0.10	0.44	< 0.02	0.83	< 0.02	0.09	< 0.02	0.07	0.21	< 0.02	0.18
LOI 925C	14.10	7.51	22.40	19.10	19.10	32.00	12.90	9.97	14.00	21.10	32.20	9.48	38.70	7.87
Total	98.28	100.28	99.68	100.34	98.18	100.43	97.99	96.42	97.54	100.2	100.41	100.11	100.74	100.94
H_2O^+	2.36	3.93	3.25	1.36	0.49	0.89	2.61	2.11	1.66	2.75	0.45	5.78	0.36	1.97
H_2O^-	1.04	2.08	4.20	2.23	2.55	0.44	5.91	0.21	7.34	13.80	6.47	3.60	0.22	4.92
CO_2	10.50	0.97	14.70	15.30	14.60	30.80	4.60	8.02	2.89	0.06	21.90	0.10	37.30	0.13
Rock type	Phosphorite cemented sandstone	Altered basalt with phosphorite veinlets	Calcite and phosphorite cemented breccia	Altered basalt with calcite infilled vesicles	Calcite and phosphorite cement of breccia	Phospha-tized micrite limestone	Phosphorite cemented breccia	Phosphorite (replaced foram sand)	Phosphorite cemented & replaced hyaloclastite	Altered hyaloclastite & reworked ash	Sandstone with calcite cement and veins	Zeolite cemented hyalo-clastite	Slightly phospha-tized limestone	Altered basalt

	D10-13[4]	D11-3E	D11-13G	D14-3B	D16-6A	D18-1B	D18-20-1	D19-1D	D19-3[3]	D19-7	D20-1	D21-2[2,4]	D21-7	D21-8
SiO_2	0.43	20.30	19.70	39.20	50.30	8.87	30.60	32.90	7.93	49.80	35.10	17.40	26.70	13.80
Al_2O_3	< 0.10	6.98	7.13	12.00	17.50	2.71	10.60	11.40	2.35	18.80	13.30	9.28	11.00	5.90
FeO	nd	nd	nd	nd	nd	nd	nd	nd	nd	nd	nd	nd	nd	nd
Fe_2O_3	0.04	6.03	6.80	10.20	10.50	1.50	8.00	8.33	1.22	9.59	9.26	43.1	9.43	26.30
MgO	0.38	1.62	1.82	2.98	1.99	0.60	2.45	2.07	0.57	2.03	2.37	1.21	0.87	1.14
CaO	55.30	28.70	25.50	8.30	5.89	44.60	23.40	16.50	45.30	5.78	15.40	8.86	23.30	23.80
Na_2O	0.46	1.32	1.53	2.14	4.25	1.54	1.92	1.85	1.34	3.86	2.41	1.77	3.16	1.68
K_2O	< 0.02	1.31	1.50	2.16	2.88	0.74	1.64	1.90	0.57	3.16	1.67	0.73	1.59	0.87
TiO_2	< 0.02	1.46	1.66	1.38	2.78	0.07	1.94	1.39	0.23	2.03	2.47	1.50	1.80	1.08
P_2O_5	12.50	15.90	15.70	4.05	1.10	20.10	1.70	9.66	28.10	0.95	0.63	5.63	13.8	15.00
MnO	< 0.02	0.43	4.85	0.20	0.08	0.52	0.21	0.41	0.06	0.11	0.13	0.83	0.07	0.28
LOI 925C	30.30	14.30	12.50	17.30	2.84	16.50	18.10	9.97	6.65	3.74	17.50	10.40	7.39	8.96
Total	99.41	98.35	98.69	99.91	100.11	97.75	100.56	96.38	94.32	99.85	100.24	100.71	99.11	98.81
H_2O^+	0.59	1.06	2.35	2.71	1.32	2.10	1.40	3.51	1.41	1.98	2.41	7.34	2.73	5.04
H_2O^-	0.13	7.64	6.72	11.1	1.36	1.60	2.30	4.20	0.40	1.46	4.87	1.72	2.54	1.55
CO_2	29.00	5.55	3.42	1	0.04	12.80	13.70	1.50	4.44	0.08	8.66	0.73	2.05	2.32
Rock type	Phospha-tized limestone	Phosphorite and calcite cemented laminated sandstone	Phosphorite cemented breccia	Phosphorite zeolite and calcite cemented hyaloclastite	Basalt	Phospha-tized limestone	Calcite, phosphorite, and zeolite cemented sandstone	Phosphorite cemented breccia	Phosphorite cemented breccia	Altered basalt	Calcite and zeolite cemented breccia	Goethite and phosphorite cemented, goethite replaced breccia-ironstone	Phosphorite cemented breccia	Phosphorite, goethite and zeolite cemented, goethite replaced breccia-ironstone

Table 11 continued

	D21-9A	D21-9B[2,4]	D21-9C	D21-12	D21-19-1	D22-1E	D23-6F	D23-10	D24-1-3	D24-1-4	D25-1B	D25-3B	D25-4A	D25-5
SiO_2	18.10	23.4	23.2	34.80	29.10	13.90	36.80	42.20	32.40	41.90	47.20	42.40	46.00	32.80
Al_2O_3	8.05	9.66	8.44	13.30	13.10	4.59	15.90	16.90	10.50	16.40	8.90	10.10	12.90	10.40
FeO	nd	nd	nd	nd	nd	nd	nd	nd	nd	nd	nd	nd	nd	nd
Fe_2O_3	20.60	35.8	9.11	14.20	8.71	4.61	11.80	11.90	8.78	14.60	15.10	16.60	14.00	10.30
MgO	1.18	1.30	1.13	1.12	0.87	1.19	1.05	1.08	2.14	2.95	7.33	6.99	6.65	2.30
CaO	20.20	9.07	25.60	14.90	20.30	35.50	7.84	10.50	17.90	2.00	6.95	13.50	7.85	17.00
Na_2O	2.01	2.17	2.31	3.56	3.10	1.35	3.40	3.75	2.02	2.51	2.12	2.31	2.79	2.07
K_2O	1.08	1.23	1.47	2.15	1.76	1.19	1.65	1.65	2.83	2.80	2.69	1.18	1.88	2.81
TiO_2	1.33	1.55	1.38	2.29	1.78	0.58	2.79	2.82	2.51	4.10	2.41	2.43	3.86	2.50
P_2O_5	12.30	5.23	15.30	8.04	11.50	22.00	2.88	4.04	0.38	0.37	0.09	1.50	0.65	0.38
MnO	3.55	0.73	1.98	0.73	0.98	0.84	0.20	0.19	0.08	0.21	0.22	0.29	0.23	0.11
LOI 925C	10.00	10.50	8.66	4.35	8.04	12.30	15.70	4.97	20.70	12.20	7.23	2.90	3.46	19.30
Total	98.40	100.64	98.58	99.44	99.24	98.05	100.01	100.00	100.24	100.04	100.24	100.20	100.27	99.97
H_2O^+	4.75	5.96	3.10	2.25	2.58	2.01	0.66	2.09	2.91	4.91	4.04	1.64	2.62	3.05
H_2O^-	2.44	3.01	2.76	0.76	3.02	5.70	10.90	1.95	2.73	4.46	2.95	0.63	0.87	2.20
CO_2	1.91	0.70	2.25	1.22	1.76	4.80	0.78	0.62	13.10	0.99	0.03	0.18	0.11	12.40
Rock type	Phosphorite and goethite cemented breccia	Phosphorite and goethite cemented goethite replaced breccia-ironstone	Phosphorite cemented breccia	Phosphorite cemented, goethite replaced basalt	Phosphorite and zeolite cemented breccia	Phospha-tized hyaloclastite	Zeolite cemented breccia with phosphorite veins	Phosphorite cemented breccia	Calcareous mudstone layer	Mudstone layer	Hyaloclastite	Altered vesicular basalt	Zeolite cemented volcani-clastic sandstone	Calcareous mudstone

	D26-9A	D27-5-1	KSD1-19B	RD33-2B	RD36-1B	RD43-1E	RD43-2C	RD44-1B	RD47B	RD48-2B	RD50E	RD59-2C	RD60F	RD63D
SiO_2	30.70	27.80	17.50	21.70	43.20	1.74	44.00	4.24	39.80	5.73	0.74	7.59	37.60	32.40
Al_2O_3	9.06	9.79	6.75	7.11	16.40	0.48	11.80	1.28	9.98	1.96	0.25	2.68	15.30	10.30
FeO	nd	nd	nd	nd	1.61	nd	0.07	-	nd	0.37	nd	nd	3.09	0.27
Fe_2O_3	11.40	9.28	7.48	7.39	9.60	0.62	11.82	1.19	16.10	3.29	0.28	2.57	9.57	8.85
MgO	1.83	2.10	1.34	2.01	4.47	0.43	2.40	0.57	2.80	1.21	0.55	0.70	5.23	6.68
CaO	19.80	20.50	32.80	28.30	8.40	51.70	4.09	49.50	1.42	45.70	54.10	45.30	13.40	13.90
Na_2O	1.87	2.50	1.31	1.54	3.12	0.98	2.78	0.93	2.27	1.25	0.55	1.03	1.66	2.21
K_2O	2.14	1.72	1.02	1.23	1.47	0.03	3.22	0.19	2.87	0.26	0.03	0.54	0.81	1.99
TiO_2	2.29	2.70	1.02	1.34	2.74	0.03	2.66	0.23	1.91	0.58	<0.02	0.29	2.73	1.13
P_2O_5	2.27	12.40	20.90	16.60	2.39	31.70	2.29	26.60	0.48	27.70	17.40	27.50	3.11	8.58
MnO	0.31	0.79	0.79	2.27	0.13	0.46	0.22	0.21	3.27	0.34	0.16	0.85	0.14	0.20
LOI 925C	18.30	9.30	8.01	8.74	6.01	7.46	14.60	11.30	17.10	8.88	24.80	7.87	6.96	13.00
Total	99.97	98.88	98.92	98.23	99.54	95.63	99.95	96.34	98.00	97.27	98.86	96.92	99.60	99.51
H_2O^+	2.34	3.54	2.96	3.65	3.92	1.88	7.49	1.99	5.46	2.18	1.29	2.00	3.17	4.87
H_2O^-	3.30	3.71	1.97	2.69	1.88	0.58	6.42	0.89	12.40	1.73	0.47	1.69	3.98	7.48
CO_2	11.70	1.86	2.82	1.48	0.33	2.60	0.35	4.12	0.33	2.52	6.30	2.48	0.33	0.85
Rock type	Calcite and phosphorite cemented breccia	Phosphorite and zeolite cemented breccia	Phosphorite cemented breccia	Phosphorite cemented sandstone	Altered basalt clast from breccia	Phosphorite	Phosphorite and zeolite cemented sandstone	Phosphorite cemented breccia	Altered hyalo-clastite	Phosphorite cement of breccia	Phosphorite cemented and replaced sandstone	Phosphorite (replaced breccia)	Altered basalt with phosphorite veins	Zeolite cemented breccia with phosphorite veins

Major oxides by X-ray fluorescence; LOI = Loss On Ignition at 925°C; Analysts: J. Taggart, A. Bartel, D. Siems, C. Papp.

[1] = Total Fe as Fe_2O_3

[2] = Semiquantiative, because Fe contents outside the range of the standard.

[3] = Contains sulfur.

[4] = Contains minor amount of sulfur.

Table 12. X-ray diffraction mineralogy of ferromanganese deposits from cruises F10-89-CP and MW-88-05.

Sample Number	Type & Interval (mm)[1]	δ–MnO_2 (%)[2]	Others(%)
	F10-89-CP		
D1-1A	Bulk Crust (0-40)	95	5 - Apatite
D1-1B	Crust Layer (0-7)	99	1 - Quartz
D1-1C	Crust Layer (7-14)	100	-
D1-1D	Crust Layer (14-40)	91	9 - Apatite
D1-3	Bulk Crust (0-20)	100	-
D1-18	Bulk Crust (0-50)	96	4 - Apatite
D3-2	Bulk Crust (0-35)	97	1 - Plagioclase, 1 - Apatite, <1 - Quartz
D4-1	Crust Surface (0-≤0.5)	99	1 - Quartz, Calcite
D4-2A	Bulk Crust (0-4)	99	1 - Quartz
D4-3A	Crust Layer (0-9)	99	1 - Quartz, Calcite
D4-3B	Crust Layer (9-27)	99	1 - Quartz
D4-3C	Crust Layer (27-37)	100	-
D4-3D	Bulk Crust (0-37)	99	1 - Quartz
D5-1-1	Bulk Crust (0-17)	100	-
D5-1-2	Bulk Crust (0-19)	100	-
D8-1-1A	Bulk Crust (0-35)	96	4 - Apatite
D8-1-1B	Crust Layer (0-7)	99	1 - Quartz
D8-1-1C	Crust Layer (7-19)	99	1 - Goethite
D8-1-1D	Crust Layer (19-35)	97	3 - Apatite
D8-1-2,3,4	Crust Surface (0-≤0.5)	100	-
D9-1A	Bulk Crust (0-70)	98	2 - Apatite
D9-1B	Crust Layer (0-3)	98	1 - Plagioclase, <1 - Quartz
D9-1C	Crust Layer (3-18)	98	1 - Plagioclase, <1 - Quartz
D9-1D	Crust Layer (18-38)	97	3 - Goethite
D9-1E	Crust Layer (38-68)	93	7 - Apatite, Trace - Quartz
D9-1F	Fossil Crust Clast in Breccia (0-17)	86	12 - Apatite, 2 - Todorokite, Trace - Quartz
D9-7A	Bulk Crust (0-75)	93	6 - Apatite, 1 - Quartz
D9-7B	Crust Layer (0-15)	97	3 - Goethite, Trace - Quartz
D9-7C	Crust Layer (15-31)	96	3 - Goethite, 1 - Plagioclase, Quartz
D9-7D	Crust Layer (31-43)	97	3 - Goethite, <1 - Apatite
D9-7E	Crust Layer (43-67)	90	10 - Apatite
D9-7F	Crust Layer (67-75)	88	12 - Apatite
D10-1-1A	Bulk Crust (0-30)	92	4 - Apatite, 4 - Goethite, <1 - Quartz
D10-1-1B	Crust Layer (0-22)	99	1 - Plagioclase, Trace - Quartz
D10-1-1C	Crust Layer (22-30)	83	11 - Apatite, 6 - Goethite, Trace - Quartz
D10-2-1	Bulk Crust (0-35)	98	1 - Plagioclase, 1 - Quartz
D11-3A	Bulk Crust (0-78)	97	3 - Apatite, Trace - Quartz
D11-3B	Crust Layer (0-25)	98	1 - Plagioclase, <1 - Quartz
D11-3C	Crust Layer (25-45)	100	-
D11-3D	Crust Layer (45-79)	84	16 - Apatite
D11-13A	Bulk Crust (0-103)	93	7 - Apatite
D11-13B	Crust Layer (0-18)	99	<1 - Quartz
D11-13C	Crust Layer (18-38)	100	-
D11-13D	Crust Layer (38-53)	95	5 - Apatite
D11-13E	Crust Layer (53-78)	86	14 - Apatite
D11-13F	Crust Layer (78-104)	83	17 - Apatite
D11-15A	Bulk Crust (0-140)	95	5 - Apatite
D11-15B	Crust Layer (0-20)	100	Trace - Quartz
D11-15C	Crust Layer 20-35)	99	1 - Plagioclase, Trace - Quartz
D11-15D	Crust Layer 35-70)	96	4 - Goethite
D11-15E	Crust Layer (70-138)	87	13 - Apatite
D11-17-1	Crust Surface (0-≤0.5)	98	1 - Quartz, 1 - Plagioclase
D12-1A	Bulk Crust (0-120)	96	4 - Apatite
D12-1B	Crust Layer (0-17)	100	Trace - Quartz

Table 12 continued

D12-1C	Crust Layer (17-40)	100	-
D12-1D	Crust Layer 40-65)	96	4 - Goethite
D12-1E	Crust Layer (65-120)	89	11 - Apatite
D12-3	Crust Surface (0-≤0.5)	100	Trace - Quartz
D12-4	Bulk Nodule (0-45)	100	Trace - Quartz
D13-3A	Bulk Crust (0-55)	100	-
D13-3B	Crust Layer (0-20)	100	-
D13-3C	Crust Layer (20-43)	95	4 - Goethite, 1 - Plagioclase, Trace - Quartz
D13-3D	Crust Layer (43-55)	95	5 - Apatite, Trace - Quartz
D13-6	Crust Surface (0-≤0.5)	100	-
D14-1A	Bulk Crust (0-120)	96	4 - Apatite
D14-1B	Crust Layer (0-30)	100	-
D14-1C	Crust Layer (30-45)	100	-
D14-1D	Crust Layer (45-70)	96	3 - Goethite, 1 - Apatite
D14-1E	Crust Layer (70-120)	92	8 - Apatite
D14-4	Bulk Crust (0-19)	88	6 - Apatite, 3 - Phillipsite, 2 - Todorokite, <1 - Quartz
D15-2	Bulk Crust (0-33)	100	Trace - Quartz, Plagioclase
D16-2A	Bulk Crust (0-105)	94	6 - Apatite, Trace - Quartz
D16-2B	Crust Layer (0-5)	100	Trace - Quartz
D16-2C	Crust Layer (5-20)	98	2 - Plagioclase, Trace - Quartz
D16-2D	Crust Layer (20-31)	90	7 - Apatite, 3 - Goethite
D16-2E	Crust Layer (31-95)	89	11 - Apatite
D16-2F	Underside Crust (0-10)	93	6 - Todorokite, 1 - Plagioclase, Trace - Quartz
D16-5A	Bulk Nodule (0-43)	93	4 - Apatite, 2 - Todorokite, 1 - Plagioclase, Trace - Quartz
D16-5B	Nodule Layer (0-15)	97	2 - Todorokite, 1 - Plagioclase, Trace - Quartz
D16-5C	Nodule Layer (15-30)	86	11 - Apatite, 3 - Todorokite
D16-5D	Nodule Layer (30-42)	76	20 - Apatite, 4 - Todorokite
D16-6B	Bulk Nodule (0-55)	97	2 - Apatite, 1 - Plagioclase
D16-8-1	Bulk Crust (0-20)	97	2 - Apatite, 1 - Todorokite
D17-1	Bulk Crust (0-55)	100	Trace - Quartz
D18-1A	Bulk Crust (0-100)	98	1 - Quartz, <1 - Halite
D18-3A	Bulk Crust (0-50)	100	Trace - Quartz, Plagioclase
D18-3B	Crust Layer (0-16)	100	Trace - Quartz
D18-3C	Crust Layer (16-26)	99	1 - Plagioclase, Trace - Quartz
D18-3D	Crust Layer (26-50)	95	5 - Goethite
D18-3E	Side & Underside Crust (0-5)	100	Trace - Calcite
D18-6	Bulk Crust (0-100)	96	3 - Goethite, 1 - Quartz, Calcite
D18-18	Crust Surface (0-≤0.5)	99	1 - Calcite, Quartz
D19-1A	Bulk Crust (0-35)	94	6 - Apatite, Trace - Quartz
D19-1B	Crust Layer (0-15)	100	Trace - Quartz
D19-1C	Crust Layer (15-35)	81	17 - Apatite, 2 - Quartz
D19-2B	Bulk Crust (0-5)	100	Trace - Quartz
D20-2	Bulk Crust (0-2)	95	3 - Plagioclase, 1 - Calcite, <1 - Quartz
D20-4	Bulk Crust (0-62)	99	1 - Goethite?, Trace - Quartz?
D21-3A	Bulk Crust (0-10)	83	15 - Apatite, 1 - Plagioclase, 1 - Quartz
D21-3B	Stratabound Layer (0-10)	69[3]	27 - Apatite, 4 - Goethite
D21-4	Bulk Crust (0-20)	95	5 - Apatite
D21-10A	Bulk Crust (0-18)	95	4 - Apatite, 1 - Quartz
D21-10B	Crust Layer (0-4)	96	4 - Apatite, Trace - Quartz
D21-10C	Crust Layer (4-18)	90	10 - Apatite
D22-1A	Bulk Crust (0-64)	92	8 - Apatite
D22-1B	Crust Layer (0-13)	99	<1 - Quartz
D22-1C	Crust Layer (13-35)	93	7 - Apatite
D22-1D	Crust Layer (35-66)	91	9 - Apatite
D23-1A	Bulk Crust (0-82)	94	6 - Apatite

Table 12 continued

D23-1B	Crust Layer (0-10)	100	-
D23-1C	Crust Layer (10-27)	100	-
D23-1D	Crust Layer (27-79)	91	9 - Apatite
D23-3	Bulk Crust (0-25)	98	2 - Apatite
D23-6A	Bulk Crust (0-85)	95	5 - Apatite
D23-6B	Crust Layer (0-10)	100	-
D23-6C	Crust Layer (10-22)	100	-
D23-6D	Crust Layer (22-34)	98	2 - Apatite
D23-6E	Crust Layer (34-84)	91	9 - Apatite
D24-1-5	Bulk Crust (0-1)	100	-
D25-3A	Crust Surface (0-≤0.5)	100	Trace - Calcite
D25-3C	Bulk Crust (0-2)	94	3 - Plagioclase, 3 - Pyroxene
D26-5-1	Bulk Crust (0-33)	95	3 - Apatite, 1 - Plagioclase, <1 - Quartz
D26-8-2	Bulk Crust (0-7)	99	1 - Plagioclase, Trace - Quartz
D27-2-1	Bulk Crust (0-63)	93	7 - Apatite
D27-2-2A	Crust Layer (0-25)	100	-
D27-2-2B	Crust Layer (25-45)	93	7 - Apatite
D27-2-2C	Crust Layer (45-65)	92	8 - Apatite
D27-2-3	Metallic patina at base of crust	90	10 - Apatite
KSD1-10A	Bulk Crust (0-47)	95	5 - Apatite
KSD1-10B	Crust Layer (0-11)	99	<1 - Quartz, Plagioclase
KSD1-10C	Crust Layer (11-32)	94	5 - Apatite, 1 - Quartz
KSD1-10D	Crust Layer (32-47)	91	9 - Apatite
KSD1-19A	Bulk Crust (0-16)	97	3 - Apatite
KSD1-25A	Bulk Crust (0-43)	96	4 - Apatite
KSD1-25B	Crust Layer (0-15)	99	1 - Apatite
KSD1-25C	Crust Layer (15-43)	95	5 - Apatite
	MW8805		
RD33-1A	Bulk Crust (0-17)	95	4 - Todorokite, 1 - Apatite, Trace - Quartz
RD33-2A	Bulk Nodule (0-53)	93	7 - Apatite, Trace - Quartz
RD33-3	Bulk Nodule (0-30)	85	13 - Apatite, 2 - Todorokite?
RD34A	Bulk Crust (0-6)	100	Trace - Quartz
RD35A	Bulk Crust (0-83)	94	6 - Apatite
RD36-1A	Bulk Crust (0-35)	90	10 - Apatite
RD36-1C	Crust Layer (0-10)	100	-
RD36-1D	Crust Layer (10-26)	92	8 - Apatite
RD36-1E	Crust Layer (26-34)	84	15 - Apatite, 1 - Todorokite?
RD38A	Bulk Nodule (0-50)	93	7 - Apatite
RD40-1	Bulk Crust (0-67)	86	12 - Apatite, 2 - Todorokite?
RD41	Bulk Crust (0-23)	98	1 - Apatite, <1 - Quartz
RD43-1A	Crust Layer (0-5)	99	<1 - Quartz
RD43-1B	Crust Layer (5-30)	100	Trace - Quartz
RD43-1C	Crust Layer (30-32)	100	-
RD43-1D	Crust Layer (32-42)	97	2 - Apatite, 1 - Goethite
RD43-1F	Bulk Crust (0-42)	100	Trace - Quartz
RD43-2A	Bulk Crust (0-4)	99	<1 - Quartz
RD43-3	Bulk Crust (0-12)	91	9 - Apatite
RD44-1A	Bulk Crust (0-30)	100	Trace - Quartz
RD47A	Bulk Crust (0-17)	99	1 - Plagioclase, Trace - Quartz
RD48A	Bulk Crust (0-58)	94	3 - Todorokite, 3 - Apatite
RD48-2A	Bulk Crust (0-9)	99	<1 - Quartz
RD50A	Bulk Crust (0-63)	90	10 - Apatite
RD50B	Crust Layer (0-7)	100	Trace - Quartz
RD50C	Crust Layer (7-26)	100	-
RD50D	Crust Layer (26-53)	87	13 - Apatite
RD53-3C	Bulk Crust (0-33)	98	1 - Apatite, 1 - Goethite, Trace - Quartz
RD53-3D	Crust Layer (0-10)	100	-
RD53-3E	Crust Layer (10-25)	99	1 - Goethite
RD53-3F	Crust Layer (25-32)	94	5 - Apatite, 1 - Goethite

Table 12 continued

RD56-1	Bulk Crust (0-53)	92	3 - Apatite, 2 - Phillipsite, 1 - Plagioclase, 1 - Goethite, <1 - Quartz
RD59-1	Bulk Crust (0-52)	95	4 - Apatite, 1 - Quartz
RD59-2A	Bulk Crust (0-65)	96	2 - Apatite, 1 - Plagioclase, 1 - Quartz
RD59-2B	Underside Bulk Crust (0-65)	90	10 - Apatite
RD59-2D	Crust Layer (0-10)	98	1 - Quartz, <1 - Plagioclase
RD59-2E	Crust Layer (10-35)	99	<1 - Quartz
RD59-2F	Crust Layer (35-45)	99	1 - Apatite
RD59-2G	Crust Layer (45-60)	88	12 - Apatite
RD59-2H	Crust Layer (60-65)	89	11 - Apatite
RD59-2I	Underside Crust Layer (0-7)	100	-
RD59-2J	Underside Crust Layer (7-21)	85	13 - Apatite, 2 - Todorokite
RD59-2K	Underside Crust Layer (21-53)	87	13 - Apatite
RD59-2L	Underside Crust Layer (53-63)	83	14 - Apatite, 3 - Todorokite
RD59-3	Bulk Crust (0-26)	87	13 - Apatite
RD60-A	Bulk Crust (0-105)	88	12 - Apatite
RD60-B	Crust Layer (0-5)	98	1 - Quartz, 1 - Plagioclase
RD60-C	Crust Layer (5-39)	100	Trace - Quartz
RD60-D	Crust Layer (39-69)	88	12 - Apatite
RD60-E	Crust Layer (69-100)	86	14 - Apatite
RD63-A	Bulk Crust (0-60)	96	4 - Apatite, Trace - Quartz
RD63-B	Crust Layer (0-24)	100	-
RD63-C	Crust Layer (24-54)	94	6 - Apatite

[1]Intervals measured from the outer surface of crusts and nodules.

[2]Percentages were determined by using the following weighting factors relative to quartz set at 1: δ-MnO_2 75; Todorokite 10; Birnessite 12 (Hein et al., 1988); Carbonate fluorapatite 3.1; Plagioclase 2.8; Calcite 1.65; Smectite 3.0; Goethite 7.0; Phillipsite 17.0; Illite 6.0, Pyroxene 5.0, Halite 2.0 (From Cook et al., 1975). The limit of detection for each mineral falls between 0.2 and 1.0%, except the manganese minerals which are greater, perhaps as much as 10% for δ-MnO_2. Apatite always refers to carbonate fluorapatite.

[3] Stratabound layer sandwiched between Fe-oxide-phosphorite substrate and phosphorite-rich Fe-Mn crust.

Table 13. Chemical composition of ferromanganese deposits in weight percent for major elements, ppm for minor elements, and ppb for platinum-group elements.

	D1-1A[1]	D1-1B	D1-1C	D1-1D	D1-3	D1-18	D1-21	D3-2	D4-1	D4-2A	D4-3A
Fe %	10.0	12.7	14.1	7.8	10.5	11.3	12.8	13.3	13.9	14.8	15.0
Mn	22.1	25.6	24.3	20.5	23.6	17.9	24.0	20.1	23.3	22.1	19.6
Mn/Fe	2.21	2.02	1.72	2.63	2.25	1.58	1.87	1.51	1.68	1.49	1.31
Si	0.93	1.54	1.59	0.55	1.00	1.59	2.20	2.52	2.57	2.76	4.07
Na	1.47	1.66	1.58	1.41	1.46	1.28	1.88	1.39	1.44	1.51	1.49
Mg	1.00	1.15	1.11	0.95	1.14	0.88	1.15	1.02	1.06	0.99	0.96
K	0.39	0.41	0.39	0.35	0.39	0.32	0.42	0.43	0.42	0.38	0.52
Ca	7.50	2.31	2.55	10.70	2.00	9.40	2.44	2.41	2.67	2.30	2.40
Ti	0.67	0.92	1.18	0.47	0.92	0.68	0.81	0.92	0.91	0.86	0.99
Al	0.15	0.36	0.33	0.21	0.29	0.44	0.35	0.83	0.33	0.43	0.92
P	2.42	0.35	0.43	3.60	0.24	3.10	0.46	0.51	0.40	0.39	0.31
H2O+	5.6	8.1	7.8	5.9	6.0	6.2	6.3	7.9	6.6	8.1	8.0
H2O-	13.5	13.2	12.7	12.5	24.3	15.4	14.7	18.5	14.4	14.3	14.0
CO2	1.30	0.44	0.47	1.80	0.31	1.60	0.58	0.45	1.00	0.62	0.86
LOI	27.5	29.8	29.4	26.8	39.1	28.8	29.7	33.5	28.3	30.6	29.0
Ba ppm	1400	1200	1600	1400	1400	1400	840	1700	910	1100	1200
Co	6900	12700	8300	4100	9500	3900	12300	5600	11000	7900	7600
Cu	550	380	670	530	800	570	200	1000	180	270	520
Mo	520	530	510	500	430	400	430	480	360	480	320
Ni	5600	5000	5100	5800	6400	4100	4600	4700	4300	3900	3800
Sr	1500	1400	1500	1500	1200	1500	1300	1300	1400	1500	1200
V	510	570	630	420	430	480	580	630	590	600	470
Y	260	140	140	320	120	250	170	150	180	190	160
Ce	900	1000	1200	830	950	780	800	790	890	740	800
As	150	250	240	130	180	140	220	210	200	260	200
Cd	3.8	4.3	3.9	4.1	4.8	2.7	4.2	3.2	4.1	3.3	3.2
Cr	6.5	6.0	4.5	4.5	3.5	10.0	6.0	9.0	4.0	4.0	16.0
Pb	1500	1900	1800	1300	1600	1200	1800	1400	1700	1600	1400
Zn	720	580	700	740	690	600	590	670	610	550	550
Au ppb	< 20	-	-	-	-	-	-	-	-	-	-
Pt	510	-	-	-	-	-	-	-	-	-	-
Pd	2.1	-	-	-	-	-	-	-	-	-	-
Rh	29.0	-	-	-	-	-	-	-	-	-	-
Ru	14.0	-	-	-	-	-	-	-	-	-	-
Ir	6.5	-	-	-	-	-	-	-	-	-	-
Interval[2]	B 0-40	L 0-7	L 7-14	L 14-40	B 0-20	B 0-50	S 0-≤0.5	B 0-35	S 0-≤0.5	B 0-4	L 0-9
Type	Crust	Crust	Crust	Crust	Crust	Crust	Crust	Crust	Crust	Crust	Crust
Comments											

Table 13 continued

	D4-3B	D4-3C	D4-3D	D5-1-1	D5-1-2	D8-1-1A	D8-1-1B	D8-1-1C	D8-1-1D	D8-1-2,3	D9-7A
Fe%	16.3	15.8	15.4	14.3	14.9	12.1	14.0	19.2	11.1	12.8	13.0
Mn	19.3	21.4	20.6	17.7	18.9	19.0	23.3	19.1	21.0	23.8	14.8
Mn/Fe	1.18	1.35	1.34	1.24	1.27	1.57	1.66	0.99	1.89	1.86	1.14
Si	4.77	2.48	3.32	3.09	2.06	1.74	2.81	3.46	1.07	2.06	2.48
Na	1.14	1.51	1.48	1.37	1.40	1.36	1.60	1.05	1.38	1.94	1.14
Mg	1.04	1.00	0.99	0.83	0.87	0.90	1.03	1.05	0.91	1.16	0.73
K	0.60	0.45	0.46	0.41	0.34	0.38	0.44	0.41	0.35	0.42	0.34
Ca	2.19	3.10	2.72	1.80	2.35	4.50	2.11	2.08	7.70	2.48	8.20
Ti	1.19	1.11	1.08	1.04	0.97	0.79	0.92	1.14	0.76	0.83	0.72
Al	1.34	0.70	0.79	0.66	0.45	0.39	0.53	0.95	0.22	0.34	0.57
P	0.32	0.66	0.54	0.29	0.46	1.35	0.36	0.43	2.51	0.44	2.83
H2O+	8.3	8.0	8.5	5.9	7.2	5.3	8.5	8.8	6.4	6.5	4.1
H2O-	10.2	10.6	12.1	23.6	20.8	21.8	12.1	10.2	13.2	15.6	18.1
CO2	0.68	0.62	0.66	0.43	0.46	0.82	0.45	0.50	1.30	0.76	1.40
LOI	24.9	26.5	27.8	36.6	35.0	34.5	28.1	25.1	27.0	30.7	29.5
Ba ppm	1500	1800	1500	1300	1600	1300	1200	1500	1500	820	1600
Co	5600	6500	7100	5900	5700	6100	10200	4600	5300	12700	2500
Cu	1000	1500	1000	740	980	570	430	740	720	150	1000
Mo	280	420	350	270	380	400	440	280	500	410	320
Ni	4200	4400	4200	3100	3500	4200	4600	3600	4700	4400	2700
Sr	1300	1500	1400	1200	1400	1400	1400	1400	1600	1400	1400
V	460	630	530	420	560	490	560	570	530	610	530
Y	160	170	170	160	200	210	150	170	210	180	260
Ce	980	1000	950	940	890	800	930	960	750	830	820
As	180	210	190	190	220	150	240	230	150	210	120
Cd	3.0	3.2	3.1	2.5	2.6	2.8	3.9	2.6	2.8	4.4	2.6
Cr	15.0	9.0	20.0	7.0	4.5	5.5	8.0	13.0	1.3	5.0	7.0
Pb	1200	1300	1400	1300	1200	1400	1800	1600	1200	1900	910
Zn	610	760	650	510	650	580	570	650	660	600	640
Au ppb	-	-	-	-	-	< 10	-	-	< 20	-	< 10
Pt	-	-	-	-	-	1000	-	-	570	-	380
Pd	-	-	-	-	-	3.7	-	-	2.2	-	3.4
Rh	-	-	-	-	-	44.0	-	-	32.0	-	18.0
Ru	-	-	-	-	-	23.0	-	-	13.0	-	11.0
Ir	-	-	-	-	-	10.0	-	-	6.8	-	4.5
Interval	L 9-27	L 27-37	B 0-37	B 0-17	B 0-19	B 0-35	L 0-7	L 7-19	L 19-35	S 0-≤0.5	B 0-75
Type	Crust	Crust	Crust	Crust	Crust	Crust	Crust	Crust	Crust	Crust	Crust
Comments											

Table 13 continued

	D9-7B	D9-7C	D9-7D	D9-7E	D9-7F	D10-1-1A	D10-1-1B	D10-1-1C	D10-1-2,	D10-2-1	D11-15A
Fe%	18.3	16.7	15.1	11.8	11.5	17.1	17.7	14.7	14.7	18.1	11.0
Mn	20.8	20.1	23.3	12.2	12.8	16.1	18.4	8.2	21.3	18.4	15.8
Mn/Fe	1.14	1.20	1.54	1.03	1.11	0.94	1.04	0.56	1.45	1.02	1.44
Si	2.62	3.09	2.10	1.92	2.90	5.10	4.58	5.70	3.41	4.25	1.50
Na	1.42	1.39	1.51	1.05	1.11	1.41	1.49	1.16	1.64	1.42	1.19
Mg	0.92	0.88	0.98	0.59	0.70	0.95	0.90	0.88	1.06	0.90	0.73
K	0.34	0.37	0.43	0.23	0.33	0.56	0.51	0.56	0.41	0.45	0.28
Ca	2.10	2.02	3.00	13.60	13.50	3.80	2.61	12.10	2.89	2.18	8.30
Ti	0.96	0.95	0.91	0.57	0.78	0.98	1.08	0.56	0.73	1.06	0.59
Al	0.50	0.59	0.50	0.46	0.78	1.37	1.15	1.87	0.50	1.06	0.30
P	0.33	0.31	0.56	4.90	4.80	0.96	0.51	4.10	0.50	0.42	2.83
H2O+	8.2	7.2	8.1	4.6	6.0	6.2	7.3	6.4	6.8	7.4	4.4
H2O-	11.4	15.0	11.3	11.6	6.8	11.2	10.2	5.4	14.3	12.2	22.0
CO2	0.45	0.43	0.56	2.20	2.30	1.00	0.68	3.10	1.20	0.46	1.40
LOI	27.0	29.6	27.4	23.1	19.2	24.2	24.6	17.8	28.7	26.2	33.3
Ba ppm	2100	1800	2100	1600	1700	2000	1800	1300	920	1800	1300
Co	4100	4100	3800	1400	2200	3200	3900	930	7300	3800	3100
Cu	1100	950	1400	1000	1300	1900	1700	1700	310	1800	650
Mo	540	460	520	250	280	260	310	110	310	340	380
Ni	3700	3500	5200	2000	2300	3300	3400	2300	4200	3400	3300
Sr	1600	1400	1500	1500	1500	1300	1400	1200	1400	1400	1400
V	770	670	700	470	500	500	540	350	600	630	480
Y	120	130	170	320	360	240	130	730	190	140	170
Ce	820	770	1200	960	1100	680	740	270	760	780	710
As	240	220	210	100	96	120	190	94	210	200	130
Cd	2.6	2.5	3.4	1.2	1.7	2.2	2.2	1.1	3.7	2.2	2.3
Cr	2.5	3.0	1.0	6.5	32.0	9.0	8.0	10.0	8.5	11.0	3.5
Pb	1200	1200	1100	920	920	1100	1300	450	1500	1200	1000
Zn	830	760	820	540	590	750	720	590	620	740	560
Au ppb	-	-	-	-	-	< 10	-	-	-	-	< 10
Pt	-	-	-	-	-	450	-	-	-	-	290
Pd	-	-	-	-	-	4.5	-	-	-	-	1.9
Rh	-	-	-	-	-	20.0	-	-	-	-	17.0
Ru	-	-	-	-	-	23.0	-	-	-	-	9.1
Ir	-	-	-	-	-	5.4	-	-	-	-	4.3
Interval	L 0-15	L 15-31	L 31-43	L 43-67	L 67-75	B 0-30	L 0-22	L 22-30	S 0-≤0.5	B 0-35	B 0-140
Type	Crust	Crust	Crust	Crust	Crust	Crust	Crust	Crust	Crust	Crust	Crust
Comments											

Table 13 continued

	D11-15B	D11-15C	D11-15D	D11-15E	D11-17A	D12-1A	D12-1B	D12-1C	D12-1D	D12-1E	D12-3
Fe%	14.9	16.5	17.6	9.3	14.5	13.1	14.1	15.6	19.6	10.3	13.7
Mn	22.7	20.2	21.2	15.5	22.6	18.2	24.3	21.0	19.9	14.3	23.7
Mn/Fe	1.52	1.22	1.20	1.67	1.56	1.39	1.72	1.35	1.02	1.39	1.73
Si	2.81	3.55	2.10	0.97	3.74	1.68	2.43	3.18	2.24	1.37	2.71
Na	1.51	1.54	1.47	1.23	1.48	1.28	1.47	1.47	1.32	1.05	1.49
Mg	0.97	0.95	1.00	0.70	1.12	0.81	1.02	0.94	0.96	0.64	1.09
K	0.42	0.44	0.35	0.27	0.41	0.32	0.42	0.45	0.31	0.24	0.39
Ca	2.18	2.07	2.18	13.30	2.42	6.80	2.25	2.11	2.43	12.40	2.56
Ti	0.91	1.15	1.04	0.48	0.69	0.72	0.90	1.09	0.89	0.49	0.65
Al	0.46	0.75	0.51	0.20	0.49	0.34	0.42	0.69	0.57	0.35	0.32
P	0.37	0.35	0.37	4.80	0.42	2.18	0.33	0.32	0.50	4.30	0.43
H2O+	7.8	7.4	8.3	4.0	8.0	6.4	8.1	7.7	8.1	4.8	6.7
H2O-	12.6	12.8	11.6	13.0	13.4	16.2	12.6	13.2	11.4	15.4	14.2
CO2	0.50	0.44	0.42	2.20	0.84	1.20	0.49	0.42	0.49	2.30	0.85
LOI	27.7	27.4	27.5	24.1	27.4	29.2	28.3	27.9	26.7	27.3	28.8
Ba ppm	1400	1700	2000	1400	900	1700	1400	1600	2100	1500	870
Co	6800	4700	4800	2300	7500	3700	7500	4800	3800	1800	8400
Cu	480	810	1200	660	330	850	730	860	1100	730	240
Mo	510	390	540	390	380	450	550	410	530	310	420
Ni	4400	3900	4200	3600	5300	3600	5200	4000	3600	2900	4900
Sr	1500	1600	1600	1500	1300	1500	1500	1500	1600	1500	1400
V	620	580	740	450	610	620	650	610	830	490	660
Y	170	150	130	210	180	190	160	150	170	220	190
Ce	780	880	750	800	740	900	680	760	680	810	670
As	250	220	250	110	220	150	220	210	260	110	220
Cd	3.0	2.5	2.9	2.2	4.0	1.9	3.9	2.7	2.7	1.5	4.5
Cr	4.0	12.0	5.0	1.8	6.0	3.5	4.0	11.0	4.5	2.0	5.0
Pb	1500	1300	1100	990	1600	1200	1500	1300	1100	980	1600
Zn	620	660	810	590	640	670	620	650	850	580	640
Au ppb	-	-	-	< 10	-	< 10	-	-	-	-	-
Pt	-	-	-	300	-	360	-	-	-	-	-
Pd	-	-	-	1.2	-	1.8	-	-	-	-	-
Rh	-	-	-	15.0	-	17.0	-	-	-	-	-
Ru	-	-	-	5.8	-	12.0	-	-	-	-	-
Ir	-	-	-	4.0	-	4.5	-	-	-	-	-
Interval	L 0-20	L 20-35	L 35-70	L 70-138	S 0-≤0.5	B 0-120	L 0-17	L 17-40	L 40-65	L 65-120	S 0-≤0.5
Type	Crust	Crust	Crust	Crust	Crust	Crust	Crust	Crust	Crust	Crust	Crust
Comments											

Table 13 continued

	D12-4	D13-3A	D13-3B	D13-3C	D13-3D	D13-6	D14-1A	D14-1B	D14-1C	D14-1D	D14-1E
Fe%	13.4	15.6	16.0	17.6	13.2	14.9	11.3	14.9	15.7	17.2	9.6
Mn	22.1	20.5	22.5	21.2	16.9	22.1	17.7	23.2	21.9	22.0	17.9
Mn/Fe	1.65	1.31	1.41	1.20	1.28	1.48	1.57	1.56	1.39	1.28	1.86
Si	2.48	2.71	3.09	2.48	2.29	2.90	1.73	2.24	2.81	1.68	1.03
Na	1.39	1.34	1.42	1.33	1.19	1.59	1.31	1.52	1.57	1.51	1.21
Mg	1.09	0.89	0.95	0.90	0.77	1.04	0.81	1.00	1.00	1.00	0.71
K	0.47	0.41	0.47	0.38	0.35	0.38	0.35	0.40	0.46	0.35	0.30
Ca	1.95	2.60	2.27	2.17	9.60	2.50	6.20	2.27	2.26	3.10	9.50
Ti	0.87	0.99	1.10	1.06	0.70	0.73	0.74	1.04	1.22	0.86	0.55
Al	0.64	0.56	0.55	0.45	0.53	0.34	0.38	0.46	0.74	0.50	0.21
P	0.30	0.52	0.36	0.34	3.20	0.44	2.00	0.33	0.31	0.65	3.30
H2O+	6.9	7.4	8.4	8.6	6.7	6.9	4.9	7.2	7.2	8.5	6.2
H2O-	17.6	15.2	12.7	12.2	8.8	14.4	21.0	15.0	13.5	13.0	15.5
CO2	0.37	0.49	0.51	0.47	1.70	0.85	1.10	0.49	0.43	0.54	1.60
LOI	32.2	29.8	28.1	27.4	22.1	29.1	33.3	29.9	29.0	29.2	29.2
Ba ppm	1700	1800	1600	2200	1800	890	1400	1300	1700	1900	1600
Co	5800	4600	5900	4300	2400	7300	4500	8000	6100	4800	3000
Cu	1100	840	530	930	1100	270	1100	690	1100	1400	940
Mo	480	480	520	550	370	330	380	460	410	580	450
Ni	6100	3900	4200	3600	3300	4200	3900	4900	4600	5200	3500
Sr	1300	1500	1600	1700	1600	1400	1300	1500	1500	1500	1400
V	640	650	670	740	550	640	470	560	580	720	480
Y	140	180	190	150	480	190	200	170	140	190	220
Ce	630	790	750	830	1100	800	880	800	910	890	1100
As	200	210	230	230	130	220	130	230	210	240	120
Cd	4.3	2.9	3.1	2.6	2.1	3.9	2.6	3.2	2.9	3.0	2.3
Cr	4.5	14.0	4.0	2.0	2.0	5.0	5.0	8.0	7.5	3.5	4.0
Pb	1400	1200	1500	1300	1200	1500	1000	1400	1200	1100	1200
Zn	780	710	660	830	670	650	650	600	680	810	590
Au ppb	-	-	-	-	-	-	< 10	-	-	-	-
Pt	-	-	-	-	-	-	470	-	-	-	-
Pd	-	-	-	-	-	-	2.5	-	-	-	-
Rh	-	-	-	-	-	-	21.0	-	-	-	-
Ru	-	-	-	-	-	-	13.0	-	-	-	-
Ir	-	-	-	-	-	-	5.1	-	-	-	-
Interval	B 0-45	B 0-55	L 0-20	L 20-43	L 43-55	S 0-≤0.5	B 0-120	L 0-30	L 30-45	L45-70	L 70-120
Type	Nodule	Crust	Crust	Crust	Crust	Crust	Crust	Crust	Crust	Crust	Crust
Comments	diameter										

Table 13 continued

	D14-3A	D14-4	D14-6	D15-2	D16-2A	D16-2B	D16-2C	D16-2D	D16-2E	D16-2F	D16-5A
Fe%	15.6	13.3	14.9	13.2	12.4	16.0	17.4	16.6	10.5	13.9	9.8
Mn	21.5	15.2	22.3	18.3	16.6	21.3	19.8	16.0	17.2	24.9	17.0
Mn/Fe	1.38	1.14	1.50	1.39	1.34	1.33	1.14	0.96	1.64	1.79	1.73
Si	3.27	4.68	3.41	2.85	1.96	3.13	4.02	2.20	1.10	2.52	1.68
Na	1.51	1.45	1.64	1.37	1.22	1.46	1.50	1.24	1.22	1.41	1.21
Mg	1.02	1.06	1.02	0.86	0.80	1.07	0.93	0.82	0.73	1.85	1.01
K	0.44	0.68	0.40	0.40	0.33	0.45	0.53	0.29	0.27	0.53	0.37
Ca	2.81	7.70	2.46	1.88	8.30	2.08	2.23	8.90	11.40	1.92	9.20
Ti	0.96	0.84	0.75	1.02	0.71	1.01	1.41	0.80	0.52	0.60	0.60
Al	0.49	1.61	0.43	0.74	0.50	0.90	1.15	0.69	0.35	1.13	0.49
P	0.41	2.50	0.43	0.27	2.86	0.41	0.36	2.92	3.90	0.43	3.30
H2O+	7.9	7.0	7.4	4.8	5.5	7.2	7.9	8.3	5.8	7.7	4.4
H2O-	13.5	10.0	14.2	26.6	15.6	14.2	11.5	9.3	13.9	10.7	17.6
CO2	1.20	1.50	0.80	0.36	1.50	0.46	0.45	1.70	1.90	0.36	1.60
LOI	28.8	23.4	29.0	38.3	27.9	29.1	26.6	24.0	26.0	26.9	29.5
Ba ppm	950	1200	900	1200	1700	1900	2000	1800	1800	2900	1500
Co	9400	4700	7700	6100	3000	7900	4300	2400	2600	6800	3600
Cu	230	1100	210	830	580	460	630	790	570	1100	780
Mo	310	250	370	310	370	430	350	380	420	380	360
Ni	3600	4300	4200	3900	3500	3200	3500	2900	3800	8900	5600
Sr	1400	1300	1400	1200	1500	1400	1500	1700	1600	1100	1400
V	560	430	620	420	540	570	590	640	560	550	480
Y	190	400	190	130	190	120	110	190	260	140	280
Ce	980	520	760	740	810	770	870	530	1100	500	520
As	210	150	230	170	140	250	210	180	140	200	120
Cd	3.4	2.6	3.8	2.7	2.6	3.0	2.7	2.1	3.0	6.7	3.1
Cr	7.5	26.0	5.5	12.0	6.5	12.0	14.0	6.0	3.0	18.0	7.0
Pb	1600	1100	1600	1100	1300	1600	1500	880	1300	1200	1000
Zn	590	640	590	510	650	550	670	700	630	1000	810
Au ppb	-	-	-	-	< 10	-	-	-	-	-	< 10
Pt	-	-	-	-	420	-	-	-	-	-	370
Pd	-	-	-	-	1.7	-	-	-	-	-	2.2
Rh	-	-	-	-	17.0	-	-	-	-	-	17.0
Ru	-	-	-	-	14.0	-	-	-	-	-	13.0
Ir	-	-	-	-	4.9	-	-	-	-	-	4.4
Interval	S 0-≤0.5	B 0-19	S 0-≤0.5	B 0-33	B 0-105	L 0-5	L 5-20	L 20-31	L 31-95	L 95-105	B 0-43
Type	Crust	Crust	Crust	Crust	Crust	Crust	Crust	Crust	Crust	Crust	Nodule
Comments											radius

Table 13 continued

	D16-5B	D16-5C	D16-5D	D16-7	D16-8-1	D17-1	D17-2-1	D18-1A	D18-3A	D18-3B	D18-3C
Fe%	14.5	10.0	5.4	14.5	11.4	15.5	14.1	14.3	15.4	12.8	17.0
Mn	21.7	16.1	12.0	22.5	22.1	19.5	22.6	20.8	18.7	22.3	17.6
Mn/Fe	1.50	1.61	2.22	1.55	1.94	1.26	1.60	1.45	1.21	1.74	1.04
Si	2.90	0.99	0.76	2.99	1.02	2.76	2.48	3.23	2.76	1.96	4.53
Na	1.51	1.21	1.05	1.72	1.45	1.37	1.67	1.45	1.34	1.45	1.43
Mg	1.16	0.97	0.88	1.07	0.96	0.88	1.03	0.90	0.84	0.90	0.80
K	0.48	0.25	0.22	0.39	0.38	0.37	0.38	0.41	0.35	0.36	0.44
Ca	2.77	14.10	21.80	2.49	3.90	2.08	2.74	2.19	1.95	2.11	1.99
Ti	1.10	0.49	0.23	0.72	0.81	1.04	0.70	0.82	0.95	0.84	1.30
Al	0.94	0.41	0.42	0.43	0.32	0.60	0.29	0.60	0.64	0.36	1.11
P	0.60	5.10	8.20	0.51	0.93	0.33	0.43	0.36	0.34	0.33	0.33
H2O+	7.8	6.0	5.1	6.8	5.2	6.1	7.0	6.5	6.8	7.2	9.3
H2O-	14.0	8.6	4.9	14.6	22.7	20.9	15.3	19.5	20.5	19.7	13.5
CO2	0.49	2.40	3.80	0.84	0.61	0.43	1.10	0.49	0.39	0.46	0.40
LOI	29.0	22.2	17.2	29.5	35.8	34.0	31.2	32.4	33.6	34.0	29.0
Ba ppm	2000	1500	1300	930	2100	1400	850	1300	1600	1200	1700
Co	6100	2500	970	8000	6700	5500	8200	6300	5100	7700	4100
Cu	960	760	740	200	780	800	210	610	960	510	860
Mo	410	370	180	350	650	380	350	500	410	500	300
Ni	5600	5700	5200	4100	5100	3500	4500	3800	3600	4900	3000
Sr	1400	1700	1700	1400	1400	1400	1300	1400	1400	1400	1400
V	580	520	320	700	590	550	600	620	580	560	510
Y	170	420	470	190	240	160	180	140	150	170	150
Ce	790	420	420	770	1000	790	720	660	720	670	900
As	200	130	59	240	200	220	220	240	220	220	200
Cd	3.7	2.9	1.9	4.0	3.4	2.4	3.9	3.0	2.5	3.3	2.3
Cr	8.5	4.0	3.0	8.5	6.5	8.0	4.0	4.5	5.0	3.5	9.0
Pb	1400	800	770	1700	1500	1200	1400	1300	1100	1300	1300
Zn	750	810	920	640	590	590	620	510	630	540	640
Au ppb	-	-	-	-	-	-	-	-	-	-	-
Pt	-	-	-	-	-	-	-	-	-	-	-
Pd	-	-	-	-	-	-	-	-	-	-	-
Rh	-	-	-	-	-	-	-	-	-	-	-
Ru	-	-	-	-	-	-	-	-	-	-	-
Ir	-	-	-	-	-	-	-	-	-	-	-
Interval	L 0-15	L 15-30	L 30-42	S 0-≤0.5	B 0-20	B 0-55	S 0-≤0.5	B 0-100	B 0-50	L 0-16	L 16-26
Type	Crust	Crust	Crust	Crust	Crust	Crust	Crust	Crust	Crust	Crust	Crust
Comments											

Table 13 continued

	D18-3D	D18-3E	D18-6	D18-18	D19-1A	D19-1B	D19-1C	D19-2A	D19-2B	D20-2	D20-4
Fe%	20.1	13.8	15.1	14.0	12.5	15.7	11.3	14.7	13.5	15.2	16.0
Mn	17.9	23.9	16.6	24.0	12.0	19.6	8.5	22.7	22.2	19.1	19.3
Mn/Fe	0.89	1.73	1.10	1.71	0.96	1.25	0.75	1.54	1.64	1.26	1.21
Si	2.99	2.24	3.51	2.43	3.55	3.88	3.93	2.76	2.48	4.82	2.81
Na	1.34	1.46	1.19	1.62	1.15	1.50	1.10	1.75	1.48	1.64	1.41
Mg	0.86	1.04	0.84	1.06	0.76	0.88	0.61	1.06	0.97	0.90	0.91
K	0.32	0.43	0.41	0.40	0.40	0.44	0.44	0.40	0.38	0.62	0.37
Ca	2.11	2.55	2.11	2.72	12.80	2.64	16.20	2.64	2.15	2.28	2.06
Ti	0.99	1.03	1.05	0.71	0.61	0.96	0.56	0.73	0.92	1.13	0.97
Al	0.82	0.35	0.90	0.27	1.04	0.78	1.21	0.35	0.43	1.17	0.63
P	0.46	0.37	0.31	0.42	4.70	0.58	6.00	0.40	0.33	0.31	0.31
H2O+	7.0	7.6	5.9	6.5	5.8	8.1	4.8	6.6	9.1	7.2	10.6
H2O-	12.5	14.6	23.0	14.7	7.5	12.8	5.8	15.2	16.5	12.9	14.8
CO2	0.43	0.79	0.82	1.00	2.10	0.60	2.70	0.92	0.50	0.79	0.41
LOI	27.4	30.4	35.2	30.2	20.2	27.7	16.4	30.6	33.3	26.6	32.4
Ba ppm	2200	1100	1300	840	1900	1300	2200	880	1200	1300	1500
Co	3500	10900	6400	8600	1900	5700	820	7500	8600	6700	5100
Cu	1600	420	660	230	1400	690	1100	300	430	920	890
Mo	430	410	240	390	200	370	130	380	450	300	410
Ni	3000	5000	3400	4900	2900	3800	1800	4400	4500	3900	3600
Sr	1500	1300	1100	1400	1400	1400	1500	1400	1400	1300	1400
V	710	520	460	630	420	570	370	610	550	470	580
Y	150	180	150	180	430	240	520	180	180	160	140
Ce	760	890	890	720	720	740	740	750	710	900	740
As	250	190	190	220	110	220	84	210	220	190	210
Cd	1.9	3.9	2.7	4.1	1.6	2.8	1.0	3.7	3.4	2.9	2.6
Cr	6.5	5.5	12.0	3.5	33 0	12.0	68.0	7.0	7.3	11.0	8.5
Pb	990	1600	1200	1500	830	1300	690	1400	1400	1200	1100
Zn	790	630	560	620	570	590	480	630	540	550	620
Au ppb	-	-	-	-	-	-	-	-	-	-	-
Pt	-	190	-	-	-	-	-	-	-	-	-
Pd	-	1.1	-	-	-	-	-	-	-	-	-
Rh	-	11.0	-	-	-	-	-	-	-	-	-
Ru	-	17.0	-	-	-	-	-	-	-	-	-
Ir	-	3.9	-	-	-	-	-	-	-	-	-
Interval	L26-50	B 0-5	B 0-100	S 0-≤0.5	B 0-35	L 0-15	L 15-35	S 0-≤0.5	B 0-5	B 0-2	B 0-62
Type	Crust	Crust	Crust	Crust	Crust	Crust	Crust	Crust	Crust	Crust	Crust
Comments		Underside									
		& side									

Table 13 continued

	D20-7	D21-4	D21-6	D21-10A	D21-10B	D21-10C	D21-11	D22-3	D23-1A	D23-1B	D23-1C
Fe%	14.9	12.4	3.3	13.2	14.8	11.6	15.0	10.8	12.4	15.6	15.4
Mn	21.0	22.8	6.4	20.3	20.8	20.0	20.7	26.5	18.9	22.3	22.5
Mn/Fe	1.41	1.84	1.94	1.54	1.41	1.72	1.38	2.45	1.52	1.43	1.46
Si	3.93	1.31	4.68	2.20	2.57	1.40	3.46	1.27	1.34	1.82	1.82
Na	1.48	1.34	1.08	1.37	1.48	1.34	1.95	1.89	1.28	1.35	1.47
Mg	0.95	0.85	1.01	0.80	0.91	0.76	1.07	1.23	0.75	0.90	0.89
K	0.40	0.38	0.61	0.35	0.39	0.34	0.39	0.41	0.30	0.36	0.39
Ca	2.68	6.70	22.40	7.20	5.00	8.90	2.85	2.58	7.70	2.27	2.38
Ti	0.70	0.66	0.28	0.88	1.03	0.80	0.69	0.72	0.78	1.01	1.18
Al	0.49	0.40	1.87	0.57	0.59	0.42	0.44	0.26	0.28	0.38	0.36
P	0.42	1.82	8.40	2.12	1.20	2.80	0.51	0.45	2.44	0.44	0.41
H2O+	6.8	6.1	3.6	7.2	7.1	6.5	6.7	7.2	5.9	8.5	9.8
H2O-	14.7	11.4	2.1	11.3	12.2	10.9	15.4	15.2	16.6	15.3	14.5
CO2	1.20	1.20	3.70	1.20	0.79	1.50	1.10	0.66	1.30	0.57	0.53
LOI	29.5	26.1	10.8	25.3	26.6	24.7	31.0	31.6	29.1	30.9	31.4
Ba ppm	870	3000	17900	2300	2500	2400	880	800	1900	1800	2100
Co	7000	4600	900	3700	3900	3900	6400	14800	3200	5400	5100
Cu	210	680	1500	1000	940	870	260	140	490	380	600
Mo	320	700	47	480	420	520	320	460	480	590	550
Ni	3700	3400	5000	3600	4300	3100	3700	5200	3600	3800	4200
Sr	1300	1800	1900	1700	1600	1800	1300	1300	1700	1700	1700
V	600	760	150	630	620	610	590	610	620	760	750
Y	180	240	580	180	130	240	180	160	180	150	110
Ce	750	1900	65	1700	1600	1700	760	650	920	870	960
As	220	190	18	180	200	160	220	210	180	270	230
Cd	3.6	3.0	2.8	2.5	2.9	2.4	3.3	5.4	2.9	2.6	3.2
Cr	7.5	16.0	210.0	12.0	12.0	17.0	13.0	4.5	5.5	5.5	4.5
Pb	1500	2800	160	1500	1500	1600	1400	1800	1200	1700	1400
Zn	580	730	740	680	730	610	580	650	640	630	690
Au ppb	-	-	-	-	-	-	-	-	-	-	-
Pt	-	-	-	-	-	-	-	-	-	-	-
Pd	-	-	-	-	-	-	-	-	-	-	-
Rh	-	-	-	-	-	-	-	-	-	-	-
Ru	-	-	-	-	-	-	-	-	-	-	-
Ir	-	-	-	-	-	-	-	-	-	-	-
Interval	S 0-≤0.5	B 0-20	B 0-7	B 0-18	L 0-4	L 4-18	S 0-≤0.5	S 0-≤0.5	B 0-82	L 0-10	L10-27
Type	Crust	Crust	Stratbound	Crust	Crust	Crust	Crust	Crust	Crust	Crust	Crust
Comments			Hydro-								
			thermal								

Table 13 continued

	D23-1D	D23-3	D25-3A	D26-5-1	D26-8-1	D26-8-2	D27-2-1	D27-2-2A	D27-2-2B	D27-2-2C	D27-3
Fe%	11.6	12.8	15.8	12.3	12.0	13.5	11.0	14.6	10.7	9.0	11.0
Mn	19.2	21.1	22.1	21.1	25.2	23.6	18.5	19.8	20.4	20.9	26.1
Mn/Fe	1.66	1.65	1.40	1.72	2.10	1.75	1.68	1.36	1.91	2.32	2.37
Si	1.14	1.59	3.04	2.24	1.82	2.52	1.68	2.66	1.29	0.98	1.54
Na	1.28	1.42	1.49	1.38	1.80	1.65	1.31	1.38	1.41	1.39	1.91
Mg	0.74	0.90	1.05	1.02	1.15	1.09	0.78	0.93	0.81	0.77	1.16
K	0.31	0.43	0.37	0.46	0.41	0.50	0.39	0.43	0.42	0.43	0.44
Ca	9.40	3.90	2.40	3.60	2.51	2.40	5.70	1.83	7.60	9.50	2.43
Ti	0.66	0.99	0.75	0.91	0.88	0.98	0.73	1.04	0.67	0.58	0.85
Al	0.24	0.37	0.36	0.61	0.27	0.48	0.22	0.45	0.12	0.08	0.24
P	3.10	1.02	0.40	0.96	0.40	0.43	1.86	0.35	2.56	3.30	0.37
H2O+	5.9	5.6	7.6	4.8	7.6	8.2	4.0	6.6	6.0	6.1	6.9
H2O-	13.8	20.0	14.8	18.8	14.8	13.0	22.8	20.0	15.1	13.0	13.8
CO2	1.60	0.70	0.76	0.63	0.74	0.49	0.95	0.30	1.20	1.50	0.70
LOI	26.6	33.3	29.4	31.4	31.7	28.9	34.2	33.5	28.6	26.4	31.0
Ba ppm	2100	2300	820	2600	850	1300	2800	2800	3000	3300	880
Co	3000	6600	5600	5400	14100	9900	5300	7400	5700	3500	16000
Cu	470	940	500	690	130	380	450	680	430	260	170
Mo	510	730	330	530	400	470	630	520	810	820	430
Ni	3700	4200	3400	5500	4900	5000	3600	4500	3800	3900	5400
Sr	1700	1500	1300	1400	1300	1400	1500	1600	1700	1700	1300
V	630	670	630	610	590	560	640	610	730	770	580
Y	210	240	170	160	170	150	150	77	240	220	160
Ce	1200	1200	770	870	810	840	1100	1000	1000	1600	770
As	160	230	210	190	200	200	140	190	150	140	200
Cd	3.2	3.0	3.3	4.6	5.1	3.8	2.7	2.8	2.9	3.3	5.3
Cr	2.0	19.0	13.0	24.0	5.0	9.5	3.5	5.5	1.5	< 1.0	3.0
Pb	1200	1400	1200	1100	1600	1700	1400	1600	1300	1500	1600
Zn	660	560	570	710	660	640	670	710	710	710	670
Au ppb	-	-	-	-	-	-	< 10	-	-	-	-
Pt	-	-	-	-	-	-	280	-	-	-	-
Pd	-	-	-	-	-	-	2.2	-	-	-	-
Rh	-	-	-	-	-	-	18.0	-	-	-	-
Ru	-	-	-	-	-	-	14.0	-	-	-	-
Ir	-	-	-	-	-	-	5.2	-	-	-	-
Interval	L 27-79	B 0-25	S 0-≤0.5	B 0-33	S 0-≤0.5	B 0-7	B 0-63	L 0-25	L 25-45	L 45-65	S 0-≤0.5
Type	Crust	Crust	Crust	Crust	Crust	Crust	Crust	Crust	Crust	Crust	Crust
Comments											

Table 13 continued

	KSD1-10A	KSD1-10B	KSD1-10C	KSD1-10D	KSD1-19A	KSD1-25A	KSD1-25B	KSD1-25C	RD33-1A	RD33-2A	RD33-3
Fe%	10.2	13.2	11.0	8.0	10.2	9.8	12.0	8.5	9.2	7.8	8.1
Mn	20.4	24.7	22.1	18.5	23.7	22.1	23.8	23.2	18.7	17.1	15.4
Mn/Fe	2.00	1.87	2.01	2.31	2.32	2.26	1.98	2.73	2.03	2.19	1.90
Si	1.29	2.06	1.01	1.37	1.45	1.05	1.29	0.64	1.07	0.87	0.72
Na	1.29	1.54	1.34	1.23	1.46	1.31	1.39	1.33	1.06	1.06	1.09
Mg	0.86	1.02	0.82	1.01	1.01	0.83	0.86	0.86	1.40	0.87	0.78
K	0.37	0.41	0.35	0.46	0.44	0.39	0.39	0.42	0.29	0.32	0.25
Ca	7.70	2.33	6.70	13.40	5.00	5.50	2.52	6.90	8.70	10.80	12.90
Ti	0.61	1.06	0.70	0.35	0.70	0.56	0.89	0.38	0.52	0.46	0.43
Al	0.47	0.53	0.39	0.59	0.51	0.24	0.24	0.14	0.73	0.33	0.26
P	2.48	0.27	1.93	4.80	1.30	1.53	0.33	2.11	2.87	3.80	4.50
H2O+	5.9	8.6	7.0	6.7	7.0	6.0	6.9	6.0	6.1	4.1	4.5
H2O-	14.3	11.9	13.2	6.3	13.7	20.9	20.0	18.0	13.6	18.0	13.9
CO2	1.20	0.41	1.10	2.10	0.77	0.84	0.41	1.10	1.60	1.90	2.30
LOI	28.5	28.3	27.9	19.8	29.0	33.9	34.3	31.6	-	-	-
Ba ppm	2700	2300	2600	3100	2200	3100	2300	2600	1700	2000	1500
Co	4300	8300	4400	2700	6700	4500	5900	3900	3300	2300	2100
Cu	680	960	650	750	870	560	700	370	1700	740	470
Mo	630	630	700	630	620	700	680	800	340	330	320
Ni	3600	4300	3100	5200	5100	3800	3600	4300	8400	5100	4000
Sr	1600	1600	1700	1500	1500	1500	1600	1500	1200	1400	1500
V	630	640	670	620	550	630	680	700	450	560	440
Y	230	100	210	310	330	180	86	190	400	270	340
Ce	1700	1700	2000	1600	1700	1800	1800	2000	470	850	750
As	140	220	160	100	160	140	170	120	100	86	86
Cd	2.9	3.3	2.6	3.9	3.7	3.2	3.6	3.6	4.1	2.5	2.5
Cr	23.0	4.0	8.0	99.0	8.5	2.3	1.0	2.0	95.0	6.5	96.0
Pb	1900	1900	2200	2000	2200	2300	2000	2500	1000	1200	1100
Zn	730	700	680	1000	760	710	650	880	1100	850	720
Au ppb	-	-	-	-	-	< 10	< 10	< 10	-	-	-
Pt	-	-	-	-	-	220	260	140	-	-	-
Pd	-	-	-	-	-	4.6	3.8	4.7	-	-	-
Rh	-	-	-	-	-	8.2	10.0	5.6	-	-	-
Ru	-	-	-	-	-	8.6	11.0	6.9	-	-	-
Ir	-	-	-	-	-	2.8	3.2	2.4	-	-	-
Interval	B 0-47	L 0-11	L 11-32	L 32-47	B 0-16	B 0-43	L 0-15	L15-43	B 0-17	B 0-53	B 0-30
Type	Crust	Crust	Crust	Crust	Crust	Crust	Crust	Crust	Crust	Nodule	Nodule
Comments											Talus

Table 13 continued

	RD34-A	RD35-A	RD36-1A	RD36-1C	RD36-1D	RD36-1E	RD38-A	RD40-1	RD41	RD43-1A	RD43-1B
Fe%	11.5	9.6	7.5	10.6	8.0	8.1	7.7	6.6	10.9	13.2	13.7
Mn	21.4	17.6	19.9	21.8	18.3	14.2	20.1	17.7	17.7	19.4	19.0
Mn/Fe	1.86	1.83	2.65	2.06	2.29	1.75	2.61	2.68	1.62	1.47	1.39
Si	1.54	0.93	0.55	0.84	0.52	0.89	0.55	0.67	1.54	2.20	2.99
Na	1.39	1.14	1.19	1.23	1.16	1.07	1.29	1.45	1.28	1.26	1.32
Mg	0.91	0.76	0.93	1.01	0.83	0.83	0.85	0.98	0.85	0.80	0.82
K	0.32	0.29	0.38	0.38	0.32	0.30	0.32	0.34	0.32	0.33	0.40
Ca	2.06	7.00	8.20	2.02	9.00	14.70	6.80	12.00	6.00	1.89	1.89
Ti	0.68	0.62	0.48	0.80	0.50	0.38	0.52	0.37	0.66	0.68	0.95
Al	0.24	0.25	0.15	0.21	0.12	0.36	0.14	0.22	0.40	0.27	0.54
P	0.38	2.23	2.52	0.30	2.81	5.10	2.11	4.20	1.88	0.33	0.28
H2O+	6.8	3.1	6.0	7.1	5.5	6.2	4.8	3.5	3.3	4.1	4.7
H2O-	17.4	25.6	20.8	27.3	22.0	11.2	23.5	19.8	21.2	24.4	23.4
CO2	0.47	1.00	1.40	0.40	1.40	2.50	1.20	1.90	1.10	0.50	0.41
LOI	-	-	33.8	40.4	34.3	25.4	-	-	-	-	-
Ba ppm	920	1300	1400	1400	1300	1400	1300	1700	1300	990	1400
Co	9600	3600	5000	9800	4700	2500	4900	3400	4100	6000	4800
Cu	250	400	460	370	440	420	400	500	700	400	920
Mo	470	420	570	520	550	380	470	380	370	440	360
Ni	4100	4100	5600	4700	4800	4000	5300	5900	4300	3300	3600
Sr	1200	1300	1400	1300	1400	1600	1300	1300	1300	1300	1300
V	530	480	450	520	470	420	430	410	460	560	480
Y	130	160	220	87	230	610	210	250	390	170	120
Ce	640	710	780	940	520	630	760	590	770	600	730
As	200	130	140	210	150	120	130	94	150	220	190
Cd	3.2	2.4	3.8	3.2	3.0	2.3	3.3	3.7	2.6	2.4	2.5
Cr	5.0	4.5	3.0	4.0	1.5	15.0	<1	9.0	1.0	<1	6.3
Pb	1600	1200	1300	1800	1000	1100	1300	1100	1300	1400	1200
Zn	520	650	740	570	560	600	690	840	620	510	580
Au ppb	-	-	<20	-	< 20	-	-	-	-	-	-
Pt	-	-	440	-	320	-	-	-	-	-	-
Pd	-	-	< 3	-	< 3	-	-	-	-	-	-
Rh	-	-	27.0	-	22.0	-	-	-	-	-	-
Ru	-	-	9.4	-	7.7	-	-	-	-	-	-
Ir	-	-	7.0	-	4.9	-	-	-	-	-	-
Interval	B 0-6	B 0-83	B 0-35	L 0-10	L 10-26	L 26-34	B 0-50	B? 0-67	B 0-23	L 0-5	L 5-30
Type	Crust	Crust	Crust	Crust	Crust	Crust	Nodule	Nucleated	Crust	Crust	Crust
Comments								on older			
								crust			

Table 13 continued

	RD43-1C	RD43-1D	RD43-1F	RD43-2A	RD43-3	RD44-1A	RD47-A	RD48-A	RD48-2A	RD50-A	RD50-B
Fe%	12.5	14.8	13.4	14.1	11.1	12.0	12.0	9.3	13.5	9.1	10.8
Mn	20.7	17.1	18.9	18.1	15.3	17.2	17.1	17.7	24.1	18.1	21.3
Mn/Fe	1.66	1.16	1.41	1.28	1.38	1.43	1.43	1.90	1.79	1.99	1.97
Si	1.92	2.01	2.71	2.90	1.50	3.04	3.51	0.95	2.10	0.94	1.31
Na	1.33	1.16	1.34	1.19	1.11	1.21	1.35	1.14	1.60	1.28	1.35
Mg	0.88	0.81	0.88	0.83	0.66	0.83	0.81	0.72	1.08	0.84	0.90
K	0.39	0.31	0.44	0.31	0.25	0.46	0.48	0.26	0.44	0.36	0.32
Ca	1.96	3.50	2.23	1.81	8.40	2.15	1.69	8.10	2.31	6.80	1.88
Ti	0.99	0.70	0.92	0.69	0.59	0.93	0.91	0.49	0.83	0.63	0.68
Al	0.46	0.53	0.55	0.37	0.37	0.69	0.82	0.15	0.30	0.21	0.21
P	0.26	0.97	0.40	0.36	2.80	0.35	0.22	2.60	0.39	2.03	0.31
H2O+	5.5	5.3	7.3	5.0	4.5	6.4	4.9	4.4	8.1	5.1	4.8
H2O-	17.2	21.0	22.8	20.1	21.7	25.4	25.9	23.8	14.7	25.1	22.3
CO2	0.43	0.70	0.44	0.52	1.40	0.43	0.32	1.40	0.51	1.10	0.46
LOI	-	-	36.3	-	-	37.7			30.8	37.2	-
Ba ppm	1600	1600	1400	1000	1600	4300	1500	1400	1100	1200	950
Co	5700	3400	5000	5200	2800	5000	4700	3100	10800	5500	10300
Cu	1500	1500	1100	380	960	1800	2300	420	270	480	270
Mo	410	400	380	370	330	330	280	460	510	430	460
Ni	4200	3400	3700	2800	2900	4100	3800	4000	4700	4500	4400
Sr	1300	1300	1300	1300	1400	1300	1100	1400	1400	1300	1200
V	490	530	490	590	450	550	480	480	580	430	500
Y	80	190	140	170	180	82	98	170	150	190	130
Ce	790	570	720	650	1000	740	700	840	740	740	690
As	190	190	190	220	110	160	130	130	240	140	180
Cd	2.6	2.4	2.5	2.4	1.8	2.8	2.3	2.5	3.4	3.0	3.3
Cr	3.0	6.0	8.5	3.0	1.5	6.5	15.0	1.0	3.0	5.0	2.0
Pb	1100	840	1100	1400	1000	950	940	1200	1800	1200	1500
Zn	670	680	590	530	540	680	590	640	560	610	490
Au ppb	-	-	<20	-	-	< 20	-	-	-	< 20	-
Pt	-	-	320	-	-	600	-	-	-	380	-
Pd	-	-	< 3	-	-	3.8	-	-	-	< 3	-
Rh	-	-	16.0	-	-	26.0	-	-	-	26.0	-
Ru	-	-	18.0	-	-	23.0	-	-	-	10.0	-
Ir	-	-	4.4	-	-	6.2	-	-	-	6.8	-
Interval	L 30-32	L 32-42	B 0-42	B 0-4	B 0-12	B 0-30	B 0-17	B 0-58	B 0-9	B 0-63	L 0-7
Type	Crust	Crust	Crust	Crust	Crust	Crust	Crust	Crust	Crust	Crust	Crust
Comments							Talus				

Table 13 continued

	RD50-C	RD50-D	RD53-3C	RD53-3D	RD53-3E	RD53-3F	RD56-1	RD59-1	RD59-2A	RD59-2B	RD59-2D
Fe%	12.2	6.7	12.7	11.8	12.2	11.3	12.7	10.2	11.0	7.2	12.9
Mn	19.3	18.0	19.3	21.1	20.1	18.5	13.9	18.0	18.1	14.6	18.1
Mn/Fe	1.58	2.69	1.52	1.79	1.65	1.64	1.09	1.76	1.65	2.03	1.40
Si	1.59	0.36	1.92	1.40	1.64	1.40	4.21	2.10	2.10	1.10	3.74
Na	1.24	1.14	1.30	1.42	1.30	1.34	1.17	1.25	1.25	1.09	1.36
Mg	0.85	0.78	0.89	0.88	0.89	0.85	0.73	0.80	0.83	0.72	0.83
K	0.34	0.29	0.40	0.34	0.35	0.31	0.51	0.37	0.39	0.33	0.42
Ca	1.88	9.60	2.51	1.94	2.01	4.60	5.60	5.30	5.20	12.10	1.81
Ti	0.91	0.42	0.87	0.80	0.83	0.64	0.83	0.68	0.71	0.55	0.72
Al	0.38	0.09	0.49	0.30	0.42	0.38	1.16	0.46	0.46	0.33	0.61
P	0.31	3.10	0.50	0.29	0.30	1.32	1.73	1.54	1.43	3.90	0.28
H2O+	4.1	3.6	6.6	4.5	5.3	3.6	5.1	4.7	6.0	4.9	5.8
H2O-	26.1	23.8	25.6	22.7	21.1	18.9	21.6	24.8	24.8	20.9	26.1
CO2	0.41	1.60	0.43	0.42	0.43	0.84	0.80	0.91	0.86	2.50	0.37
LOI	-	-	37.9	-	-	-	-	-	37.0	32.4	37.7
Ba ppm	1200	1200	1600	1500	1700	1600	1900	1300	1300	1400	1100
Co	6300	4000	4400	5700	4400	3400	2100	4100	4300	2800	5800
Cu	450	440	930	84	990	1000	2300	800	710	870	440
Mo	350	480	470	540	530	480	240	360	380	280	390
Ni	3800	5300	4300	4600	4600	4500	2600	4000	4000	3700	3400
Sr	1200	1300	1300	1300	1200	1300	1200	1200	1300	1300	1200
V	470	400	620	640	640	580	470	430	450	380	480
Y	120	220	120	77	88	320	270	270	280	340	130
Ce	810	580	740	800	700	700	1000	870	880	880	660
As	170	86	190	160	200	160	76	120	150	92	210
Cd	2.5	3.3	2.5	2.8	2.7	2.8	1.5	4.1	2.6	2.3	2.5
Cr	4.5	1.0	9.0	1.5	17.0	3.0	12.0	5.0	5.0	4.0	8.0
Pb	1400	990	1200	1400	1100	1000	1200	1300	1200	1000	1400
Zn	530	680	730	650	740	720	640	600	610	610	490
Au ppb	-	-	< 20	-	-	-	-	-	< 20	< 20	< 20
Pt	-	-	480	-	-	-	-	-	540	950	190
Pd	-	-	< 3	-	-	-	-	-	< 3	< 3	< 3
Rh	-	-	28.0	-	-	-	-	-	26.0	33.0	13.0
Ru	-	-	17.0	-	-	-	-	-	12.0	9.7	18.0
Ir	-	-	7.5	-	-	-	-	-	7.1	9.0	4.4
Interval	L 7-26	L 26-53	B 0-33	L 0-10	L 10-25	L 25-32	B 0-53	B 0-52	B 0-65	B 0-65	L 0-10
Type	Crust	Crust	Crust	Crust	Crust	Crust	Crust	Crust	Crust	Crust	Crust
Comments										Underside	

Table 13 continued

	RD59-2E	RD59-2F	RD59-2G	RD59-2H	RD59-2I	RD59-2J	RD59-2K	RD59-2L	RD59-3	RD60-A	RD60-B
Fe%	13.3	9.0	8.2	6.4	9.9	7.6	6.6	6.8	6.9	8.3	12.2
Mn	17.6	20.9	15.0	18.4	21.3	17.1	12.2	15.7	13.9	16.6	17.5
Mn/Fe	1.32	2.32	1.83	2.87	2.15	2.25	1.85	2.31	2.01	2.00	1.43
Si	3.27	0.94	0.85	0.73	1.25	0.89	1.34	0.86	0.74	1.27	3.51
Na	1.29	1.24	1.16	1.19	1.25	1.14	1.06	1.11	1.10	1.23	1.46
Mg	0.87	0.92	0.69	0.83	0.93	0.85	0.63	0.71	0.63	0.79	0.88
K	0.48	0.38	0.28	0.37	0.40	0.34	0.32	0.31	0.25	0.35	0.36
Ca	1.83	3.60	11.70	10.20	2.03	9.60	15.20	12.00	13.40	8.90	1.67
Ti	0.90	0.72	0.51	0.55	0.83	0.54	0.51	0.59	0.44	0.58	0.59
Al	0.75	0.25	0.19	0.21	0.30	0.30	0.40	0.25	0.21	0.33	0.53
P	0.29	0.78	3.80	3.30	0.26	2.92	5.00	3.90	4.60	2.81	0.33
H2O+	5.8	5.5	4.1	5.5	5.9	5.2	4.0	4.9	3.3	5.0	5.1
H2O-	26.7	28.8	21.9	19.3	28.5	23.0	17.6	20.6	19.1	24.1	23.8
CO2	0.35	0.51	1.90	1.60	0.32	2.00	3.00	2.10	2.60	1.50	0.40
LOI	38.2	40.7	32.8	32.6	41.5	34.9	28.7	31.8	-	35.8	-
Ba ppm	1300	1600	1300	1800	1600	1500	1300	1600	1200	1300	870
Co	4400	5700	2500	5800	6600	3200	2000	4100	2500	3800	5700
Cu	750	1000	720	910	1100	1100	710	840	690	800	440
Mo	330	490	300	430	500	380	200	320	270	380	370
Ni	3600	5500	3500	4500	5400	5400	2600	3400	3200	4100	3700
Sr	1200	1200	1400	1300	1200	1200	1400	1400	1300	1300	1100
V	450	480	400	440	540	430	320	420	360	420	480
Y	130	190	520	580	76	240	360	490	440	210	140
Ce	770	880	1100	1300	870	740	960	1200	930	820	630
As	190	150	100	98	170	110	72	84	62	130	180
Cd	2.5	3.8	2.0	2.6	4.1	3.6	1.5	2.7	1.8	2.3	2.7
Cr	10.0	2.0	4.0	5.0	2.0	2.5	3.0	7.5	2.5	6.5	4.5
Pb	1200	1300	1100	1300	1300	1000	920	1100	940	1100	1500
Zn	570	760	590	790	770	730	510	660	550	630	510
Au ppb	< 20	< 20	< 20	-	< 20	< 20	< 20	< 20	-	< 20	-
Pt	430	780	970	-	860	650	1000	550	-	480	-
Pd	< 3	< 3	< 3	-	< 3	< 3	< 3	< 3	-	< 3	-
Rh	22.0	31.0	36.0	-	38.0	25.0	40.0	22.0	-	28.0	-
Ru	16.0	14.0	9.9	-	17.0	12.0	8.2	11.0	-	14.0	-
Ir	6.6	7.4	8.6	-	8.7	6.8	8.6	6.8	-	6.9	-
Interval	L 10-35	L 35-45	L 45-60	L60-65	L 0-7	L 7-21	L 21-53	L 53-63	B? 0-26	B 0-105	L 0-5
Type	Crust	Crust	Crust	Crust	Crust	Crust	Crust	Crust	Crust	Crust	Crust
Comments					Underside	Underside	Underside	Underside	Outer layers		
									missing		

Table 13 continued

	RD60-C	RD60-D	RD60-E	RD63-A	RD63-B	RD63-C
Fe %	12.2	7.8	5.5	9.4	13.9	8.2
Mn	18.6	17.5	14.9	19.0	24.7	21.5
Mn/Fe	1.52	2.24	2.71	2.02	1.78	2.62
Si	2.62	0.72	0.54	1.10	1.50	0.64
Na	1.49	1.28	1.17	1.23	1.52	1.41
Mg	0.89	0.79	0.65	0.86	1.14	1.01
K	0.46	0.30	0.26	0.35	0.48	0.43
Ca	1.90	9.00	13.80	5.10	2.29	11.00
Ti	0.81	0.56	0.43	0.63	1.04	0.59
Al	0.69	0.22	0.16	0.24	0.34	0.20
P	0.31	2.88	4.60	1.42	0.33	3.60
H2O+	4.0	4.2	3.5	5.7	8.4	6.6
H2O-	27.0	23.1	20.5	26.9	13.4	9.6
CO2	0.39	1.70	2.60	0.84	0.43	1.80
LOI	-	-	-	39.2	29.6	24.2
Ba ppm	1200	1300	1300	1200	1500	1700
Co	4300	3400	3000	5700	9700	3800
Cu	830	970	610	550	760	1100
Mo	350	370	290	450	480	470
Ni	3700	4900	3400	4600	5400	6300
Sr	1200	1300	1300	1300	1400	1600
V	430	420	350	450	560	440
Y	110	210	300	200	140	570
Ce	670	630	1000	810	1100	1200
As	190	96	66	170	220	120
Cd	2.4	2.5	1.9	2.8	3.7	3.9
Cr	7.0	3.5	3.5	2.5	7.5	8.0
Pb	1200	950	1000	1400	1800	1600
Zn	530	700	630	590	670	740
Au ppb	-	-	-	< 20	-	-
Pt	-	-	-	860	-	-
Pd	-	-	-	< 3	-	-
Rh	-	-	-	30.0	-	-
Ru	-	-	-	6.0	-	-
Ir	-	-	-	6.5	-	-
Interval	L 5-39	L 39-69	L 69-100	B 0-60	L 0-24	L 24-54
Type	Crust	Crust	Crust	Crust	Crust	Crust
Comments						

•Major and minor elements determined by Inductively Coupled Plasma - Atomic Emission Spectrometry (ICP-AES): except K, Zn, Pb by Flame Atomic - Absorption Spectroscopy, and As, Cr, Cd by Graphite-Furnace Atomic Absorption Spectroscopy. Samples were air dried before being ground. Pt group elements determined by ICP - Mass Spectroscopy.

•Analysts: Herbert Kirschenbaum, Hezekiah Smith, C.L. Prosser, J.W. Marinenko, G.O. Riddle, Norma Rait, and R.R. Carlson.

[1]Sample numbers which are identical except for suffixes -A, -B, -C, and -D represent different sample intervals from the same crust.

[2]Intervals measured from the outer surface of crust; B = bulk, which means the entire crust thickness was sampled and analyzed; L = layer; N = nodule; S = scraped surface, ≤ 0.5mm. Top crust is on the top side of substrate rock, at seawater substrate contact; underside crust is from bottom side of substrate, not in direct (or most recent) contact with seawater.

Table 14. Statistics for 61 bulk crusts from the Marshall Islands, data from Table 13.

Element	N	Mean	Median	SD[1]	Min[2]	Max[3]	NM[4]
Fe (Wt%)	61	12.2	12.4	2.47	7.2	18.1	16.6
Mn	61	18.8	18.7	2.6	12.0	24.1	25.6
Mn/Fe	61	1.54[5]	-	-	-	-	-
Si	61	2.19	2.10	1.09	0.55	5.10	2.98
Na	61	1.32	1.34	0.14	1.06	1.65	1.80
Mg	61	0.89	0.87	0.12	0.66	1.40	1.21
K	61	0.39	0.38	0.08	0.25	0.68	0.53
Ca	61	5.15	4.50	3.15	1.69	12.90	7.02
Ti	61	0.79	0.81	0.18	0.43	1.13	1.08
Al	61	0.53	0.45	0.30	0.14	1.61	0.72
P	61	1.51	1.35	1.22	0.22	4.70	2.06
H2O+	61	6.0	5.9	1.4	3.1	10.6	8.17
H2O-	61	19.0	20.0	4.9	7.5	26.9	-
CO2	61	0.95	0.82	0.52	0.31	2.50	1.29
LOI	48	31.9	32.4	4.4	20.2	39.2	-
Ba (ppm)	61	1597	1400	542	920	4300	2176
Co	61	5136	5000	2102	1900	10900	6997
Cu	61	841	780	454	250	2300	1146
Mo	61	410	400	108	200	730	559
Ni	61	4166	4000	988	2600	8400	5675
Sr	61	1367	1400	130	1100	1800	1862
V	61	524	510	81.9	380	760	714
Y	61	204	180	75.9	82	430	278
Ce	61	835	790	221.6	470	1900	1138
As	61	166	170	43.8	76	260	226
Cd	61	2.9	2.7	0.67	1.5	4.8	4.0
Cr	60	11.1	6.5	16.9	1.0	96.0	15.1
Pb	61	1273	1200	284.9	830	2800	1734
Zn	61	643	640	96	510	1100	876
Pt (ppb)	20	489	445	216.6	190	1000	666
Pd	12	2.6	2.2	1.0	1.1	4.5	3.5
Rh	20	23.5	23.5	7.7	11.0	44.0	32.0
Ru	20	14.1	13.5	4.8	6.0	23.0	19.2
Ir	20	6.0	5.8	1.7	3.9	10.0	8.2
Depth[6]	61	1813.1	1863.0	299.4	1114.0	2553.0	-
Thickness[7]	61	44.66	35.00	32.27	2.00	140.00	-

[1]Standard deviation; [2]Minimum; [3]Maximum; [4]Normalized mean for 0% H_2O^-, adsorbed water; [5]Ratio of the Fe and Mn means, not a mean of the summation of the ratios; [6]Water depth in meters; [7]Crust thickness in millimeters.

Table 15. Mean concentrations of selected elements in various groups of ferromanganese crusts, in weight percent except Pt in ppm. Data from Table 13.

	Fe	Mn	Mn/Fe	Al	P	Co	Cu	Ni	Pt
All bulk crusts, n=61 (Pt=20)	12.2	18.8	1.54	0.53	1.51	0.51	0.08	0.42	0.49
Crust surfaces ≤0.5 mm, n=17	13.8	23.2	1.68	0.36	0.43	0.99	0.02	0.45	--
Bulk crusts ≤20 mm thick, n=18	12.9	20.3	1.57	0.56	0.96	0.67	0.08	0.44	--
Bulk crusts ≥20 mm thick, n=47 (Pt=19)	11.9	18.4	1.55	0.51	1.66	0.46	0.09	0.41	0.50
Bulk crusts ≥100 mm thick, n=7 (Pt=5)	12.2	17.5	1.43	0.48	1.91	0.44	0.08	0.37	0.40
Bulk crusts with Co ≥0.95%, n=6 (Pt=1)	12.2	23.1	1.89	0.31	0.35	1.01	0.04	0.50	0.19
Central Pacific average[1], n=311 (Pt=29)	15.7	23.0	1.46	--	0.91	0.79	0.12	0.47	0.24

[1]Hein et al. (1990c)

Table 16. Statistics for 17 crust surfaces (≤ 0.5mm) from the Marshall Islands, data from Table 13.

Element	N	Mean	Median	SD[1]	Min[2]	Max[3]	NM[4]
Fe (Wt%)	17	13.8	14.1	1.4	10.8	15.6	17.3
Mn	17	23.2	22.7	1.6	21.0	26.5	29.1
Mn/Fe	17	1.69[5]	-	-	-	-	-
Si	17	2.67	2.71	0.75	1.27	3.93	3.35
Na	17	1.67	1.64	0.17	1.44	1.94	2.09
Mg	17	1.08	1.06	0.07	0.95	1.23	1.35
K	17	0.41	0.41	0.018	0.38	0.44	0.51
Ca	17	2.59	2.56	0.14	2.42	2.89	3.25
Ti	17	0.77	0.73	0.09	0.65	0.96	0.97
Al	17	0.36	0.34	0.09	0.24	0.50	0.45
P	17	0.43	0.43	0.04	0.37	0.51	0.54
H2O+	17	7.0	6.8	0.5	6.3	8.0	8.8
H2O-	17	14.5	14.6	0.61	13.4	15.6	-
CO2	17	0.90	0.85	0.19	0.58	1.20	1.13
LOI	17	29.8	29.5	1.2	27.4	31.7	-
Ba (ppm)	17	876	880	40.15	800	950	1099
Co	17	9871	8400	2986	7000	16000	12382
Cu	17	218	210	58.2	130	330	273
Mo	17	377	380	45.0	310	460	473
Ni	17	4518	4400	522	3600	5400	5667
Sr	17	1359	1400	50.7	1300	1400	1705
V	17	611	610	32.95	560	700	766
Y	17	180	180	10.0	160	190	226
Ce	17	775	760	77.6	650	980	972
As	17	215	220	10.7	200	240	270
Cd	17	4.2	4.0	0.59	3.4	5.4	5.3
Cr	17	5.6	5.0	1.7	3.0	8.5	7.0
Pb	17	1606	1600	139.1	1400	1900	2015
Zn	17	624	620	27.1	580	670	783
Depth[6]	17	1784.7	1863.0	244.9	1263.0	2090.0	-

[1]Standard deviation; [2]Minimum; [3]Maximum; [4]Normalized mean for 0% H_2O^-, adsorbed water; [5]Ratio of the Fe and Mn means, not a mean of the summation of the ratios; [6]Water depth in meters.

Table 17. Concentrations of rare earth elements (ppm) in ferromanganese crusts.

	D1-1A	D1-1B	D1-1C	D1-1D	D8-1-1A	D8-1-1B	D8-1-1C	D8-1-1D	D9-7A	D9-7B	D9-7C	D9-7D	D9-7E	D9-7F
La	230	190	200	270	210	200	220	230	260	260	250	240	290	300
Ce	640	770	1100	510	770	860	880	560	580	670	620	1100	690	820
Pr	33	29	31	36	32	30	31	36	41	45	42	42	42	41
Nd	150	130	140	170	140	140	130	160	190	210	200	180	190	180
Sm	27	25	26	28	27	26	25	29	34	42	39	36	34	33
Eu	8.1	7.1	7.3	7.9	7.0	6.8	6.6	7.4	9.0	9.8	9.4	8.9	8.4	8.3
Gd	31	26	29	32	29	29	29	31	36	41	37	38	41	38
Tb	5.0	4.7	4.2	5.9	4.7	4.4	4.8	5.3	5.8	6.6	6.1	6.3	5.8	6.2
Dy	33	28	25	36	30	31	29	32	36	37	36	38	37	36
Ho	7.2	6.3	5.4	8.6	7.2	6.1	6.8	7.1	8.0	7.7	7.1	7.4	8.7	7.9
Er	21	19	16	27	20	19	20	20	21	20	20	21	25	24
Tm	3	2.6	2.4	3.7	2.9	2.8	2.9	3	3.2	3	2.9	2.9	3.9	3.3
Yb	20	18	14	24	19	19	20	19	21	20	20	19	24	23
Σ REE	1208.3	1255.7	1600.3	1159.1	1298.8	1374.1	1405.1	1139.8	1245.0	1372.1	1289.5	1739.5	1399.8	1520.7
Ce*	0.73	1.05	1.42	0.51	0.95	1.12	1.06	0.62	0.57	0.64	0.62	1.13	0.63	0.73
Interval	B[1] 0-40	L 0-7	L 7-14	L 14-40	B 0-35	L 0-7	L 7-19	L 19-35	B 0-75	L 0-15	L 15-31	L 31-43	L 43-67	L 67-75

	D10-1-1A	D10-1-1B	D10-1-1C	D11-15A	D11-15B	D11-15C	D11-15D	D11-15E	D12-1A	D12-1B	D12-1C	D12-1D	D12-1E	D12-4
La	230	220	460	220	190	240	250	220	230	210	250	300	220	200
Ce	570	540	190	520	520	650	470	620	490	440	600	580	470	490
Pr	38	36	66	36	30	39	42	34	37	34	43	48	32	33
Nd	170	160	320	170	140	180	190	160	180	150	200	220	150	160
Sm	32	31	58	30	26	34	34	27	29	30	37	41	25	30
Eu	8.3	7.7	16.0	7.9	7.0	9.4	8.3	7.4	7.8	8.1	9.3	9.7	7.2	7.4
Gd	35	35	79	33	29	36	34	32	33	31	37	45	25	32
Tb	5.5	5.3	12.0	4.9	5.4	6.4	6.1	5.0	5.5	5.4	6.5	6.8	4.3	5.2
Dy	35	35	77	33	34	35	37	33	33	35	37	40	30	30
Ho	7.5	7.1	18.0	6.7	6.8	7.0	6.7	6.9	6.6	7.4	7.5	8.4	6.5	6.6
Er	20	20	53	19	18	20	18	21	19	20	22	23	19	19
Tm	2.9	3.0	7.6	2.6	3.2	3.1	2.7	3.0	2.9	3.2	3.3	3.5	3.1	2.7
Yb	18	18	47	18	18	19	17	18	18	20	19	20	18	18
ΣREE	1172.2	1118.1	1403.6	1101.1	1027.4	1278.9	1115.8	1187.3	1091.8	994.1	1271.6	1345.4	1010.1	1033.9
Ce*	0.63	0.62	0.11	0.6	0.7	0.69	0.47	0.73	0.54	0.53	0.6	0.49	0.56	0.62
Interval	B 0-30	L 0-22	L 22-30	B 0-140	L 0-20	L 20-35	L 35-70	L 70-138	B 0-120	L 0-17	L 17-40	L 40-65	L 65-120	B 0-45

Table 17 continued

	D13-3A	D14-1A	D14-1B	D14-1C	D14-1D	D14-1E	D16-2A	D16-2C	D16-2D	D16-2E	D16-2F	D16-5A	D16-5B	D16-5C	D16-5D
La	270	220	240	260	240	270	200	200	230	270	170	230	170	290	290
Ce	640	750	490	730	690	900	390	740	370	700	480	430	520	270	300
Pr	46	35	39	46	40	43	29	32	36	37	26	31	27	37	35
Nd	200	160	190	200	180	190	140	150	160	170	130	140	130	180	170
Sm	37	30	35	39	35	35	24	29	28	29	24	26	23	29	28
Eu	10.0	7.1	9.7	9.1	8.5	9.2	5.6	7.7	7.6	7.1	6.0	6.8	6.5	10.0	8.2
Gd	39	30	35	42	34	35	28	32	35	36	27	30	27	43	42
Tb	6.8	5.0	6.2	6.7	5.7	6.1	4.6	4.6	5.4	5.4	4.5	5.1	4.3	6.8	6
Dy	38	32	40	41	37	37	31	32	34	35	27	35	27	45	38
Ho	8.1	7.0	7.9	7.7	7.4	8.0	5.9	6.4	7.3	8.7	6.5	7.9	5.8	10.0	9.6
Er	23	19	24	21	22	24	19	16	21	24	18	23	16	29	28
Tm	3.2	2.9	3.2	2.9	2.8	3.4	2.5	2.9	2.7	3.3	2.4	2.9	2.4	4.4	4.1
Yb	21	18	23	21	19	23	18	17	20	23	17	23	17	30	26
ΣREE	1342.1	1316.0	1143.0	1426.4	1321.4	1583.7	897.6	1269.6	957.0	1348.5	938.4	990.7	976.0	984.2	984.9
Ce*	0.59	0.87	0.52	0.69	0.72	0.85	0.51	0.94	0.41	0.69	0.73	0.5	0.78	0.25	0.29
Interval	B 0-55	B 0-120	L 0-30	L 30-45	L 45-70	L 70-120	B 0-105	L 5-20	L 20-31	L 31-95	L 95-105	B 0-43	L 0-15	L 15-30	L 30-42

	D27-2-1	D27-2-2A	D27-2-2B	D27-2-2C	KSD1-25A	KSD1-25B	KSD1-25C	RD36-1A	RD36-1C	RD36-1D	RD36-1E	RD43-1A	RD43-1B
La	250	250	290	210	210	150	240	270	180	290	560	260	250
Ce	1000	1100	770	1100	1500	1500	1400	1200	1600	920	1200	550	1100
Pr	39	41	43	32	28	25	28	42	32	46	77	40	41
Nd	180	180	200	140	120	100	120	190	130	210	360	180	170
Sm	31	34	33	25	19	18	19	32	23	36	57	31	31
Eu	8.9	8.8	9.6	6.3	5.3	4.6	5.4	8.1	5.4	8.7	15.0	8.0	7.4
Gd	34	34	42	29	24	18	23	35	23	40	77	37	32
Tb	5.5	6.1	7.1	4.7	3.9	3.1	3.7	5.6	4.0	6.1	11.0	5.5	5.3
Dy	35	35	43	29	25	18	24	36	24	40	71	36	31
Ho	7	6.8	9.9	6.5	6	3.9	5.8	7.8	4.8	8.2	16	7.1	6.1
Er	21	19	28	20	18	12	18	24	15	24	48	21	18
Tm	3.1	2.5	4.3	3.0	2.7	1.7	2.6	3.3	2.0	3.3	6.1	2.7	2.4
Yb	21	19	27	18	19	13	18	21	13	21	37	17	17
Σ REE	1635.5	1736.2	1506.9	1623.5	1980.9	1867.3	1907.5	1874.8	2056.2	1653.3	2535.1	1195.3	1711.2
Ce*	1.03	1.11	0.69	1.36	1.92	2.51	1.63	1.14	2.19	0.81	0.57	0.55	1.11
Interval	B 0-63	L 0-25	L 25-45	L 45-65	B 0-43	L 0-15	L 15-43	B 0-35	L 0-10	L 10-26	L 26-34	L 0-5	L 5-30

Table 17 continued

	RD43-1C	RD43-1D	RD43-1F	RD44-1A	RD50A	RD50B	RD50C	RD50D	RD53-3C	RD53-3D	RD53-3E	RD53-3F	RD59-2A	RD59-2D	RD59-2E
La	220	320	250	200	250	240	220	300	250	280	240	360	370	250	270
Ce	1700	1100	1300	1400	1600	1600	1800	1100	1500	1500	1400	1300	1900	1200	1400
Pr	44	51	44	38	38	39	39	44	46	55	44	57	59	41	48
Nd	180	230	190	160	170	180	170	190	200	230	190	260	260	180	210
Sm	33	39	35	31	28	30	31	33	34	41	34	44	44	33	38
Eu	7.4	8.8	7.3	6.2	6.4	6.9	6.2	6.7	6.9	7.8	6.2	8.4	9.9	6.3	7.2
Gd	30	46	37	30	30	35	31	38	34	39	31	51	51	35	39
Tb	4.9	6.6	5.6	4.7	5.2	5.5	5.1	6.3	5.6	6.9	5.2	7.7	8.1	5.8	6.2
Dy	28	45	34	28	32	34	29	37	35	37	29	48	50	33	36
Ho	5.5	9.7	7.1	5.5	7.1	7.3	6.3	9.0	7.0	7.4	6.1	11.0	11.0	7.5	7.4
Er	15	29	20	15	20	21	17	25	19	18	16	30	32	21	20
Tm	2.2	4.2	2.7	2.4	2.9	3.3	2.6	3.8	2.8	2.7	2.2	4.4	4.4	3.0	2.9
Yb	14	27	17	15	19	20	16	24	16	17	14	25	28	18	19
ΣREE	2284.0	1916.3	1949.7	1935.8	2208.6	2222.0	2373.2	1816.8	2156.3	2241.8	2017.7	2206.5	2827.4	1833.6	2103.7
Ce*	1.82	0.88	1.28	1.68	1.66	1.69	2.02	0.96	1.46	1.27	1.42	0.92	1.31	1.21	1.28
Interval	L 30-32	L 32-42	B 0-42	B 0-30	B 0-63	L 0-7	L 7-26	L 26-53	B 0-33	L 0-10	L 10-25	L 25-32	B 0-64	L 0-10	L 10-35

	RD59-2F	RD59-2G	RD59-2H	RD59-2I	RD59-2J	RD59-2K	RD59-2L	RD60A	RD60B	RD60C	RD60D	RD60E	RD63A	RD63B	RD63C
La	240	490	620	210	280	350	530	270	280	260	250	330	290	250	390
Ce	1800	2100	1900	1900	1600	1900	2400	1400	1100	1400	1300	2400	1700	1800	2200
Pr	41	69	82	36	40	44	77	43	50	47	39	49	46	46	56
Nd	180	320	370	150	180	210	350	190	220	200	170	220	210	200	250
Sm	32	52	60	26	30	32	57	33	38	34	30	36	35	34	42
Eu	6.1	12.0	13.0	5.8	6.9	8.0	13.0	7.4	9.3	8.0	7.0	9.3	8.8	8.4	10.0
Gd	31	63	79	25	37	42	67	38	40	36	34	42	40	34	53
Tb	5.6	10.0	12.0	4.2	5.5	6.3	11.0	5.8	6.9	5.9	5.4	6.9	6.4	5.8	8.5
Dy	32	63	77	24	36	43	67	36	42	35	33	44	40	36	53
Ho	6.5	15.0	19.0	4.9	8.1	9.9	15.0	7.3	8.0	6.1	6.9	9.2	8.3	6.6	12.0
Er	20	45	56	14	25	30	46	23	25	19	22	29	25	21	37
Tm	2.8	6.1	7.9	1.9	3.3	4.4	6.1	3.1	3.1	2.6	2.8	3.7	3.4	2.8	4.9
Yb	18	38	46	12	21	26	38	19	21	17	18	24	22	19	33
ΣREE	2415.0	3283.1	3341.9	2413.8	2272.8	2705.6	3677.1	2075.6	1843.3	2070.6	1918.1	3203.1	2434.9	2463.6	3149.4
Ce*	1.87	1.14	0.83	2.25	1.51	1.49	1.19	1.32	0.97	1.32	1.34	1.9	1.5	1.75	1.49
Interval	L 35-45	L 45-60	L 60-65	L 0-7	L7-21	L 21-53	L 53-63	B 0-105	L 0-5	L 5-39	L 39-69	L 69-100	B 0-60	L 0-24	L 24-54

By inductively coupled plasma-atomic emission spectrometry-mass spectroscopy. Analyst: G. Riddle.

[1] B = Bulk, L = Layer.

*Ce anomaly from chondrite normalized data = Ce/La+Pr.

Table 18. Correlation coefficient matrix for 61 bulk crusts and nodules listed in Table 13; n = 61, except for Cr = 60, LOI = 48, Pt, Rh, Ru, and Ir = 20, Pd = 12; the zero correlation for 61 points at the 99% confidence level is ±0.326.

	Depth	Lat.	Long.	Fe	Mn	Mn/Fe	Si	Na	Mg	K	Ca	Ti	Al	P	H2O+	H2O-	CO2	LOI	Ba
Lat.	-0.001																		
Long.	-0.117	0.002																	
Fe	0.388	-0.131	-0.181																
Mn	-0.342	-0.221	0.163	0.190															
Mn/Fe	-0.576	0.005	0.210	-0.806	0.378														
Si	0.545	-0.015	-0.169	0.787	-0.196	-0.815													
Na	-0.112	-0.171	0.069	0.577	0.706	-0.140	0.389												
Mg	-0.189	-0.208	0.088	0.143	0.594	0.222	0.060	0.471											
K	0.189	-0.099	-0.015	0.492	0.121	-0.363	0.759	0.604	0.359										
Ca	-0.145	0.022	-0.086	-0.684	-0.565	0.314	-0.467	-0.676	-0.323	-0.438									
Ti	0.260	-0.124	-0.062	0.851	0.350	-0.588	0.696	0.706	0.253	0.633	-0.811								
Al	0.472	-0.039	-0.241	0.588	-0.342	-0.703	0.897	0.205	0.171	0.749	-0.215	0.522							
P	-0.126	0.003	-0.081	-0.668	-0.591	0.280	-0.448	-0.687	-0.327	-0.441	0.997	-0.809	-0.200						
H2O+	0.061	-0.007	-0.116	0.619	0.495	-0.265	0.408	0.645	0.460	0.401	-0.529	0.595	0.288	-0.545					
H2O-	-0.119	0.329	0.182	-0.379	-0.113	0.261	-0.330	-0.308	-0.343	-0.280	-0.176	-0.128	-0.384	-0.177	-0.479				
CO2	-0.115	0.030	-0.122	-0.621	-0.562	0.272	-0.382	-0.632	-0.278	-0.371	0.972	-0.750	-0.144	0.964	-0.467	-0.257			
LOI	-0.215	0.307	0.183	-0.321	0.158	0.368	-0.431	-0.165	-0.854	-0.325	-0.383	0.014	-0.480	-0.392	-0.188	0.953	-0.448		
Ba	0.155	-0.248	0.144	0.043	-0.047	-0.090	0.047	-0.129	-0.095	0.125	0.048	0.085	0.119	0.046	-0.073	-0.066	0.003	-0.079	
Co	-0.253	-0.134	0.166	0.275	0.813	0.179	0.050	0.770	0.543	0.304	-0.663	0.490	-0.156	-0.677	0.519	-0.038	-0.610	0.245	-0.258
Cu	0.541	0.144	-0.114	0.265	-0.419	-0.454	0.547	-0.123	0.011	0.416	-0.074	0.266	0.681	-0.062	0.025	-0.062	-0.087	-0.234	0.386
Mo	-0.512	-0.317	0.179	-0.109	0.702	0.469	-0.489	0.319	0.187	-0.151	-0.157	-0.052	-0.555	-0.181	0.101	0.025	-0.230	0.148	0.250
Ni	-0.404	-0.165	0.134	-0.402	0.482	0.667	-0.419	0.102	0.799	0.009	0.027	-0.184	-0.216	0.015	0.054	-0.023	0.017	0.229	-0.043
Sr	-0.159	-0.302	-0.040	0.067	0.216	0.034	-0.251	0.088	-0.152	-0.236	0.302	-0.131	-0.279	0.288	0.130	-0.492	0.265	-0.492	0.365
V	0.022	-0.364	0.029	0.473	0.507	-0.184	0.076	0.353	0.132	0.073	-0.368	0.329	-0.053	-0.367	0.367	-0.310	-0.393	-0.198	0.459
Y	-0.008	0.066	-0.154	-0.375	-0.441	0.101	-0.124	-0.391	0.052	-0.078	0.701	-0.507	0.147	0.701	-0.302	-0.347	0.723	-0.501	-0.071
Ce	-0.008	-0.065	0.011	0.027	0.225	0.070	-0.152	0.097	-0.270	-0.058	0.064	0.083	-0.163	0.026	-0.015	-0.114	0.038	-0.142	0.438
As	-0.087	-0.141	0.001	0.649	0.702	-0.217	0.251	0.721	0.333	0.237	-0.779	0.660	0.005	-0.785	0.651	-0.115	-0.746	0.157	-0.073
Cd	-0.403	-0.206	0.228	-0.141	0.727	0.539	-0.279	0.393	0.718	0.120	-0.270	0.094	-0.256	-0.288	0.203	-0.040	-0.260	0.183	-0.035
Cr	0.191	-0.231	-0.067	-0.163	-0.176	0.058	-0.045	-0.253	0.323	-0.068	0.335	-0.204	0.199	0.337	-0.022	-0.350	0.359	-0.539	0.092
Pb	-0.262	-0.089	0.090	0.087	0.706	0.292	-0.188	0.449	0.264	0.059	-0.253	0.089	-0.272	-0.287	0.264	-0.222	-0.246	-0.087	0.069
Zn	-0.036	-0.167	-0.005	-0.256	0.017	0.313	-0.232	-0.293	0.475	-0.060	0.313	-0.282	0.044	0.312	-0.072	-0.257	0.299	-0.248	0.323
Pt	-0.285	0.608	-0.050	-0.330	-0.189	0.218	-0.173	-0.235	-0.149	-0.078	0.139	-0.211	-0.048	0.101	-0.099	0.307	0.179	0.279	-0.028
Pd	0.341	0.494	0.133	0.440	-0.474	-0.535	0.692	-0.073	-0.081	0.589	-0.361	0.337	0.725	-0.333	-0.081	0.132	-0.382	0.050	0.418
Rh	-0.481	0.596	0.163	-0.431	-0.023	0.400	-0.321	-0.093	-0.054	-0.059	0.095	-0.285	-0.197	0.053	-0.118	0.405	0.063	0.391	-0.068
Ru	0.292	-0.055	0.216	0.643	0.138	-0.493	0.696	0.518	0.359	0.740	-0.636	0.778	0.631	-0.615	0.414	-0.223	-0.517	-0.157	0.476
Ir	-0.491	0.591	0.203	-0.436	-0.035	0.410	-0.303	-0.127	-0.079	-0.024	0.115	-0.258	-0.177	0.057	-0.062	0.399	0.121	0.388	-0.085
Thick	-0.121	0.067	-0.261	-0.185	-0.380	-0.046	-0.193	-0.408	-0.442	-0.324	0.321	-0.273	-0.176	0.330	-0.318	0.266	0.281	0.134	-0.036

	Co	Cu	Mo	Ni	Sr	V	Y	Ce	As	Cd	Cr	Pb	Zn	Pt	Pd	Rh	Ru	Ir
Co	-0.391																	
Mo	0.360	-0.459																
Ni	0.311	-0.112	0.282															
Sr	-0.149	-0.306	0.540	-0.161														
V	0.176	-0.063	0.648	-0.080	0.608													
Y	-0.440	0.098	-0.248	0.135	0.075	-0.371												
Ce	-0.013	-0.056	0.437	-0.249	0.557	0.401	-0.066											
As	0.682	-0.290	0.451	-0.027	0.171	0.601	-0.537	0.082										
Cd	0.594	-0.324	0.448	0.776	-0.058	0.118	-0.126	-0.048	0.303									
Cr	-0.239	0.221	-0.180	0.331	0.004	-0.144	0.477	-0.130	-0.288	0.084								
Pb	0.527	-0.402	0.623	0.122	0.400	0.492	-0.161	0.592	0.441	0.384	-0.161							
Zn	-0.314	0.293	0.046	0.629	0.104	0.116	0.308	-0.061	-0.362	0.285	0.495	-0.047						
Pt	-0.110	0.048	-0.225	0.041	-0.218	-0.405	0.320	0.022	-0.194	-0.134	-0.191	0.013	-0.255					
Pd	-0.355	0.766	-0.510	-0.337	-0.424	-0.190	0.032	-0.311	-0.392	-0.339	0.575	-0.441	0.149	0.596				
Rh	-0.013	-0.088	0.040	0.210	-0.168	-0.361	0.207	0.039	-0.109	0.023	-0.133	0.122	-0.172	0.874	0.522			
Ru	0.203	0.580	-0.265	-0.101	-0.134	0.333	-0.376	-0.163	0.275	-0.044	0.652	0.029	0.203	0.048	0.665	0.097		
Ir	-0.016	-0.113	0.026	0.177	-0.223	-0.363	0.248	0.094	-0.129	0.004	-0.112	0.130	-0.161	0.829	0.510	0.959	0.104	
Thick	-0.438	-0.065	-0.074	-0.233	0.055	-0.087	-0.044	-0.072	-0.295	-0.303	-0.183	-0.337	-0.021	-0.137	-0.318	-0.196	-0.484	-0.248

Table 19. Correlation coefficient matrix for 17 crust surfaces (≤ 0.5mm) listed in Table 13 and oxygen data from CTD casts; n = 17, except Top of O_2 min. = 16, and Lowest O_2 content and Depth of lowest O_2 = 15; the zero correlation for 17 points at the 95% level is ł0.481ł; Depth, Lat., and Long. apply to the dredge sites.

	Top of O_2 min. zone	Lowest O_2 content	Depth of lowest O_2	Depth	Lat.	Long.	Fe	Mn	Mn/Fe	Si	Na	Mg	K	Ca	Ti	Al	P
O_2 content	0.777																
Depth O_2	0.364	-0.048															
Depth	0.432	0.255	0.344														
Lat.	0.760	0.702	-0.092	0.053													
Long.	-0.592	-0.760	-0.318	-0.402	-0.355												
Fe	0.565	0.570	0.321	0.751	0.389	-0.748											
Mn	-0.579	-0.572	-0.411	-0.685	-0.446	0.693	-0.950										
Mn/Fe	-0.588	-0.612	-0.306	-0.728	-0.465	0.723	-0.990	0.972									
Si	0.636	0.508	0.545	0.648	0.391	-0.641	0.895	-0.919	-0.901								
Na	-0.582	-0.337	-0.433	-0.764	-0.271	0.459	-0.729	0.656	0.703	-0.753							
Mg	-0.509	-0.477	-0.423	-0.848	-0.166	0.595	-0.865	0.859	0.862	-0.790	0.714						
K	-0.276	-0.512	-0.080	-0.355	-0.051	0.562	-0.349	0.306	0.367	-0.257	0.256	0.365					
Ca	0.306	0.400	0.042	0.454	0.150	-0.375	0.418	-0.447	-0.412	0.276	-0.396	-0.491	-0.016				
Ti	-0.469	-0.563	-0.155	-0.102	-0.154	0.577	-0.174	0.169	0.187	-0.278	0.158	0.148	0.769	0.045			
Al	0.497	0.363	0.523	0.325	0.406	-0.513	0.734	-0.824	-0.748	0.889	-0.519	-0.546	0.040	0.259	-0.073		
P	0.130	0.417	-0.131	-0.269	0.343	-0.407	0.211	-0.307	-0.259	0.218	0.087	-0.005	-0.368	0.118	-0.388	0.385	
H2O+	-0.314	-0.540	0.396	0.089	-0.418	-0.016	0.128	-0.086	-0.062	0.252	-0.265	-0.004	0.191	-0.049	0.194	0.337	-0.221
H2O-	0.037	0.423	-0.383	-0.280	0.123	-0.052	-0.285	0.224	0.228	-0.441	0.519	0.186	-0.363	0.054	-0.187	-0.447	0.190
CO2	0.435	0.457	0.306	0.704	0.207	-0.520	0.696	-0.739	-0.697	0.635	-0.666	-0.787	-0.115	0.862	-0.029	0.528	0.035
LOI	-0.510	-0.281	-0.348	-0.437	-0.539	0.364	-0.666	0.632	0.661	-0.768	0.760	0.438	0.002	-0.073	0.084	-0.713	-0.187
Ba	0.099	-0.004	0.212	0.555	0.044	-0.240	0.676	-0.644	-0.640	0.661	-0.582	-0.560	0.117	0.255	0.227	0.667	0.109
Co	-0.671	-0.711	-0.313	-0.714	-0.391	0.837	-0.922	0.877	0.921	-0.870	0.703	0.803	0.612	-0.363	0.534	-0.640	-0.321
Cu	0.584	0.519	0.187	0.554	0.356	-0.571	0.680	-0.631	-0.665	0.693	-0.522	-0.425	-0.274	0.264	-0.447	0.563	0.169
Mo	-0.286	-0.306	-0.346	-0.735	-0.159	0.511	-0.843	0.899	0.849	-0.774	0.630	0.843	0.207	-0.586	-0.044	-0.696	-0.215
Ni	-0.366	-0.431	-0.392	-0.470	-0.278	0.494	-0.727	0.798	0.744	-0.594	0.379	0.753	0.108	-0.467	-0.198	-0.615	-0.284
Sr	0.273	0.388	0.048	0.382	0.351	-0.473	0.540	-0.411	-0.509	0.288	-0.293	-0.359	-0.144	0.281	0.044	0.218	0.239
V	0.141	0.434	0.001	0.010	0.068	-0.450	0.191	-0.103	-0.185	0.149	-0.109	-0.087	-0.694	-0.252	-0.633	0.007	0.527
Y	0.435	0.516	0.349	0.611	0.413	-0.716	0.884	-0.830	-0.884	0.754	-0.635	-0.705	-0.426	0.324	-0.206	0.620	0.391
Ce	-0.175	-0.228	0.007	0.198	0.107	0.190	0.303	-0.304	-0.297	0.158	-0.163	-0.230	0.560	0.167	0.865	0.299	-0.201
As	0.254	0.539	0.124	0.039	0.174	-0.661	0.480	-0.434	-0.480	0.481	-0.198	-0.370	-0.611	-0.191	-0.605	0.380	0.598
Cd	-0.593	-0.629	-0.217	-0.662	-0.493	0.714	-0.961	0.952	0.969	-0.850	0.611	0.841	0.249	-0.469	0.111	-0.739	-0.235
Cr	0.424	0.386	0.288	0.148	0.266	-0.448	0.576	-0.676	-0.597	0.647	-0.215	-0.386	-0.061	0.285	-0.105	0.829	0.584
Pb	-0.268	-0.197	-0.177	-0.802	0.247	0.366	-0.506	0.454	0.478	-0.428	0.453	0.648	0.442	-0.472	0.348	-0.122	0.229
Zn	-0.531	-0.479	-0.214	-0.170	-0.582	0.382	-0.513	0.577	0.551	-0.490	0.270	0.525	-0.121	-0.324	-0.150	-0.527	-0.136

	H2O+	H2O-	CO2	LOI	Ba	Co	Cu	Mo	Ni	Sr	V	Y	Ce	As	Cd	Cr	Pb
H2O-	-0.552																
CO2	0.100	-0.158															
LOI	-0.190	0.686	-0.335														
Ba	0.338	-0.696	0.498	-0.686													
Co	-0.024	0.166	-0.623	0.603	-0.498												
Cu	0.118	-0.413	0.419	-0.639	0.492	-0.764											
Mo	-0.191	0.265	-0.837	0.484	-0.720	0.716	-0.480										
Ni	0.068	-0.041	-0.625	0.302	-0.510	0.533	-0.130	0.793									
Sr	-0.251	-0.039	0.290	-0.382	0.446	-0.446	0.291	-0.369	-0.466								
V	-0.240	0.138	-0.143	-0.135	0.069	-0.404	0.141	0.003	0.006	0.405							
Y	0.051	-0.235	0.550	-0.643	0.638	-0.835	0.547	-0.722	-0.658	0.739	0.436						
Ce	0.203	-0.300	0.257	-0.264	0.521	0.080	-0.102	-0.444	-0.546	0.290	-0.466	0.233					
As	-0.052	-0.016	0.010	-0.303	0.178	-0.612	0.267	-0.219	-0.276	0.197	0.710	0.527	-0.311				
Cd	-0.006	0.176	-0.703	0.599	-0.594	0.861	-0.640	0.823	0.775	-0.466	-0.041	-0.787	-0.352	-0.433			
Cr	0.121	-0.137	0.396	-0.384	0.548	-0.522	0.436	-0.576	-0.632	0.243	0.172	0.520	0.197	0.381	-0.595		
Pb	-0.116	0.145	-0.602	0.060	-0.310	0.600	-0.578	0.533	0.162	-0.052	-0.002	-0.315	0.177	-0.064	0.445	-0.097	
Zn	0.158	-0.082	-0.413	0.321	-0.120	0.356	-0.043	0.384	0.687	-0.206	0.282	-0.368	-0.376	-0.241	0.662	-0.345	-0.105

Table 20. Correlation coefficient matrix for 18 bulk crusts and nodules with thicknesses ≤ 20mm listed in Table 13; n = 18; the zero correlation for 18 points at the 95% confidence level is |0.468|.

	Depth	Lat.	Long.	Fe	Mn	Mn/Fe	Si	Na	Mg	K	Ca	Ti	Al	P	H2O+	H2O-
Lat.	0.256															
Long.	0.024	0.052														
Fe	0.212	0.216	-0.073													
Mn	-0.607	-0.271	0.040	0.031												
Mn/Fe	-0.620	-0.315	0.067	-0.677	0.703											
Si	0.437	0.011	-0.131	0.645	-0.447	-0.772										
Na	-0.393	-0.236	-0.041	0.552	0.552	0.017	0.374									
Mg	-0.409	-0.376	0.014	-0.350	0.374	0.572	-0.188	0.121								
K	0.024	-0.300	-0.219	0.402	-0.085	-0.334	0.789	0.652	0.154							
Ca	0.174	-0.259	-0.229	-0.482	-0.400	0.026	-0.197	-0.558	0.082	-0.133						
Ti	-0.027	0.081	-0.142	0.672	0.206	-0.296	0.539	0.752	-0.089	0.591	-0.610					
Al	0.349	-0.160	-0.327	0.185	-0.604	-0.544	0.790	0.100	0.103	0.773	0.304	0.233				
P	0.195	-0.234	-0.186	-0.491	-0.463	-0.013	-0.179	-0.600	0.078	-0.150	0.995	-0.637	0.318			
H2O+	-0.287	-0.280	-0.144	0.488	0.541	0.047	0.197	0.676	0.353	0.306	-0.264	0.443	0.014	-0.294		
H2O-	0.094	0.558	0.288	-0.230	-0.204	0.025	-0.232	-0.258	-0.318	-0.350	-0.414	0.051	-0.339	-0.374	-0.599	
CO2	0.223	-0.288	-0.303	-0.332	-0.409	-0.079	-0.022	-0.490	0.136	-0.003	0.958	-0.524	0.424	0.952	-0.155	-0.561
LOI	-0.501	0.510	0.248	-0.306	0.262	0.397	-0.537	-0.135	0.156	-0.549	-0.693	0.196	-0.581	-0.681	-0.284	0.965
Ba	0.122	-0.111	-0.329	-0.285	0.053	0.229	-0.390	-0.246	-0.190	-0.200	0.546	-0.272	-0.073	0.486	-0.290	-0.141
Co	-0.636	-0.181	0.149	0.225	0.782	0.408	-0.082	0.711	0.339	0.185	-0.683	0.441	-0.391	-0.705	0.601	-0.046
Cu	0.558	0.095	-0.126	-0.404	-0.578	-0.122	0.149	-0.419	0.021	0.116	0.351	-0.109	0.484	0.368	-0.495	0.266
Mo	-0.439	-0.267	-0.107	-0.134	0.725	0.594	-0.612	0.207	0.029	-0.300	0.013	-0.228	-0.604	-0.052	0.160	-0.198
Ni	-0.377	-0.362	-0.026	-0.612	0.325	0.717	-0.385	-0.054	0.921	-0.025	0.190	-0.183	0.001	0.182	0.138	-0.127
Sr	0.018	-0.141	-0.184	0.221	0.301	0.025	-0.217	0.096	-0.271	-0.154	0.372	-0.135	-0.209	0.309	0.252	-0.528
V	-0.026	-0.155	-0.102	0.217	0.493	0.168	-0.297	0.126	-0.217	-0.247	0.014	-0.184	-0.435	-0.043	0.207	-0.359
Y	0.058	-0.293	-0.379	-0.268	-0.328	-0.026	0.024	-0.350	0.487	0.142	0.721	-0.421	0.513	0.729	-0.023	-0.476
Ce	0.010	-0.007	-0.249	0.044	0.237	0.119	-0.280	0.006	-0.436	-0.169	0.287	0.010	-0.232	0.215	-0.092	-0.190
As	-0.336	0.167	0.052	0.668	0.590	-0.032	0.055	0.618	-0.071	0.030	-0.656	0.390	-0.387	-0.679	0.572	-0.117
Cd	-0.635	-0.327	0.060	-0.330	0.737	0.816	-0.415	0.312	0.822	0.015	-0.197	0.091	-0.278	-0.231	0.377	-0.131
Cr	0.147	-0.278	-0.173	-0.526	-0.229	0.245	-0.126	-0.478	0.653	-0.061	0.565	-0.451	0.346	0.577	-0.098	-0.296
Pb	-0.379	-0.192	-0.060	0.075	0.690	0.428	-0.362	0.282	-0.003	-0.080	-0.057	-0.087	-0.435	-0.126	0.233	-0.352
Zn	0.002	-0.276	-0.116	-0.573	0.013	0.458	-0.372	-0.425	0.676	-0.171	0.578	-0.419	0.131	0.565	-0.072	-0.296
Thick.	-0.029	0.130	-0.232	-0.443	-0.245	0.152	-0.292	-0.310	0.026	-0.047	0.469	-0.186	0.169	0.458	-0.435	0.222

	CO2	LOI	Ba	Co	Cu	Mo	Ni	Sr	V	Y	Ce	As	Cd	Cr	Pb	Zn
LOI	-0.851															
Ba	0.417	-0.213														
Co	-0.624	0.364	-0.518													
Cu	0.287	-0.157	0.292	-0.639												
Mo	-0.086	0.032	0.549	0.272	-0.452											
Ni	0.182	0.376	-0.026	0.206	0.218	0.053										
Sr	0.332	-0.510	0.681	-0.174	-0.324	0.675	-0.312									
V	-0.022	-0.313	0.549	0.043	-0.378	0.826	-0.288	0.824								
Y	0.775	-0.499	0.235	-0.452	0.257	-0.085	0.421	0.097	-0.093							
Ce	0.198	-0.250	0.831	-0.243	-0.071	0.566	-0.331	0.799	0.629	-0.155						
As	-0.606	0.285	-0.246	0.611	-0.763	0.445	-0.305	0.311	0.516	-0.389	0.055					
Cd	-0.186	0.444	-0.112	0.629	-0.236	0.325	0.817	-0.151	-0.047	0.061	-0.159	0.158				
Cr	0.598	-0.744	0.187	-0.413	0.531	-0.201	0.705	-0.182	-0.228	0.733	-0.241	-0.591	0.261			
Pb	-0.077	-0.172	0.464	0.331	-0.534	0.819	-0.101	0.665	0.777	-0.138	0.637	0.467	0.290	-0.253		
Zn	0.560	-0.256	0.399	-0.329	0.462	0.035	0.762	0.030	-0.037	0.646	0.025	-0.517	0.435	0.899	-0.017	
Thick.	0.283	0.154	0.641	-0.500	0.547	0.086	0.166	0.124	-0.039	0.369	0.366	-0.438	-0.059	0.271	0.008	0.426

Table 21. Correlation coefficient matrix for 47 crusts and nodules ≥ 20mm in thickness listed in Table 13; n =47, except for Cr = 46, LOI = 38, Pt, Rh, Ru, and Ir = 19, Pd = 11; the zero correlation for 47 points at the 99% confidence level is |0.366|.

	Depth	Lat.	Long.	Fe	Mn	Mn/Fe	Si	Na	Mg	K	Ca	Ti	Al	P	H2O+	H2O-	CO2	LOI	Ba
Lat.	-0.046																		
Long.	-0.170	0.033																	
Fe	0.391	-0.183	-0.236																
Mn	-0.395	-0.185	0.174	0.129															
Mn/Fe	-0.577	0.076	0.250	-0.835	0.381														
Si	0.599	0.010	-0.151	0.816	-0.259	-0.848													
Na	-0.129	-0.124	0.118	0.564	0.738	-0.145	0.290												
Mg	-0.297	-0.090	0.163	0.230	0.714	0.177	0.059	0.686											
K	0.309	0.022	0.145	0.560	0.158	-0.404	0.748	0.522	0.459										
Ca	-0.181	0.046	-0.063	-0.669	-0.538	0.344	-0.508	-0.721	-0.48	-0.614									
Ti	0.292	-0.141	-0.002	0.861	0.316	-0.631	0.712	0.685	0.406	0.683	-0.861								
Al	0.552	0.024	-0.168	0.730	-0.312	-0.789	0.956	0.208	0.111	0.742	-0.393	0.632							
P	-0.157	0.016	-0.066	-0.646	-0.564	0.305	-0.481	-0.723	-0.478	-0.606	0.996	-0.848	-0.367						
H2O+	0.061	0.104	-0.128	0.631	0.345	-0.352	0.429	0.532	0.418	0.405	-0.512	0.587	0.380	-0.521					
H2O-	-0.111	0.251	0.202	-0.389	0.051	0.333	-0.281	-0.149	-0.164	-0.123	-0.268	-0.058	-0.345	-0.282	-0.375				
CO2	-0.161	0.065	-0.089	-0.611	-0.559	0.300	-0.441	-0.710	-0.464	-0.571	0.977	-0.803	-0.327	0.969	-0.464	-0.315			
LOI	-0.201	0.236	0.197	-0.337	0.256	0.403	-0.368	-0.002	0.081	-0.120	-0.416	0.078	-0.422	-0.438	-0.115	0.963	-0.451		
Ba	0.199	-0.324	0.242	0.153	0.091	-0.134	0.168	0.041	0.024	0.339	-0.112	0.187	0.173	-0.110	0.066	-0.172	-0.118	-0.129	
Co	-0.322	-0.059	0.213	0.182	0.790	0.221	-0.056	0.747	0.693	0.311	-0.664	0.505	-0.126	-0.679	0.325	0.264	-0.649	0.506	-0.028
Cu	0.631	0.165	-0.035	0.452	-0.317	-0.553	0.763	0.127	-0.009	0.717	-0.320	0.460	0.784	-0.302	0.222	-0.125	-0.302	-0.293	0.310
Mo	-0.513	-0.351	0.165	-0.109	0.754	0.443	-0.485	0.413	0.303	-0.086	-0.154	-0.038	-0.531	-0.179	0.061	0.037	-0.215	0.144	0.275
Ni	-0.532	-0.044	0.276	-0.423	0.619	0.720	-0.507	0.256	0.739	-0.001	-0.074	-0.162	-0.433	-0.084	-0.049	0.183	-0.106	0.326	-0.071
Sr	-0.233	-0.389	-0.083	0.046	0.243	0.053	-0.300	0.065	-0.066	-0.324	0.337	-0.204	-0.320	0.329	0.112	-0.595	0.309	-0.545	0.336
V	0.047	-0.434	-0.031	0.509	0.511	-0.248	0.151	0.438	0.257	0.232	-0.379	0.395	0.097	-0.373	0.389	-0.357	-0.389	-0.241	0.537
Y	-0.062	0.139	-0.103	-0.380	-0.444	0.124	-0.202	-0.432	-0.259	-0.266	0.729	-0.559	-0.070	0.727	-0.378	-0.368	0.732	-0.516	-0.142
Ce	-0.057	-0.129	0.079	-0.019	0.336	0.144	-0.192	0.129	-0.072	0.014	0.040	-0.006	-0.165	0.002	-0.015	-0.166	0.037	-0.123	0.416
As	-0.138	-0.226	-0.074	0.616	0.703	-0.224	0.213	0.730	0.500	0.282	-0.749	0.693	0.112	-0.756	0.615	-0.030	-0.729	0.212	0.105
Cd	-0.443	-0.121	0.309	-0.177	0.728	0.521	-0.335	0.419	0.700	0.109	-0.261	0.069	-0.324	-0.276	0.053	0.118	-0.274	0.251	0.043
Cr	0.223	-0.216	-0.013	-0.057	-0.210	-0.060	0.014	-0.174	-0.075	-0.088	0.297	-0.118	0.101	0.303	-0.024	-0.369	0.312	-0.505	0.076
Pb	-0.265	-0.046	0.026	-0.010	0.639	0.310	-0.269	0.342	0.294	0.028	-0.125	-0.013	-0.233	-0.164	0.108	-0.154	-0.136	-0.055	0.217
Zn	-0.052	-0.141	0.090	-0.131	0.161	0.281	-0.143	-0.100	0.371	0.087	0.176	-0.203	-0.041	0.182	0.013	-0.350	0.176	-0.300	0.290
Pt	-0.268	0.588	-0.135	-0.271	0.012	0.243	-0.154	-0.108	0.001	-0.016	0.041	-0.070	-0.074	-0.013	0.066	0.230	0.135	0.246	-0.092
Pd	0.410	0.484	0.041	0.642	-0.248	-0.505	0.790	0.175	0.185	0.776	-0.727	0.829	0.754	-0.721	0.291	0.010	-0.613	0.033	0.347
Rh	-0.482	0.576	0.084	-0.374	0.288	0.448	-0.312	0.091	0.151	0.017	-0.030	-0.129	-0.242	-0.093	0.079	0.326	0.000	0.365	-0.149
Ru	0.282	-0.028	0.258	0.634	0.066	-0.503	0.693	0.512	0.335	0.734	-0.629	0.814	0.649	-0.610	0.398	-0.190	-0.506	-0.139	0.514
Ir	-0.486	0.570	0.145	-0.391	0.197	0.441	-0.291	0.007	0.071	0.037	0.021	-0.138	-0.207	-0.054	0.097	0.337	0.076	0.363	-0.147
Thick	-0.020	0.019	-0.320	-0.056	-0.309	-0.130	-0.106	-0.316	-0.469	-0.426	0.233	-0.219	-0.204	0.241	-0.122	0.102	0.241	0.020	-0.284

	Co	Cu	Mo	Ni	Sr	V	Y	Ce	As	Cd	Cr	Pb	Zn	Pt	Pd	Rh	Ru	Ir	
Cu	-0.177																		
Mo	0.438	-0.459																	
Ni	0.525	-0.337	0.385																
Sr	-0.174	-0.379	0.546	-0.104															
V	0.155	0.036	0.618	-0.045	0.594														
Y	-0.491	-0.099	-0.193	-0.106	0.179	-0.350													
Ce	0.144	-0.105	0.530	-0.137	0.493	0.435	0.104												
As	0.661	-0.096	0.497	0.125	0.169	0.624	-0.548	0.125											
Cd	0.639	-0.355	0.477	0.795	-0.008	0.117	-0.215	0.090	0.324										
Cr	-0.229	0.025	-0.151	-0.103	0.175	-0.062	0.316	0.029	-0.185	-0.097									
Pb	0.375	-0.271	0.630	0.203	0.455	0.464	-0.029	0.808	0.309	0.353	-0.068								
Zn	-0.193	0.055	0.105	0.448	0.238	0.275	0.049	0.028	-0.207	0.245	0.099	0.172							
Pt	0.236	-0.031	-0.235	0.133	-0.301	-0.407	0.306	0.083	-0.069	0.034	-0.207	0.208	-0.303						
Pd	0.028	0.741	-0.557	-0.224	-0.713	-0.236	-0.026	-0.267	-0.093	-0.096	0.621	-0.264	0.082	0.512					
Rh	0.487	-0.197	0.046	0.341	-0.264	-0.365	0.183	0.114	0.058	0.266	-0.150	0.384	-0.226	0.858	0.426				
Ru	0.149	0.637	-0.269	-0.142	-0.110	0.328	-0.367	-0.192	0.240	-0.134	0.661	-0.047	0.219	0.101	0.797	0.165			
Ir	0.361	-0.198	0.030	0.273	-0.299	-0.361	0.230	0.154	-0.006	0.187	-0.122	0.334	-0.199	0.811	0.444	0.958	0.155		
Thick	-0.273	-0.272	-0.146	-0.343	0.037	-0.099	-0.116	-0.144	-0.135	-0.301	-0.261	-0.268	-0.253	-0.296	-0.648	-0.398	-0.470	-0.409	

Table 22. Correlation coefficient matrix for 7 bulk crusts ≥ 100mm in thickness from Table 13; n = 7, except for Pt, Rh, Ru, and Ir = 5, Pd = 4; the zero correlation for 7 points at the 95% confidence level is |0.753|.

	Depth	Lat.	Long.	Fe	Mn	Mn/Fe	Si	Na	Mg	K	Ca	Ti	Al	P	H2O+	H2O-	CO2	LOI	Ba
Lat.	-0.644																		
Long.	-0.605	0.985																	
Fe	0.634	-0.756	-0.784																
Mn	0.452	-0.294	-0.355	0.444															
Mn/Fe	-0.535	0.793	0.777	-0.888	-0.028														
Si	0.464	-0.539	-0.572	0.86	0.453	-0.657													
Na	0.411	-0.268	-0.310	0.287	0.972	0.111	0.330												
Mg	0.373	-0.367	-0.467	0.637	0.840	-0.234	0.772	0.757											
K	0.278	-0.234	-0.320	0.547	0.549	-0.209	0.841	0.471	0.891										
Ca	-0.664	0.520	0.548	-0.827	-0.594	0.560	-0.948	-0.487	-0.821	-0.853									
Ti	0.541	-0.575	-0.625	0.850	0.250	-0.729	0.908	0.107	0.651	0.778	-0.881								
Al	0.286	-0.453	-0.498	0.764	0.150	-0.661	0.931	0.017	0.614	0.803	-0.821	0.944							
P	-0.629	0.449	0.483	-0.790	-0.594	0.505	-0.940	-0.485	-0.830	-0.879	0.996	-0.871	-0.820						
H2O+	0.325	-0.299	-0.414	0.725	0.725	-0.406	0.622	0.549	0.815	0.595	-0.641	0.568	0.484	-0.645					
H2O-	-0.043	0.478	0.540	-0.356	-0.301	0.368	0.050	-0.236	-0.153	0.228	-0.113	0.043	0.135	-0.163	-0.485				
CO2	-0.706	0.488	0.509	-0.745	-0.769	0.416	-0.853	-0.697	-0.855	-0.797	0.959	-0.721	-0.639	0.955	-0.647	-0.067			
LOI	0.045	0.442	0.488	-0.270	-0.174	0.346	0.144	-0.125	-0.013	0.350	-0.233	0.138	0.205	-0.286	-0.358	0.987	-0.194		
Ba	-0.139	-0.254	-0.333	0.131	-0.018	-0.238	-0.285	-0.090	-0.091	-0.373	0.356	-0.132	-0.233	0.391	0.319	-0.903	0.374	-0.912	
Co	0.551	-0.324	-0.361	0.653	0.562	-0.345	0.893	0.480	0.823	0.928	-0.962	0.825	0.794	-0.978	0.552	0.318	-0.924	0.441	-0.515
Cu	0.340	0.054	0.042	-0.355	0.020	0.380	-0.428	0.113	-0.117	-0.123	0.177	-0.166	-0.409	0.170	-0.241	0.145	0.103	0.182	0.034
Mo	0.081	0.053	0.037	-0.085	0.721	0.341	-0.214	0.768	0.268	-0.136	0.084	-0.457	-0.526	0.088	0.330	-0.449	-0.180	-0.405	0.207
Ni	-0.231	0.479	0.397	-0.520	0.368	0.816	-0.262	0.466	0.297	0.282	0.113	-0.290	-0.304	0.060	0.010	0.249	-0.021	0.311	-0.188
Sr	-0.222	-0.041	-0.049	-0.144	0.222	0.117	-0.476	0.248	-0.176	-0.581	0.500	-0.605	-0.631	0.532	0.127	-0.789	0.339	-0.825	0.685
V	0.350	-0.422	-0.471	0.564	0.732	-0.360	0.262	0.635	0.498	0.080	-0.300	0.118	0.003	-0.269	0.766	-0.787	-0.426	-0.713	0.519
Y	-0.501	0.486	0.449	-0.793	-0.433	0.651	-0.865	-0.335	-0.544	-0.541	0.823	-0.653	-0.695	0.804	-0.473	-0.053	0.798	-0.108	0.381
Ce	0.100	-0.011	-0.090	0.013	-0.353	-0.121	-0.140	-0.429	-0.115	0.004	0.091	0.275	0.104	0.083	0.059	-0.063	0.247	-0.035	0.407
As	0.415	-0.362	-0.401	0.739	0.763	-0.396	0.879	0.661	0.877	0.793	-0.886	0.648	0.671	-0.889	0.748	-0.043	-0.915	0.069	-0.289
Cd	0.182	-0.488	-0.491	0.423	0.423	-0.239	0.717	0.465	0.643	0.719	-0.649	0.515	0.629	-0.636	0.179	0.157	-0.645	0.204	-0.442
Cr	-0.061	-0.093	-0.144	0.349	-0.303	-0.373	0.592	-0.406	0.253	0.610	-0.452	0.736	0.837	-0.473	0.125	0.382	-0.201	0.407	-0.250
Pb	-0.129	-0.283	-0.397	0.601	0.487	-0.391	0.571	0.343	0.673	0.499	-0.415	0.431	0.517	-0.411	0.815	-0.575	-0.373	-0.508	0.406
Zn	-0.280	0.163	0.092	-0.419	-0.338	0.267	-0.672	-0.320	-0.388	-0.472	0.645	-0.371	-0.497	0.648	-0.154	-0.398	0.669	-0.424	0.716
Pt	-0.297	0.192	0.074	-0.437	0.306	0.609	-0.035	0.487	0.699	0.979	-0.074	0.219	0.362	-0.207	0.034	0.208	-0.031	0.274	-0.071
Pd	0.727	-0.468	-0.303	-0.566	0.307	0.981	-0.182	0.660	0.210	0.504	-0.730	0.315	-0.215	-0.693	-0.420	0.639	-0.762	0.731	-0.574
Rh	-0.470	0.773	0.725	-0.902	-0.071	0.989	-0.711	0.086	0.171	0.651	0.329	-0.463	-0.267	0.110	-0.275	0.734	0.230	0.776	-0.585
Ru	-0.465	0.119	-0.041	-0.185	0.336	0.380	0.200	0.363	0.802	0.911	0.039	0.331	0.619	-0.057	0.347	-0.163	0.153	-0.108	0.313
Ir	-0.643	0.766	0.690	-0.848	-0.100	0.940	-0.598	0.004	0.249	0.695	0.445	-0.428	-0.074	0.239	-0.162	0.584	0.389	0.618	-0.420
Thick.	0.203	0.032	0.169	-0.338	-0.384	0.050	-0.606	-0.295	-0.768	-0.841	0.506	-0.552	-0.663	0.540	-0.597	0.016	0.421	-0.075	0.026

	Co	Cu	Mo	Ni	Sr	V	Y	Ce	As	Cd	Cr	Pb	Zn	Pt	Pd	Rh	Ru	Ir
Cu	-0.091																	
Mo	-0.127	0.051																
Ni	0.098	0.528	0.365															
Sr	-0.638	-0.130	0.738	-0.053														
V	0.116	-0.234	0.713	-0.155	0.655													
Y	-0.719	0.596	0.005	0.479	0.255	-0.373												
Ce	-0.072	0.565	-0.510	0.062	-0.295	-0.254	0.494											
As	0.844	-0.446	0.246	-0.034	-0.183	0.524	-0.858	-0.424										
Cd	0.671	-0.309	-0.061	0.075	-0.352	0.015	-0.599	-0.446	0.664									
Cr	0.519	-0.228	-0.841	-0.161	-0.797	-0.463	-0.261	0.404	0.222	0.367								
Pb	0.323	-0.615	0.207	-0.104	0.254	0.637	-0.423	-0.141	0.645	0.355	0.235							
Zn	-0.641	0.566	-0.033	0.242	0.341	-0.082	0.881	0.722	-0.742	-0.644	-0.175	-0.167						
Pt	0.610	0.485	-0.311	0.889	-0.534	-0.427	0.945	0.542	-0.253	0.460	0.786	0.087	0.579					
Pd	0.884	0.877	-0.238	0.770	-0.945	-0.622	0.498	0.308	-0.605	0.405	-0.024	-0.727	0.061	0.555				
Rh	0.473	0.325	-0.287	0.898	-0.782	-0.741	0.808	0.126	-0.525	0.109	0.573	-0.280	0.061	0.721	0.974			
Ru	0.306	0.185	-0.170	0.694	-0.123	-0.104	0.861	0.580	0.102	0.348	0.849	0.517	0.746	0.898	0.084	0.505		
Ir	0.326	0.161	-0.314	0.867	-0.629	-0.660	0.842	0.134	-0.411	0.144	0.726	-0.045	0.157	0.764	0.559	0.968	0.647	
Thick.	-0.591	0.273	0.118	-0.361	0.313	-0.088	0.230	-0.091	-0.576	-0.553	-0.610	-0.727	0.153	-0.798	-0.489	-0.972	-0.665	0.170	

Table 23. Correlation coefficient matrix of selected elements from Table 13 and REEs from Table 17 for 20 bulk crusts. The zero correlation for 20 points at the 95% confidence level is |0.442|.

	La	Ce	Pr	Nd	Sm	Eu	Gd	Tb	Dy	Ho	Er	Tm	Yb	REE*	Ce*	Fe
Ce	0.653															
Pr	0.905	0.736														
Nd	0.915	0.665	0.978													
Sm	0.839	0.595	0.961	0.944												
Eu	0.691	0.108	0.639	0.69	0.718											
Gd	0.926	0.547	0.925	0.943	0.937	0.762										
Tb	0.935	0.504	0.907	0.926	0.907	0.787	0.962									
Dy	0.958	0.479	0.840	0.868	0.811	0.736	0.931	0.940								
Ho	0.903	0.398	0.732	0.745	0.732	0.721	0.843	0.876	0.937							
Er	0.906	0.423	0.684	0.713	0.645	0.653	0.826	0.847	0.934	0.945						
Tm	0.931	0.471	0.756	0.789	0.729	0.745	0.851	0.886	0.928	0.950	0.942					
Yb	0.779	0.223	0.489	0.534	0.476	0.651	0.668	0.727	0.836	0.897	0.928	0.891				
REE*	0.744	0.991	0.811	0.751	0.680	0.220	0.647	0.609	0.585	0.501	0.520	0.570	0.318			
Ce*	0.360	0.937	0.501	0.401	0.357	-0.148	0.248	0.200	0.152	0.088	0.108	0.169	-0.067	0.886		
Fe	-0.241	-0.420	-0.024	-0.035	0.139	0.169	0.011	0.047	-0.112	-0.120	-0.304	-0.226	-0.294	-0.393	-0.420	
Mn	0.014	0.077	0.031	0.022	0.031	0.146	0.013	0.097	-0.031	0.035	0.094	0.092	0.035	0.072	0.081	-0.056
Mn/Fe	0.250	0.392	0.064	0.067	-0.080	-0.022	0.029	0.031	0.116	0.156	0.342	0.273	0.277	0.372	0.383	-0.865
Si	-0.163	-0.230	0.046	-0.003	0.212	0.102	0.091	0.060	-0.046	-0.054	-0.230	-0.172	-0.239	-0.214	-0.216	0.866
Ca	0.050	-0.241	-0.279	-0.197	-0.375	-0.081	-0.149	-0.166	0.070	0.077	0.209	0.115	0.318	-0.224	-0.303	-0.601
Al	-0.190	-0.245	-0.016	-0.062	0.134	-0.001	0.039	0.011	-0.061	-0.048	-0.208	-0.187	-0.235	-0.235	-0.231	0.792
P	-0.005	-0.308	-0.333	-0.250	-0.416	-0.100	-0.196	-0.209	0.032	0.044	0.165	0.070	0.300	-0.292	-0.362	-0.557
H2O-	0.360	0.822	0.464	0.414	0.348	-0.111	0.261	0.195	0.194	0.126	0.159	0.188	0.041	0.786	0.844	-0.527
Ba	-0.321	0.019	-0.101	-0.168	-0.052	-0.153	-0.213	-0.232	-0.339	-0.440	-0.463	-0.345	-0.356	-0.028	0.195	0.244
Co	-0.021	0.315	-0.028	-0.085	-0.065	-0.003	-0.096	-0.060	-0.141	-0.027	0.016	0.056	-0.002	0.269	0.408	-0.279
Cu	-0.286	-0.103	-0.015	-0.086	0.131	-0.127	-0.055	-0.114	-0.231	-0.241	-0.413	-0.320	-0.451	-0.123	0.001	0.628
Ni	-0.070	0.058	-0.190	-0.204	-0.222	-0.165	-0.162	-0.104	-0.093	0.034	0.142	0.030	0.143	0.030	0.092	-0.445
Pt	0.059	0.276	0.057	-0.008	0.056	-0.003	0.055	0.066	0.034	0.157	0.147	0.182	0.090	0.249	0.309	-0.083
Thick.	-0.058	-0.253	-0.128	-0.009	-0.133	-0.043	-0.036	-0.074	-0.015	-0.138	-0.063	-0.069	-0.044	-0.232	-0.307	-0.143
Depth	-0.123	-0.218	0.103	0.087	0.273	0.135	0.084	0.070	-0.094	-0.115	-0.317	-0.200	-0.247	-0.196	-0.196	0.652
Lat.	0.404	0.559	0.458	0.424	0.402	0.033	0.451	0.346	0.343	0.334	0.313	0.318	0.092	0.563	0.475	-0.164
Long.	0.075	0.432	0.163	0.088	0.083	-0.016	0.012	-0.060	-0.070	-0.130	-0.114	-0.030	-0.118	0.391	0.525	-0.189

	Mn	Mn/Fe	Si	Ca	Al	P	H2O-	Ba	Co	Cu	Ni	Pt	Thick.	Depth	Lat.
Mn/Fe	0.476														
Si	-0.271	-0.799													
Ca	-0.423	0.357	-0.551												
Al	-0.299	-0.725	0.968	-0.458											
P	-0.444	0.296	-0.523	0.994	-0.437										
H2O-	-0.075	0.324	-0.403	-0.135	-0.431	-0.166									
Ba	-0.113	-0.281	0.414	-0.386	0.318	-0.362	0.060								
Co	0.820	0.565	-0.352	-0.373	-0.402	-0.398	0.233	0.023							
Cu	-0.263	-0.601	0.854	-0.517	0.855	-0.504	-0.218	0.551	-0.266						
Ni	0.710	0.706	-0.411	-0.015	-0.295	-0.039	-0.008	-0.151	0.620	-0.238					
Pt	0.291	0.157	-0.072	-0.308	-0.033	-0.324	0.266	-0.053	0.489	-0.043	0.228				
Thick.	-0.447	-0.149	-0.277	0.526	-0.299	0.535	0.007	-0.262	-0.497	-0.243	-0.452	-0.338			
Depth	-0.361	-0.772	0.641	-0.365	0.527	-0.321	-0.156	0.379	-0.431	0.638	-0.563	-0.305	0.093		
Lat.	-0.054	0.103	-0.038	-0.100	0.035	-0.154	0.413	-0.277	0.071	0.083	0.016	0.516	-0.06	-0.102	
Long.	0.212	0.217	-0.099	-0.231	-0.237	-0.240	0.369	0.416	0.473	-0.070	-0.001	-0.168	-0.357	-0.056	-0.073

Table 24. Correlation coefficient matrix of major and minor elements from Table 13 and REEs from Table 17 for 5 layers from crust D9-7; the zero correlation for 5 points at the 95% confidence level is |0.883|.

	La	Ce	Pr	Nd	Sm	Eu	Gd	Tb	Dy	Ho	Er	Tm	Yb	REE*	Ce*	Fe	Mn	Mn/Fe	Si	Na	Mg	K
Ce	-0.294																					
Pr	-0.357	-0.315																				
Nd	-0.281	-0.733	0.834																			
Sm	-0.631	-0.377	0.864	0.891																		
Eu	-0.697	-0.318	0.816	0.847	0.994																	
Gd	0.310	-0.304	0.617	0.410	0.181	0.083																
Tb	-0.431	0.177	0.678	0.395	0.672	0.680	0.046															
Dy	-0.485	0.679	0.276	-0.183	0.065	0.074	0.319	0.205														
Ho	0.758	-0.175	-0.087	-0.177	-0.517	-0.602	0.727	-0.523	0.079													
Er	0.865	0.017	-0.562	-0.572	-0.864	-0.912	0.285	-0.695	-0.127	0.861												
Tm	0.774	-0.259	-0.272	-0.226	-0.605	-0.679	0.567	-0.728	-0.070	0.962	0.905											
Yb	0.944	-0.334	-0.411	-0.283	-0.679	-0.746	0.370	-0.672	-0.386	0.863	0.934	0.924										
REE*	-0.190	0.992	-0.314	-0.758	-0.432	-0.383	-0.226	0.166	0.673	-0.073	0.109	-0.173	-0.240									
Ce*	-0.476	0.980	-0.236	-0.628	-0.234	-0.165	-0.345	0.217	0.730	-0.304	-0.147	-0.378	-0.489	0.950								
Fe	-0.782	-0.197	0.774	0.771	0.973	0.991	0.009	0.700	0.158	-0.669	-0.952	-0.747	-0.828	-0.270	-0.035							
Mn	-0.967	0.351	0.457	0.296	0.685	0.747	-0.274	0.642	0.490	-0.791	-0.911	-0.864	-0.991	0.260	0.512	0.830						
Mn/Fe	-0.766	0.831	-0.082	-0.363	0.080	0.165	-0.480	0.339	0.656	-0.607	-0.491	-0.650	-0.767	0.760	0.922	0.297	0.779					
Si	-0.007	-0.429	-0.030	0.306	0.314	0.344	-0.557	0.308	-0.809	-0.607	-0.415	-0.523	-0.2.00	-0.467	-0.412	0.308	0.075	-0.204				
Na	-0.953	0.347	0.453	0.296	0.690	0.753	-0.303	0.675	0.450	-0.819	-0.923	-0.893	-0.997	0.256	0.503	0.835	0.998	0.772	0.129			
Mg	-0.904	0.368	0.437	0.266	0.673	0.737	-0.344	0.747	0.392	-0.850	-0.922	-0.936	-0.993	0.284	0.509	0.818	0.979	0.764	0.212	0.990		
K	-0.769	0.594	0.023	-0.132	0.315	0.406	-0.661	0.589	0.287	-0.889	-0.732	-0.923	-0.887	0.512	0.692	0.513	0.841	0.873	0.283	0.862	0.899	
Ca	0.935	-0.059	-0.561	-0.535	-0.841	-0.891	0.237	-0.629	-0.277	0.815	0.983	0.859	0.956	0.038	-0.236	-0.943	-0.954	-0.571	-0.253	-0.956	-0.933	-0.728
Ti	-0.751	0.106	0.434	0.404	0.738	0.796	-0.432	0.794	0.025	-0.922	-0.948	-0.980	-0.909	0.026	0.230	0.843	0.853	0.525	0.558	0.883	0.924	0.835
Al	0.485	0.004	-0.527	-0.381	-0.396	-0.371	-0.560	0.047	-0.705	-0.185	0.215	-0.124	0.254	0.029	-0.112	-0.385	-0.380	-0.194	0.693	-0.323	-0.203	0.115
P	0.940	-0.082	-0.552	-0.516	-0.831	-0.882	0.245	-0.634	-0.290	0.820	0.981	0.865	0.962	0.014	-0.259	-0.936	-0.961	-0.590	-0.245	-0.962	-0.941	-0.742
H2O+	-0.816	0.309	0.537	0.337	0.723	0.775	-0.254	0.861	0.337	-0.810	-0.916	-0.932	-0.955	0.240	0.430	0.840	0.934	0.667	0.273	0.952	0.981	0.854
H2O-	-0.678	-0.359	0.280	0.558	0.577	0.602	-0.096	-0.132	0.074	-0.395	-0.574	-0.277	-0.467	-0.456	-0.173	0.610	0.506	0.152	0.039	0.474	0.368	0.145
CO2	0.944	-0.060	-0.564	-0.537	-0.839	-0.888	0.217	-0.606	-0.302	0.797	0.975	0.839	0.951	0.037	-0.240	-0.940	-0.955	-0.575	-0.218	-0.954	-0.925	-0.713
LOI	-0.923	-0.078	0.452	0.547	0.754	0.798	-0.182	0.279	0.280	-0.662	-0.852	-0.631	-0.811	-0.185	0.123	0.842	0.839	0.472	0.089	0.819	0.745	0.518
Ba	-0.772	0.432	0.630	0.283	0.663	0.696	0.000	0.857	0.597	-0.587	-0.787	-0.768	-0.882	0.386	0.536	0.765	0.899	0.691	-0.034	0.904	0.918	0.746
Co	-0.868	0.074	0.512	0.490	0.816	0.871	-0.344	0.724	0.149	-0.893	-0.994	-0.943	-0.957	-0.018	0.230	0.920	0.927	0.557	0.420	0.943	0.951	0.798
Cu	-0.075	0.914	-0.255	-0.693	-0.366	-0.321	-0.276	0.376	0.463	-0.160	0.055	-0.289	-0.238	0.935	0.842	-0.227	0.220	0.653	-0.197	0.238	0.313	0.559
Mo	-0.902	0.210	0.630	0.465	0.814	0.858	-0.138	0.769	0.417	-0.754	-0.948	-0.862	-0.967	0.132	0.363	0.917	0.972	0.637	0.153	0.976	0.970	0.765
Ni	-0.914	0.618	0.274	0.009	0.447	0.518	-0.325	0.572	0.643	-0.712	-0.753	-0.796	-0.936	0.537	0.749	0.628	0.953	0.926	-0.095	0.947	0.934	0.890
Sr	0.137	0.091	0.699	0.271	0.287	0.220	0.756	0.606	0.423	0.350	0.000	0.083	0.000	0.167	0.033	0.189	0.049	-0.107	-0.330	0.052	0.087	-0.146
V	-0.849	0.097	0.714	0.569	0.880	0.912	-0.061	0.807	0.348	-0.721	-0.955	-0.839	-0.929	0.026	0.245	0.954	0.931	0.527	0.206	0.938	0.936	0.694
Y	0.905	0.069	-0.647	-0.650	-0.898	-0.934	0.107	-0.582	-0.267	0.725	0.961	0.768	0.896	0.161	-0.114	-0.969	-0.907	-0.459	-0.209	-0.903	-0.865	-0.601
As	-0.902	0.008	0.658	0.609	0.893	0.932	-0.127	0.679	0.289	-0.758	-0.978	-0.826	-0.931	-0.079	0.180	0.972	0.936	0.508	0.232	0.937	0.915	0.669
Cd	-0.908	0.548	0.298	0.072	0.513	0.587	-0.392	0.654	0.519	-0.804	-0.825	-0.885	-0.971	0.465	0.680	0.689	0.968	0.887	0.067	0.972	0.975	0.934
Cr	0.790	0.026	-0.538	-0.501	-0.628	-0.640	-0.216	-0.119	-0.574	0.256	0.586	0.274	0.594	0.099	-0.151	-0.674	-0.682	-0.387	0.363	-0.638	-0.527	-0.226
Pb	-0.843	-0.165	0.635	0.696	0.923	0.958	-0.170	0.620	0.102	-0.778	-0.982	-0.810	-0.873	-0.256	0.010	0.980	0.862	0.372	0.378	0.868	0.848	0.599
Zn	-0.900	0.235	0.594	0.431	0.793	0.841	-0.189	0.778	0.396	-0.786	-0.952	-0.890	-0.976	0.156	0.385	0.904	0.975	0.658	0.187	0.982	0.981	0.800

	Ca	Ti	Al	P	H2O+	H2O-	CO2	LOI	Ba	Co	Cu	Mo	Ni	Sr	V	Y	As	Cd	Cr	Pb
Ti	-0.892																			
Al	0.367	0.070																		
P	1.000	-0.895	0.363																	
H2O+	-0.903	0.945	-0.136	-0.909																
H2O-	-0.646	0.316	-0.608	-0.635	0.257															
CO2	0.999	-0.872	0.405	0.999	-0.890	-0.669														
LOI	-0.914	0.660	-0.575	-0.910	0.660	0.892	-0.928													
Ba	-0.813	0.786	-0.336	-0.822	0.944	0.165	-0.809	0.581												
Co	-0.974	0.971	-0.157	-0.975	0.946	0.507	-0.964	0.815	0.815											
Cu	0.048	0.165	0.301	0.025	0.326	-0.649	0.062	-0.315	0.421	0.047										
Mo	-0.967	0.894	-0.364	-0.970	0.966	0.463	-0.964	0.809	0.934	0.955	0.147									
Ni	-0.819	0.736	-0.340	-0.832	0.871	0.330	-0.822	0.691	0.885	0.795	0.466	0.879								
Sr	0.005	0.022	-0.247	0.003	0.232	-0.437	0.007	-0.223	0.461	0.000	0.274	0.208	0.056							
V	-0.958	0.896	-0.353	-0.959	0.954	0.457	-0.954	0.790	0.918	0.952	0.069	0.990	0.806	0.271						
Y	0.985	-0.827	0.470	0.982	-0.839	-0.722	0.989	-0.941	-0.766	-0.935	0.190	-0.938	-0.741	-0.032	-0.945					
As	-0.992	0.880	-0.404	-0.991	0.904	0.623	-0.992	0.894	0.835	0.964	-0.076	0.974	0.786	0.102	0.979	-0.991				
Cd	-0.862	0.835	-0.226	-0.874	0.930	0.315	-0.859	0.695	0.899	0.868	0.447	0.914	0.986	0.041	0.853	-0.777	0.830			
Cr	0.710	-0.317	0.895	0.706	-0.439	-0.837	0.740	-0.879	-0.513	-0.534	0.332	-0.652	-0.584	-0.014	-0.632	0.782	-0.719	-0.518		
Pb	-0.973	0.879	-0.325	-0.968	0.841	0.682	-0.970	0.898	0.720	0.956	-0.229	0.914	0.668	0.000	0.934	-0.983	0.979	0.733	-0.672	
Zn	-0.964	0.914	-0.313	-0.969	0.978	0.437	-0.959	0.793	0.934	0.963	0.182	0.998	0.888	0.184	0.985	-0.926	0.966	0.929	-0.614	0.908

Table 25. Correlation coefficient matrix of major and minor elements from Table 13 and REEs from Table 17 for 4 layers from crust D11-15; the zero correlation for 4 points at the 95% confidence level is |0.962|.

	La	Ce	Pr	Nd	Sm	Eu	Gd	Tb	Dy	Ho	Er	Tm	Yb	REE*	Ce*	Fe	Mn	Mn/Fe	Si	Na	Mg	K
Ce	0.030																					
Pr	0.984	-0.115																				
Nd	0.994	-0.045	0.997																			
Sm	0.912	-0.023	0.948	0.942																		
Eu	0.786	0.380	0.775	0.793	0.904																	
Gd	0.907	0.378	0.866	0.894	0.905	0.956																
Tb	0.680	-0.022	0.752	0.734	0.920	0.889	0.772															
Dy	0.701	-0.591	0.817	0.770	0.819	0.517	0.507	0.770														
Ho	0.000	0.981	-0.121	-0.058	0.030	0.448	0.389	0.101	-0.529													
Er	0.126	0.883	-0.052	0.025	-0.115	0.182	0.316	-0.287	-0.618	0.775												
Tm	-0.758	0.513	-0.784	-0.765	-0.568	-0.217	-0.413	-0.265	-0.723	0.598	0.206											
Yb	-0.154	0.872	-0.230	-0.184	0.000	0.421	0.273	0.191	-0.478	0.949	0.544	0.756										
REE*	0.612	0.807	0.494	0.554	0.542	0.792	0.845	0.425	-0.033	0.785	0.745	-0.020	0.624									
Ce*	-0.638	0.750	-0.744	-0.695	-0.639	-0.251	-0.320	-0.500	-0.935	0.745	0.618	0.878	0.751	0.214								
Fe	0.408	-0.460	0.553	0.500	0.713	0.546	0.387	0.870	0.861	-0.312	-0.722	-0.272	-0.122	-0.078	-0.660							
Mn	-0.158	-0.593	0.014	-0.053	0.207	0.065	-0.165	0.498	0.540	-0.424	-0.901	0.099	-0.131	-0.516	-0.389	0.833						
Mn/Fe	-0.724	0.225	-0.816	-0.787	-0.934	-0.806	-0.720	-0.974	-0.895	0.118	0.421	0.441	0.035	-0.285	0.682	-0.916	-0.542					
Si	0.029	0.105	0.119	0.097	0.425	0.562	0.295	0.744	0.321	0.295	-0.360	0.403	0.539	0.157	0.014	0.739	0.722	-0.636				
Na	0.076	-0.253	0.214	0.168	0.473	0.454	0.203	0.768	0.563	-0.064	-0.657	0.164	0.202	-0.100	-0.291	0.905	0.903	-0.739	0.934			
Mg	0.164	-0.555	0.329	0.266	0.507	0.338	0.141	0.730	0.756	-0.392	-0.844	-0.123	-0.148	-0.295	-0.574	0.966	0.948	-0.780	0.753	0.938		
K	-0.114	0.005	-0.008	-0.039	0.298	0.414	0.130	0.649	0.279	0.201	-0.462	0.461	0.477	-0.006	0.033	0.725	0.801	-0.555	0.985	0.947	0.783	
Ca	-0.129	0.427	-0.285	-0.228	-0.502	-0.398	-0.174	-0.760	-0.682	0.250	0.772	-0.003	-0.008	0.210	0.456	-0.954	-0.941	0.776	-0.847	-0.981	-0.988	-0.869
Ti	0.386	-0.210	0.507	0.469	0.727	0.676	0.481	0.928	0.735	-0.044	-0.556	-0.079	0.153	0.113	-0.459	0.962	0.779	-0.911	0.878	0.949	0.915	0.843
Al	0.385	0.098	0.464	0.447	0.720	0.797	0.594	0.931	0.554	0.263	-0.296	0.096	0.434	0.357	-0.223	0.834	0.616	-0.849	0.934	0.892	0.760	0.869
P	-0.128	0.431	-0.283	-0.227	-0.500	-0.394	-0.170	-0.758	-0.683	0.254	0.775	-0.001	-0.004	0.214	0.458	-0.954	-0.943	0.774	-0.844	-0.980	-0.988	-0.867
H2O+	0.165	-0.589	0.332	0.268	0.500	0.314	0.124	0.714	0.768	-0.430	-0.862	-0.150	-0.188	-0.323	-0.599	0.963	0.948	-0.773	0.726	0.923	0.999	0.758
H2O-	-0.486	0.852	-0.615	-0.556	-0.530	-0.126	-0.162	-0.444	-0.910	0.830	0.750	0.794	0.788	0.381	0.982	-0.691	-0.517	0.634	-0.029	-0.360	-0.652	-0.042
CO2	-0.164	0.435	-0.319	-0.263	-0.531	-0.418	-0.201	-0.777	-0.708	0.260	0.770	0.032	0.009	0.196	0.485	-0.965	-0.933	0.797	-0.837	-0.976	-0.990	-0.855
LOI	0.062	-0.470	0.223	0.164	0.437	0.324	0.096	0.706	0.655	-0.293	-0.810	0.027	-0.024	-0.284	-0.444	0.935	0.965	-0.728	0.827	0.973	0.989	0.862
Ba	0.855	-0.434	0.933	0.903	0.901	0.629	0.670	0.776	0.968	-0.405	-0.406	-0.806	-0.426	0.174	-0.910	0.753	0.325	-0.887	0.215	0.413	0.592	0.136
Co	-0.404	-0.507	-0.244	-0.306	-0.031	-0.106	-0.361	0.310	0.302	-0.337	-0.839	0.327	-0.022	-0.593	-0.160	0.670	0.965	-0.326	0.701	0.837	0.836	0.806
Cu	0.907	-0.393	0.951	0.931	0.839	0.551	0.670	0.616	0.884	-0.417	-0.245	-0.922	-0.520	0.222	-0.901	0.550	0.085	-0.745	-0.041	0.153	0.365	-0.131
Mo	-0.072	-0.985	0.089	0.014	0.051	-0.324	-0.371	0.114	0.612	-0.933	-0.951	-0.411	-0.776	-0.810	-0.718	0.565	0.722	-0.298	0.060	0.406	0.674	0.165
Ni	-0.306	-0.763	-0.130	-0.204	-0.005	-0.217	-0.407	0.249	0.460	-0.627	-0.968	0.044	-0.350	-0.749	-0.412	0.685	0.953	-0.340	0.490	0.730	0.844	0.606
Sr	0.873	-0.069	0.923	0.911	0.996	0.894	0.870	0.948	0.845	0.000	-0.192	-0.535	0.000	0.487	-0.652	0.775	0.297	-0.963	0.492	0.552	0.585	0.375
V	0.343	-0.799	0.505	0.437	0.547	0.220	0.138	0.616	0.910	-0.702	-0.888	-0.516	-0.546	-0.402	-0.864	0.894	0.800	-0.755	0.399	0.692	0.897	0.427
Y	-0.553	0.498	-0.689	-0.638	-0.797	-0.581	-0.474	-0.877	-0.943	0.378	0.683	0.452	0.239	0.030	0.780	-0.981	-0.735	0.950	-0.614	-0.805	-0.911	-0.583
As	0.047	-0.610	0.219	0.153	0.395	0.217	0.013	0.636	0.697	-0.446	-0.894	-0.070	-0.184	-0.408	-0.538	0.925	0.979	-0.695	0.723	0.921	0.992	0.774
Cd	-0.204	-0.824	-0.025	-0.102	0.073	-0.182	-0.347	0.289	0.554	-0.698	-0.992	-0.083	-0.442	-0.740	-0.524	0.723	0.940	-0.401	0.443	0.712	0.861	0.550
Cr	0.446	0.416	0.465	0.474	0.711	0.898	0.732	0.871	0.359	0.551	0.045	0.175	0.648	0.637	-0.012	0.616	0.326	-0.738	0.849	0.701	0.496	0.746
Pb	-0.585	-0.124	-0.474	-0.512	-0.202	-0.092	-0.381	0.196	-0.050	0.052	-0.535	0.685	0.363	-0.395	0.253	0.440	0.793	-0.121	0.771	0.758	0.617	0.865
Zn	0.710	-0.660	0.816	0.770	0.754	0.404	0.446	0.640	0.980	-0.635	-0.592	-0.838	-0.627	-0.094	-0.985	0.750	0.429	-0.796	0.126	0.399	0.642	0.089

	Ca	Ti	Al	P	H2O+	H2O-	CO2	LOI	Ba	Co	Cu	Mo	Ni	Sr	V	Y	As	Cd	Cr	Pb
Ti	-0.945																			
Al	-0.833	0.952																		
P	1.000	-0.944	-0.830																	
H2O+	-0.981	0.900	0.735	-0.981																
H2O-	0.531	-0.475	-0.209	0.534	-0.678															
CO2	0.999	-0.952	-0.836	0.999	-0.984	0.554														
LOI	-0.997	0.916	0.791	-0.997	0.983	-0.533	-0.994													
Ba	-0.522	0.646	0.509	-0.522	0.602	-0.840	-0.554	0.480												
Co	-0.848	0.643	0.508	-0.850	0.833	-0.314	-0.831	0.885	0.066											
Cu	-0.277	0.422	0.291	-0.277	0.380	-0.803	-0.313	0.234	0.963	-0.176										
Mo	-0.563	0.339	0.039	-0.567	0.703	-0.836	-0.567	0.606	0.430	0.644	0.344									
Ni	-0.804	0.569	0.350	-0.807	0.855	-0.567	-0.794	0.848	0.224	0.944	0.026	0.860								
Sr	-0.581	0.787	0.768	-0.579	0.577	-0.557	-0.608	0.520	0.905	0.063	0.820	0.110	0.082							
V	-0.819	0.739	0.499	-0.821	0.913	-0.919	-0.833	0.823	0.779	0.629	0.640	0.851	0.783	0.604						
Y	0.878	-0.914	-0.770	0.878	-0.913	0.785	0.896	-0.853	-0.866	-0.535	-0.703	-0.575	-0.599	-0.845	-0.918					
As	-0.975	0.861	0.691	-0.976	0.993	-0.637	-0.974	0.986	0.510	0.891	0.281	0.729	0.906	0.477	0.888	-0.858				
Cd	-0.806	0.584	0.344	-0.809	0.875	-0.667	-0.801	0.846	0.330	0.901	0.146	0.909	0.992	0.156	0.849	-0.660	0.915			
Cr	-0.597	0.798	0.941	-0.593	0.463	0.049	-0.602	0.540	0.387	0.235	0.216	-0.296	0.024	0.734	0.207	-0.562	0.406	0.008		
Pb	-0.688	0.518	0.504	-0.688	0.600	0.107	-0.661	0.721	-0.259	0.907	-0.505	0.280	0.727	-0.115	0.269	-0.258	0.673	0.639	0.339	
Zn	-0.544	0.584	0.377	-0.545	0.661	-0.955	-0.573	0.522	0.963	0.187	0.926	0.649	0.400	0.769	0.880	-0.860	0.590	0.508	0.183	-0.200

Table 26. Correlation coefficient matrix of major and minor elements from Table 13 and REEs from Table 17 for 4 layers from crust D12-1; the zero correlation for 4 points at the 95% confidence level is |0.962|.

	La	Ce	Pr	Nd	Sm	Eu	Gd	Tb	Dy	Ho	Er	Tm	Yb	REE*	Ce*	Fe	Mn	Mn/Fe	Si	Na	Mg	K
Ce	0.806																					
Pr	0.946	0.895																				
Nd	0.950	0.933	0.993																			
Sm	0.884	0.847	0.983	0.958																		
Eu	0.842	0.855	0.969	0.944	0.996																	
Gd	0.917	0.780	0.975	0.943	0.987	0.969																
Tb	0.797	0.825	0.945	0.913	0.987	0.996	0.956															
Dy	0.805	0.705	0.920	0.869	0.972	0.969	0.975	0.975														
Ho	0.828	0.609	0.890	0.832	0.935	0.916	0.969	0.916	0.980													
Er	0.904	0.875	0.992	0.975	0.998	0.992	0.983	0.978	0.956	0.917												
Tm	0.942	0.744	0.964	0.932	0.964	0.936	0.994	0.917	0.952	0.967	0.962											
Yb	0.388	0.121	0.496	0.391	0.622	0.618	0.672	0.657	0.787	0.829	0.572	0.663										
REE*	0.933	0.956	0.984	0.997	0.945	0.934	0.919	0.903	0.843	0.794	0.964	0.904	0.338									
Ce*	-0.461	0.140	-0.290	-0.221	-0.296	-0.223	-0.444	-0.208	-0.409	-0.581	-0.275	-0.524	-0.636	-0.152								
Fe	0.868	0.691	0.934	0.886	0.967	0.949	0.990	0.945	0.988	0.994	0.954	0.984	0.769	0.855	-0.516							
Mn	-0.017	0.016	0.230	0.131	0.404	0.450	0.380	0.521	0.577	0.532	0.347	0.318	0.839	0.103	-0.154	0.479						
Mn/Fe	-0.925	-0.758	-0.790	-0.834	-0.667	-0.614	-0.701	-0.546	-0.524	-0.555	-0.708	-0.743	-0.024	-0.831	0.330	-0.615	0.394					
Si	0.220	0.581	0.525	0.494	0.633	0.702	0.522	0.748	0.650	0.498	0.611	0.424	0.466	0.512	0.345	0.525	0.727	0.047				
Na	0.094	0.285	0.387	0.312	0.543	0.603	0.476	0.667	0.655	0.556	0.498	0.392	0.725	0.304	0.071	0.537	0.946	0.259	0.911			
Mg	0.281	0.254	0.501	0.407	0.651	0.682	0.638	0.737	0.793	0.757	0.601	0.585	0.921	0.376	-0.286	0.718	0.955	0.103	0.762	0.935		
K	-0.118	0.235	0.206	0.154	0.357	0.436	0.252	0.505	0.439	0.299	0.318	0.150	0.482	0.166	0.367	0.295	0.850	0.410	0.927	0.951	0.780	
Ca	-0.398	-0.442	-0.632	-0.554	-0.764	-0.798	-0.730	-0.845	-0.864	-0.802	-0.723	-0.670	-0.860	-0.533	0.190	-0.785	-0.897	0.033	-0.851	-0.942	-0.979	-0.802
Ti	0.348	0.594	0.630	0.583	0.744	0.799	0.659	0.843	0.784	0.662	0.716	0.574	0.631	0.586	0.138	0.677	0.793	-0.039	0.977	0.940	0.864	0.890
Al	0.614	0.916	0.821	0.830	0.844	0.883	0.746	0.886	0.762	0.627	0.851	0.676	0.303	0.854	0.261	0.692	0.367	-0.453	0.859	0.627	0.534	0.605
P	-0.379	-0.428	-0.616	-0.538	-0.750	-0.786	-0.716	-0.834	-0.853	-0.790	-0.709	-0.654	-0.858	-0.516	0.181	-0.772	-0.905	0.012	-0.853	-0.948	-0.981	-0.812
H2O+	0.416	0.375	0.621	0.535	0.754	0.778	0.743	0.823	0.873	0.838	0.710	0.695	0.923	0.504	-0.321	0.810	0.902	-0.042	0.769	0.906	0.989	0.732
H2O-	-0.654	-0.425	-0.753	-0.670	-0.840	-0.830	-0.877	-0.850	-0.941	-0.965	-0.806	-0.867	-0.945	-0.626	0.602	-0.936	-0.715	0.322	-0.539	-0.685	-0.881	-0.430
CO2	-0.410	-0.460	-0.645	-0.569	-0.774	-0.809	-0.739	-0.854	-0.870	-0.806	-0.734	-0.678	-0.852	-0.548	0.182	-0.791	-0.888	0.048	-0.857	-0.940	-0.974	-0.801
LOI	-0.766	-0.423	-0.521	-0.562	-0.377	-0.298	-0.463	-0.222	-0.261	-0.362	-0.417	-0.544	0.075	-0.545	0.522	-0.396	0.582	0.912	0.441	0.559	0.330	0.728
Ba	0.982	0.683	0.874	0.874	0.804	0.747	0.866	0.697	0.740	0.801	0.822	0.910	0.392	0.847	-0.599	0.828	-0.081	-0.925	0.052	-0.024	0.214	-0.264
Co	-0.259	-0.218	-0.022	-0.122	0.162	0.212	0.141	0.291	0.356	0.319	0.100	0.080	0.738	-0.149	-0.092	0.254	0.968	0.607	0.606	0.869	0.852	0.816
Cu	0.993	0.755	0.943	0.934	0.898	0.855	0.942	0.816	0.846	0.881	0.911	0.968	0.489	0.909	-0.542	0.909	0.071	-0.882	0.230	0.152	0.364	-0.084
Mo	0.309	0.023	0.410	0.301	0.542	0.537	0.599	0.580	0.723	0.774	0.489	0.593	0.995	0.245	-0.652	0.706	0.844	0.052	0.413	0.704	0.903	0.464
Ni	-0.312	-0.280	-0.084	-0.185	0.101	0.149	0.083	0.229	0.300	0.269	0.038	0.025	0.713	-0.211	-0.093	0.200	0.950	0.650	0.560	0.837	0.819	0.789
Sr	0.907	0.483	0.773	0.749	0.724	0.657	0.819	0.615	0.714	0.815	0.730	0.878	0.522	0.706	-0.788	0.815	0.004	-0.815	-0.058	-0.025	0.274	-0.308
V	0.802	0.467	0.811	0.745	0.851	0.816	0.917	0.813	0.918	0.978	0.830	0.935	0.853	0.696	-0.737	0.956	0.484	-0.541	0.327	0.446	0.704	0.158
Y	-0.265	-0.453	-0.547	-0.482	-0.684	-0.737	-0.615	-0.791	-0.765	-0.663	-0.646	-0.534	-0.728	-0.476	-0.046	-0.658	-0.890	-0.079	-0.944	-0.983	-0.933	-0.913
As	0.634	0.481	0.769	0.690	0.864	0.866	0.881	0.891	0.958	0.956	0.830	0.857	0.928	0.652	-0.494	0.934	0.758	-0.292	0.643	0.760	0.916	0.531
Cd	-0.101	-0.154	0.108	0.000	0.286	0.322	0.287	0.394	0.486	0.473	0.224	0.239	0.853	-0.036	-0.263	0.403	0.981	0.471	0.582	0.866	0.912	0.754
Cr	0.238	0.728	0.511	0.528	0.558	0.628	0.417	0.651	0.483	0.300	0.561	0.319	0.100	0.571	0.601	0.365	0.391	-0.106	0.914	0.668	0.444	0.765
Pb	-0.361	-0.206	-0.093	-0.180	0.090	0.153	0.041	0.236	0.264	0.195	0.032	-0.034	0.609	-0.193	0.100	0.141	0.934	0.681	0.661	0.875	0.789	0.880
Zn	0.947	0.617	0.888	0.858	0.865	0.816	0.932	0.785	0.858	0.922	0.866	0.967	0.623	0.819	-0.691	0.928	0.175	-0.794	0.182	0.191	0.450	-0.083

	Ca	Ti	Al	P	H2O+	H2O-	CO2	LOI	Ba	Co	Cu	Mo	Ni	Sr	V	Y	As	Cd	Cr	Pb		
Ti	-0.939																					
Al	-0.696	0.855																				
P	1.000	-0.939	-0.688																			
H2O+	-0.990	0.882	0.613	-0.989																		
H2O-	0.883	-0.706	-0.530	0.876	-0.928																	
CO2	1.000	-0.944	-0.710	0.999	-0.988	0.882																
LOI	-0.257	0.335	-0.048	-0.277	0.205	0.151	-0.248															
Ba	-0.303	0.202	0.454	-0.284	0.346	-0.633	-0.313	-0.842														
Co	-0.757	0.649	0.160	-0.770	0.767	-0.544	-0.746	0.728	-0.305													
Cu	-0.462	0.377	0.587	-0.443	0.492	-0.731	-0.472	-0.734	0.983	-0.167												
Mo	-0.823	0.578	0.215	-0.823	0.893	-0.909	-0.813	0.119	0.326	0.766	0.416											
Ni	-0.714	0.600	0.098	-0.728	0.727	-0.502	-0.701	0.748	-0.350	0.998	-0.219	0.748										
Sr	-0.311	0.125	0.273	-0.293	0.387	-0.696	-0.316	-0.810	0.965	-0.190	0.936	0.476	-0.225									
V	-0.717	0.516	0.453	-0.705	0.780	-0.956	-0.718	-0.429	0.815	0.293	0.867	0.812	0.252	0.876								
Y	0.971	-0.983	-0.749	0.974	-0.931	0.748	0.972	-0.414	-0.138	-0.771	-0.313	-0.690	-0.729	-0.107	-0.541							
As	-0.932	0.791	0.617	-0.926	0.960	-0.992	-0.932	-0.075	0.588	0.582	0.704	0.887	0.537	0.627	0.920	-0.824						
Cd	-0.817	0.663	0.188	-0.827	0.845	-0.682	-0.806	0.583	-0.131	0.981	0.000	0.875	0.974	0.000	0.464	-0.788	0.704					
Cr	-0.593	0.833	0.910	-0.593	0.476	-0.256	-0.606	0.308	0.048	0.263	0.200	0.031	0.214	-0.149	0.096	-0.735	0.375	0.209				
Pb	-0.710	0.663	0.195	-0.725	0.695	-0.417	-0.699	0.833	-0.431	0.981	-0.284	0.636	0.980	-0.350	0.141	-0.769	0.476	0.929	0.366			
Zn	-0.509	0.357	0.476	-0.491	0.563	-0.813	-0.515	-0.694	0.964	-0.045	0.978	0.565	-0.091	0.971	0.940	-0.330	0.770	0.136	0.073	-0.189		

Table 27. Correlation coefficient matrix of major and minor elements from Table 13 and REEs from Table 17 for 5 layers from crust RD59-2; the zero correlation for 5 points at the 95% confidence level is |0.883|.

	La	Ce	Pr	Nd	Sm	Eu	Gd	Tb	Dy	Ho	Er	Tm	Yb	REE*	Ce*	Fe	Mn	Mn/Fe	Si	Na	Mg	K
Ce	0.689																					
Pr	0.995	0.690																				
Nd	0.994	0.711	0.999																			
Sm	0.992	0.675	0.999	0.998																		
Eu	0.985	0.732	0.989	0.995	0.991																	
Gd	0.997	0.647	0.997	0.995	0.996	0.984																
Tb	1.000	0.695	0.996	0.996	0.994	0.989	0.997															
Dy	1.000	0.700	0.996	0.997	0.994	0.989	0.997	1.000														
Ho	0.999	0.674	0.990	0.991	0.988	0.984	0.996	0.998	0.998													
Er	0.997	0.714	0.985	0.988	0.981	0.983	0.989	0.996	0.997	0.998												
Tm	0.998	0.690	0.987	0.987	0.983	0.978	0.992	0.997	0.997	0.999	0.999											
Yb	0.998	0.727	0.991	0.994	0.988	0.990	0.992	0.998	0.999	0.997	0.999	0.997										
REE*	0.918	0.920	0.917	0.929	0.908	0.936	0.894	0.921	0.924	0.909	0.929	0.916	0.937									
Ce*	-0.758	-0.095	-0.763	-0.754	-0.782	-0.746	-0.799	-0.760	-0.755	-0.774	-0.735	-0.749	-0.731	-0.467								
Fe	-0.801	-0.891	-0.772	-0.777	-0.746	-0.767	-0.754	-0.795	-0.799	-0.791	-0.825	-0.817	-0.820	-0.914	0.235							
Mn	-0.421	-0.244	-0.453	-0.483	-0.489	-0.550	-0.456	-0.443	-0.442	-0.440	-0.423	-0.401	-0.440	-0.375	0.609	0.001						
Mn/Fe	0.662	0.660	0.627	0.613	0.592	0.564	0.617	0.646	0.649	0.645	0.671	0.681	0.660	0.708	-0.142	-0.907	0.364					
Si	-0.644	-0.955	-0.629	-0.641	-0.603	-0.640	-0.591	-0.642	-0.648	-0.626	-0.670	-0.654	-0.675	-0.866	-0.010	0.952	-0.038	-0.830				
Na	-0.759	-0.983	-0.773	-0.790	-0.762	-0.804	-0.728	-0.766	-0.771	-0.740	-0.770	-0.751	-0.789	-0.951	0.214	0.870	0.315	-0.644	0.919			
Mg	-0.552	-0.467	-0.553	-0.590	-0.577	-0.665	-0.561	-0.572	-0.571	-0.578	-0.581	-0.551	-0.586	-0.563	0.560	0.284	0.923	0.112	0.229	0.486		
K	-0.584	-0.842	-0.548	-0.586	-0.541	-0.644	-0.539	-0.593	-0.596	-0.598	-0.641	-0.606	-0.635	-0.774	0.145	0.748	0.421	-0.430	0.758	0.771	0.719	
Ca	0.907	0.881	0.899	0.919	0.896	0.945	0.887	0.914	0.916	0.909	0.928	0.910	0.933	0.974	-0.530	-0.850	-0.527	0.582	-0.786	-0.902	-0.726	-0.853
Ti	-0.792	-0.762	-0.743	-0.766	-0.733	-0.798	-0.755	-0.794	-0.795	-0.810	-0.839	-0.819	-0.823	-0.840	0.436	0.836	0.373	-0.603	0.727	0.721	0.678	0.915
Al	-0.636	-0.903	-0.595	-0.613	-0.568	-0.626	-0.576	-0.633	-0.638	-0.633	-0.681	-0.661	-0.673	-0.830	0.030	0.949	0.000	-0.800	0.952	0.832	0.337	0.870
P	0.917	0.864	0.910	0.929	0.908	0.954	0.899	0.924	0.926	0.919	0.936	0.919	0.941	0.970	-0.560	-0.837	-0.546	0.569	-0.765	-0.890	-0.737	-0.840
H2O+	-0.473	-0.777	-0.477	-0.521	-0.486	-0.597	-0.451	-0.493	-0.496	-0.483	-0.514	-0.474	-0.527	-0.687	0.152	0.507	0.688	-0.102	0.584	0.748	0.850	0.898
H2O-	-0.973	-0.543	-0.966	-0.966	-0.971	-0.964	-0.982	-0.975	-0.973	-0.981	-0.969	-0.972	-0.967	-0.825	0.877	0.665	0.537	-0.511	0.468	0.623	0.635	0.524
CO2	0.906	0.849	0.900	0.920	0.900	0.950	0.890	0.914	0.916	0.910	0.926	0.908	0.931	0.957	-0.572	-0.809	-0.588	0.525	-0.736	-0.875	-0.772	-0.845
LOI	-0.929	-0.561	-0.929	-0.939	-0.940	-0.957	-0.942	-0.937	-0.935	-0.942	-0.931	-0.926	-0.933	-0.814	0.863	0.594	0.705	-0.358	0.427	0.636	0.789	0.602
Ba	0.564	0.589	0.556	0.533	0.523	0.467	0.529	0.548	0.551	0.531	0.550	0.566	0.551	0.619	-0.061	-0.792	0.449	0.944	-0.762	-0.607	0.297	-0.204
Co	-0.227	-0.473	-0.276	-0.315	-0.303	-0.393	-0.239	-0.253	-0.255	-0.228	-0.236	-0.200	-0.267	-0.396	0.154	0.071	0.841	0.329	0.198	0.507	0.788	0.519
Cu	0.277	0.634	0.294	0.282	0.263	0.235	0.236	0.268	0.274	0.232	0.263	0.266	0.280	0.492	0.315	-0.644	0.469	0.741	-0.766	-0.633	0.366	-0.181
Mo	-0.148	-0.002	-0.204	-0.228	-0.246	-0.290	-0.199	-0.172	-0.170	-0.160	-0.132	-0.115	-0.158	-0.098	0.462	-0.304	0.934	0.616	-0.291	0.094	0.735	0.119
Ni	-0.032	0.361	-0.059	-0.073	-0.101	-0.124	-0.092	-0.050	-0.045	-0.062	-0.021	-0.016	-0.027	0.167	0.573	-0.502	0.814	0.709	-0.598	-0.283	0.619	-0.084
Sr	0.777	0.800	0.779	0.811	0.788	0.864	0.767	0.792	0.794	0.787	0.803	0.776	0.813	0.864	-0.508	-0.655	-0.743	0.294	-0.625	-0.819	-0.895	-0.869
V	-0.702	-0.692	-0.740	-0.766	-0.759	-0.814	-0.713	-0.721	-0.722	-0.700	-0.701	-0.678	-0.727	-0.770	0.539	0.457	0.845	-0.100	0.464	0.765	0.855	0.647
Y	0.972	0.823	0.961	0.971	0.955	0.977	0.955	0.974	0.975	0.971	0.983	0.975	0.985	0.976	-0.623	-0.877	-0.437	0.678	-0.767	-0.861	-0.625	-0.753
As	-0.861	-0.959	-0.857	-0.870	-0.843	-0.876	-0.828	-0.864	-0.867	-0.849	-0.877	-0.862	-0.885	-0.990	0.339	0.946	0.277	-0.753	0.928	0.971	0.493	0.797
Cd	-0.452	-0.032	-0.478	-0.494	-0.515	-0.542	-0.501	-0.469	-0.465	-0.476	-0.442	-0.433	-0.451	-0.274	0.794	-0.090	0.943	0.364	-0.215	0.130	0.825	0.222
Cr	-0.276	-0.766	-0.228	-0.248	-0.196	-0.262	-0.203	-0.271	-0.277	-0.270	-0.330	-0.307	-0.320	-0.558	-0.369	0.782	-0.275	-0.695	0.866	0.645	0.071	0.743
Pb	-0.322	-0.616	-0.388	-0.416	-0.406	-0.467	-0.330	-0.344	-0.348	-0.303	-0.313	-0.284	-0.353	-0.526	0.105	0.226	0.677	0.106	0.385	0.676	0.605	0.454
Zn	0.460	0.617	0.447	0.429	0.410	0.370	0.415	0.445	0.449	0.427	0.456	0.466	0.456	0.577	0.106	-0.792	0.525	0.936	-0.802	-0.606	0.339	-0.251

	Ca	Ti	Al	P	H2O+	H2O-	CO2	LOI	Ba	Co	Cu	Mo	Ni	Sr	V	Y	As	Cd	Cr	Pb
Ti	-0.907																			
Al	-0.804	0.863																		
P	0.999	-0.903	-0.784																	
H2O+	-0.787	0.714	0.630	-0.779																
H2O-	-0.854	0.762	0.498	-0.870	0.441															
CO2	0.997	-0.902	-0.762	0.999	-0.799	-0.869														
LOI	-0.880	0.776	0.469	-0.897	0.590	0.974	-0.906													
Ba	0.439	-0.352	-0.636	0.427	0.046	-0.389	0.377	-0.220												
Co	-0.496	0.278	0.153	-0.497	0.842	0.241	-0.531	0.436	0.342											
Cu	0.297	-0.135	-0.570	0.274	-0.065	-0.054	0.228	0.056	0.876	0.115										
Mo	-0.232	0.019	-0.312	-0.253	0.492	0.275	-0.297	0.454	0.605	0.825	0.523									
Ni	-0.005	-0.057	-0.518	-0.034	0.189	0.237	-0.082	0.379	0.763	0.493	0.843	0.877								
Sr	0.946	-0.842	-0.664	0.948	-0.914	-0.766	0.962	-0.863	0.141	-0.724	0.076	-0.491	-0.249							
V	-0.831	0.589	0.413	-0.838	0.840	0.701	-0.857	0.816	-0.054	0.850	-0.067	0.702	0.395	-0.927						
Y	0.978	-0.885	-0.775	0.980	-0.640	-0.921	0.971	-0.904	0.549	-0.337	0.330	-0.138	0.038	0.871	-0.756					
As	-0.949	0.831	0.888	-0.941	0.689	0.742	-0.923	0.726	-0.667	0.365	-0.580	0.001	-0.288	-0.827	0.712	-0.942				
Cd	-0.424	0.297	-0.160	-0.452	0.445	0.611	-0.492	0.735	0.447	0.621	0.599	0.886	0.900	-0.602	0.710	-0.395	0.148			
Cr	-0.513	0.637	0.915	-0.483	0.490	0.107	-0.458	0.079	-0.559	0.024	-0.622	-0.515	-0.715	-0.385	0.118	-0.456	0.662	-0.482		
Pb	-0.542	0.225	0.240	-0.540	0.767	0.268	-0.556	0.412	0.032	0.928	-0.227	0.678	0.244	-0.686	0.859	-0.416	0.512	0.446	0.110	
Zn	0.397	-0.342	-0.686	0.378	0.011	-0.264	0.328	-0.106	0.983	0.338	0.920	0.677	0.858	0.108	0.006	0.482	-0.649	0.567	-0.672	0.034

Table 28. Suggested resource potential of Co-rich crusts within the EEZ of Pacific nations, Hawaii, and U.S. territories and possessions

Area	Relative Ranking	Potential[1]
R. of Marshall Islands	1	High
Johnston Island	2	High
French Polynesia	3	High
Kiribati	4	High
Hawaii	5	Medium
F.S. of Micronesia	6	Medium
Kingman-Palmyra	7	Medium
Howland-Baker	8	Medium
Wake	9	Medium
Northern Mariana Is	10	Low
Jarvis	11	Low
Tokelau	12	Low
Samoa	13	Low
Belau (Palau)	14	Low
Guam	15	Low

[1]Based on 11 criteria presented by Hein et al. (1988, 1990c)

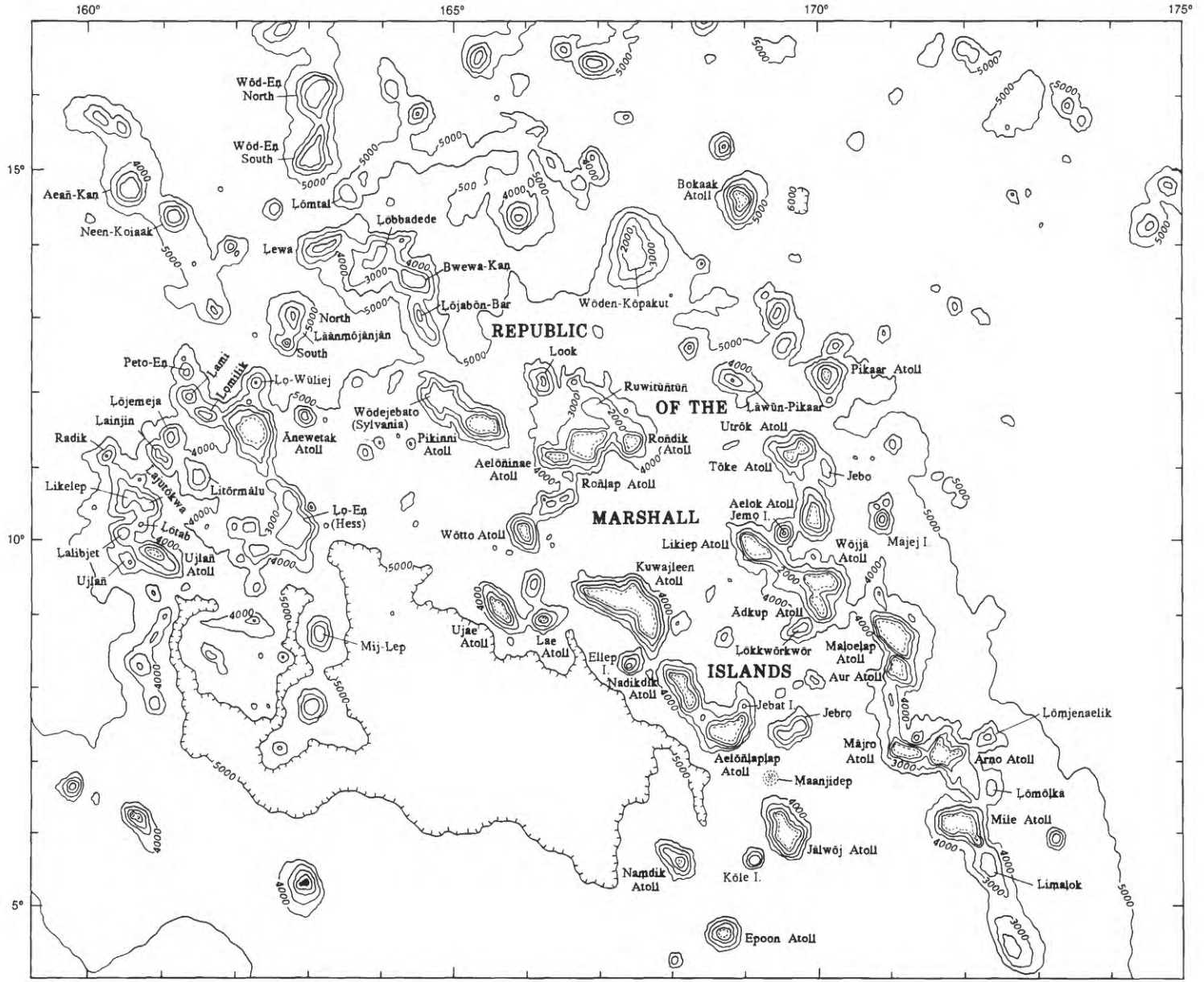

Figure 1. Atoll, island, and seamount names within the Exclusive Economic Zone of the Republic of the Marshall Islands. Dashed lines indicate atolls, except for Maanjidep Seamount, which was discovered on cruise F10-89-CP with only one line crossing it, so it is dashed. Common names used in previous publications for seamounts include: Sylvania for Wōdejebato; Hess for Ḷo-Eṇ; and Van Valtier for Ḷōmjenaelik. Contour interval = 1000 m, modified from Chase and Menard (1973).

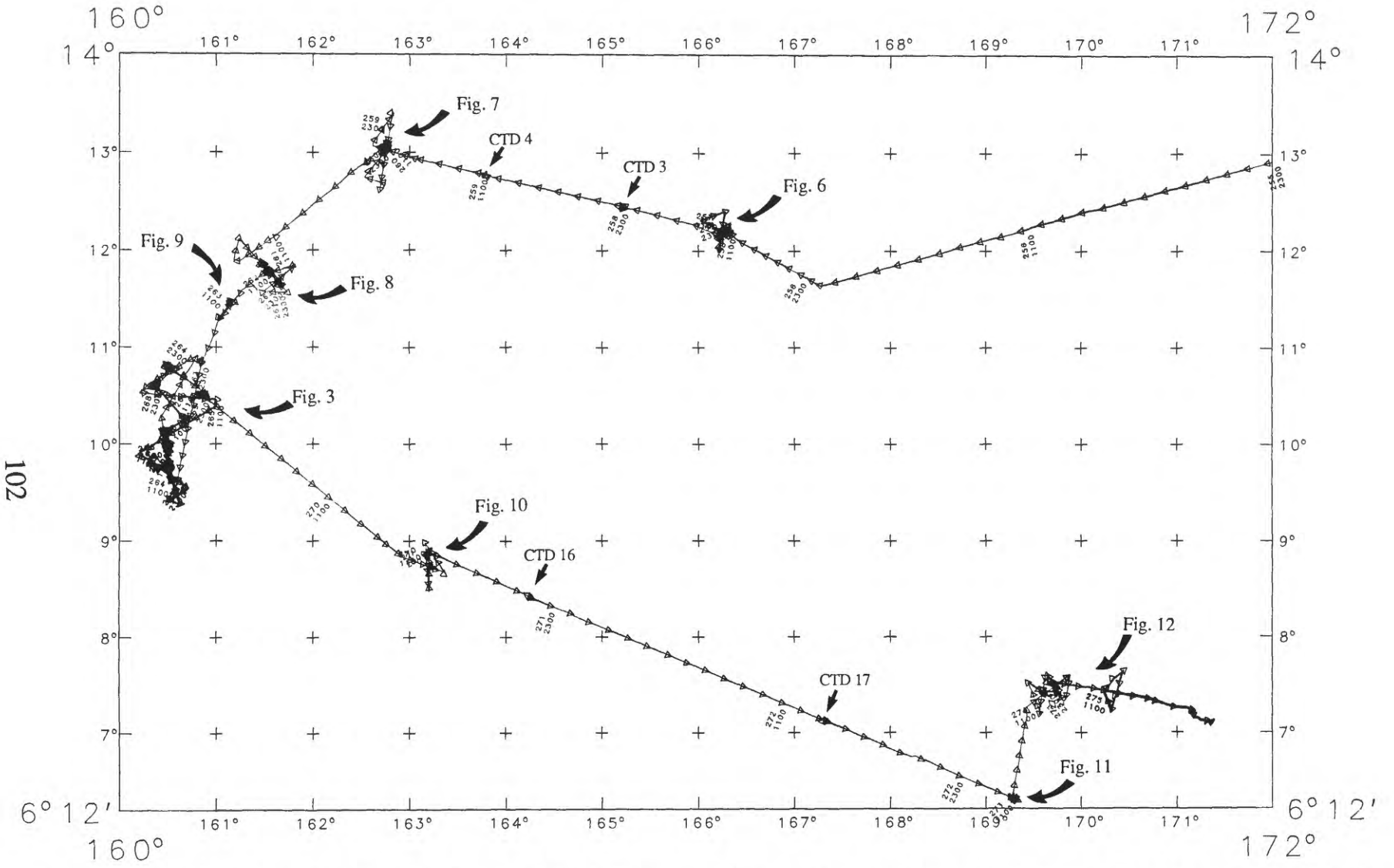

Figure 2. Trackline chart of cruise F10-89-CP. Seismic lines, tracklines, and stations for each seamount studied are detailed in the individual figures indicated. Note the location of open ocean CTD stations 3, 4, 16, and 17. Numbers along the trackline are the Julian day and hour of passage.

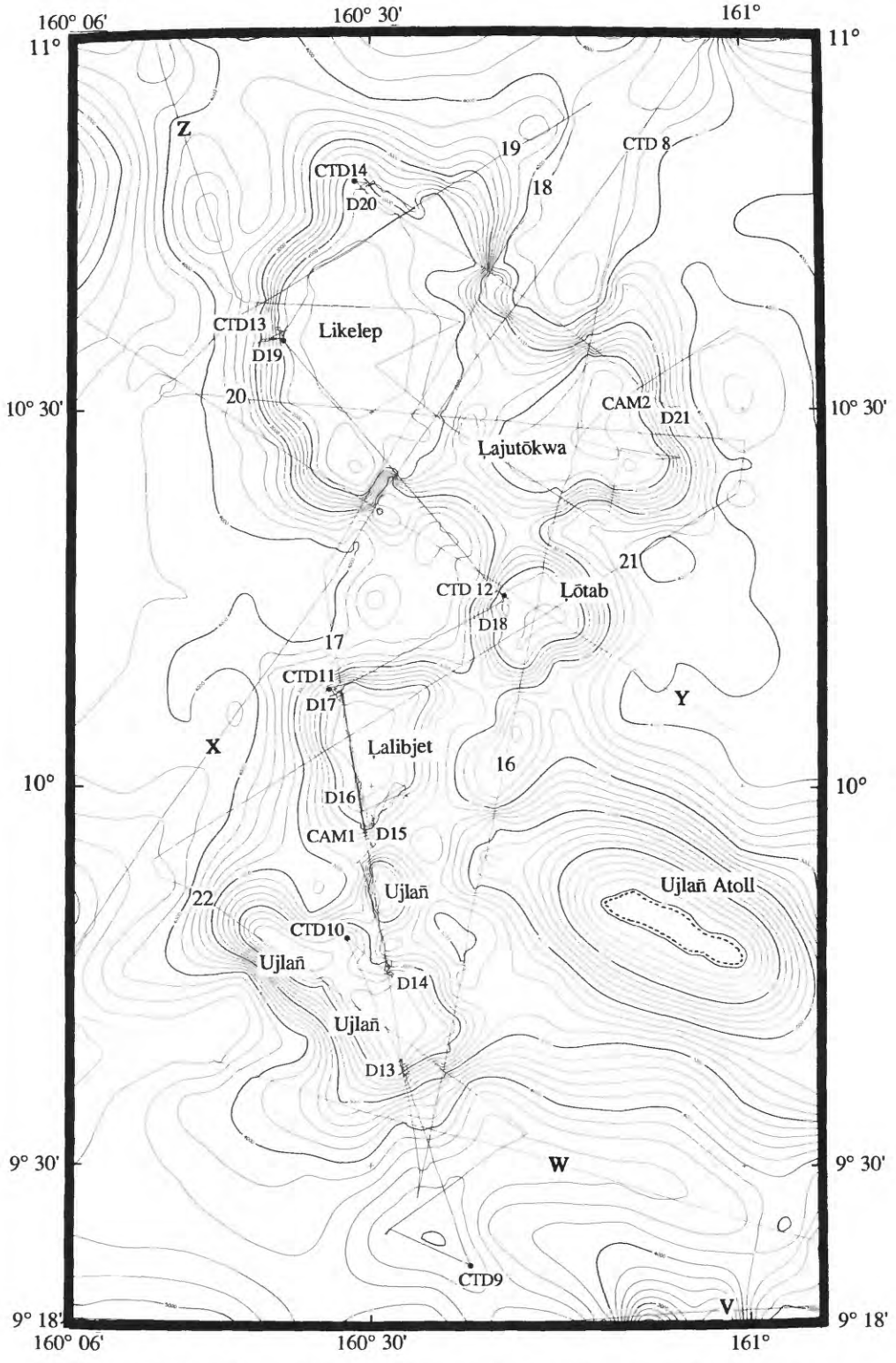

Figure 3. Trackline and station map for the Ujlañ volcanic complex. The bathymetry used for this figure is from our seven seismic lines (16-22), from transit lines between stations, and from 5 lines obtained from the National Geophysical Data Center (NGDC): **V**, Scripps Institution of Oceanography Argo Cruise A5-69-NP, D. Karig, Chief; **W**, Deep Sea Drilling Project Glomar Challenger Cruise Leg 61, R.L. Larson, S.O. Schlanger, Chiefs; **X**, U.S. Geological Survey Cruise L8-82-NP, D. Clague, Chief; **Y**, Deep Sea Drilling Project Cruise Leg 89, R. Moberly and S.O. Schlanger, Chiefs; **Z**, Lamont-Doherty Geological Observatory Cruise V1-77-SP, B. Heezen, Chief. Areas of no data filled in with NGDC, ETOPO5. Notice that Ujlañ Seamount consists of three peaks whereas the other seamounts consist of one. D = Dredge, Cam = Camera-video survey, CTD = Temperature-oxygen profile. Contour interval is 200m.

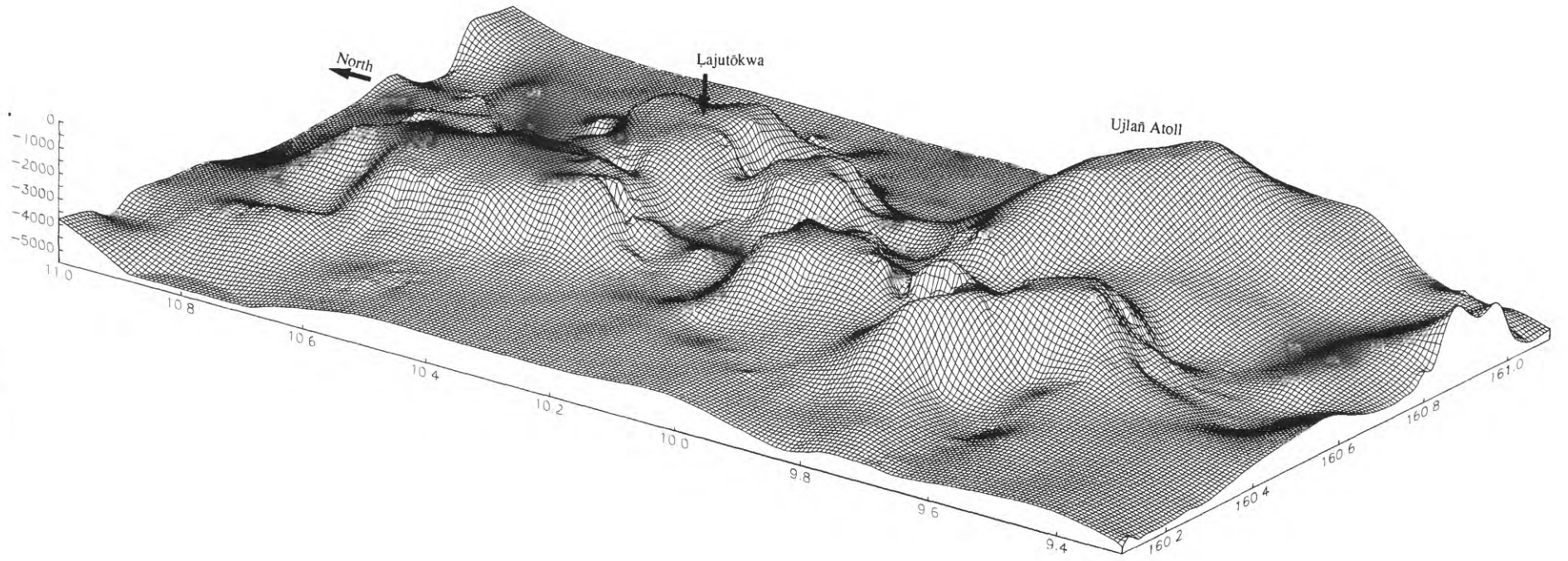

Figure 4. Computer generated physiographic map of Ujlañ volcanic complex derived from the bathymetry in Figure 3. View looking to the northeast from 235° azimuth at 20° elevation; vertical exaggeration is 4 times.

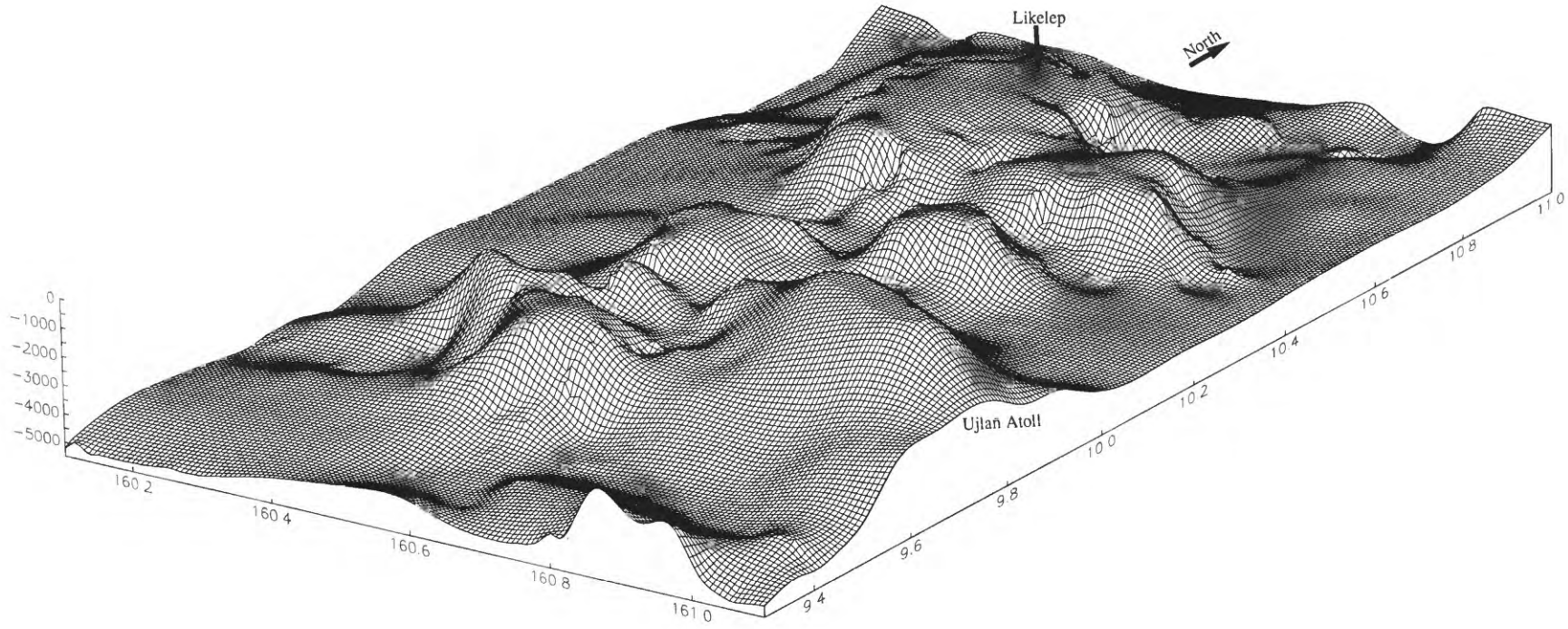

Figure 5. Same as Figure 4 except looking to the northwest from 145° azimuth. Note the three peaks of Ujlañ Seamount.

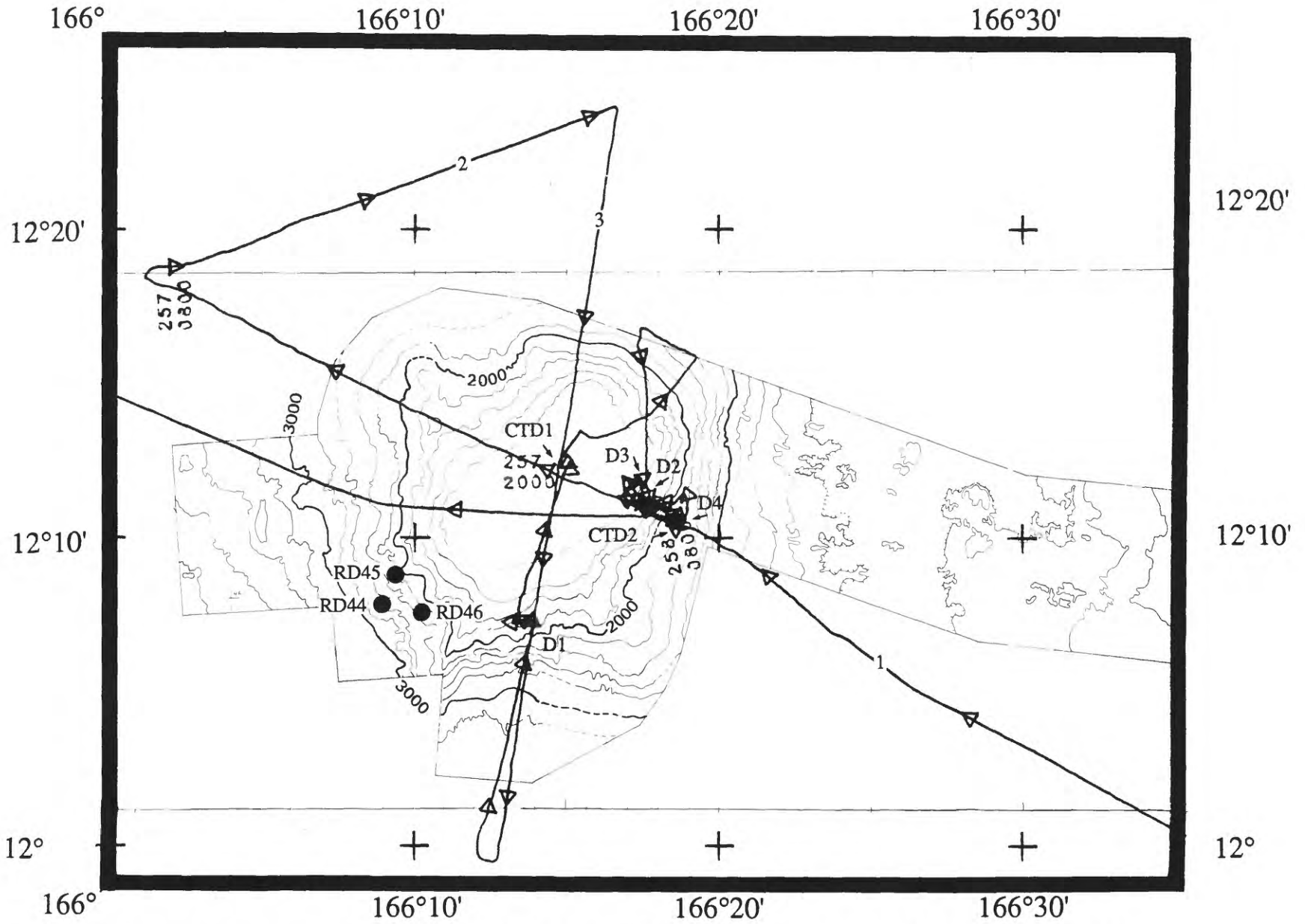

Figure 6. Trackline and station map for Look Seamount; bathymetry from Duennebier and Schlanger (1988). D = Dredge from F10-89-CP; RD = Dredge from MW-88-05; CTD = Temperature-oxygen profile. Contour interval is 200m.

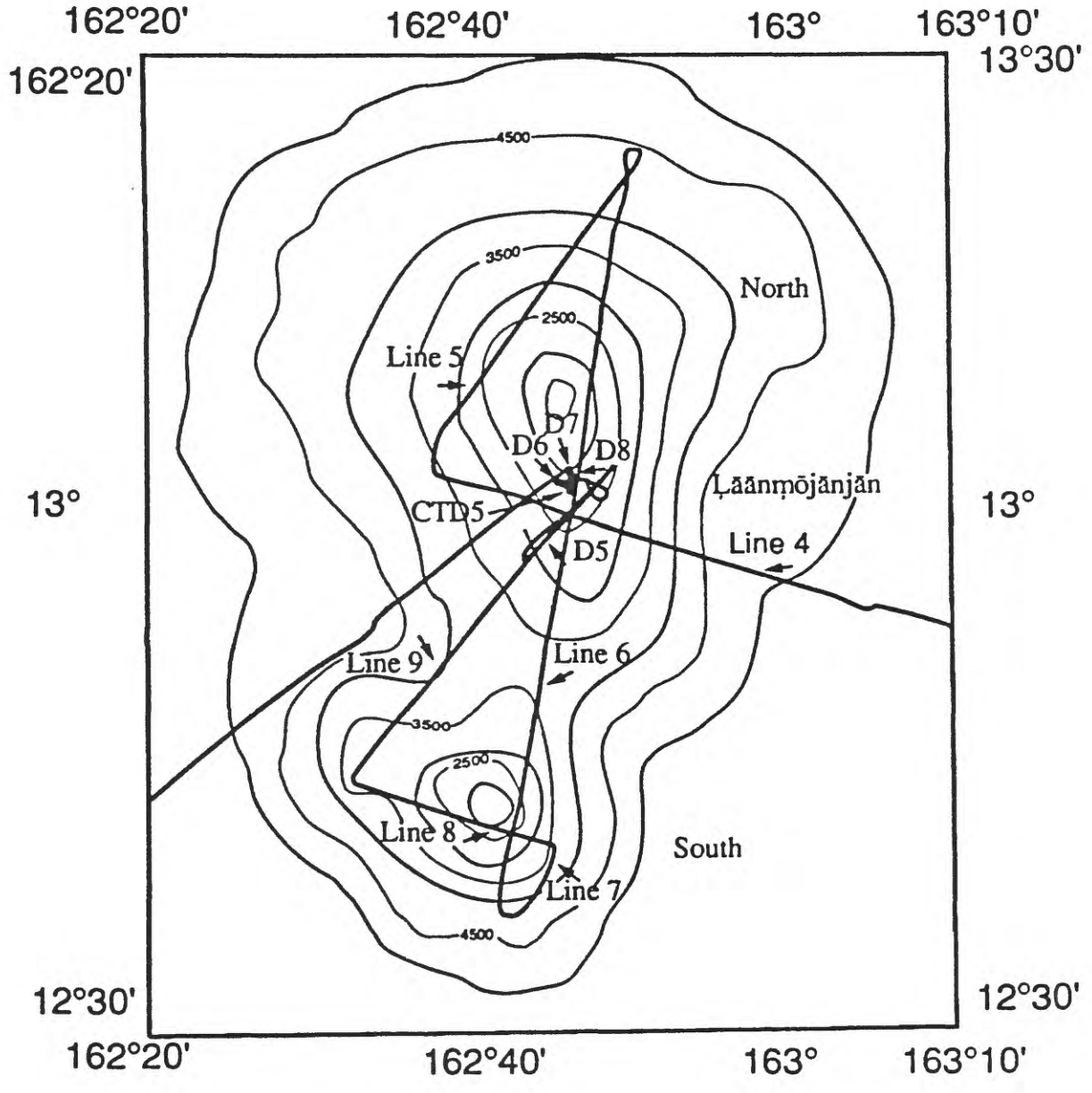

Figure 7. Trackline and station map for North and South Ļāānmōjānjān Seamounts; bathymetry modified from Chase and Menard (1973). The summit of South Ļāānmōjānjān Seamount is 7 km west northwest of the summit indicated on this topographic map. D = Dredge, CTD = Temperature-oxygen profile. Contour interval is 500 m.

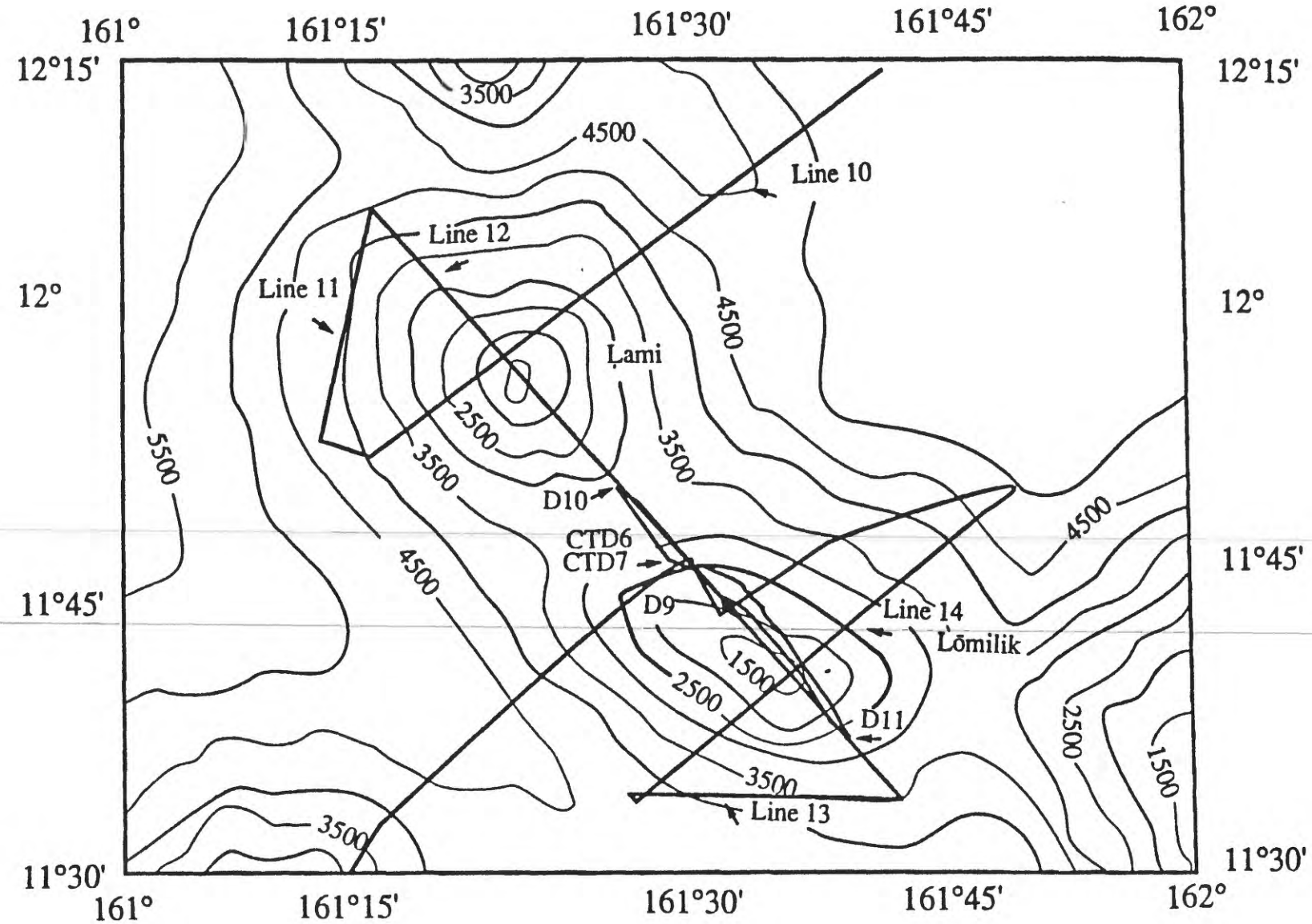

Figure 8. Trackline and station map for Lami and Lomilik Seamounts; bathymetry modified from Chase and Menard (1973). D = Dredge, CTD = Temperature-oxygen profile. Contour interval is 500 m.

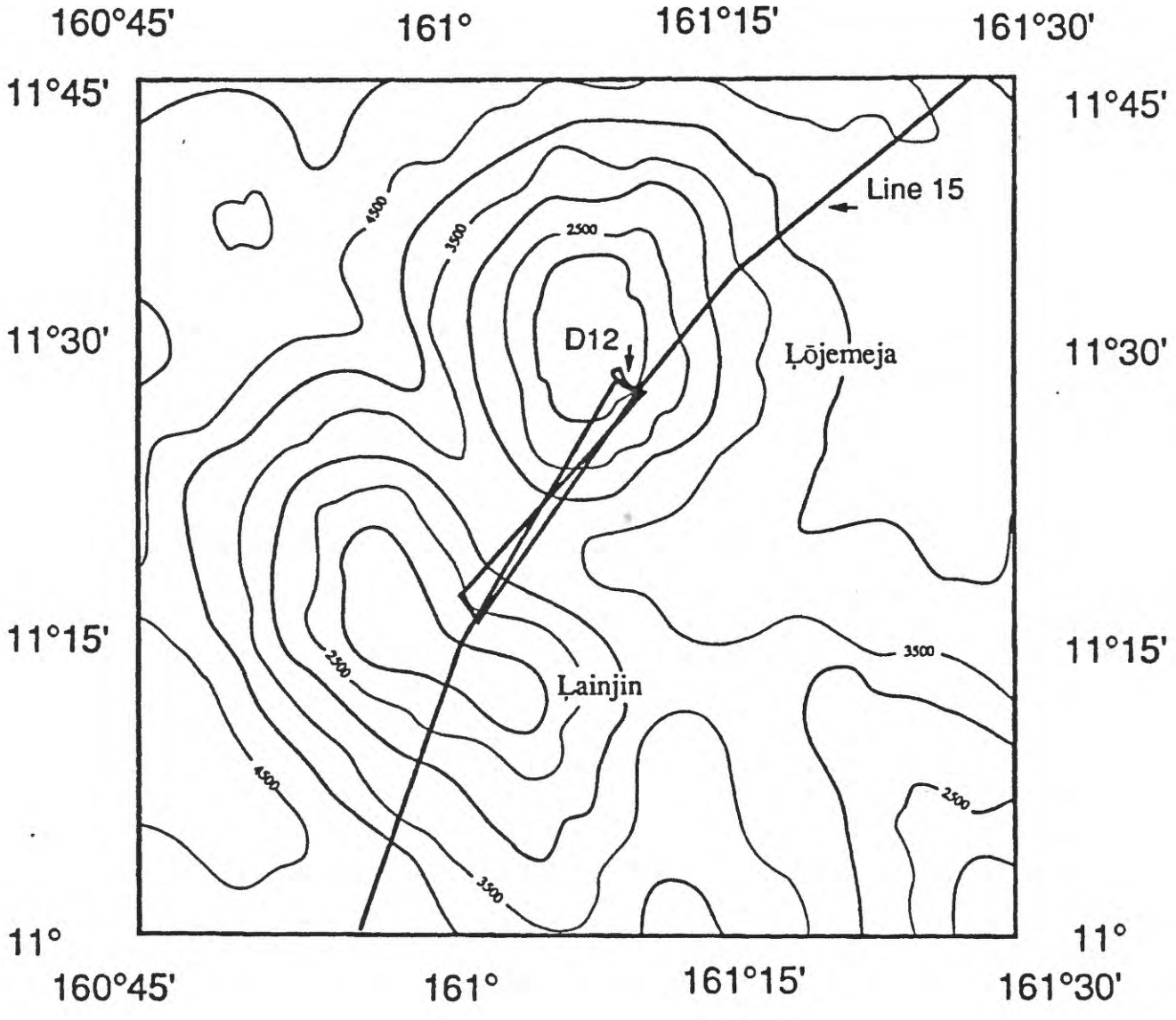

Figure 9. Trackline and station map for Ļōjemeja and Ļainjin Seamounts; bathymetry modified from Chase and Menard (1973). D = Dredge, CTD = Temperature-oxygen profile. Contour interval is 500 m.

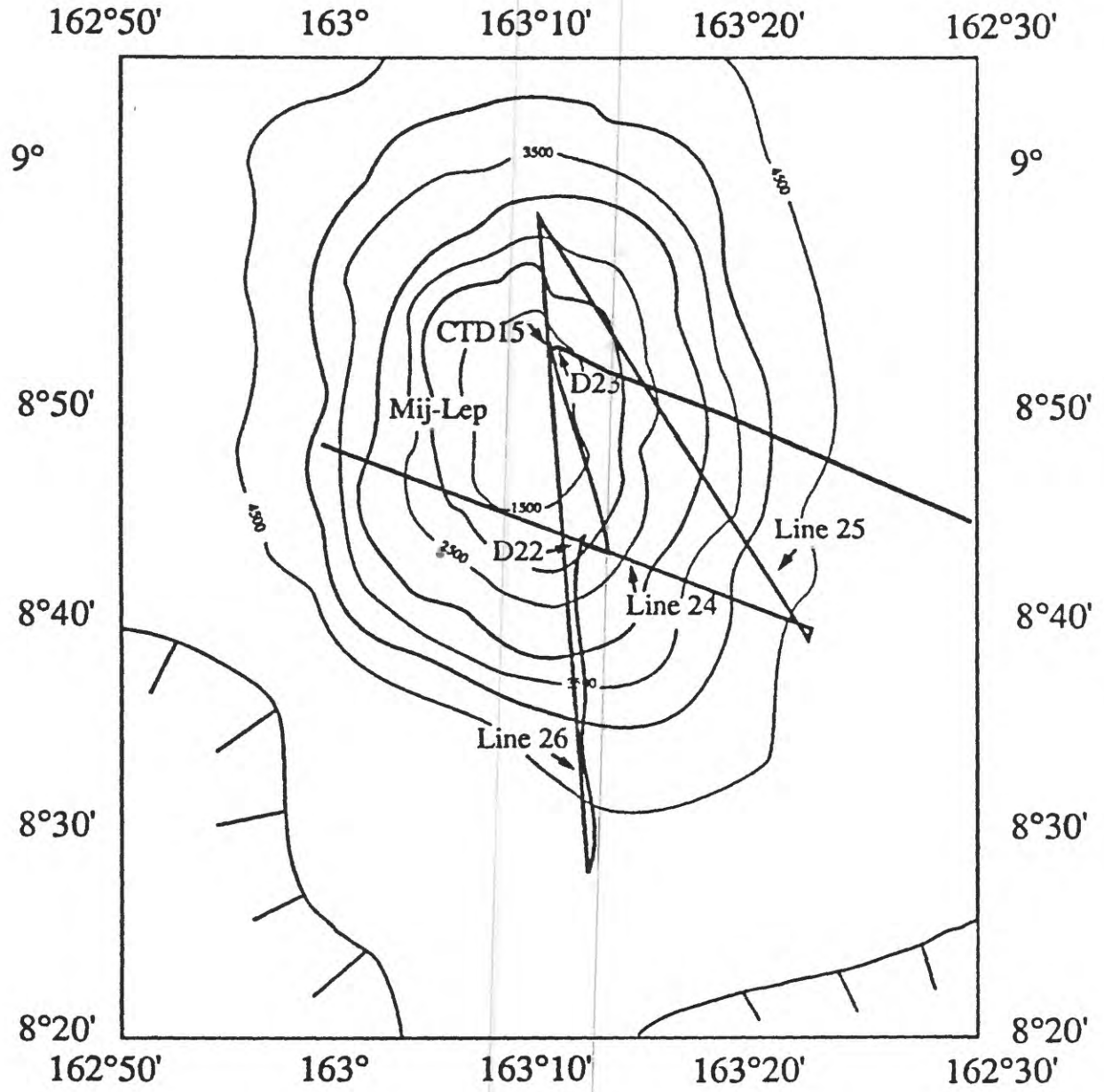

Figure 10. Trackline and station map for Mij-Lep Seamount; bathymetry modified from Chase and Menard (1973). D = Dredge, CTD = Temperature-oxygen profile. Contour interval is 500 m.

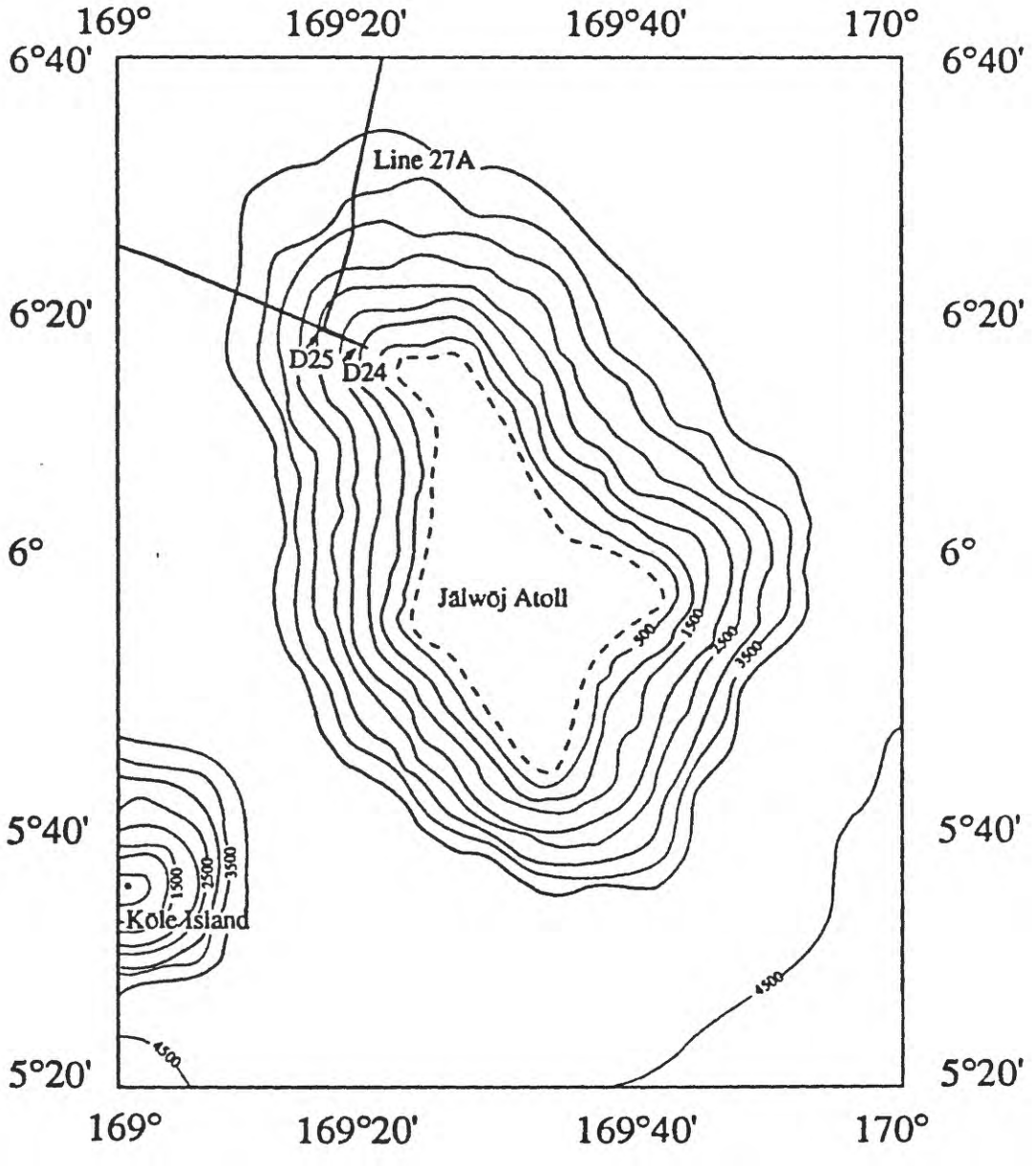

Figure 11. Trackline and station map for Jālwōj Seamount; bathymetry modified from Chase and Menard (1973). D = Dredge, CTD = Temperature-oxygen profile. Contour interval is 500 m.

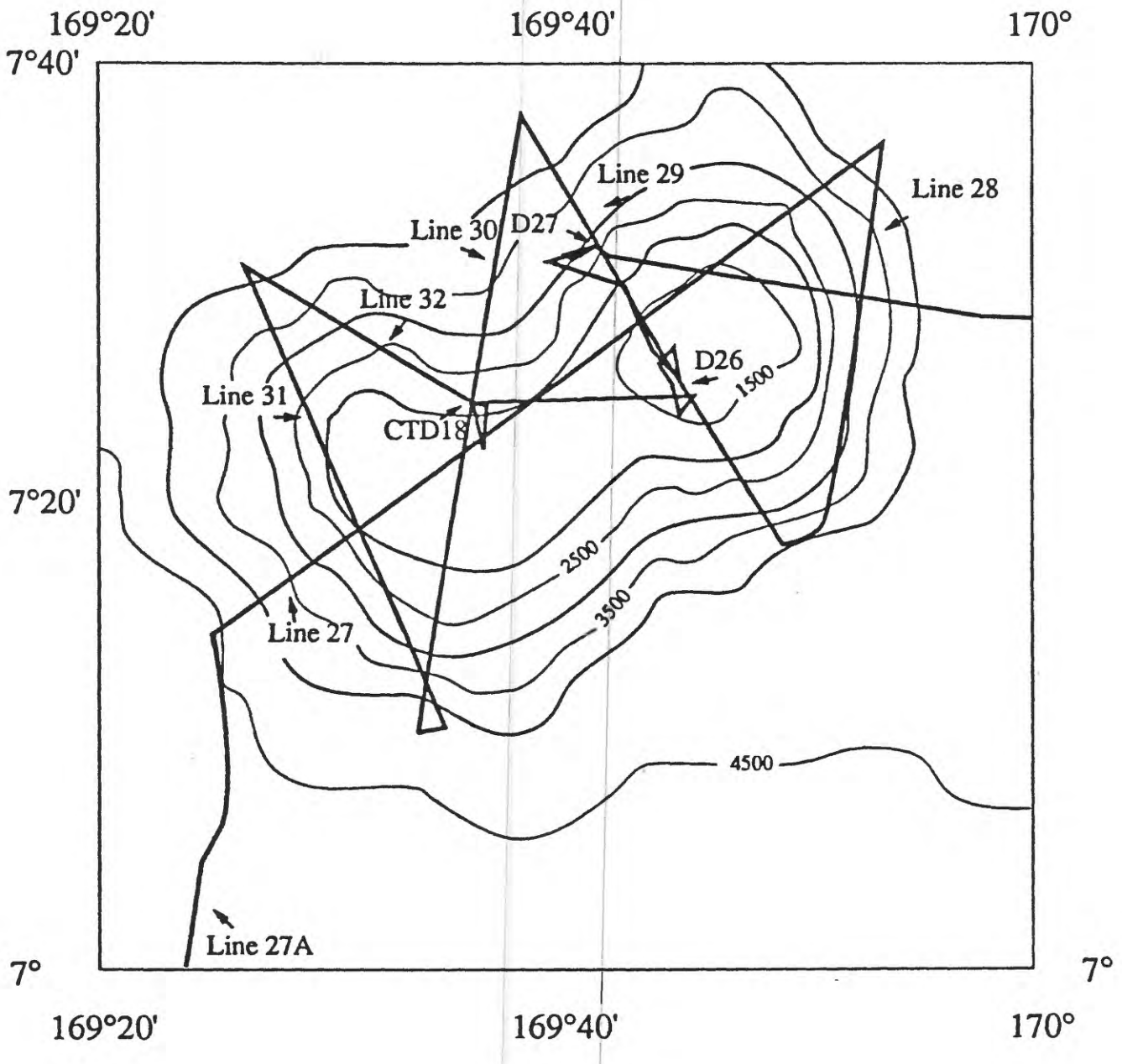

Figure 12. Trackline and station map for Jebro Seamount; bathymetry modified from Chase and Menard (1973). D = Dredge, CTD = Temperature- oxygen profile. Contour interval is 500 m.

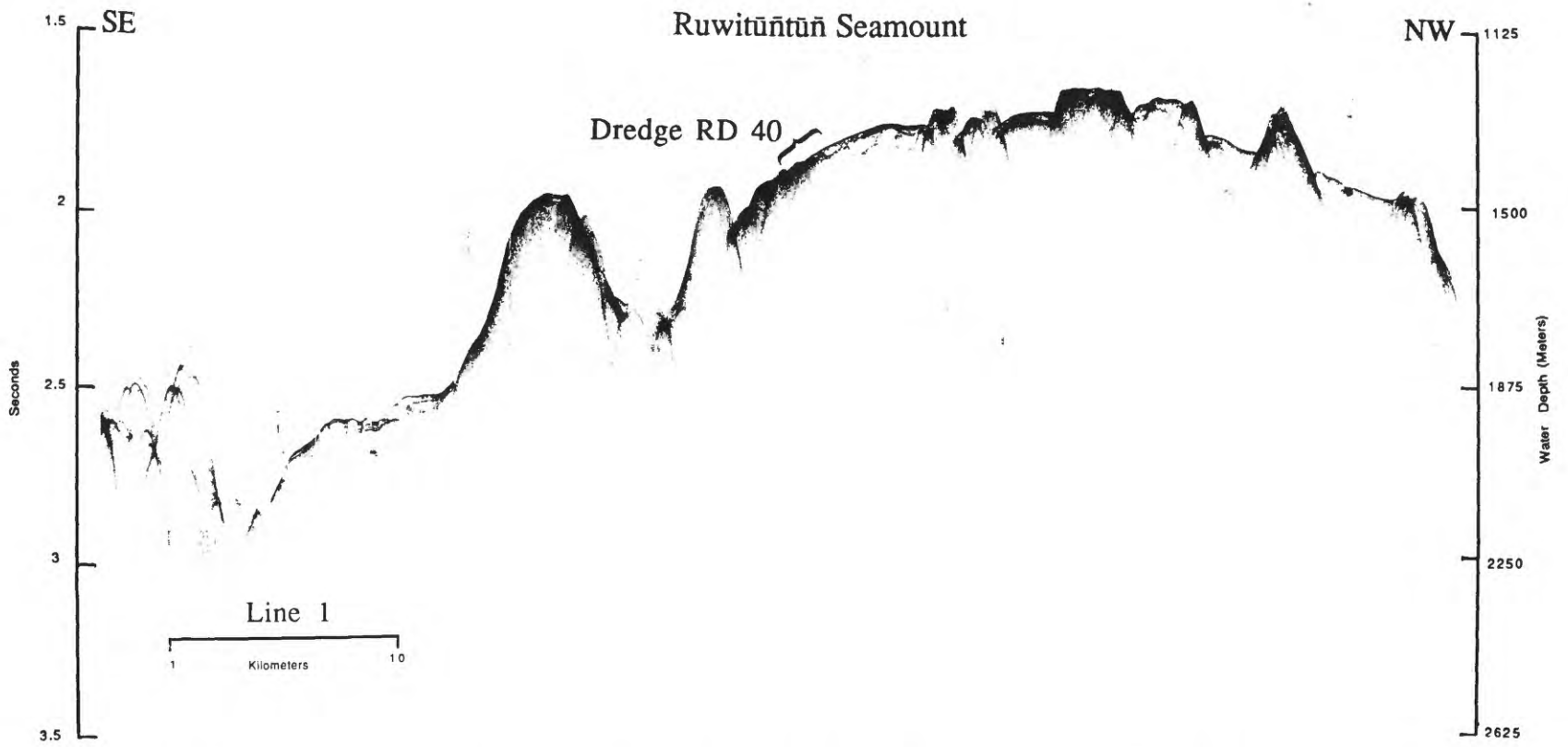

Figure 13. Ruwitūñtūñ Seamount, southeast third of 3.5 kHz line 1. MW-88-05 dredge RD40 is located on the southeast flank.

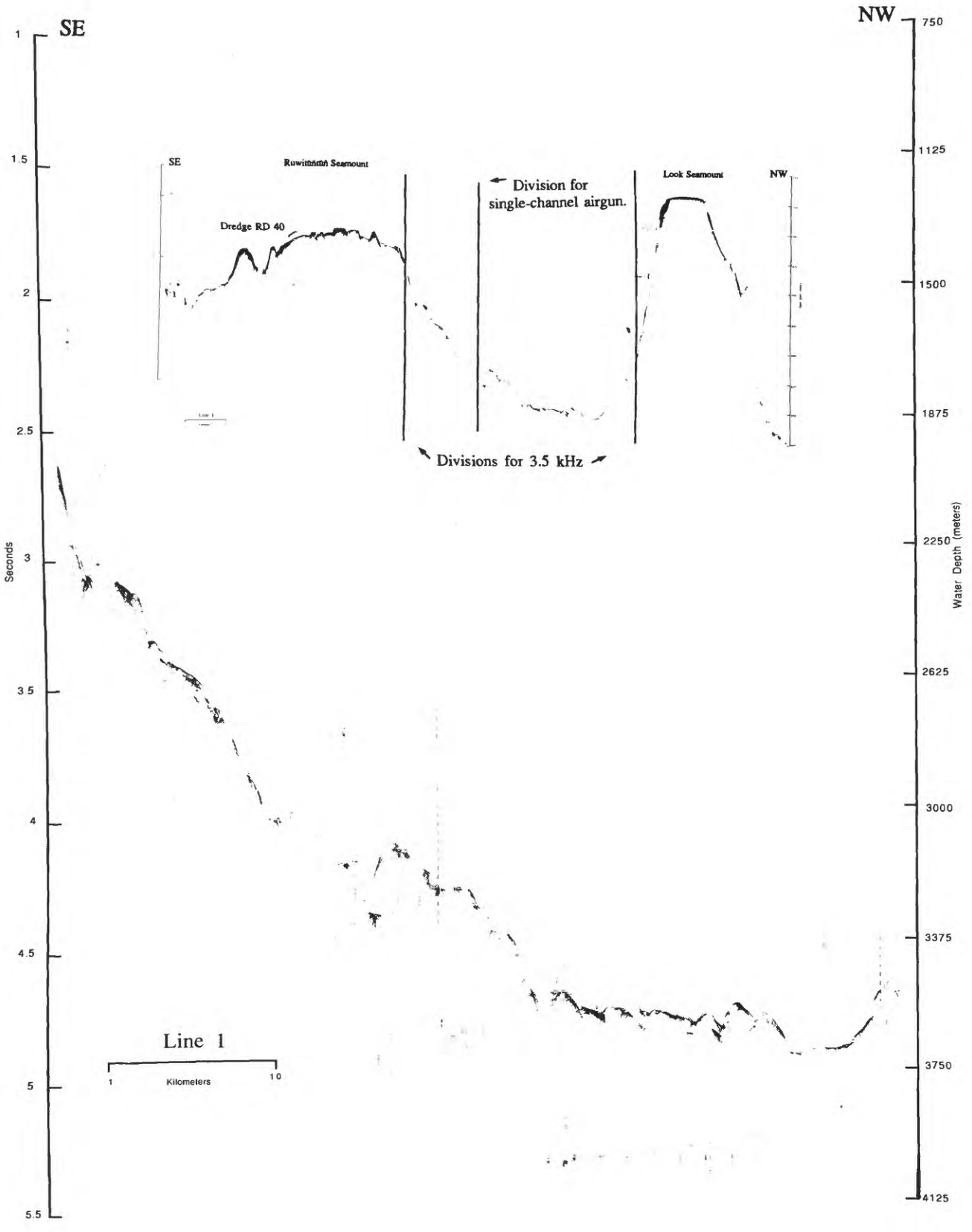

Figure 14. Saddle between Ruwitūntūn and Look Seamounts, central third of 3.5 kHz line 1. Inset shows the complete line 1 and places it was divided for Figures 13, 14, and 15.

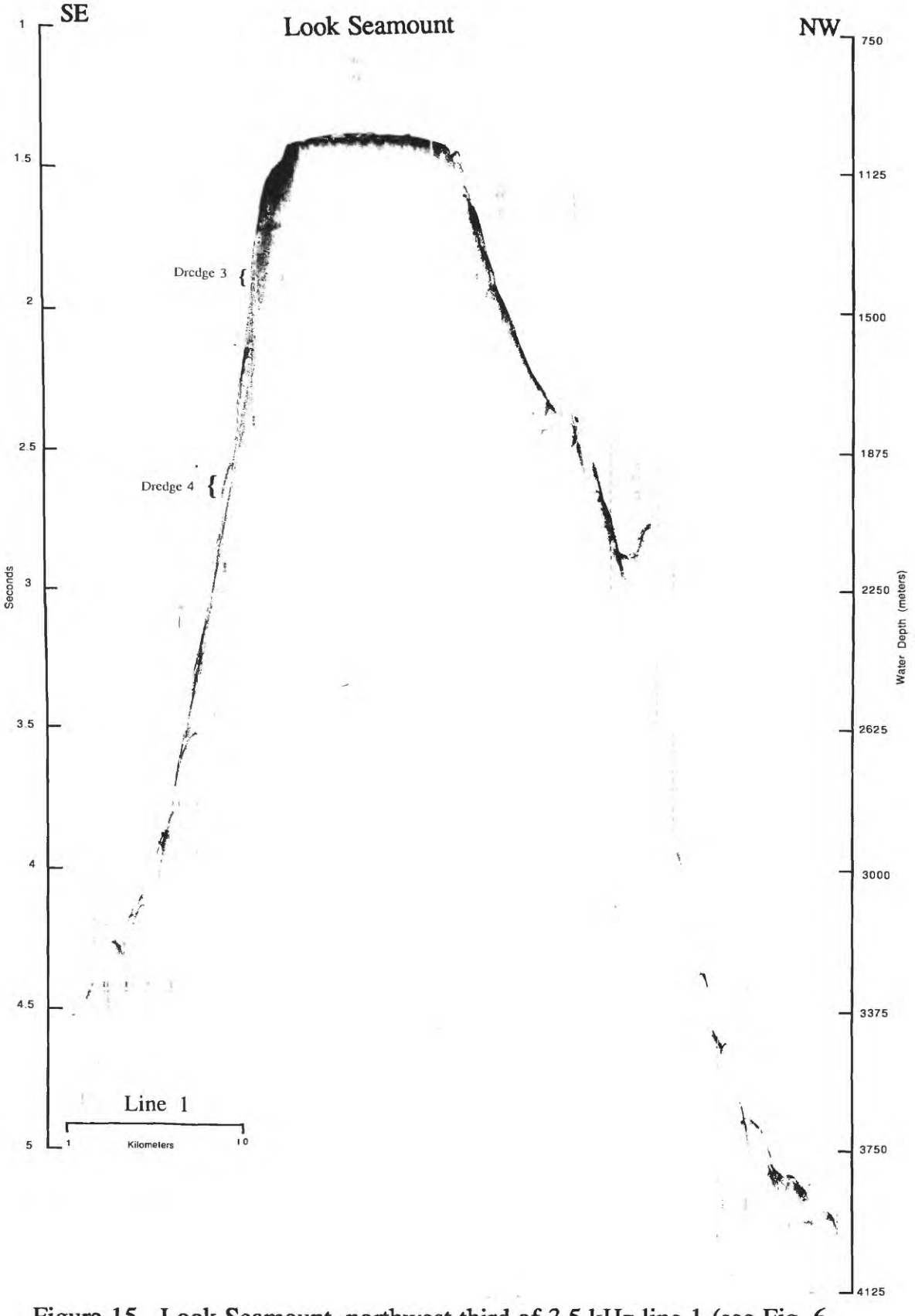

Figure 15. Look Seamount, northwest third of 3.5 kHz line 1 (see Fig. 6 for location). Dredges D3 and D4 are located on the southeast flank.

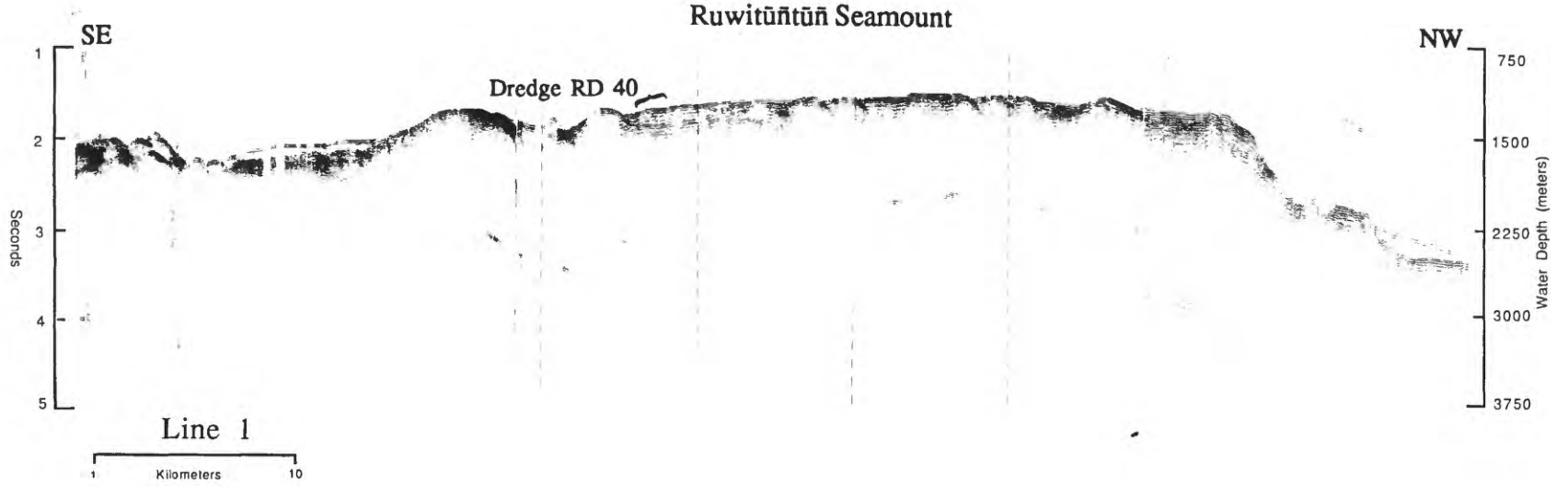

Figure 16. Ruwitūñtūñ Seamount, southeast half of 40 in^3, single-channel airgun line 1. Note location of dredge RD40.

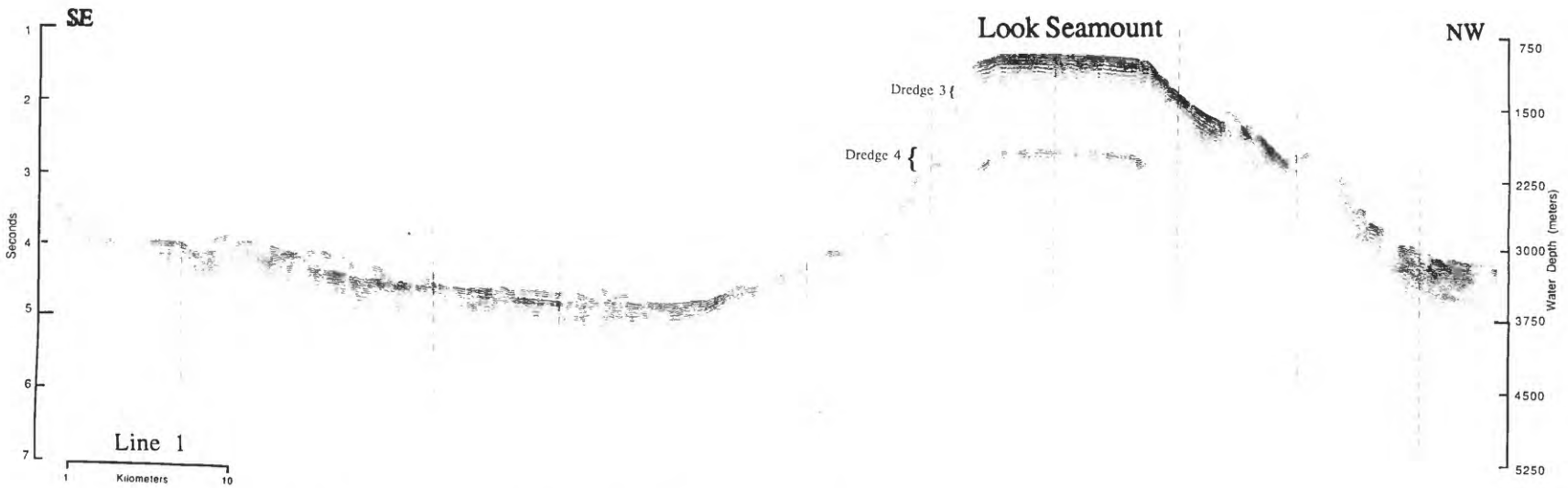

Figure 17. Look Seamount and saddle between Look and Ruwitūñtūñ Seamounts, northwest half of 40 in^3, single-channel airgun line 1 (see Fig. 6 for location). Note location of dredges D3 and D4.

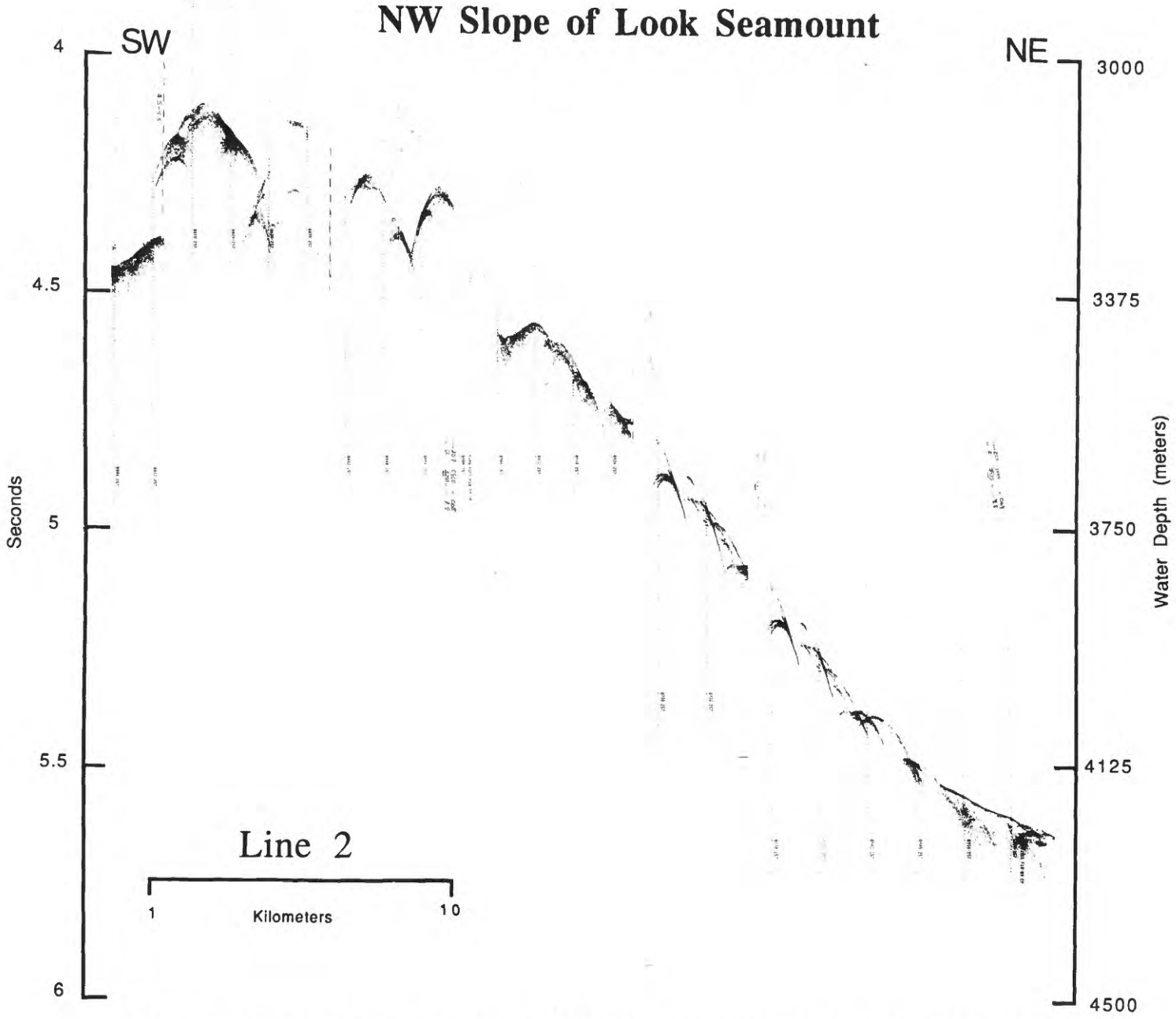

Figure 18. Lower northwest flank of Look Seamount, 3.5 kHz line 2 (see Fig. 6 for location).

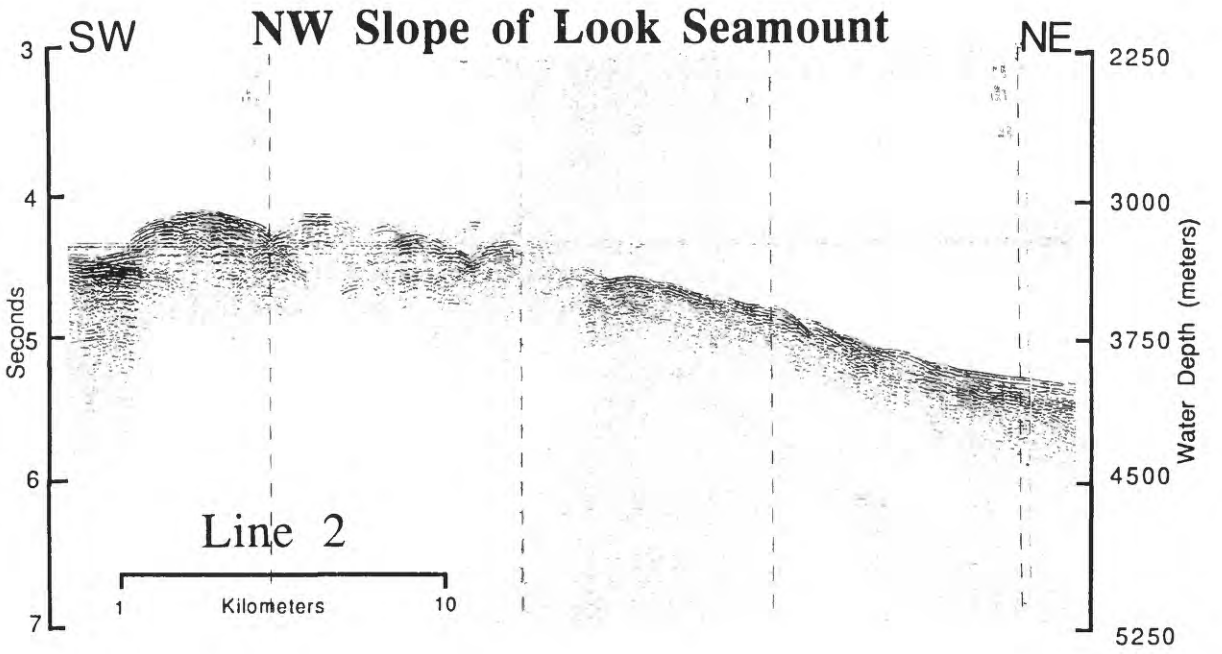

Figure 19. Lower northwest flank of Look Seamount, 40 in^3 single-channel airgun line 2.

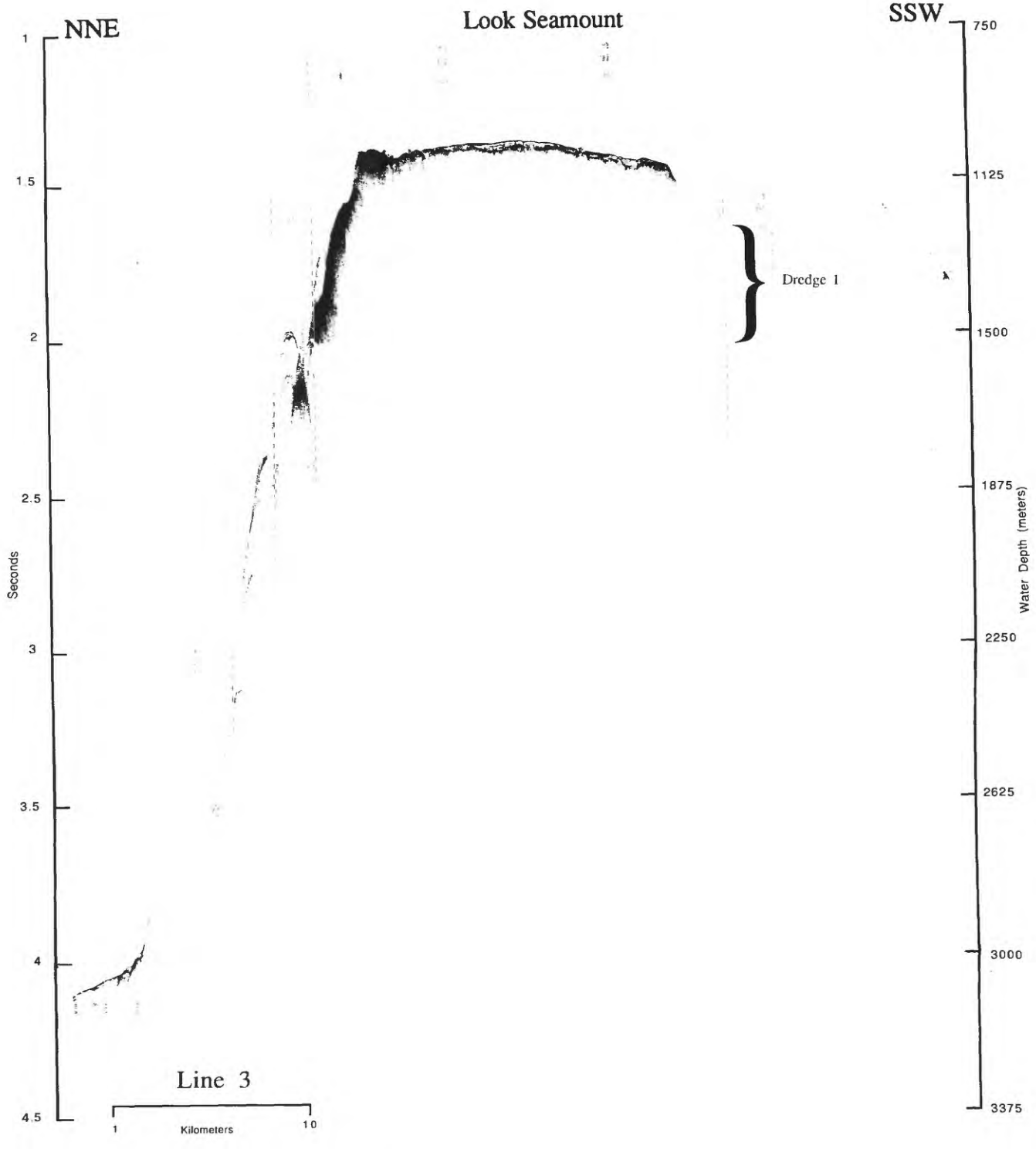

Figure 20. Look Seamount, 3.5 kHz line 3 (see Fig. 6 for location). Note location of dredge 1.

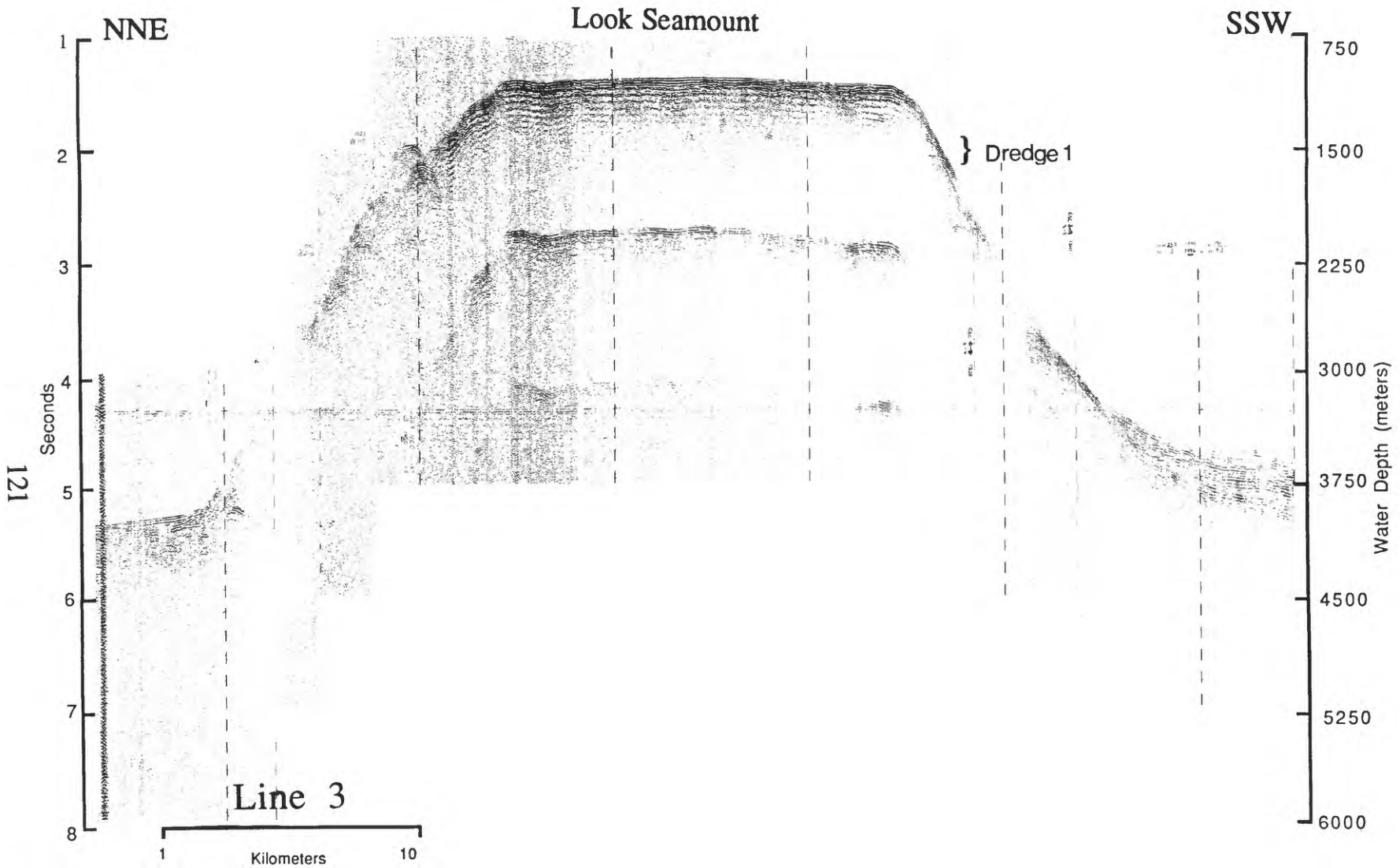

Figure 21. Look Seamount, 40 in^3 single-channel airgun line 3.

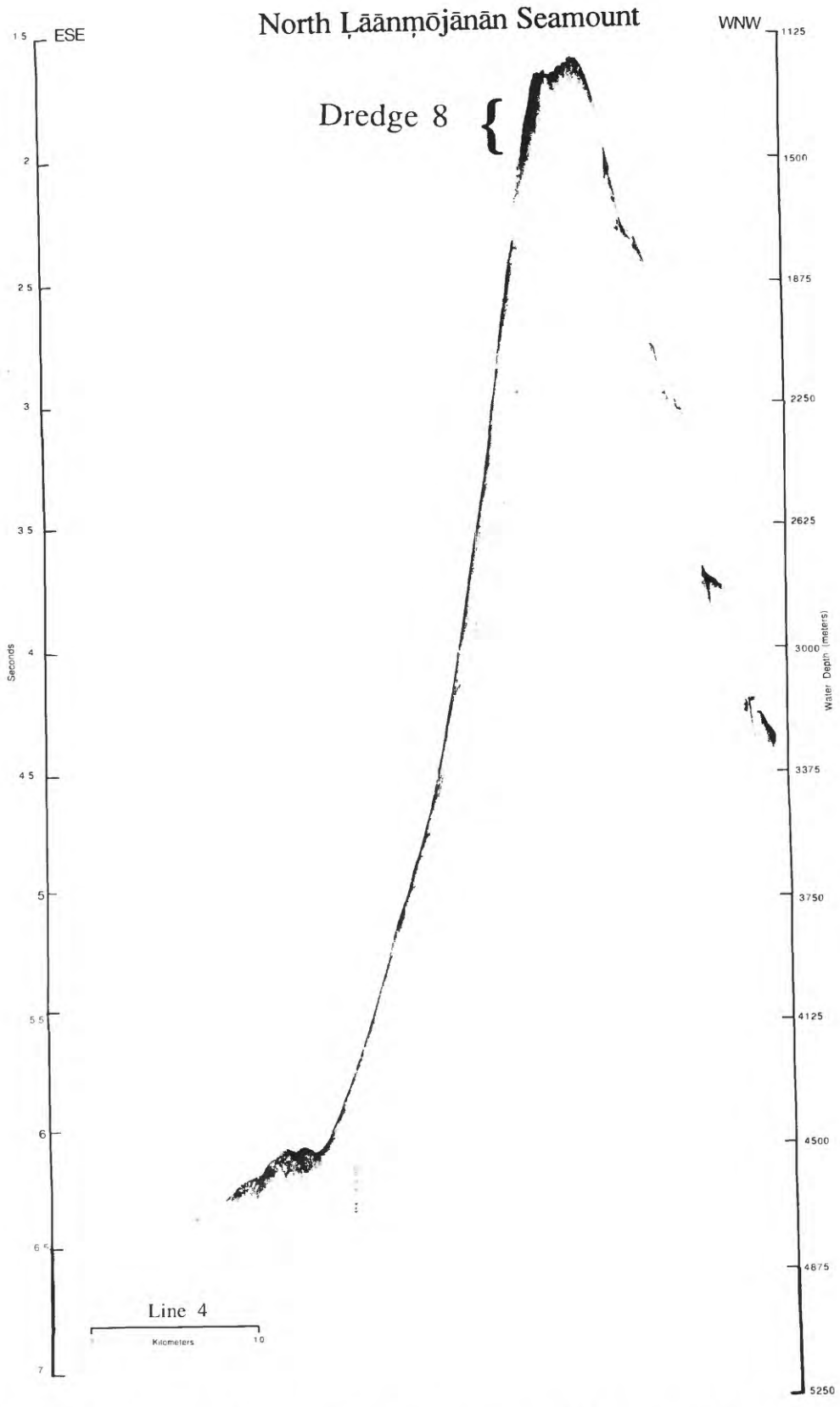

Figure 22. North Ḷāānṃōjānjān Seamount, 3.5 kHz line 4 (see Fig. 7 for location). Note location of dredge D8.

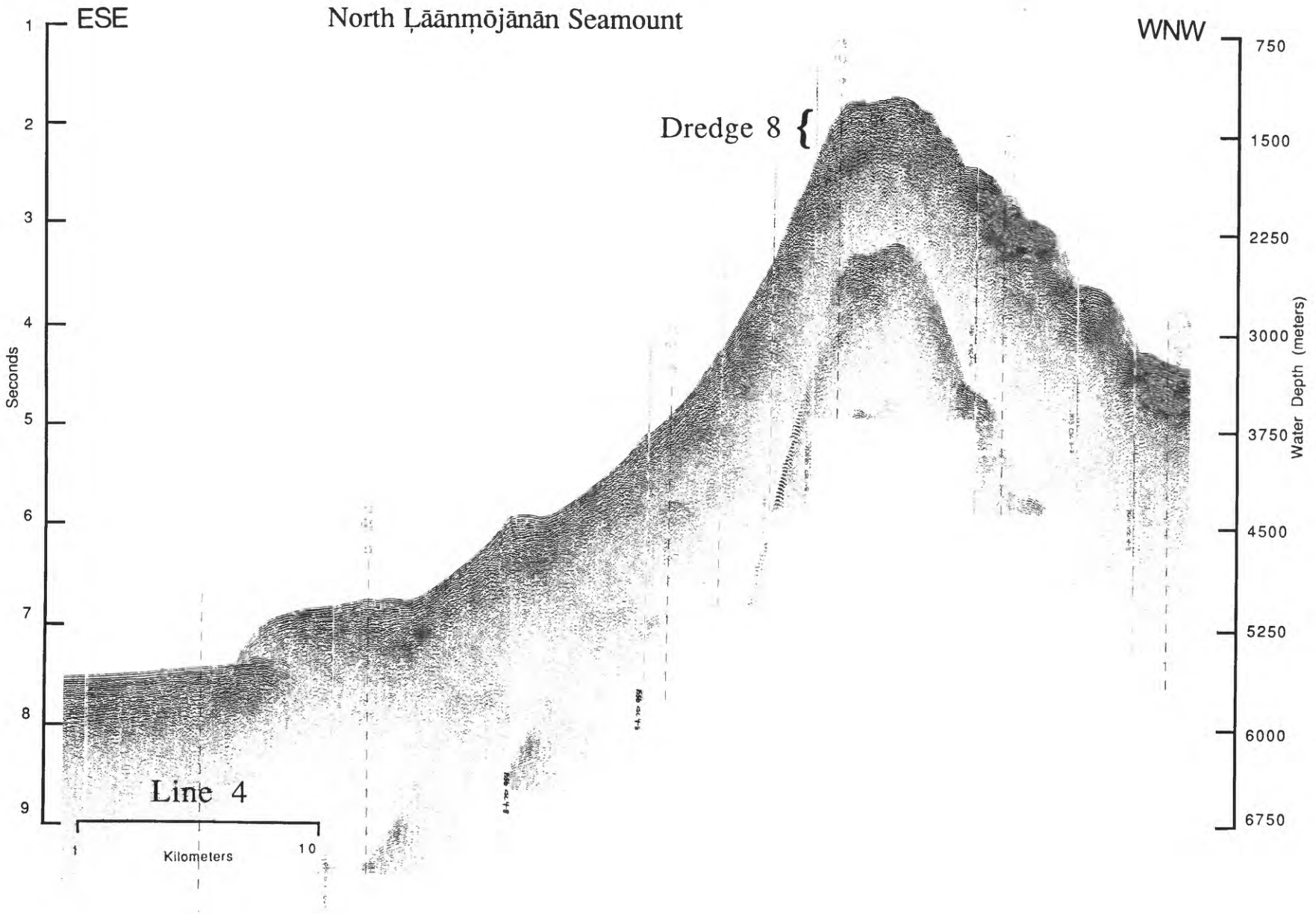

Figure 23. North Ļāānṃōjānjān Seamount, 160 in^3 single-channel airgun line 4.

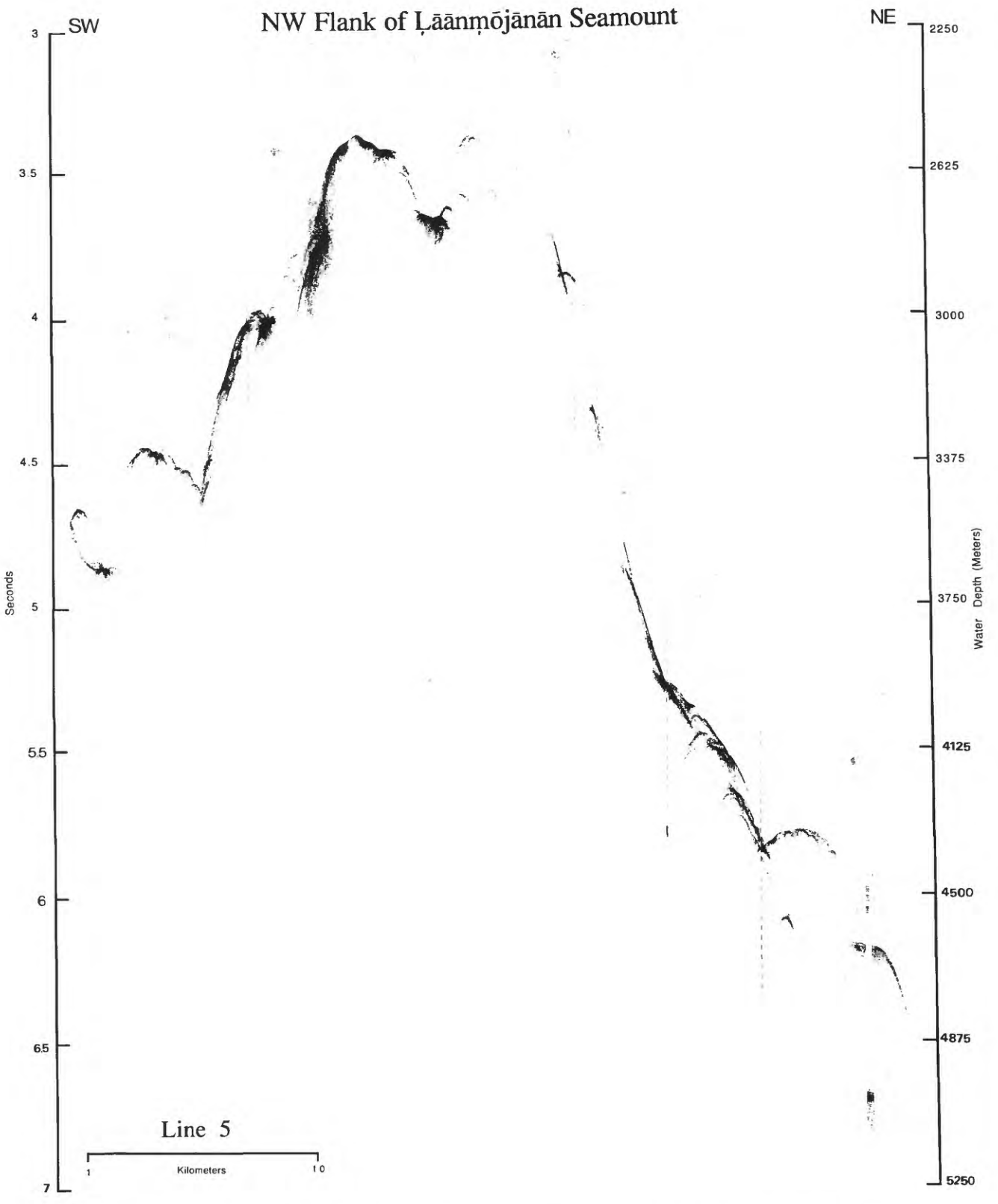

Figure 24. Northwest flank of North Ļāānṃōjānjān Seamount, 3.5 kHz line 5 (see Fig. 7 for location).

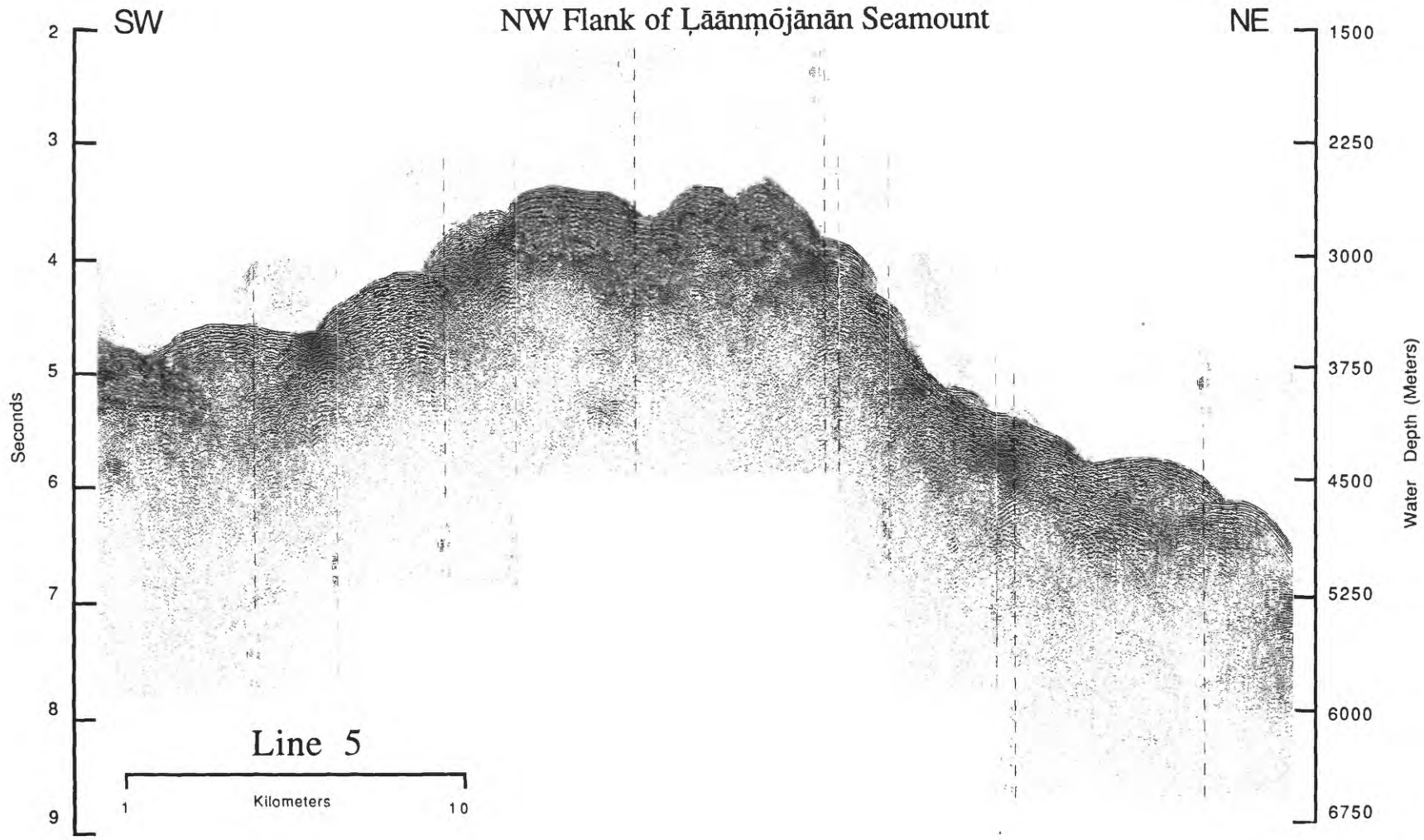

Figure 25. Northwest flank of North Ļāānṃōjānjān Seamount, 160 in^3 single-channel airgun line 5.

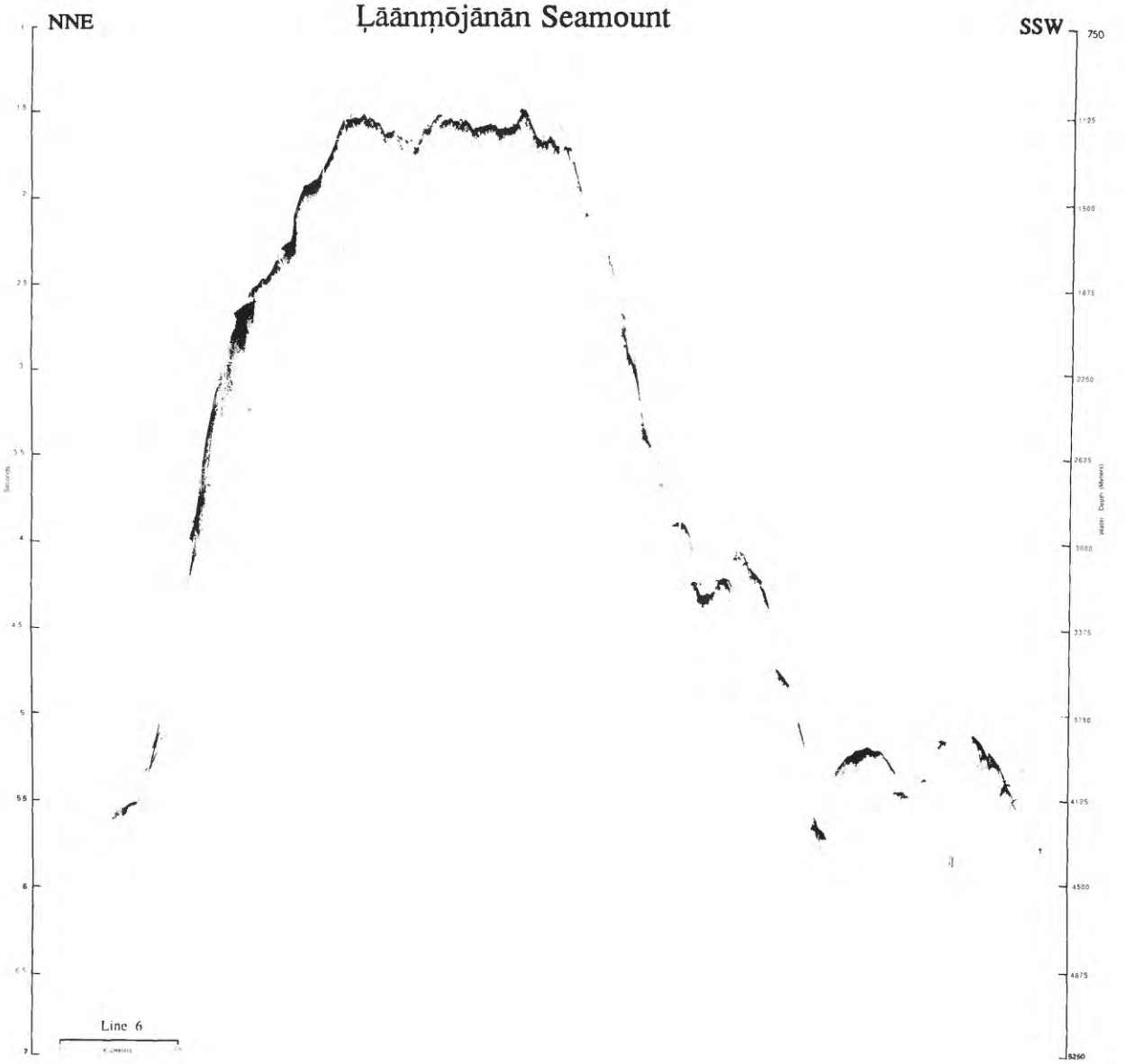

Figure 26. North Ļāānmōjānjān Seamount and southeast flank of South Ļāānmōjānjān Seamount, 3.5 kHz line 6 (see Fig. 7 for location).

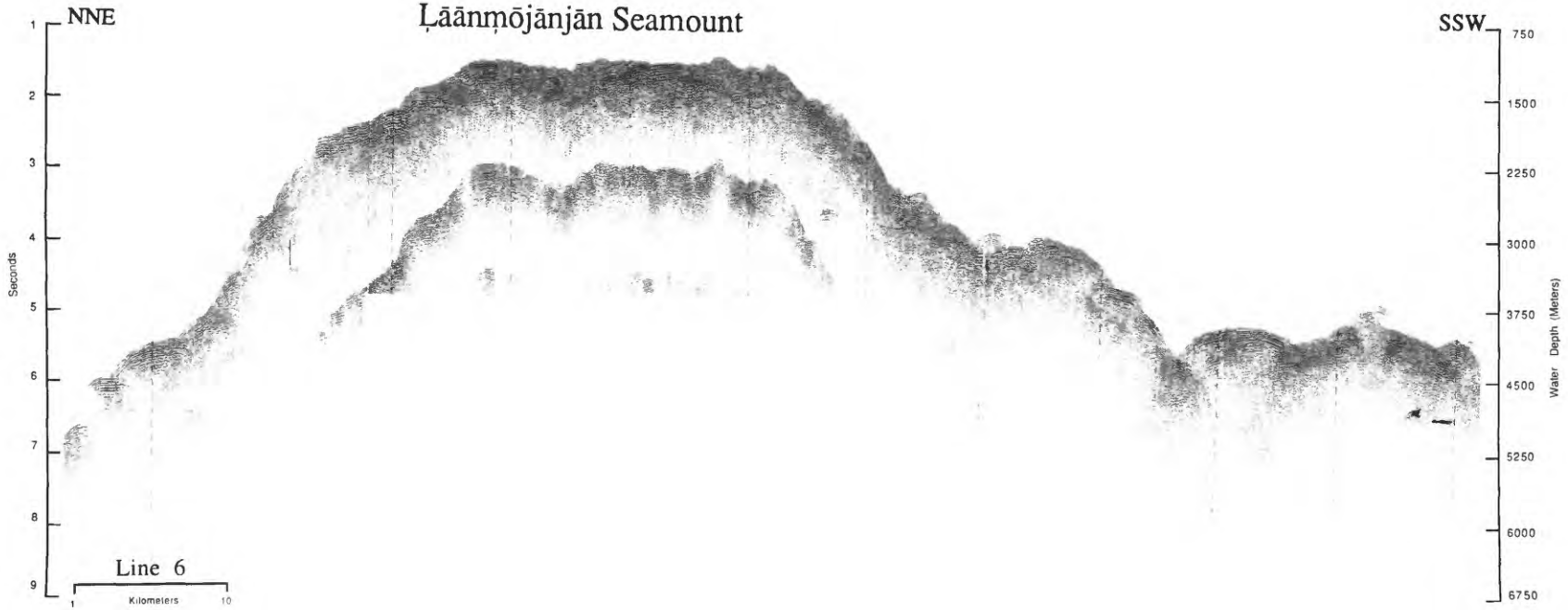

Figure 27. North Ļāānmōjānjān Seamount and southeast flank of South Ļāānmōjānjān Seamount, 160 in^3 single-channel airgun line 6.

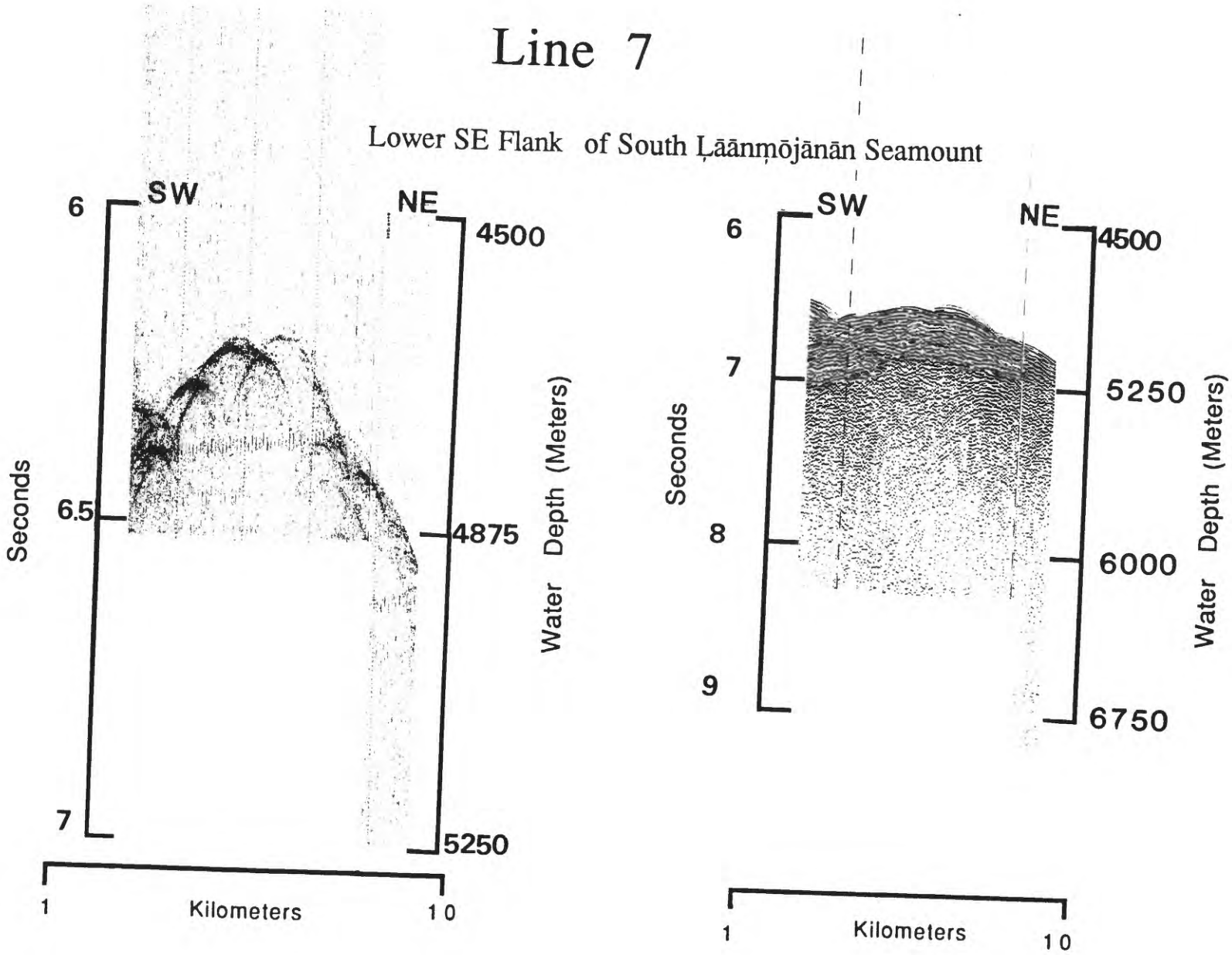

Figure 28. Lower southeast flank of South Ḷāānṃōjānjān Seamount, 3.5 kHz (left) and 160 in^3 single-channel airgun (right) line 7 (see Fig. 7 for location).

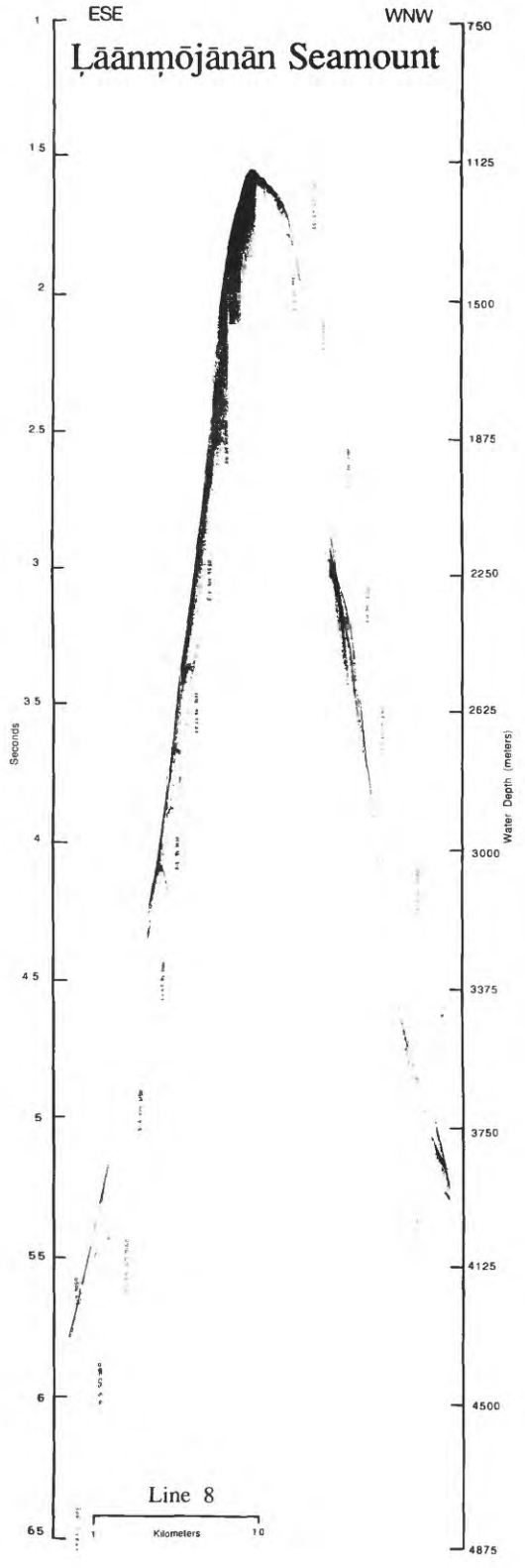

Figure 29. South Ļāānṃōjānjān Seamount, 3.5 kHz line 8 (see Fig. 7 for location).

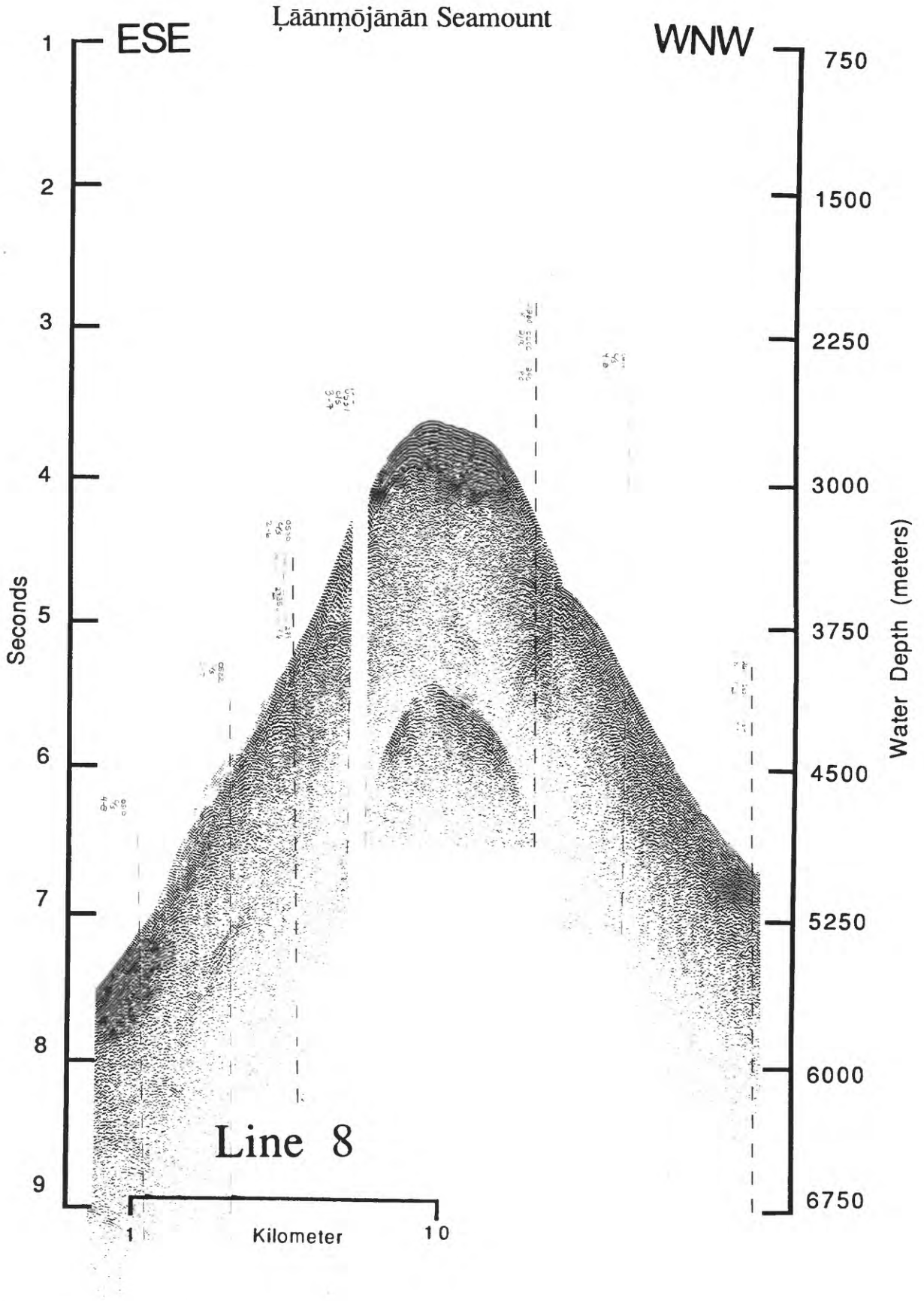

Figure 30. South Ļāānṃōjānjān Seamount, 160 in^3 single-channel airgun line 8.

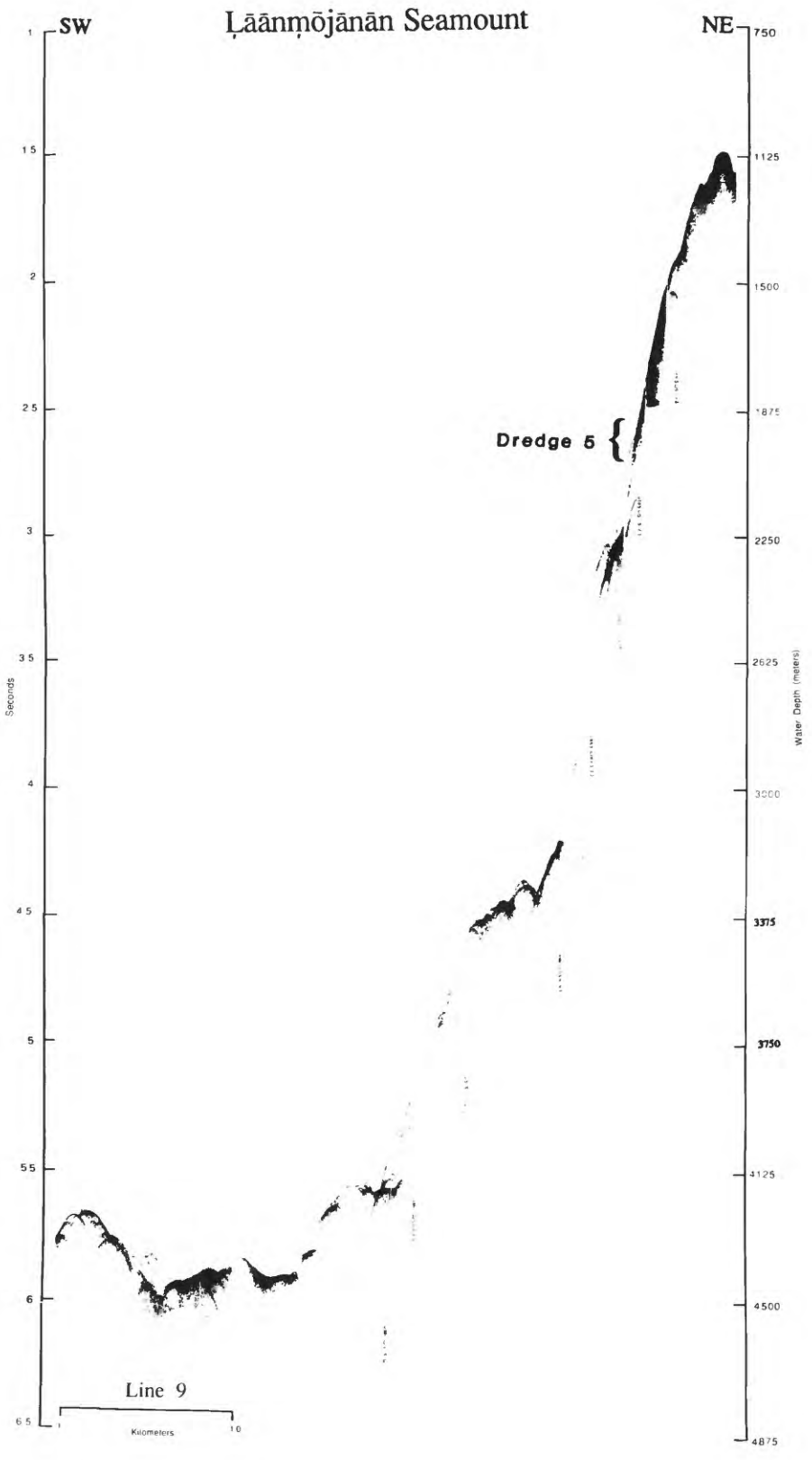

Figure 31. Southwest flank of North Ļāānṃōjānjān Seamount, 3.5 kHz line 9 (see Fig. 7 for location). Note location of dredge D5.

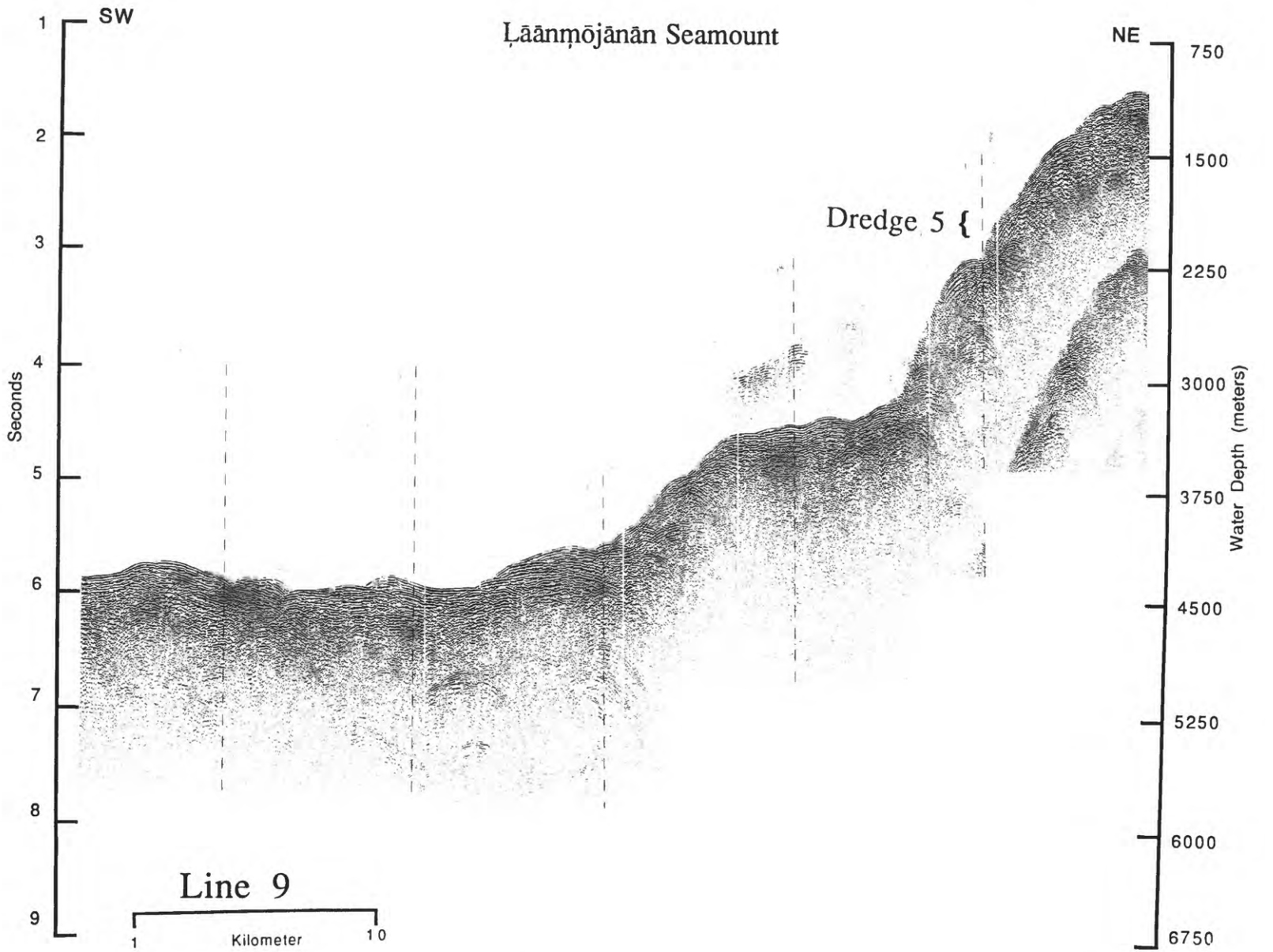

Figure 32. Southwest flank of North Ļāānṃōjānjān Seamount, 160 in^3 single-channel airgun line 9.

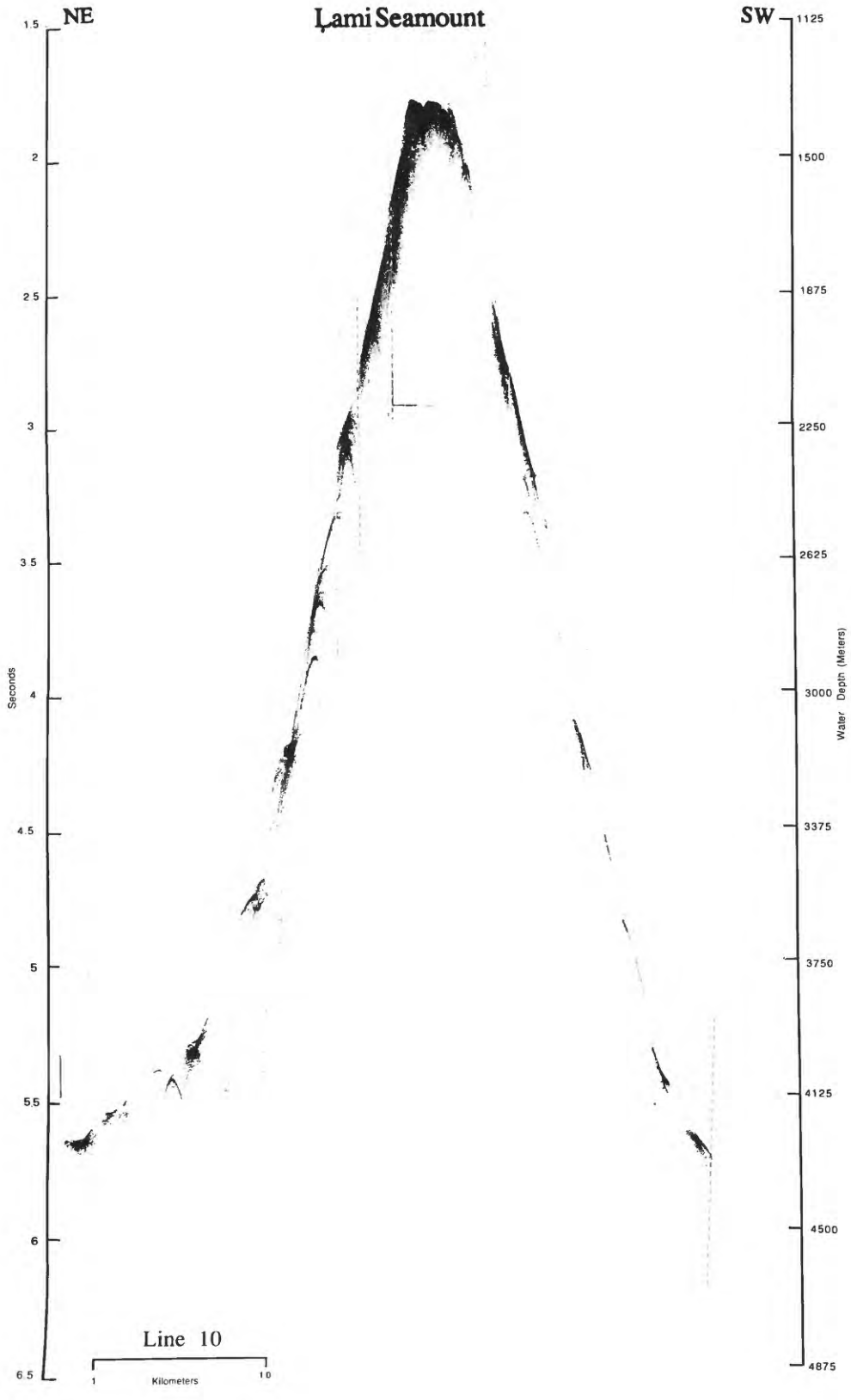

Figure 33. Ḷami Seamount, 3.5 kHz line 10 (see Fig. 8 for location).

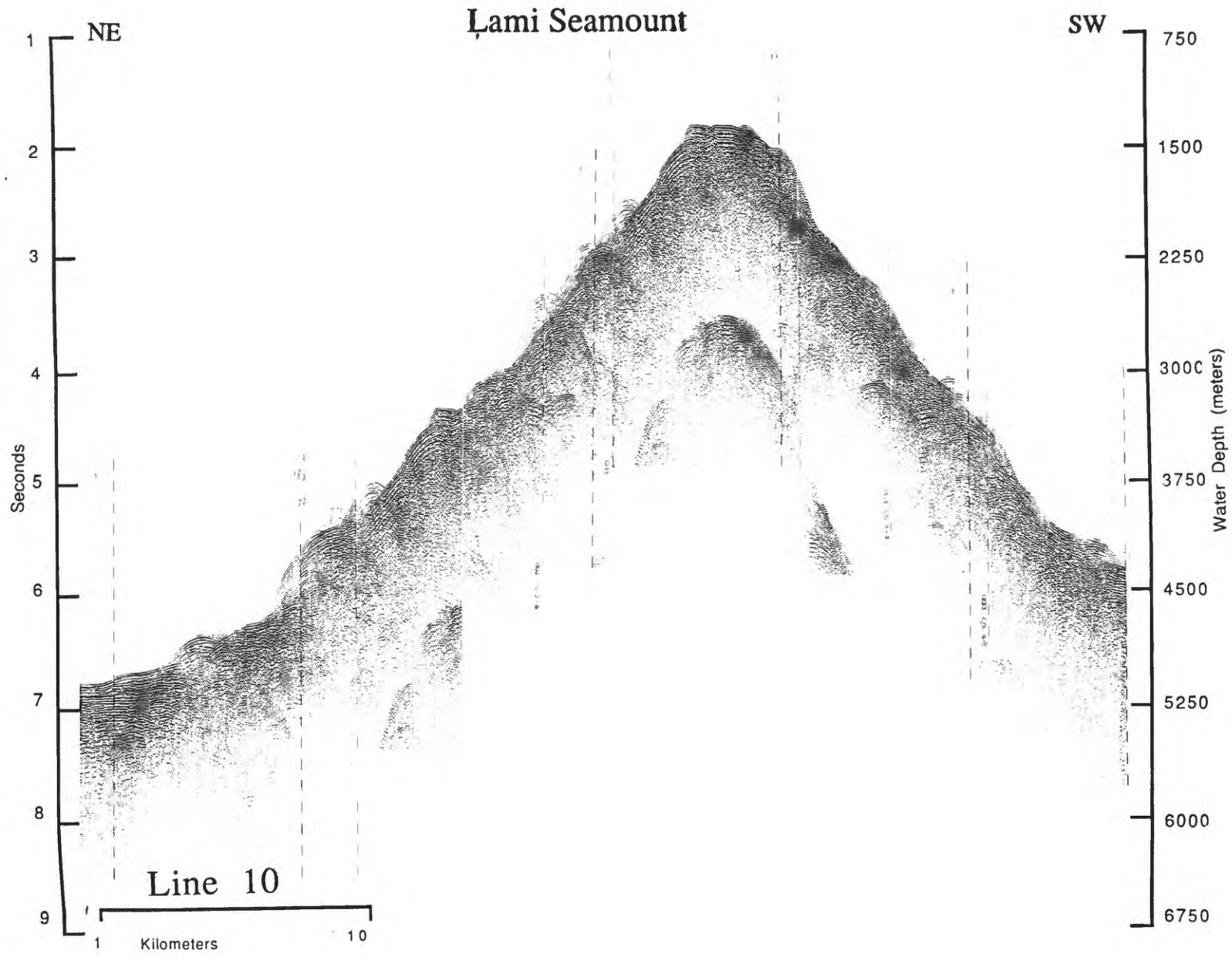

Figure 34. Ļami Seamount, 160 in^3 single-channel airgun line 10.

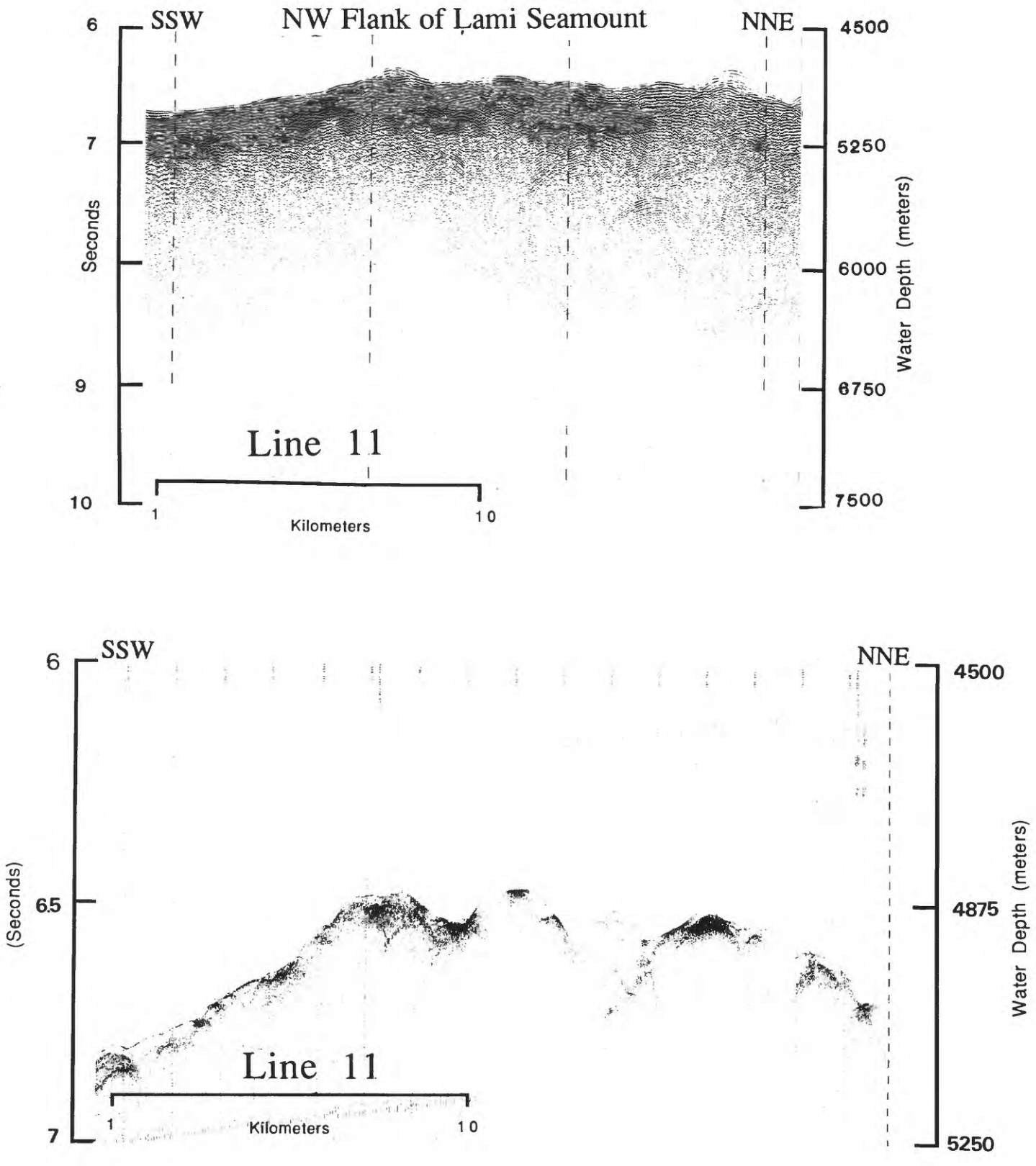

Figure 35. Lower northwest flank of Lami Seamount, 3.5 kHz (bottom) and 160 in^3 single-channel airgun (top) line 11 (see Fig. 8 for location).

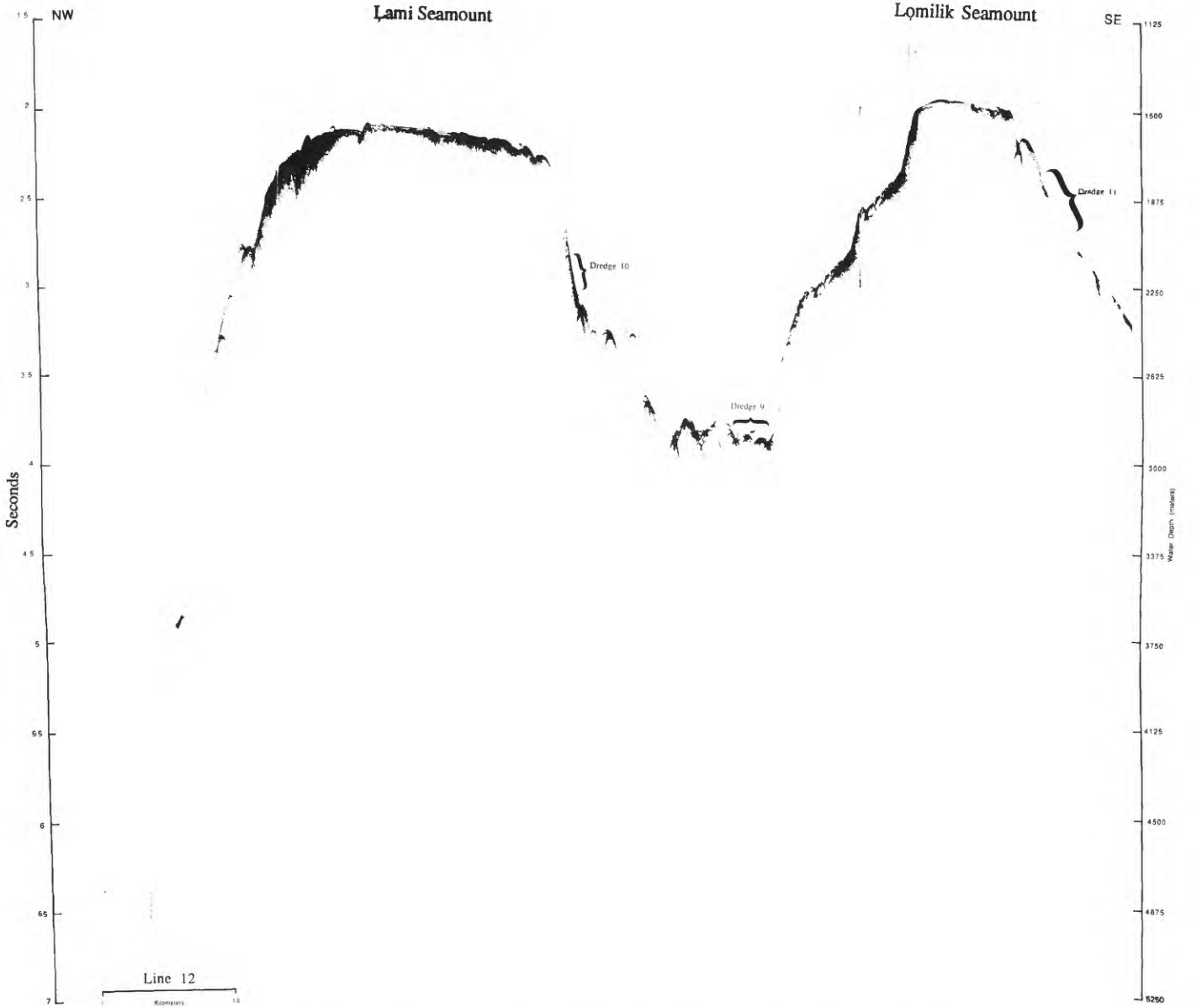

Figure 36. Ḷami and Ḷomilik Seamounts, 3.5 kHz line 12 (see Fig. 8 for location). Note location of dredges D9, D10, and D11.

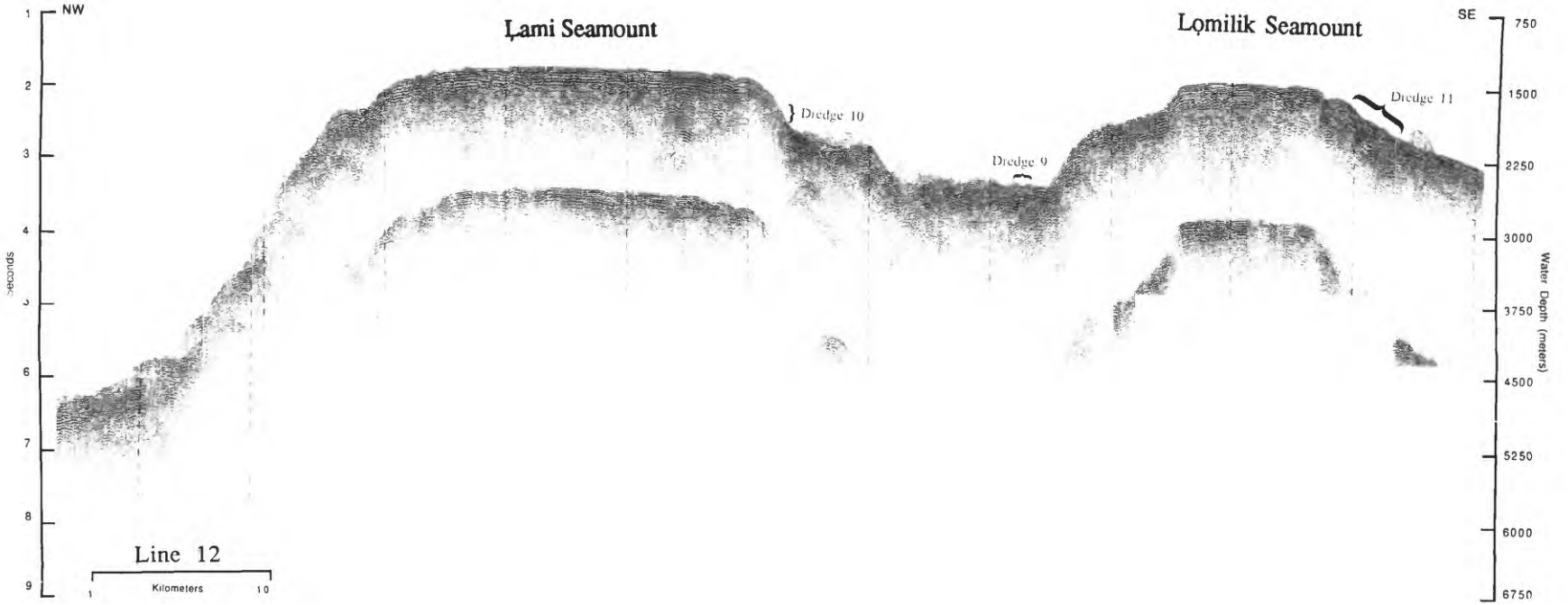

Figure 37. Ḷami and Ḷomilik Seamounts, 160 in^3 single-channel airgun line 12.

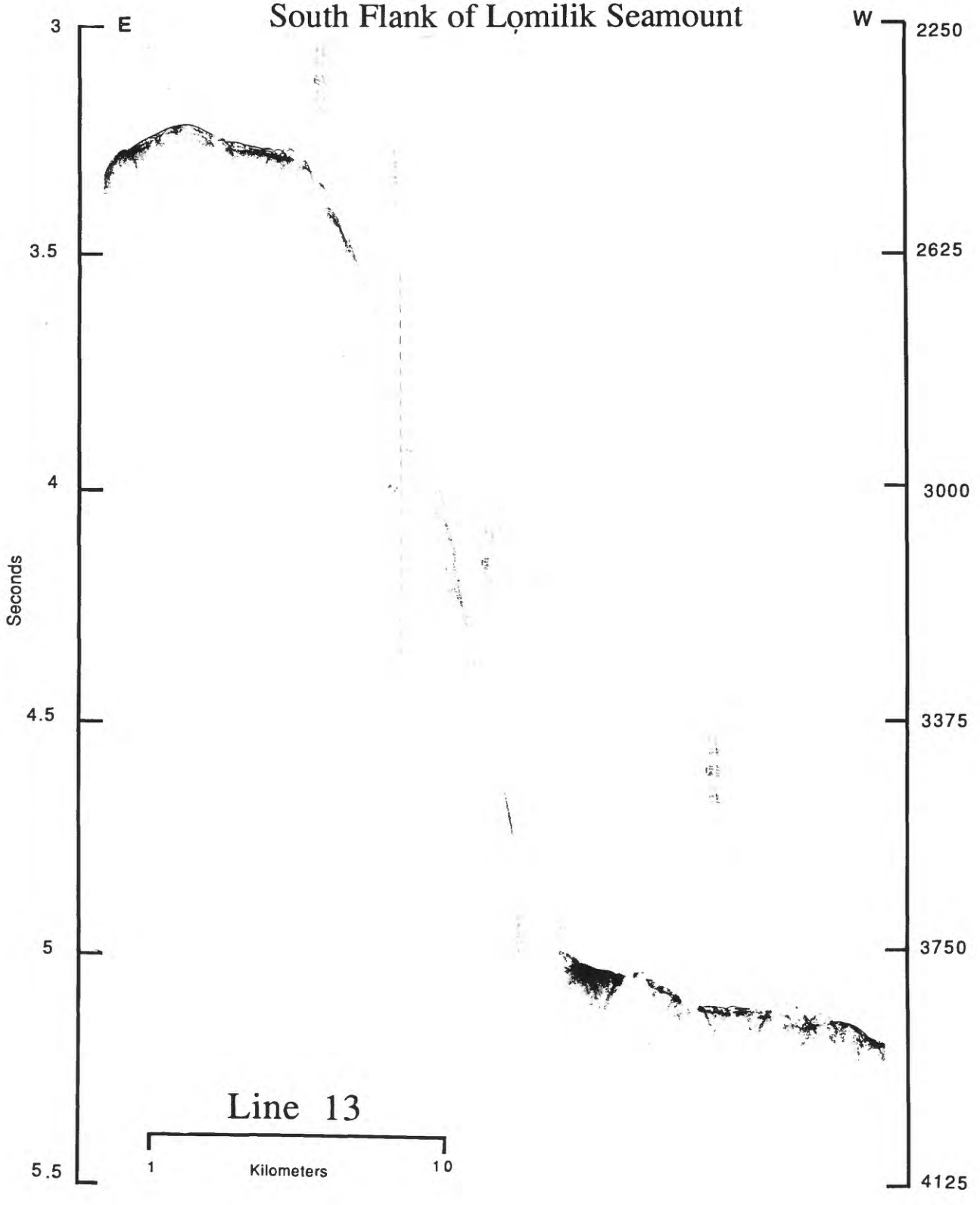

Figure 38. Southern flank of Lọmilik Seamount, 3.5 kHz line 13 (see Fig. 8 for location).

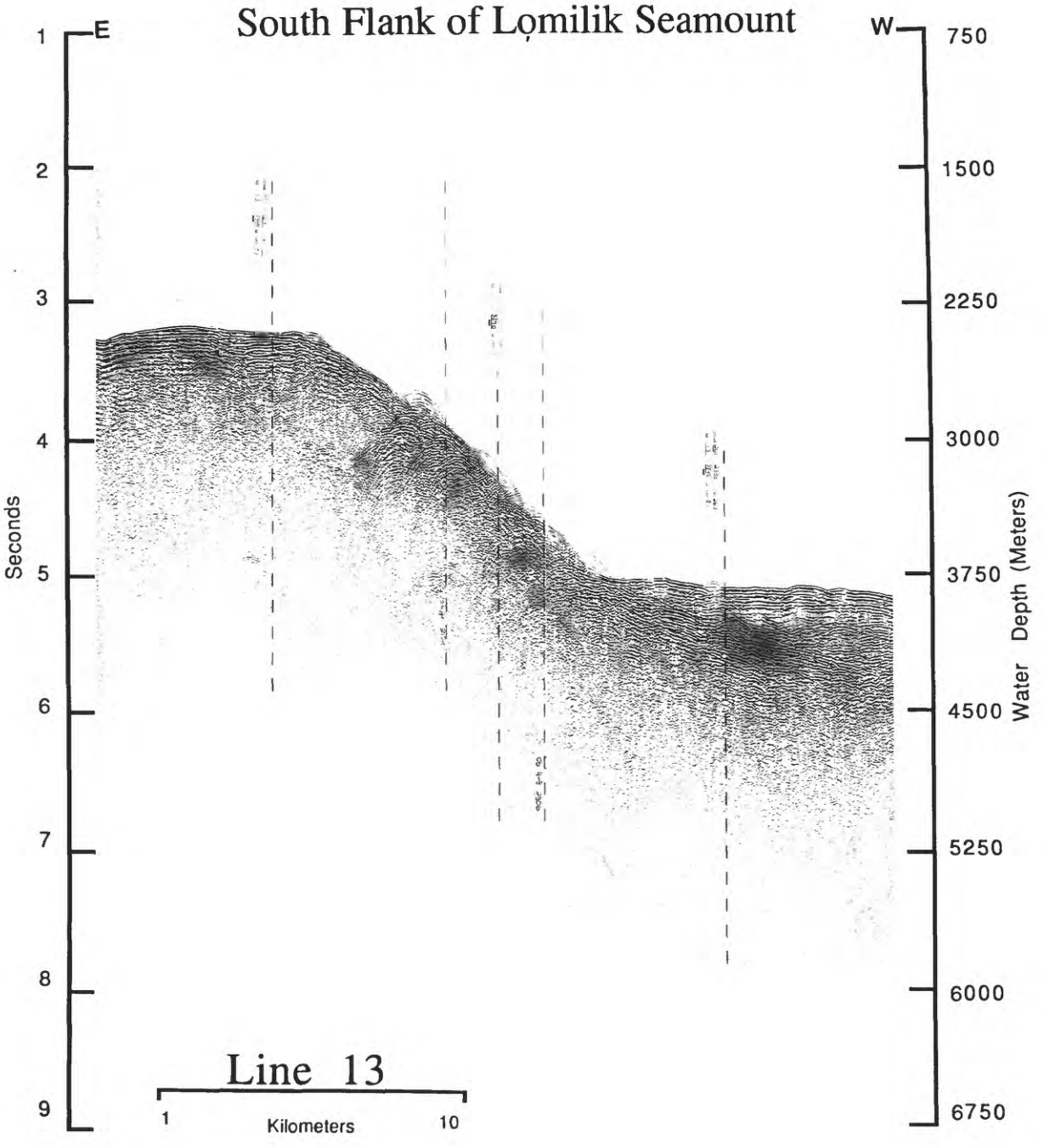

Figure 39. Southern flank of Lọmilik Seamount, 160 in^3 single-channel airgun line 13.

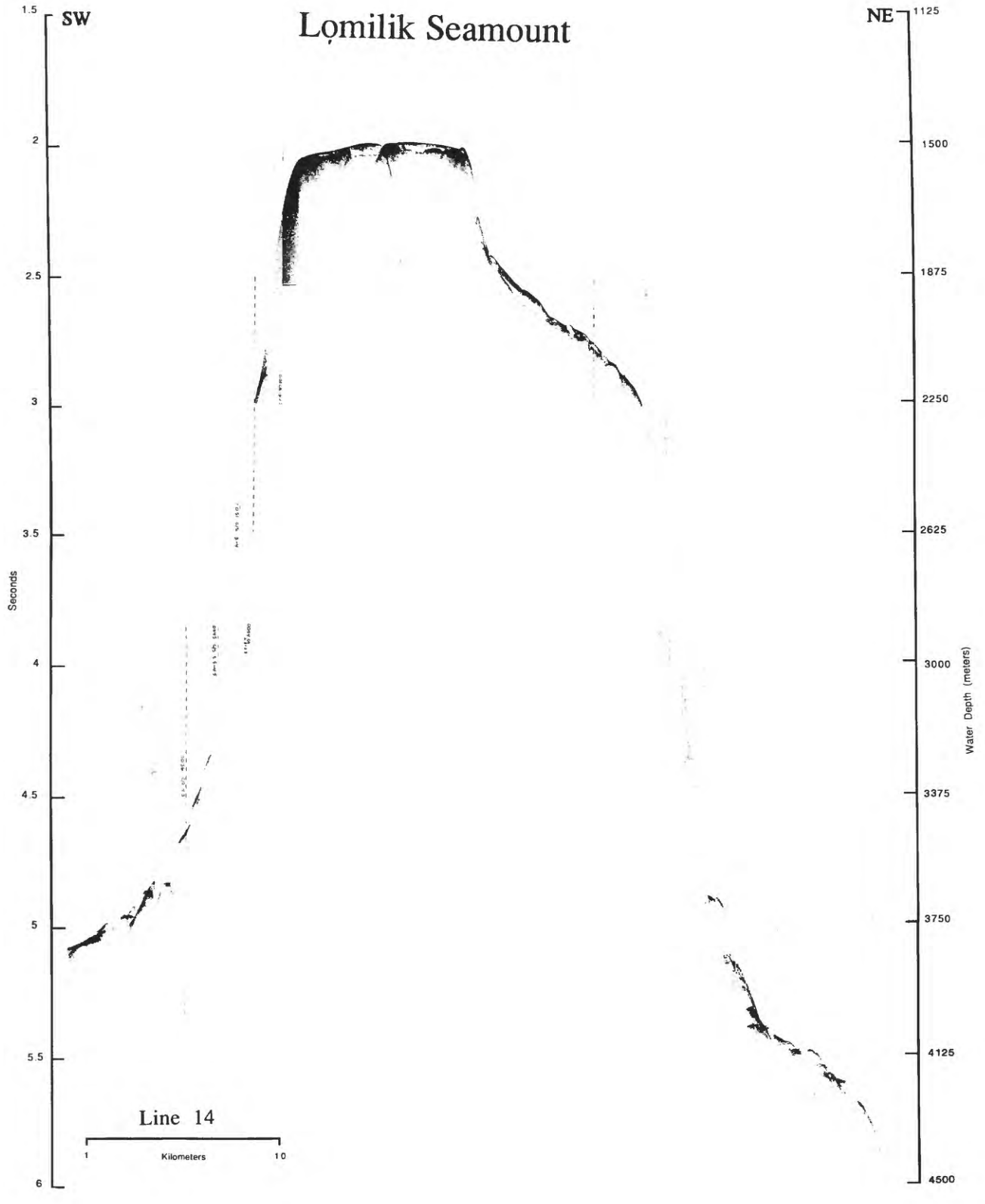

Figure 40. Lọmilik Seamount, 3.5 kHz line 14 (see Fig. 8 for location).

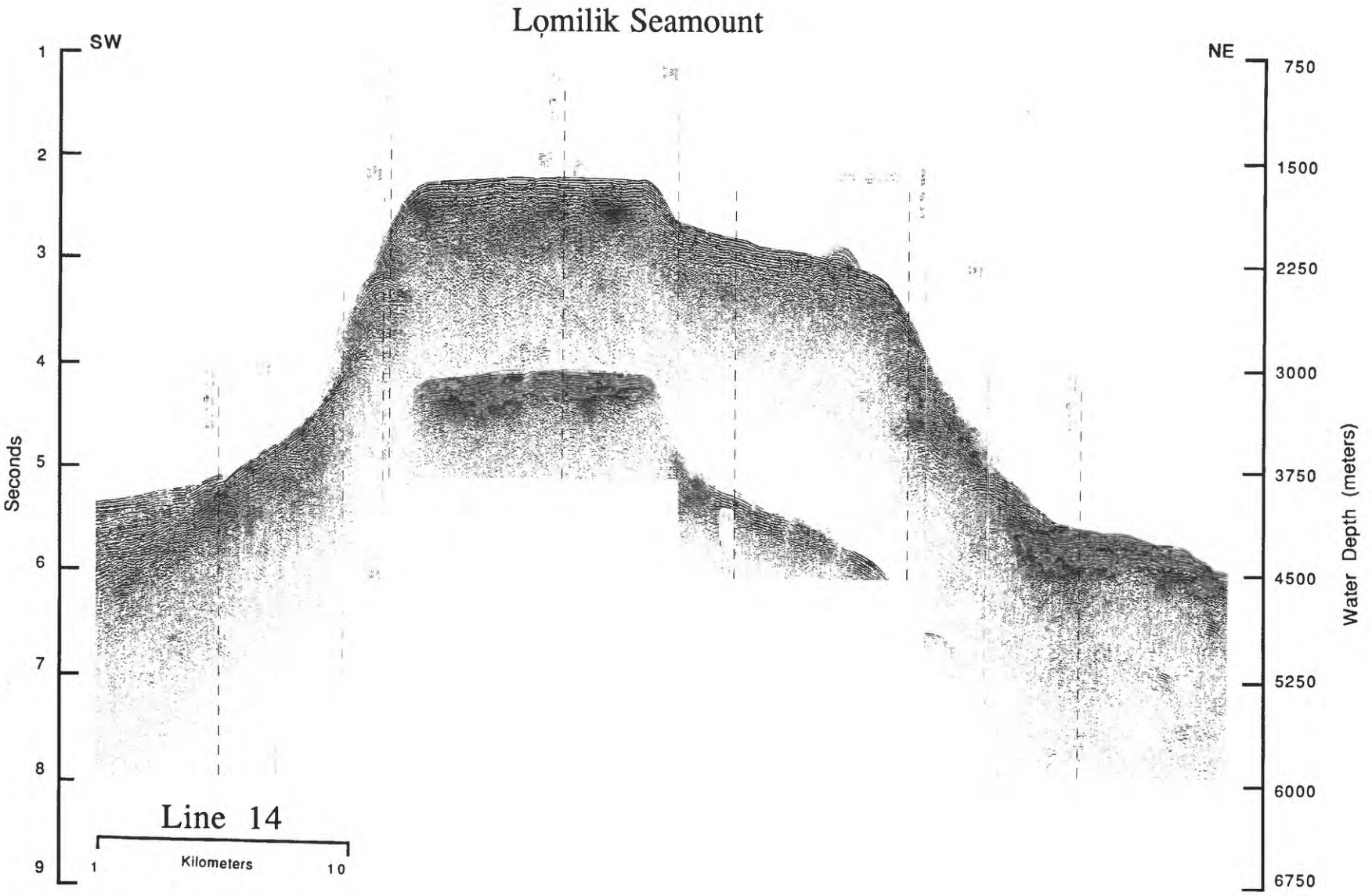

Figure 41. Lomilik Seamount, 160 in^3 single-channel airgun line 14.

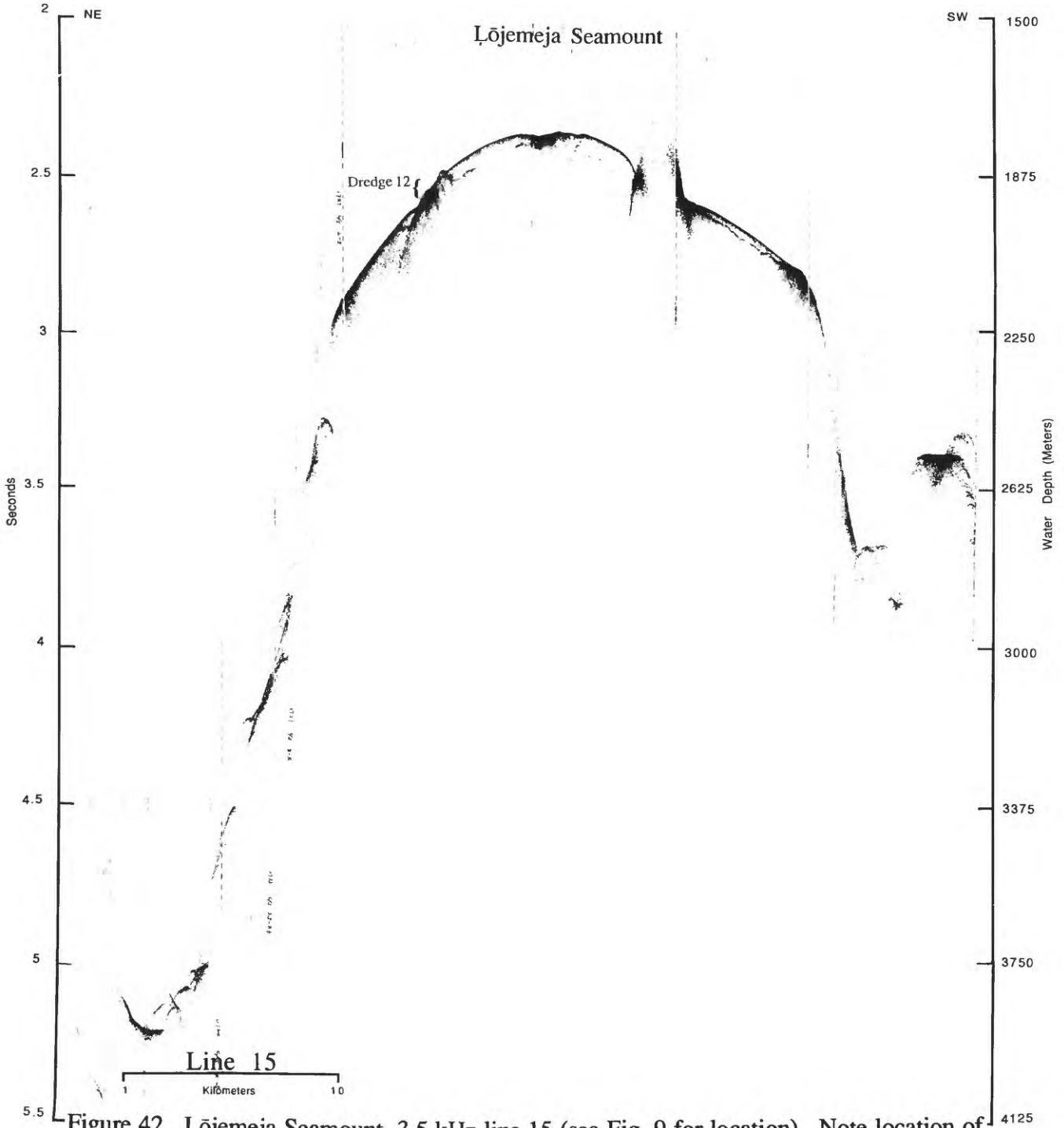

Figure 42. Ļōjemeja Seamount, 3.5 kHz line 15 (see Fig. 9 for location). Note location of dredge D12.

Figure 43. Ļajutōkwa and Ļōtab Seamounts of the Ujlañ volcanic complex, north half of 3.5 kHz line 16 (see Fig. 3 for location). Note location of dredge D18.

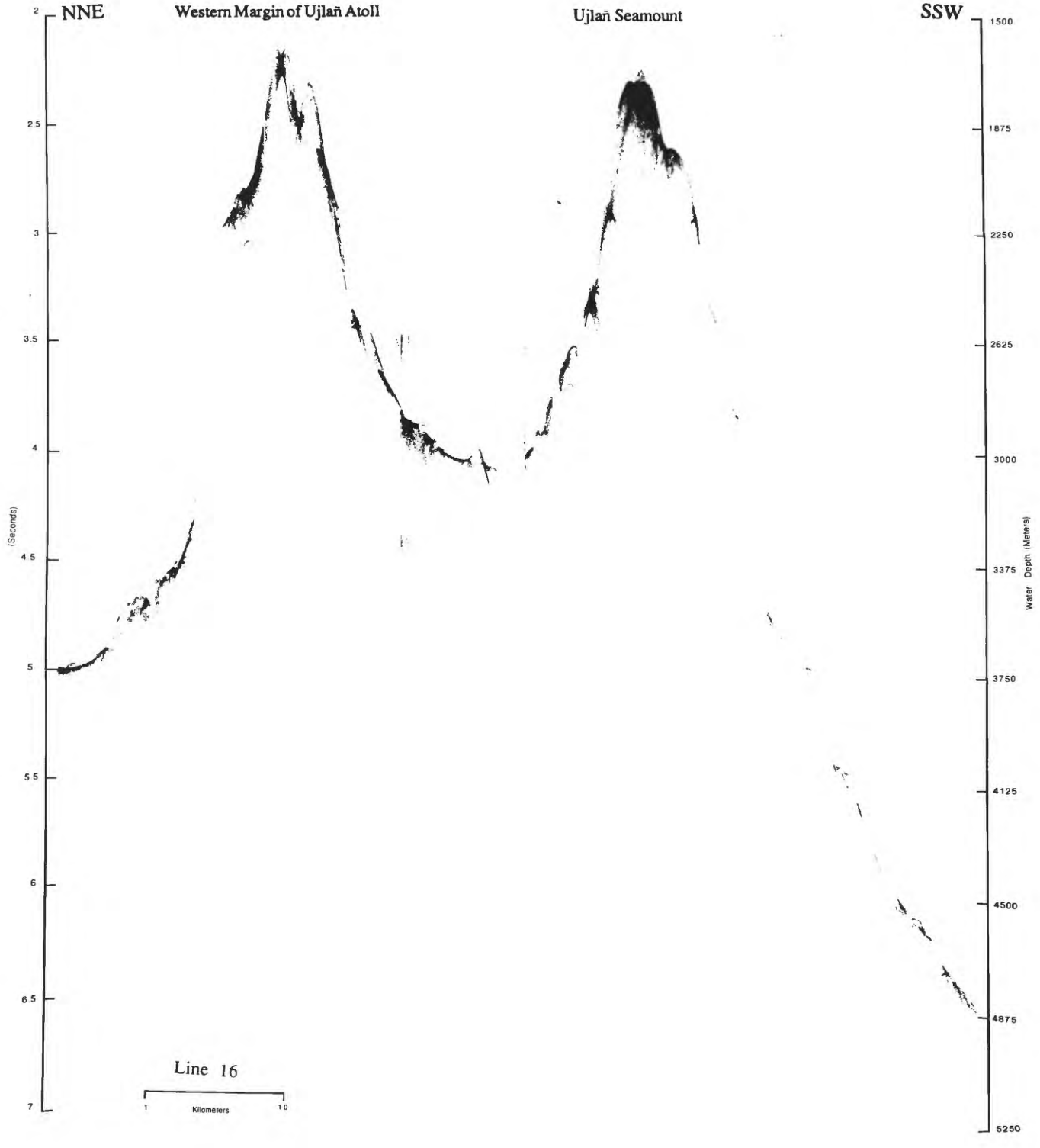

Figure 44. Ujlañ Seamount and west flank of Ujlañ Atoll, south half of 3.5 kHz line 16.

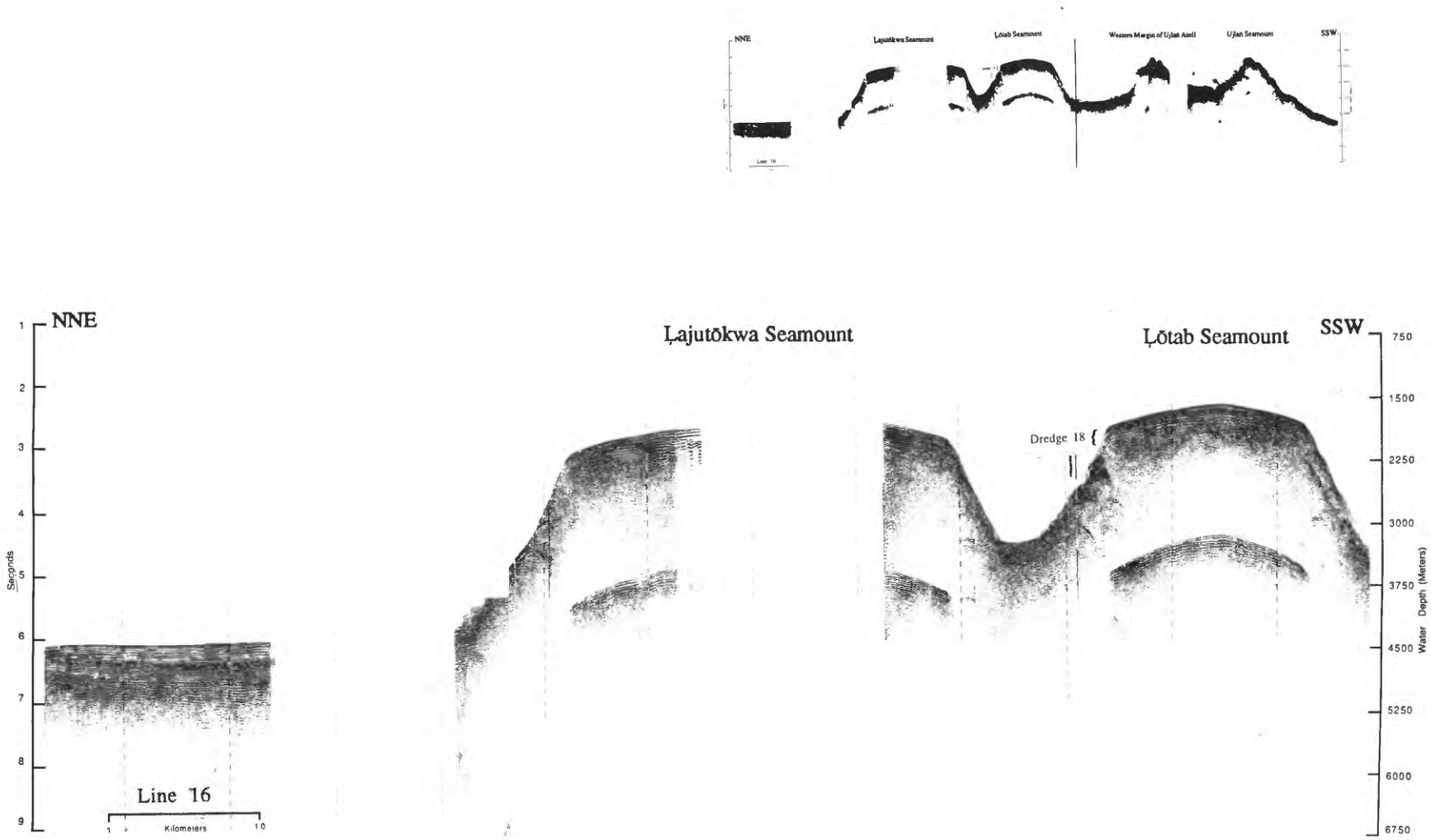

Figure 45. Ļajutōkwa and Ļōtab Seamounts, north half of 160 in3 single-channel airgun line 16. The inset shows the complete line and where it was divided for Figs. 43-46.

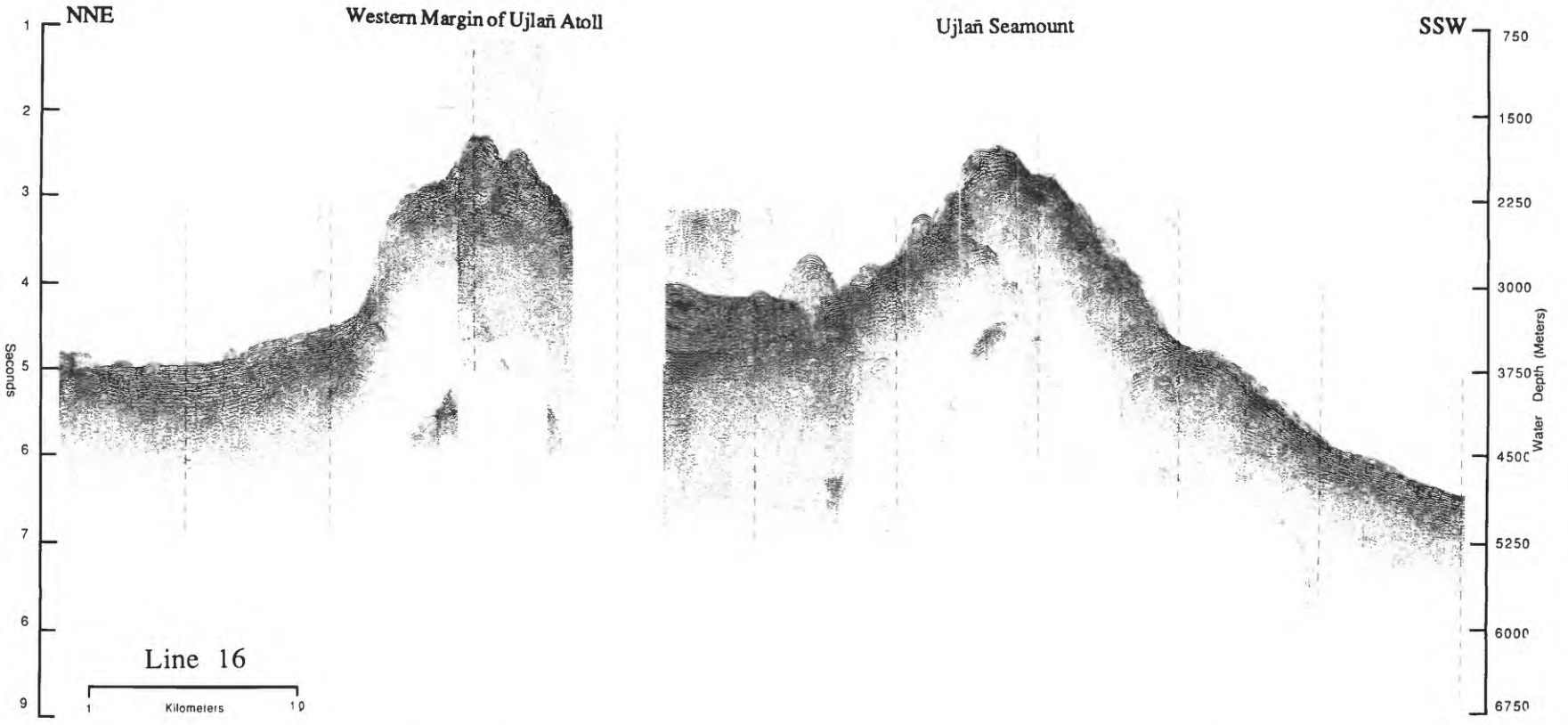

Figure 46. Ujlañ Seamount and west flank of Ujlañ Atoll, south half of 160 in^3 single-channel airgun line 16.

Figure 47. North and south peaks of Ujlañ Seamount and Ļalibjet Seamount, 3.5 kHz line 17 (see Fig. 3 for location). Note the location of dredges D13-D17.

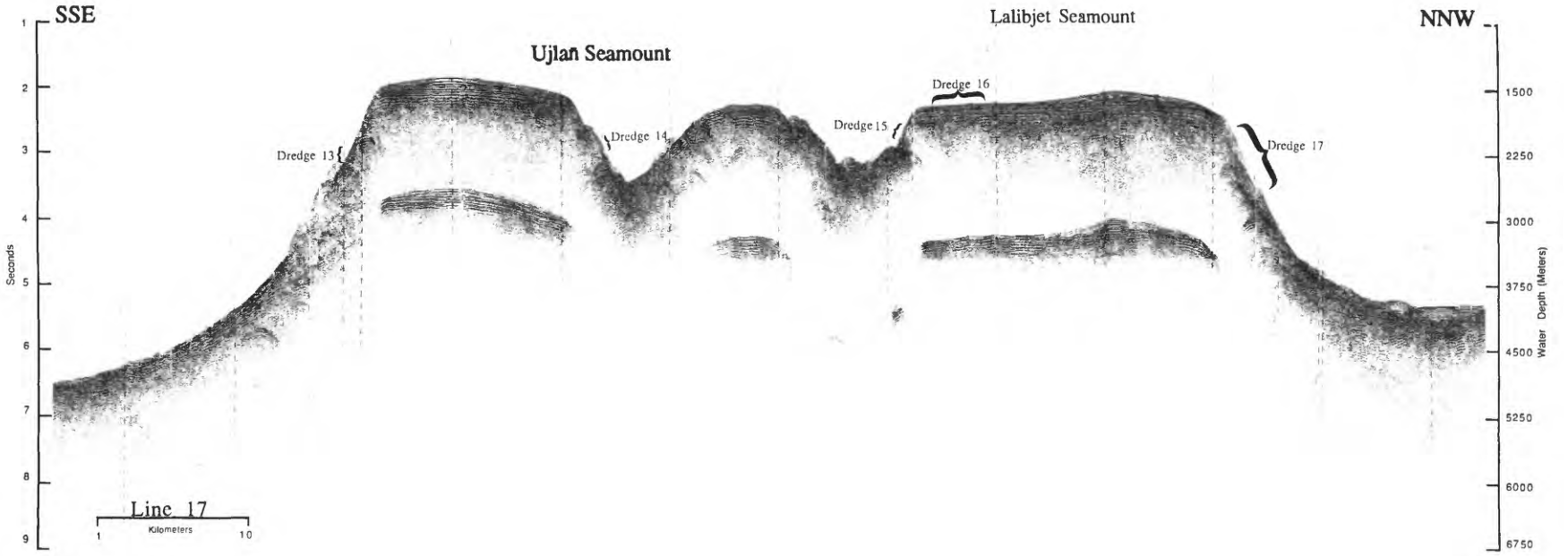

Figure 48. North and south peaks of Ujlaŋ Seamount and Ļalibjet Seamount, 160 in^3 single-channel airgun line 17.

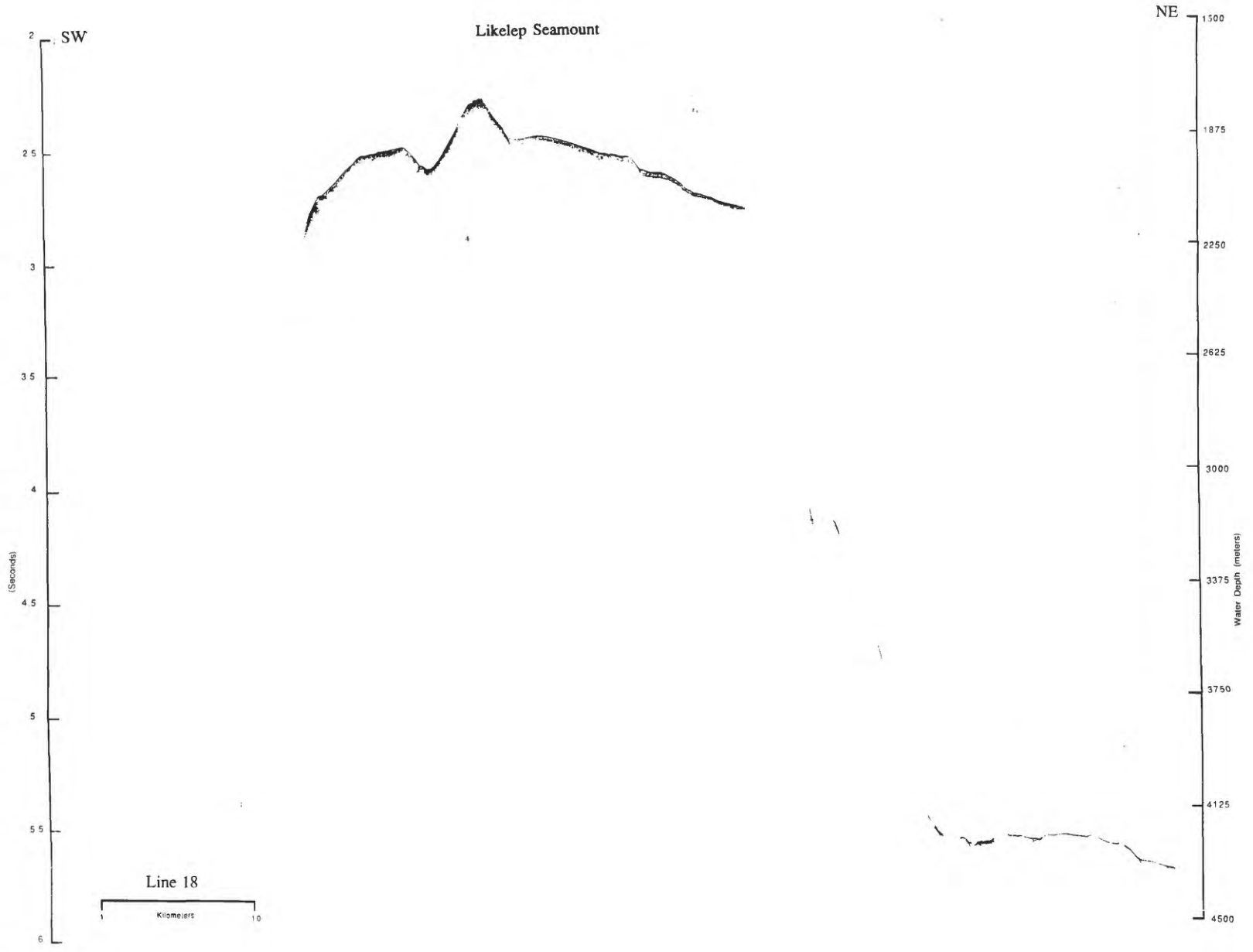

Figure 49. Likelep Seamount of the Ujlañ volcanic complex, 3.5 kHz line 18 (see Fig. 3 for location).

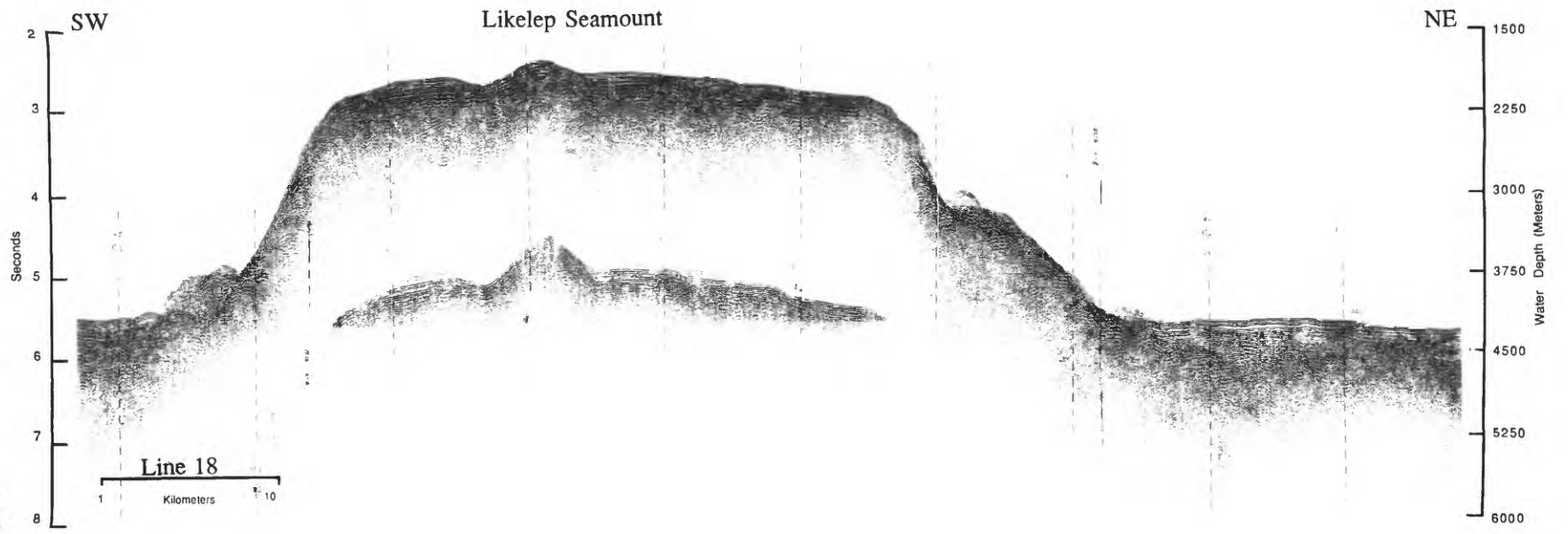

Figure 50. Likelep Seamount, 160 in^3 single-channel airgun line 18.

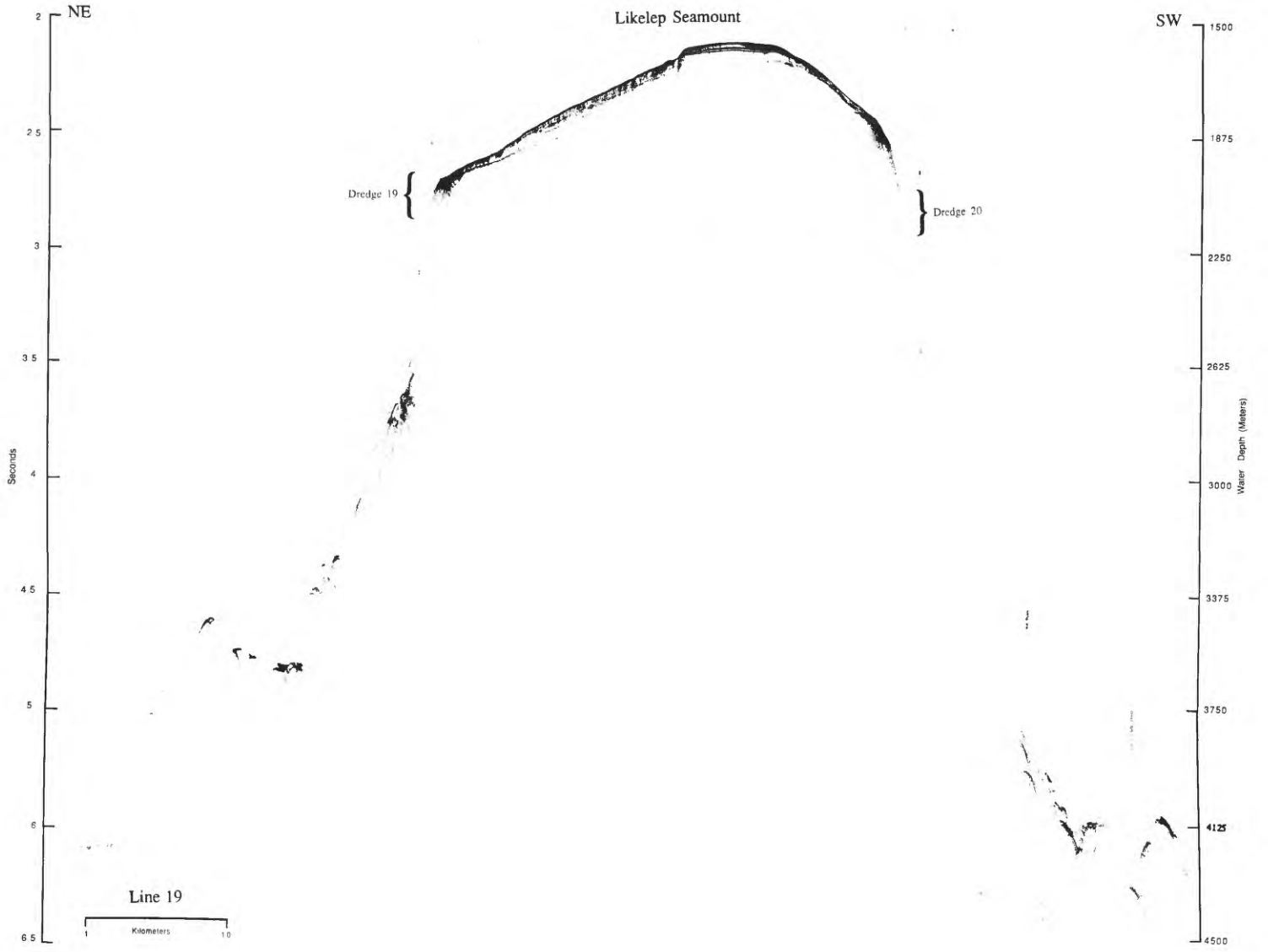

Figure 51. Likelep Seamount of the Ujlañ volcanic complex, 3.5 kHz line 19 (see Fig. 3 for location). Note the location of dredges D19 and D20.

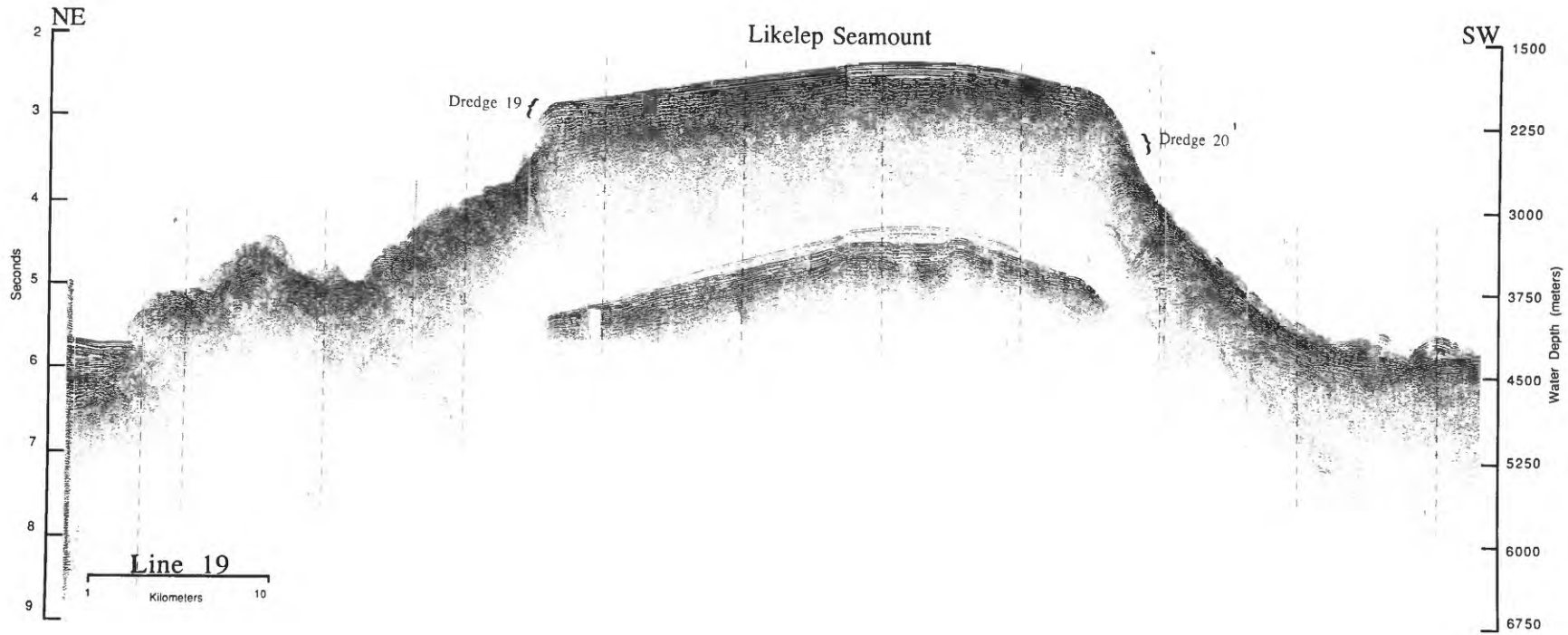

Figure 52. Likelep Seamount, 160 in^3 single-channel airgun line 19.

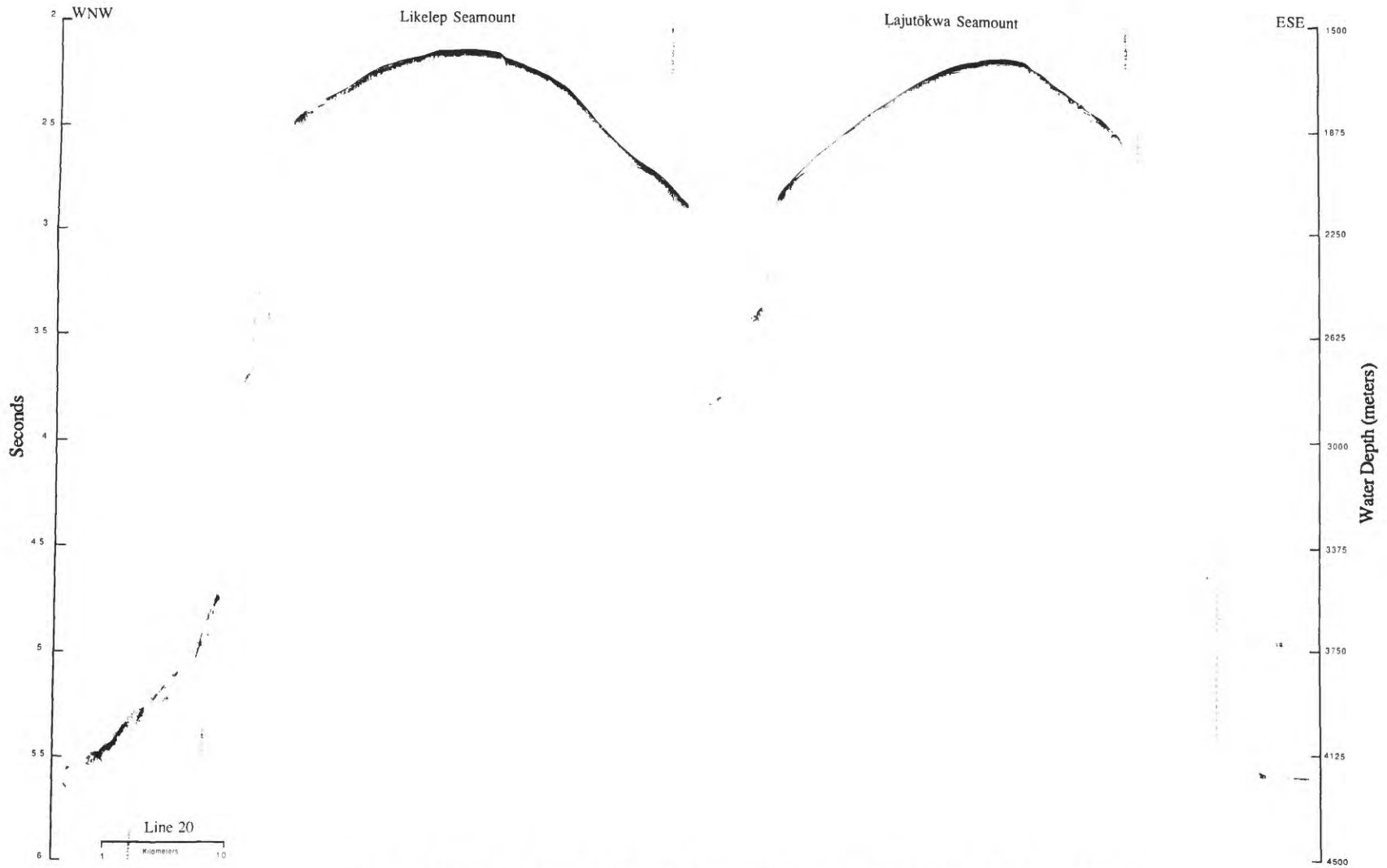

Figure 53. Likelep and Ļajutōkwa Seamounts of the Ujlañ volcanic complex, 3.5 kHz line 20 (see Fig. 3 for location).

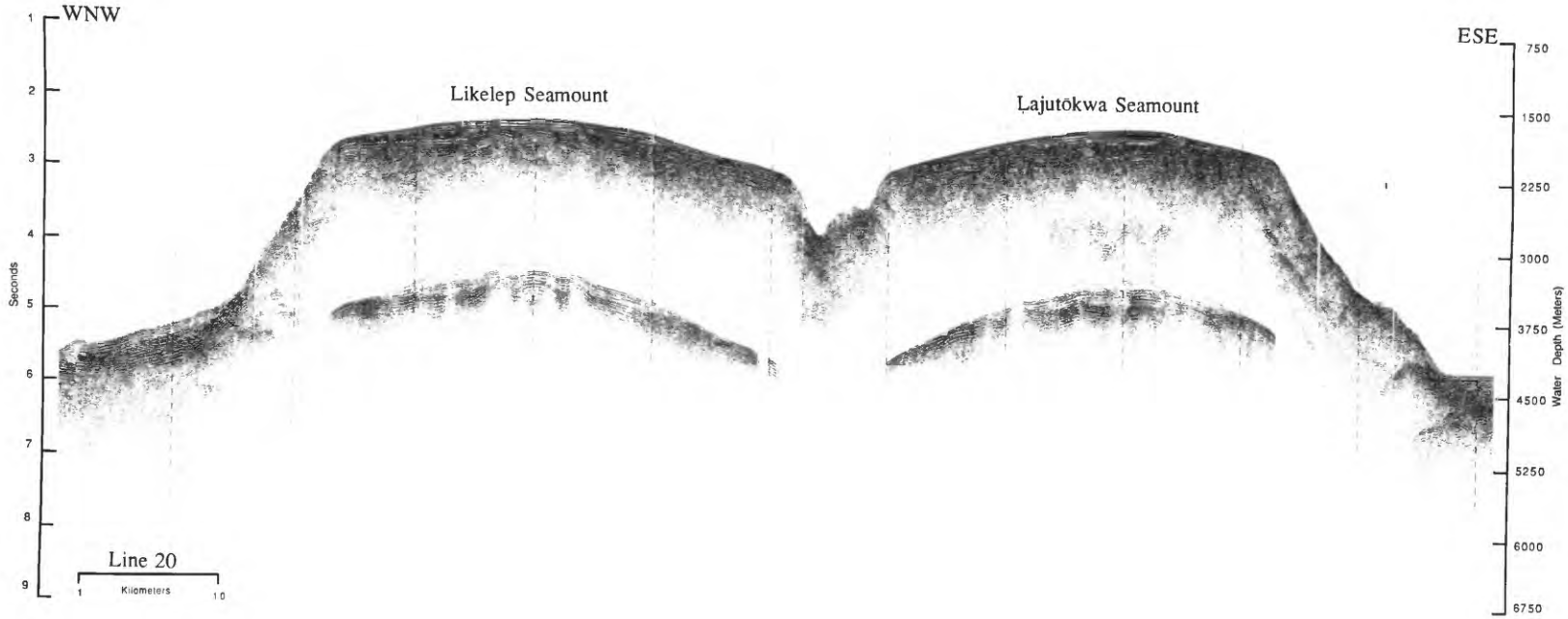

Figure 54. Likelep and Lajutōkwa Seamounts, 160 in^3 single-channel airgun line 20.

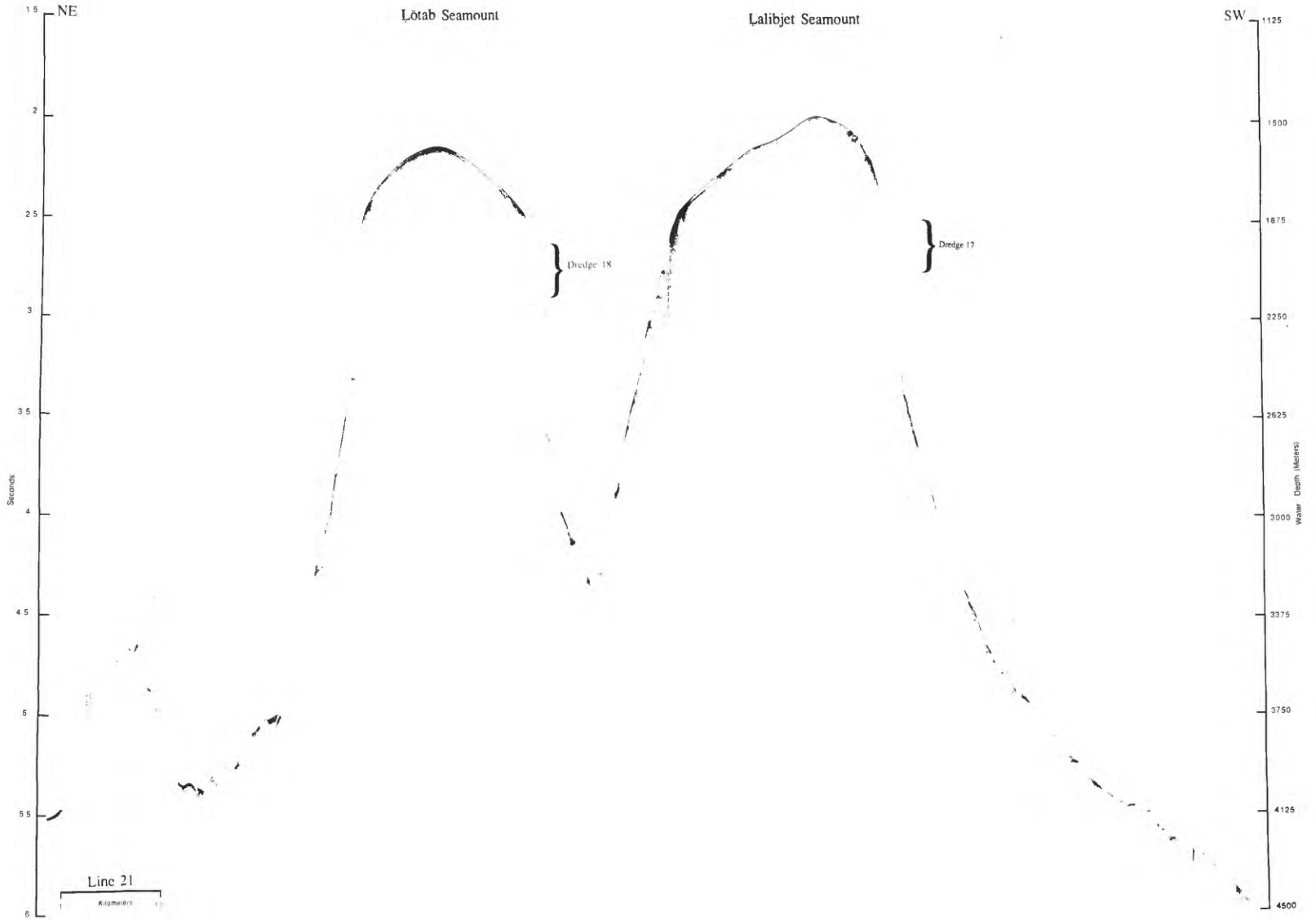

Figure 55. Ļōtab and Ļalibjet Seamounts of the Ujlañ volcanic complex, 3.5 kHz line 21 (see Fig. 3 for location). Note the location of dredges D17 and D18.

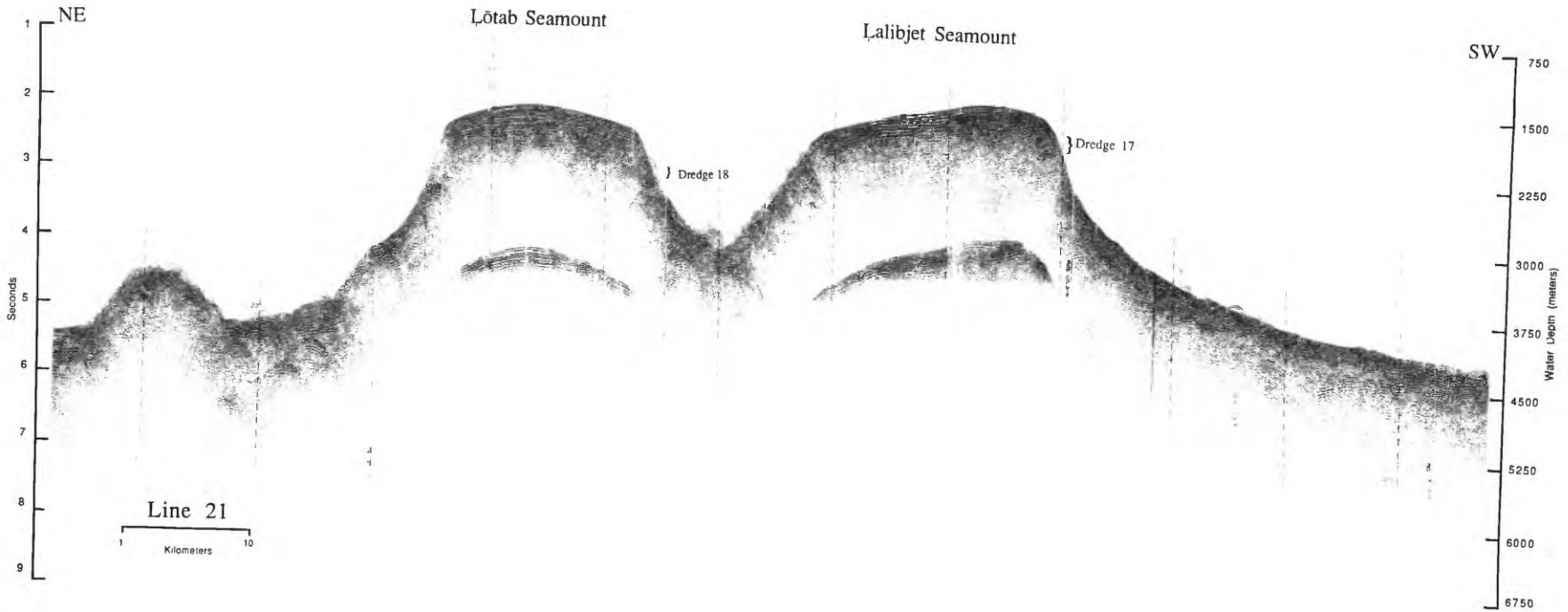

Figure 56. Ļōtab and Ļalibjet Seamounts, 160 in^3 single-channel airgun line 21.

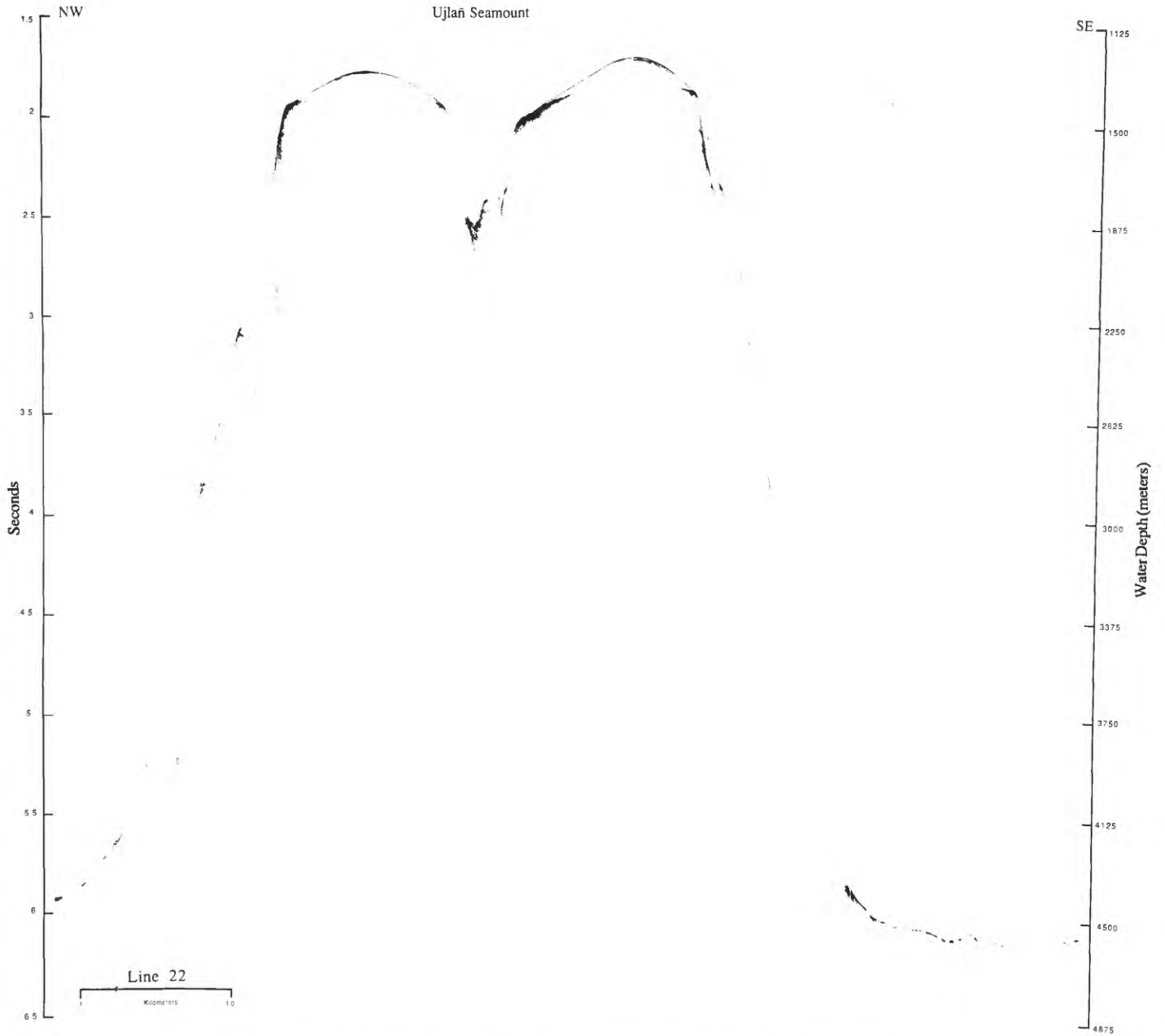

Figure 57. Northwest and south peaks of Ujlañ Seamount, 3.5 kHz line 22 (see Fig. 3 for location).

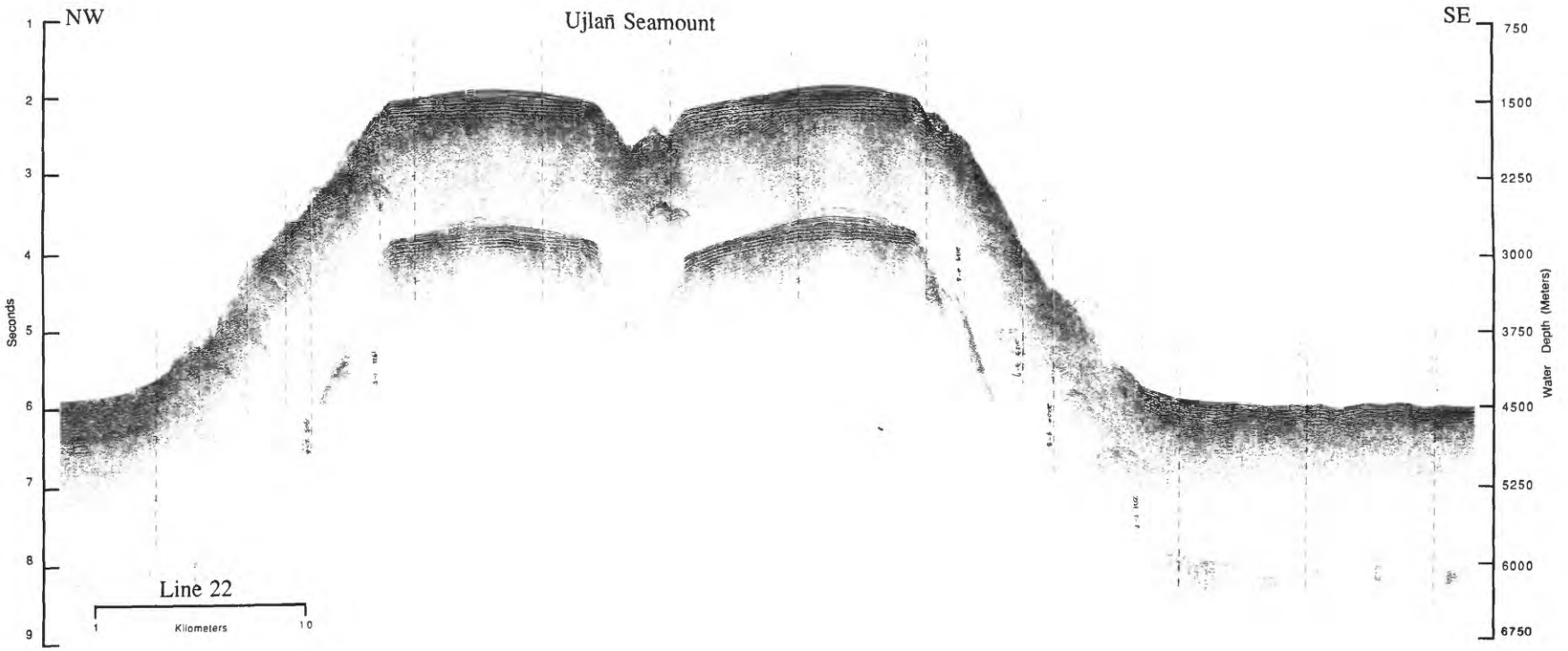

Figure 58. Northwest and south peaks of Ujlañ Seamount, 160 in^3 single-channel airgun line 22.

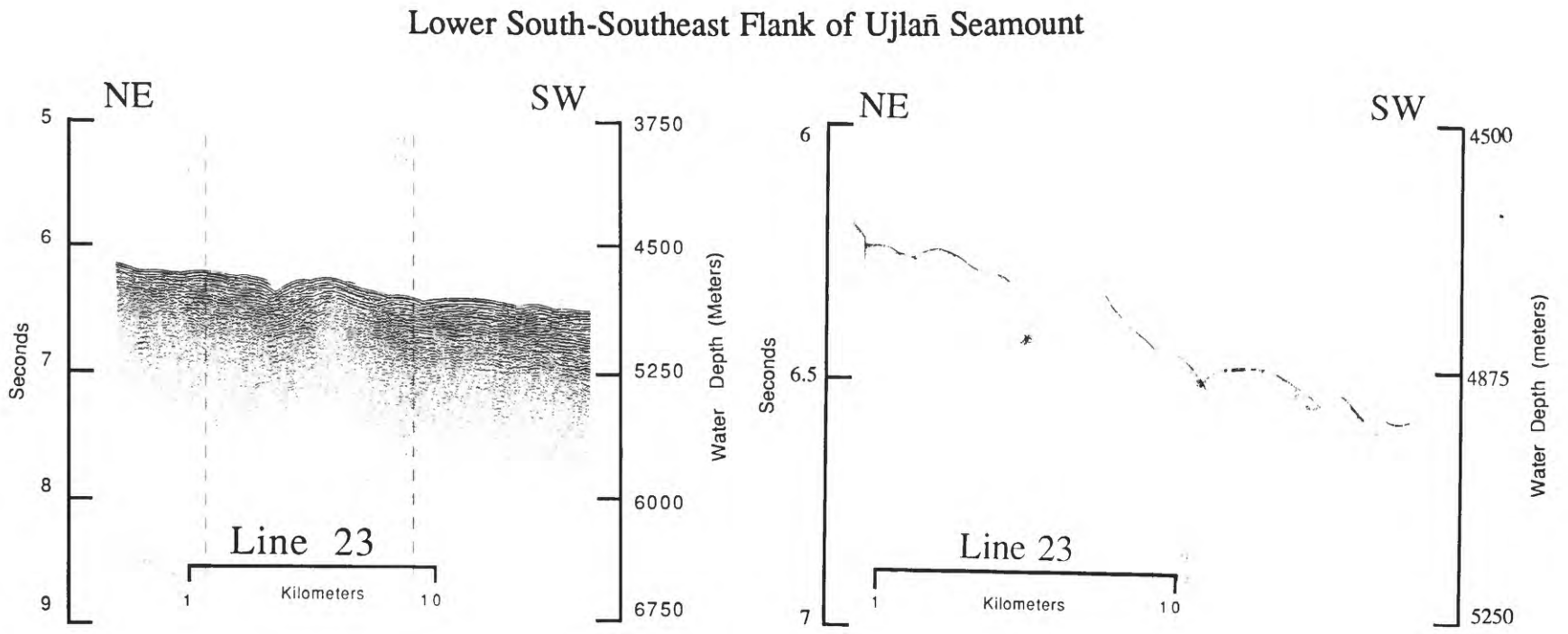

Figure 59. Lower south flank of Ujlañ Seamount, 3.5 kHz (right) and 160 in^3 single-channel airgun (left) line 23 (see Fig. 3 for location).

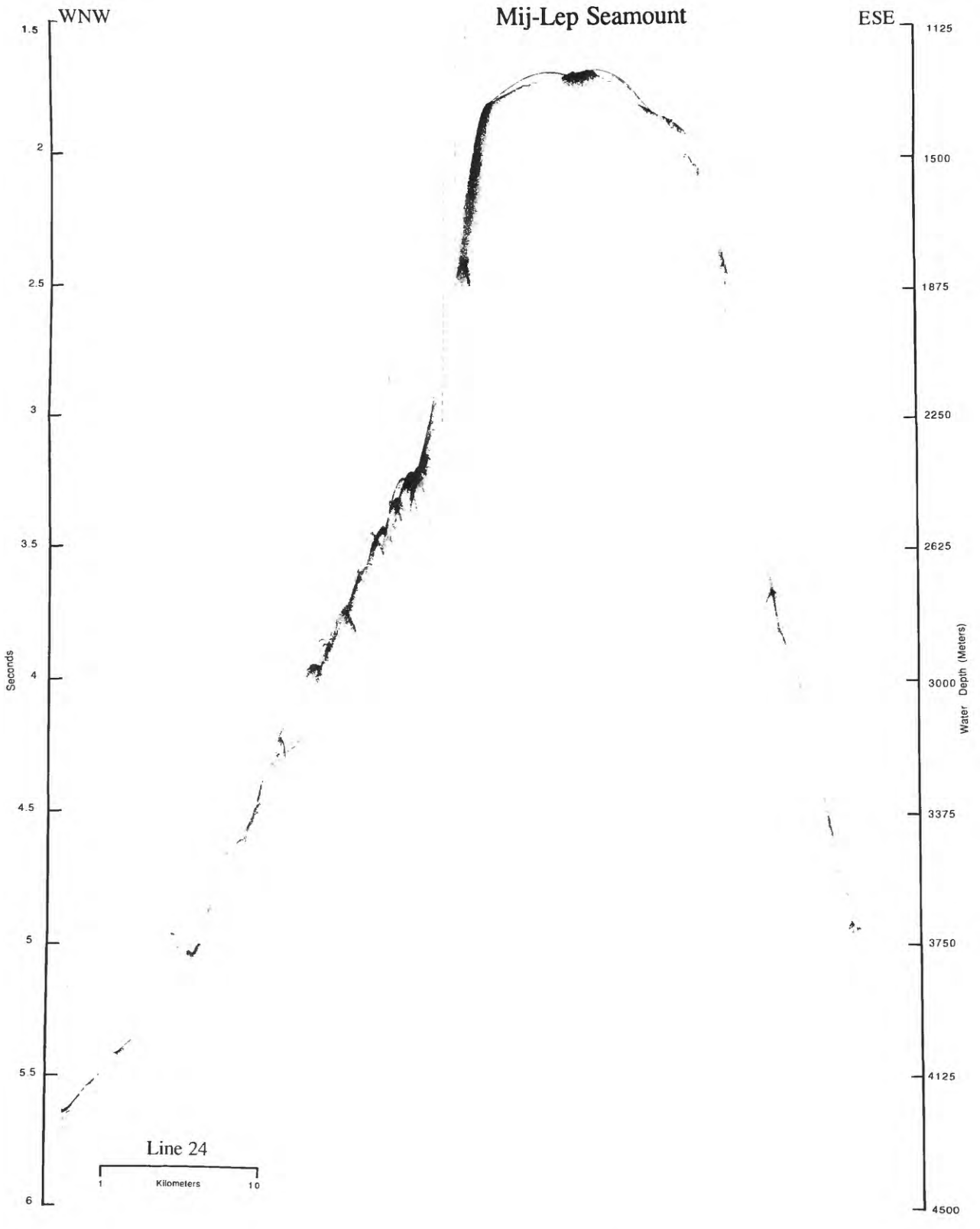

Figure 60. Mij-Lep Seamount, 3.5 kHz line 24 (see Fig. 10 for location).

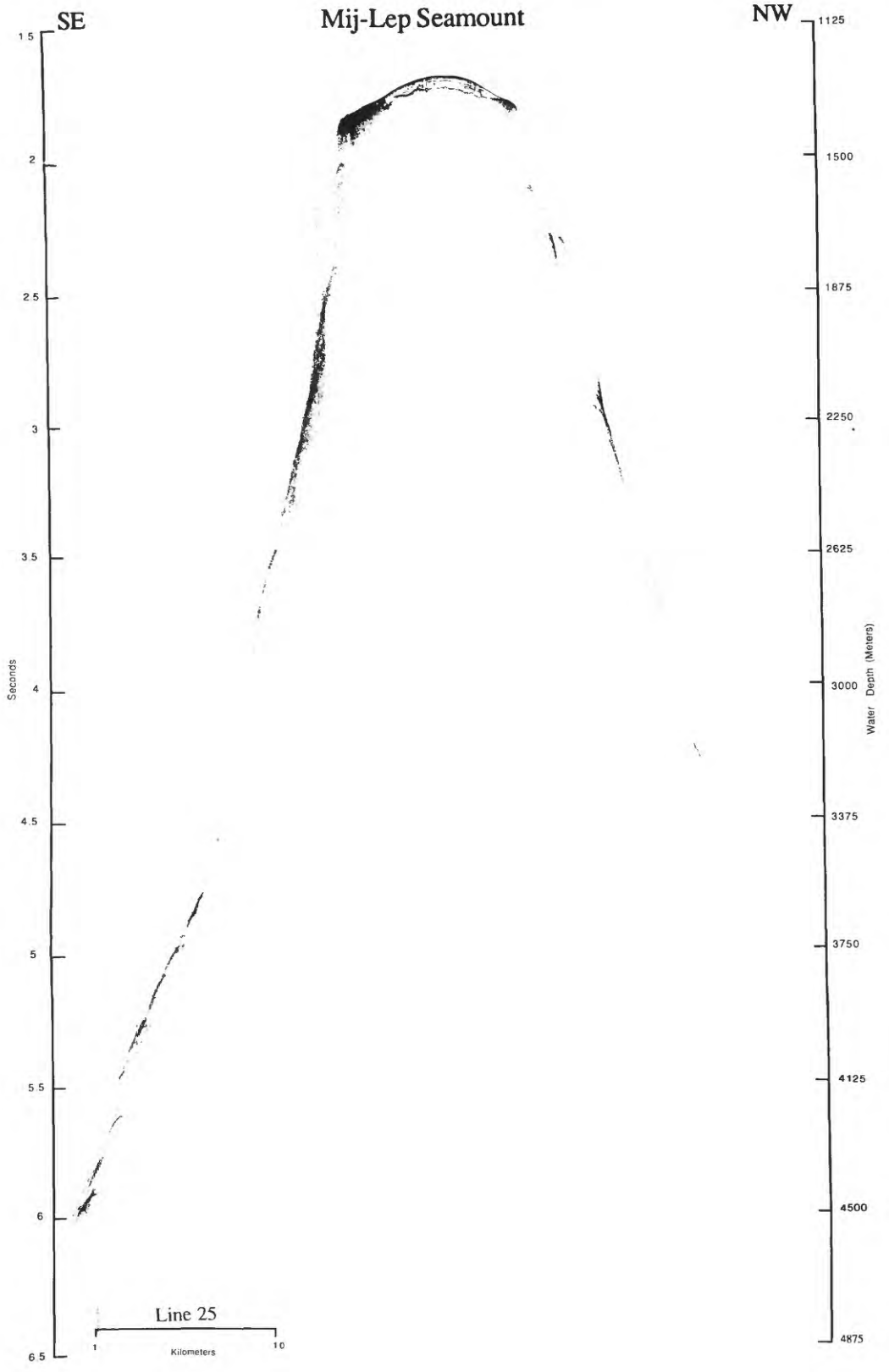

Figure 61. Mij-Lep Seamount, 3.5 kHz line 25 (see Fig. 10 for location).

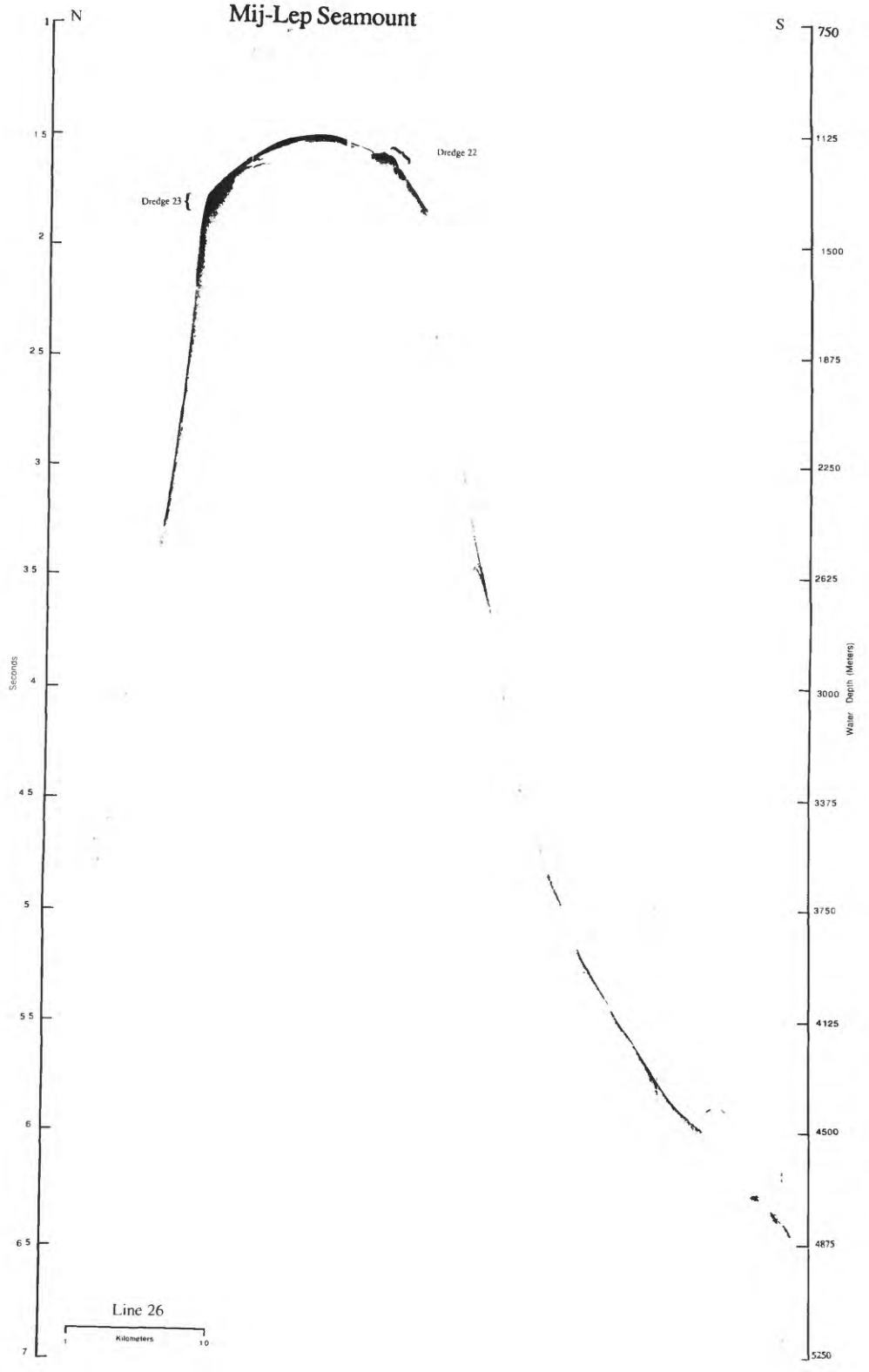

Figure 62. Mij-Lep Seamount, 3.5 kHz line 26 (see Fig. 10 for location). Note the location of dredges D22 and D23.

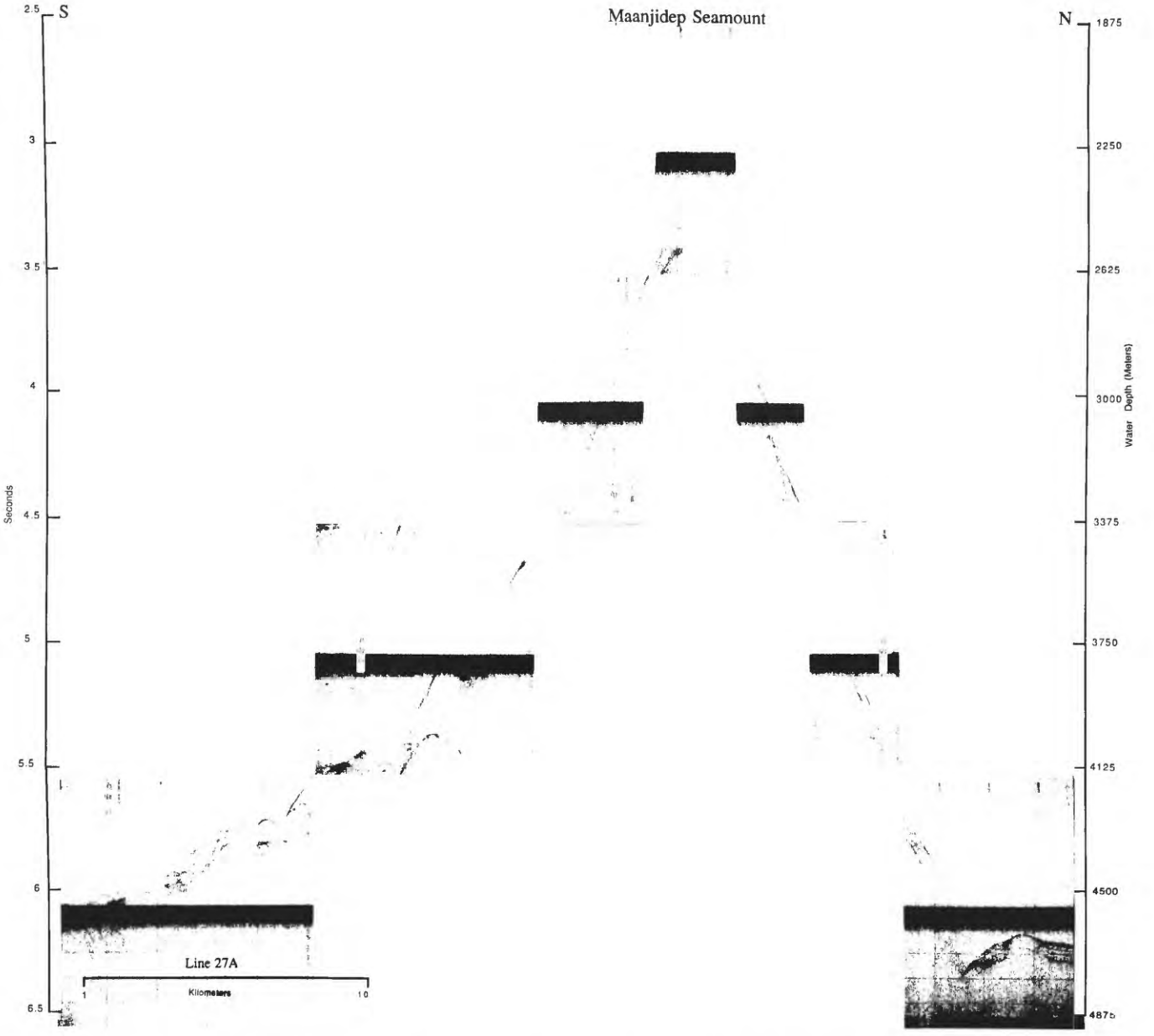

Figure 63. Maanjidep Seamount, discovered on cruise F10-89-CP, central part of 3.5 kHz line 27A, which ran from Jālwōj Atoll to Jebro Seamount.

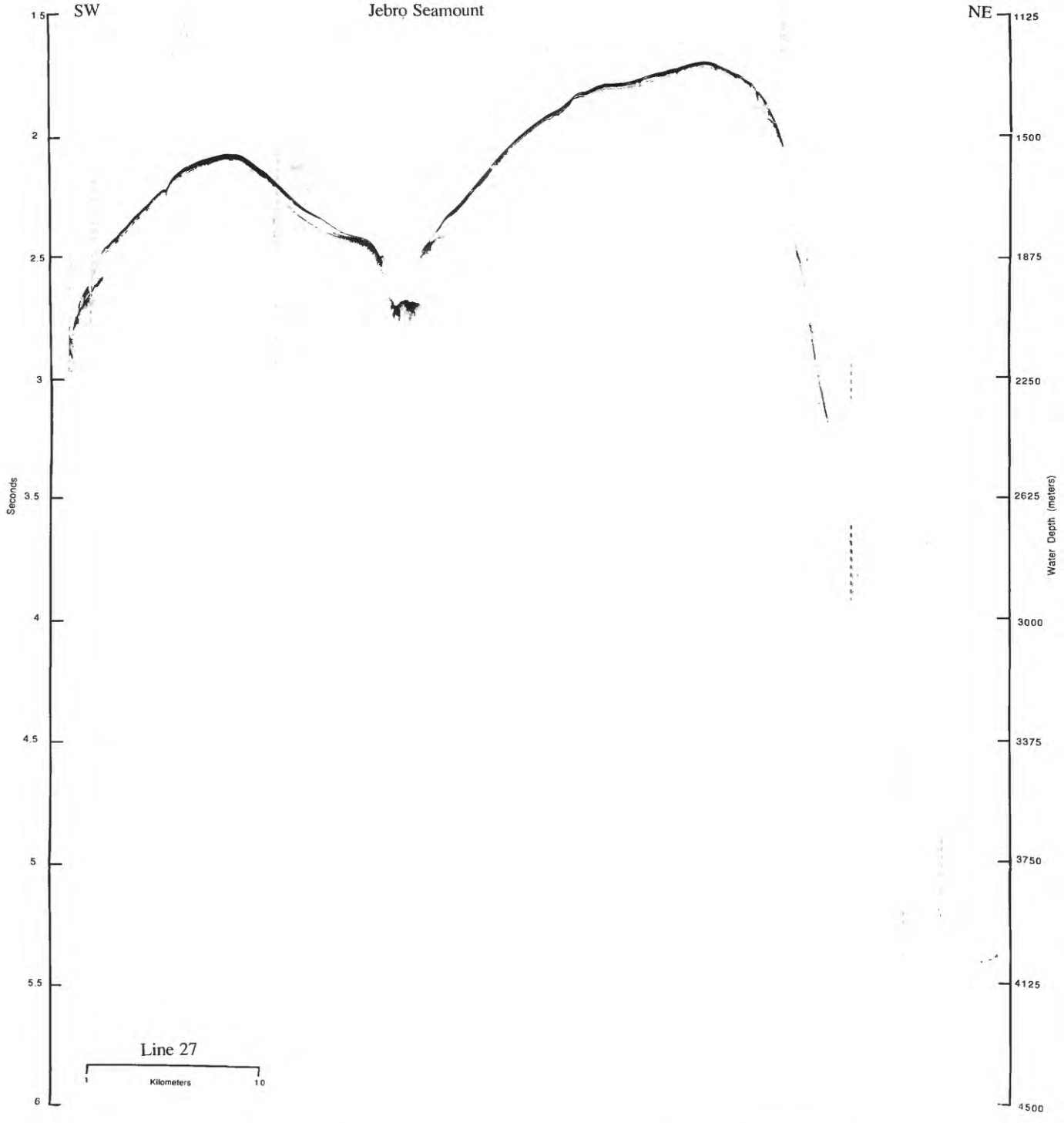

Figure 64. Southwest and northeast peaks of Jebro Seamount, 3.5 kHz line 27 (see Fig. 12 for location).

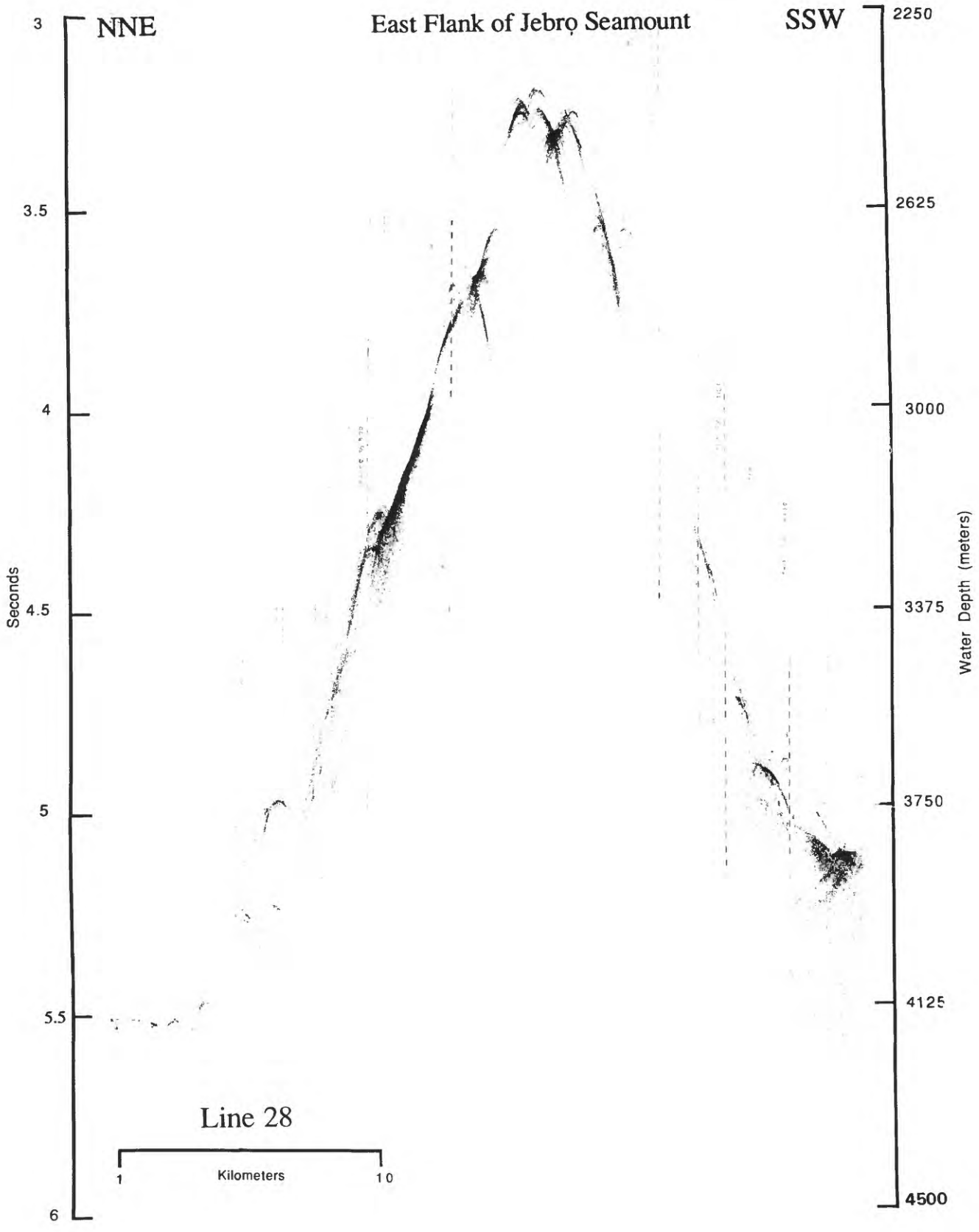

Figure 65. East flank of the northeast peak of Jebro Seamount, 3.5 kHz line 28 (see Fig. 12 for location).

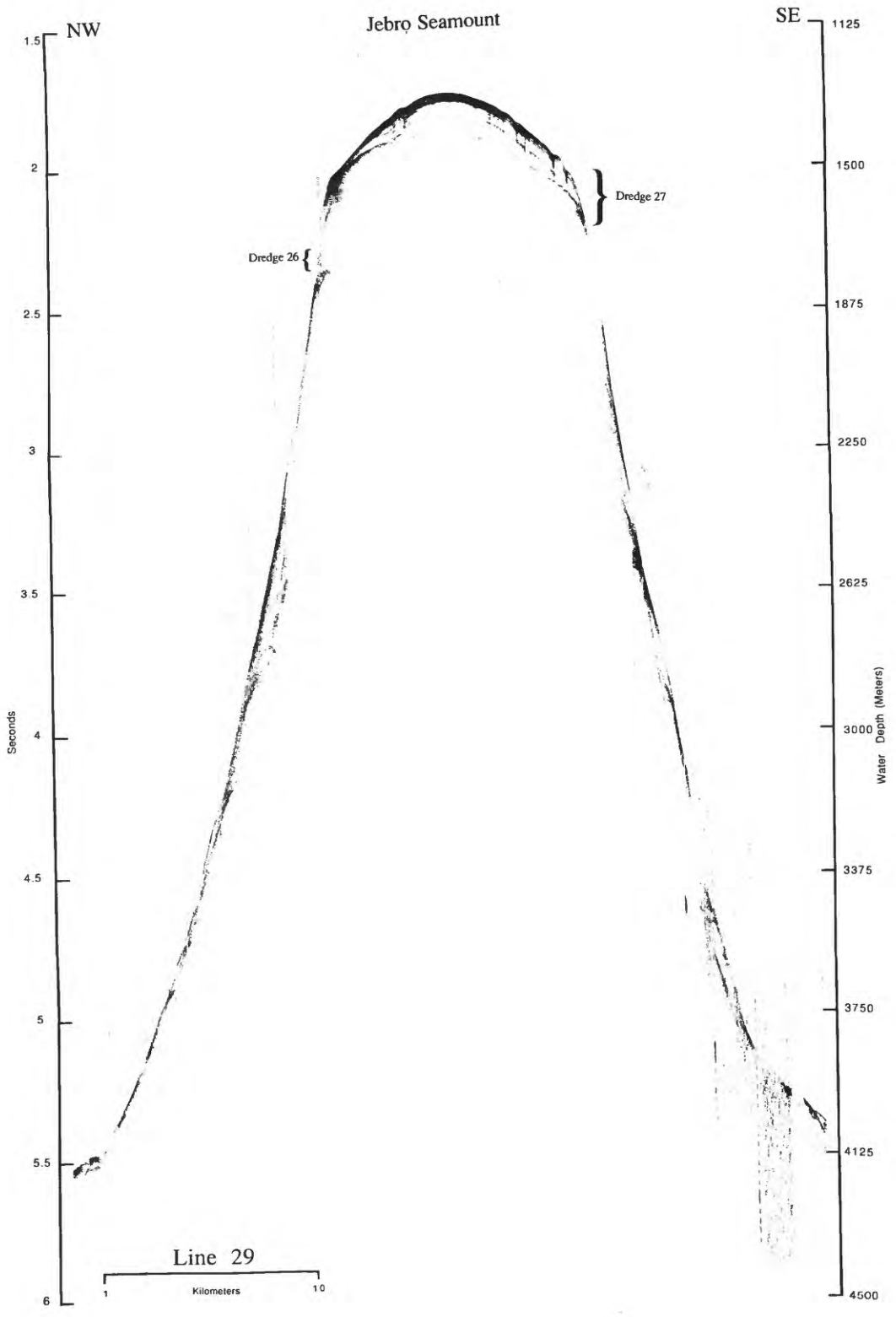

Figure 66. Northeast peak of Jebro Seamount, 3.5 kHz line 29 (see Fig. 12 for location). Note location of dredges D26 and D27.

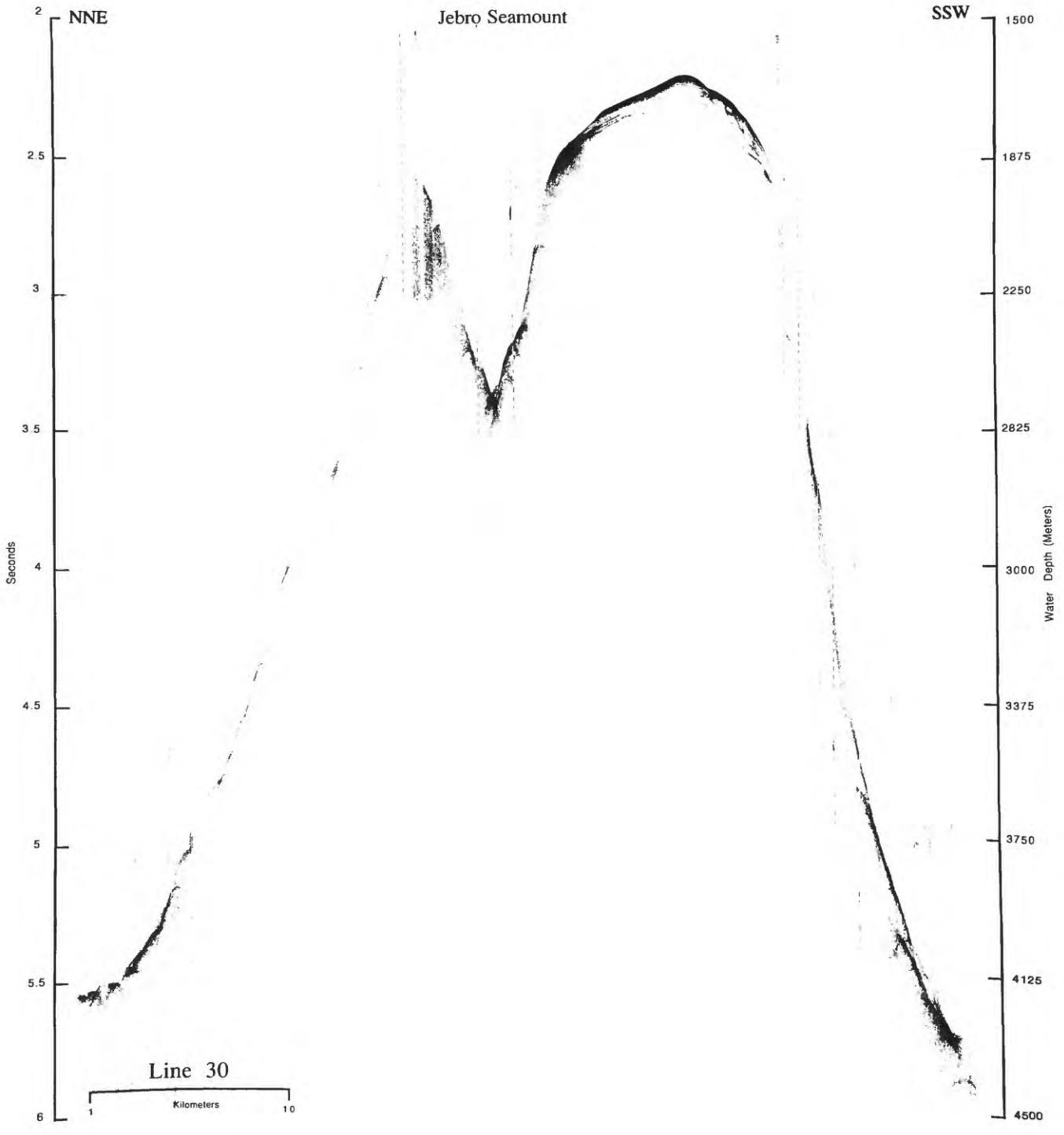

Figure 67. Northwest flank of the northeast peak and the southwest peak of Jebro Seamount, 3.5 kHz line 30 (see Fig. 12 for location).

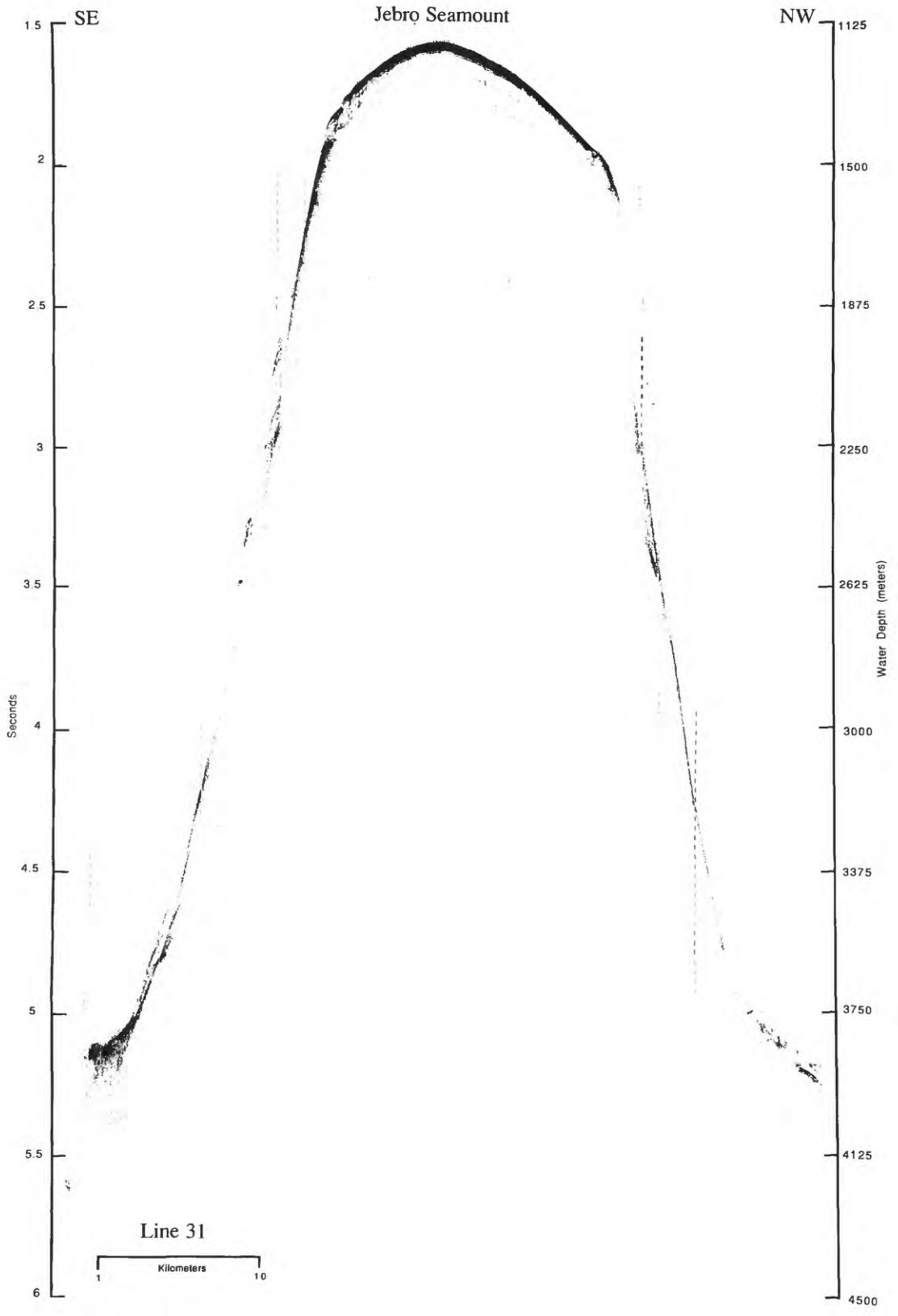

Figure 68. Southwest peak of Jebro Seamount, 3.5 kHz line 31 (see Fig. 12 for location).

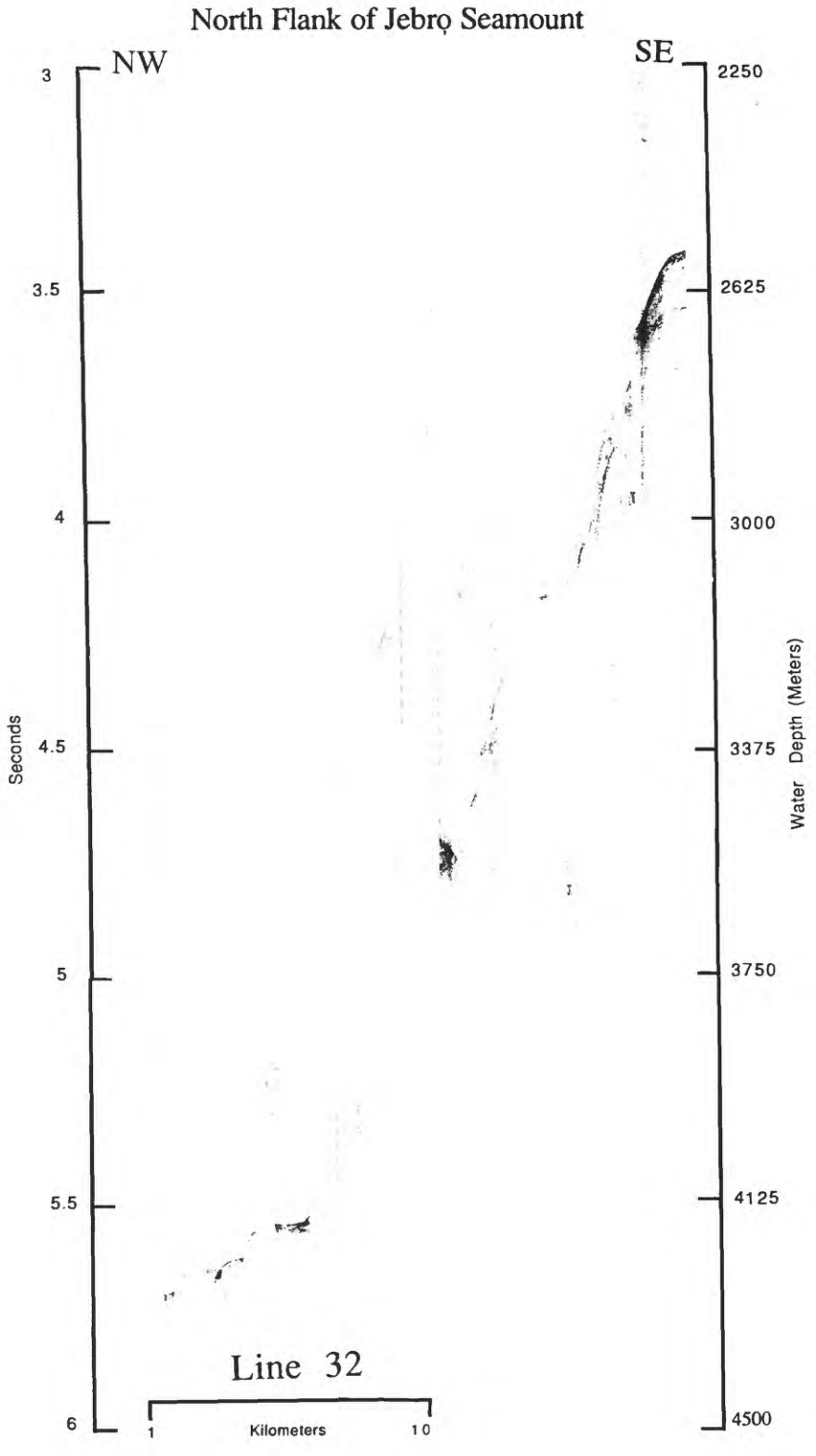

Figure 69. North flank of the southwest peak of Jebro Seamount, 3.5 kHz line 32 (see Fig. 12 for location).

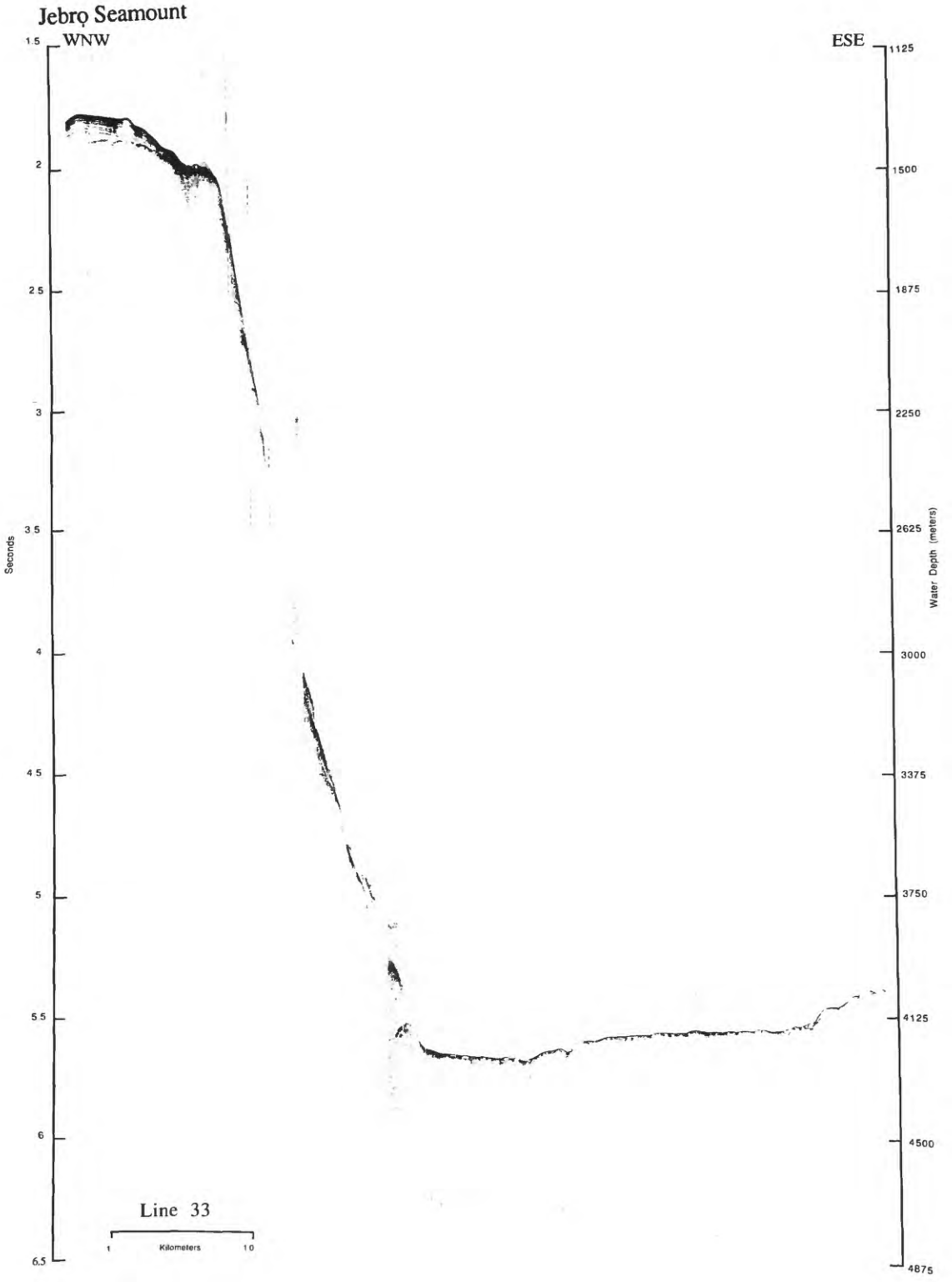

Figure 70. Northeast peak of Jebro Seamount and the archipelagic apron between Aelōnļapļap and Majro Atolls, 3.5 kHz line 33 (see Fig. 12 for location).

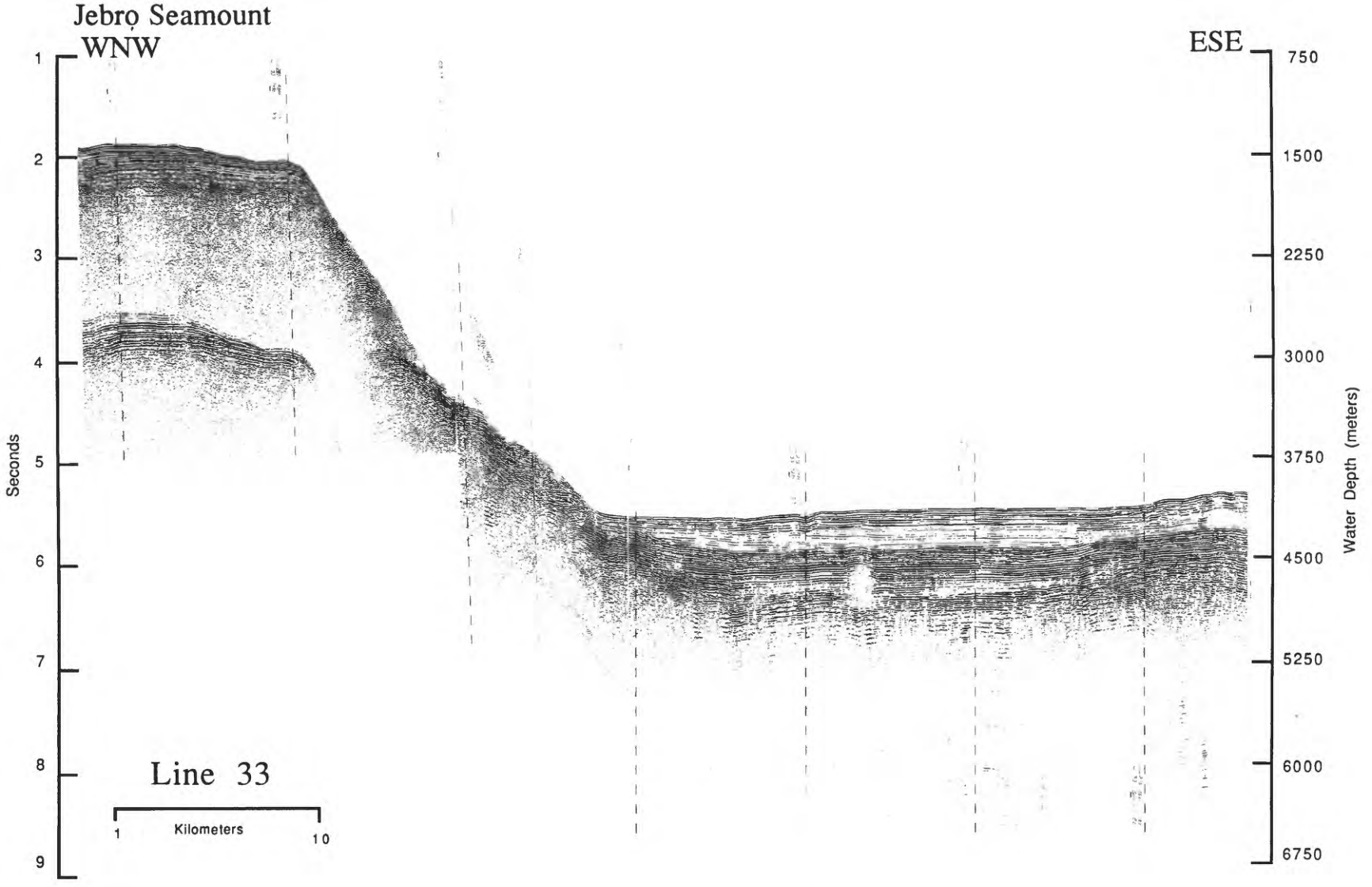

Figure 71. Northeast peak of Jebro Seamount and the archipelagic apron between Aelōñļapļap and Mājro Atolls, 160 in^3 single-channel airgun line 33.

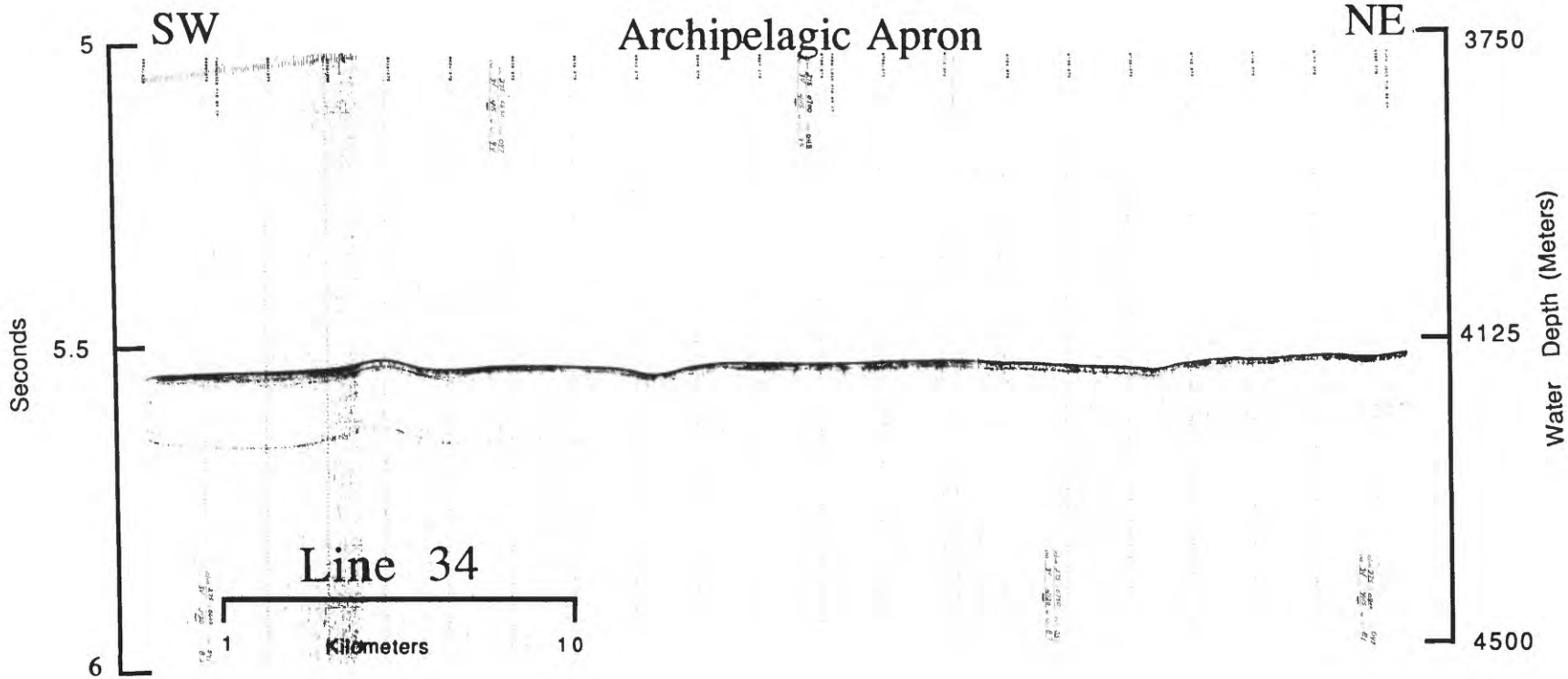

Figure 72. Archipelagic apron between Aelōṇlapḷap and Mājro Atolls, 3.5 kHz line 34 (see Fig. 12 for location).

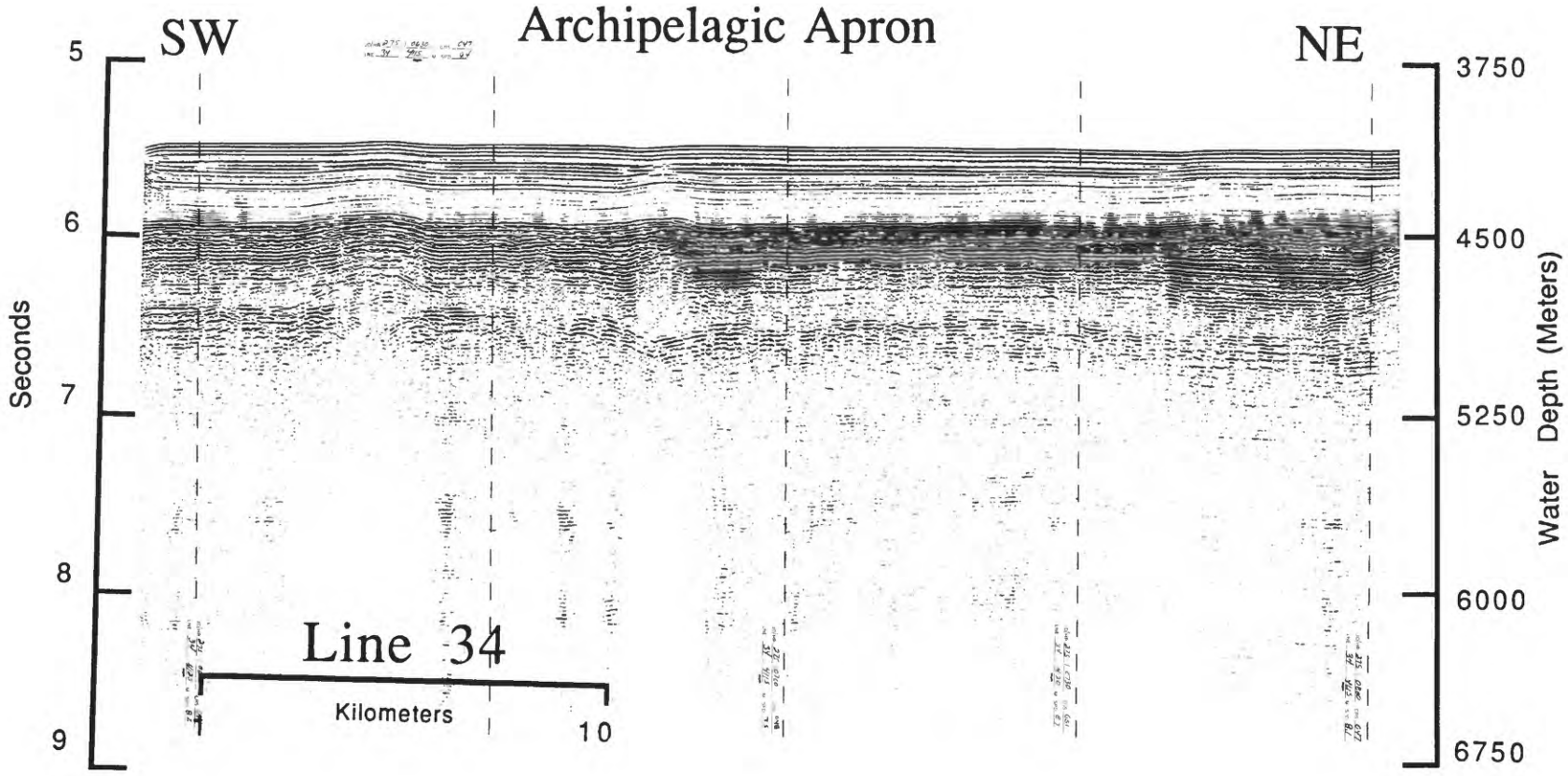

Figure 73. Archipelagic apron between Aelōñļapļap and Mājro Atolls, 160 in^3 single-channel airgun line 34.

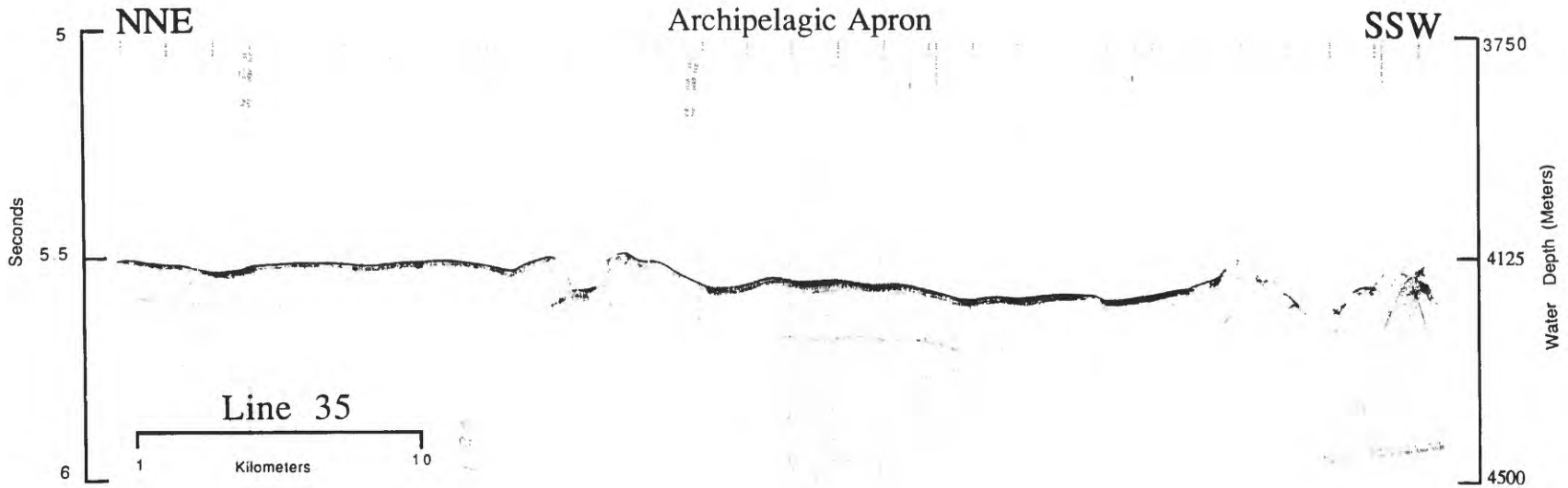

Figure 74. Archipelagic apron between Aelōñļapļap and Mājro Atolls, 3.5 kHz line 35 (see Fig. 12 for location).

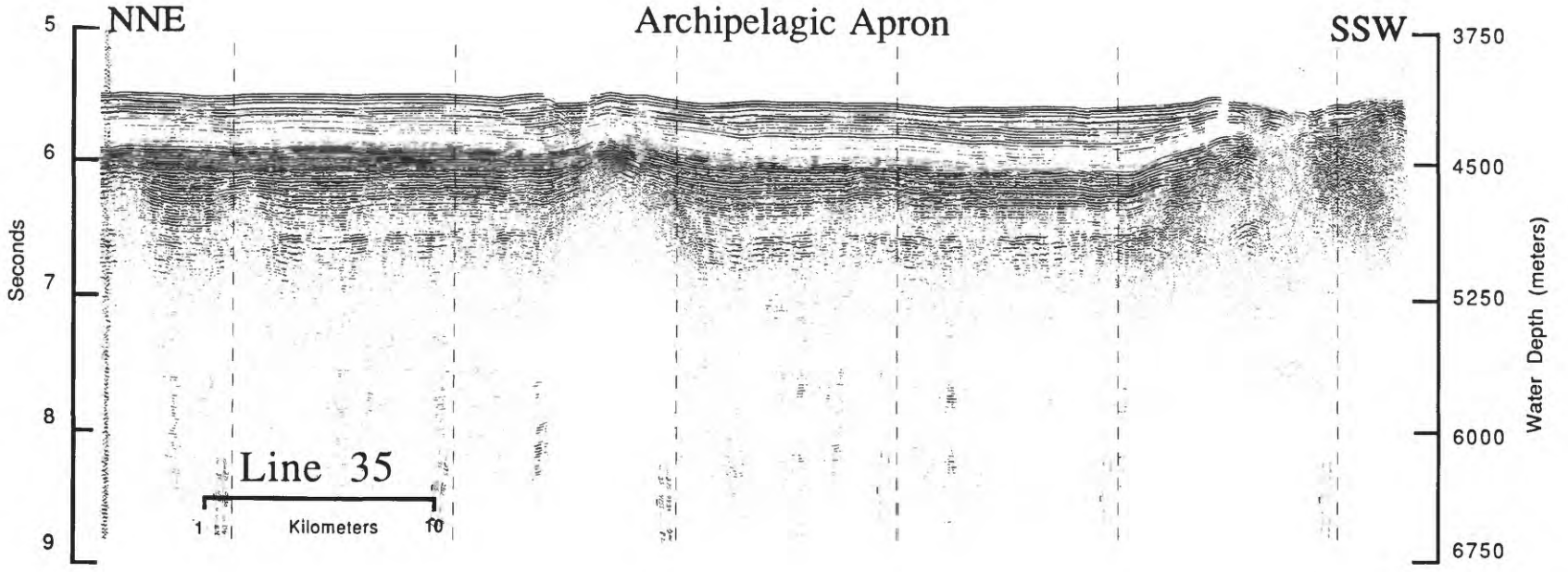

Figure 75. Archipelagic apron between Aelōñļapļap and Mājro Atolls, 160 in^3 single-channel airgun line 35.

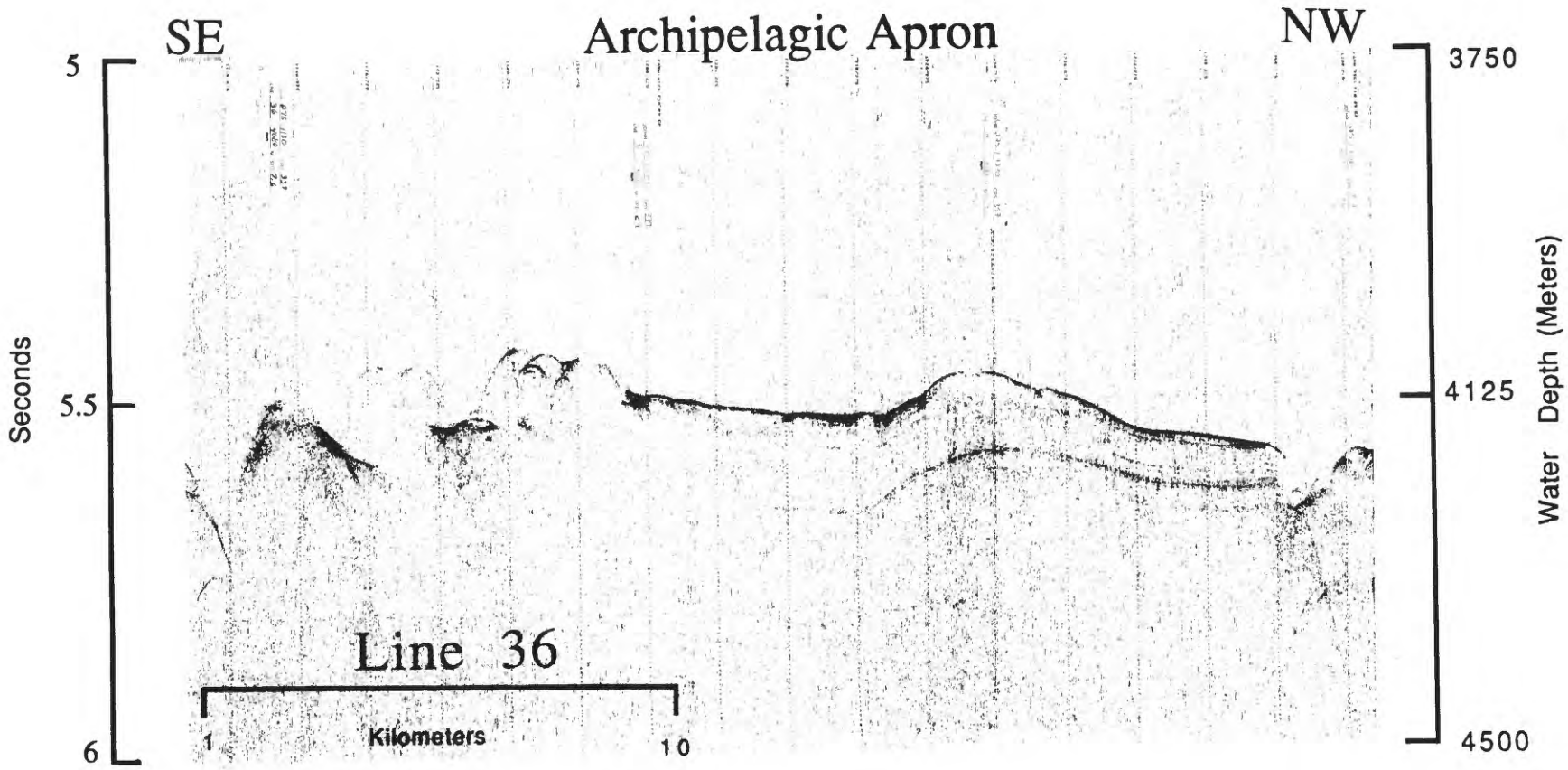

Figure 76. Archipelagic apron between Aelōñļapļap and Mājro Atolls, 3.5 kHz line 36 (see Fig. 12 for location).

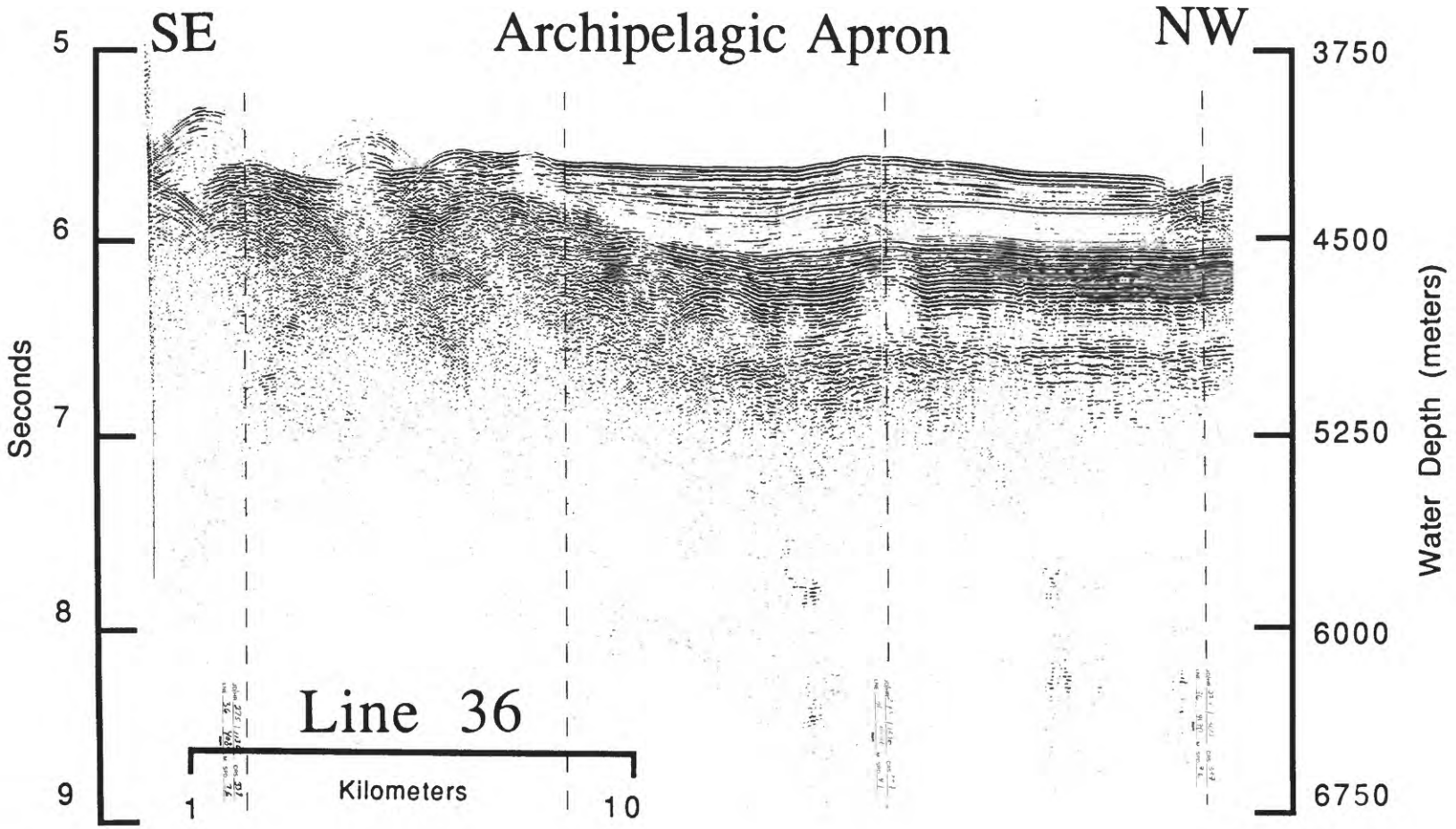

Figure 77. Archipelagic apron between Aelōñļapļap and Mājro Atolls, 160 in^3 single-channel airgun line 36.

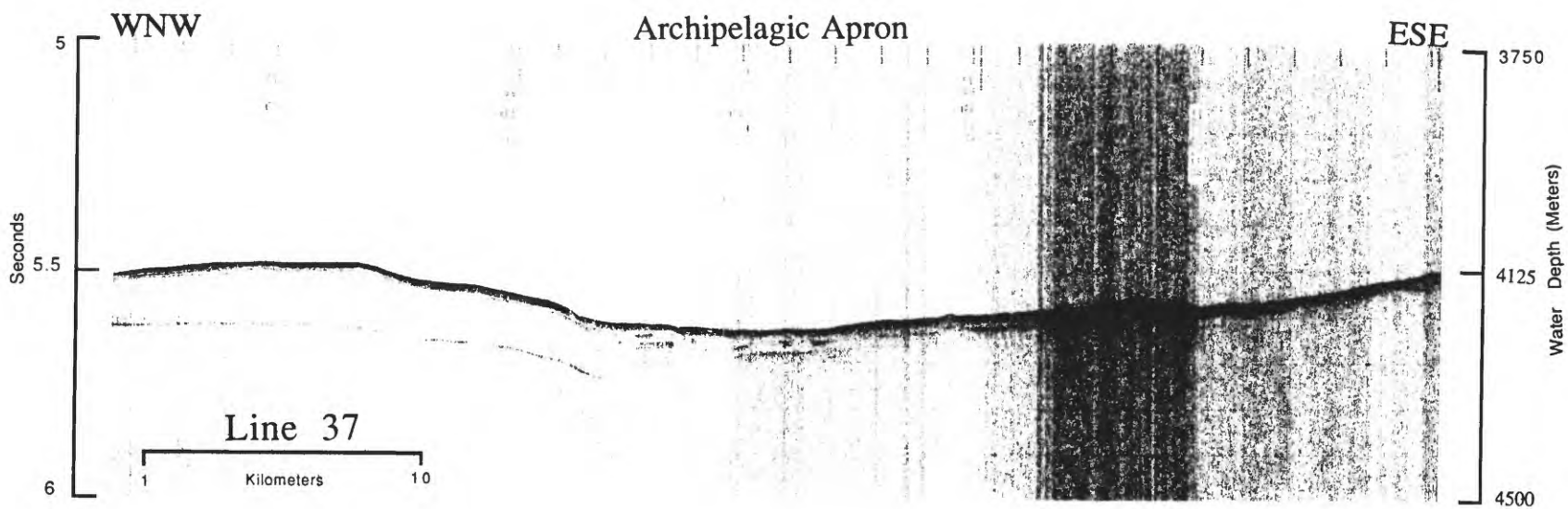

Figure 78. Archipelagic apron between Aelōñlapļap and Mājro Atolls, 3.5 kHz line 37 (see Fig. 12 for location).

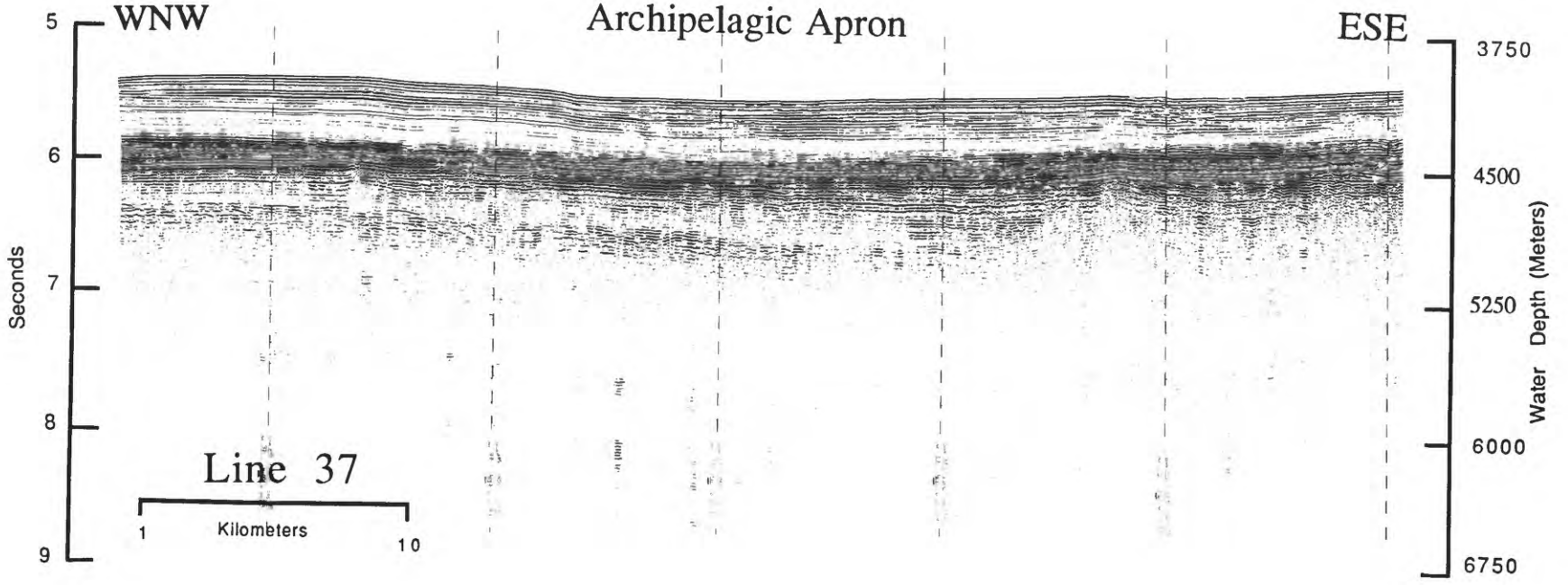

Figure 79. Archipelagic apron between Aelōñḷapḷap and Mājro Atolls, 160 in^3 single-channel airgun line 37.

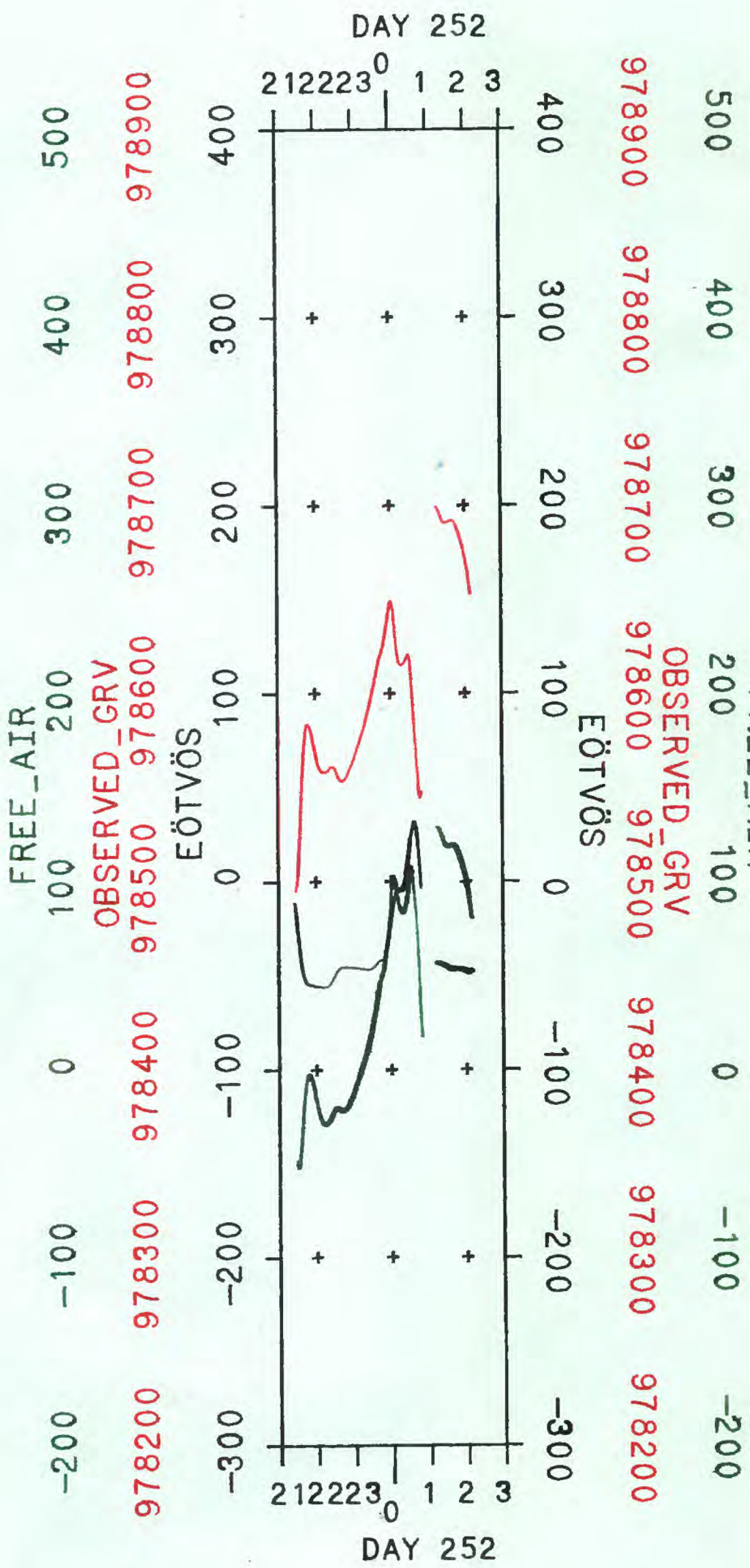

Figure 80. Gravity profiles for line KS1 over Karin Seamount near Johnston Island. Each division on the vertical scale equals 100 mGal.

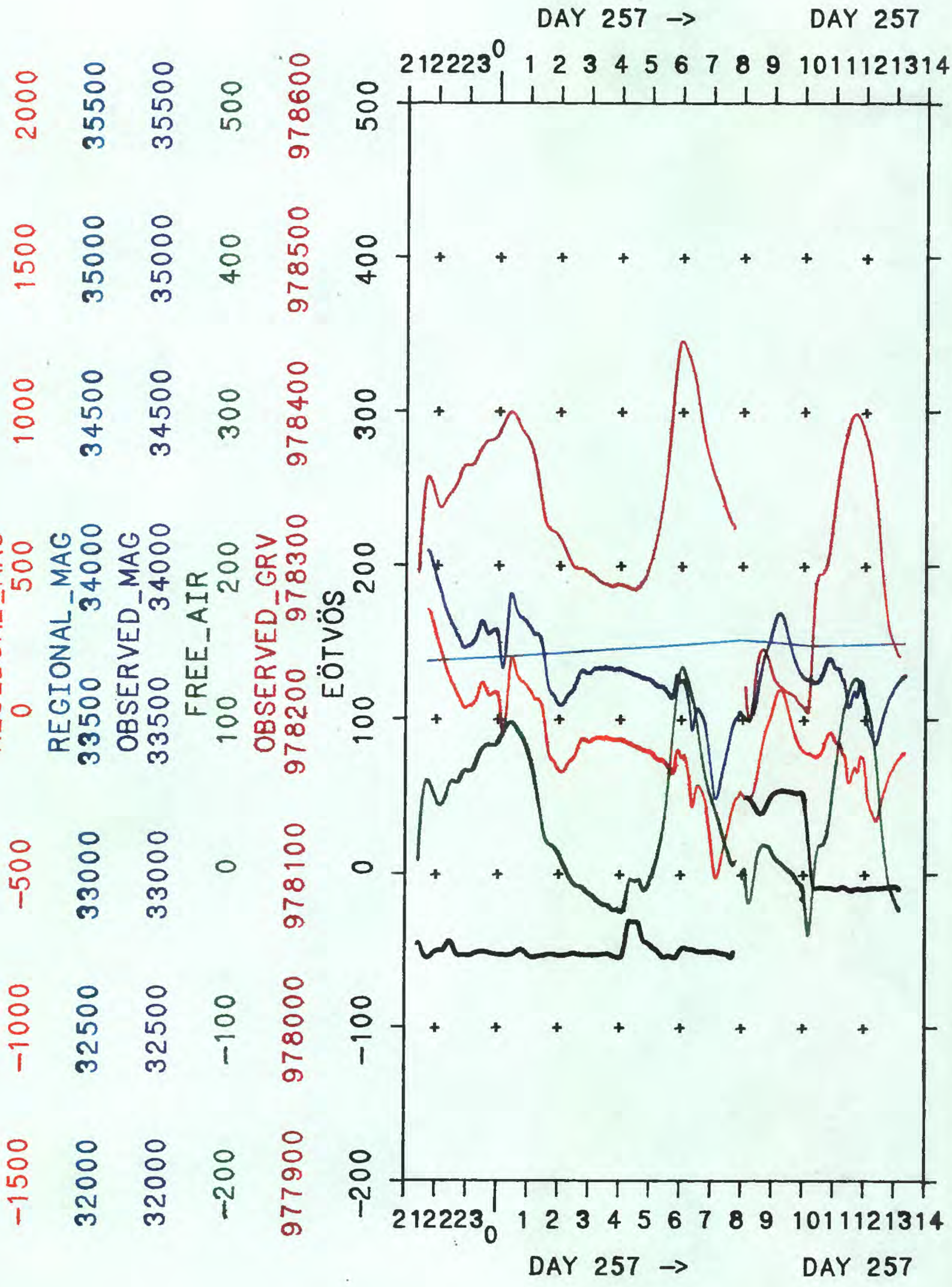

Figure 81. Gravity and magnetic profiles for lines 1-3 over Ruwitūñtūñ and Look Seamounts. Line 2 begins at Julian day 257, 0805 and line 3 at Julian day 257, 1010. Each division on the vertical scale equals 100 mGal or 500 gammas.

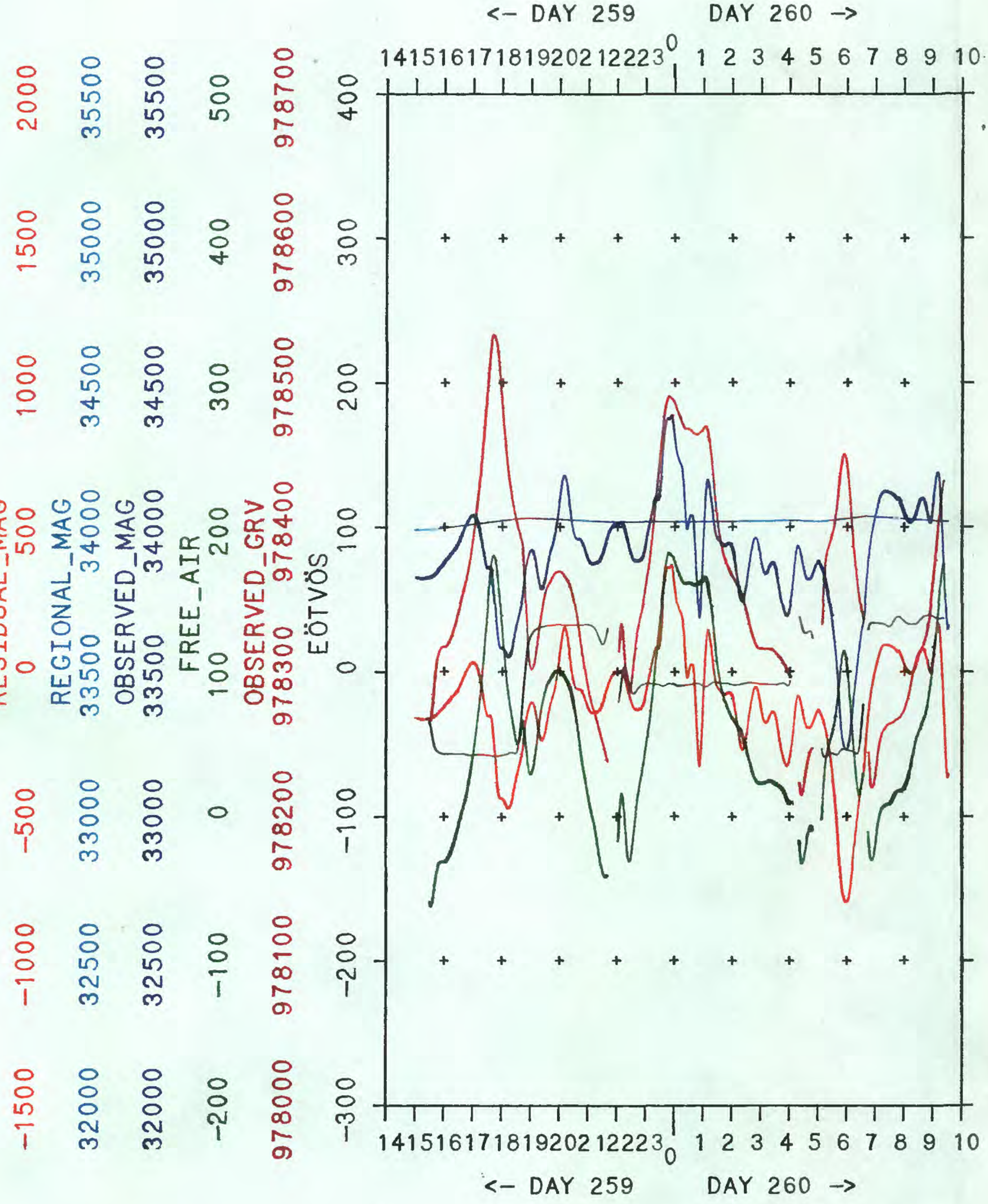

Figure 82. Gravity and magnetic profiles for lines 4-9 over Ḷāānṃōjānjān Seamount. Lines 5, 6, 7, 8, and 9 begin at Julian day 259 (1835), JD 259 (2200),JD 260 (0425), JD 260 (0503), and JD 260 (0700), respectively. Each division on the vertical scale equals 100 mGal or 500 gammas.

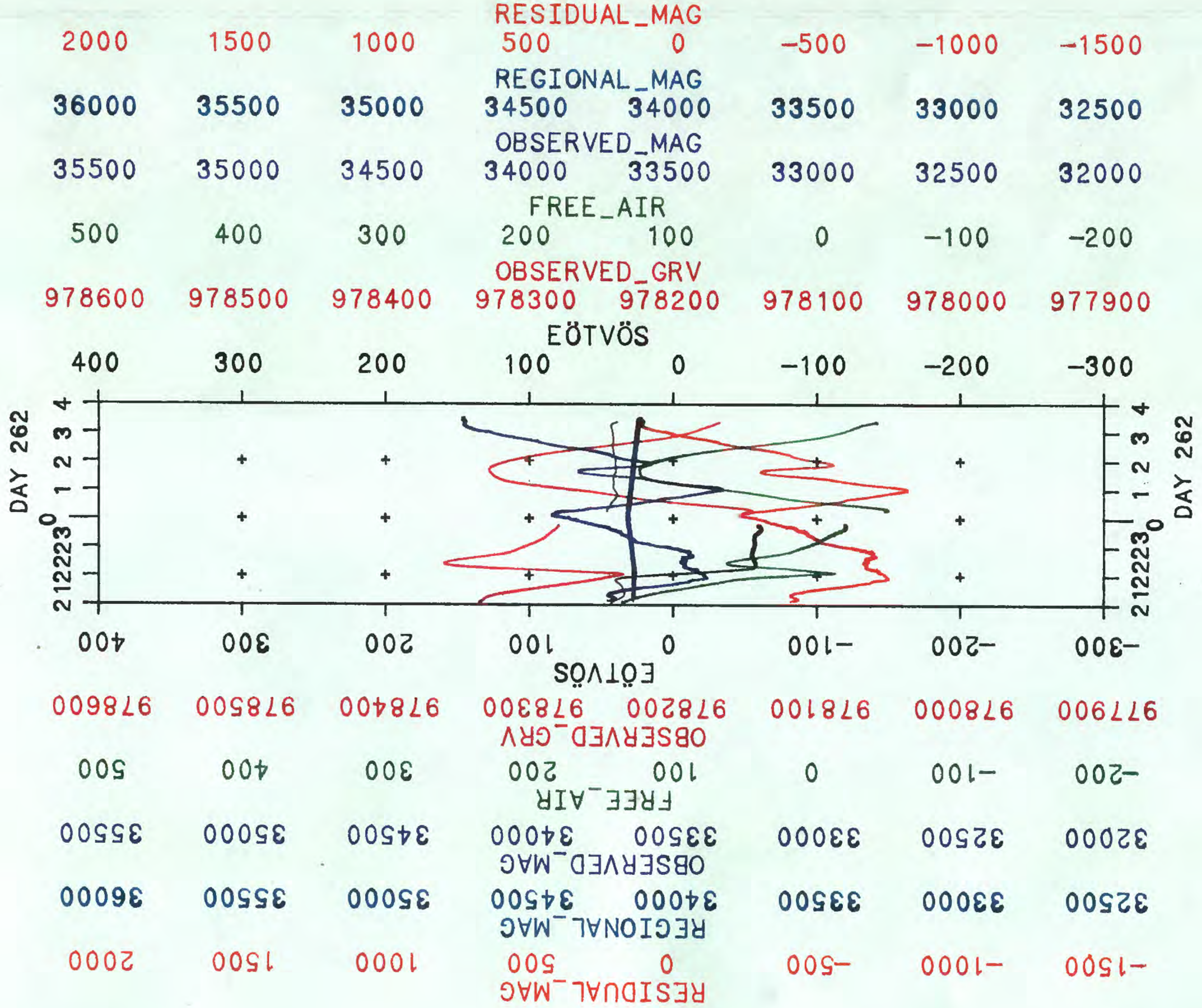

Figure 83. Gravity and magnetic profiles for lines 12-14 over Lomilik Seamount. Lines 13 and 14 begin at JD 261 (2206) and JD 262 (0008), respectively. Each division on the vertical scale equals 100 mGals or 500 gammas.

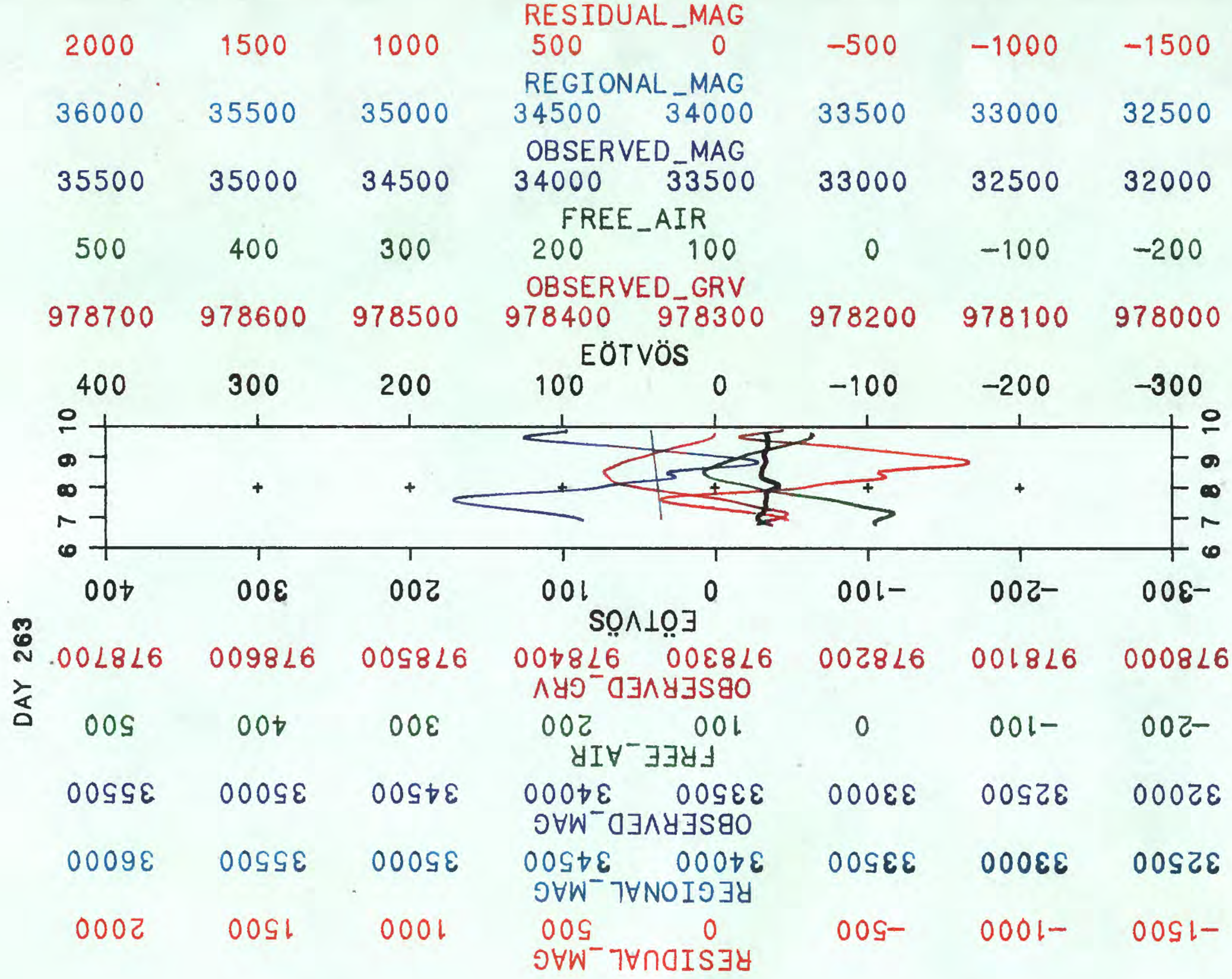

Figure 84. Gravity and magnetic profiles for line 15 over Lõjemeja Seamount. Each division on the vertical scale equals 100 mGal or 500 gammas.

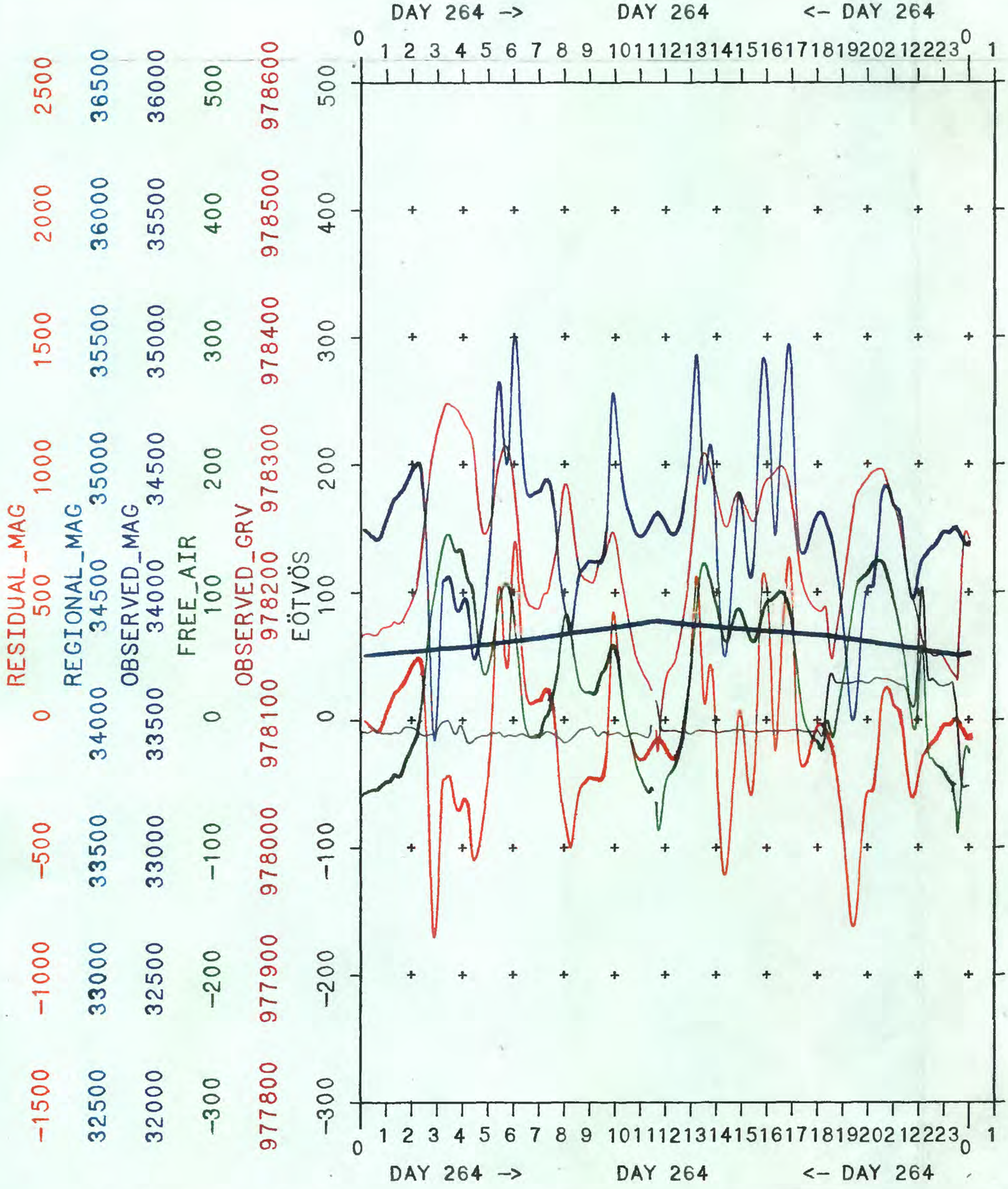

Figure 85. Gravity and magnetic profiles for lines 16 through first part of 19 over the Ujlañ volcanic complex. Lines 17, 18, and 19 begin at JD 264 (1140), JD264 (1820), and JD 264 (2334), respectively. Each division on the vertical scale equals 100 mGal or 500 gammas.

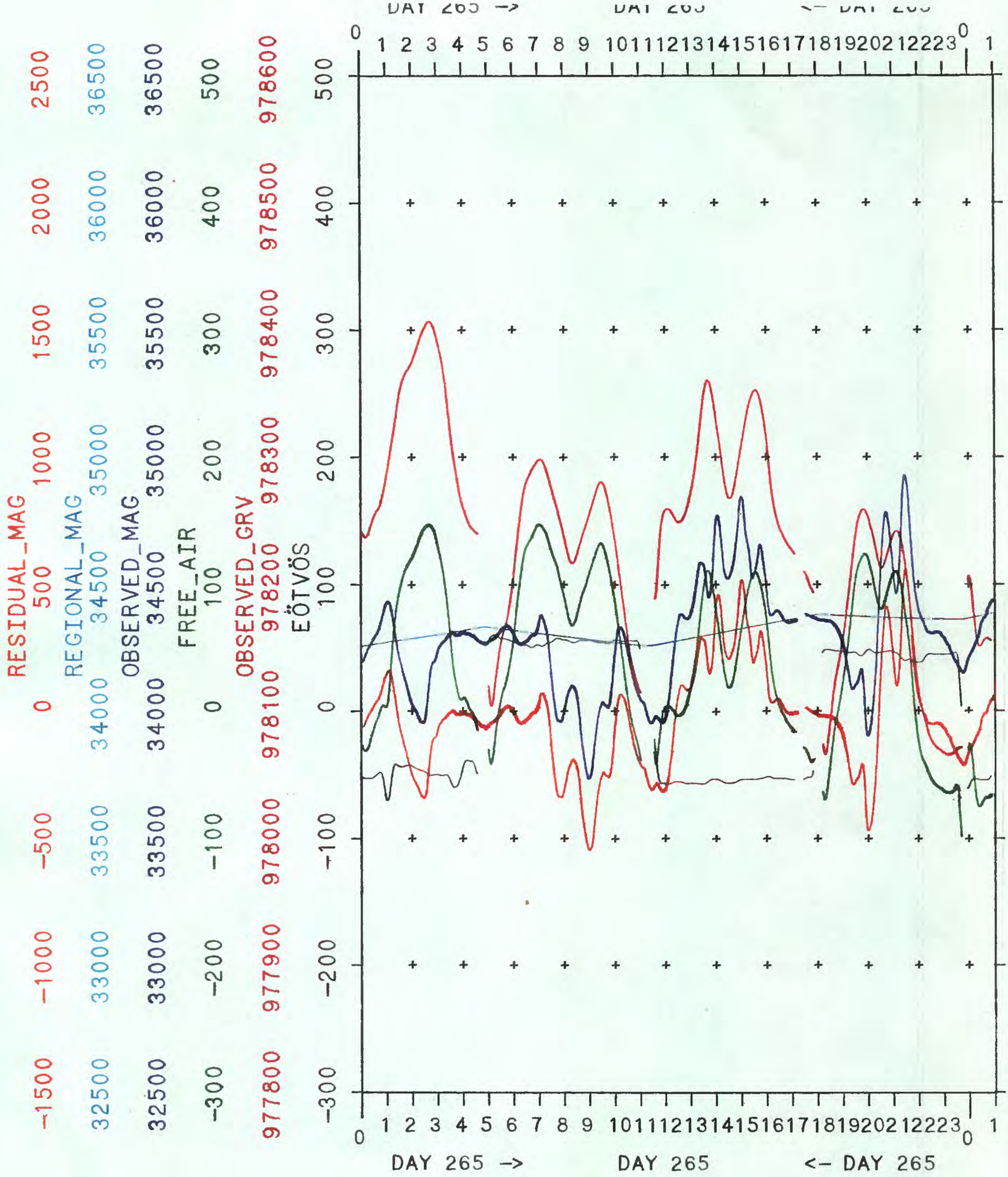

Figure 86. Gravity and magnetic profiles for lines 19-23 over the Ujlañ volcanic complex. Lines 20, 21, 22, and 23 begin at JD 265 (0501) JD 265 (1137), JD 265 (1808), and JD 265 (2346), respectively. Each division on the vertical scale equals 100 mGal or 500 gammas.

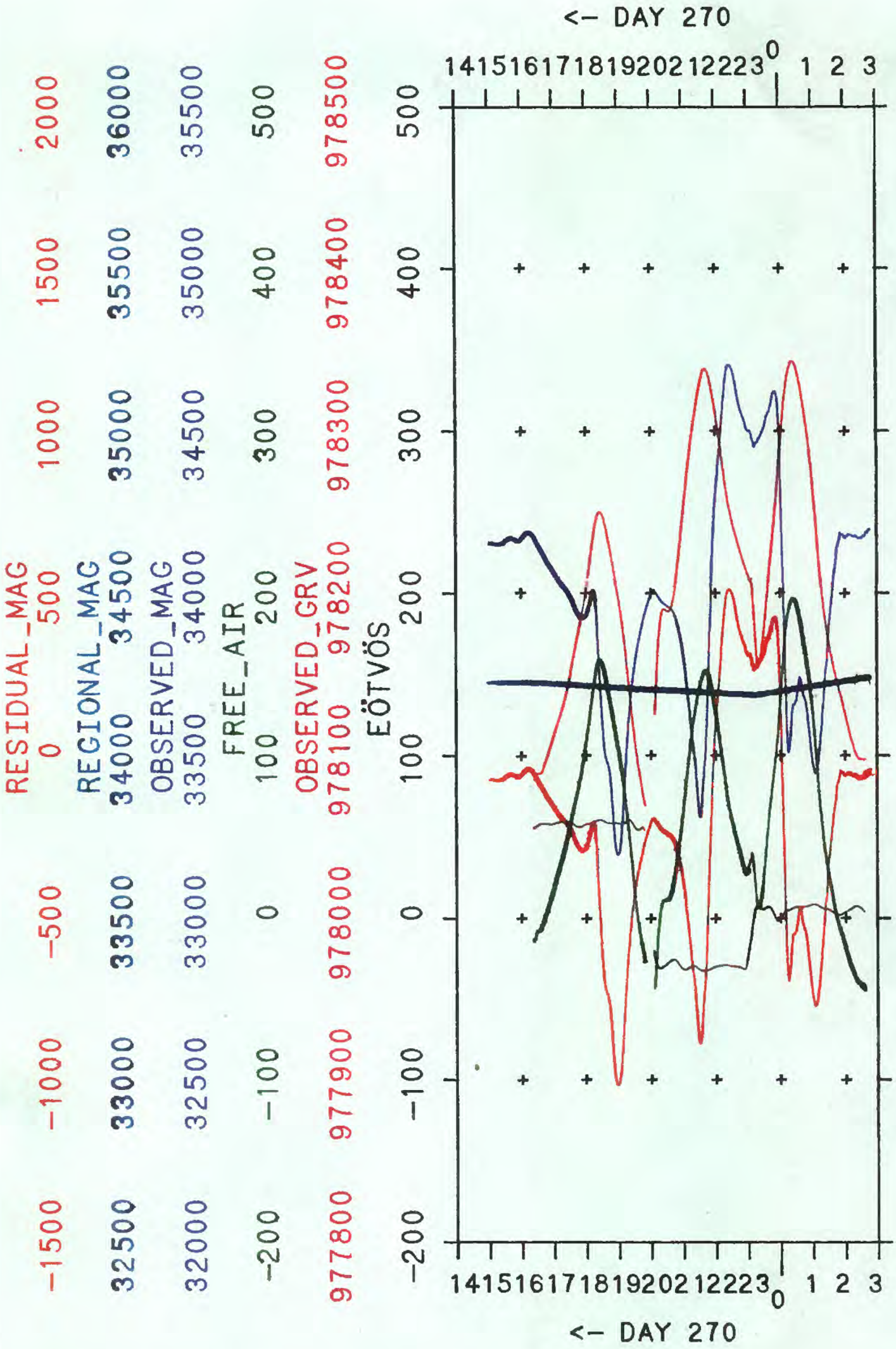

Figure 87. Gravity and magnetic profiles for lines 24-26 over Mij-Lep Seamount. Lines 25 and 26 begin at JD270 (2004) and JD 270 (2310), respectively. Each division on the vertical scale equals 100 mGal or 500 gammas.

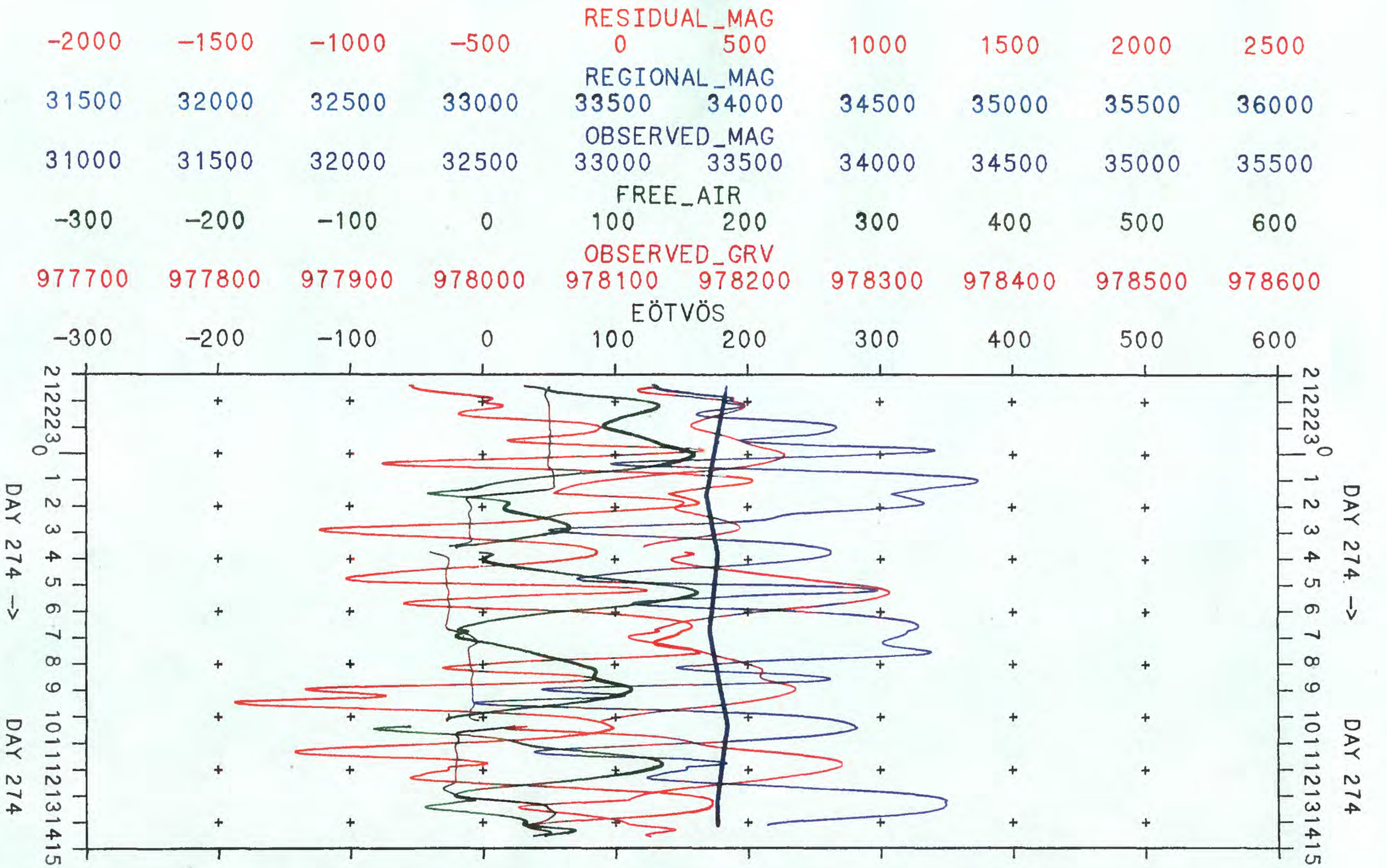

Figure 88. Gravity and magnetic profiles for lines 27-32 over Jebro Seamount. Lines 28, 29, 30, 31, and 32 begin at JD 273 (0132), JD 274 (0348), JD 274 (0644), JD 274 (1025), and JD 274 (1311), respectively. Each division on the vertical scale equals 100 mGal or 500 gammas.

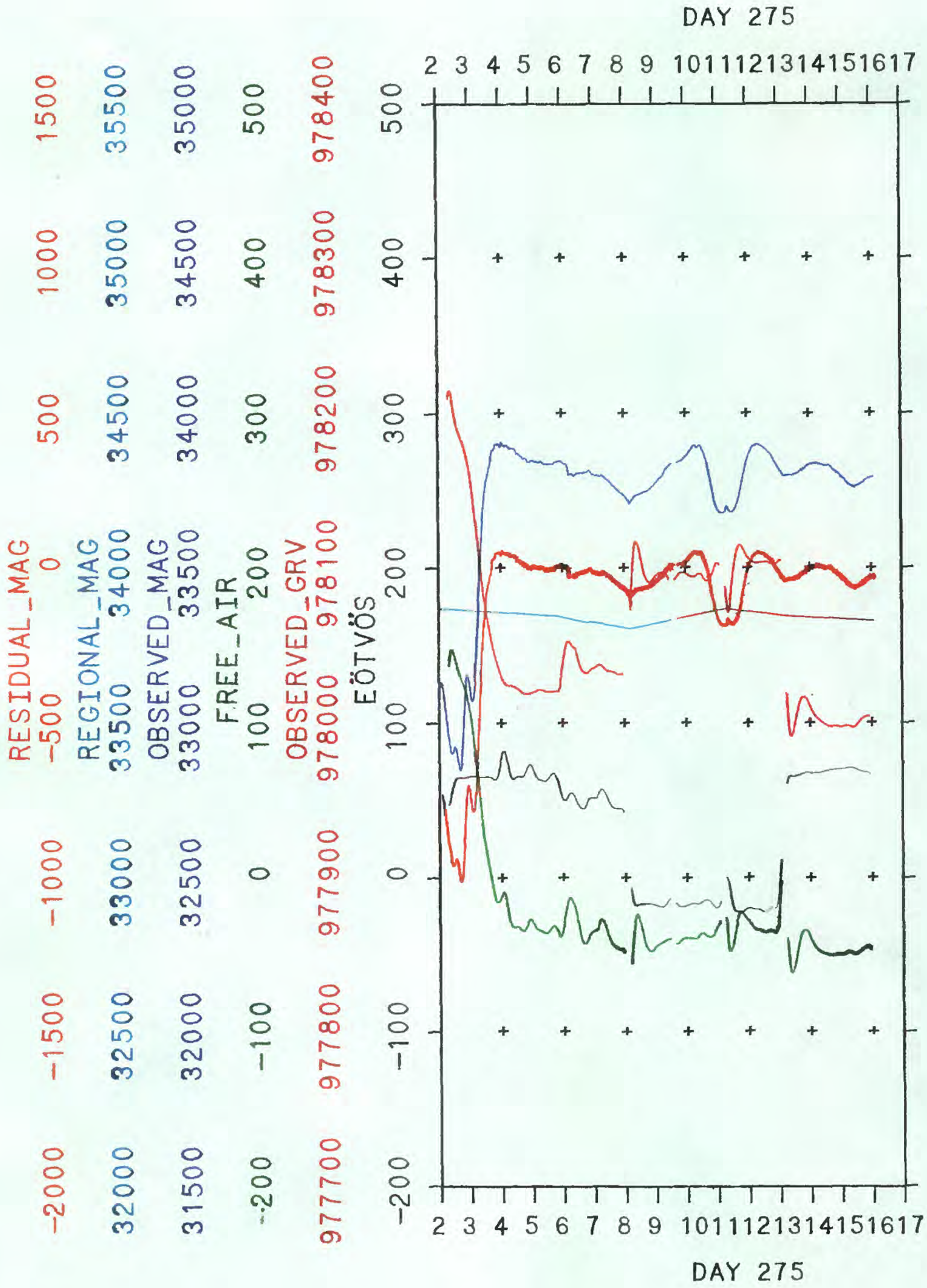

Figure 89. Gravity and magnetic profiles for lines 33-37 over the archipelagic apron. Lines 34, 35, 36, and 37 begin at JD 275 (0554), JD 275 (0812), JD 275 (1120) and JD 275 (1308). Each division on the vertical scale equals 100 mGal or 500 gammas.

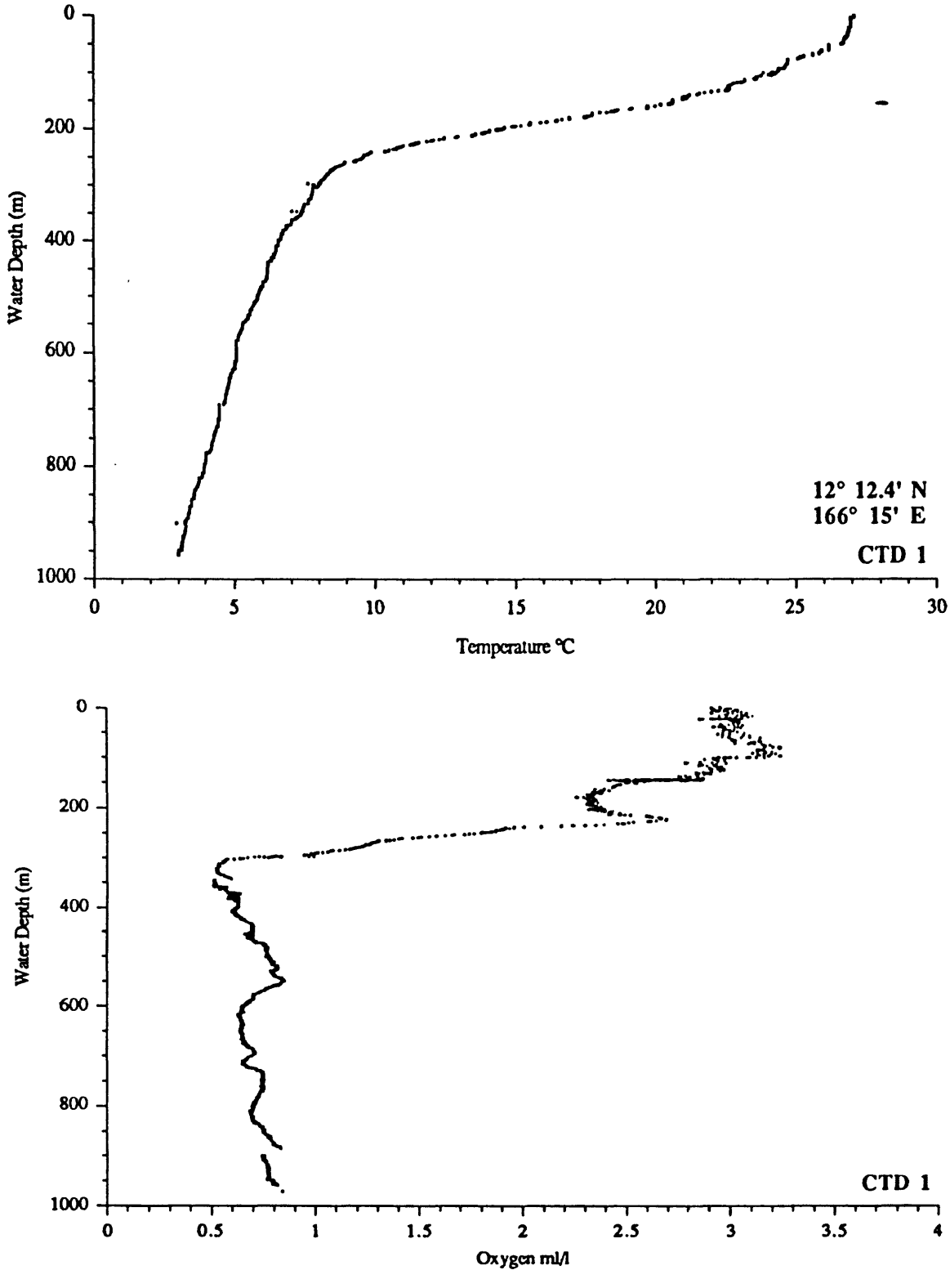

Figure 90. Temperature and oxygen content versus water depth for CTD 1, Look Seamount. Water depth at station is 1000 meters.

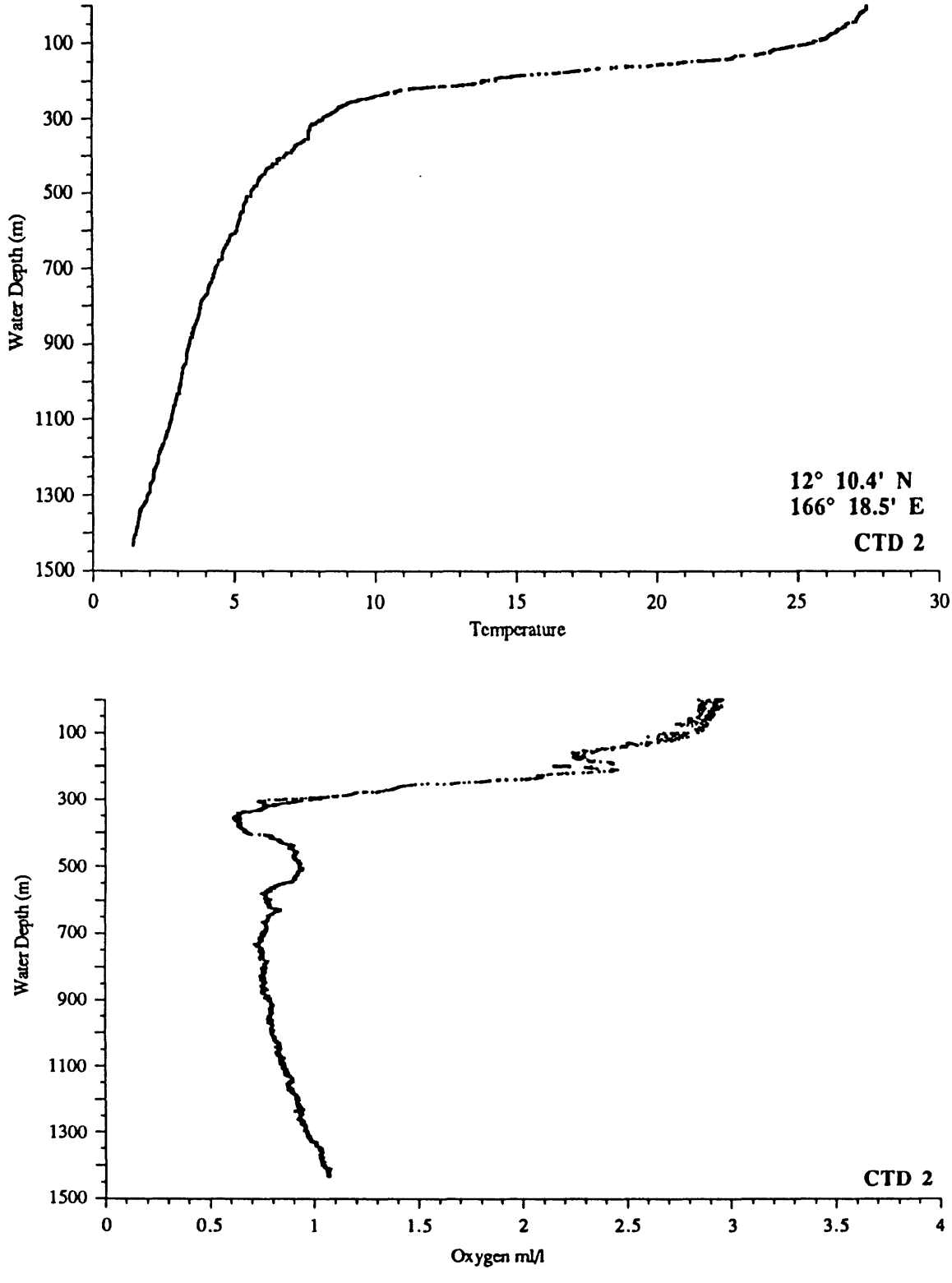

Figure 91. Temperature and oxygen content versus water depth for CTD 2, Look Seamount. Water depth at station is 2000 meters.

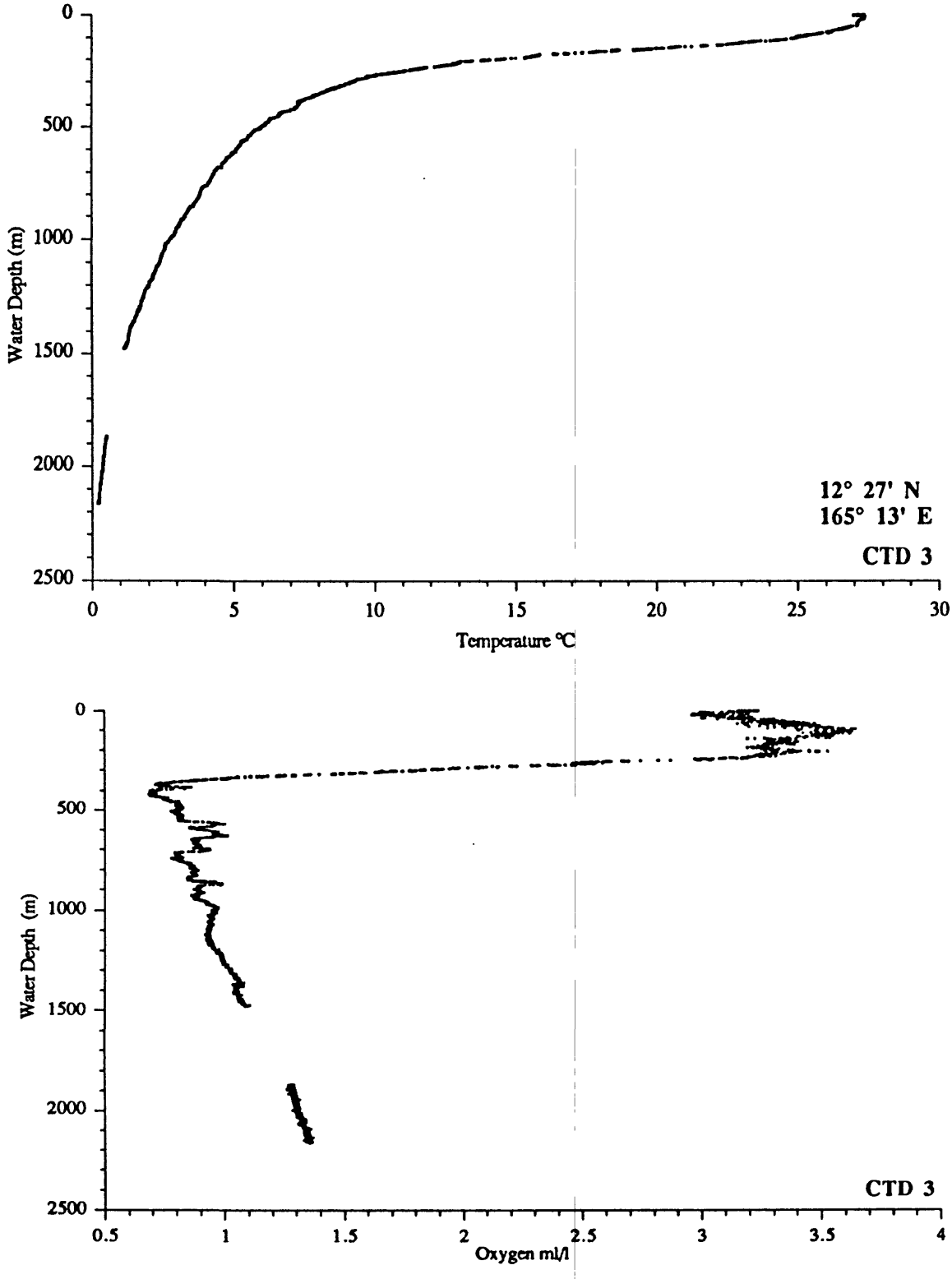

Figure 92. Temperature and oxygen content versus water depth for CTD 3, open ocean. Water depth at station is 4758 meters.

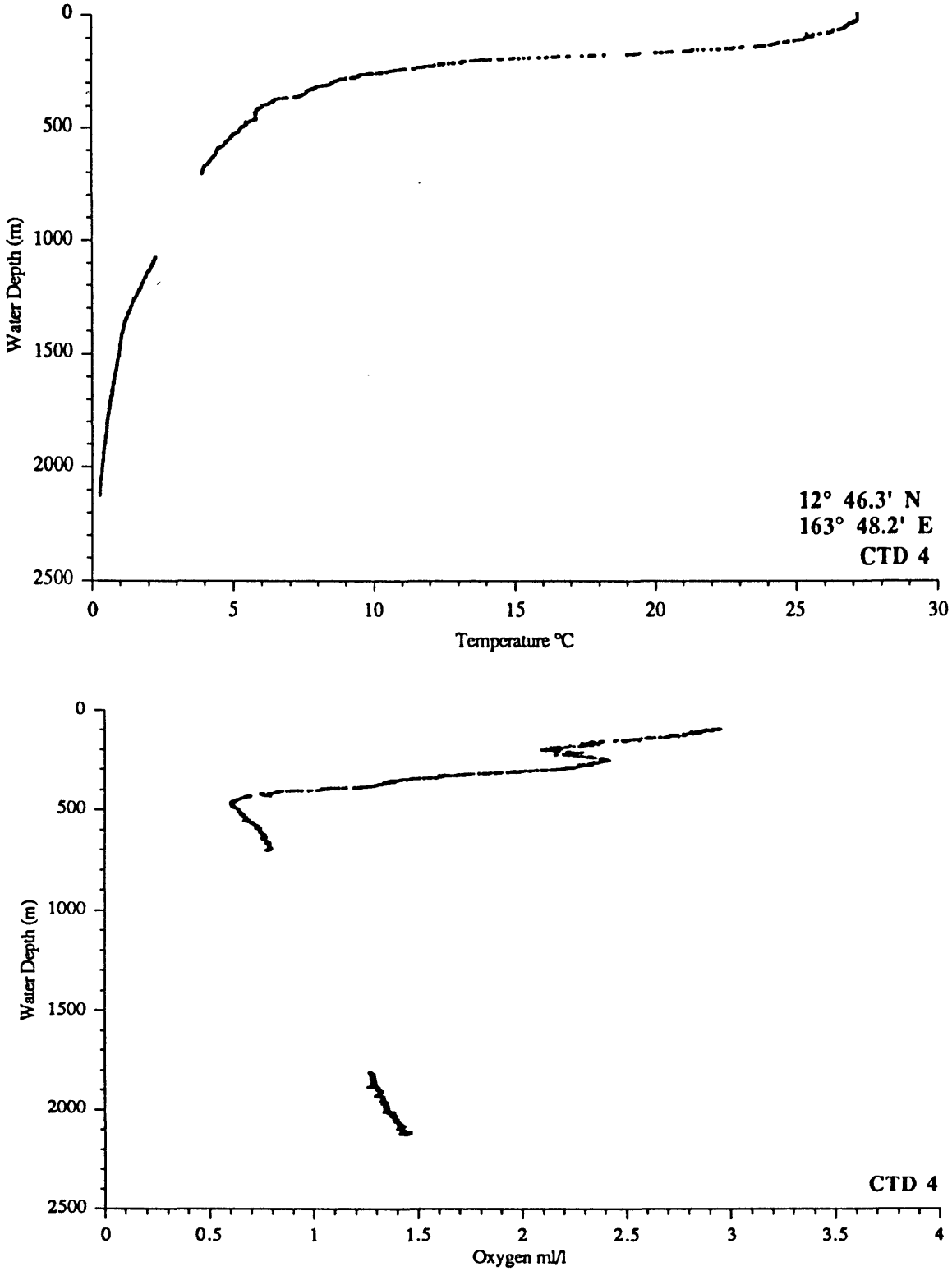

Figure 93. Temperature and oxygen content versus water depth for CTD 4, open ocean. Water depth at station is 5600 meters.

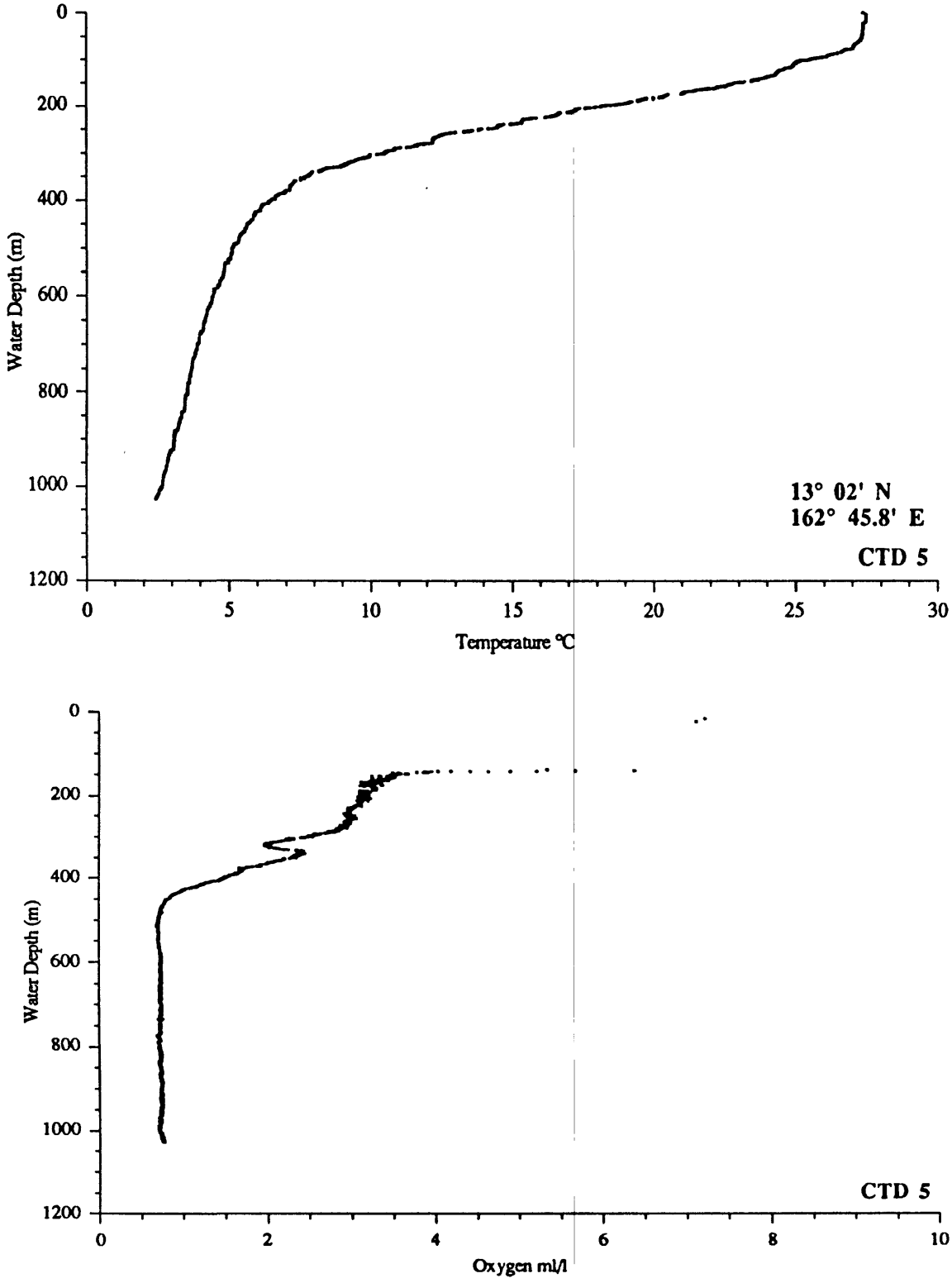

Figure 94. Temperature and oxygen content versus water depth for CTD 5, North Ļāānṃōjānjān Seamount. Water depth at station is 1090 meters.

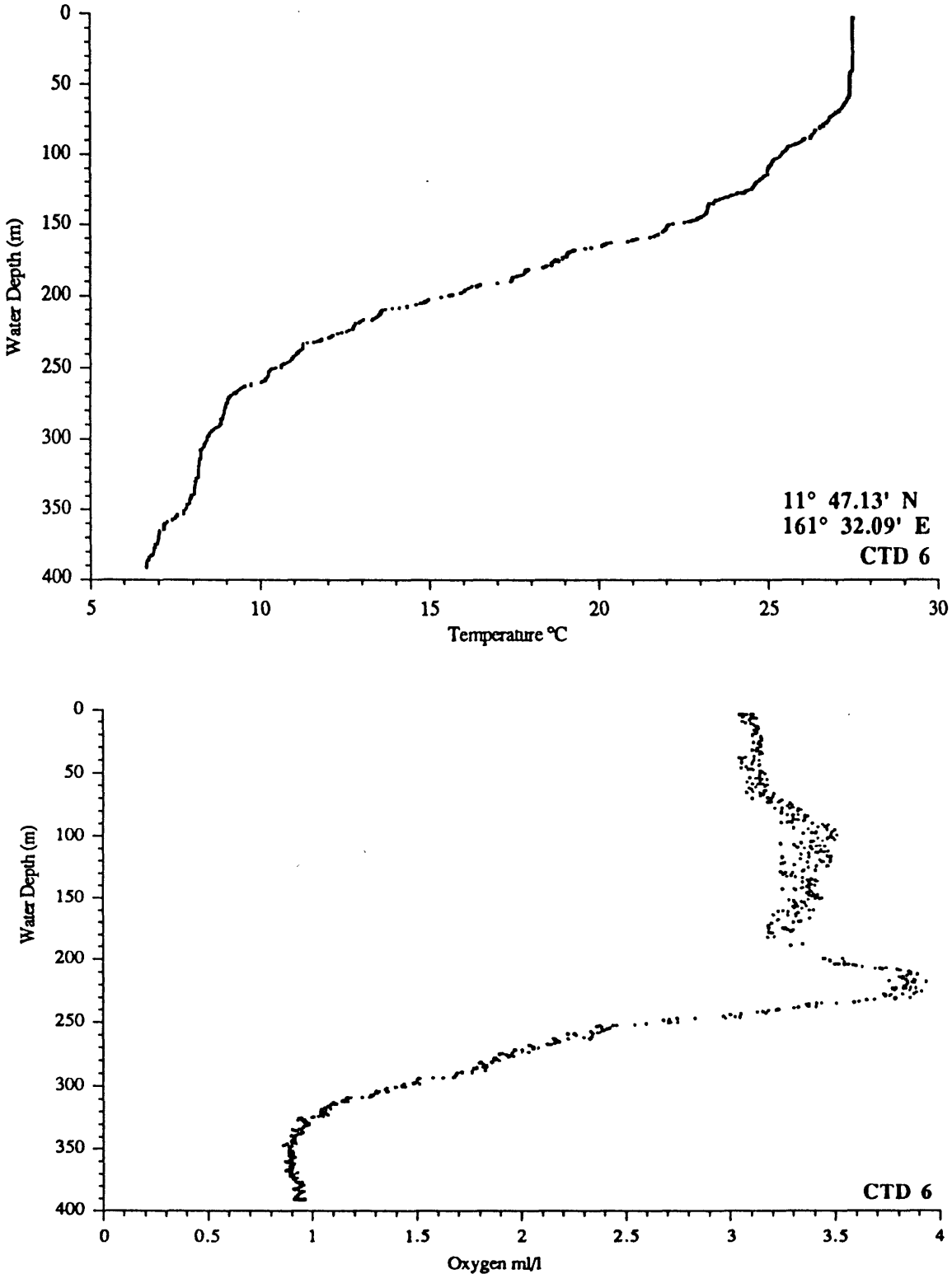

Figure 95. Temperature and oxygen content versus water depth for CTD 6, Lomilik Seamount. Water depth at station is 2505 meters.

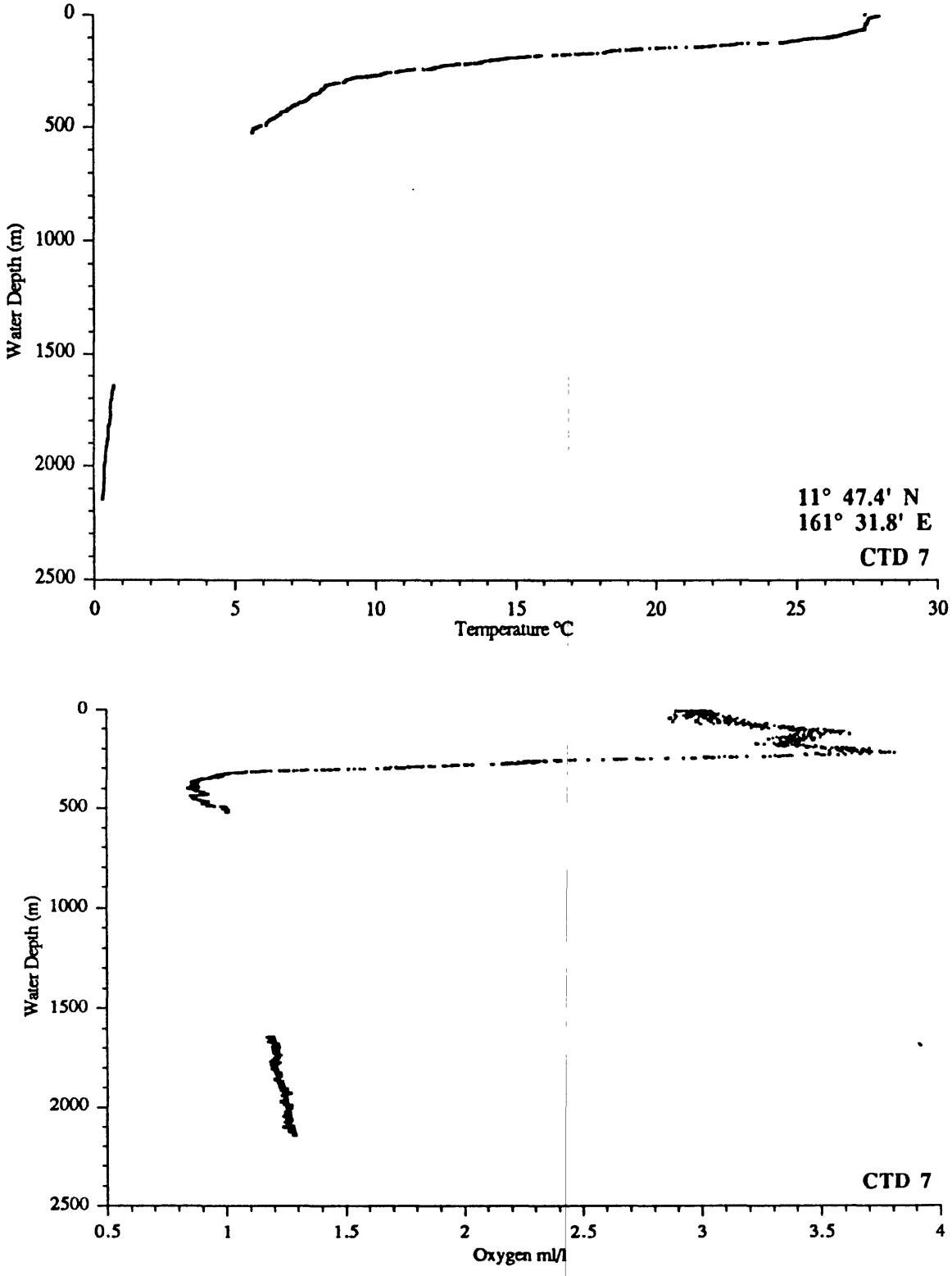

Figure 96. Temperature and oxygen content versus water depth for CTD 7, Lọmilik Seamount. Water depth at station is 2525 meters.

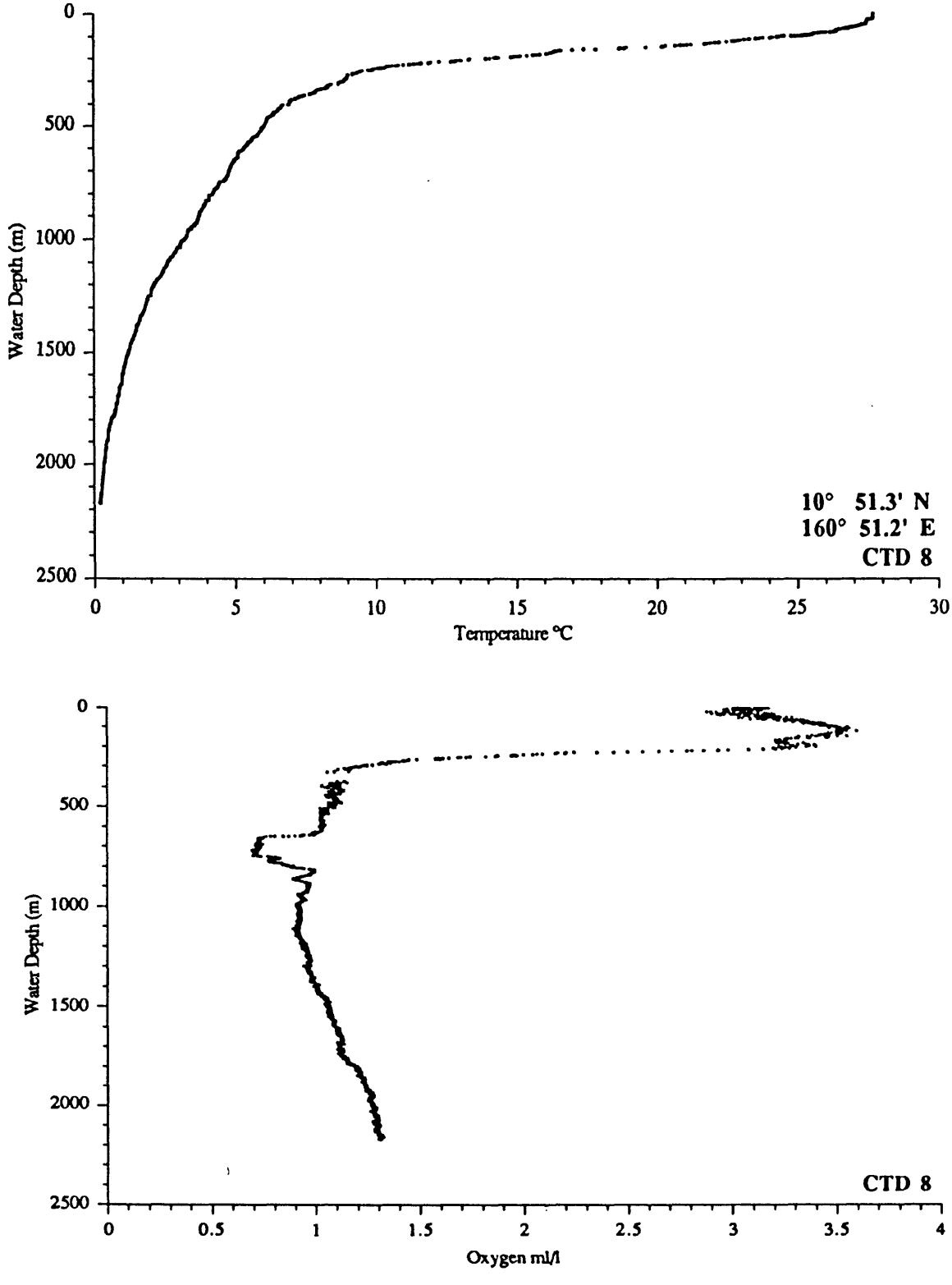

Figure 97. Temperature and oxygen content versus water depth for CTD 8, open ocean. Water depth at station is 4340 meters.

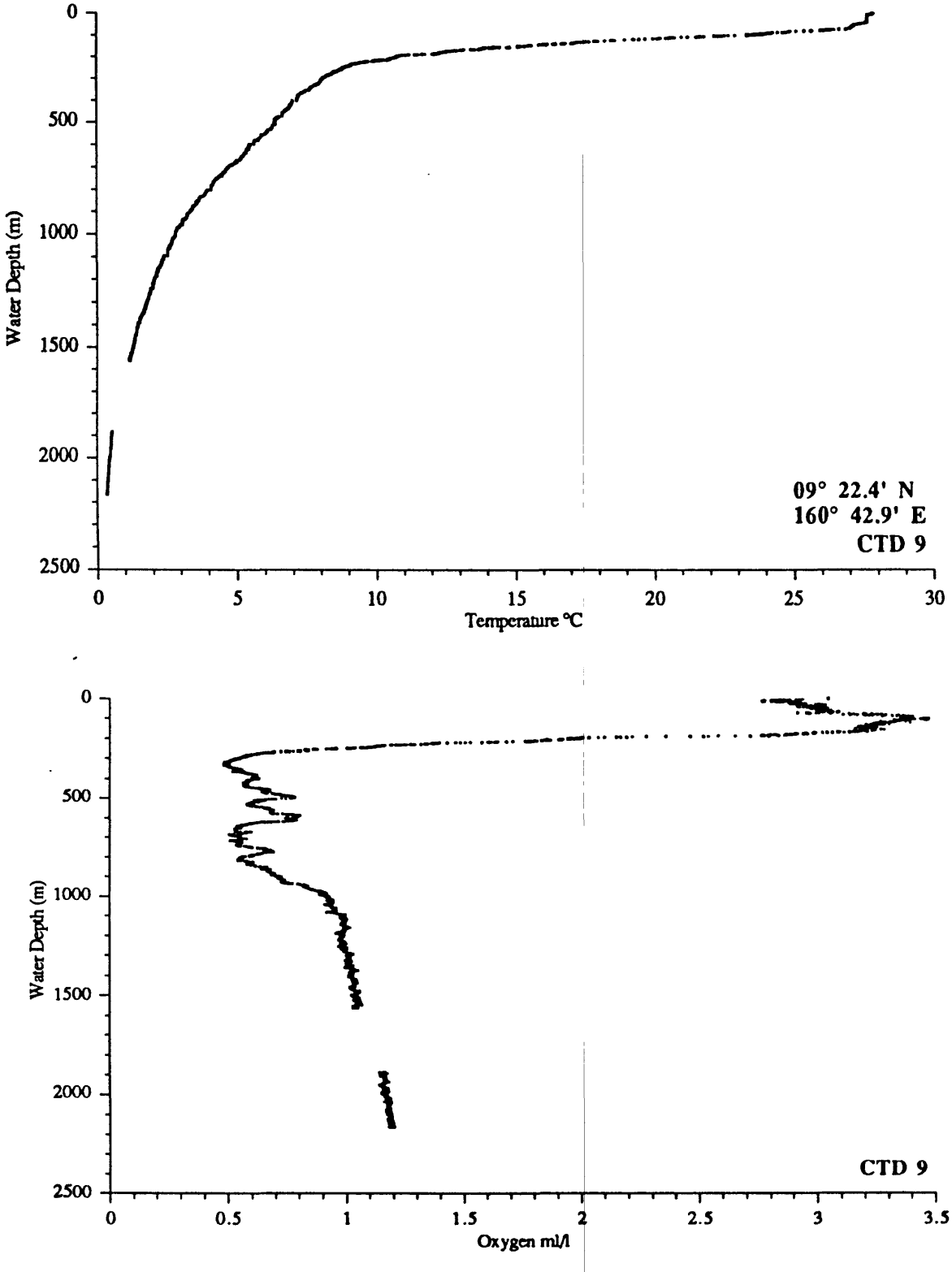

Figure 98. Temperature and oxygen content versus water depth for CTD 9, open ocean. Water depth at station is 4950 meters.

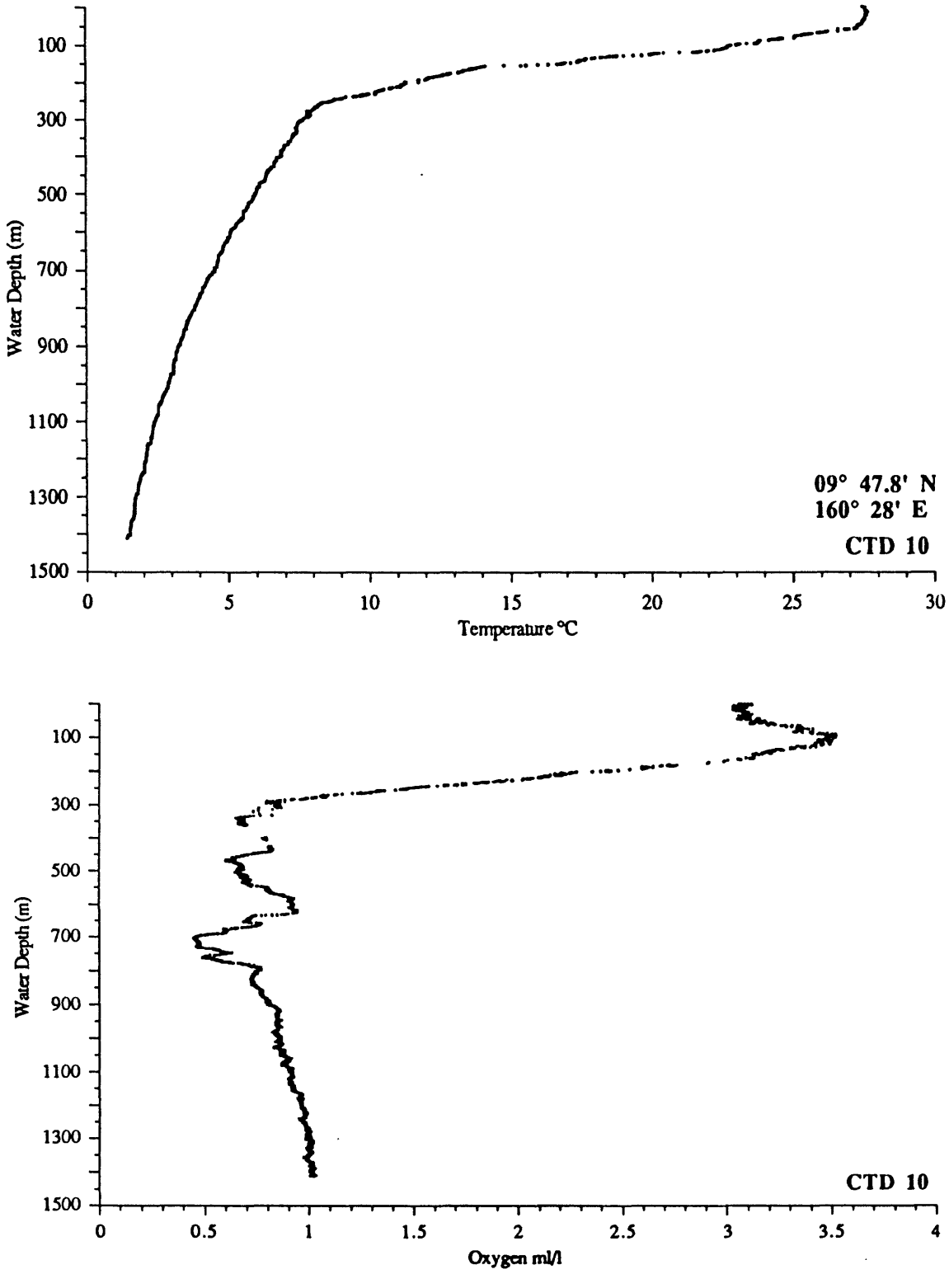

Figure 99. Temperature and oxygen content versus water depth for CTD 10, Ujlañ Seamount. Water depth at station is 1445 meters.

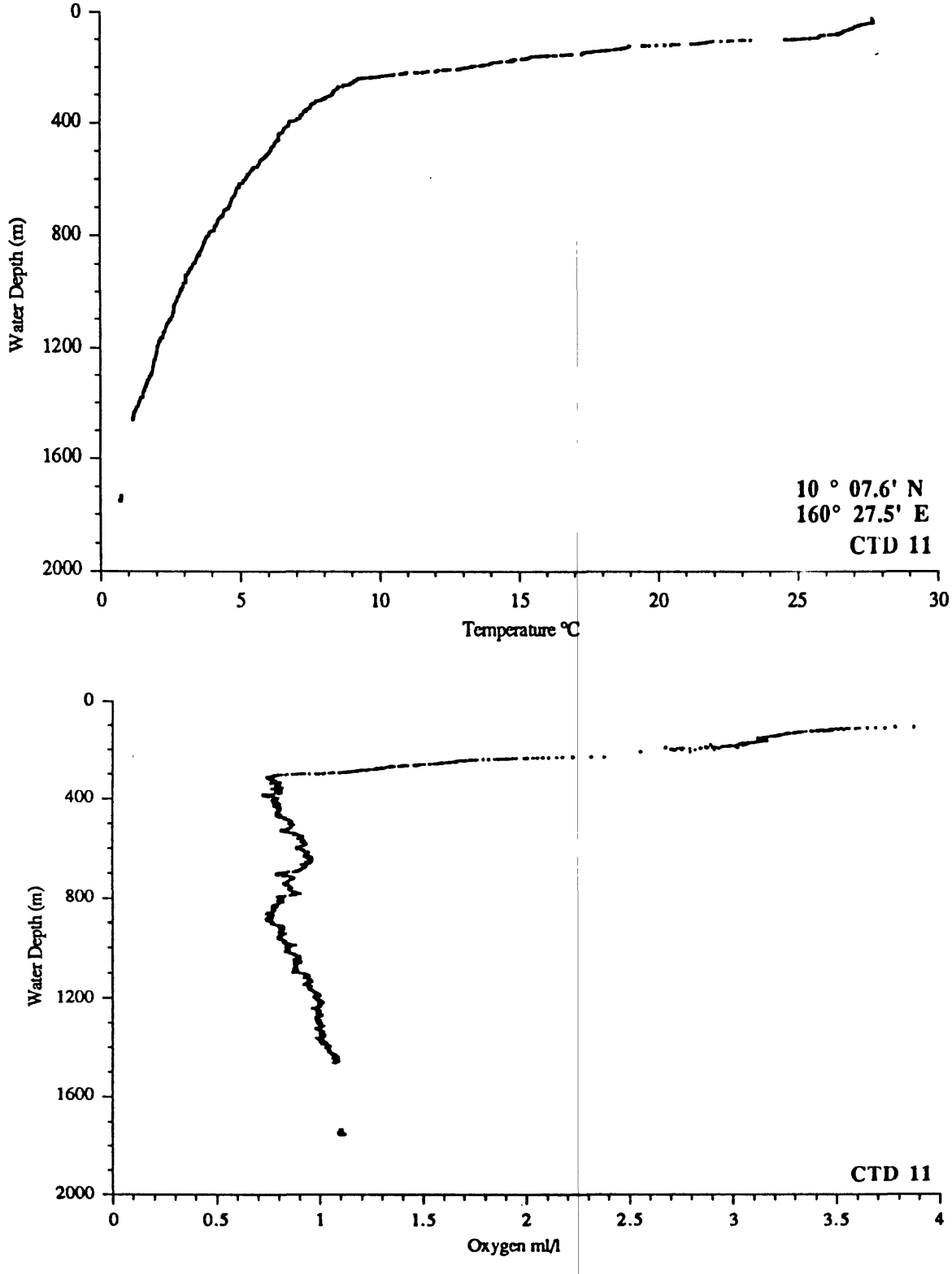

Figure 100. Temperature and oxygen content versus water depth for CTD 11, Ļalibjet Seamount. Water depth at station is 1900 meters.

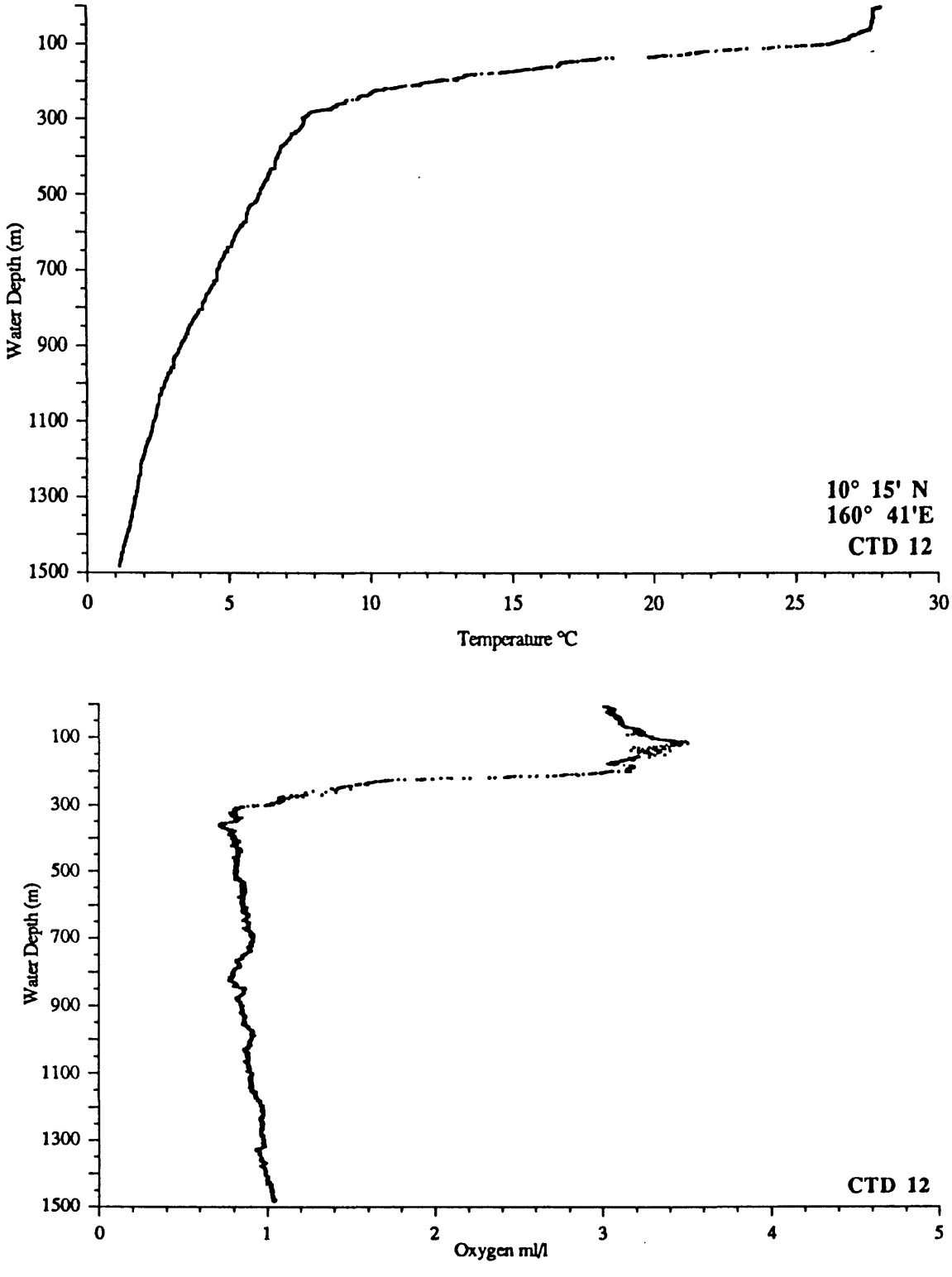

Figure 101. Temperature and oxygen content versus water depth for CTD 12, Ḷōtab Seamount. Water depth at station is 1715 meters.

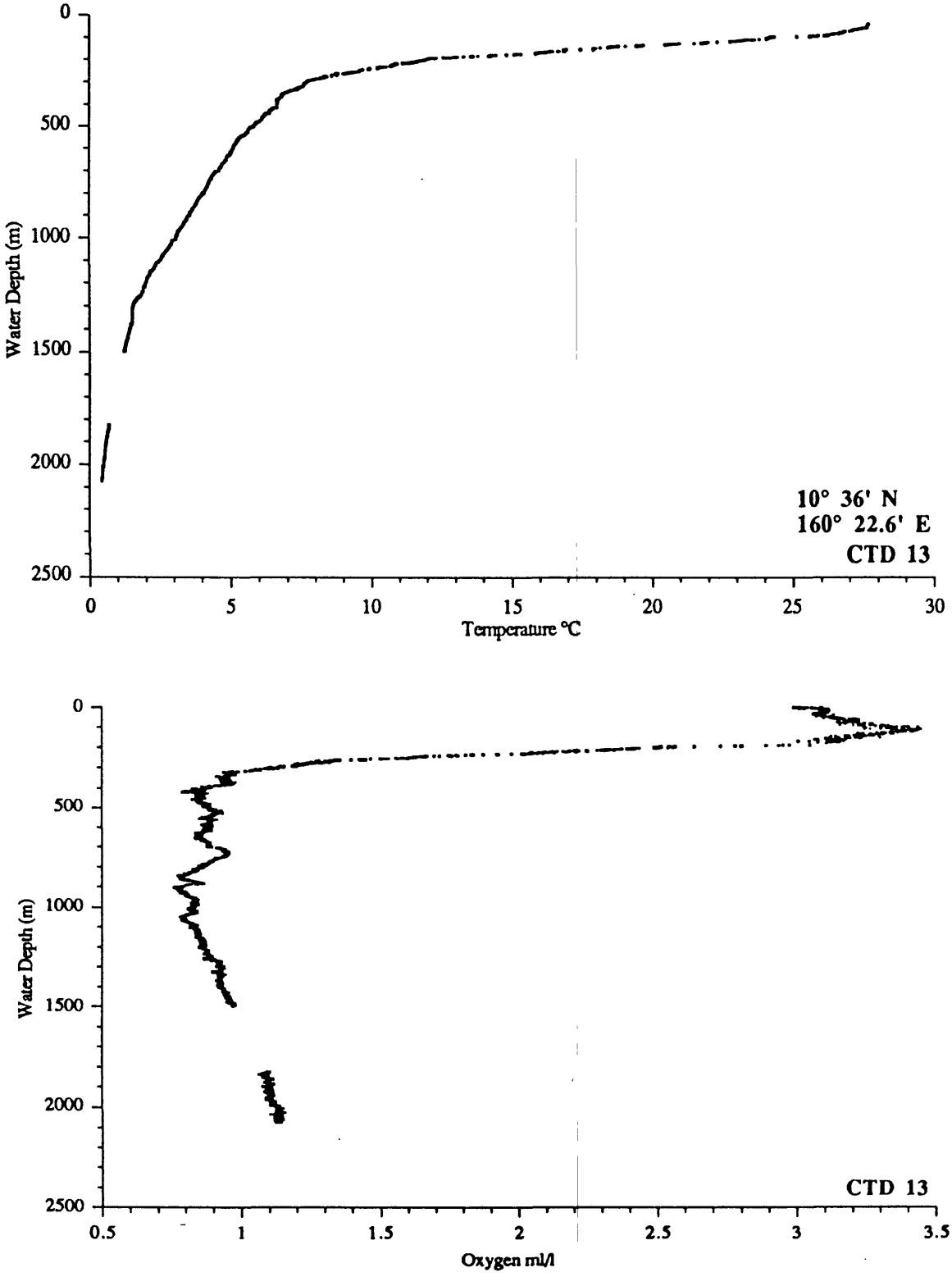

Figure 102. Temperature and oxygen content versus water depth for CTD 13, Likelep Seamount. Water depth at station is 2520 meters.

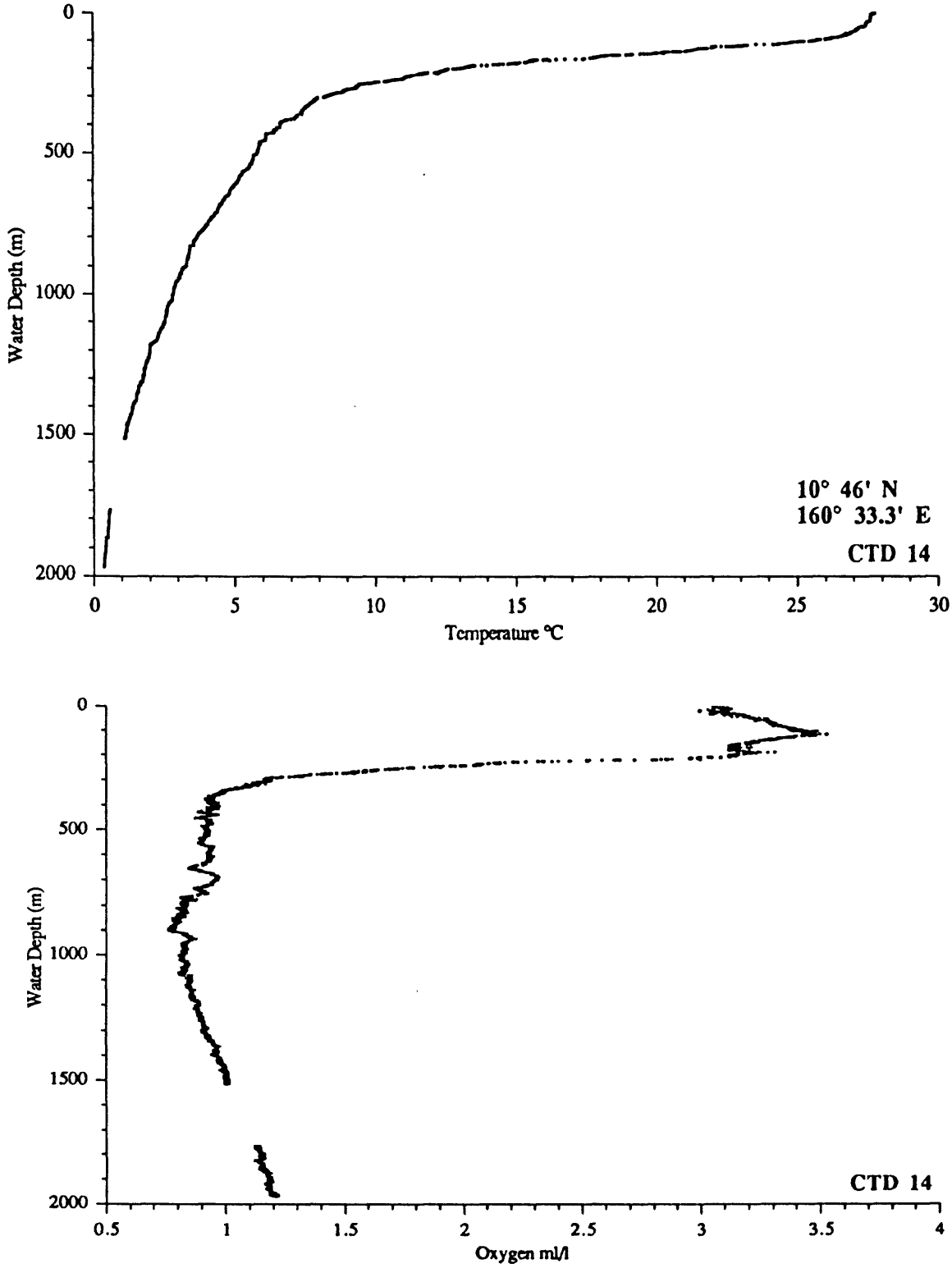

Figure 103. Temperature and oxygen content versus water depth for CTD 14, Likelep Seamount. Water depth at station is 2280 meters.

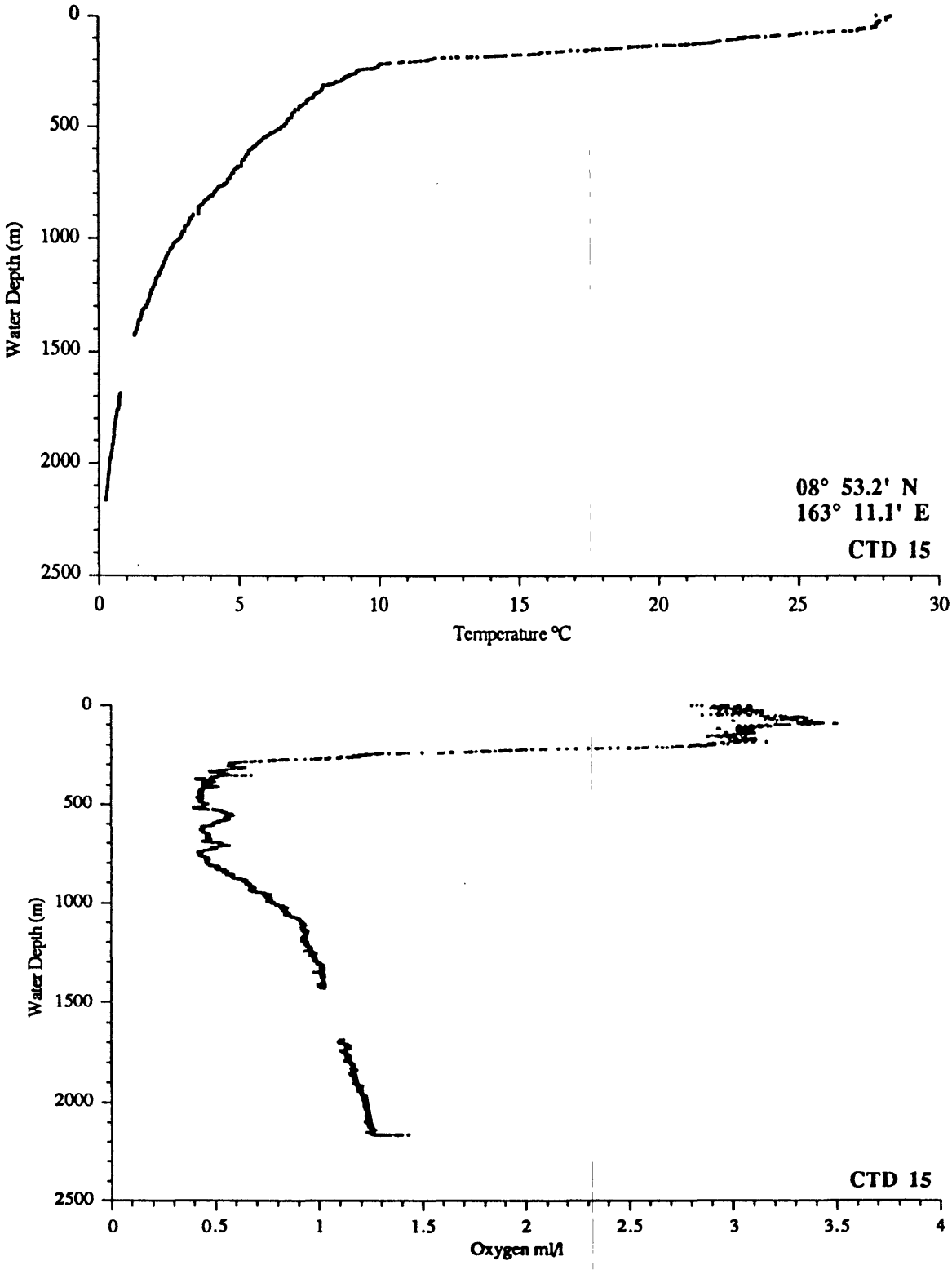

Figure 104. Temperature and oxygen content versus water depth for CTD 15, Mij-Lep Seamount. Water depth at station is 2295 meters.

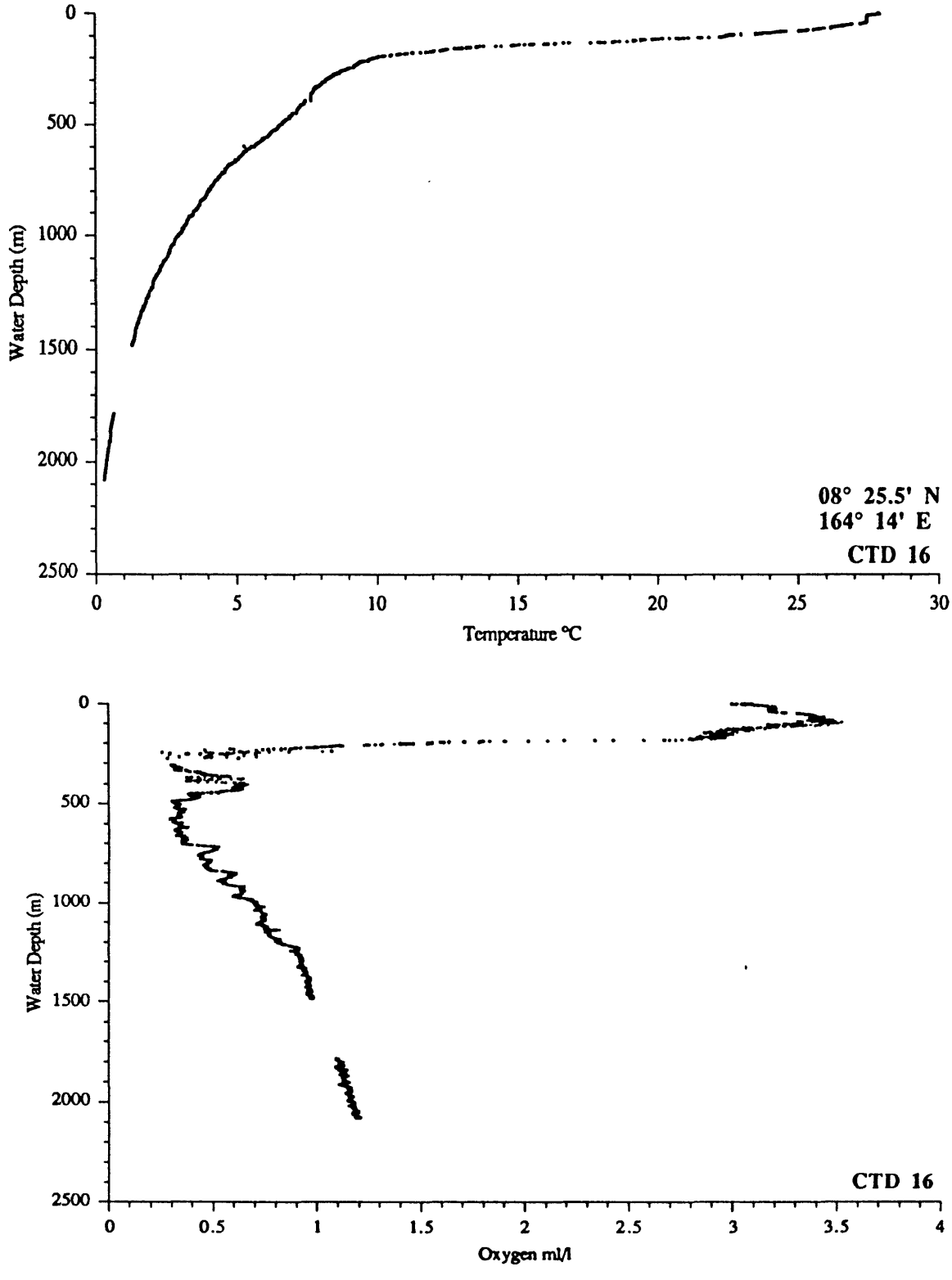

Figure 105. Temperature and oxygen content versus water depth for CTD 16, open ocean. Water depth at station is 5000 meters.

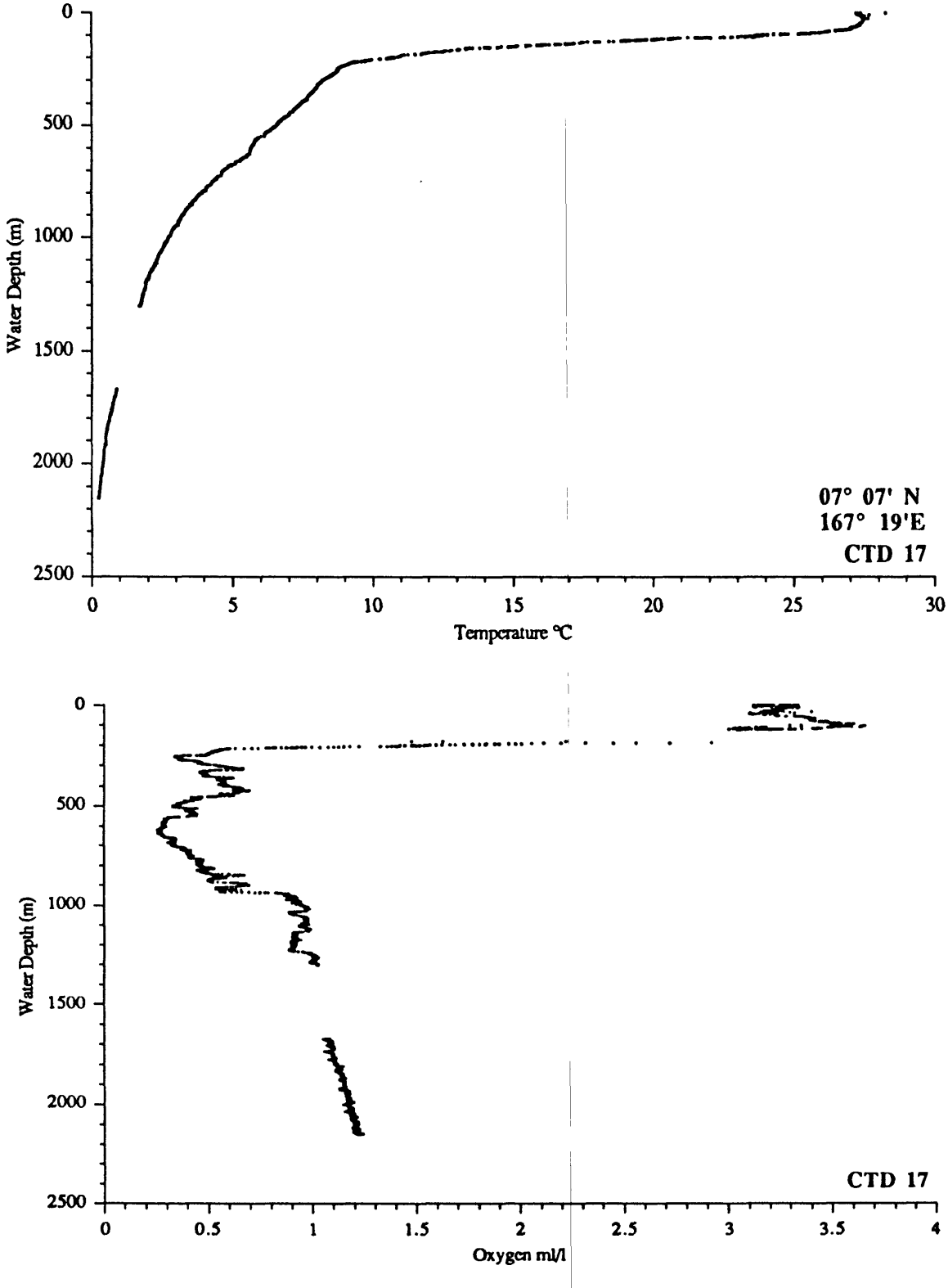

Figure 106. Temperature and oxygen content versus water depth for CTD 17, open ocean. Water depth at station is 5000 meters.

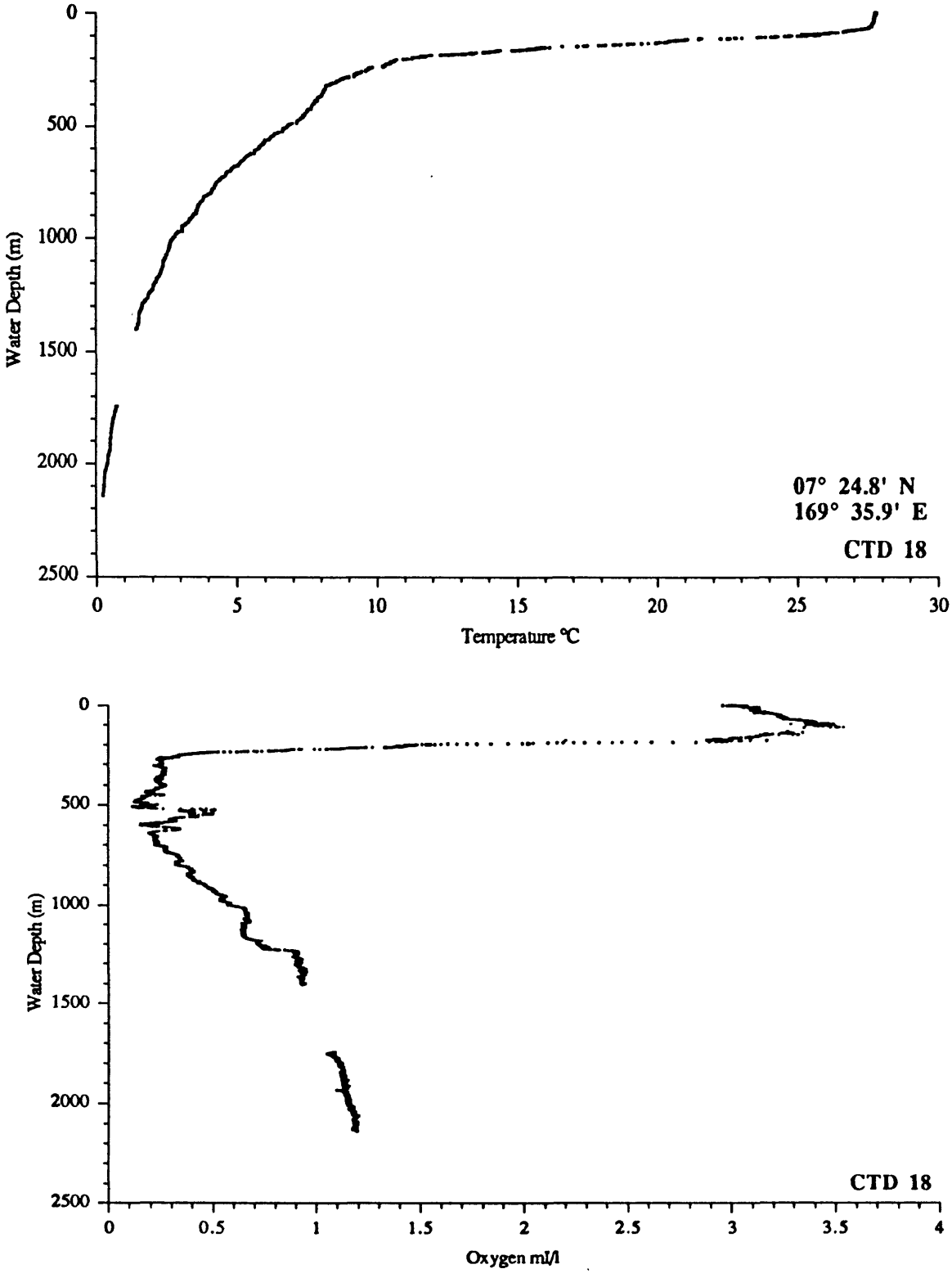

Figure 107. Temperature and oxygen content versus water depth for CTD 18, Jebro Seamount. Water depth at station is 2350 meters.

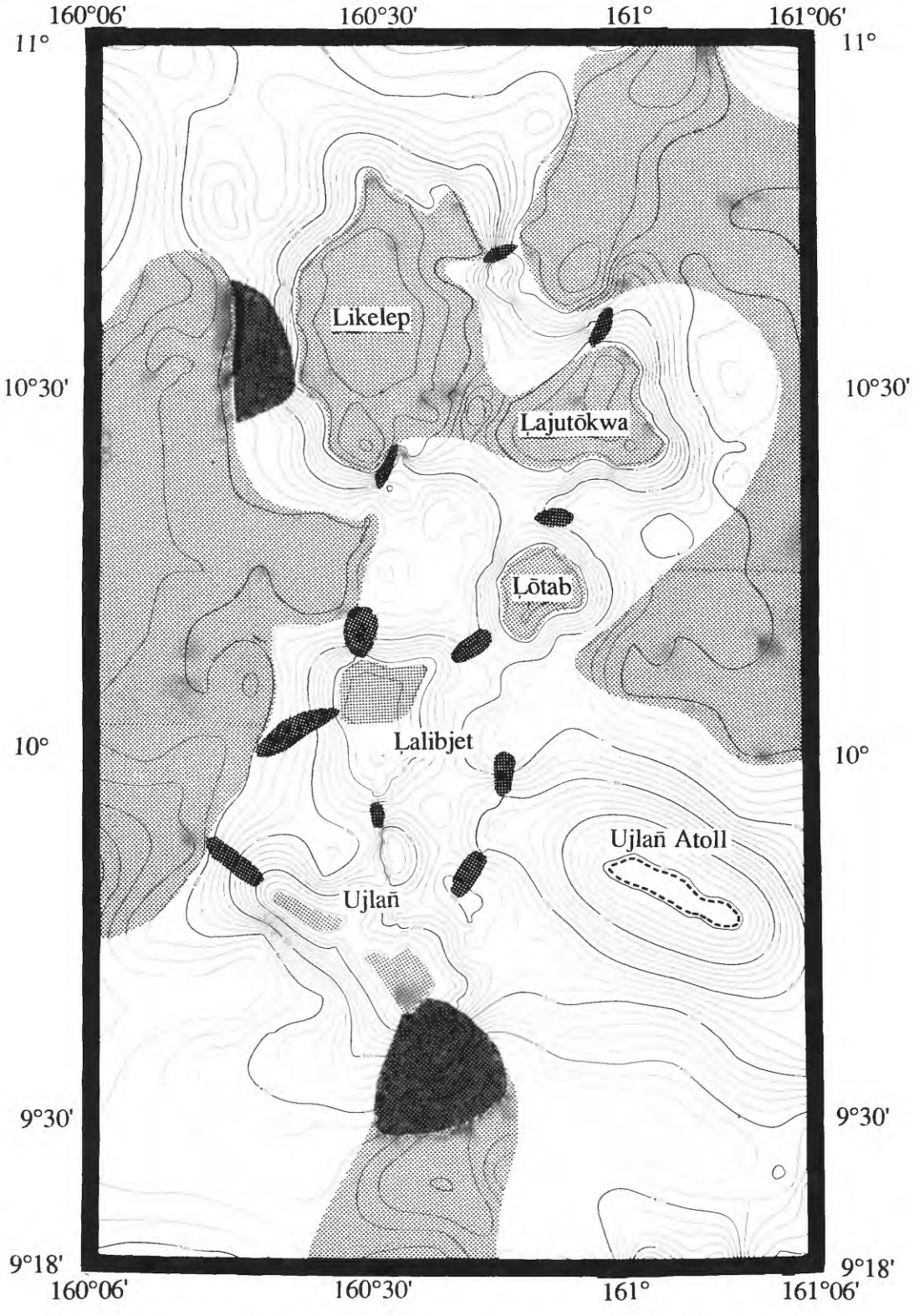

Figure 108. Sediment (light stippling) and talus (dark stippling) cover of Ujlañ volcanic complex. Sediment cap size and thickness decrease to the south. Talus and slumps probably occur at the base of the many of the seamount flanks. The abyssal sediment undoubtedly extends to the south and northwest. Note that the southern half of the sediment cap on Ļalibjet is gone.

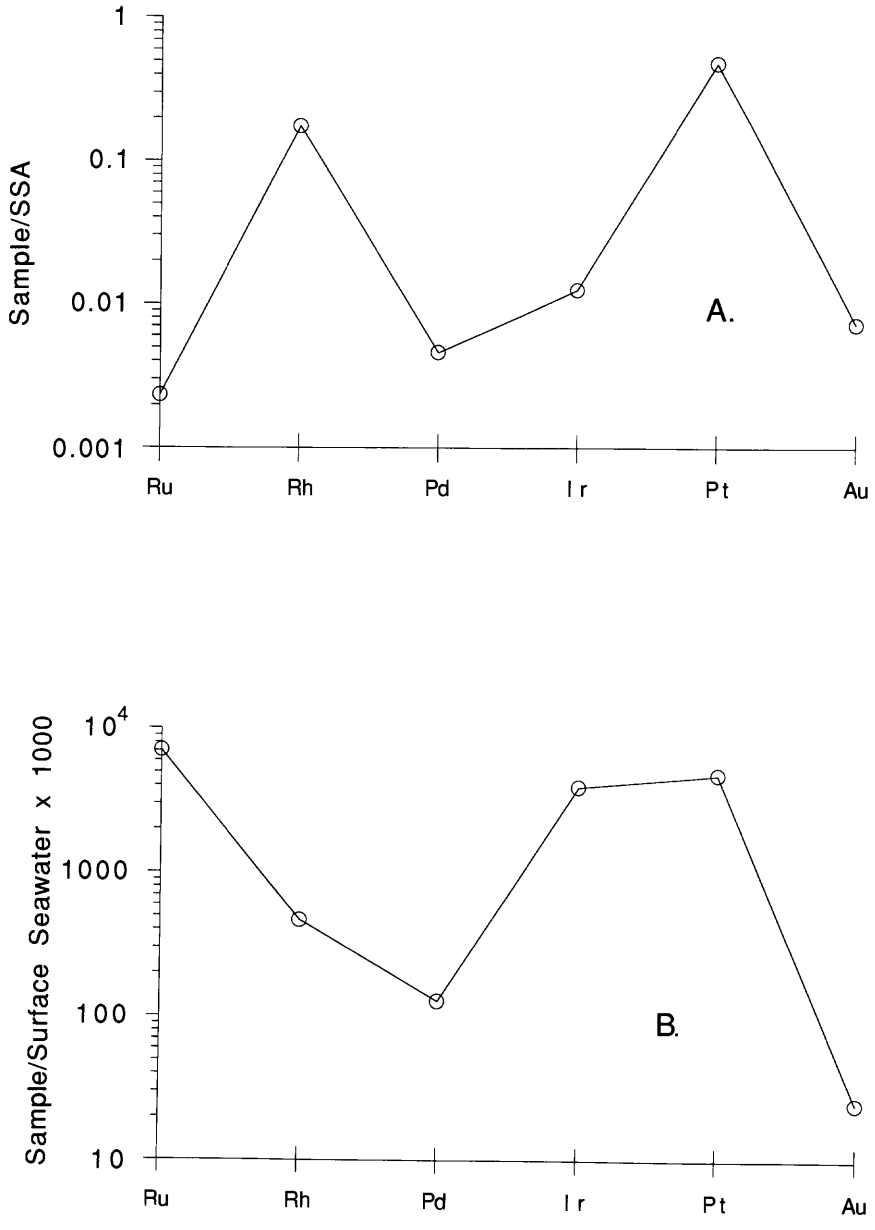

Figure 115. **A**. Mean PGE and Au concentrations in bulk crusts normalized to their solar system abundances (same as C1 chondrite concentrations) taken from Anders and Ebihara (1982). **B**. Mean PGE and Au concentrations in bulk crusts normalized to their surface seawater abundances taken from Goldberg (1987), except Rh, which is arbitrarily set at 50 pg/l, half the value of Pt. Au in crusts for both plots is set at 1.0 ppb.

p209 to 214 ARE HARD COPY

Figure 116. Chondrite-normalized REE plot. Shaded field represents complete data set of 86 samples (see Table 17). Chondrite composition for Figures 116-137 from Haskin et al. (1968).

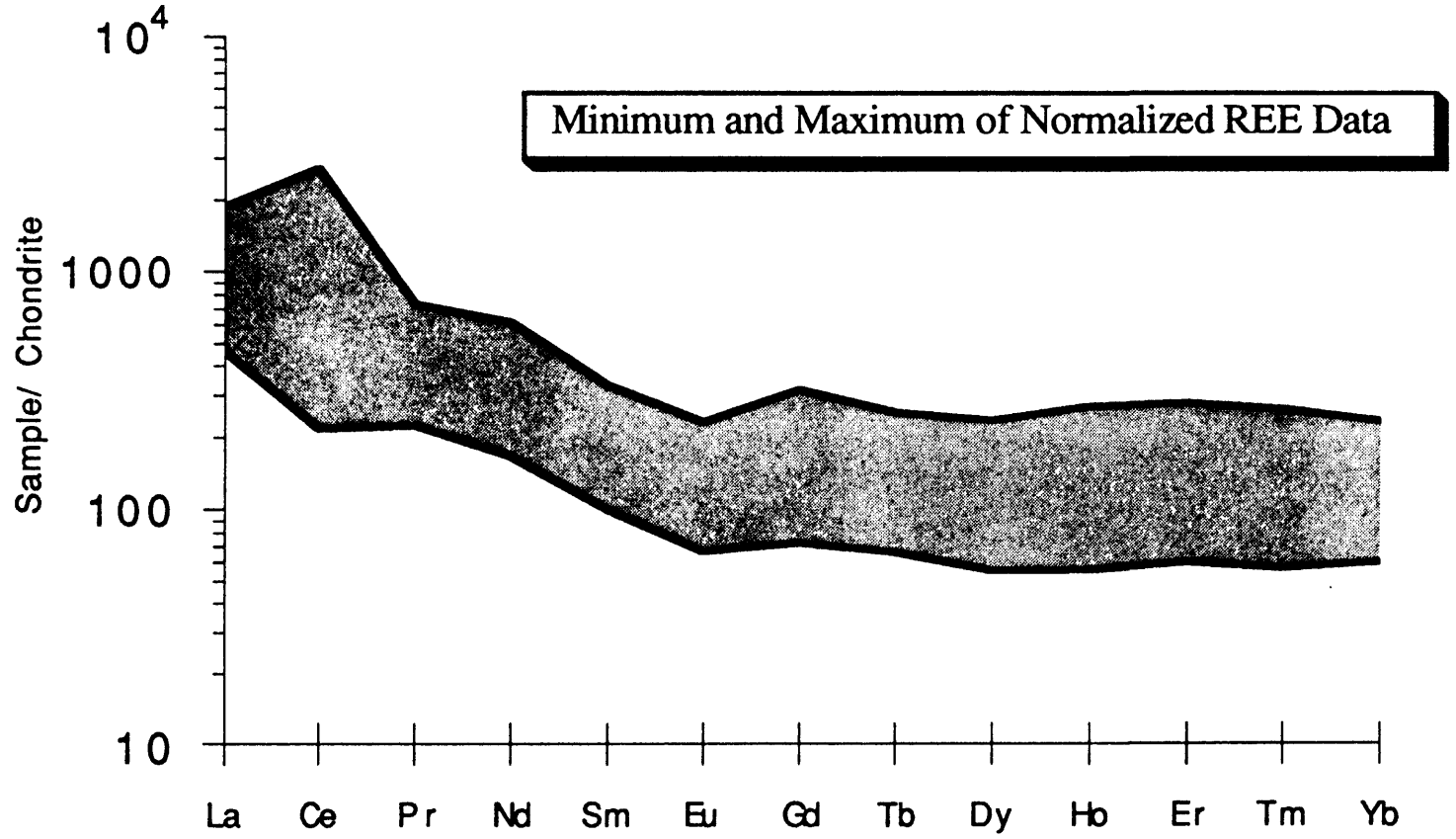

Figure 117. Chondrite-normalized REE plot of a layered crust from dredge D1. In Figures 117-137, B = bulk, L = layer, and N = nodule followed by interval in millimeters.

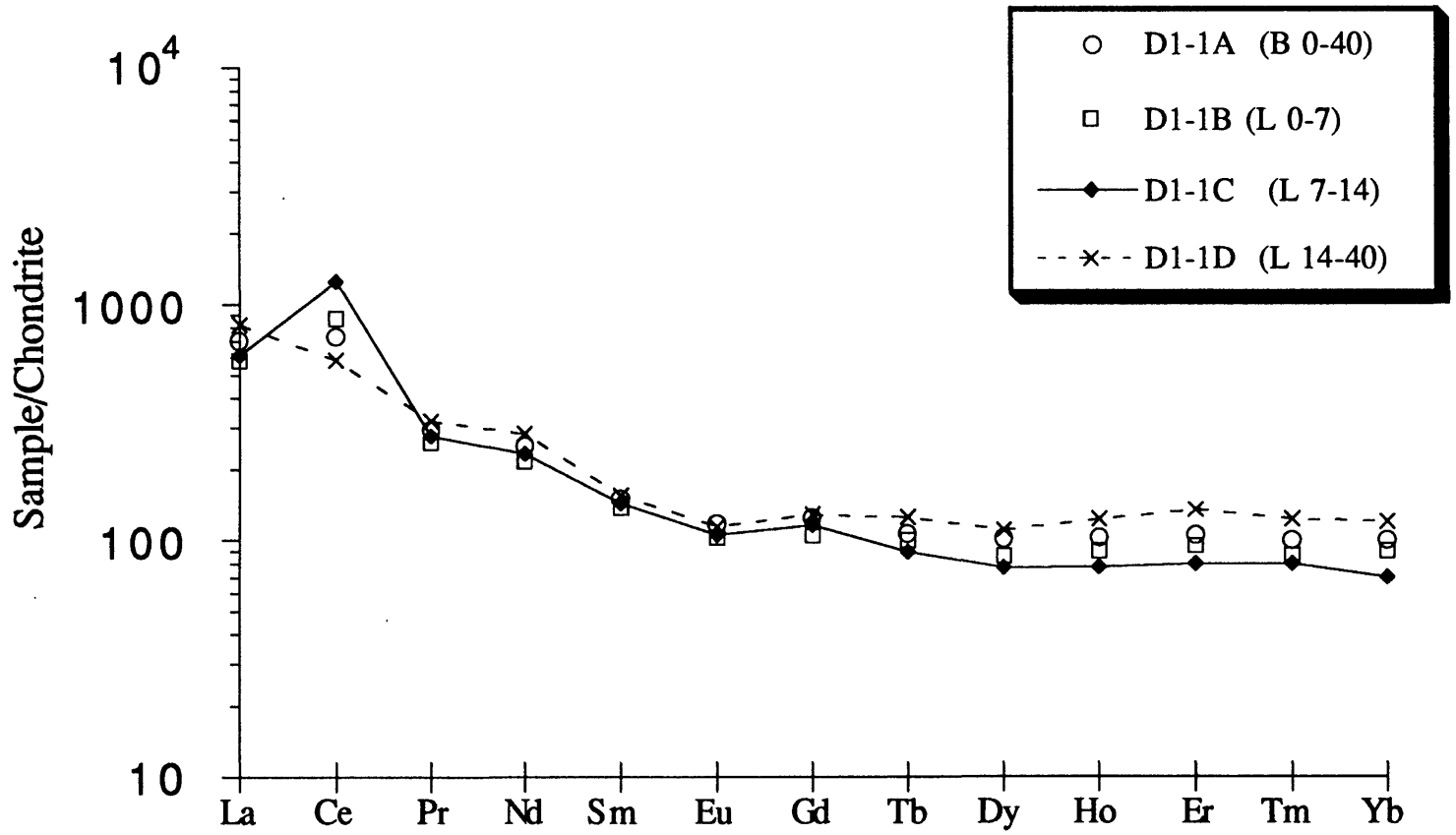

Figure 118. Chondrite-normalized REE plot of a layered crust from dredge D8.

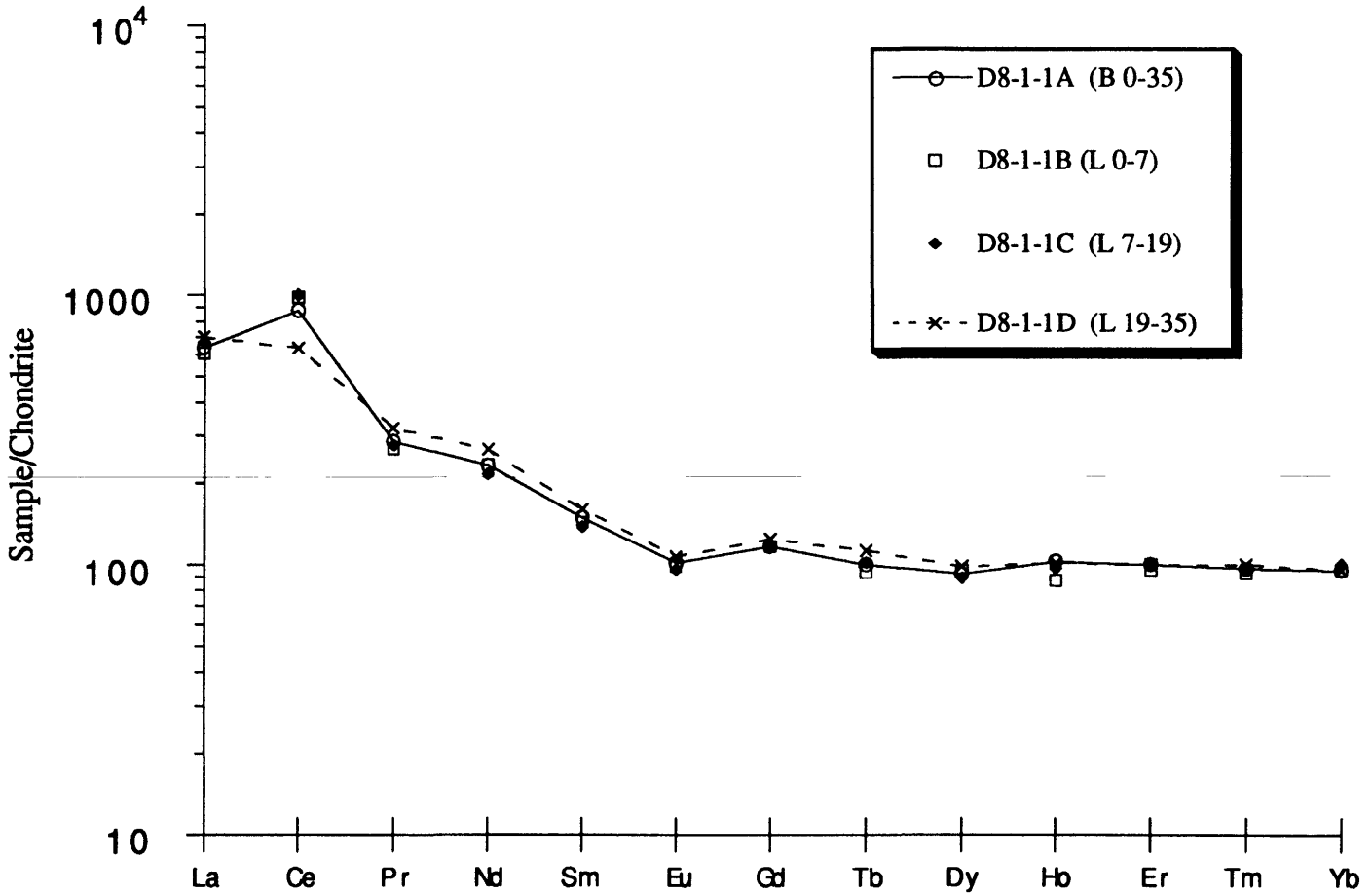

Figure 119. Chondrite-normalized REE plot of a layered crust from dredge D9.

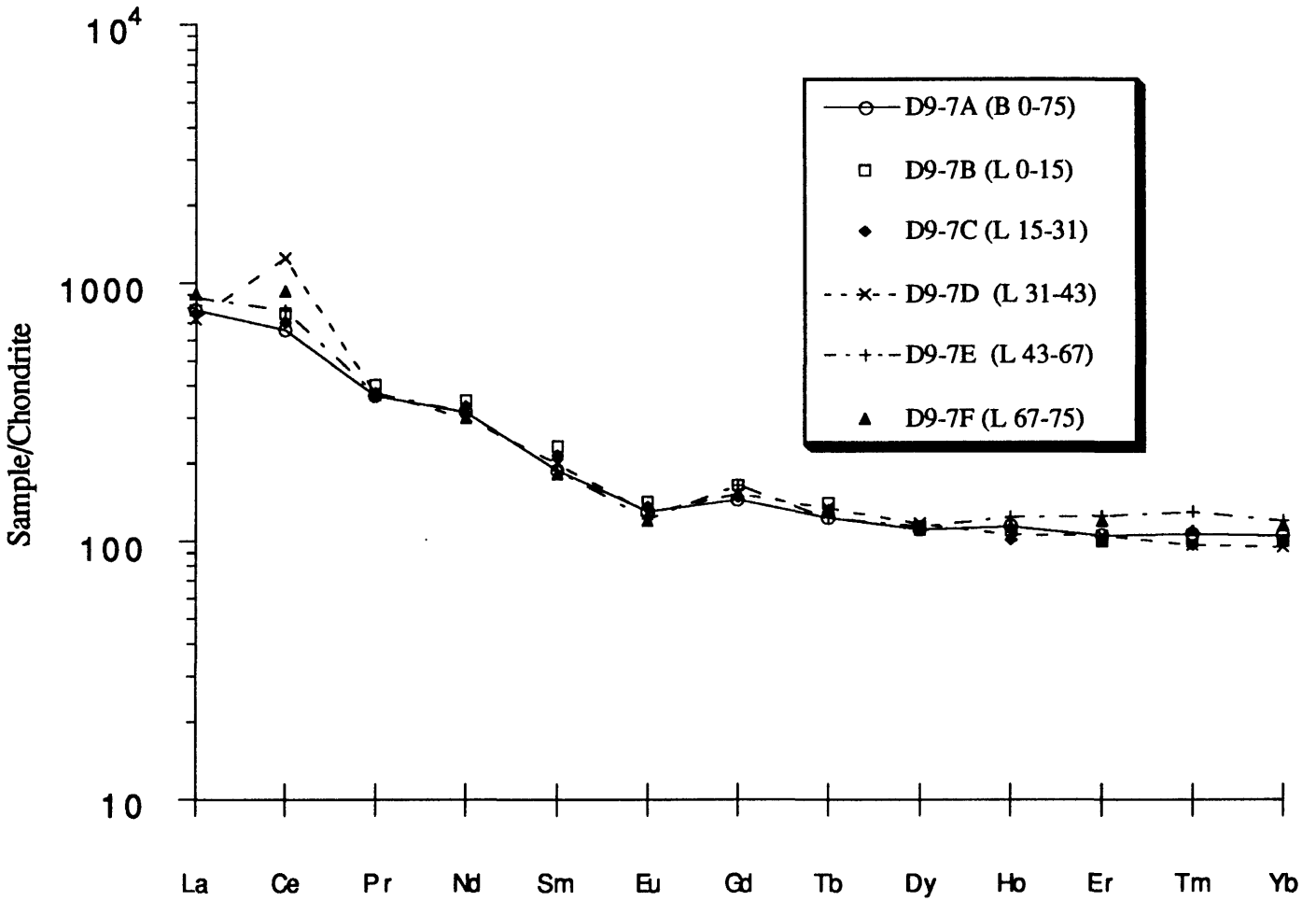

Figure 120. Chondrite-normalized REE plot of a layered crust from dredge D10.

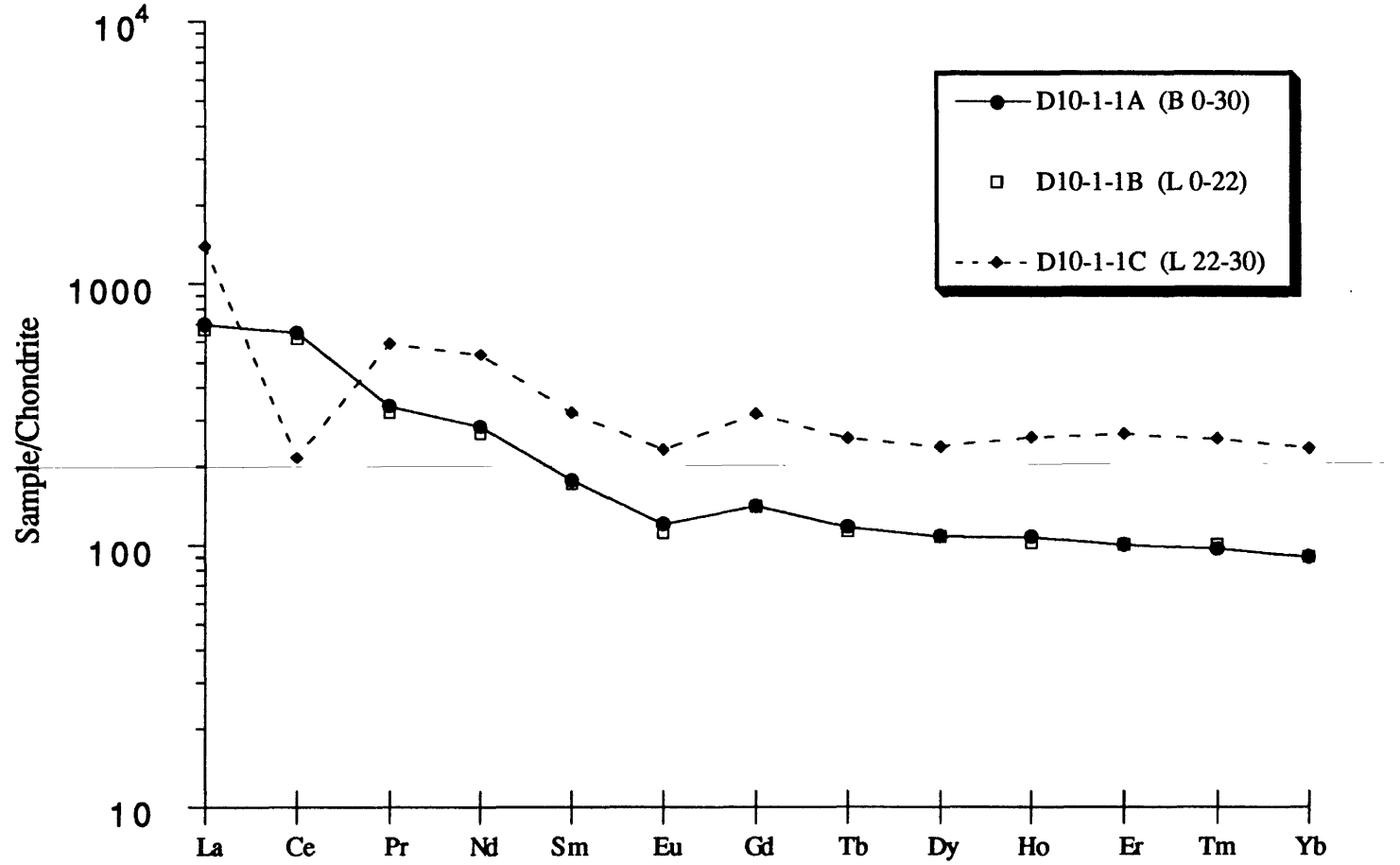

Figure 121. Chondrite-normalized REE plot of a layered crust from dredge D11.

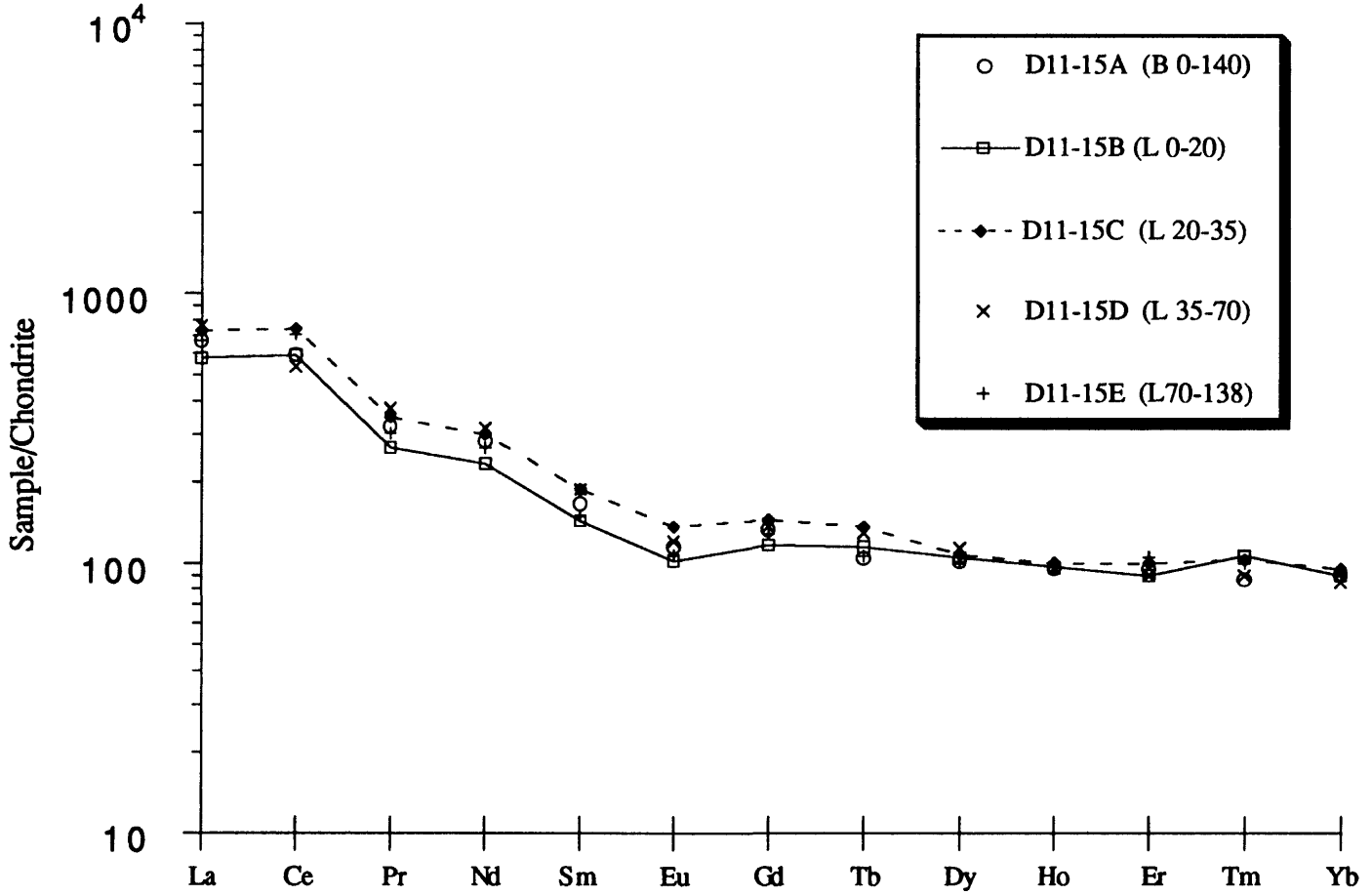

Figure 122. Chondrite-normalized REE plot of a layered crust from dredge D12.

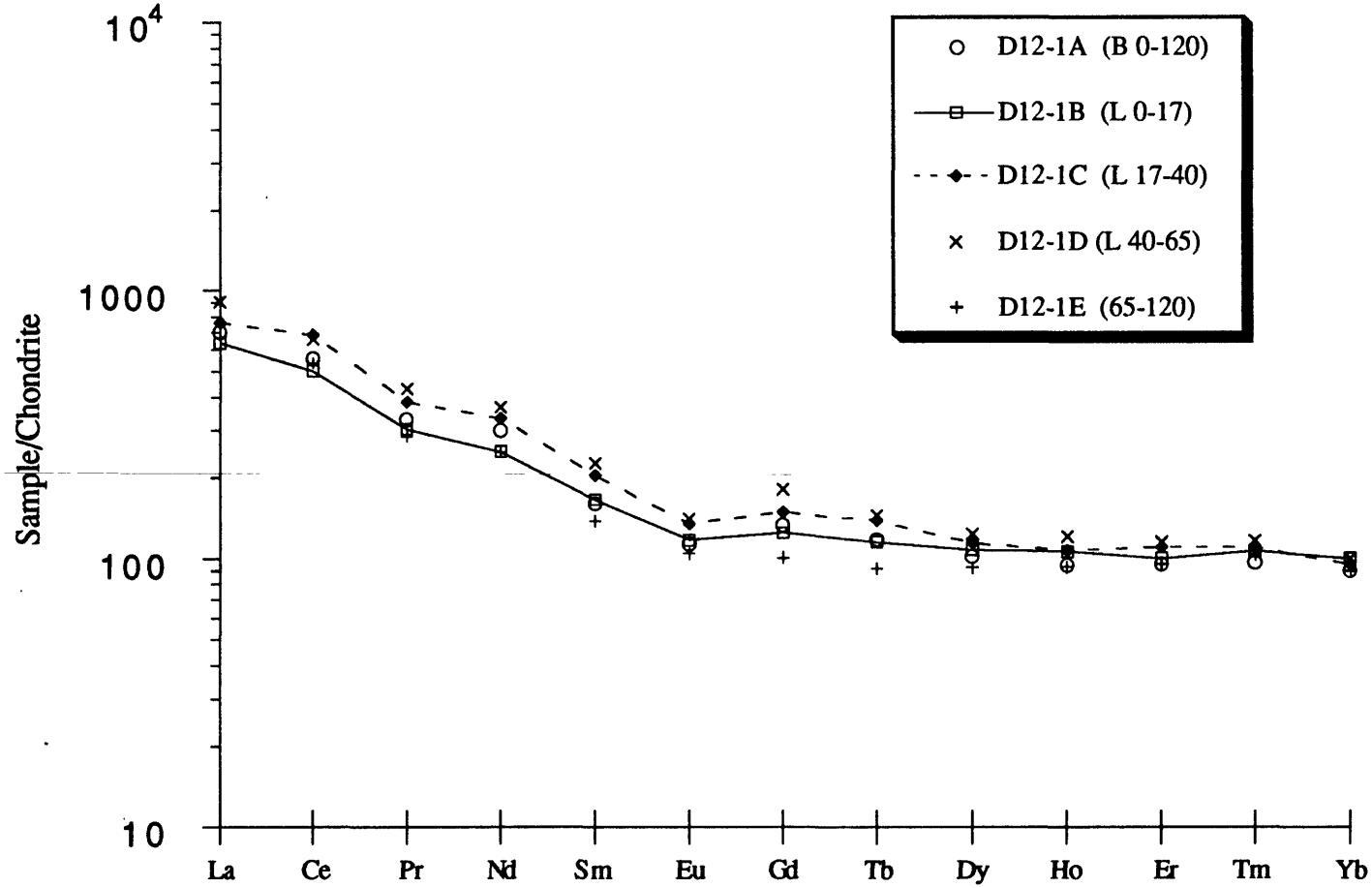

Figure 123. Chondrite-normalized REE plot of a bulk crust and nodule from dredges D12 and D13.

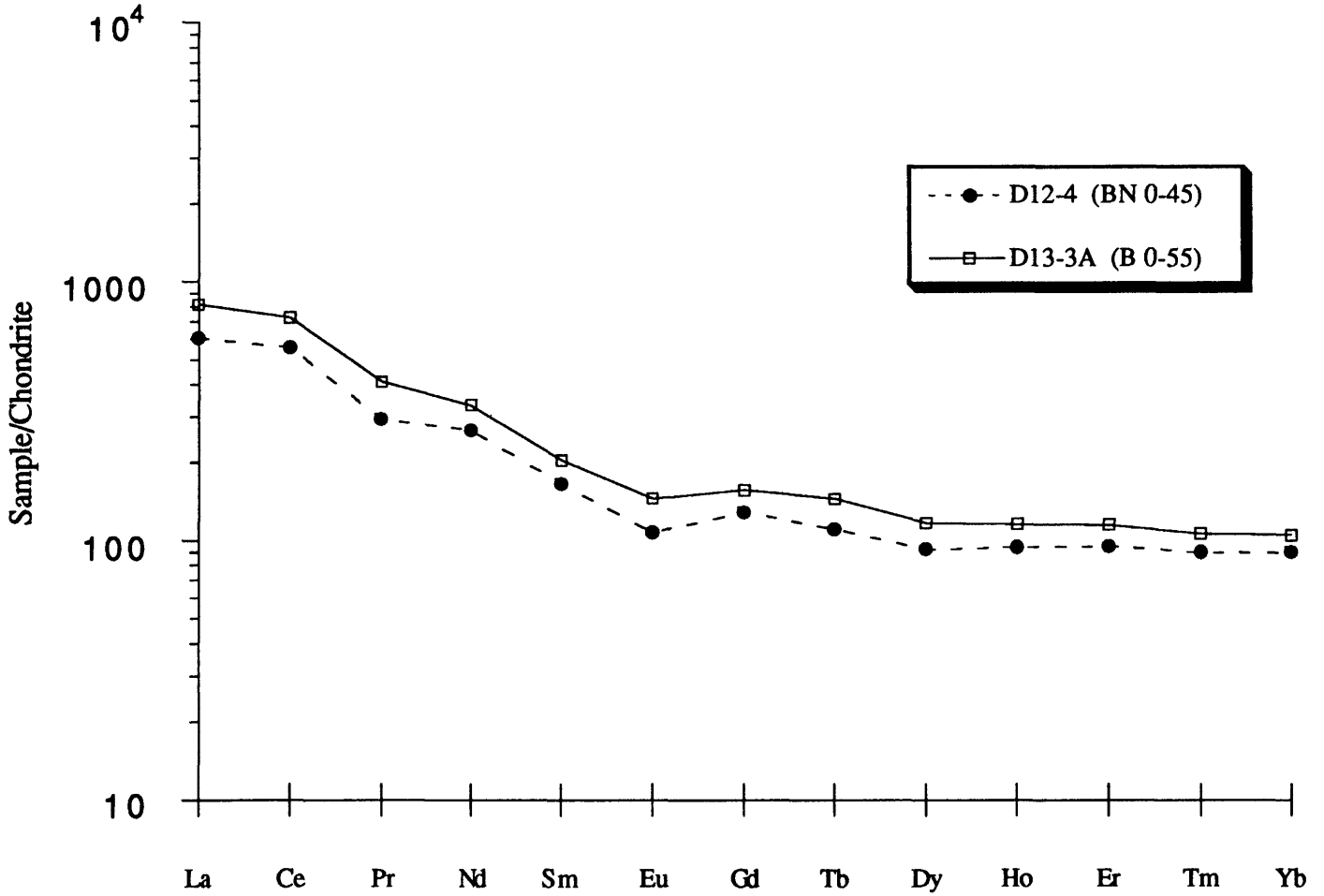

Figure 124. Chondrite-normalized REE plot of layered crust from dredge D14.

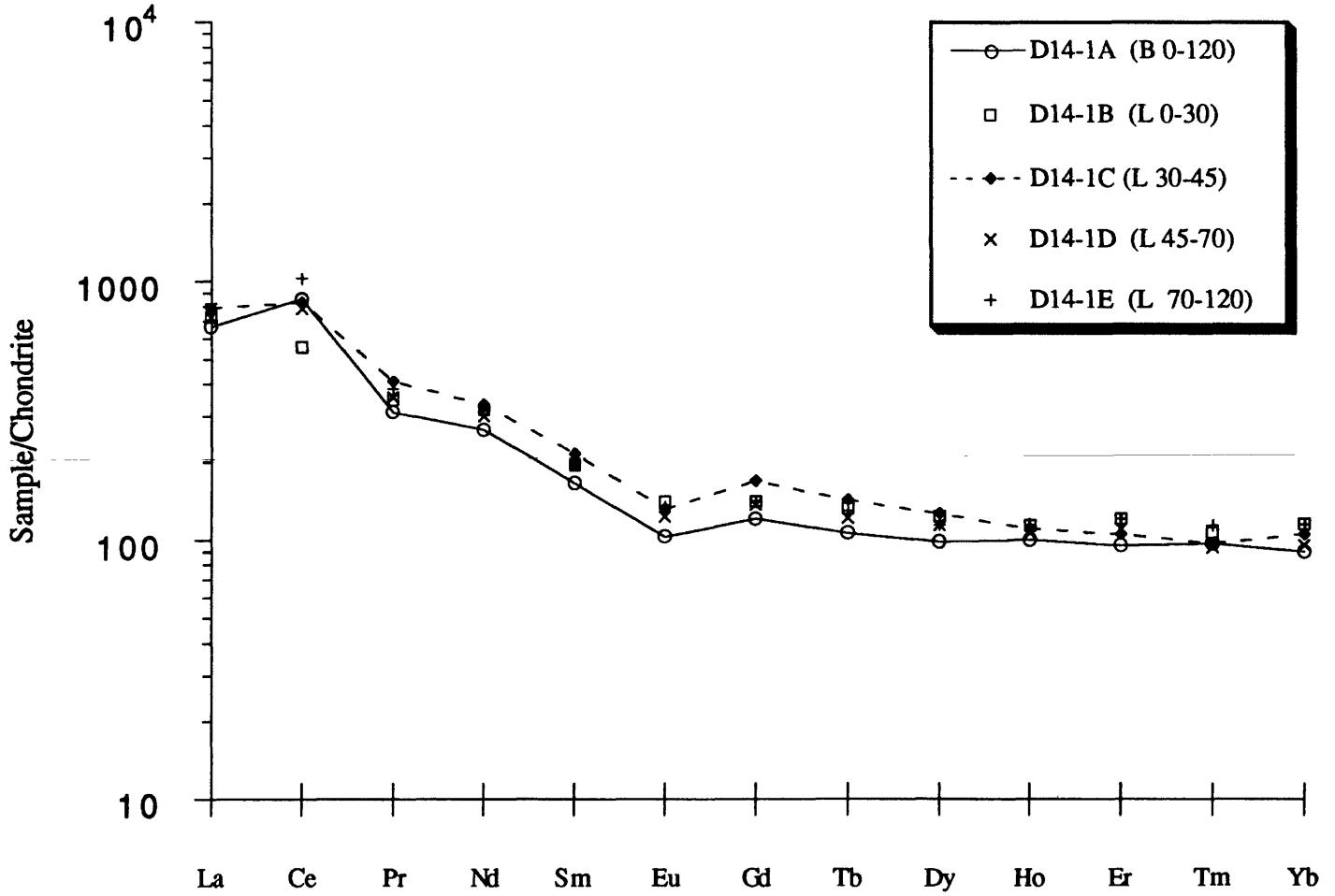

Figure 125. Chondrite-normalized REE plot of a bulk crust and nodule from dredge D16.

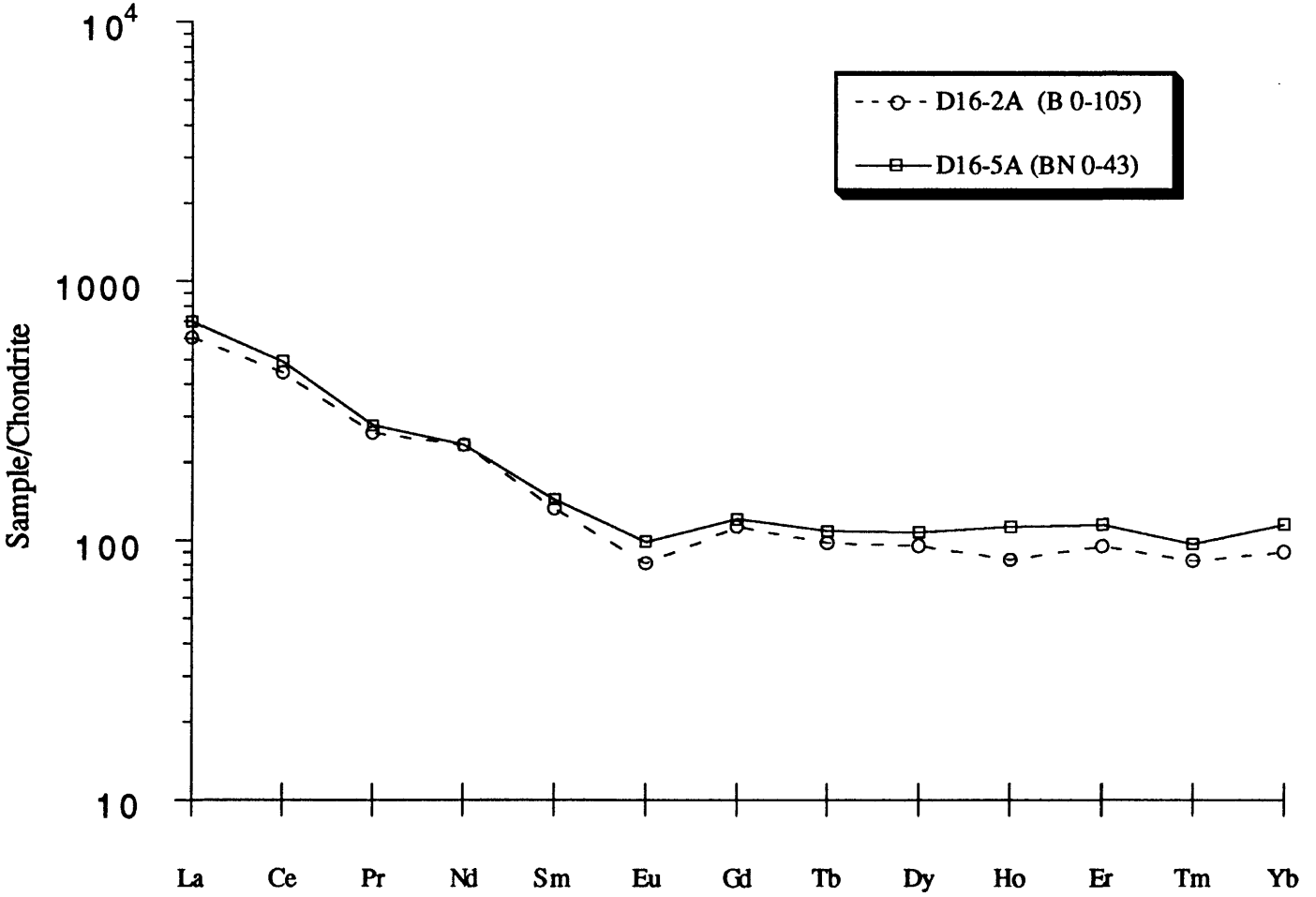

Figure 126. Chondrite-normalized REE plot of a layered crust from dredge D16.

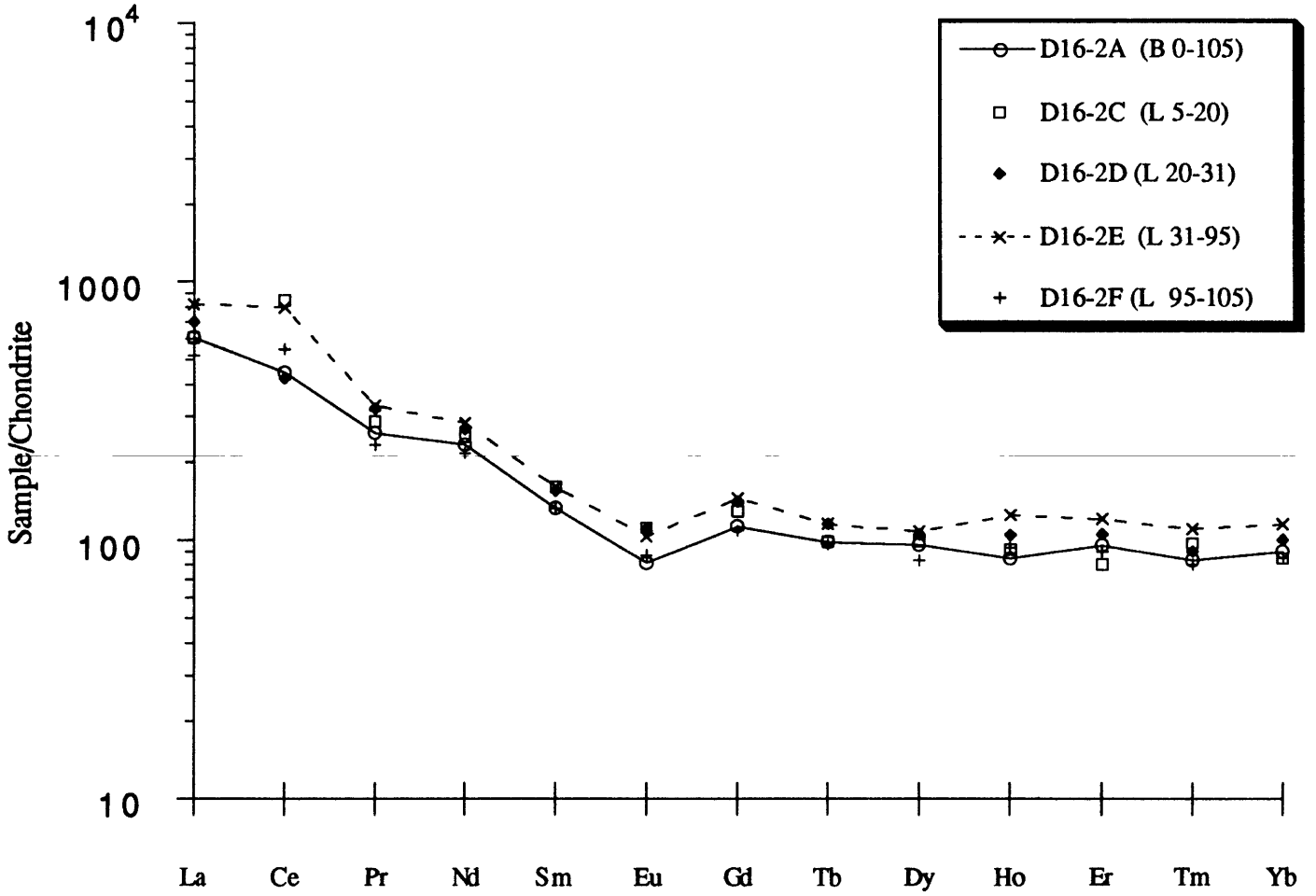

Figure 127. Chondrite-normalized REE plot of a layered nodule from dredge D16.

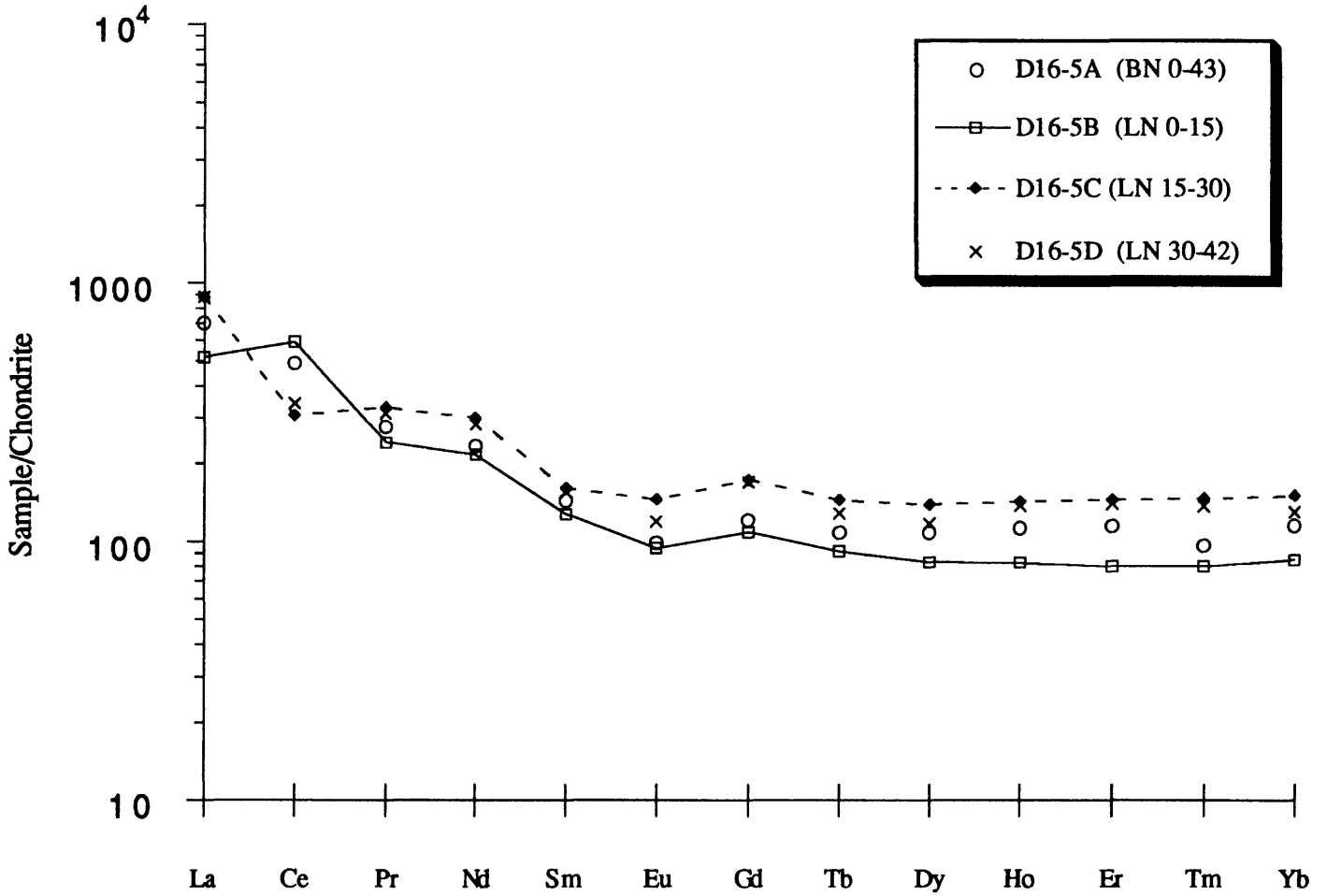

Figure 128. Chondrite-normalized REE plot of a layered crust from dredge D27.

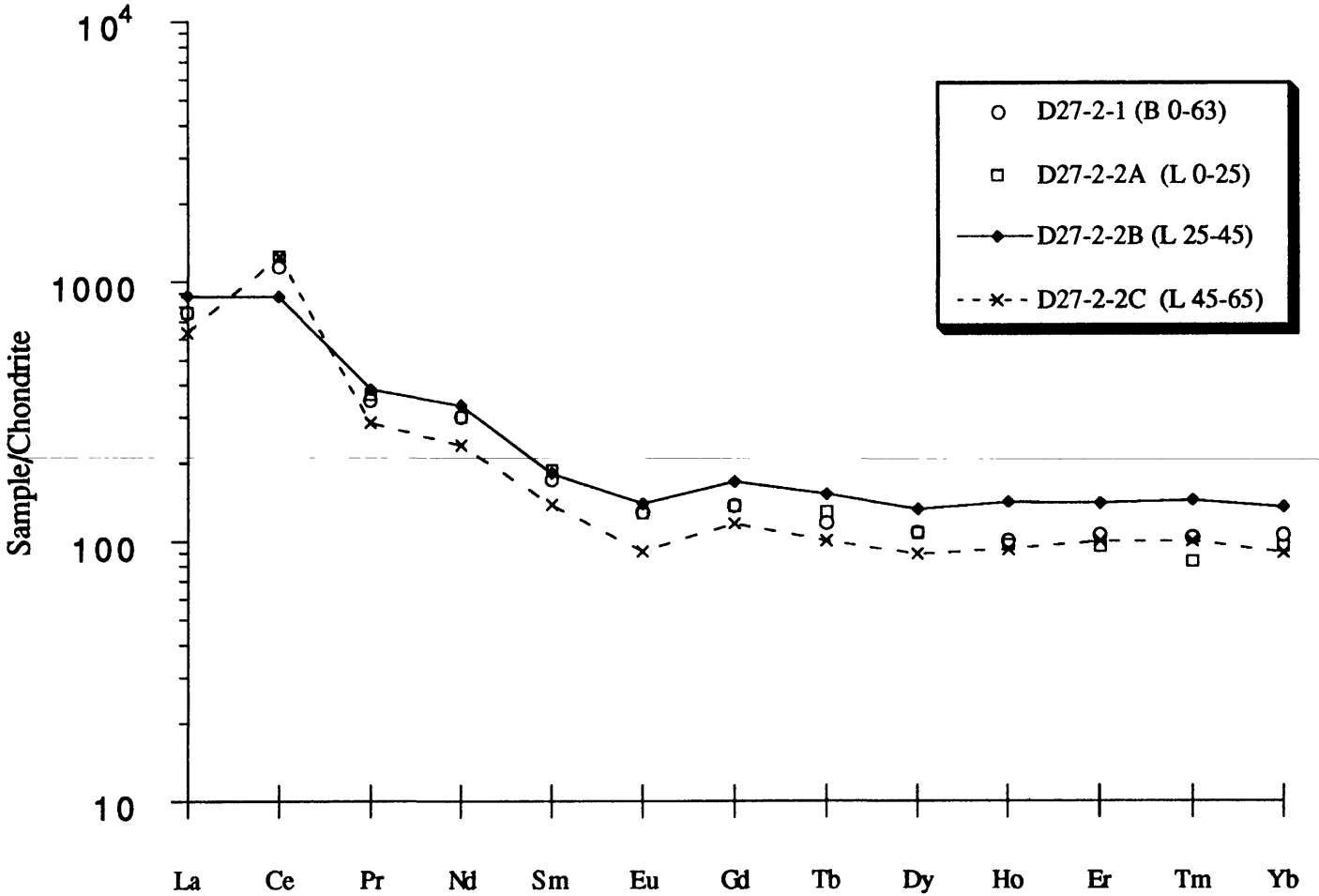

Figure 129. Chondrite-normalized REE plot of a layered crust from dredge KSD1.

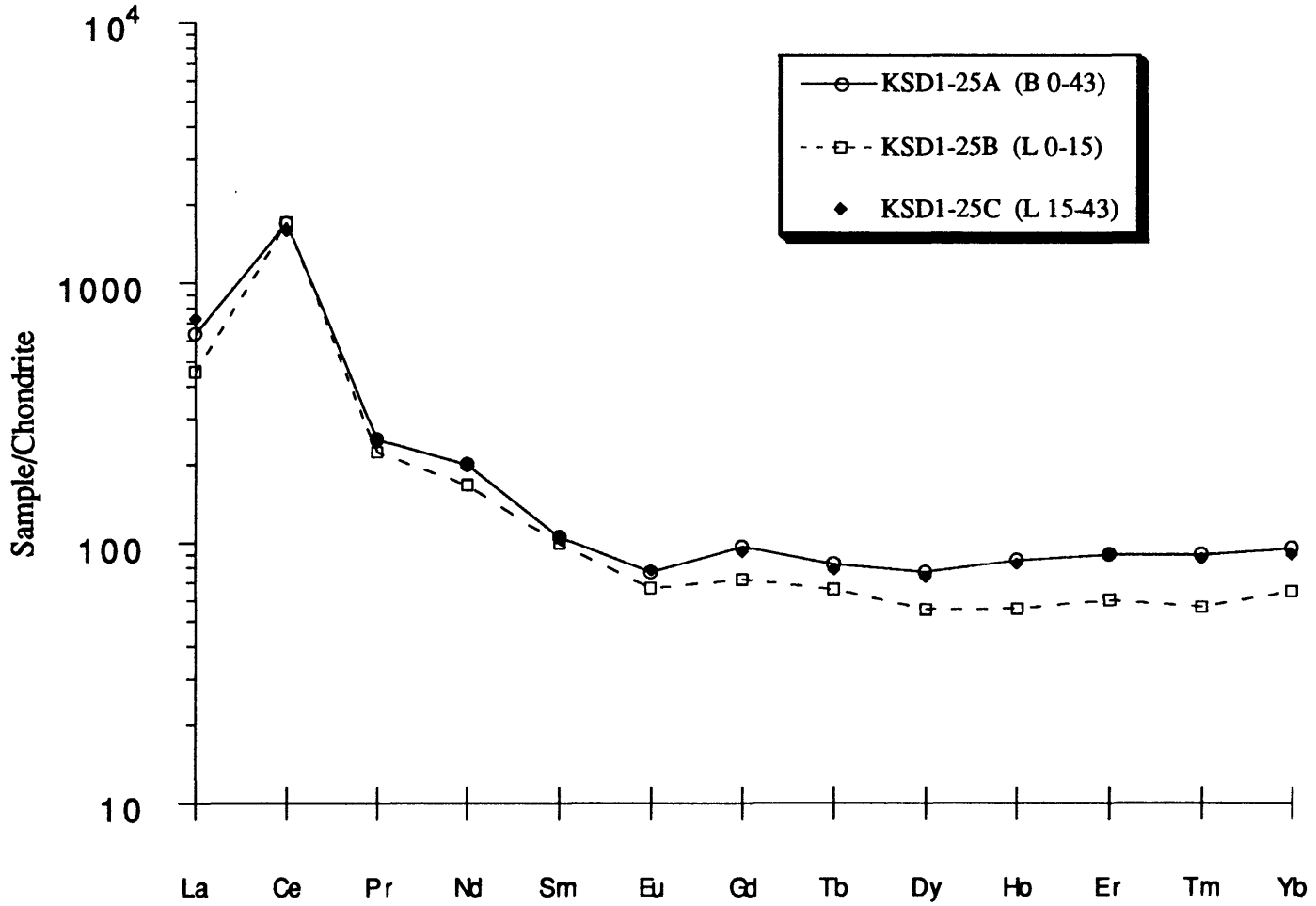

Figure 130. Chondrite-normalized REE plot of a layered crust from dredge RD36.

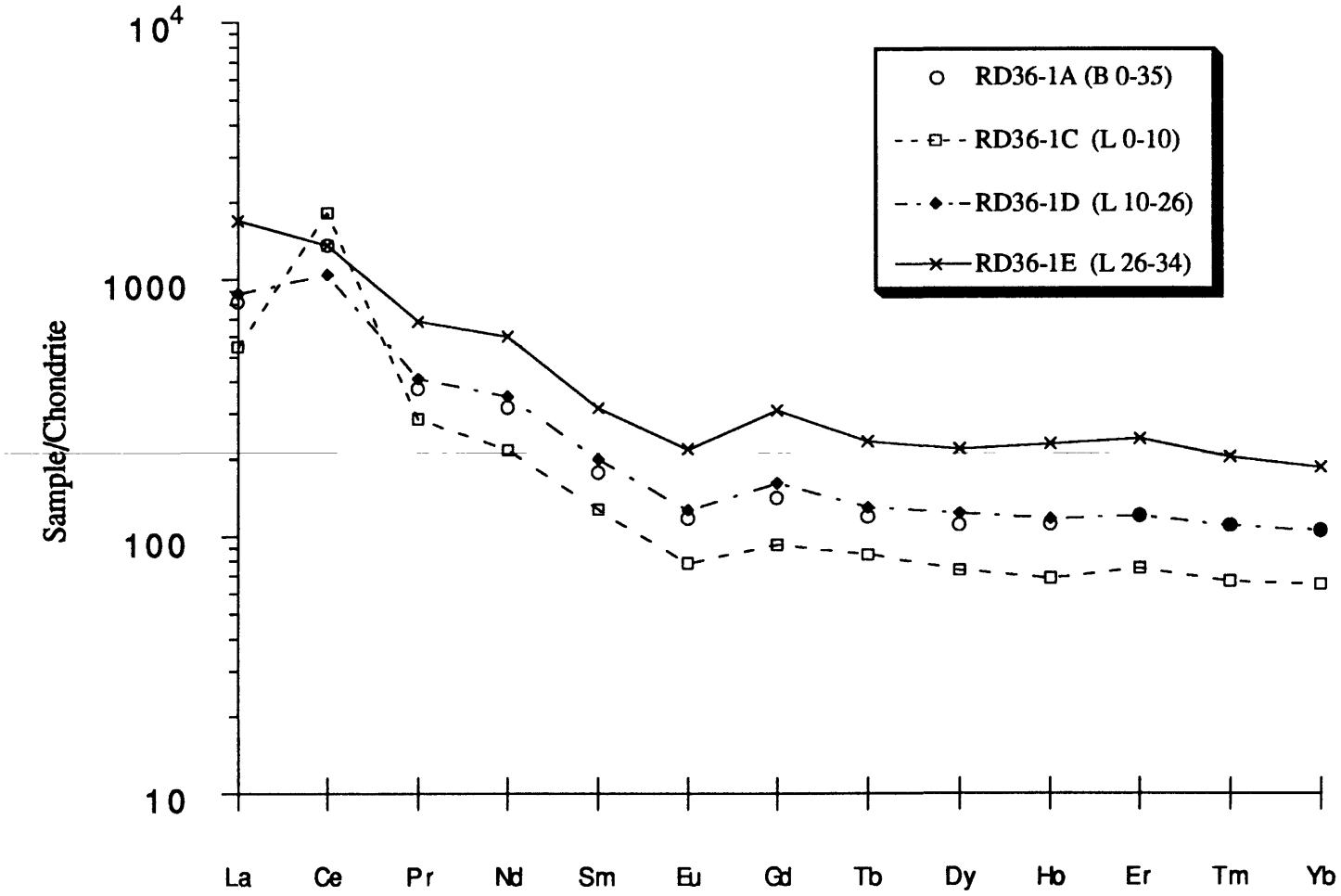

Figure 131. Chondrite-normalized REE plot of one layered crust and one bulk crust from dredges RD 43 and RD44, respectively.

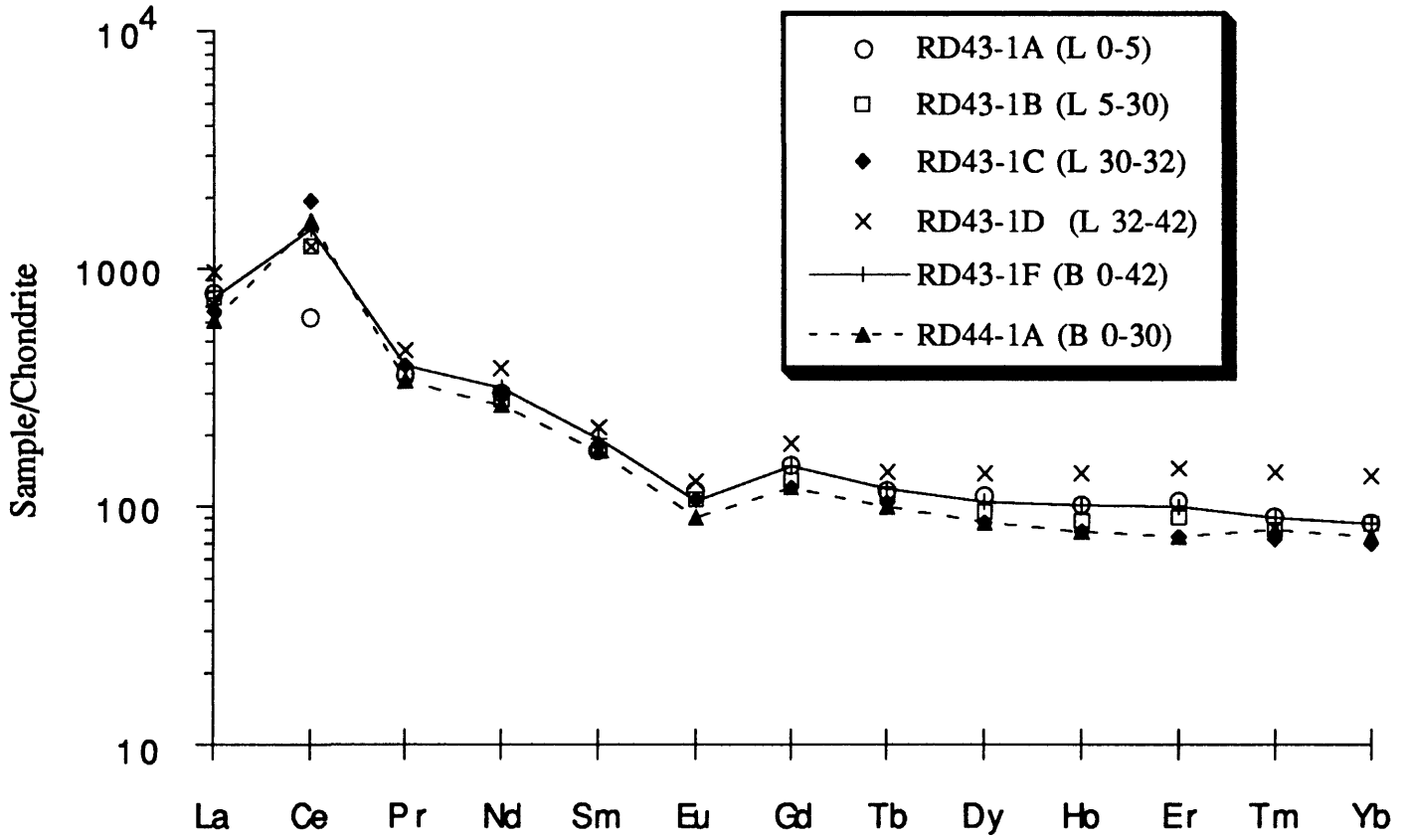

Figure 132. Chondrite-normalized REE plot of a layered crust from dredge RD50.

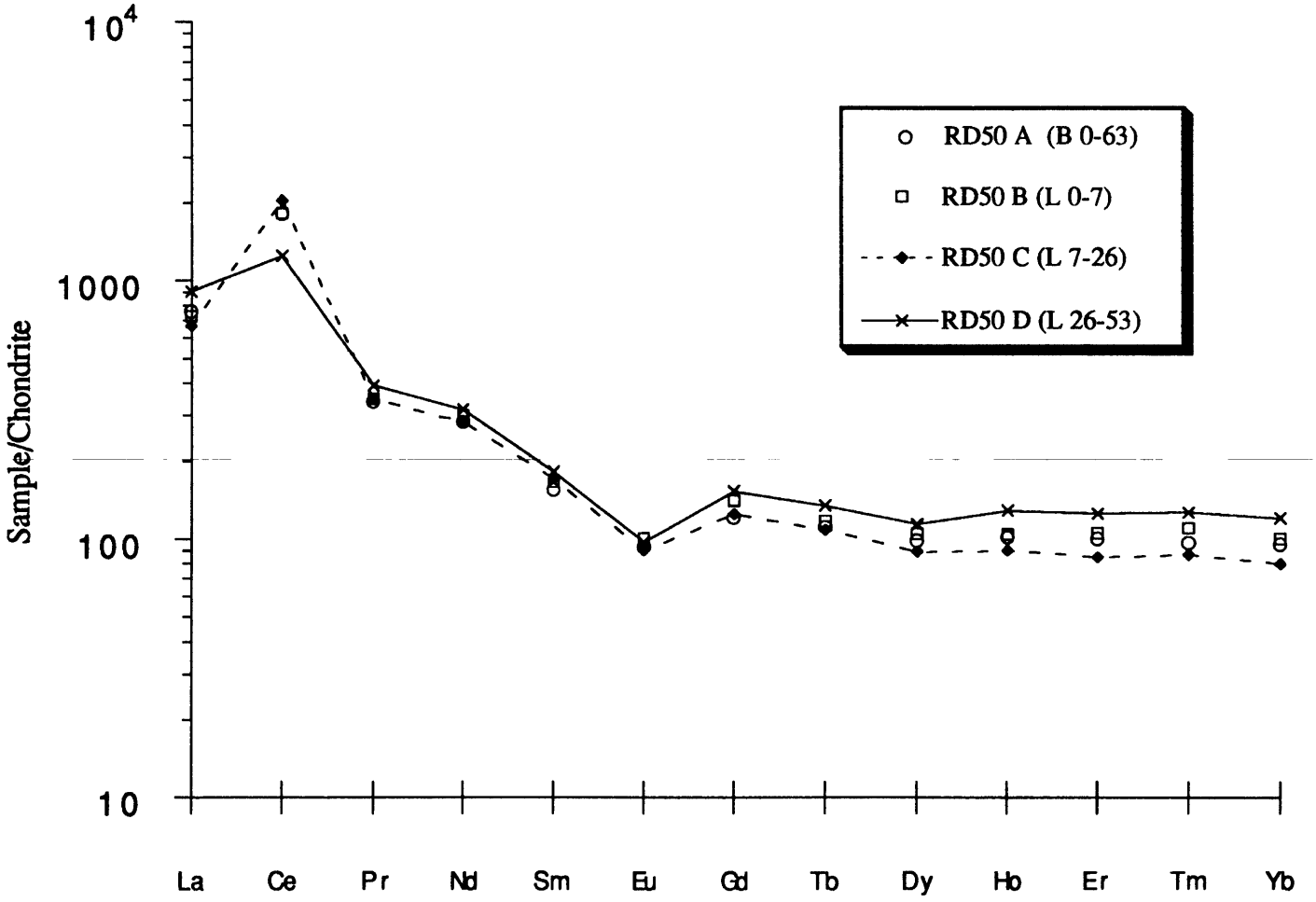

Figure 133. Chondrite-normalized REE plot of a layered crust from dredge RD53.

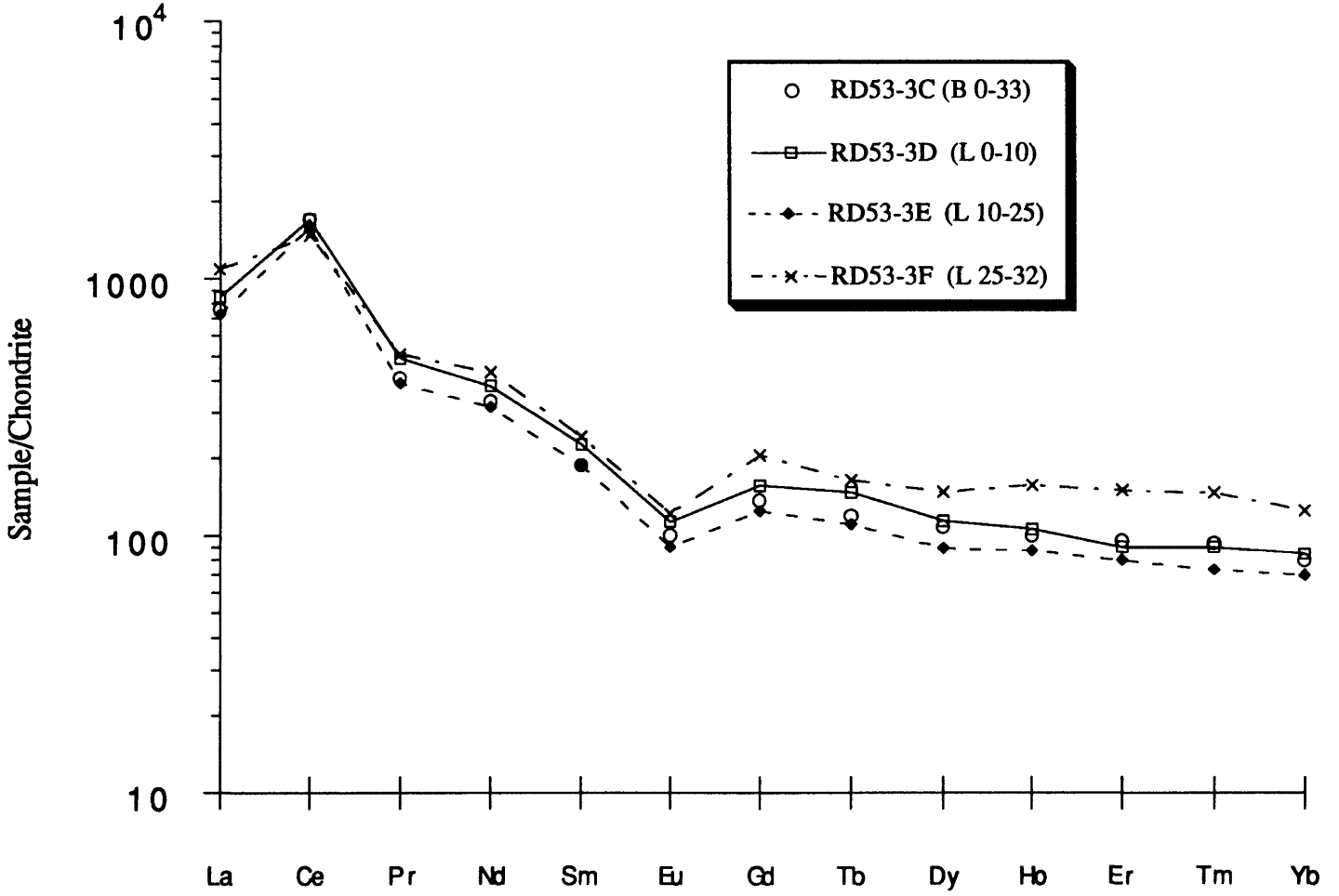

Figure 134. Chondrite-normalized REE plot of a layered crust from dredge RD59.

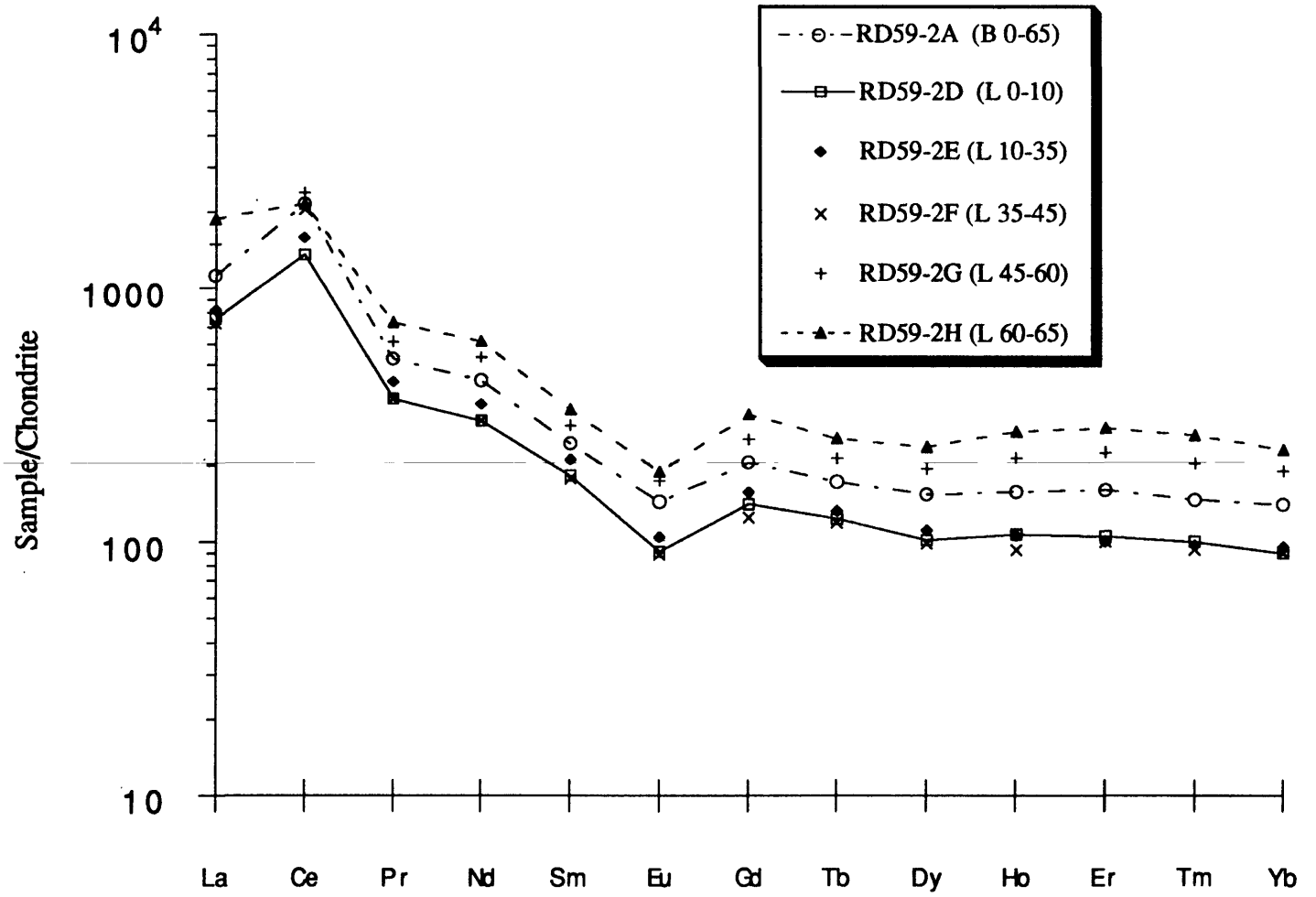

Figure 135. Chondrite-normalized REE plot of a layered underside crust from dredge RD59.

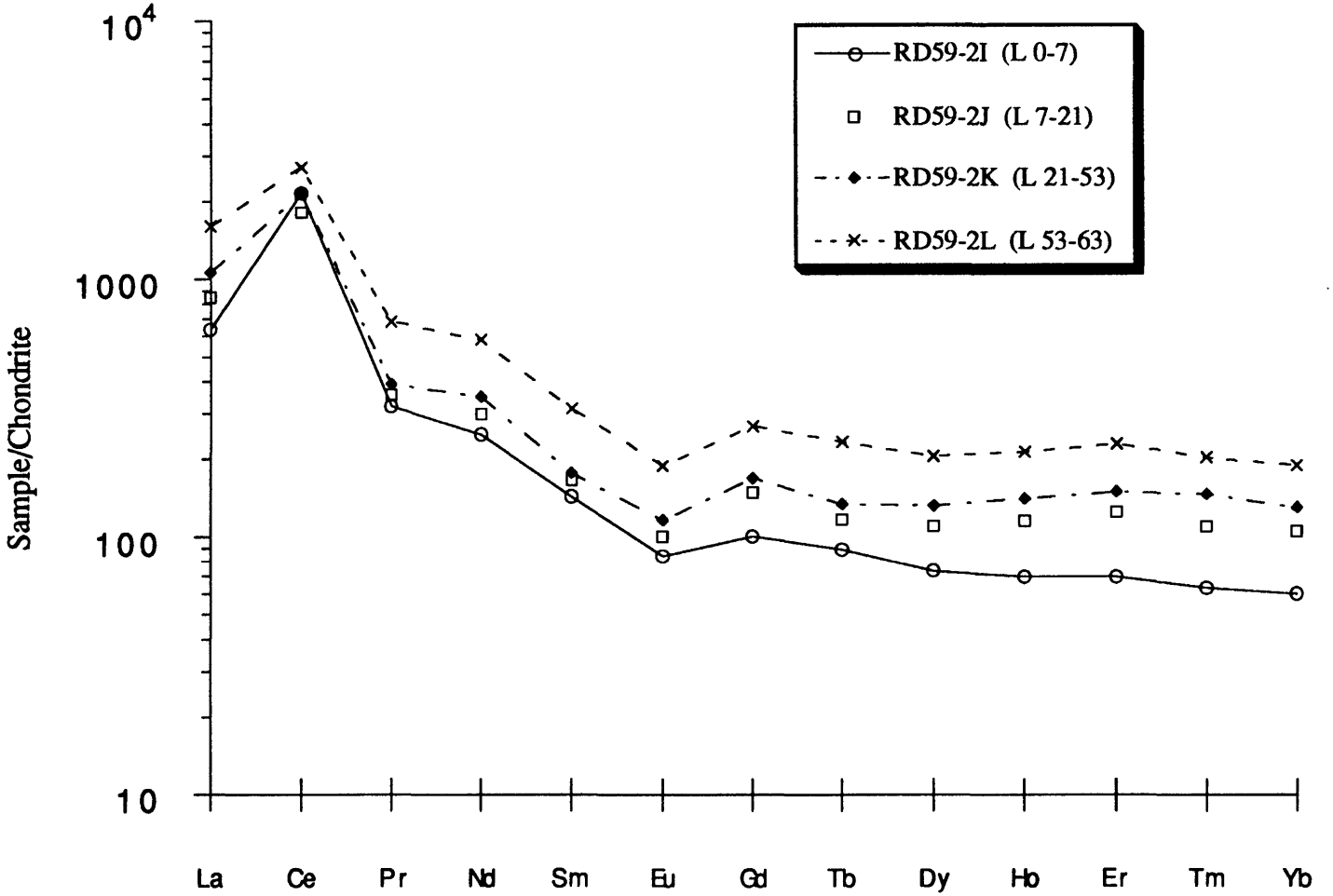

Figure 136. Chondrite-normalized REE plot of a layered crust from dredge RD60.

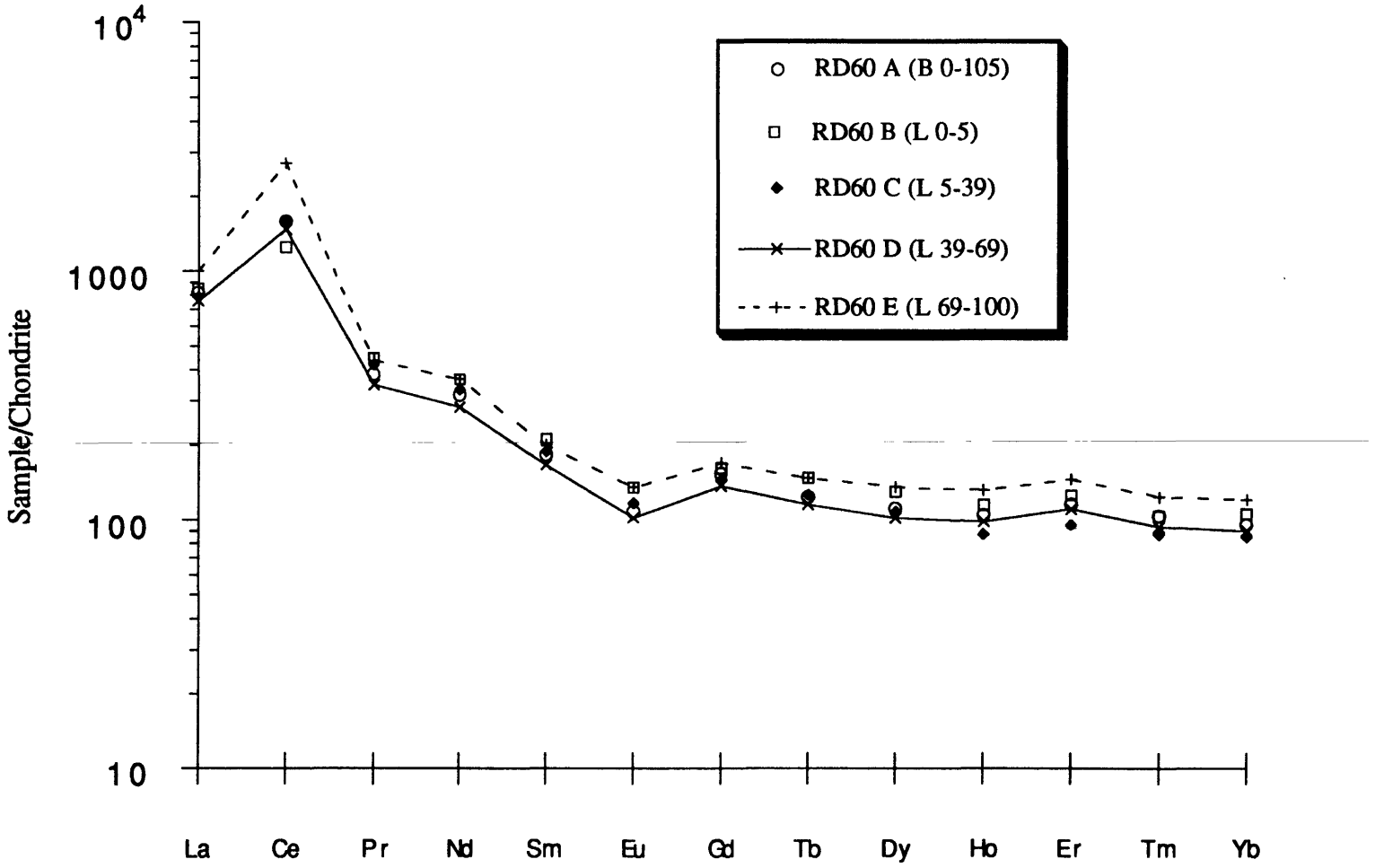

Figure 137. Chondrite-normalized REE plot of a layered crust from dredge RD63.

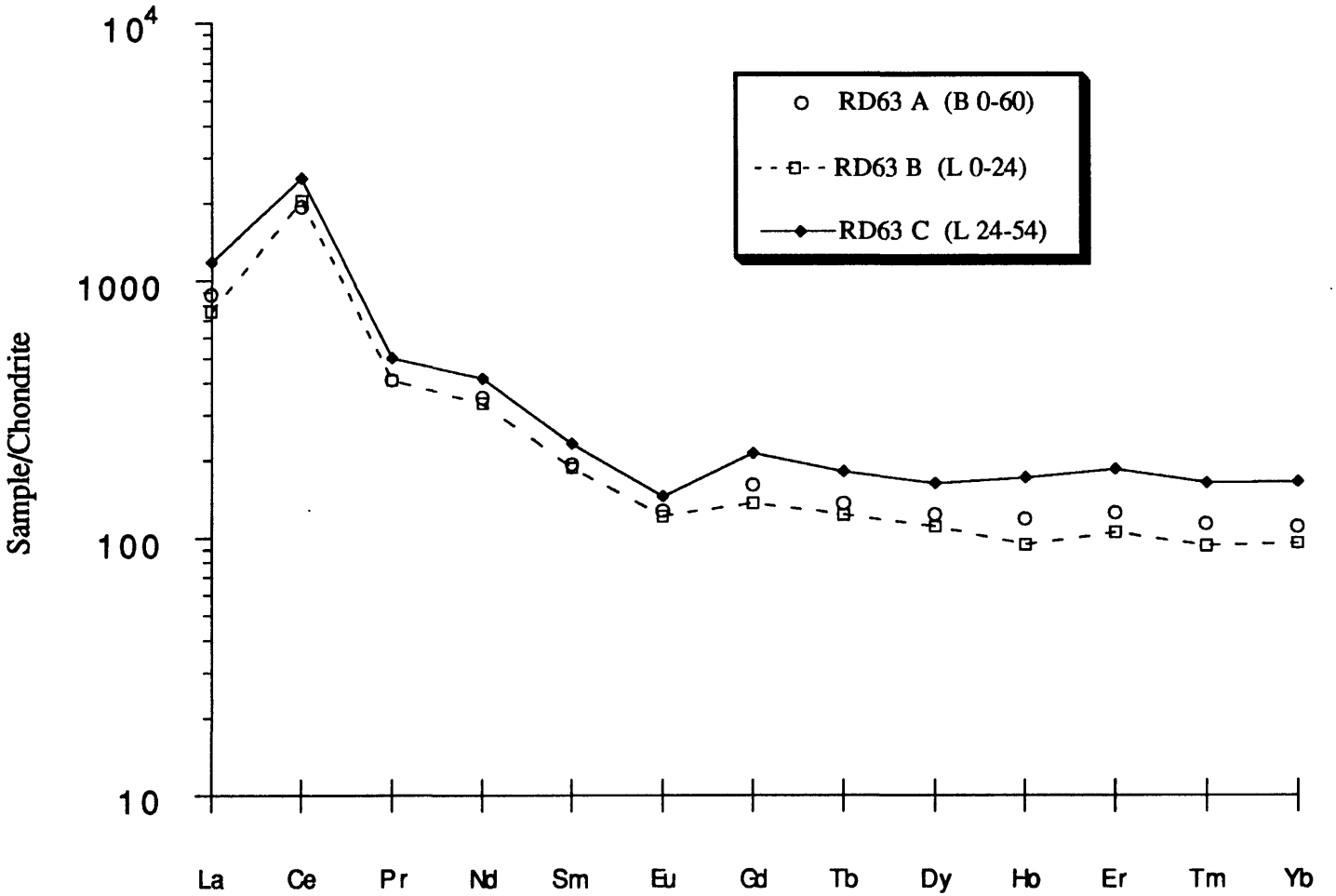

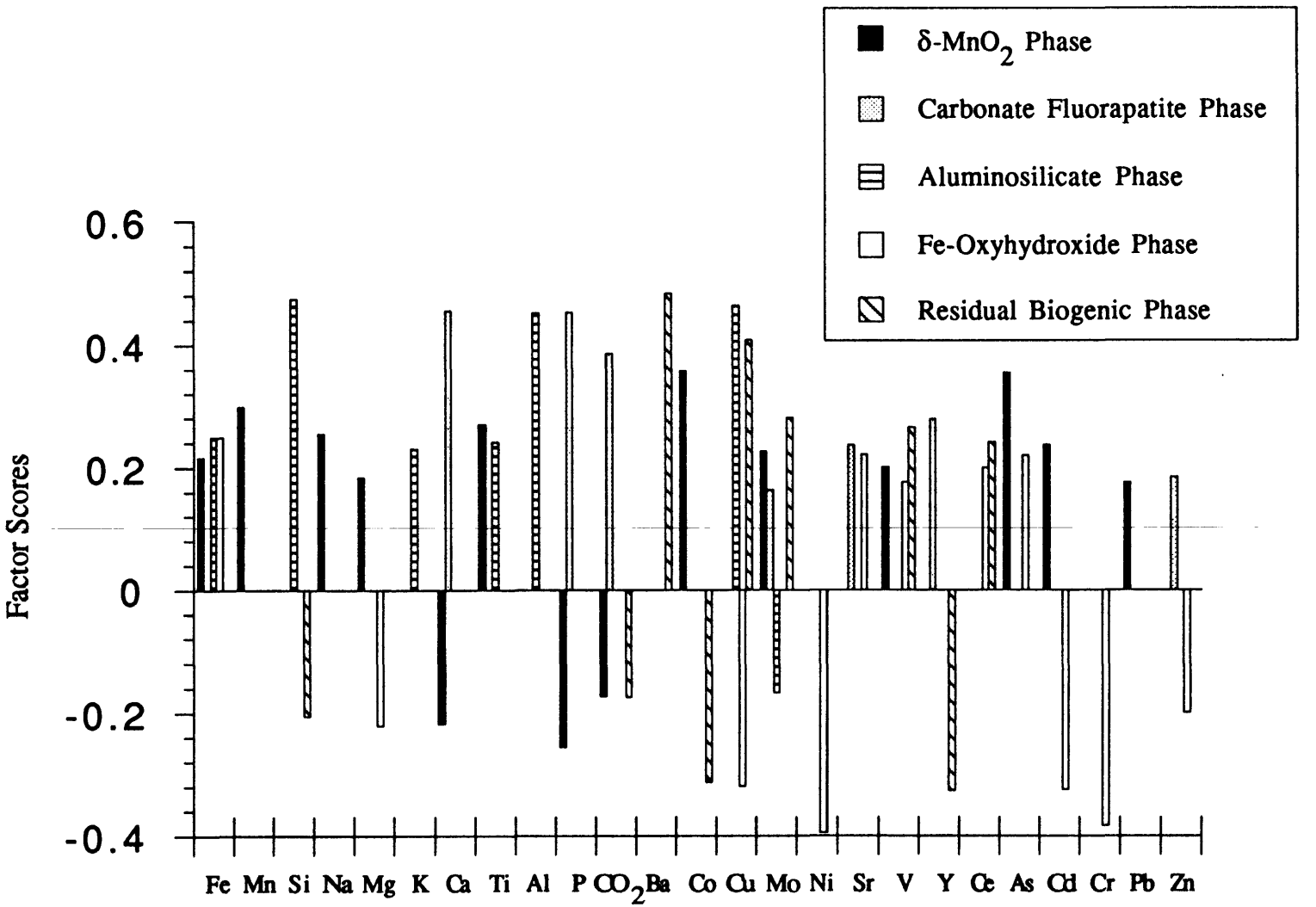

Figure 138. Q-mode factor scores for 60 bulk crusts and nodules. Factor scores between 0 and|0.160| are not included, because random noise makes it difficult to resolve the orientation of the factor to within 10° of an absolute direction in variable space. The five factors account for 99.0% of the data set.

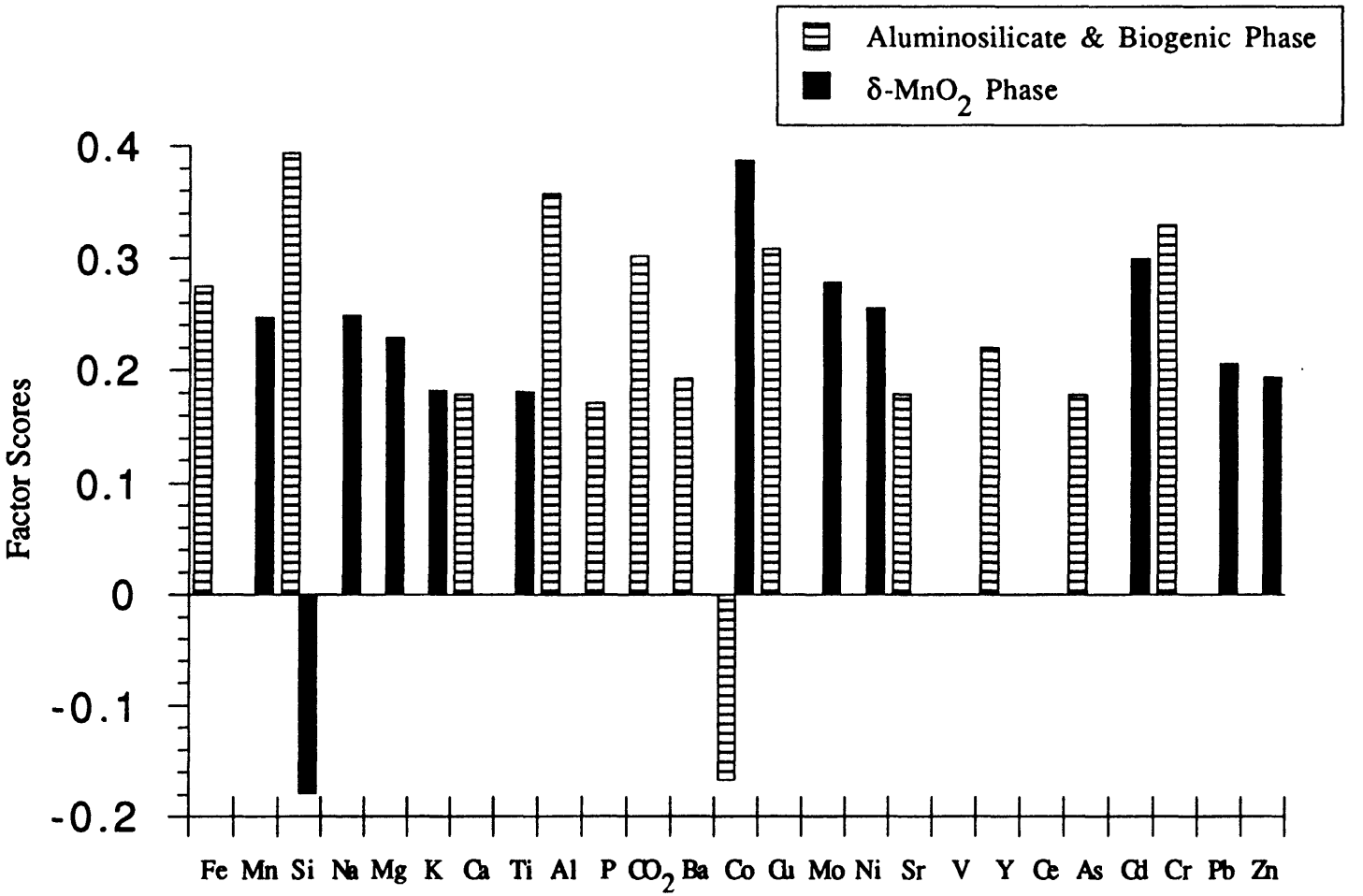

Figure 139. Q-mode factor scores for 17 crust surfaces. Factor scores between 0 and |0.160| are not included, because random noise makes it difficult to resolve the orientation of the factor to within 10° of an absolute direction in variable space. The two factors account for 99.5% of the data set.

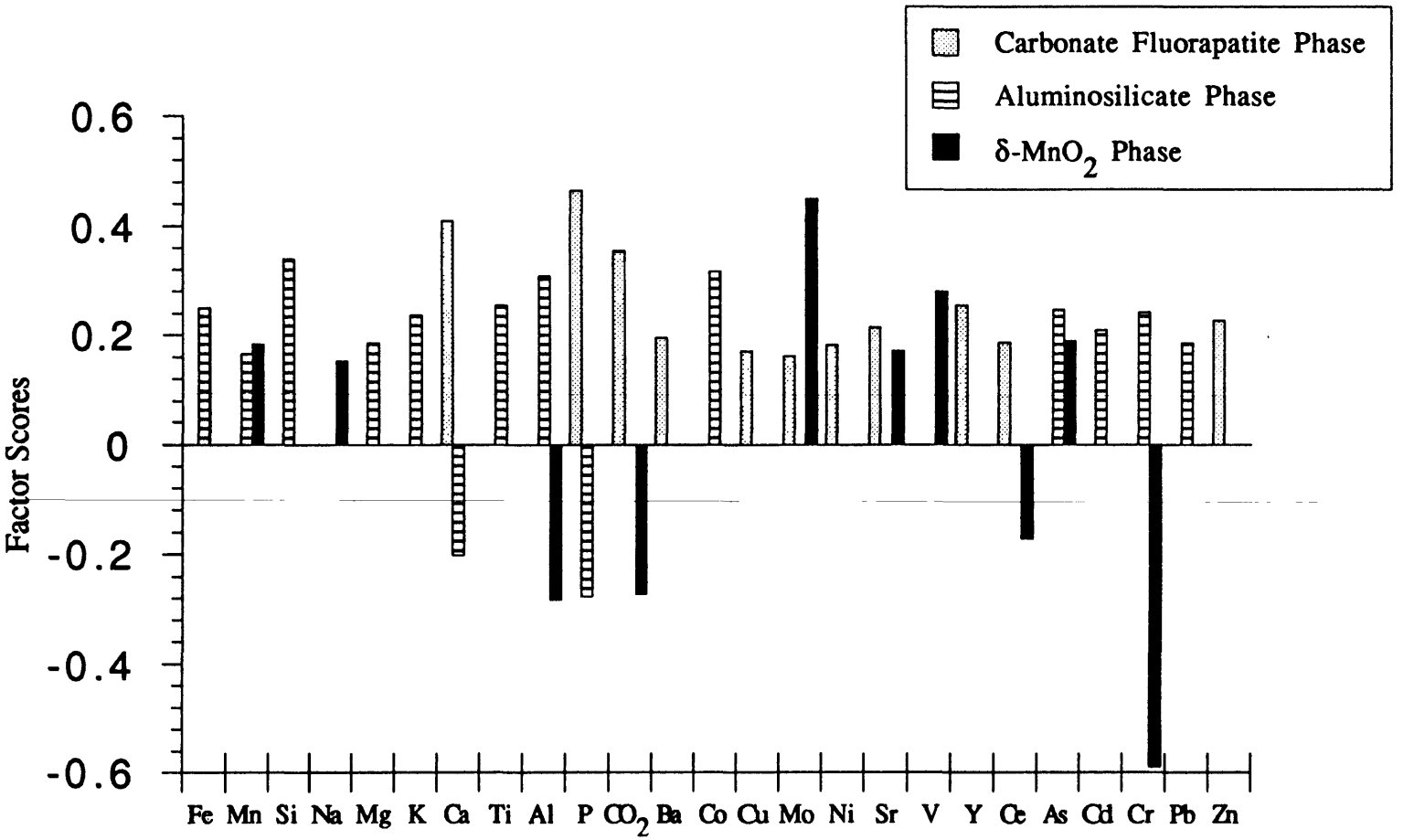

Figure 140. Q-mode factor scores for 11 bulk crusts ≥ 100mm. Factor scores between 0 and |0.160| are not included, because random noise makes it difficult to resolve the orientation of the factor to within 10° of an absolute direction in variable space. The three factors account for 99.4% of the data set.

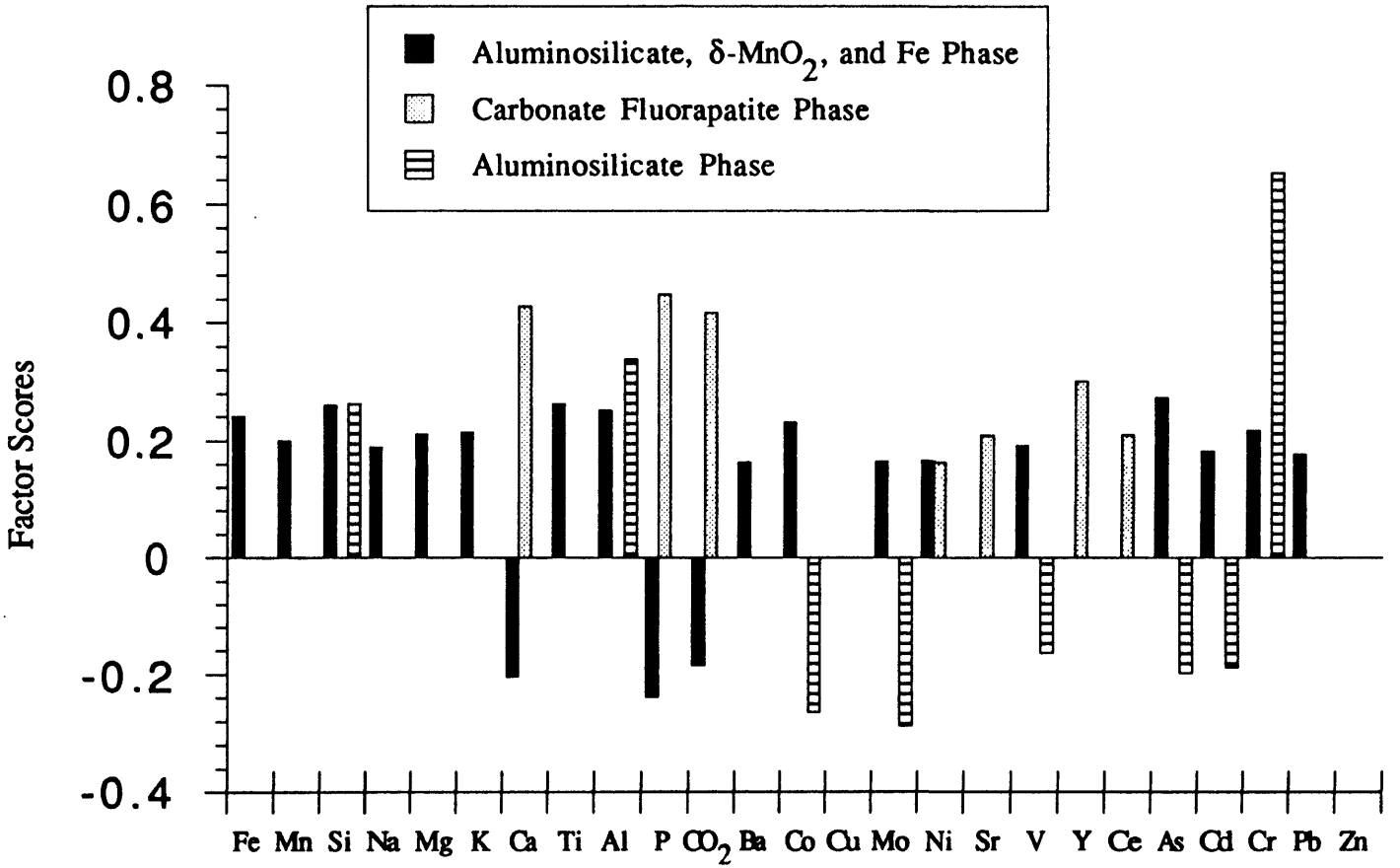

Figure 141. Q-mode factor scores for crust D11-15. Factor scores between 0 and |0.160| are not included, because random noise makes it difficult to resolve the orientation of the factor to within 10° of an absolute direction in variable space. The three factors account for 99.4% of the data set.

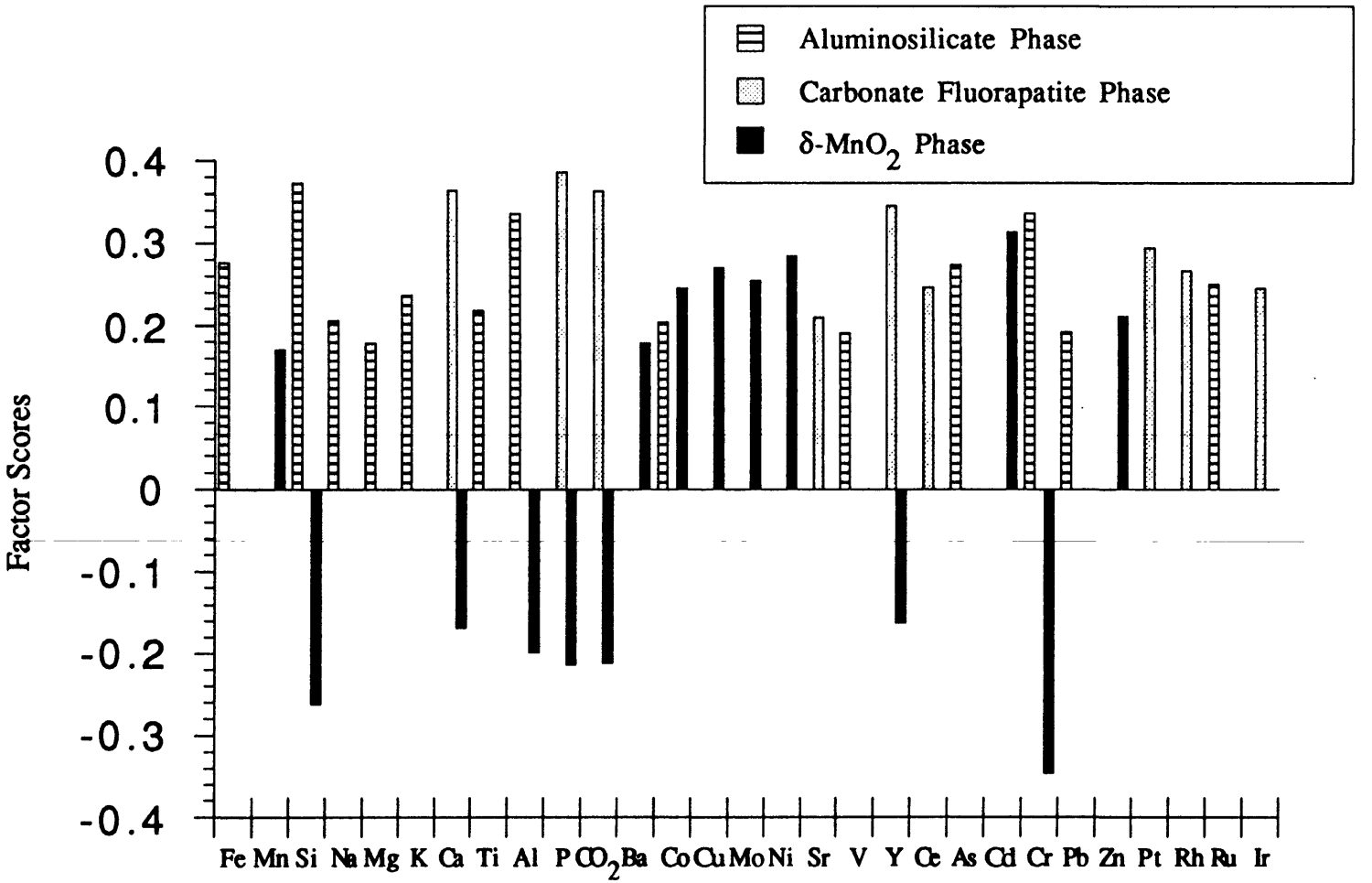

Figure 142. Q-mode factor scores for crust RD59-2. Factor scores between 0 and |0.160| are not included, because random noise makes it difficult to resolve the orientation of the factor to within 10° of an absolute direction in variable space. The three factors account for 99.6% of the data set.

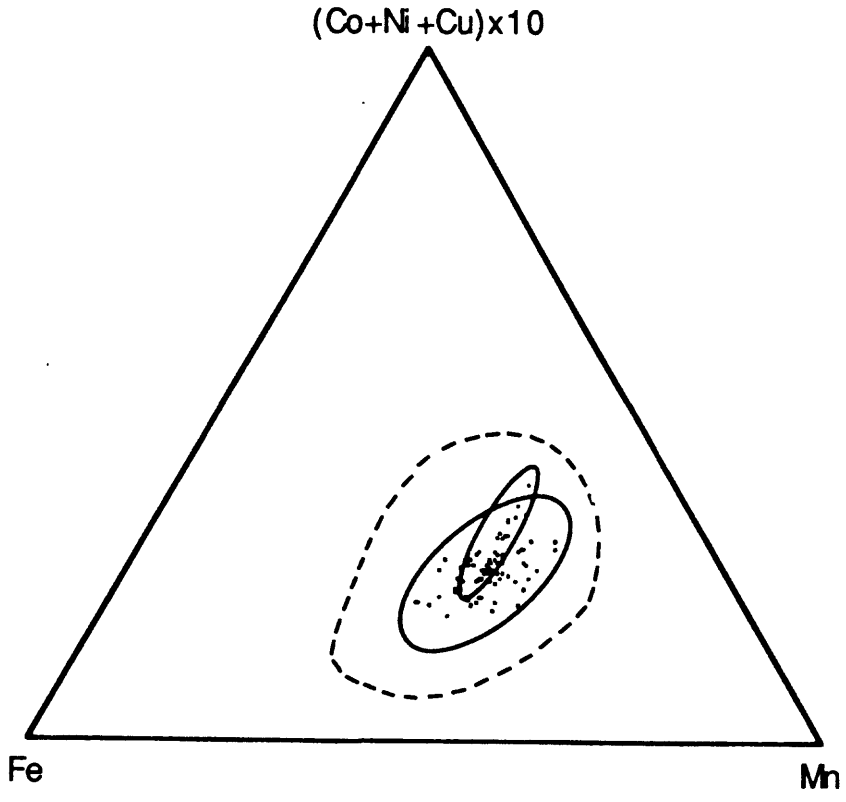

Figure 143. Ternary diagram after Bonatti et al. (1972) for 61 bulk crusts (large ellipse) and 17 crust surfaces (≤ 0.5 mm, small ellipse) from the Marshall Islands. Field enclosed in dashed line is for 308 central Pacific bulk crusts (from Hein et al., 1990c).

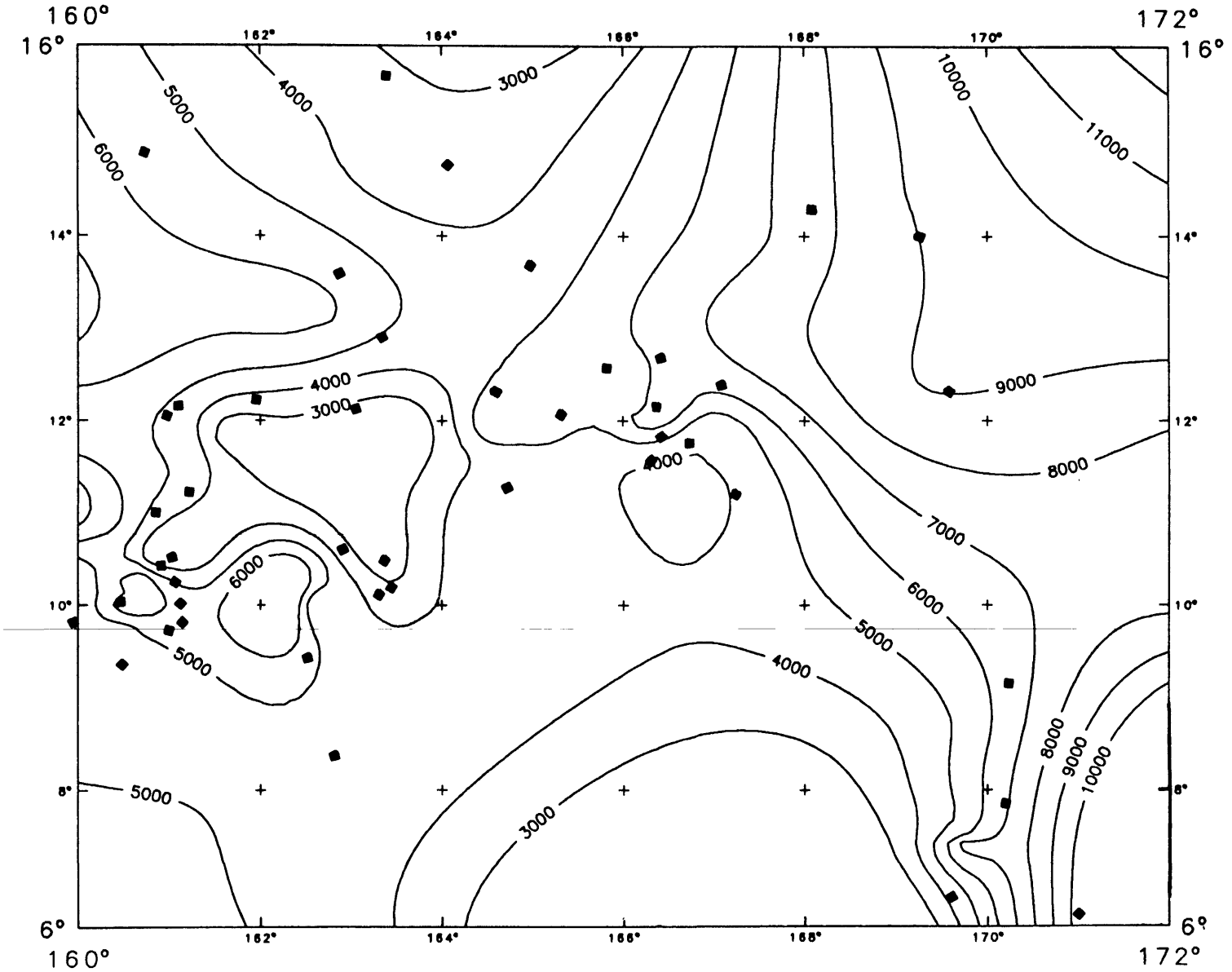

Figure 144. Map of cobalt concentration in the Marshall Islands EEZ. Contour interval 1000 ppm Co. Squares are data points where Co in bulk crusts were averaged for each dredge. Data in eastern part of area from Hein et al. (1988).

APPENDIX

Prepared by

Alfred Capelle
Alele Museum and National Archives
Republic of the Marshall Islands

A concise description of the pronunciation of the Marhallese language can be found in Abo, et al., 1976, Marshallese-English Dictionary, University Press of Hawaii. Also, the Marshallese names used in this paper follow the spelling in that dictionary.

Atoll (Aelōñ)	Associated seamounts (Koṃlōñ)	Meaning of Seamount Names
Ānewetak	Ļami	Legendary giant from Ānewetak
	Lọmilik	Best fishing site in the atoll
	Peto-Eṇ	A channel taboo to everyone but members of the Pako (shark) clan
	Ļọ-Eṇ	Site named in honor ot the ever so useful hibiscus tree, whose bark is used for traditional dress
	Ļọ-Wūliej	Traditional cape on the windward side of Ānewetak Atoll
	Neen-Koiaak	The fastest Marshallese runner from tradition
	Aeañ-Kaṇ	A taboo fishing spot reserved for traditional chiefs (irooj) in the northern part of Ānewetak
Ujlañ	Ļōjemeja	A prehistoric chief of Ujlañ
	Likelep	Traditional site at Ujlañ where the technique for extracting the arrowroot starch was first acquired
	Mij-Lep	Longest gap between islets in Ujlañ
	Radik	A prehistoric chief of Ujlañ
	Ļalibjet	A god of the sea
	Ļajutōkwa	First chief to navigate to northern seas of the islands
	Litōrmālu	Legendary navigator who passed on the knowledge to Ļainjin
	Ļōtab	A descendant of Litōrmālu, who made a name for himself in navigational skill and prowess
	Ļainjin	Son of legendary navigator who managed to mentally map the entire archipelago

Jālwōj	Maanjidep	A prehistoric chief of Jālwōj
Bokaak	Wōden-Kōpakut	A coral head that represents both good and bad luck depending on ones behavior toward local traditions
Pikaar	Ļāwūn-Pikaar	Legendary chief of Pikaar
Arṇo	Ļōṃjenaelik	A legendary chief of Arṇo
Mile	Ļōmōļkā	A traditional chief of Mile
	Limaļok	A traditional chieftess of Mile
Aelōṇļapļap	Jebrọ	Legendary chief who was shown how to use the sail on the outrigger canoe of Aelōṇļapļap
Pikinni	Wōdejebato	Most feared and respected of the sea gods of Pikinni
	Ļōbbadede	Popular prehistoric chieftain of Pikinni, known for his unusual physical characteristics
	Ļōjabōn-Bar	Physically powerful traditional personage of Pikinni
	Ļāānṃōjānjān	Site named in recognition of the props used in the canoe building tradition of Pikinni, where the first knowledge of the canoe building techniques was brought from heaven
	Bwewa-Kaṇ	Site in recognition of the canoe keels, which Ļetao (Marshallese traditional version of the universal trickster) used to build his canoe
	Ļewa	One of the first two Marshallese who received the canoe-building knowledge from heaven
	Ļōmtal	One of the first two Marshallese who received the canoe-building knowledge from heaven
	Wōd-Eṇ	A coral head which the Ri-Pako clan members used to feed on

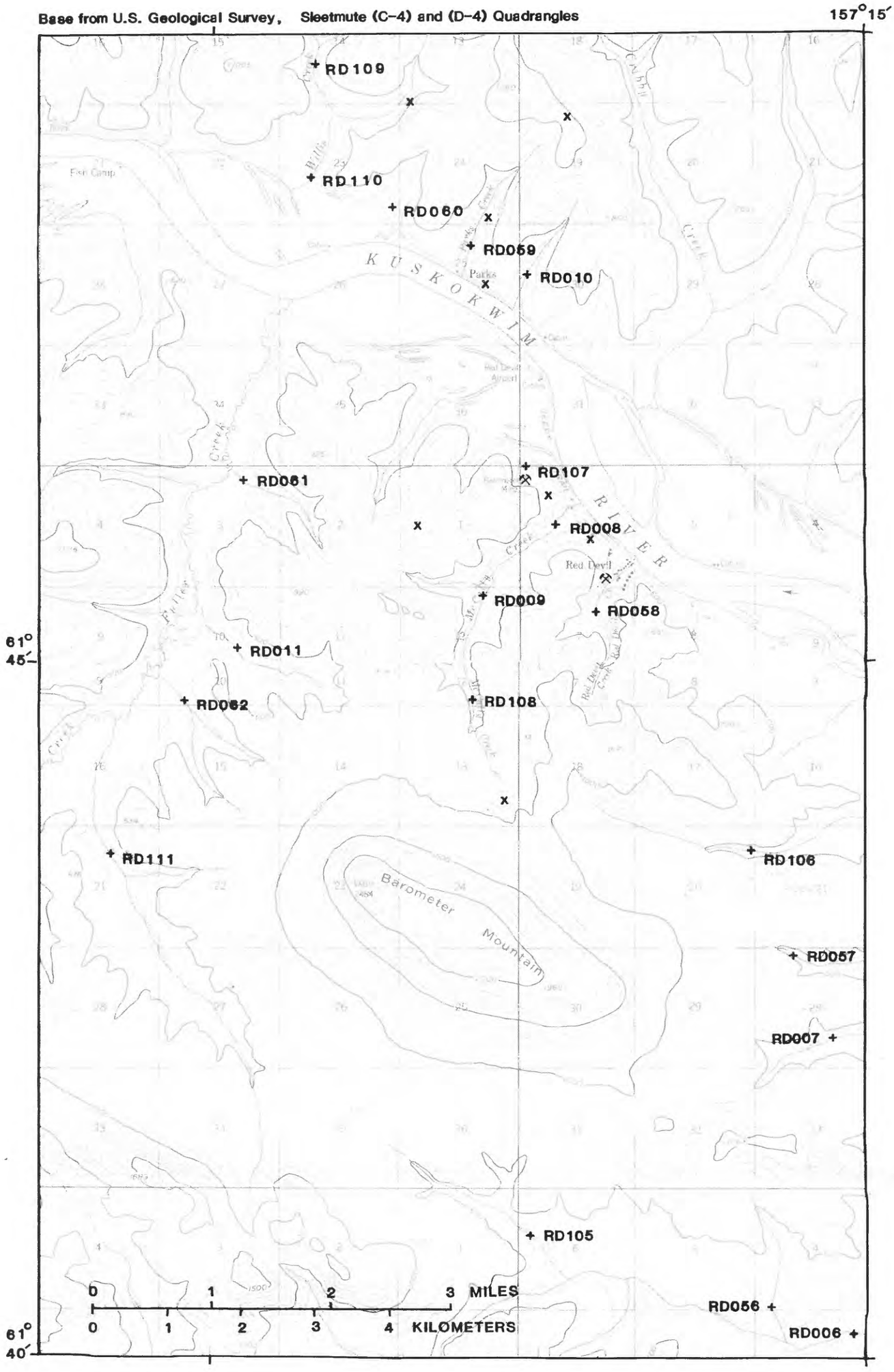

Figure 2. Localities of samples from the Red Devil area.
⚒ - Mines as labeled, x - mineral prospects.